



The
University
Of
Sheffield.

Peptidoglycan Dynamics in *Staphylococcus aureus* using Super-Resolution Microscopy

By:

Victoria A Lund BSc (Hons)

(University of Sheffield)

A thesis submitted for the degree of Doctor of Philosophy

March 2016

Department of Molecular Biology and Biotechnology, University of
Sheffield, Firth Court, Western Bank, Sheffield, S10 2TN

Abstract

Peptidoglycan is the major structural component of the bacterial cell wall; essential for viability and shape determination. This crucial function makes peptidoglycan synthesis an important target for antibiotics such as penicillin. In order to develop novel antimicrobials, especially against drug resistant *Staphylococcus aureus* it is important to understand peptidoglycan dynamics at the molecular level. *S. aureus* makes peptidoglycan primarily during septation and divides on 3 orthogonal planes resulting in cell wall sectoring, with each cell having material of different ages. However, how peptidoglycan is biosynthesised at the molecular level is still not understood.

In order to approach the issue of peptidoglycan synthesis I have used a combination of novel probes and fluorescence microscopy. A range of fluorescent probes, based on analogues of peptidoglycan constituents were used in order to allow imaging. I have used 2 new microscopy approaches, structured illumination microscopy (SIM) and stochastic optical reconstruction microscopy (STORM). Previously unresolved features of peptidoglycan synthesis were revealed. Firstly, peptidoglycan synthesis occurs as a zone across the septum, secondly, there is an apparent split in the septum at the mother cell wall-septum interface and finally synthesis is not confined to the septum but occurs throughout the cell wall.

As well as molecular level information my study has given cellular level insights. The dynamics of peptidoglycan insertion showed progression of synthesis during a division cycle and the inheritance of material over several generations. It was observed that within a population there is a degree of heterogeneity in peptidoglycan insertion both at the cellular and population level. The existence of transiently non-growing cells within larger exponentially growing population alluded to the presence of potential persisters, able to withstand environmental assault. My work has led to a reassessment of models of growth and division of *S. aureus* from the molecular to population level.

Acknowledgements

Firstly, I would like to thank the MRC and Prof. Simon Foster for giving me the opportunity to carry out my PhD. Thanks also to Simon for his continued support and guidance throughout.

I am grateful to the many people who gave me technical advice. Thanks must go to Dr Simon Jones and Dr Dan Cox for production of probes and to Dr Stéphane Mesnage for assistance with the HPLC and Mass Spec. Thanks also to Irene Johnson for use of the Scintillation Counter and Darren Robinson at the Light Microscopy Facility. I am indebted to the many hours both Dr Robert Turner & Dr Christa Walther have put in towards the use of the super-resolution microscopes during my PhD. I would also like to thank Bob for the many useful discussions.

Thanks to all members of the Foster lab, both past and present, not only for scientific help but also for making the experience a lot more enjoyable. Particularly to Ashley Davies for helping when I started out, Kasia Wacnik for creation of strains and Sam Fenn for providing an extra pair of hands. Thanks to Bryony Cotterell for her friendship and encouragement for many hours sat at the HPLC and for basically being my personal chemist.

Thanks to all my friends I've made during my time here in Sheffield particularly to Amy, Claudine, Emily, Jason & Oishek for board games nights and dragging me to the cinema. Special thanks to Hayley for always knowing when I needed a cup of tea.

Thanks to my extended family, who have supported me for the duration. Also to my parents who have always been at the other end of the phone no matter what time of day or night.

Last but by no means least, to Michael White who has helped me in countless ways. Thank you.

List of Abbreviations

%	Percentage
~	Approximately
°	Degree
°C	Degree Celsius
µg	Microgram
µl	Microliter
µM	Micromolar
µm	Micrometre/microns
2D	Two dimensional
3D	Three dimensional
Å	Angstrom
ADA	3-Azido-D-alanine
ADEP	Acyldepsipeptide
AFM	Atomic force microscopy
Ami	Amidase
BHI	Brain Heart Infusion
CDM	Chemically defined media
ColM	Colicin M
CPase	Carboxypeptidase
CTCF	Corrected total cell fluorescence
D-ala	D-alanine
Ddl	D-ala-D-ala ligase
D-glu	D-glutamic acid
dH ₂ O	Distilled water
DMSO	Dimethyl sulphoxide
DNA	Deoxyribonucleic acid
DPM	Disintegrations per minute
dSTORM	Direct STORM
ECT	Electron cryo tomography
EM	Electron microscopy
EMS	Ethyl methanesulphoxide
EPase	Endopeptidase
Ery	Erythromycin
eYFP	Enhanced yellow fluorescent protein
FDAAs	Fluorescent D-amino acids
FWHM	Full-width half maxima
g	Grams
GlcN	Deacetylated GlcNAc
GlcNAc	N-acetyl glucosamine
GTP	Guanosine triphosphate
h	Hour
HADA	Hydroxycoumarin 3-amino-D-alanine
HDZ	High density zone
HF	Hydrofluoric acid

HMW	High molecular weight
HPLC	High performance liquid chromatography
IPTG	Isopropyl beta-D-1-thiogalactopyranoside
l	Litre
L-ala	L-alanine
Ldt	L,D-transpeptidase
LDZ	Low density zone
Lin	Lincomycin
LMW	Low molecular weight
LTA	Lipoteichoic acid
M	Molar
mA	Milliamps
ManNAc	N-acetylmannosamine
m-DAP	meso-diaminopimelate
MEA	Mercaptoethylamine
mg	Milligram
MIC	Minimum inhibitory concentration
min	Minute
ml	Millilitre
mM	Millimolar
MRSA	Methicillin resistant <i>Staphylococcus aureus</i>
MS	Mass spectrometry
MurN	Deacetylated MurNAc
MurNAc	N-acetyl muramic acid
mW	Milliwatts
n	Number
NA	Numerical aperture
NADA	Nitrobenzofurazan 3-amino-D-alanine
NCDAAs	Non-canonical D-amino acid
nm	Nanometres
NMR	Nuclear magnetic resonance
OD _x	Optical density at wavelength x (nm)
PALM	Photoactivated localisation microscopy
PBP	Penicillin binding protein
PBS	Phosphate buffered saline
polyGroP	Polyglycerol phosphate
polyRboP	Polyribitol phosphate
ppGpp	Guanosine tetraphosphate
PSF	Point spread function
P _{Spac}	Spac promoter
RNA	Ribonucleic acid
rpm	Revolutions per min
S ₀	Ground state
S ₁ /S ₂	Excited singlet state
SDS	Sodium dodecyl sulphate
SEDS	Shape, elongation, division & sporulation
SIM	Structured illumination microscopy
Spec	Spectinomycin
SSIM	Saturated SIM

STED	Stimulated emission depleted microscopy
STORM	Stochastic optical reconstruction microscopy
T	Triplet state
TA	Toxin-Antitoxin
TADA	Tetramethylrhodamine 3-amino-D-alanine
TCA	Trichloroacetic acid
TEM	Transmission EM
TES	Tris-EDTA NaCl
TGase	Transglycosylase
TMR	Tetramethylrhodamine
TPase	Transpeptidase
Tris	Tris (hydroxymethyl) aminomethane
tRNA	Transfer RNA
UDP	Uridine diphosphate
UV	Ultra violet
v/v	Volume for volume
VISA	Vancomycin intermediate <i>Staphylococcus aureus</i>
VRSA	Vancomycin resistant <i>Staphylococcus aureus</i>
w/v	Weight for volume
WGA	Wheat Germ Agglutinin
WTA	Wall teichoic acid
x	Times
λ	Wavelength

Table of Contents

Abstract	i
Acknowledgements	iii
List of Abbreviations	iv
Table of Contents	vii
List of Figures	xii
List of Tables	xvi
Chapter 1	1
Introduction	1
1.1 The bacterial cell envelope	1
1.1.1 Gram negative.....	1
1.1.2 Gram positive	1
1.2 Chemical structure of peptidoglycan.....	3
1.2.1 Glycan strands.....	3
1.2.2 Peptide sidechains	6
1.3 Teichoic acids	6
1.4 Peptidoglycan synthesis.....	9
1.4.1 Cytoplasmic steps of precursor biosynthesis.....	12
1.4.2 Translocation of lipid II.....	12
1.4.3 Incorporation of Lipid II into peptidoglycan	13
1.5 Peptidoglycan hydrolysis	14
1.5.1 Glycosidases	14
1.5.2 Amidases and peptidases.....	16
1.5.3 The physiological role of peptidoglycan hydrolases	16
1.6 Cell division	18
1.6.1 Cell division in rod-shaped bacteria.....	18
1.6.2 Cell division in coccoid bacteria	21
1.7 Cell division machinery	23
1.7.1 The z-ring.....	23
1.7.2 FtsZ interacting proteins	26
1.7.3 Septal biosynthesis machinery.....	29
1.8 Cell division as an antibiotic drug target.....	31
1.9 Peptidoglycan dynamics	33
1.9.1 Synthesis of peptidoglycan	33

1.9.2	Enlargement of the sacculus	34
1.9.3	Daughter cell splitting & septum expansion	36
1.10	Peptidoglycan architecture	39
1.10.1	Models of peptidoglycan architecture	39
1.10.2	New models of peptidoglycan architecture	42
1.10.3	Models of peptidoglycan architecture in Gram negative bacteria.....	42
1.10.4	Models of peptidoglycan architecture in Gram positive rods.....	44
1.10.5	Models of peptidoglycan architecture in ovococci	47
1.10.6	Models of peptidoglycan architecture in <i>S. aureus</i>	47
1.11	Methods of peptidoglycan analysis.....	51
1.12	<i>Staphylococcus aureus</i>	52
1.13	Antibiotic resistance	53
1.14	Project Aims.....	54
Chapter 2	57
Materials and Methods	57
2.1	Media.....	57
2.1.1	Brain Heart Infusion (BHI).....	57
2.1.2	Chemically defined media (CDM)	57
2.2	Antibiotics.....	59
2.3	Buffers & Solutions	59
2.3.1	Phosphate Buffered Saline	59
2.3.2	Borate Buffer	59
2.3.3	HPLC buffers	61
2.3.4	Fixative preparation.....	61
2.3.5	Click-iT® reaction buffer mix.....	62
2.3.6	STORM imaging buffers.....	62
2.3.7	Tris/EDTA/NaCl Buffer (TES)	63
2.4	Bacterial strains and growth.....	63
2.5	Chemicals & enzymes	63
2.6	Centrifugation.....	63
2.7	Determination of bacterial cell density	63
2.7.1	Optical density measurements.....	63
2.8	Antibiotic minimum inhibitory concentration (MIC) determination.....	67
2.9	Growth of <i>S. aureus</i> with antibiotic treatment	67
2.10	Labelling peptidoglycan.....	67
2.10.1	Labelling with fluorescent D-amino acids (FDAAs)	67
2.10.2	Click-iT® reaction	67

2.10.3	Labelling the cell surface with NHS-ester dyes	68
2.10.4	Vancomycin labelling	68
2.11	Labelling Protocols	68
2.11.1	Labelling 5 minutes peptidoglycan synthesis with FDAAs for diffraction limited microscopy & STORM	68
2.11.2	Labelling 5 minutes peptidoglycan synthesis with FDAAs for SIM	68
2.11.3	Labelling 2 minutes peptidoglycan synthesis with FDAAs for STORM.....	69
2.11.4	Labelling peptidoglycan synthesis during antibiotic treatment.....	69
2.11.5	Labelling nascent peptidoglycan synthesis with vancomycin.....	69
2.11.6	Labelling whole peptidoglycan with vancomycin	69
2.11.7	Dual labelling with dipeptide & vancomycin	70
2.11.8	Chemical treatment of labelled samples	70
2.11.9	Labelling mutant strains to determine off-septal percentage.....	70
2.11.10	Using the FtsZ-eYFP strain to determine the effect of PC190723	71
2.11.11	Dual Labelling.....	71
2.12	Preparation of samples for fluorescence microscopy	72
2.12.1	Fixation.....	72
2.12.2	Sample preparation for diffraction limited microscopy	72
2.12.3	Sample preparation for STORM	73
2.12.4	Sample preparation for SIM.....	74
2.13	Fluorescence microscopy.....	74
2.13.1	DeltaVision microscopy.....	74
2.13.2	Nikon dual-camera microscopy	74
2.13.3	OMX microscopy	74
2.13.4	Image rendering.....	75
2.13.5	Stochastic optical reconstruction microscopy (STORM).....	75
2.14	Purification of cell walls	78
2.14.1	Extraction of cell walls	78
2.14.2	Breaking cells for imaging	79
2.15	Preparation of cell walls for biochemical analysis	79
2.15.1	Preparation of fluorescently labelled sacculi.....	79
2.15.2	Digestion of peptidoglycan to produce soluble muropeptides	79
2.15.3	Sodium borohydride reduction of soluble peptidoglycan material.....	79
2.15.4	HPLC separation of muropeptides	80
2.16	Incorporation of ¹⁴ C-labelled <i>N</i> -acetylglucosamine into cell wall peptidoglycan.....	80
Chapter 3	81

Use of fluorescent D-amino acids to analyse peptidoglycan synthesis in <i>Staphylococcus aureus</i>	81
3.1 Introduction.....	81
3.1.1 Labelling peptidoglycan synthesis	81
3.1.2 Super resolution microscopy.....	82
3.1.3 Aims of the chapter	89
3.2 Results	89
3.2.1 Fluorescent D-amino acid labelling in <i>S. aureus</i>	89
3.2.2 Using STORM in <i>Staphylococcus aureus</i>	108
3.2.3 Using SIM in <i>Staphylococcus aureus</i>	118
3.3 Discussion	122
3.3.1 Labelling peptidoglycan synthesis in <i>S. aureus</i>	122
3.3.2 Using super-resolution microscopy in <i>S. aureus</i>	130
Chapter 4	133
Analysis of the pattern of peptidoglycan synthesis in <i>Staphylococcus aureus</i>	133
4.1 Introduction.....	133
4.1.1 Cell wall architecture in <i>S. aureus</i>	133
4.1.2 <i>S. aureus</i> divisome	135
4.1.3 Aims of the Chapter.....	136
4.2 Results	136
4.2.1 Localisation of peptidoglycan synthesis in <i>S. aureus</i>	136
4.2.2 Peptidoglycan synthesis occurs as a zone at the septum.....	145
4.2.3 Apparent splitting of septum prior to daughter cell separation	145
4.2.4 Peptidoglycan insertion is not confined to the septum	172
4.2.5 Role of peptidoglycan synthesis enzymes in off-septal labelling of peptidoglycan	173
4.2.6 Role of penicillin binding proteins in synthesis of peptidoglycan	178
4.2.7 Effect of inhibition of FtsZ by PC190723 on peptidoglycan insertion	189
4.3 Figure 4.32. Effect of PC190723 on peptidoglycan synthesis in 4424 (<i>pbp3pbp4</i>). 5	
minute windows of peptidoglycan synthesis were labelled by HADA (500 μ M) during	
treatment with 10 μ g ml ⁻¹ PC190723. (Scale Bar 5 μ m).Discussion	228
4.3.1 Model of septal peptidoglycan synthesis	229
4.3.2 Contribution of off-septal synthesis to growth in <i>S. aureus</i>	231
4.3.3 Response to treatment of <i>S. aureus</i> with FtsZ inhibitor PC190723	232
Chapter 5	234
Dynamics of peptidoglycan insertion in <i>Staphylococcus aureus</i>	234
5.1 Introduction.....	234

5.1.1	Aims of the Chapter	238
5.2	Results	241
5.2.1	Dynamics of synthesis by pulse labelling	241
5.2.2	Septal dynamics by virtual time-lapse	245
5.2.3	Inheritance of peptidoglycan over several generations	253
5.2.4	Dynamics reveals heterogeneity in peptidoglycan synthesis	258
5.3	Discussion.....	275
5.3.1	Septation dynamics.....	275
5.3.2	Inheritance of peptidoglycan in sectors.....	276
5.3.3	Heterogeneity in peptidoglycan synthesis.....	277
5.3.4	Bacterial persistence	279
Chapter 6.....		286
General Discussion		286
6.1	Growth & division in <i>S. aureus</i>	286
6.1.1	Selection of division plane	286
6.1.2	Peptidoglycan synthesis.....	291
6.1.3	Splitting of daughter cells	292
6.1.4	Requirement of peptidoglycan hydrolysis in cell growth	293
6.1.5	Inheritance of cell wall material	294
6.1.6	Model of septum formation in <i>S. aureus</i>	296
6.2	Heterogeneity of <i>S. aureus</i> populations	301
6.3	Future Directions	301
6.3.1	Shape change in <i>S. aureus</i>	301
6.3.2	Future insights into peptidoglycan using microscopy.....	302
6.3.3	Role of <i>S. aureus</i> division proteins.....	302
6.3.4	Effect of antibiotic treatment and resistance	305
References		306
Appendix I - Pattern of FDAA labelling over time.....		327
Appendix II - Fourier transform of SIM images		331
Appendix III - Stills from movies 1 & 2		345
Appendix IV - Frequency tables for FtsZ & HADA localisations		347
Appendix V - Quantification of population heterogeneity		348

Enclosed CD-ROM contains an electronic copy of this thesis and Movies 1 & 2. Some images may be clearer on the electronic version.

List of Figures

Figure 1.1. General Structure of the Gram positive and Gram negative cell envelopes..	2
Figure 1.2. Muropeptide structure of <i>S. aureus</i>	4
Figure 1.3. Modifications of glycan residues	8
Figure 1.4 Chemical structures of <i>S. aureus</i> teichoic acids.....	10
Figure 1.5. Peptidoglycan biosynthetic pathway.....	11
Figure 1.6. Action of peptidoglycan hydrolases on the glycan backbone (A) and peptide sidechains (B)	15
Figure 1.7 Division process in rod-shaped & coccoid bacteria.	19
Figure 1.8. Schematic of 3 orthogonal planes in a spherical object.....	22
Figure 1.9. Schematic of cell division machinery (divisome) from (A) <i>E. coli</i> , (B) <i>B. subtilis</i> and (C) <i>S. aureus</i>	24
Figure 1.10 Schematic of z-ring positioning in rod-shaped and coccoid bacteria.....	25
Figure 1.11. Structure of EzrA.....	28
Figure 1.12. Three-for-one model of peptidoglycan insertion.	35
Figure 1.13. Models of peptidoglycan architecture.	40
Figure 1.14. Model of Gram negative peptidoglycan architecture.	43
Figure 1.15. Peptidoglycan architecture of <i>B. subtilis</i>	45
Figure 1.16. Peptidoglycan architecture of <i>S. aureus</i>	48
Figure 1.17. Model of specification of division plane by architectural features in <i>S. aureus</i>	50
Figure 3.1. Jablonski diagram showing energy levels occupied by an excited electron within a fluorescent molecule.	83
Figure 3.2. Diagram depicting the general features of a fluorescence microscope.	85
Figure 3.3. Chemical structures of FDAAs & Alkyne Dyes.	90
Figure 3.4. Testing increasing concentrations of HADA to determine optimal labelling conditions.....	92
Figure 3.5. Testing increasing concentrations of NADA to determine optimal labelling conditions.....	93
Figure 3.6. Testing increasing concentrations of TADA to determine optimal labelling conditions.....	94

Figure 3.7. Testing increasing concentrations of ADA to determine optimal labelling conditions.....	95
Figure 3.8. Testing increasing concentrations of alkyne Alexa Fluor 647 in the click reaction with ADA at 500 μM to determine optimal conditions for labelling.....	96
Figure 3.9. Testing increasing concentrations of dipeptide to determine optimal conditions for labelling peptidoglycan insertion.	97
Figure 3.10. Incorporation of ADA over time..	98
Figure 3.11. Labelling of peptidoglycan sacculi.	100
Figure 3.12. FDAA labelling requires active growth. <i>S. aureus</i> SH1000 in stationary phase was labelled with ADA for 5 min (500 μM) and click labelled to Alexa Fluor 647 post fixation.	103
Figure 3.13. Labelling peptidoglycan synthesis in <i>S. aureus</i> SH1000 with HADA (500 μM) during treatment with 10 x MIC penicillin G (5 $\mu\text{g ml}^{-1}$).	104
Figure 3.14. Labelling peptidoglycan synthesis in <i>S. aureus</i> SH1000 with dipeptide (1 mM) during treatment with 10 x MIC penicillin G (5 $\mu\text{g ml}^{-1}$).	105
Figure 3.15. Labelling peptidoglycan synthesis in <i>S. aureus</i> SH1000 with HADA (500 μM) during treatment with 10 x MIC moenomycin (5 $\mu\text{g ml}^{-1}$).	106
Figure 3.16. Labelling peptidoglycan synthesis in <i>S. aureus</i> SH1000 with dipeptide (1 mM) during treatment with 10 x MIC moenomycin (5 $\mu\text{g ml}^{-1}$).	107
Figure 3.17. Labelling <i>S. aureus</i> SH1000 peptidoglycan synthesis with HADA (500 μM) during treatment with D-cycloserine at 10 x MIC (500 $\mu\text{g ml}^{-1}$).	109
Figure 3.18. Labelling <i>S. aureus</i> SH1000 peptidoglycan synthesis with dipeptide (1 mM) during treatment with D-cycloserine at 10 x MIC (500 $\mu\text{g ml}^{-1}$).	110
Figure 3.19. Biochemistry of FDAA labelling of <i>S. aureus</i> peptidoglycan.....	111
Figure 3.20. Testing fluorescent dyes in STORM.	114
Figure 3.21. Autofluorescence detection in STORM..	117
Figure 3.22. Determining crosstalk of Alexa Fluor 647 and Amersham Cy3B.	119
Figure 3.23. STORM of SH1000 labelled by the Click reaction in the absence of Click compatible FDAA.....	120
Figure 3.24. Testing peptidoglycan labels in structured illumination microscopy.....	121
Figure 3.25. Fourier transforms can detect underlying structure in SIM images	124
Figure 4.1 Localisation of FDAA Incorporation over 5 minutes.....	138
Figure 4.2. Localisation of ADA incorporation over 5 minutes.....	141

Figure 4.3. 2D images and 3D projections of selected cells to highlight features of peptidoglycan incorporation.....	143
Figure 4.4. Localisation of dipeptide incorporation over 5 minutes..	148
Figure 4.5. Fluorescent vancomycin labelling of nascent peptidoglycan following incubation in excess D-serine demonstrates septal and off-septal labelling.	151
Figure 4.6. Reduced labelling time shows zone of synthesis at septum.	154
Figure 4.7. Cells show gap in peptidoglycan synthesis labelling at septum & mother cell interface prior to cell splitting..	156
Figure 4.8. The gap in the septum is not apparent in cells when cell wall is labelled with vancomycin.	161
Figure 4.9. STORM of cells dual labelled with dipeptide and vancomycin.....	167
Figure 4.10. STORM of dual dipeptide and vancomycin labelled <i>S. aureus</i>	170
Figure 4.11. Measurement of gap between two areas of peptidoglycan synthesis... ..	171
Figure 4.12. Chemical treatment of <i>S. aureus</i> to investigate off-septal labelling.	175
Figure 4.13. Contribution of teichoic acids to off-septal labelling.	177
Figure 4.14. Off-septal labelling in Nebraska library mutants.....	180
Figure 4.15. Role of PBP3 and PBP4 in off-septal labelling..	182
Figure 4.16. Quantification the role of PBP3 and PBP4.....	185
Figure 4.17. Role of PBP3 and PBP4 in off-septal labelling measured via dipeptide incorporation..	187
Figure 4.18. SIM of 5 minute HADA labelled PBP mutants..	191
Figure 4.19. STORM of ADA labelled PBP mutants.....	194
Figure 4.20. STORM of dipeptide labelled PBP mutants.	197
Figure 4.21. Effect of PC190723 on growth and cell diameter.	202
Figure 4.22. Effect of PC190723 on FtsZ localisation in <i>S. aureus</i>	206
Figure 4.23. Quantification of localisation of FtsZ during PC190723 treatment.....	207
Figure 4.24. Effect of PC190723 on peptidoglycan synthesis in FtsZ-eYFP <i>S. aureus</i> ..	210
Figure 4.25. Quantification of localisation of peptidoglycan synthesis during inhibition by PC190723 in the FtsZ-eYFP strain.	211
Figure 4.26. Effect of PC190723 on peptidoglycan synthesis in SH1000.	214
Figure 4.27. Quantification of localisation of PG synthesis during inhibition by PC190723 in SH1000.....	218
Figure 4.28. Localisation of peptidoglycan synthesis during PC190723 treatment.	221

Figure 4.29. Quantification of off-septal labelling during the first 20 minutes of PC190723 treatment.....	222
Figure 4.30. Effect of PC190723 on localisation of peptidoglycan synthesis in 4421 (<i>pbp3</i>).....	224
Figure 4.31. Effect of PC190723 on peptidoglycan synthesis in 4425 (<i>pbp4</i>).....	226
Figure 4.32. Effect of PC190723 on peptidoglycan synthesis in 4424 (<i>pbp3pbp4</i>).....	228
Figure 4.33. Peptidoglycan synthesis occurs as a zone at the septum.....	230
Figure 5.1. Model of dynamics of nascent peptidoglycan insertion..	239
Figure 5.2. Schematic of peptidoglycan age by sectoring of cell-wall during multiple cell division cycles.....	240
Figure 5.3. Localisation of nascent peptidoglycan synthesis using dual labelling.....	244
Figure 5.4. Localisation of 2 minutes nascent peptidoglycan synthesis using dual labelling.....	246
Figure 5.5. Septal dynamics by virtual time-lapse.....	249
Figure 5.6. Features of dynamics in septal formation. .	252
Figure 5.7. Fields of cells labelled consecutively with ADA-647 (blue), NADA (green) and HADA (red) for 30 minutes each (All at 500 μ M).....	254
Figure 5.8. Inheritance of peptidoglycan over 3 generations..	257
Figure 5.9. 3D Maximum intensity projections of cells labelled for consecutive 30 minute windows with ADA-647 (blue), NADA (green) & HADA (red) (all at 500 μ M)...	259
Figure 5.10. Heterogeneity in peptidoglycan synthesis during the cell cycle..	262
Figure 5.11. Heterogeneous peptidoglycan synthesis within sister cells.....	265
Figure 5.12 Dynamics of peptidoglycan synthesis reveals heterogeneity across a <i>S. aureus</i> population.....	268
Figure 5.13 Population heterogeneity in peptidoglycan incorporation.....	274
Figure 5.14 Whole population versus single cell analysis.....	280
Figure 6.1. General Schematic of cell division in <i>S. aureus</i>	287
Figure 6.2. Schematic of the piecrust and its subsequent inheritance.	290
Figure 6.3 Models of cell wall inheritance.....	295
Figure 6.4 Model of <i>S. aureus</i> cell division.	300
Figure 6.5 Interaction map of proteins involved in the division process.	304

List of Tables

Table 2.1 Antibiotics used in this study.	60
Table 2.2 <i>S. aureus</i> strains used in this study.	64
Table 2.3 Chemicals & enzymes used in this study.	65
Table 2.4 Centrifuges used in this study.	66
Table 2.5 Minimum inhibitory concentrations (MICs).....	66
Table 2.6 DeltaVision Filters.....	77
Table 2.7 OMX Filters.....	77
Table 2.8 OMX SIM Laser Lines.....	77
Table 2.9. Details for Laser lines used in BigSTORM.....	77
Table 5.1. Distribution of FDAA incorporation over 3 generations in <i>Staphylococcus aureus</i>	269

Chapter 1

Introduction

1.1 The bacterial cell envelope

Bacterial cells exist within demanding and dynamic environments. To survive they have evolved a sophisticated, multi-layered structure to protect them, yet permit interaction with the environment e.g. for nutrient acquisition and waste removal (Silhavy et al., 2010). Species within the bacterial kingdom fall mainly into one of two groups due to the structure of the cell envelope; Gram negative and Gram positive (Figure 1.1).

1.1.1 Gram negative

The Gram negative cell wall consists of three primary layers; the outer membrane, the peptidoglycan, and the cytoplasmic membrane (Figure 1.1 A). The two membranes define the periplasm, a cellular compartment containing a specific set of proteins and processes (Hoppert and Mayer, 1999). The cytoplasmic membrane, common to both Gram positive and negative bacteria, is composed of a phospholipid bilayer and is the site of many important cellular processes such as energy production and lipid biosynthesis (Silhavy et al., 2010). In comparison, the outer membrane of Gram negative bacteria is composed of a mixture of phospholipids comprising the inner leaflet and lipopolysaccharide composing the outer leaflet (Kamio and Nikaido, 1976). The peptidoglycan is an essential, more rigid exoskeleton which is required to withstand internal turgor pressure to maintain cell shape (Vollmer and Höltje, 2004). Peptidoglycan is a polymer containing glycan strands crosslinked by peptide sidechains (Vollmer et al., 2008a). In Gram negative bacteria this peptidoglycan layer is approximately 2-6 nm thick (Vollmer and Seligman, 2010).

1.1.2 Gram positive

The Gram positive cell envelope differs from that of the Gram negative bacteria mainly due to the lack of an outer membrane (Figure 1.1 B). The role of the outer membrane

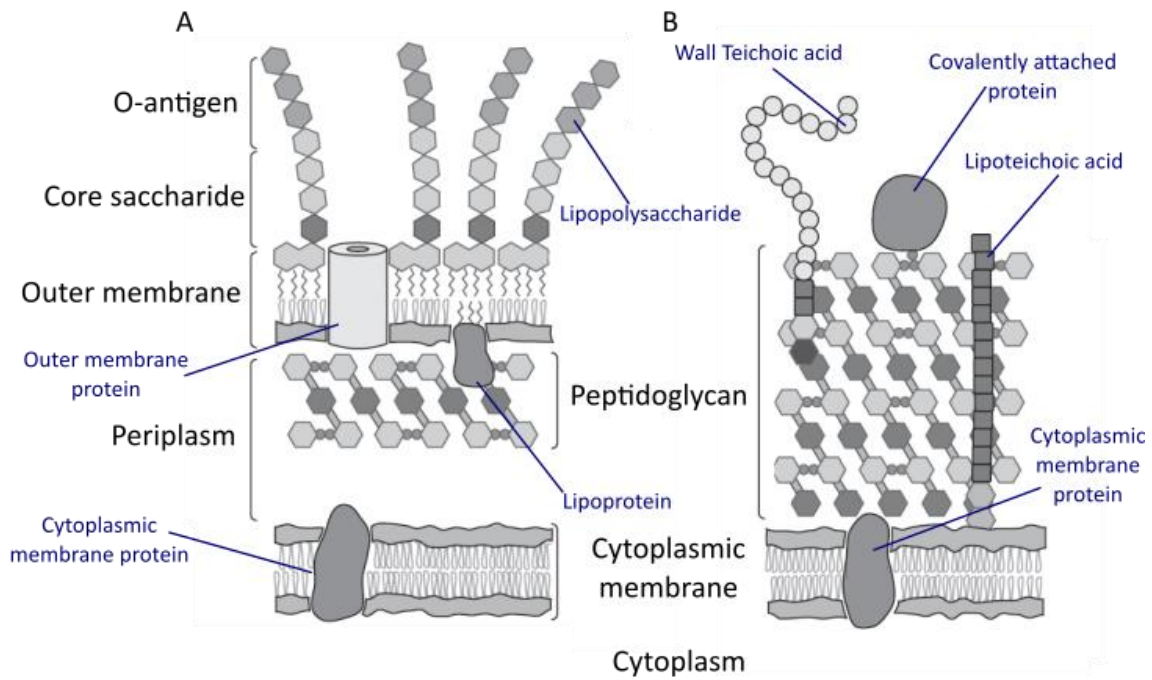


Figure 1.1. General Structure of the Gram positive and Gram negative cell envelopes.

(A) Gram negative, (B) Gram positive. Adapted from (Silhavy et al., 2010).

is the protection of Gram negative bacteria from the environment. To replicate this the peptidoglycan layer of Gram positive bacteria is many times thicker than that of Gram negatives (Silhavy et al., 2010). In fact, Gram positive peptidoglycan comprises approximately 30-70% of the cell wall and it is ~ 20-35 nm thick (Schleifer and Kandler, 1972). The cell wall of the Gram positive bacteria is often decorated with secondary anionic polymers called teichoic acids (Navarre and Schneewind, 1999). These can either be covalently attached to the peptidoglycan (wall teichoic acids, WTAs) or anchored via the head groups of the membrane lipids (lipoteichoic acids, LTAs) (Neuhaus and Baddiley, 2003). It was initially thought that Gram positive bacteria would lack a periplasm however, a periplasmic space exists between the cytoplasmic membrane and the peptidoglycan of the cell wall (Matias and Beveridge, 2007).

1.2 Chemical structure of peptidoglycan

Peptidoglycan is composed of polymeric glycan strands crosslinked by peptide sidechains. Glycan strands are comprised of alternating *N*-acetylglucosamine (GlcNAc) and *N*-acetylmuramic acid (MurNAc) residues linked by β 1-4 glycosidic bonds. The lactyl group of the MurNAc residue is substituted by a peptide side chain consisting of both D- and L- isoforms of amino acids (Vollmer et al., 2008a). The mucopeptide structure of *Staphylococcus aureus* is shown in Figure 1.2.

1.2.1 Glycan strands

The glycan strands are produced via oligomerisation of lipid II through the transglycosylation reaction. This glycan strand structure is conserved among bacterial species and the major variation comes from distribution of glycan chain length. The average glycan chain length does not correlate with cell wall thickness as *Staphylococcus aureus* has characteristic short glycan chains while *Bacillus subtilis* has long glycan chains despite peptidoglycan of relatively similar thicknesses (Boneca et al., 2000; Hayhurst et al., 2008). *S. aureus* glycans have been shown to contain approximately 3 – 10 disaccharides with the average glycan chain containing 6 disaccharides (Boneca et al., 2000). In addition, 10-15% of *S. aureus* glycan chains contained more than 26 disaccharides. However, *B. subtilis* has glycan strands up to 5 μ m in length which are longer than the bacterium itself (Hayhurst et al., 2008). Glycan strands may terminate with a variety of different residues (Vollmer et al., 2008a). For

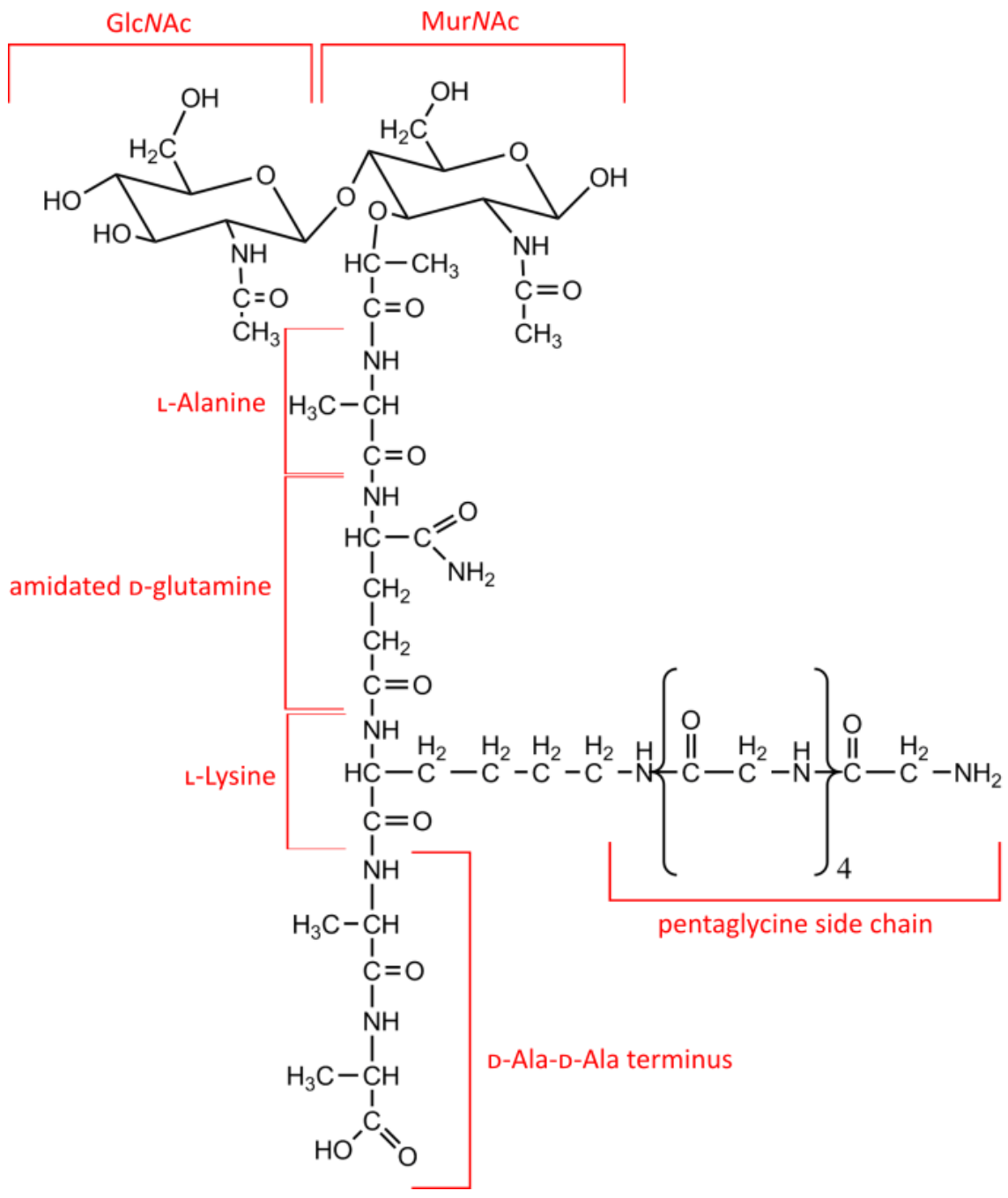


Figure 1.2. Muropeptide structure of *S. aureus*. Monomer of peptidoglycan as achieved from non-crosslinked material by digestion with Mutanolysin.

example, *S. aureus* may have either MurNAc or GlcNAc at the reducing terminus, suggesting enzymatic cleavage of glycan strands (Boneca et al., 2000). In all Gram negatives and some Gram positives glycan strands can be terminated by 1,6-anhydroMurNAc (Figure 1.3; red box)(Vollmer and Bertsche, 2008). 1,6-anhydroMurNAc can be produced by a lytic transglycosylase reaction converting the glycosidic bond between MurNAc and GlcNAc but whether termination of glycan strands occurs via lytic transglycosylation of the polymerised strand or formed at the growing end of the strand remains unclear (Höltje, 1998; Höltje et al., 1975). MltG, an endolytic transglycosylase, was recently discovered to play a role in termination of *Escherichia coli* glycan strands via association with the biosynthetic machinery and cleavage of nascent peptidoglycan (Yunck et al., 2015).

The glycan chains of bacteria also show some specific modifications in addition to diversity in glycan chain length distribution (Figure 1.3). Glycan strands have been shown to be *N*-deacetylated at both residues, *O*-acetylated and *N*-glycolylated at MurNAc, all of which have different physiological effects (Vollmer, 2008). Deacetylated peptidoglycan is a poor substrate for lysozyme (a host defence enzyme) as well as increasing the positive charge of the peptidoglycan, potentially also effecting interaction with the host (Atilano et al., 2010; Vollmer, 2008). *N*-glycolylation causes the acetate group of MurNAc to be modified to a glycolyl group (Figure 1.3; red circle), occurring mainly in bacteria containing mycolic acid e.g. *Mycobacteria* (Vollmer, 2008). The physiological effect of this is not understood although the addition of an extra hydroxyl group increases the hydrogen bonding potential and may influence cell envelope stability (Brennan and Nikaido, 1995). *O*-acetylation occurs on the C6-OH of MurNAc and has not been found on GlcNAc residues (Figure 1.3; green circle)(Vollmer, 2008). It renders peptidoglycan resistant to lysozyme digestion in an *O*-acetylation concentration dependent manner (Clarke and Dupont, 1992). In addition, the *O*-acetylation levels can control endogenous peptidoglycan hydrolase activity (Moynihan and Clarke, 2011). The components involved in the *O*-acetylation process have thus been proposed as new antibiotic targets (Moynihan and Clarke, 2013).

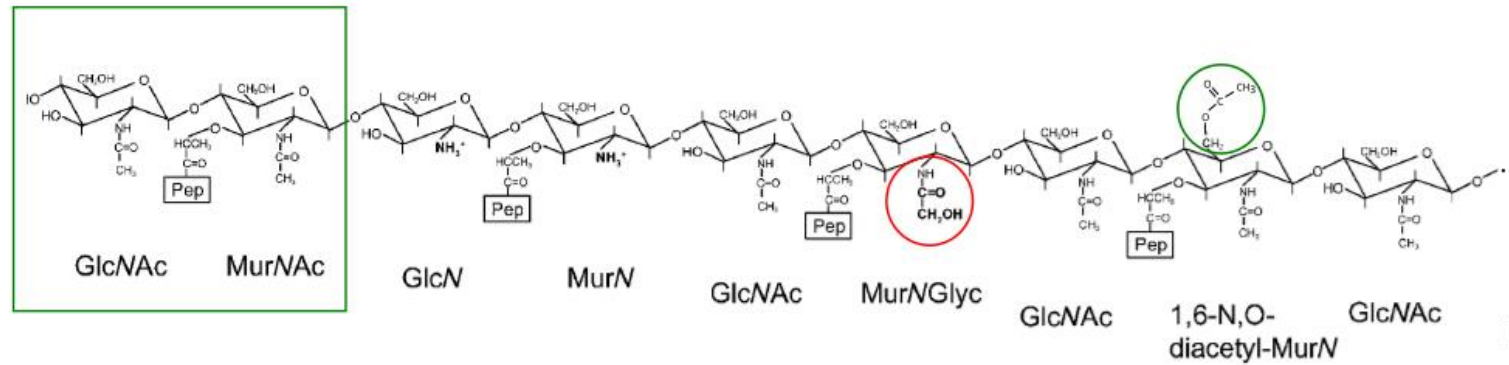
1.2.2 Peptide sidechains

There is a greater extent of variation among the peptide side chains of peptidoglycan than within the glycan strands. Variation occur either due to specificity of the peptide biosynthesis pathway or can occur at a later step during peptidoglycan assembly (Vollmer et al., 2008a). The peptide side chain generally has the composition of L-Ala- γ -D-Glu-*m*-DAP-D-Ala-D-Ala in the nascent peptidoglycan (Bouhss et al., 2008). The second amino acid, D-glutamic acid, is unusually linked via its γ -carboxyl group to the 3rd amino acid (Figure 1.2)(Schleifer and Kandler, 1972). The greatest variability occurs at the 3rd amino acid which is often L-Lysine in Gram positive bacteria (Figure 1.2), although it can also be other diamino or monoamino acids (Vollmer et al., 2008a). The terminal D-amino acid is also sometimes altered, particularly to D-Lactate which confers vancomycin resistance (Courvalin, 2006). Modifications to the peptide side chain often occur at the lipid II linked level. For example, the D-Glu α -carboxy group is amidated in *S. aureus* in an essential process mediated by the GatD/MurT enzyme (Figueiredo et al., 2012; Münch et al., 2012).

Other variations occur not within the peptide side chain but within the crossbridge (Schleifer and Kandler, 1972). Most bacterial species crosslink between the 3rd amino acid of one strand with the 4th amino acid of the next, however in coryneform bacteria this occurs between the 2nd and the 4th (Schleifer and Kandler, 1972). Some bacteria e.g. *E. coli* have a direct crosslink while other bacteria can have a cross bridge containing up to 7 amino acids, including some branched cross bridges (Vollmer et al., 2008a). *S. aureus* peptidoglycan contains a pentaglycine cross bridge forming a 3-4 crosslinkage (Shockman and Barrett, 1983). *S. aureus* also has highly crosslinked peptidoglycan, between 70-80%, mainly due to the action of PBP4 (Snowden and Perkins, 1990; Wyke et al., 1981).

1.3 Teichoic acids

Teichoic acids are anionic glycopolymers that decorate the cell envelope of Gram positive bacteria and are linked to either peptidoglycan (WTAs) or to the cytoplasmic membrane (LTAs) (Xia et al., 2010). WTAs are linked to the C6 OH group of approximately every 9th MurNAc on the *S. aureus* peptidoglycan (Figure 1.3; orange

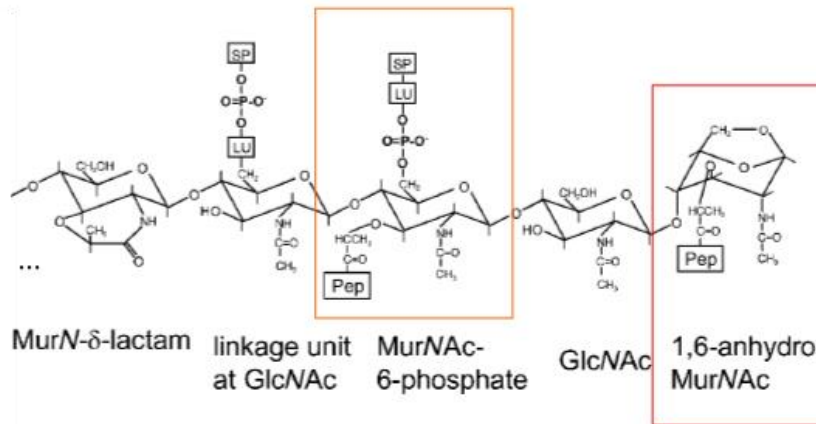


**Unmodified
disaccharide**

N-deacetylation
(GlcN, MurN or both)

N-glycolylation
(at MurN)

O-acetylation
(at MurNAc)



Muramic δ -lactam

**Attachment of
surface polymers**

1,6-Anhydro ring
(at MurNAc)

Figure 1.3. Modifications of glycan residues. Structure of unmodified residues (green box), glycan modifications and the structure of 1,6-anhydro MurNAc (red box). Adapted from (Vollmer, 2008).

box) (Brown et al., 2013). They consist of a disaccharide linkage unit appended to polyribitol phosphate (polyRboP) or polyglycerol phosphate (polyGroP) containing up to 60 repeats (Silhavy et al., 2010). In bacteria the structure of WTA varies between species and strains however, *S. aureus* WTA is linked to MurNA via GlcNAc-1-P an *N*-acetylmannosamine (ManNAc), which is followed by 2 polyGroP residues and 11-40 residues of polyRboP dependent upon the strain (Figure 1.4 A) (Xia et al., 2010). OH groups on the polyRboP are regularly decorated with substitutions e.g. *D*-alanine and glycosyl moieties, which play a role in WTA function (Silhavy et al., 2010). The LTA of *S. aureus* is linked to the cytoplasmic membrane via a glycolipid anchor which is diglucosyl diacylglycerol in the case of most staphylococci (Figure 1.4 B) (Xia et al., 2010). Most LTAs are formed of repeating polyGroP residues that can be decorated in the same manner as in WTAs (Silhavy et al., 2010).

Together WTAs and LTAs contribute to a negative charge on the cell surface. This is an important feature for bacterial survival because while bacteria can survive the deletion of WTA or LTA separately, albeit with morphological defects, they are synthetically lethal and strains cannot survive without any teichoic acids (Silhavy et al., 2010). LTA deficient *S. aureus* strains can only survive in high sucrose or salt media, due to the osmoprotectant nature of such growth conditions (Corrigan et al., 2011). Some of the roles of WTAs include regulation of cell morphology & division, regulation of peptidoglycan autolysins and protection from host defences/antibiotics (Brown et al., 2013). In particular *S. aureus* strains that lack *D*-alanine have an increased susceptibility to phagocytes and neutrophil killing (Collins et al., 2002).

1.4 Peptidoglycan synthesis

Peptidoglycan synthesis follows a common pathway across both Gram positive and Gram negative bacteria (Bugg et al., 2011; Lovering et al., 2012). The process can be split into 3 overall stages; precursors are synthesised in the cytoplasm, lipid-linked muropeptides are assembled and flipped across the membrane, monomers are polymerized and the resulting glycan strands are inserted into the mature peptidoglycan (Figure 1.5)(Typas et al., 2012). The enzymes involved in the biosynthetic pathway are essential and have no known mammalian homologs therefore they are excellent targets for broad spectrum antibiotics (Lovering et al., 2012).

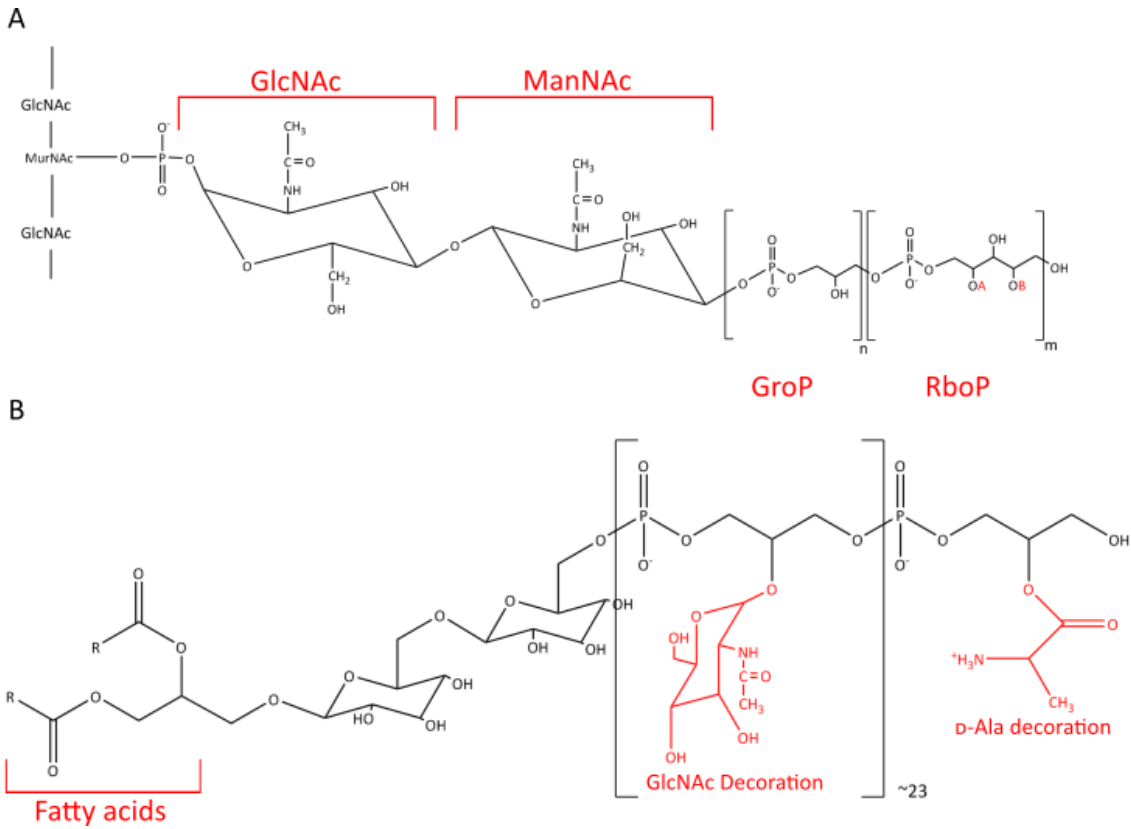


Figure 1.4 Chemical structures of *S. aureus* teichoic acids. (A) Wall teichoic acid, decorations of poly(RboP) are noted by red A & B, A= α or β GlcNAc, B=D-Alanine or Hydrogen. Based on (Swoboda et al., 2010). (B) Lipoteichoic acid, GlcNAc and D-Alanine decorations shown. Based on (Gründling and Schneewind, 2007; Morath, 2001).

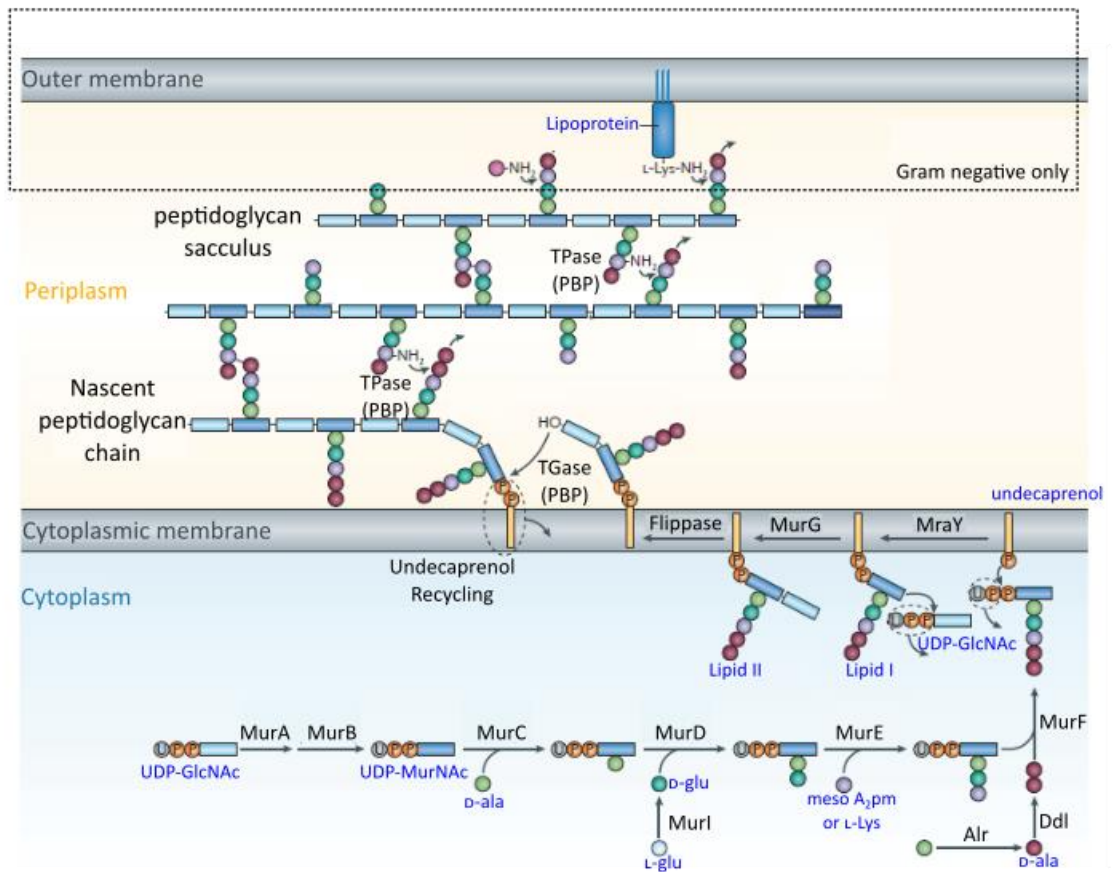


Figure 1.5. Peptidoglycan biosynthetic pathway. Precursors are synthesised in the cytoplasm, translocated across the cytoplasmic membrane and inserted into the peptidoglycan sacculus through transglycosylase (TGase) and transpeptidase (TPase) reactions. Adapted from (Typas et al., 2012).

1.4.1 Cytoplasmic steps of precursor biosynthesis

Peptidoglycan synthesis is initiated in the cytoplasm with the formation of soluble nucleotide precursors (Figure 1.5) (Bouhss et al., 2008). The first step is the transfer of an enolpyruvyl moiety to UDP-GlcNAc (Uridine diphosphate-GlcNAc) catalysed by MurA (Lovering et al., 2012). This is followed by the Flavin dependent reductase reaction of MurB to convert the MurA product into UDP-MurNAc (Bugg et al., 2011; Lovering et al., 2012). The pentapeptide is then synthesised via the ATP-dependent Mur ligases, Mur C-F, that add each amino acid in a stepwise manner (Bouhss et al., 2008; Lovering et al., 2012). UDP-MurNAc-pentapeptide is then linked to the transport lipid, undecaprenyl-phosphate (also known as bactoprenol), on the cytoplasmic side of the membrane via MraY (van Dam et al., 2009). This produces undecaprenyl-pyrophosphate -MurNAc-pentapeptide, also known as lipid I (Typas et al., 2012). Lipid I is then converted to lipid II via the transfer of GlcNAc from UDP-GlcNAc to lipid I catalysed by MurG (Bouhss et al., 2008). In *E. coli* there are only approximately 700 molecules of lipid I per cell which suggests that there is an interaction between MraY and MurG (Bouhss et al., 2004; van Heijenoort, 2007). The *S. aureus* peptidoglycan muropeptide is modified by the addition of a pentaglycine sidechain, involved in the crosslinking of peptidoglycan (Qiao et al., 2014). The *femABX* genes have been shown to be required for addition of glycines into the pentaglycine bridge with FemX catalysing the addition of the first glycine, FemA catalysing the addition of the subsequent two glycines and FemB catalysing the addition of the final two glycines (Bouhss et al., 2008). This requires both lipid II and glycyl tRNA therefore this process occurs in the cytoplasm immediately following conversion of lipid I to lipid II but prior to flipping of lipid II to the cell surface (Bouhss et al., 2008). In addition, the amidation of D-glu by GatD/MurT occurs at the lipid II level (Figueiredo et al., 2012; Münch et al., 2012).

1.4.2 Translocation of lipid II

Lipid II is entirely assembled on the inner leaflet of the cytoplasmic membrane and so this hydrophilic molecule must cross the hydrophobic cytoplasmic membrane (Figure 1.5)(van Heijenoort, 2007; Young, 2014). In addition, the pool of lipid II is limited, about 1,000-2,000 molecules in *E. coli* and while increased in other organisms with higher peptidoglycan content it remains low (van Heijenoort, 2007). In fact, in Gram

positive bacteria such as *S. aureus*, the lipid II pool is less than 1 mole percent of the phospholipid content of the cytoplasmic membrane (Ruiz, 2015). Therefore lipid II translocation must be fast and efficient and must require a flippase to act as a mechanism of passage for the hydrophilic moiety (Ruiz, 2015).

The identity of such a flippase has been the source of some controversy (Scheffers and Tol, 2015). There are two prospective candidates for the flippase, first the FtsW/RodA type and secondly the MurJ/AmJ type. FtsW/RodA are integral membrane proteins belonging to the shape, elongation, division and sporulation (SEDS) protein family (Ruiz, 2015). In addition the *ftsW* gene is found in an operon associated with peptidoglycan synthesis (Young, 2014). The evidence for FtsW as the lipid II flippase is that membrane vesicles extracted from *E. coli* have lipid II translocation that correlates with the amount of FtsW and also purified FtsW facilitates translocation of lipid II in large unilamellar vesicles (Mohammadi et al., 2011). However, in this system MurJ did not cause lipid II translocation (Mohammadi et al., 2011). The evidence for MurJ conversely comes from *in vivo* work where inactivation or depletion of *murJ* resulted in a decrease in lipid II translocation as measured by amount of colicin M (ColM) cleaved lipid II product (Sham et al., 2014). Lipid II was found to instead accumulate on the inner leaflet of the membrane (Sham et al., 2014). In the *in vivo* system, lipid II translocation was maintained on FtsW depletion in a $\Delta rodA$ background, although some remaining active FtsW could be present in this case (Sham et al., 2014). The *murJ* ortholog in Gram positive bacteria (*ytgP*) was shown to be essential in *S. aureus* and *Streptococcus pneumoniae* but not in *B. subtilis* as a strain missing all four *ytgP* homologs remained viable. However a protein with redundancy to YtgP called AmJ was discovered to be synthetically lethal, therefore suggesting that MurJ/AmJ could in fact be the flippase (Ruiz, 2015). Both the experimental systems used have limitations and it remains a possibility that both the FtsW/RodA and MurJ/AmJ proteins could act as the lipid II flippases *in vivo*.

1.4.3 Incorporation of Lipid II into peptidoglycan

Once lipid II has been translocated to the outer leaflet, it is polymerized into glycan strands by transglycosylase activity (Figure 1.5)(Lovering et al., 2012). There are two types of transglycosylases in bacteria, monofunctional and bifunctional enzymes, bifunctional enzymes usually also possess transpeptidase activity and are therefore

called Class A PBPs (Lovering et al., 2012; Typas et al., 2012). *S. aureus* possesses one bifunctional PBP (PBP2) and two monofunctional transglycosylases (MGT and SgtA) (Reed et al., 2015). Polymerisation occurs via the formation of a glycosidic bond between the lipid-anchored MurNAc on the growing nascent glycan strand and the GlcNAc on the lipid II molecule (Fuchs-Cleveland and Gilvarg, 1976; Ward and Perkins, 1973). At this point undecaprenyl-pyrophosphate is released from the peptidoglycan subunit and transported back to the cytoplasmic side. It is then dephosphorylated and recycled back into the synthesis pathway to form new lipid I molecules (van Dam et al., 2009).

Once glycan strands have been polymerised, crosslinking occurs via the transpeptidase activity of PBPs linking peptide units in adjacent glycan strands (Figure 1.5) (Lovering et al., 2012). This reaction occurs via the hydrolysis of the terminal D-ala of the donor strand forming an acyl-enzyme intermediate. This is resolved by the crosslinking with the amino group either from the third amino acid in the peptide strand of an acceptor strand or the N-terminal peptide of the acceptor strand crossbridge (Lovering et al., 2012).

1.5 Peptidoglycan hydrolysis

Hydrolases exist that are able to specifically cleave the many different bonds found within bacterial peptidoglycan (Ghuysen, 1968). These can originate from the bacterium on which they act and are termed autolysins. They are also produced by other organisms, including other bacteria and eukaryotes (Ghuysen, 1968). There are examples of peptidoglycan hydrolases for every glycosidic and amide bond within peptidoglycan although not every species contains each of them (Figure 1.6)(Vollmer et al., 2008b).

1.5.1 Glycosidases

Enzymes which catalyse the cleavage of the glycan backbone are known as glycosidases and fall into two main categories; glucosaminidases and muramidases depended on which of the two bonds they break (Figure 1.6 A)(Vollmer et al., 2008b). Glucosaminidases hydrolyse the bond between GlcNAc and MurNAc resulting in a reducing terminal GlcNAc (Wheeler et al., 2015). Glucosaminidases are widespread in

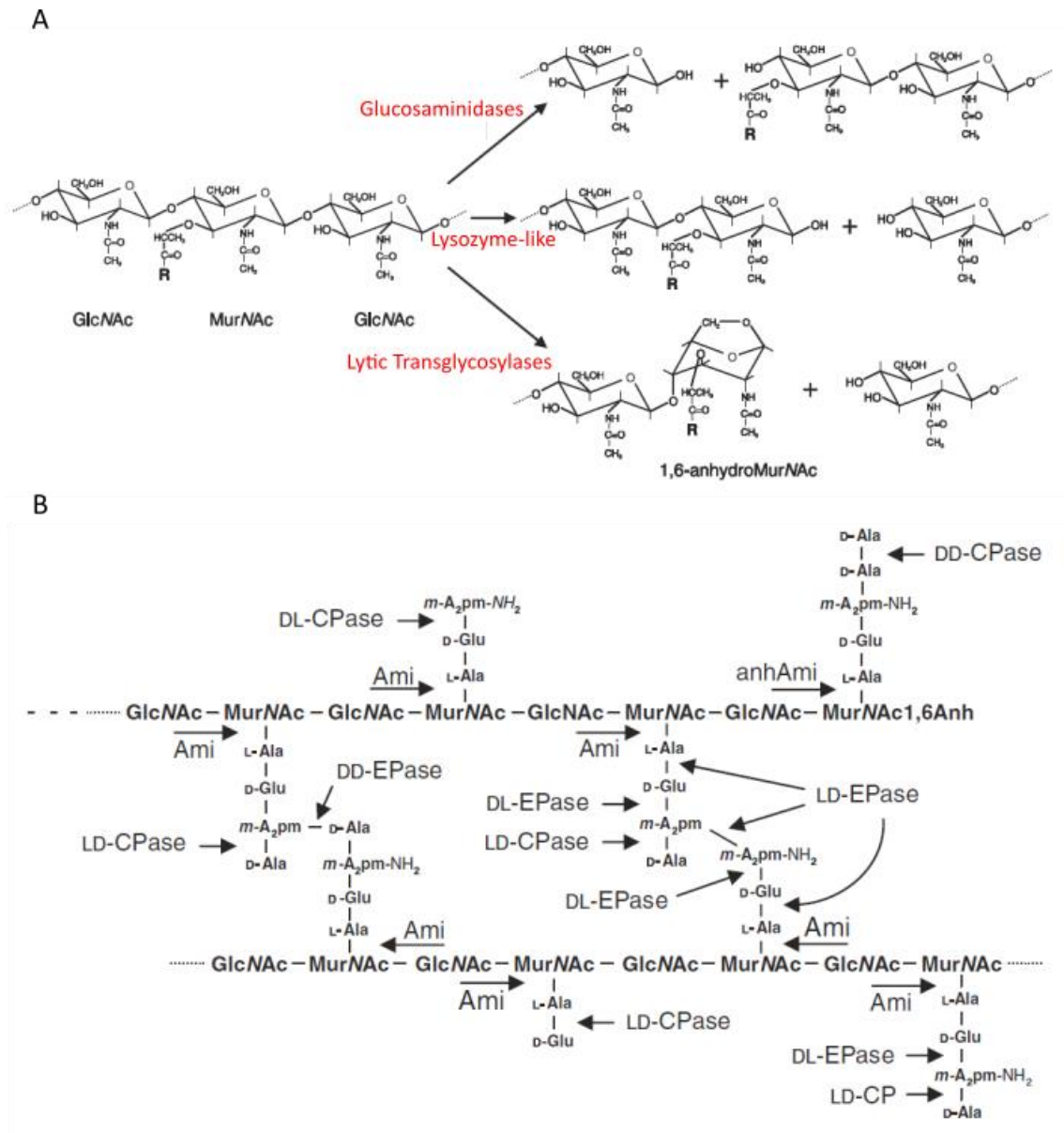


Figure 1.6. Action of peptidoglycan hydrolases on the glycan backbone (A) and peptide sidechains (B). Taken from (Vollmer et al., 2008b).

bacteria and are found not only as peptidoglycan hydrolases but also able to cleave the bond between *N*-acetyl glucosamine residues and adjacent monosaccharides in several polymers (Vollmer et al., 2008b). Muramidases cleave the β 1,4-glycosidic bond between MurNAc and GlcNAc and can use one of two different mechanisms for this; Lysozyme-like enzymes that result in a terminal reducing MurNAc or lytic transglycosylases that cleave the bond with an intramolecular transglycosylase reaction resulting in the formation of the 1,6-anhydroMurNAc residue (Vollmer et al., 2008b).

1.5.2 Amidases and peptidases

Within the peptide side chain there are two bond types for which peptidoglycan hydrolases exist; the amide bond between MurNAc and the peptide side chain and the peptide bonds within the sidechain itself (Figure 1.6 B). Hydrolases that cleave the amide bond are known as *N*-acetyl-L-alanine amidases (Ami)(Heidrich et al., 2001). Many species encode several versions of this protein, e.g. *E. coli* has five homologs within its genome (Heidrich et al., 2001; Uehara and Park, 2007). These amidases have been shown to play an important role in septum cleavage during cell division (Heidrich et al., 2001). Alternatively, the enzymes that cleave bonds between amino acids in both peptidoglycan and soluble peptidoglycan fragments are known as peptidases. These are known as carboxypeptidases (CPases) and endopeptidases (EPases) which catalyse the removal of the C-terminal amino acid and cleavage within the peptide respectively (Vollmer et al., 2008b).

1.5.3 The physiological role of peptidoglycan hydrolases

There is a great deal of redundancy among the peptidoglycan hydrolases suggesting important or essential roles in many bacterial functions (Typas et al., 2012). The majority of these functions are within vegetative growth and division of bacteria but they are also involved in more specialised processes such as interactions between bacteria & their hosts and differentiation (Smith et al., 2000; Stapleton et al., 2007). A number of different studies have shown that hydrolases play a role in shape determination, peptidoglycan thickness and are essential for daughter cell separation during cell division (Typas et al., 2012).

During vegetative growth, *E. coli* removes up to 40-50% of total peptidoglycan during each generation via peptidoglycan turnover (Höltje and Heidrich, 2001). This value is reduced in hydrolase mutants, suggesting a role of these proteins in the turnover process (Kraft et al., 1999). This suggests a system of tightly coordinated peptidoglycan synthesis and hydrolysis and therefore growth should cease on hydrolase inactivation (Höltje, 1998). However due to the high degree of redundancy within the hydrolase system and essentiality of the synthesis and hydrolysis processes in cell growth it is difficult to assess the contributions of individual enzymes.

E. coli encodes 3 hydrolytic enzymes that were found to act as endopeptidases. They are redundantly essential for growth and viability, as a conditional triple mutant is unable to incorporate new peptidoglycan and undergoes rapid lysis (Singh et al., 2012). Two enzymes, MepS and MepH (formally Spr & YdhO respectively) were found to be members of the NlpC/P60 peptidase superfamily while the third, MepM (formally YebA) was part of the lysostaphin superfamily (Singh et al., 2012, 2015). These enzymes act to cleave the peptidoglycan cross-links therefore this process is thought to be essential for cell wall expansion (Singh et al., 2012). MepS was found to be modulated by rapid proteolytic degradation by a membrane lipoprotein/periplasmic protease system known as Nlpl-Prc (Singh et al., 2015). Nlpl-Prc may also have a role in the formation of cross links suggesting that the Nlpl-Prc control system may facilitate the concomitant cleavage and synthesis of cross links allowing expansion of the sacculus (Singh et al., 2015).

Two endopeptidases from *B. subtilis*, CwlO & LytE were also shown to be synthetic lethal partners. A double mutant is not viable and depletion of either protein within a conditional mutant leads to defects in lateral cell wall synthesis (Bisicchia et al., 2007). This was shown to be due to the lack of D,L-endopeptidase activity at the cylinder as the synthetic lethality could be suppressed by localisation of alternative D,L-endopeptidases, LytE & CwlS at the cylinder (Hashimoto et al., 2012). Similarly, *S. aureus* expresses 4 synthetically lethal glucosaminidases that are required for growth (Wheeler et al., 2015).

Another role is the regulation of cell growth by DD-carboxypeptidases. In *B. subtilis* PBP5 (DacA) acts as a DD-carboxypeptidase and controls the amount of tetrapeptide

sidechains in peptidoglycan (Atrih et al., 1999). This suggests a role of PBP5 in the maturation of *B. subtilis* peptidoglycan. Deletion of PBP5 does not affect either the growth or morphology of vegetative cells however spores of the mutant were 10-fold less heat resistant and had an altered spore cortex structure suggesting an additional role of PBP5 in cortex synthesis (Todd et al., 1986). In *E. coli*, deletion of DD-carboxypeptidase activity results in alteration of cell shape and aberrant z-ring formation (Nelson and Young, 2001; Potluri et al., 2012). In addition to cell growth and maintenance of cell shape, peptidoglycan hydrolases are also essential to the cell splitting process (Chapter 1.9.3).

1.6 Cell division

Cell division is a fundamental process by which a parental cell divides into 2 daughter cells (Figure 1.7). Genetic information must be faithfully copied and equally divided between the daughter cells. Within the bacteria this process involves the coordinated action of multiple proteins forming a complex known as the divisome (Wu and Errington, 2011).

1.6.1 Cell division in rod-shaped bacteria

Cell division in bacteria is a complex process which requires not only the replication and division of the intracellular contents such as DNA etc. but also the formation of a new cell envelope barrier between the daughter cells (Errington et al., 2003).

Therefore, the entirety of the cell envelope layers must be remodelled to form the septum. In rod shaped bacteria, prior to cell division cells elongate to increase cell size while maintaining a constant diameter. This elongation is mediated by a version of the divisome known as the elongasome that directs lateral insertion of peptidoglycan along the long axis of the cell (Szwedziak and Löwe, 2013).

Only once rod-shaped bacteria such as *E. coli* and *B. subtilis* reach a minimum cell length will cell division take place (Donachie and Begg, 1989; Sharpe et al., 1998). At this point the replicated chromosomes will separate to opposite poles of the dividing bacteria allowing the formation of a septum at the midcell (Donachie and Begg, 1989; Errington et al., 2003). Following septal completion, daughter cells are split due to the action of peptidoglycan hydrolases (Heidrich et al., 2002).

Rod-Shaped Bacteria

Coccioid Bacteria

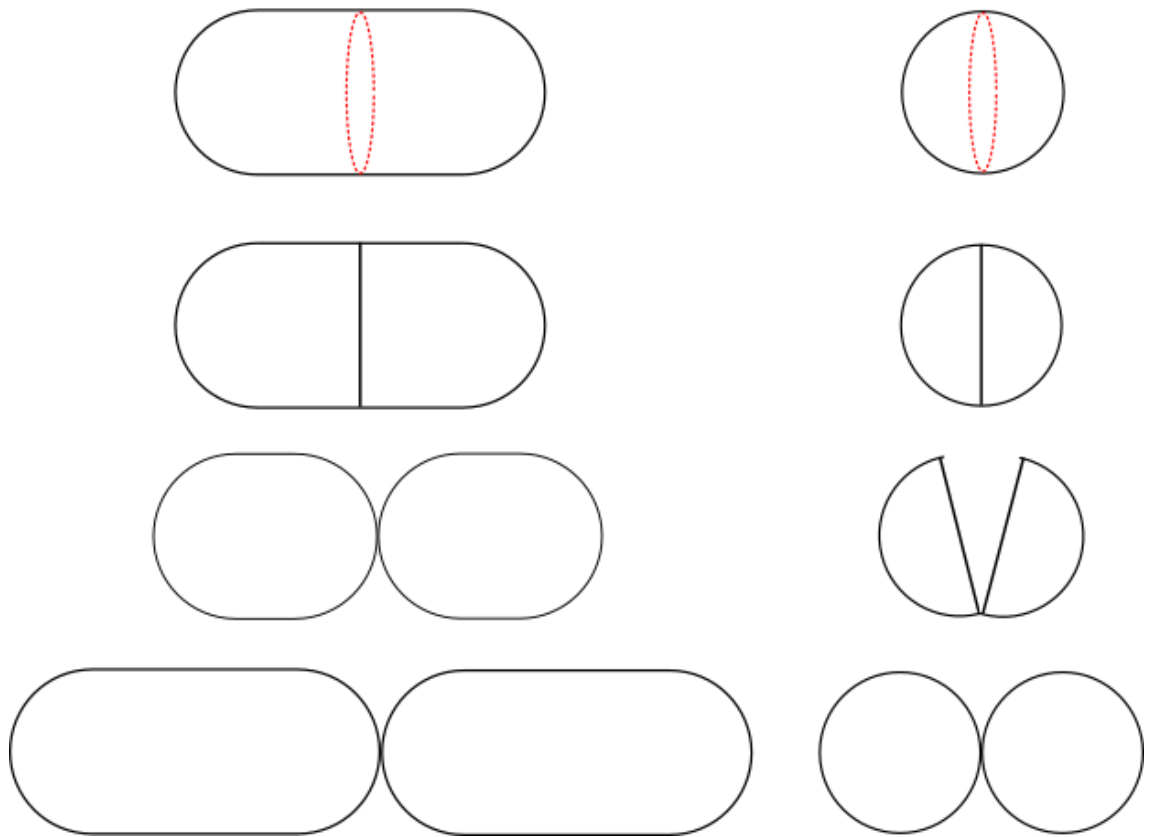


Figure 1.7 Division process in rod-shaped & coccoid bacteria.

1.6.1.1 Selection of division plane in rod shaped bacteria

Determination of division plane selection needs to be controlled both temporally and spatially. Temporal selection ensures the correct cell length is reached and therefore requires coordination between growth rate and cell size. Nutrient availability is a strong determinant of cell size (Weart et al., 2007). Bacteria require the ability to determine when they have reached an appropriate size for a given growth rate and then transmit this to the divisome in order to initiate cell division (Weart et al., 2007). One such mechanism is the effector UgtP in *B. subtilis* that localises to the division site in a nutrient dependent manner & inhibits the assembly of FtsZ (Weart et al., 2007). When there are high levels of nutrients UgtP is highly expressed and distributed throughout the cell where it may inhibit FtsZ assembly or prolong the period between FtsZ ring formation and cytokinesis however, when nutrient levels are low, UgtP is not as highly expressed therefore FtsZ mediated division continues without inhibition allowing division at a smaller cell size (Weart et al., 2007).

In theory cell division could take place at any point along the length of the rod-shaped cell however in practice localisation of FtsZ occurs at the midcell with high accuracy (Migocki et al., 2002). Therefore, control mechanism(s) must exist that ensure midcell placement. One such mechanism is the Min system, that when deleted leads to the formation of mini cells due to the placement of division septa towards the pole (de Boer et al., 1989). In *E. coli* this system consists of three proteins MinC, MinD and MinE. MinCD forms a complex which is a negative regulator of the z-ring. This is spatially regulated by MinE, a topological specificity factor that prevents MinC activity at the midcell (Raskin and de Boer, 1997). MinC and MinD oscillate from pole to pole in an MinE dependent manner, thereby the time-integrated concentration of MinC is highest at cell poles causing pole-specific negative regulation of FtsZ (Hu and Lutkenhaus, 1999). In *B. subtilis* homologs of MinCD are present, but not a homolog of MinE. However the topological specificity factor has been identified as DivIVA, which similarly to MinE has an affinity for phospholipids however, binds preferentially to strongly curved cell membranes and thus recruits MinCD to the poles (Bramkamp et al., 2008; Lenarcic et al., 2009). However the Min system has been shown to be not required for the precise placement of the midcell ring instead acts as a block to z-ring formation at the cell poles (Migocki et al., 2002).

A second system known as nucleoid occlusion inhibits division near the chromosome and thus prevents bisection of the nucleoid (Wu and Errington, 2011). Nucleoid occlusion factors, Noc in *B. subtilis* and SlmA in *E. coli*, prevent FtsZ ring formation over the chromosome through binding to specific DNA sequences and effecting FtsZ polymerisation (Bernhardt and De Boer, 2005; Wu and Errington, 2011).

1.6.2 Cell division in coccoid bacteria

A lot of previous work has been carried out in rod shaped bacteria, however the use of the coccoid shaped organisms is becoming more popular due to the apparently simpler mode of division. Rod-shaped bacteria maintain two modes of cell wall synthesis; elongation and septation, however in cocci, FtsZ dependent cell wall synthesis is predominant (Pinho and Errington, 2003). In addition, many coccoid bacteria are important human pathogens. Therefore, understanding the division process within these bacteria may lead to identification of novel antimicrobial targets.

Selection of division plane in coccoid bacteria is more complex than within rod-shaped bacteria due to the potential to divide in an infinite number of planes whereas rod-shaped organisms must divide parallel to the short axis of the bacterium. Some coccoid species division occurs on one plane as in rod-shaped bacteria e.g. enterococci, streptococci (Zapun et al., 2008a). However some divide on more than one plane usually either two or three alternating planes (Zapun et al., 2008a). *S. aureus* divides on three perpendicular or orthogonal planes in a regular sequence (Figure 1.8)(Tzagoloff and Novick, 1977). Thus the specification of the plane of division is not only determined by features of the cell but also by the positioning of the division plane for the two previous divisions (Tzagoloff and Novick, 1977). There must therefore be some internal indicator of geometric orientation to complete this. It is unlikely to be a genetic signal since it must be maintained over several generations, yet must change with each division.

In addition to determining the geometric position of the division plane cocci do not possess a Min system for FtsZ ring placement at the midcell therefore nuclear occlusion is thought to play a greater role (Wu and Errington, 2011). Noc deletion in *S. aureus* results in the formation of multiple FtsZ rings and DNA breaks however

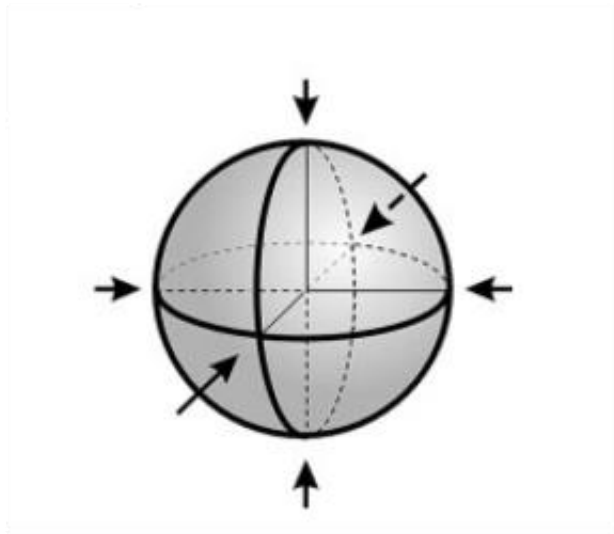


Figure 1.8. Schematic of 3 orthogonal planes in a spherical object. (Dmitriev et al., 2004).

chromosome replication and segregation occur as normal (Veiga et al., 2011; Wu and Errington, 2011). The multiple z rings arising from Noc deletion are not placed in the division plane suggesting a role of nucleoid occlusion in determining the plane of septum formation (Veiga et al., 2011). Additionally, a model of division plane selection based on the inheritance of peptidoglycan architectural features, known as ribs, has been proposed (Turner et al., 2010a). These ribs (thickenings of the peptidoglycan) are produced at the site of septation and are faithfully inherited at each division, thereby they could mark the localisation of previous division planes.

1.7 Cell division machinery

The cell division machinery comprises of a number of different proteins, many of which are conserved among different bacterial species (Typas et al., 2012). Together these proteins form the divisome complex which provides both the constriction force and enzymatic actions required for completion of division (Wu and Errington, 2011). Using mutant and lethality studies, *in vivo* imaging, structure determination, biochemical assays and two-hybrid systems many members of the divisome of different organisms have been identified and characterised, particularly in rod-shaped organisms although also for *S. aureus* (Figure 1.9).

1.7.1 The z-ring

FtsZ is the most highly conserved among the division proteins and has been shown to be involved in the first known stage of the *E. coli* division process (Margolin, 2000). FtsZ forms a ring at the division site (Figure 1.10)(Scheffers and Driessen, 2010). In the presence of GTP, FtsZ hydrolyses GTP and polymerises into thin protofilaments (Scheffers and Driessen, 2010). The z-ring is continuously remodelled by polymerisation and depolymerisation with a protein turnover time of a few seconds (Mingorance et al., 2010). FtsZ can provide the force to generate a constrictive force in liposomes without the interactions of other division proteins, suggesting that within bacteria FtsZ directs constriction during division (Osawa et al., 2008).

FtsZ has weak homology to eukaryotic tubulin yet the 3D structure is similar to that of α - & β - tubulin (Löwe and Amos, 1998). The GTPase domain and C-terminal domain of unknown function are arranged around a central helix. The C-terminal tail acts as a linker to other components of the divisome (Szwedziak et al., 2014).

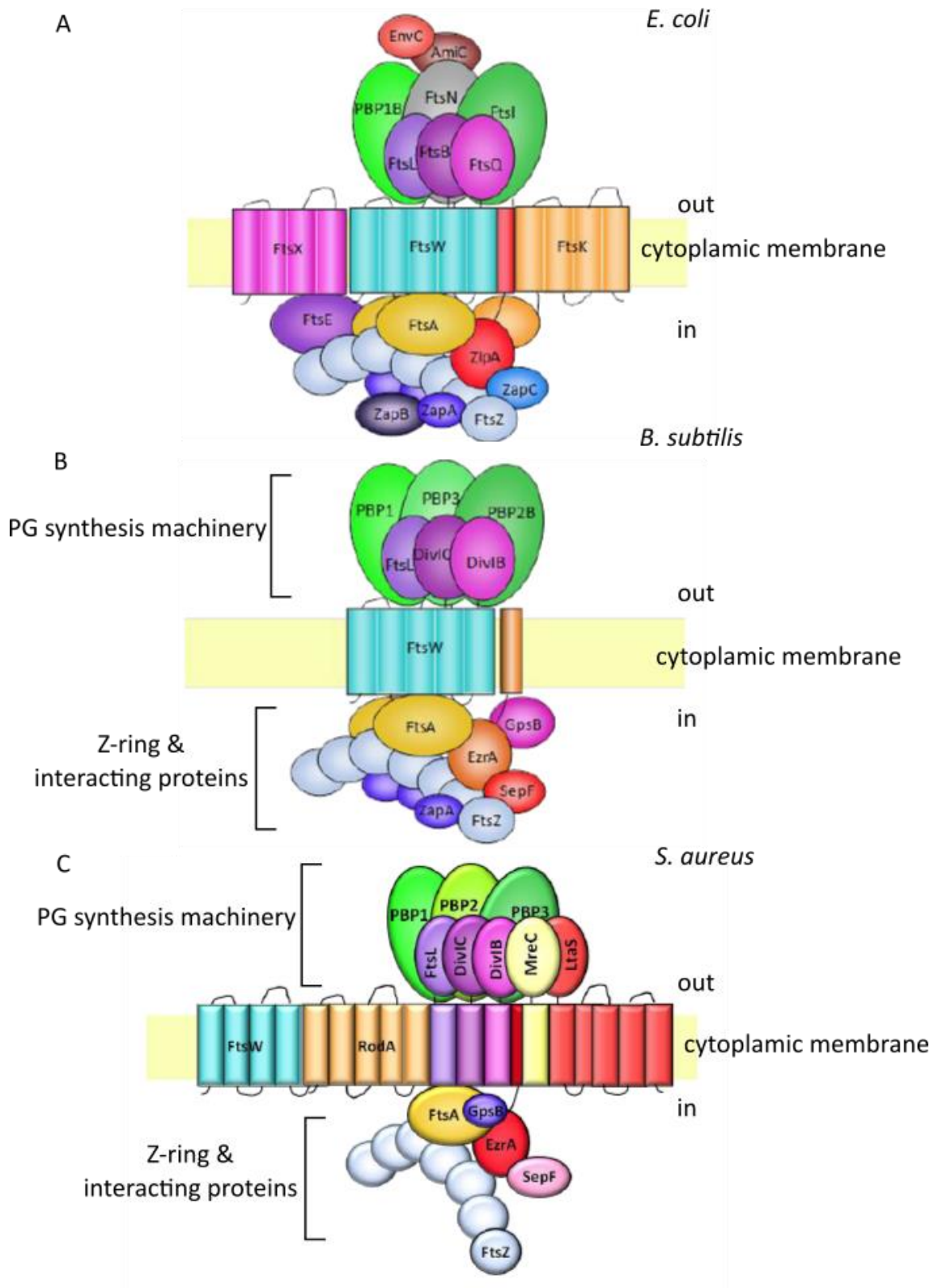


Figure 1.9. Schematic of cell division machinery (divisome) from (A) *E. coli*, (B) *B. subtilis* and (C) *S. aureus*. Taken from (Bottomley, 2011).

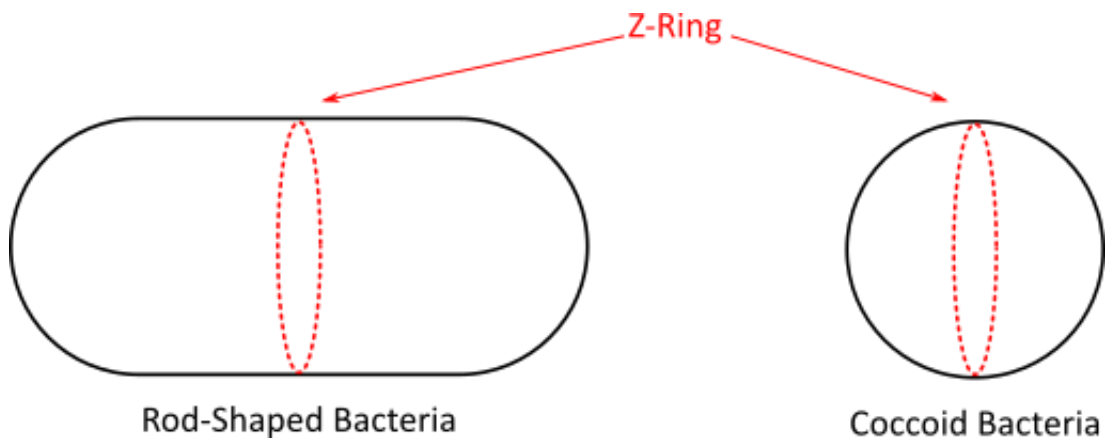


Figure 1.10 Schematic of z-ring positioning in rod-shaped and coccoid bacteria.

Initial diffraction limited fluorescence microscopy of tagged FtsZ suggested FtsZ formed a thick band at the mid-cell, however electron cryo-tomography (ECT) of *Caulobacter crescentus* revealed the presence of short (~100 nm) filaments near the division site (Li et al., 2007). 2D single molecule super resolution imaging of FtsZ in *E. coli* showed a continuous ring formed of loose overlapping bundles (Buss et al., 2013; Fu et al., 2010). FtsZ in *C. crescentus* was initially determined to have a continuous structure (Biteen et al., 2012) however recent work revealed intensity variation suggesting the ring may be discontinuous (Holden et al., 2014). In Gram positives, 3D structured illumination microscopy (SIM) has shown a dynamic bead-like structure of FtsZ (Strauss et al., 2012).

Reconstruction of FtsZ & its interacting partner FtsA in liposomes revealed the z-ring to be composed of a small single layered band of filaments that overlap via lateral filament contacts to form a continuous ring (Szwedziak et al., 2014). Self-arrangement of these filaments caused spontaneous constriction of liposomes independent of nucleotide hydrolysis, therefore not due to shortening of the filaments (Szwedziak et al., 2014). A model of filament sliding to constrict the z-ring was proposed. This would require a closed ring to generate force and this mechanism produces self-regulation since constriction cannot occur until a complete ring has formed (Szwedziak et al., 2014).

1.7.2 FtsZ interacting proteins

There are a number of different proteins that interact with FtsZ to maintain correct z-ring function (Figure 1.9). The first of these, FtsA, is a membrane associated protein that interacts with FtsZ and enables FtsZ polymers to assemble at the membrane (Figure 1.9)(Loose and Mitchison, 2014; Wang et al., 1997). The cellular ratio of FtsA:FtsZ molecules is speculated to be an important feature, and is not constant across bacterial species (Feucht et al., 2001). It is thought that FtsA individually is not able to provide strong enough attachments to the membrane but that an FtsZ-filament-FtsA complex allows multiple bonds for membrane association (Loose and Mitchison, 2014). Additionally, in *E. coli*, ZipA also recruits FtsZ to the membrane through interaction with the same part of the FtsZ molecule as FtsA (Loose and Mitchison, 2014). Z-ring formation requires the presence of only one of FtsA or ZipA however they are both required for septal constriction (Pichoff and Lutkenhaus, 2002).

ZipA and FtsA are also both required for the recruitment of FtsK and subsequent division proteins (Pichoff and Lutkenhaus, 2002). Additional FtsZ interacting proteins include ZapA, ZapB & ZapC (*E. coli*) and SepF (*B. subtilis* & *S. aureus*) which together with previously mentioned proteins help stabilise and maintain correct z-ring conformation throughout the cell cycle (Durand-Heredia et al., 2011; Galli and Gerdes, 2010; Hamoen et al., 2006). ZapA & ZapB may act to align FtsZ clusters consisting of several proto-filaments since super-resolution microscopy determined that the abnormal septa and highly dynamic FtsZ in $\Delta zapA$ or $\Delta zapB$ strains was due to the disordered arrangement of the FtsZ clusters (Buss et al., 2013).

EzrA is a member of the Gram positive divisome (Steele et al., 2011). It was shown to cause the destabilisation of FtsZ filaments in *B. subtilis* (Levin et al., 1999). Interaction between EzrA and FtsZ is through the same C-terminal tail as FtsA suggesting binding may be in competition with the positive regulator (Singh et al., 2007). While EzrA is non-essential in *B. subtilis* it was found to have an essential role in *S. aureus* (Levin et al., 1999; Steele et al., 2011). In *S. aureus* EzrA was shown to not only be essential for cell growth but depletion of the protein resulted in the delocalisation of cell division machinery and an inhibition of peptidoglycan synthesis (Steele et al., 2011).

The EzrA protein consists of an N-terminal transmembrane helix and a cytoplasmic domain consisting of five linear repeats of an unusual triple helical bundle (Cleverley et al., 2014). The 3D structure of *B. subtilis* EzrA (minus the N-terminal transmembrane helix) was resolved and revealed the triple helical bundles bent into a semicircle of 120Å diameter (Figure 1.11 A)(Cleverley et al., 2014). The orientation of EzrA was therefore proposed to result in the cytoplasmic domain of EzrA forming an arch over the membrane surface with the N-terminal domain within the membrane and the C-terminal domain positioned close to the membrane surface (Figure 1.11 B) (Cleverley et al., 2014). This allows interaction of the C-terminal to the membrane or specific membrane associated proteins. This led to 2 possible models of EzrA regulation of FtsZ (Figure 1.11 B). The first suggesting regulation occurs through trapping of FtsZ filaments under the EzrA arch thereby disrupting lateral interactions and also anchoring the proto-filaments to the membrane. Alternatively, FtsA & FtsZ could

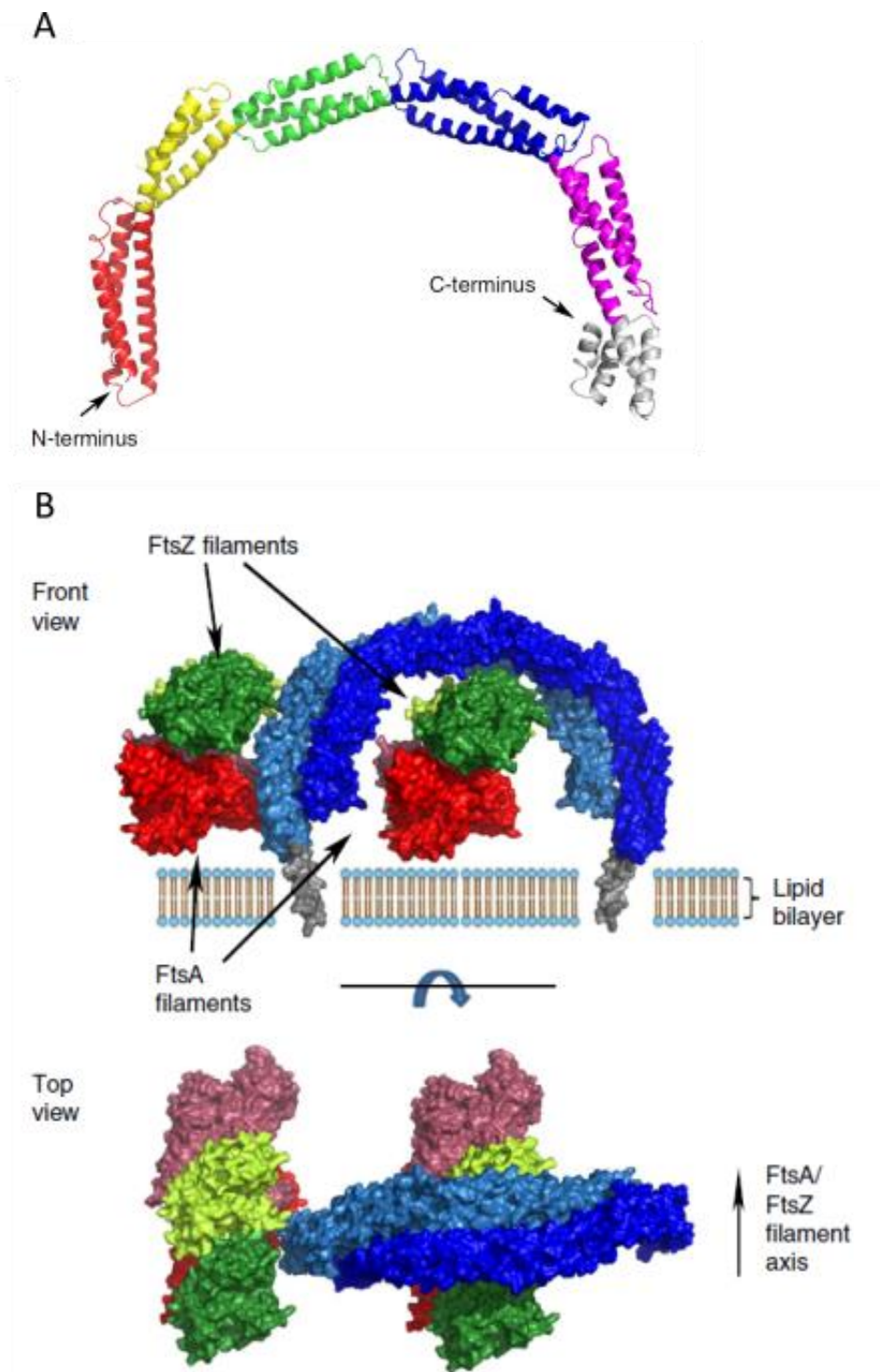


Figure 1.11. Structure of EzrA. (A) Ribbon structure of *B. subtilis* monomer, each triple helical bundle repeat separately coloured. (B) Models of EzrA (light & dark blue) interaction with FtsZ (light & dark green) & FtsA (light & dark red). Taken from (Cleverley et al., 2014).

interact with the outer surface of EzrA leaving the inner surface for alternative interactions (Cleverley et al., 2014).

1.7.3 Septal biosynthesis machinery

There are multiple proteins that belong to the divisome that are involved in the synthesis, remodelling and degradation of the peptidoglycan sacculus. In *E. coli* these are mainly integral membrane proteins and are recruited in the following order; FtsK, FtsQ, FtsL, FtsW, FtsI, FtsN (Pichoff and Lutkenhaus, 2002). The putative flippase FtsW is not only required for this function but it is also involved in FtsI recruitment (Mercer and Weiss, 2002) and together these are required for the recruitment of monofunctional transglycosylases to the divisome (Derouaux et al., 2008). Many important components of the divisome, such as FtsZ, remain conserved across bacterial species while others have diverged significantly (Angert, 2005). Within Gram positives homologs or all genes required for vegetative cell division in *B. subtilis* are conserved in *S. aureus* (Steele et al., 2011).

An additional trimeric complex of proteins, DivIB, DivIC & FtsL (FtsQ, FtsB & FtsL respectively in Gram negatives), are conserved among species. It is thought that this trimer acts as a scaffold for other division proteins (Figure 1.9)(Daniel and Errington, 2000). These genes are often found within operons containing genes involved in peptidoglycan precursor synthesis and mutants exhibit abnormal cell wall phenotypes suggesting a role in the mechanics of the cell wall (Le Gouëllec et al., 2008; Zapun et al., 2008a). Recently DivIB in *S. aureus* has been shown to act as a morphological checkpoint during cell division (Bottomley et al., 2014).

1.7.3.1 Penicillin-binding proteins

Penicillin binding proteins (PBPs) catalyse both the polymerisation of the glycan strands (transglycosylation) and crosslinking of glycan strands (transpeptidation) of peptidoglycan (Chapter 1.4.3) (Sauvage et al., 2008). In addition, some catalyse the hydrolysis of the terminal D-alanine or the peptide crosslinkage. The PBPs can be divided into 2 main groups; high molecular weight (HMW) and low molecular weight (LMW). The HMW PBPs are multimodular with a cytoplasmic tail, transmembrane anchor and 2 domains on the outer surface linked by a β -sheet rich linker (Sauvage et al., 2008). These fall into two classes (A & B), both have transpeptidase activity on the

C-terminal domain. The N-terminal domain of class A has transglycosylase activity while the N-terminal domain of class B is thought to play a role in cell morphogenesis. The LMW PBPs usually have carboxypeptidase or endopeptidase activities.

Lipid II is polymerised to form the glycan backbone of peptidoglycan by the transglycosylase reaction, catalysed either by the monofunctional transglycosylases or the bifunctional Class A PBPs (Lovering et al., 2012). Transglycosylation has 2 modes; initiation where two lipid II molecules are joined together to form lipid IV and elongation where processive addition of lipid II to the growing glycan strand occurs (Lovering et al., 2012). Enzymatically they are essentially identical only differing in the length of glycan strand substrate. Determination of the structure of the transglycosylase domain revealed that lipid II is the acceptor i.e. it maintains its undecaprenoyl-pyrophosphate group while the same group is lost from the glycan chain (Lovering et al., 2007). This occurs via the deprotonation of the lipid II GlcNAc by a glutamate residue within the transglycosylase domain and subsequent reaction with the MurNAc C1 of the glycan chain to form a β 1,4-glycosidic linkage (Lovering et al., 2007, 2012). In addition to class A PBPs, bacteria contain monofunctional transglycosylases capable of carrying out the transglycosylase reaction but do not contain a transpeptidase domain and are therefore not strictly PBPs (Spratt et al., 1996). *S. aureus* has two non-essential monofunctional transglycosylases; SgtA and MGT (Reed et al., 2011).

Transpeptidation occurs via three common steps; first a non-covalent complex is formed between the donor peptide strand and the enzyme transpeptidase domain, then the active site serine attacks the carbonyl carbon of the C-terminal D-alanine forming an acyl-enzyme complex. At this point the terminal D-alanine is released. Finally, the acyl-enzyme complex either undergoes hydrolysis to release a tetrapeptide product or a crosslinkage is formed due to reaction between an amino group on an acceptor peptide sidechain (Lovering et al., 2012; McDonough et al., 2002). The transpeptidase has a common structure whereby two subdomains, a 5 stranded β -sheet covered by 3 α -helices and an all helical subdomain exist with the active site within the cleft between the two (Lovering et al., 2012). The active site contains 3 conserved sequences including the SXXK motif which contains the active site serine.

Bacterial species contain a range of PBPs of the different classifications as well as monofunctional transglycosylases (Sauvage et al., 2008). For example, *E. coli* contains 12 PBPs while *B. subtilis* has 16 (Sauvage et al., 2008). In this respect *S. aureus* provides a minimalist system in that it contains only 4 PBPs (Canepari et al., 1985). PBP2 is the only class A bifunctional PBP, PBP1 and PBP3 are both HMW PBPs containing transpeptidase activity only. *S. aureus* has one LMW PBP, PBP4 (Scheffers and Pinho, 2005). PBP4 is an unusual LMW PBP in that it has transpeptidase activity, this contributes to the high degree of crosslinking in *S. aureus* peptidoglycan (Wyke et al., 1981; Zapun et al., 2008b). In addition, methicillin resistant *S. aureus* (MRSA) strains have an additional PBP, MecA/PBP2A (Zapun et al., 2008b). PBP2A has a lower affinity for β -lactam antibiotics than the native PBPs of *S. aureus* i.e. the acylation rate of PBP2A is negligible at therapeutic concentrations (Zapun et al., 2008b). Therefore, PBP2A can restore transpeptidase function to *S. aureus*. However, the transglycosylase reaction of PBP2 is still required along with the activities of a number of additional proteins, e.g the Fem proteins. Following removal of β -lactam selective pressure native PBPs are quickly restored suggesting use of PBP2A in cell wall synthesis bears a significant cost in the absence of antibiotics (Zapun et al., 2008b).

Of the PBPs, only PBP1 and PBP2 have been shown to be essential, in fact *S. aureus* has been shown to survive when PBP1 & 2 are the only known peptidoglycan synthesis enzymes, however these strains have impaired survival in challenging environments (Reed et al., 2015). It has also been suggested that the essentiality of PBP1 may be independent of its enzymatic activity, however, the reason for this is unclear (Pereira et al., 2009). Both PBP1 and PBP2 have been localised to the septum where peptidoglycan synthesis is believed to mostly occur (Pereira et al., 2009; Pinho and Errington, 2003).

1.8 Cell division as an antibiotic drug target

The unique and universal chemical structure of peptidoglycan in bacteria makes it an ideal target for antibiotics as inactivation of peptidoglycan generally leads to cell death (Coyette and van der Ende, 2008). Due to the increased prevalence of antibiotic resistance there is an urgent need for the creation of new agents for the inhibition of bacterial cell wall synthesis (Bugg et al., 2011). The essentiality of proteins involved in all stages of peptidoglycan synthesis make them ideal targets for antibiotic

development although most current antibiotics are targeted to the later lipid-linked steps (Bugg et al., 2011; Lovering et al., 2012). Recent structure based drug design and targeted library screening has produced new lead compounds for targeting cytoplasmic steps in addition to fosfomycin and D-cycloserine, current inhibitors of MurA and D-ala-D-ala ligase respectively (Bugg et al., 2011).

Lipid II is an attractive antibiotic target since it is highly conserved and any modification to the structure is difficult (Scheffers and Tol, 2015). Vancomycin, a current antibiotic in clinical use, targets lipid II by binding to the D-ala-D-ala motif in the pentapeptide stem of lipid II (Reynolds, 1989). This produces steric hindrance and prevents the activity of transpeptidases in the synthesis of peptidoglycan (Lovering et al., 2012; Reynolds, 1989).

The major class of antibiotics targeting peptidoglycan synthesis are β -lactams, that mimic the D-ala-D-ala dipeptide (Lovering et al., 2012). These target the transpeptidase active site of PBPs (Waxman and Strominger, 1983). The transpeptidase active-site serine attacks the β -lactam ring, as it would the D-ala-D-ala substrate under normal conditions, forming a long-lived covalent acyl enzyme complex, this impairs PBP activity and thus PG crosslinking is reduced (Lovering et al., 2012). Resistance against β -lactams is highly prevalent, one mechanism is the acquisition of insensitive PBPs, such as PBP2A in *S. aureus*, in which the active site serine is in a poor position for a nucleophilic attack (Lovering et al., 2012). Another means of resistance is the acquisition of β -lactamases, enzymes that break down β -lactam antibiotics thereby reducing the effective concentration of β -lactams so that PBP transpeptidase activity is able to continue (Zapun et al., 2008b).

Peptidoglycan synthesis is not the only process within cell division which can be targeted by antibiotics. There are a number of other essential proteins that make up the bacterial divisome and are required for correct localisation of peptidoglycan synthesis and progression of cell division that also provide attractive targets for antibiotics (Bottomley et al., 2014; Steele et al., 2011; Vollmer, 2006). In particular FtsZ has proved a promising drug target (Andreu et al., 2010; Haydon et al., 2008; Tan et al., 2012).

1.9 Peptidoglycan dynamics

1.9.1 Synthesis of peptidoglycan

The localisation of peptidoglycan synthesis in the sacculus is important for the determination of cell shape as well as growth of the organism. Using a fluorescent derivative of vancomycin, which binds to the terminal D-ala-D-ala of pentapeptides, present in nascent peptidoglycan and lipid II precursors only, it is possible to visualise synthesis using fluorescence microscopy (Daniel and Errington, 2003). In *B. subtilis* vancomycin labelling was shown to occur in a helical pattern on the cell cylinder as well as the expected intense staining at the active or recent division site (Daniel and Errington, 2003; Tiyanont et al., 2006). This helical pattern was reminiscent of the pattern seen in bacterial cytoskeletal proteins.

Similar to *B. subtilis* a roughly helical pattern of new peptidoglycan synthesis was seen on the cylinder of *E. coli* when labelled with fluorescent immunodetection of D-cysteine (Varma et al., 2007). New peptidoglycan insertion occurred as short arcs separating older material and despite a lack of defined periodicity this was ascribed to a helical distribution of peptidoglycan insertion sites (Varma et al., 2007). However recent super-resolution microscopy of *E. coli* sacculi labelled with fluorescent vancomycin revealed peptidoglycan insertion to occur as multiple discrete foci over the cylinder of the cell (Turner et al., 2013). This was unexpected since the elongation machinery in *E. coli* moves in a helical manner (van Teeffelen et al., 2011) however Lpo proteins, which are also required for peptidoglycan synthesis, have been shown to exist in patches (Paradis-Bleau et al., 2010; Typas et al., 2010). Therefore it is possible that there is additional control over peptidoglycan synthesis during elongation in *E. coli* rather than simply the localisation of the elongation machinery (Turner et al., 2014).

Several cytoskeletal proteins have been identified in bacteria as determinants of cell shape. Deletions of the genes encoding these proteins in rod-shaped organisms cause spherical growth (Leaver and Errington, 2005). MreB and its paralogs in *B. subtilis* (MreB, Mbl & MreBH) form dynamic helical cables which suggests that they may direct peptidoglycan synthesis on the cylinder of the cell (Daniel and Errington, 2003; Jones et al., 2001). However more recent work has suggested that all three MreB homologs in *B. subtilis* were shown to form discrete structures that move independently with no underlying tracks or filaments (Domínguez-Escobar et al., 2011; Garner et al., 2011).

MreC & D are thought to stabilise the MreB cytoskeleton (Leaver and Errington, 2005). In *C. crescentus* MreC binds to the penicillin binding protein PBP2 thereby MreB & MreC are thought to control cell shape through localisation of the peptidoglycan synthesis machinery (Divakaruni et al., 2007). Additionally, in *B. subtilis* MreB interacts with Dapl, a protein required for *m*-DAP synthesis (Rueff et al., 2014). While peptidoglycan biosynthesis proteins do not move with MreB they are thought to dynamically associate with them as recruitment platforms (Chastanet and Carballido-López, 2012). Some Mur enzymes have also been shown to display MreB like localisation (Divakaruni et al., 2007). Therefore MreB may contribute to tight coupling between peptidoglycan precursors and cell wall synthesis complexes (Rueff et al., 2014).

Determination of peptidoglycan synthesis localisation in the coccoid bacterium *S. aureus* showed that synthesis occurred primarily at the division site (Pinho and Errington, 2003). This is directed by FtsZ since deletion of FtsZ results in delocalisation of peptidoglycan synthesis, presumably due to the delocalisation of biosynthetic enzymes (Pinho and Errington, 2003). *S. aureus* can therefore act as a simpler model of peptidoglycan synthesis and dynamics due to the presence of a single cell wall synthesis machine. In addition, such a model of division within *S. aureus* may lead to the identification of novel drug targets in a clinically relevant organism.

1.9.2 Enlargement of the sacculus

Peptidoglycan hydrolases are essential for bacterial survival and are thought to play a role in cell wall growth (Lee and Huang, 2013). It has been proposed that hydrolysis of existing bonds may allow for the growth of the sacculus but this may compromise cell wall integrity, therefore strict control between the synthesis and hydrolysis processes must exist. A three-for-one model of peptidoglycan insertion was postulated (Figure 1.12 A); in this model, 3 new peptidoglycan strands are crosslinked together to form peptidoglycan triplet, this triplet is cross linked to free amino groups on the crossbridges of a single docking strand of peptidoglycan within the cell wall (Höltje and Heidrich, 2001). The docking strand is stress bearing while the triplet remains unstressed. Specific removal of the docking strand by hydrolase activity results in the insertion of the peptidoglycan triplet into the stress bearing layer (Figure 1.12 A)(Höltje and Heidrich, 2001). While this model was postulated on an assumption of a single

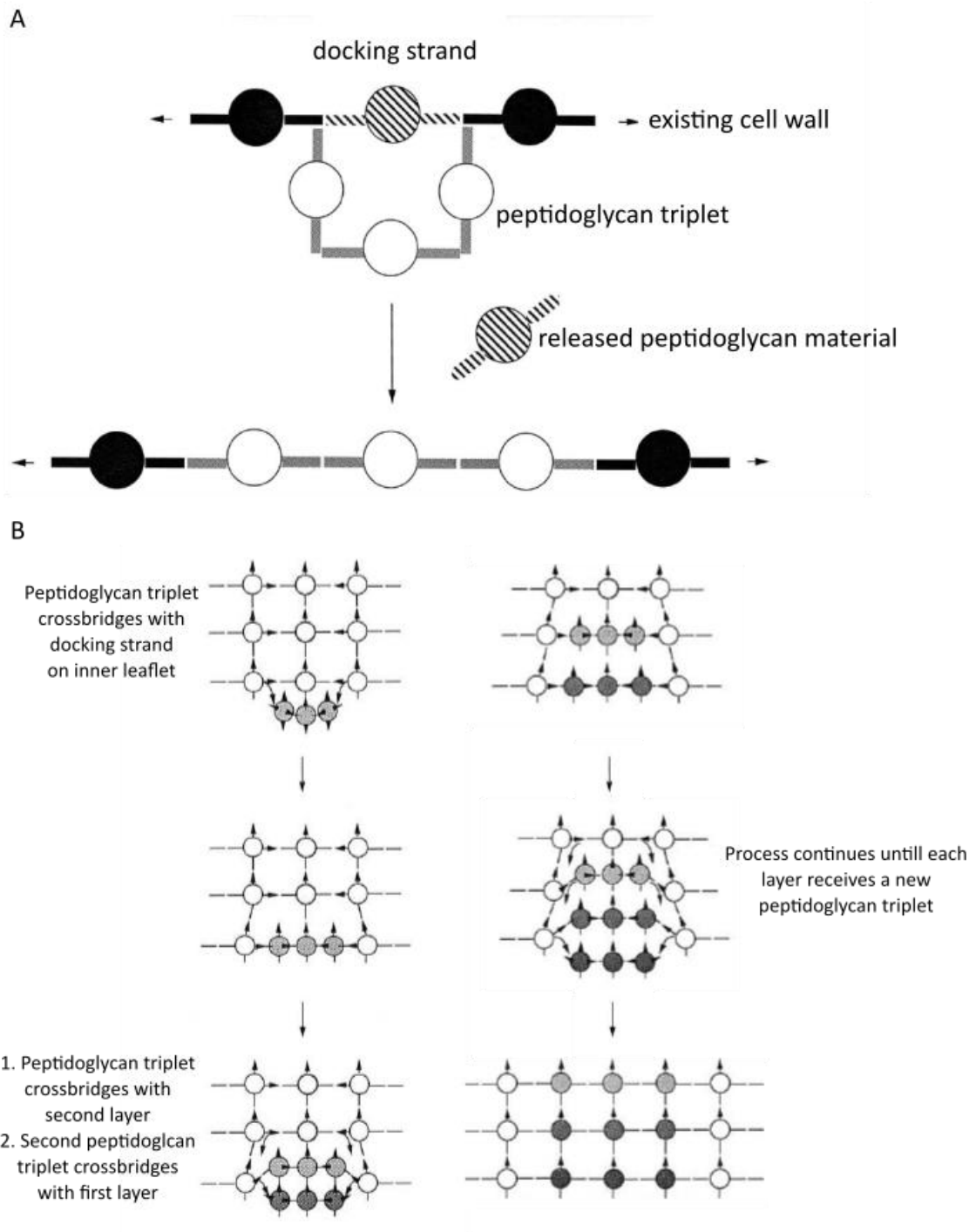


Figure 1.12. Three-for-one model of peptidoglycan insertion. (A) Model in a single layer. (B) Schematic of how the three-for-one model may be applied in Gram positive bacteria. Adapted from (Höltje and Heidrich, 2001).

layer of peptidoglycan however it can still occur in multi-layered peptidoglycan such as that found in Gram positive bacteria. Peptidoglycan is generally believed to expand from the inside out and with the three-for-one model newly synthesised peptidoglycan can be inserted “pack by pack” and transferred from the inner layer through the peptidoglycan such that each layer receives a new peptidoglycan triplet (Figure 1.12 B)(Höltje and Heidrich, 2001).

1.9.3 Daughter cell splitting & septum expansion

1.9.3.1 Role of hydrolysis in cell splitting

Both hydrolysis and synthesis of peptidoglycan important in the growth of a bacterial cell, however the coupling between the two processes is still not fully understood (Lee and Huang, 2013). During the cell cycle the septum must be synthesised and then the daughter cells split from one another, this splitting is thought to involve the action of peptidoglycan hydrolases (Giesbrecht et al., 1997; Heidrich et al., 2001; Ohnishi et al., 1999). Gram negative bacteria such as *E. coli* require the additional constriction and separation of the outer membrane in addition to the peptidoglycan layer (Goley et al., 2010).

Recent work in *C. crescentus* discovered that the DipM protein plays a role in envelope invagination (Goley et al., 2010; Moll et al., 2010; Poggio et al., 2010). DipM contains 4 LysM domains for peptidoglycan binding and is a putative LytM endopeptidase with peptidoglycan hydrolase activity (Moll et al., 2010). DipM was found to localise to the midcell in an FtsZ (Goley et al., 2010; Moll et al., 2010; Poggio et al., 2010) and FtsN dependent manner(Moll et al., 2010). Interaction between DipM and FtsN was detected suggesting a role for DipM in the divisome of *C. crescentus* (Moll et al., 2010). DipM is non-essential, except in fast growth conditions (Poggio et al., 2010), and mutants were found to have thickened peptidoglycan and blebbing of the outer membrane at division sites (Goley et al., 2010). This indicates that DipM is required for normal envelope invagination during division and to maintain a sacculus of a constant thickness, through direct hydrolysis of peptidoglycan. Additionally, a number of peptidoglycan hydrolases which cleave a variety of bonds are involved in the process (Chapter 1.5.3).

Many peptidoglycan hydrolases play a role in daughter cell separation and are localised to the division septa, although direct interaction between hydrolases and the divisome has not been demonstrated. *E. coli* contains three amidases AmiA, AmiB & AmiC, that are involved in splitting of the septum (Heidrich et al., 2001). Cell splitting can occur with only one amidase, although at a reduced rate (Höltje and Heidrich, 2001). AmiC is localised to the midcell in a FtsN dependent manner, although direct interaction between the proteins was not shown (Bernhardt and De Boer, 2003). In addition to amidases both lytic transglycosylases (Slf70, MltA & MltB) and endopeptidases (MepA, PBP4, PBP7) are able to cleave the septum, although amidases are presumed to be the major proteins involved since the effect of the other protein families are only apparent following deletion of the amidase activity (Heidrich et al., 2002). In *B. subtilis* a number of different peptidoglycan hydrolases are involved in cell separation including LytF(CwlW) and CwlF (Ohnishi et al., 1999).

In *S. aureus* there are a various autolysins involved in daughter cell splitting including Atl, Sle1, IsaA and SceD (Biswas et al., 2006; Kajimura et al., 2005; Stapleton et al., 2007; Wheeler et al., 2015). Atl is the major autolysin in both *S. aureus* (AtlA) and *Staphylococcus epidermidis* (AtlE). Atl is a bifunctional enzyme composed of amidase and glucosaminidase domains which undergoes proteolytic processing to generate two extracellular peptidoglycan hydrolases (Biswas et al., 2006; Yamada et al., 1996). Atl has been shown to localise to the division septa and split into two rings on adjacent daughter cells during cell splitting (Yamada et al., 1996). On completion of cell splitting AtlA already starts to align at the site where the next division will occur, suggesting that whatever mechanism specifies division planes is already in place (Yamada et al., 1996).

1.9.3.2 Daughter cell splitting in *S. aureus*

Initial EM data suggested that the staphylococcal cell wall was composed of two parts; a transitory and a permanent part. The transitory part was thought to comprise approximately 1/3 of the cell wall and was lost during cell separation (Giesbrecht et al., 1997). Two compatible mechanisms for cell separation were proposed, both initiated by lysis of the mature cell wall in a punctate pattern, thought to be due to the presence of vesicular wall organelles called murosomes (Giesbrecht et al., 1997). The first mechanism involved continued lysis of the septum by murosomes while the

second involved the action of the splitting system as a mechanical aid to separation of the daughter cells by application of physical forces (Giesbrecht et al., 1997). Cell splitting in this manner could theoretically occur “suddenly” and the force used may force daughter cells to pop apart (Giesbrecht et al., 1997). Recent live-cell microscopy has shown that daughter cell separation does indeed occur on a millisecond timescale (Zhou et al., 2015). However, more recent EM work questioned the presence of a splitting system, although this does not negate the role of mechanical forces in the splitting of daughter cells (Giesbrecht et al., 1997; Matias and Beveridge, 2007). The growing septum was seen to consist of 5 distinct layers in EM, two high density zones (HDZ) sandwiched by low density zones (LDZ) i.e. membrane, LDZ, HDZ, LDZ, HDZ, LDZ, membrane (Matias and Beveridge, 2007). These LDZ’s were confirmed to be a “periplasmic space” and comprised of soluble components while the HDZ’s were that of the peptidoglycan cell wall (Matias and Beveridge, 2007). This firstly confirmed the existence of a periplasmic space within Gram positive bacteria and secondly proposed that the septum existed as 2 separate entities prior to cell separation (Matias and Beveridge, 2006, 2007). This suggests that the newly synthesised septum is rapidly separated into two separate parts due to autolysis activity, indeed many peptidoglycan hydrolases, not just Atl, have been localised to the septum of *S. aureus* (Frankel and Schneewind, 2012).

Cell splitting has been shown to be due to the action of hydrolases. Null mutants of *atl* and *sle1*, an *N*-acetylmuramyl-L-alanine amidase, produce clusters of cells that have failed to separate, suggesting the role of these enzymes in daughter cell separation (Kajimura et al., 2005; Takahashi et al., 2002). Additionally, using fluorescence microscopy, Atl amidase and glucosaminidase proteins have been localised to the septum, in particular in association with a raised architectural feature that surrounds the nascent septum known as the piecrust (Chapter 1.10.6.1)(Kent, 2013). This may implicate Atl in the hydrolysis of this feature required for cell splitting to take place. As in *E. coli*, the deletion of two putative lytic transglycosylases from *S. aureus*, IsaA and SceD caused impaired cell separation (Stapleton et al., 2007).

1.9.3.3 Septum expansion in *S. aureus*

Nascent cell wall exposed on cell splitting was found to be stiffer than the rest of the cell wall, and this stiffness was seen to decrease as the expansion of the cell wall

occurred (Bailey et al., 2014). *S. aureus* has characteristic short glycan chains, average 6 disaccharides long, which have been processed to give reducing terminal *N*-acetyl glucosamines (Boneca et al., 2000). This explains the need for glucosaminidase activity in the growth of *S. aureus* (Wheeler et al., 2015). The *S. aureus* genome contains 4 putative glucosaminidases; *atl*, *sagA*, *scaH*, *sagB* (Wheeler et al., 2015). The 4 encoded proteins are synthetically lethal and cells that lack all four, due to the use of a conditional mutant, were seen to have a defect in cell expansion, increased surface stiffness and increased glycan chain length. Interestingly despite redundancy in glucosaminidases, SagB is the most dominant enzyme with important roles in both cell stiffness and glycan chain length (Wheeler et al., 2015). The nascent cell wall expansion due to hydrolysis of glycan strands & concomitant decrease in stiffness apparently accounts for the growth mode of *S. aureus* (Bailey et al., 2014; Wheeler et al., 2015).

1.10 Peptidoglycan architecture

While the chemical structure of peptidoglycan has been well studied it is only recently that we have had the techniques available to begin to understand the 3D architecture of the peptidoglycan sacculus. A number of architectural models have been proposed concerning glycan strand orientation. In addition recent applications of electron cryo tomography (ECT) and atomic force microscopy (AFM) have revealed large scale architectural features of peptidoglycan across species (Amako et al., 1982; Andre et al., 2010; Hayhurst et al., 2008; Plomp et al., 2007; Touhami et al., 2004; Turner et al., 2010a, 2013; Wheeler et al., 2011).

1.10.1 Models of peptidoglycan architecture

1.10.1.1 Planar vs. scaffold model of glycan chains

Glycan strand orientation modelling has proposed two opposing ideas; the planar and scaffold models (Figure 1.13 A & B). In the planar model glycan chains are orientated parallel to the cytoplasmic membrane (Koch, 1998a). The planar model, within Gram negative bacteria would consist of a single stress bearing layer with newly synthesised material on the innermost side and mostly degraded material on the outermost side both loosely crosslinked to the stress bearing layer (Figure 1.13 B)(Dmitriev et al., 2003). These glycans were thought to be arranged circumferentially first due to EM images of digested or sonicated sacculi and later due to AFM measurements which

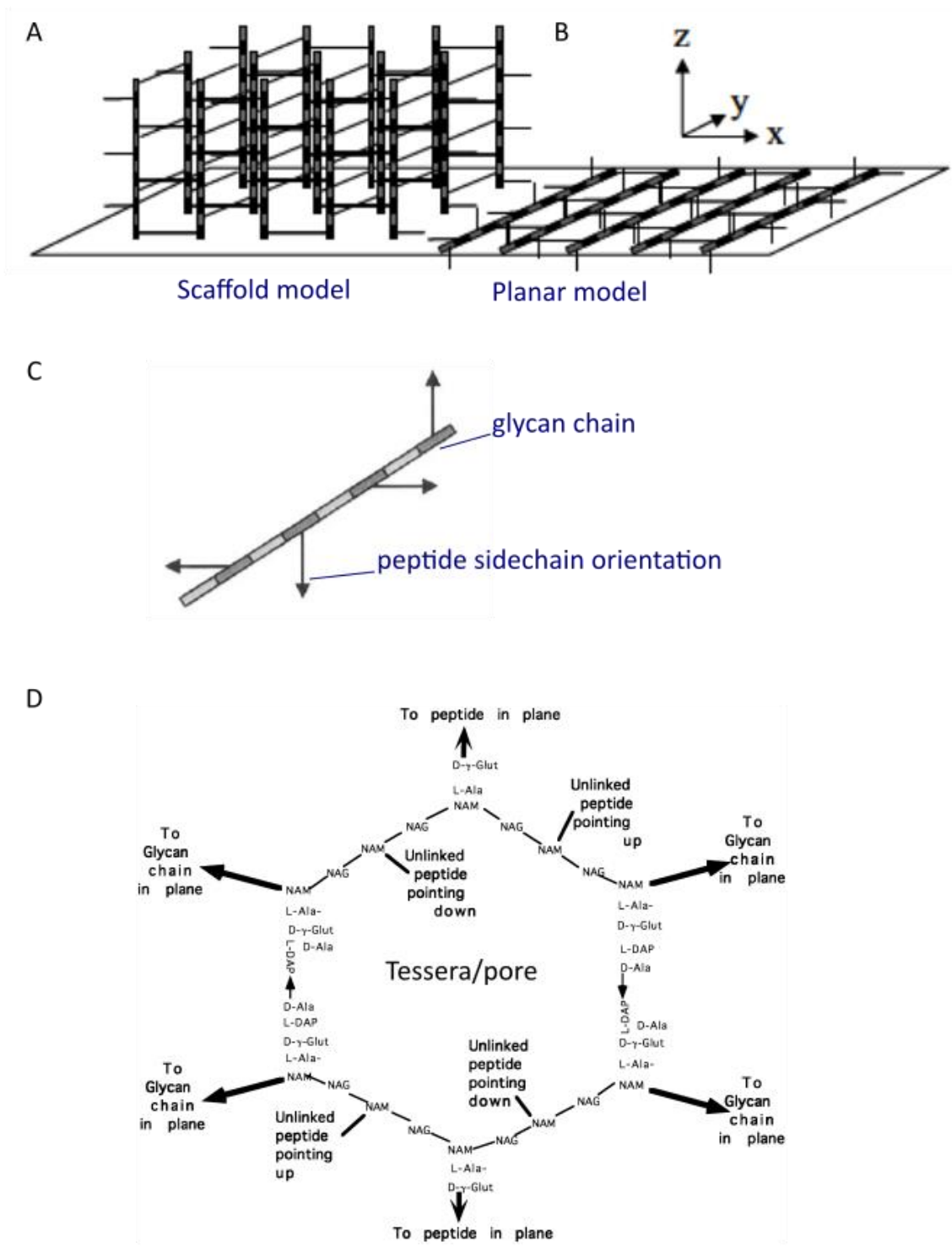


Figure 1.13. Models of peptidoglycan architecture. (A) Scaffold model. (B) Planar Model. (C) Helical glycan strands. (D) Tessera structure. Adapted from (Koch, 1998b; Vollmer and Höltje, 2004).

showed sacculi to be less elastic in the circumferential direction compared with the longitudinal direction (Koch, 1998a; Yao et al., 1999). Glycan chains form an extended helix with peptides extending in a clockwise manner, perpendicular to each other (Figure 1.13 C) (Vollmer and Höltje, 2004). Therefore, in a theoretically perfect monolayer would be 50% crosslinked, close to the 40-50% crosslinked experimental value. A modification of this model proposed by Koch (1998b) suggested that glycans would follow a zig-zag as opposed to a straight line forming small pores in the sacculus known as tessera (Figure 1.13 D)(Koch, 1998b). Since glycan strands are often shorter than the dimensions of the cell and the percentage crosslinks is lower than the theoretical value, holes or slits are thought to exist within the sacculus formed of fused hexagonal tessera (Vollmer and Höltje, 2004). If these are distributed across the peptidoglycan layer it is not thought that the presence of such holes will decrease overall peptidoglycan stability. In Gram positive bacteria the peptidoglycan layer is thought to consist of several layers of peptidoglycan in this formation linked to one another (Dmitriev et al., 2003).

An alternative model for glycan chain orientation was proposed by Dmitriev et al (2003) where glycan strands are arranged perpendicular to the cytoplasmic membrane (Figure 1.13 A). Glycans extend vertically from the cytoplasmic membrane and crosslinked by peptides parallel to the surface. The peptidoglycan would be highly crosslinked near the cytoplasmic membrane and have reduced crosslinking at the outer membrane (Dmitriev et al., 2003). This model was also later applied to Gram positives in the form of *S. aureus* where it could account for high cross-linking as well as division on consecutive planes (Dmitriev et al., 2004). The planar model of division was thought to result in sectors of peptidoglycan with glycan chains running in multiple directions and would require consecutive turns of the biosynthetic machinery whereas the scaffold model poses a simpler system (Dmitriev et al., 2004). While the short glycan chains of *S. aureus* would permit the scaffold architecture, sacculi of *E. coli* are thin and for the scaffold model to exist glycan chains would have an average length of 2.5 saccharides and a maximum length of 7 disaccharides (Vollmer and Höltje, 2004). However, in reality *E. coli* has an average glycan chain length of 25-30 disaccharides with a high proportion over 30 disaccharides, which would not fit a scaffold model of arrangement. Additionally, even if was assumed that peptidoglycan

with vertically orientated glycan strands were to exist entirely in the maximally stretched conformation there is not enough peptidoglycan material in the *E. coli* sacculus to cover the entire cell surface (Vollmer and Höltje, 2004). This makes it unlikely that the scaffold model exists in Gram negative bacteria.

1.10.2 New models of peptidoglycan architecture

Recent work, mainly using EM and AFM, has revealed a number of different architectural features of peptidoglycan. While these have been useful in determining small scale features of peptidoglycan it has not yet been possible to confirm visualisation of glycan strands and crosslinks within sacculi (Turner et al., 2014).

1.10.3 Models of peptidoglycan architecture in Gram negative bacteria

Electron cryo tomography (ECT) of sacculi from both *E. coli* and *C. crescentus* revealed a mostly single layer of peptidoglycan although in some parts this extended up to three layers thick (Gan et al., 2008). In addition, thin “tubes” of electron density were observed in the plane of the peptidoglycan and mostly perpendicular to the long axis of the cell. These were attributed to single glycan chains (Gan et al., 2008). This showed that the scaffold model is indeed not possible in Gram negative bacteria. The architecture of the glycan strands were uniform across the sidewall, indicating a lack of growth zones however they were irregularly spaced and not perfectly parallel, although a mostly circumferential organisation was observed (Gan et al., 2008). More recently AFM was used on Gram negative sacculi which revealed features in the plane of the sacculus however in many directions in relation to the axis of the cell (Turner et al., 2013). In addition, bands were seen to run approximately circumferential to the long axis (Figure 1.14 A), however these were too large to account for individual glycan strands. High resolution AFM showed these bands to contain pores and form a lattice like structure (Figure 1.14 A), however these pores were too large to be compatible with tessera (Koch, 1998b; Turner et al., 2013; Vollmer and Höltje, 2004). Additionally, hydrolase digestion of these features showed that glycans have little or no general orientation. This architectural landscape was common to all Gram negative species tested (*E. coli*, *C. crescentus*, *Pseudomonas aeruginosa* & *Campylobacter jejuni*)(Turner et al., 2013).

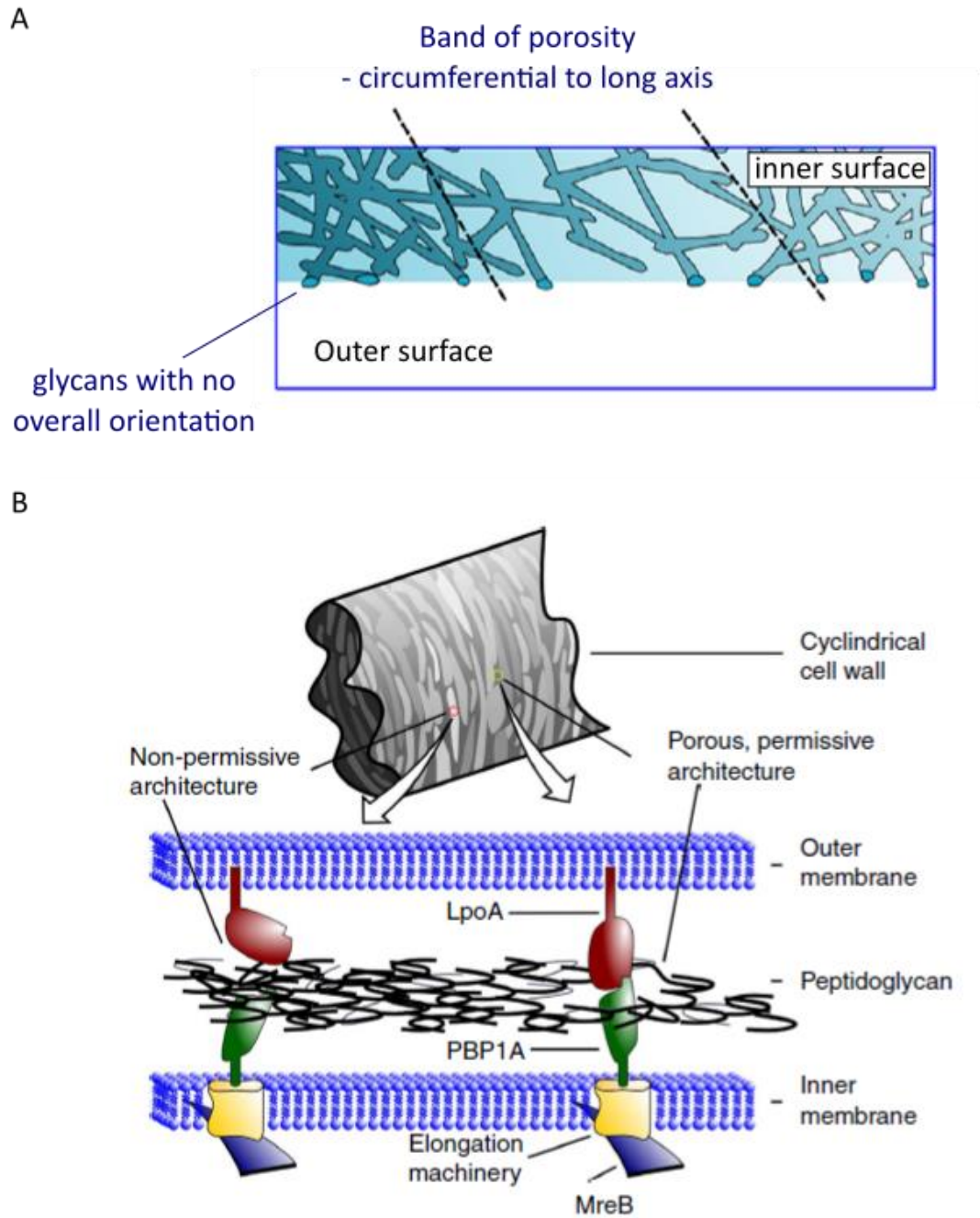


Figure 1.14. Model of Gram negative peptidoglycan architecture. (A) Model of architecture including randomly oriented glycan strands and bands of porosity circumferential to long axis. (B) “Architecture -regulated” model of growth. Adapted from (Turner et al., 2013, 2014).

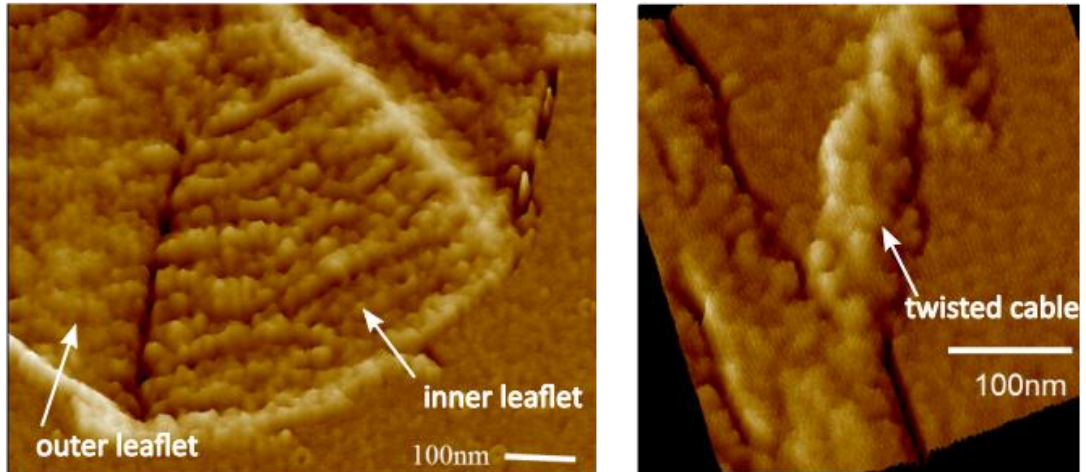
These architectural features in addition to super-resolution observations of insertion patterns (Chapter 1.9.1) has led to a model of “architecture-regulated” growth (Turner et al., 2013). Insertion of peptidoglycan into areas that already contain higher peptidoglycan levels would result in dense, thick peptidoglycan that was unable to expand (non-permissive architecture). The new model proposes that insertion would occur primarily in areas with the most pores (permissive architecture), likely directed by LpoA, the outer membrane protein required for synthesis as it would span the peptidoglycan in areas where the pores exist (Figure 1.14 B). The mechanism of growth for elongation occurs when the areas with higher peptidoglycan content are hydrolysed and stretched due to turgor pressure to become permissive (Turner et al., 2013).

1.10.4 Models of peptidoglycan architecture in Gram positive rods

Organisation of peptidoglycan in Gram positive rods, particularly *B. subtilis* have long been thought to also have a layered architecture however composed of multiple layers to explain peptidoglycan thickness. AFM observations of *Lactobacillus helveticus* revealed ~26 nm thick twisted fibres within the cell wall, this was attributed to glycan strands however this is not unequivocal due to limitations in the nanosurgery technique used (Firtel et al., 2004). Alternatively *B. subtilis* sacculi had a striated appearance perpendicular to the short axis in EM images which was thought to be due to glycan strands (Verwer and Nanninga, 1976). The glycan strands were proposed to be organised in an irregular pattern but predominantly tangentially.

A more recent AFM study of *B. subtilis* revealed a number of features in the peptidoglycan. Firstly *B. subtilis* was shown to have exceedingly long glycan chains (Hayhurst et al., 2008). Approximately 25% of glycan material was found to be over 500 disaccharides in length and some were measured to be of up to 5 µm in length, corresponding to 5,000 disaccharides. The inner surface of the peptidoglycan sacculus was shown to have a regular macrostructure with ~50 nm wide cables running across the short axis (Figure 1.15 A) (Hayhurst et al., 2008). This architecture was also maintained in the septum. The proposed model is that during biosynthesis a peptidoglycan rope is formed from the polymerisation and crosslinking of a small number of glycan strands. This rope is subsequently coiled into a ~50nm wide helical

A



B

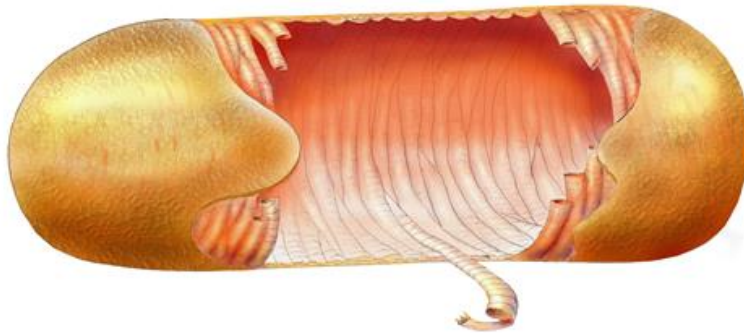


Figure 1.15. Peptidoglycan architecture of *B. subtilis*. (A) AFM phase images of cell wall features, outer vs. inner leaflet and possible twisted cables. (B) Model of peptidoglycan architecture in *B. subtilis*. Adapted from (Hayhurst et al., 2008).

cable which is inserted into the cell wall via crosslinks with 2 existing cables (Figure 1.15 B). The interface is cleaved by hydrolases and flattened due to turgor which allows for growth (Hayhurst et al., 2008). This model not only allows for the long glycan chains but predicts that the cell wall is composed of one intact cable with partially hydrolysed cables present externally, explaining why the architecture is only observed on the inner leaflet (Hayhurst et al., 2008; Smith et al., 2000). Both *E. coli* and *B. subtilis* have been shown to twist during growth, albeit in a different direction, this suggested that helical peptidoglycan insertion may contribute to peptidoglycan architecture by chiral self-organization of the peptidoglycan network (Wang et al., 2012b).

Beeby et al. (2013) were unable to discern a structure representing the coiled cable architecture using ECT. Instead peptidoglycan was seen to be uniformly dense with the inner surface smooth and flush with the inner membrane (Beeby et al., 2013). During sporulation *B. subtilis* was shown to produce a thin “Gram negative” style peptidoglycan. The authors therefore rejected the coiled coil model since the uniform density does not allow for hollow cables. Additionally, the modification of peptidoglycan thickness during sporulation, in other species and due to the environment is unlikely to be possible with the cabled conformation (Beeby et al., 2013; Cheng and Costerton, 1977; Hanaki et al., 1998; Tocheva et al., 2013). Instead a model of circumferentially arranged glycan chains in multiple layers was posed, similar to a suggested model for Gram negative bacteria which would be assembled from inside to out due to deposition of material at the inner membrane and degradation of the outer layer (Beeby et al., 2013). This can then be “thinned” by hydrolase activity. However this interpretation comes from ECT where signal:noise ratio limitations can make internal structure difficult to discern. In addition, the proposed model does not appear to accommodate the AFM data from Hayhurst et al (2008) in particular the long glycan chains. It is possible that the observed thinner peptidoglycan may have a different architecture, particularly as these observations were made during either different growth phases or in different species. Unlike Gram negative bacteria, a number of different architectural features have been seen among Gram positive species (Chapter 1.10.5 & 1.10.6).

1.10.5 Models of peptidoglycan architecture in ovococci

Unlike “true” cocci such as *S. aureus* which have an apparent “spherical” shape, ovococci are slightly elongated (Zapun et al., 2008a). Examples of ovococci include *S. pneumoniae*, *Enterococcus faecalis* and *Lactococcus lactis*. Using AFM Wheeler et al. (2011) determined the architectural features of ovococci peptidoglycan. Glycan strands were found to be preferentially orientated circumferentially and parallel to the short axis of the cell. Distinct ring structures were associated with growth and division from septa and equatorial rings were also observed (Wheeler et al., 2011). A single growth annulus was seen in *L. lactis* and *E. faecalis*, however up to three were observed in *S. pneumoniae*. Parallel bands of material attributed to several intertwined glycan bands were seen in *S. pneumoniae* but not in *L. lactis* or *E. faecalis*, probably due to the overlapping rounds of division in *S. pneumoniae*. This showed that ovococci have a peptidoglycan architecture distinct from that of other Gram positive species (*B. subtilis* and *S. aureus*) as well as variation between ovococci species, though to be due to differences in spatial and temporal regulation of the cell cycle.

1.10.6 Models of peptidoglycan architecture in *S. aureus*

Atomic force microscopy (AFM) has been applied to both whole cells and extracted peptidoglycan sacculi to determine the surface architecture of *S. aureus* (Touhami et al., 2004; Turner et al., 2010a). The mature peptidoglycan surface within whole cells were shown to have both contoured and smooth structures with different adhesive properties (Touhami et al., 2004). At higher resolution this peptidoglycan has been proposed to have a network or honeycomb-like structure (Figure 1.16 A) (Giesbrecht et al., 1998; Touhami et al., 2004; Turner et al., 2010b). However, these were not visible in extracted sacculi suggesting that the other components of the cell wall, proteins, teichoic acids etc., may contribute to these structures (Turner et al., 2010a). Instead older cell wall was seen to have a knobbly architecture (Figure 1.16 B)(Turner et al., 2010a). The knobbly architecture was thought to occur due to rearrangement of the nascent peptidoglycan architecture through the action of hydrolases.

New cell wall material visualised just after cell separation was seen to consist of concentric surface rings and a central depression consistent with previous SEM (Figure 1.16 B & C) (Amako et al., 1982; Touhami et al., 2004). In addition, AFM on sacculi revealed a thicker band of peptidoglycan encircling the cell on the inner leaflet of the

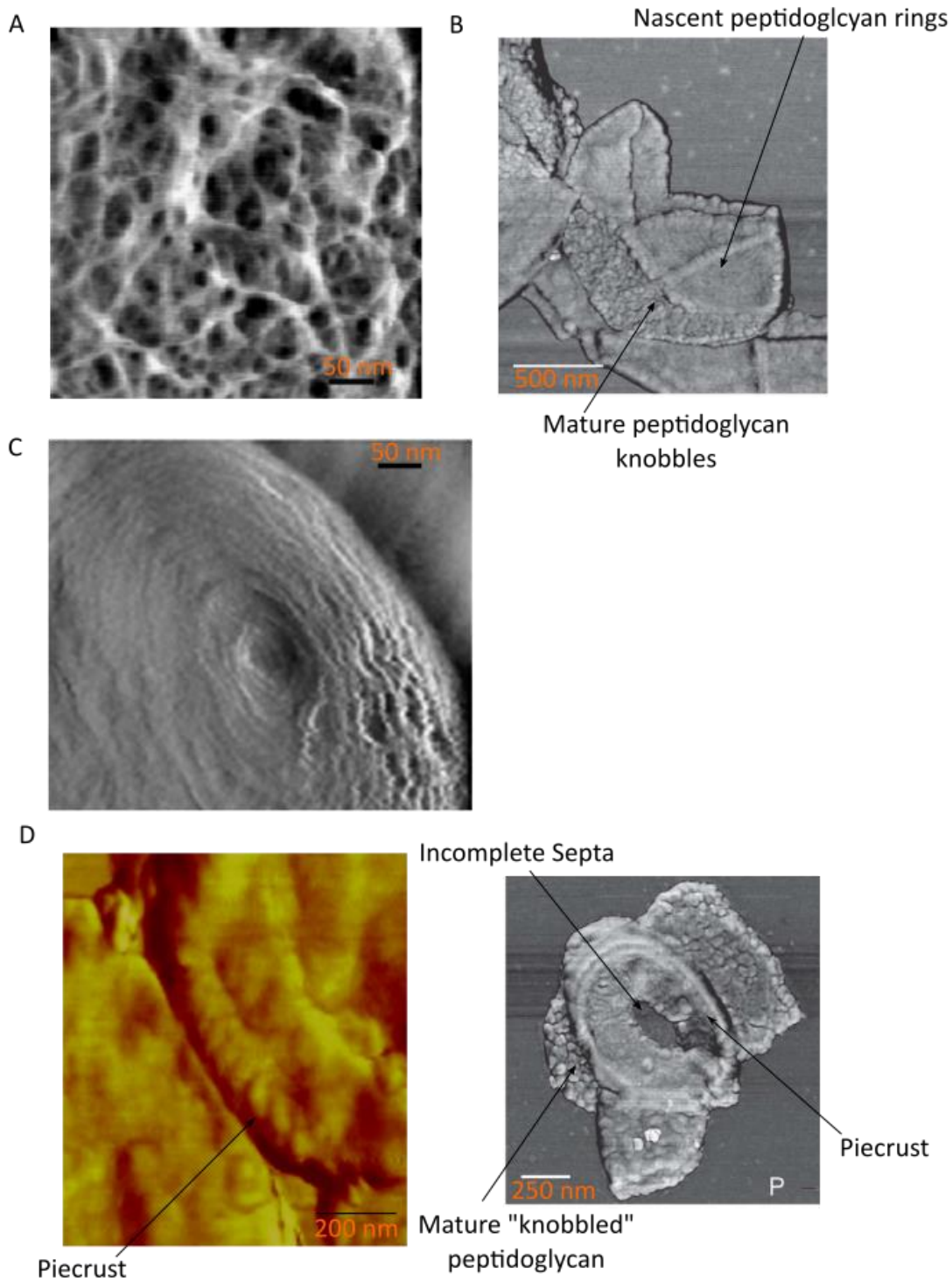


Figure 1.16. Peptidoglycan architecture of *S. aureus*. (A) High resolution AFM of mature cell wall. (B) Mature and nascent peptidoglycan architecture in sacculi. (C) Nascent septum architecture. (D) Piecrust feature under AFM. Adapted from (Touhami et al., 2004; Turner et al., 2010a).

peptidoglycan layer (Figure 1.16 D)(Turner et al., 2010a). This band, known as the piecrust, is proposed to denote the division planes (Chapter 1.10.6.1). Since this feature was seen surrounding incomplete septa it was proposed that this was synthesised prior to the rest of the septum. Spacing between the rings on the newly exposed septa were seen to vary from 13-25 nm on average although some longer spacings were also present (Touhami et al., 2004). As the rings were positioned closer to the centre of the septum the height increased from ~1 nm to ~2 nm (Touhami et al., 2004). The central depression had a depth of at least 30 nm, the presence of this depression is likely due to the completion of the septal plate, an important step where peptidoglycan alignment and bonding is subtly different from normal peptidoglycan (Matias and Beveridge, 2007; Touhami et al., 2004). It is very rare for both the ring and knobbly architectures to occur in the same areas of the peptidoglycan sacculi suggests that the rings are remodelled into knobbles, likely by discontinuous autolysis of the peptidoglycan rings (Turner et al., 2010a).

1.10.6.1 Model of specification of division planes by recognition of specific architectural features

On division of *S. aureus*, the piecrust architectural feature is split and each daughter cell receives half. This led to the proposal of a model of specification of division planes by architectural features (Turner et al., 2010a). Indeed, bands less distinct than the piecrust, known as ribs, were observed and understood to be remnants of the piecrust. When more than one band was present on a sacculi fragment they were approximately perpendicular and formed cross or T-junctions. A model of how the piecrust feature is inherited over several generations was proposed (Figure 1.17)(Turner et al., 2010a). Immediately after division a cell contains a whole rib derived from the piecrust that marks the plane of division that had just taken place. On division in the next plane, the rib will be bisected by the new piecrust such that each daughter cell will receive half the rib, in addition to a new whole rib. Cross junctions occurred when a piecrust intersected a rib, once the cells split at the piecrust, these cross junctions become T-junctions (Turner et al., 2010a). This process will repeat on the third division plane resulting in daughter cells with a whole rib, a half rib and a quarter rib. At this point the next division plane will be the same as the first division plane i.e. the plane of the quarter rib. It is proposed that *S. aureus* can sense the plane

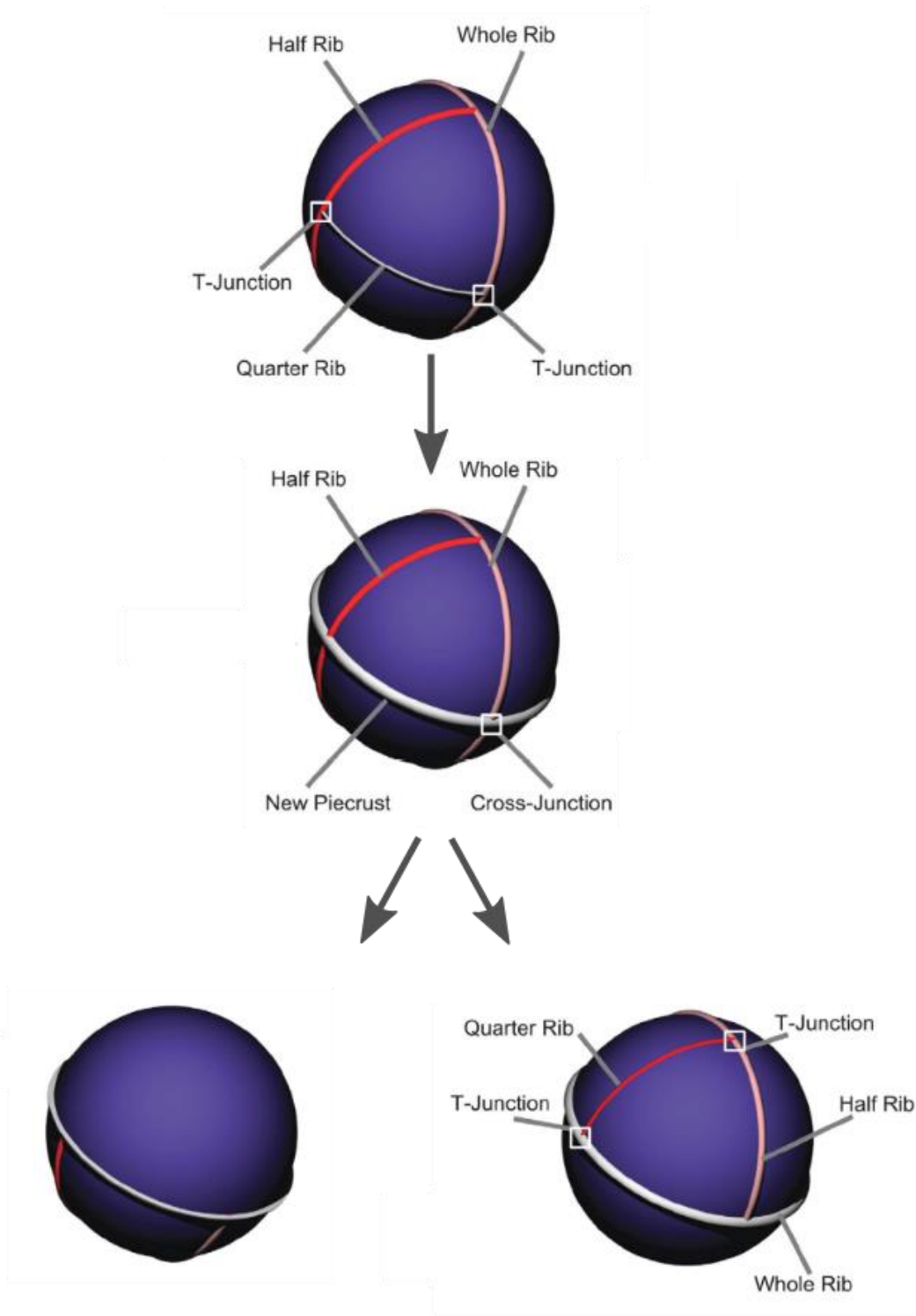


Figure 1.17. Model of specification of division plane by architectural features in *S. aureus*. Note that although the piecrust and rib features are shown on the outer surface these would in fact be present on the inner leaflet of the cell wall. Adapted from (Turner et al., 2010a).

of the quarter rib and form a piecrust in this plane. Therefore, *S. aureus* can faithfully divide in 3 orthogonal planes.

1.11 Methods of peptidoglycan analysis

Peptidoglycan has been analysed on three levels; peptidoglycan chemistry by high performance liquid chromatography (HPLC), architecture by EM and AFM and subcellular localisation of features by fluorescence microscopy. HPLC muropeptide analysis has been beneficial in determining the chemical composition of both the muropeptide building block but also how these are assembled including glycan chain length and mechanism of crosslinking (Boneca et al., 2000; Desmarais et al., 2013; Glauner et al., 1988; Harz et al., 1990; Snowden and Perkins, 1990). This could also be applied to determine mechanisms of actions of numerous peptidoglycan interacting enzymes through a combination of HPLC with genetic mutations or recombinant enzyme digestion (Atrih et al., 1996, 1999; Snowden and Perkins, 1990). HPLC relies on the extraction of vast quantities of peptidoglycan which are then solubilized and pumped through a column such that fragments are separated based on their chemical properties (Desmarais et al., 2013). Therefore, this is a population average method and may disguise individual differences. It is also currently impossible to determine the muropeptide profile of subcellular compartments, for example is the septum more or less crosslinked than the rest of the cell wall?

In order to determine both the overall morphology of the cell wall and the subcellular architectural features, various imaging techniques have been applied, namely EM and AFM. Since peptidoglycan has a high degree of heterogeneity it is not easily applied to methods that require a high degree of order such as X-ray diffraction. However, certain aspects of the architecture of muropeptides have been revealed using nuclear magnetic resonance (NMR)(Kim et al., 2013, 2014; Romaniuk and Cegelski, 2015). Electron microscopy uses electrons instead of light to produce an image, therefore has a greater resolving power than light. Peptidoglycan has been studied using both transmission and scanning EM methods as well as electron cryo tomography (ECT) in more recent years (Beeby et al., 2013; Gan et al., 2008; Popham, 2013). In ECT, samples are plunge frozen in liquid ethane & propane so that the water molecules do not have time to rearrange into crystalline ice therefore the cellular structure is preserved in vitreous ice. Samples are then imaged using transmission EM as they are

tilted in order to produce of 3D tomogram (Gan and Jensen, 2012). Another common method of architecture determination is the use of atomic force microscopy (AFM) a high resolution form of scanning probe microscopy that can achieve resolution up to fractions of a nanometre. AFM uses a sharp tip that scans the sample. The deflection of the tip is translated into a topological image, in addition phase shift of the tip can be converted into information concerning chemical and mechanical properties of the sample.

While EM and AFM can both produce images with greater resolution than microscopy techniques based on light, the resulting images do not contain any information on the identification of the structures observed. In conjunction with chemical probes and reporter proteins fluorescence microscopy is able to localise structures to subcellular localisations. This has been particularly useful with fluorescent proteins (Hu and Lutkenhaus, 1999; Pinho and Errington, 2005). However conventional microscopy is limited by the resolution limit of light (~250 nm)(Huang et al., 2010). Therefore, new microscopy techniques have been developed that allow this resolution limit to be passed, including the use of structured illumination microscopy (SIM) and stochastic optical reconstruction microscopy (STORM) (Chapter 3.1.2). In recent years these have begun to be applied to microbiological samples, in particular to the study of peptidoglycan and cell division dynamics (Turner et al., 2013; Wheeler et al., 2011).

1.12 *Staphylococcus aureus*

Staphylococci are Gram positive, non-motile, facultative anaerobes. They are roughly spherical in shape with diameter of 0.7-1.2 μm . Taxonomically *Staphylococci* lie within the Firmicutes, within the Bacillales order due to ribosomal RNA sequences (Kuroda et al., 2001). The genome of *S. aureus* is AT rich, with a GC content of ~30% (Wang et al., 2012a). *Staphylococci* are important human and animal opportunistic pathogens, in particular *Staphylococcus epidermidis* and *Staphylococcus aureus* are important human pathogens.

S. aureus is the most prevalent staphylococcal human pathogen. It is characterised by the gold pigmentation of its colonies due to the production of carotenoids including staphyloxanthin and its production of coagulase, a blot clotting factor (Marshall and Wilmoth, 1981). *S. aureus* is a commensal organism the resides primarily in the

anterior nares, the channels of the nose i.e. the nostrils. Approximately 20% of the population are permanent carriers of *S. aureus* while a further 30% are transitory carriers (Wertheim et al., 2005). It is unsurprising therefore that it is the most common cause of hospital-acquired infections.

S. aureus can cause a large number of nosocomial and community-acquired infections. These generally occur via a breach in an outer barrier, skin or mucosal surface, that allows access of *S. aureus* to soft tissue and the bloodstream. *S. aureus* infections can range in severity from simple skin infections, boils and impetigo to more serious, even life threatening infections including bacteraemia, pneumonia, endocarditis and septic arthritis. In 2014, there were 9,100 reported cases of *S. aureus* bacteraemia in the UK, a reduction of 40% from 2004 (Public Health England, 2015). Of these 9.4% were due to MRSA. Intravenous catheters and other surgical implants are prone to *S. aureus* infections since they are rapidly coated in serum constituents such as fibrinogen and fibronectin allowing *S. aureus* adherence.

There are many virulence factors expressed by *S. aureus* including surface proteins that play a role in adhesion, host immune system inhibition and toxins. Adhesion proteins are able to mediate host colonisation and infection by binding to the extracellular matrix mediated by MSCRAMMs (microbial surface components recognising adhesive matrix molecules)(Foster and Hook, 1998). *S. aureus* also excretes a number of enzymes thought to play a role in virulence and infection progression including catalase, coagulase, proteolytic enzymes and lipases. *Staphylococci* also produce a number of different toxins including cytotoxins, haemolysins and leukotoxins to lyse host cells and superantigens which bind MHC (major histocompatibility complex) Class II proteins causing over activation of the host immune system and host mediated cell damage, particularly from cytokine release (Llewelyn and Cohen, 2002).

1.13 Antibiotic resistance

As rapidly as new antibiotics have been introduced to combat *S. aureus* infections strains have arisen that have reduced susceptibility to the antimicrobial agents. Resistance to penicillin was seen almost immediately after penicillin was first used in 1941. Resistance was caused by the expression of a β -lactamase that degrades penicillin and related antibiotics. Additionally, staphylococcal isolates were found that

were resistant to numerous other antimicrobial agents targeting different systems. Mechanisms of resistance include inactivation of antimicrobials by destruction or modification, prevention of access to target due to permeability, presence of efflux pumps or alteration of targets (Neu, 1992). The synthetic antibiotic methicillin was a promising antibiotic until the emergence of methicillin resistant *S. aureus* (MRSA) strains. These strains acquired an extra PBP known as MecA/PBP2A which has a low affinity for all β -lactams including methicillin (Neu, 1992; Zapun et al., 2008b). This problem is aggravated since many MRSA strains are also resistant to other antibiotics. Therefore, vancomycin and other glycopeptides have become the drugs of last resort. Inevitably resistance to vancomycin has also risen in *S. aureus* with the appearance of vancomycin-intermediate (VISA) and vancomycin-resistant (VRSA) strains. The mechanism of VISA is thought to be due to an increased cell wall thickness thereby restricting access of vancomycin to its target at the septum, combined with a reduction in PBP4 activity to increase levels of D-ala-D-ala, the target for vancomycin (Howden et al., 2010). VRSA is due to the acquisition of the *vanA* gene which allows the incorporation of D-lactate in the terminal peptide position of the pentapeptide of the peptidoglycan precursor thereby preventing vancomycin binding (Courvalin, 2006; Holmes et al., 2012).

1.14 Project Aims

Previous work has determined the architectural features of *S. aureus* peptidoglycan as well as the dynamics of synthesis using conventional fluorescence microscopy. However, this information is limited in resolution due to the use of diffraction limited microscopy. Recent developments in new probes to label peptidoglycan synthesis, based on fluorescent derivatives of D-amino acids (FDAAs), allow synthesis to be investigated for the first time in greater detail (Kuru et al., 2012). These new probes not only allow direct labelling of new peptidoglycan but also allow dynamics to be investigated by using probes with different spectral properties as a virtual time-lapse. The aim of this study was to apply novel probes and super-resolution microscopy to determine the insertion and dynamics of nascent peptidoglycan in *S. aureus* at the molecular level. This was achieved through a number of different objectives:

- Determine the ability of FDAAs to label peptidoglycan synthesis in *S. aureus* and ascertain the mechanism of labelling.
- Establish methods of super-resolution microscopy in *S. aureus* using synthetic dyes.
- Combine FDAA labelling and super-resolution microscopy to determine the localisation of peptidoglycan synthesis at the molecular level.
- Investigate the effect of FtsZ depletion on peptidoglycan synthesis localisation.
- Determine the dynamics of peptidoglycan synthesis during a single division cycle and inheritance of material over multiple cycles.

These have informed new models of peptidoglycan synthesis in *S. aureus* as well as providing further insight into the cell growth and division process of this bacterium.

Chapter 2

Materials and Methods

2.1 Media

All media was prepared using distilled water (dH₂O) and sterilised by autoclaving at 121°C, 15 pounds per square inch for 20 mins.

2.1.1 Brain Heart Infusion (BHI)

Brain Heart Infusion (Oxoid/Fluka) 37 g l⁻¹

Bacteriological Agar (VWR) was added at 1% (w/v) to produce BHI Agar.

2.1.2 Chemically defined media (CDM)

All glassware was acid washed & autoclaved before use in CDM preparation.

2.1.2.1 Solution 1

Sodium phosphate dibasic (Na₂HPO₄·2H₂O) 7 g l⁻¹

Potassium phosphate monobasic (KH₂PO₄) 3 g l⁻¹

L-Aspartic Acid 0.15 g l⁻¹

L-Alanine 0.1 g l⁻¹

L-Arginine 0.1 g l⁻¹

L-Cysteine 0.05 g l⁻¹

Glycine 0.1 g l⁻¹

L-Glutamic Acid 0.15 g l⁻¹

L-Histidine 0.1 g l⁻¹

L-Isoleucine 0.15 g l⁻¹

L-Lysine 0.1 g l⁻¹

L-Leucine 0.15 g l⁻¹

L-Methionine 0.1 g l⁻¹

L-Phenylalanine	0.1 g l ⁻¹
L-Proline	0.15 g l ⁻¹
L-Serine	0.1 g l ⁻¹
L-Threonine	0.15 g l ⁻¹
L-Tryptophan	0.1 g l ⁻¹
L-Tyrosine	0.1 g l ⁻¹
L-Valine	0.15 g l ⁻¹

Solution 1 was adjusted to pH 7.2 prior to autoclaving or mixing to produce CDM.

2.1.2.2 Solution 2 (1000x)

Biotin	0.02 g
Nicotinic Acid	0.4 g
D-Pantothenic Acid	0.4 g
Thiamine HCl	0.4 g
Pyridoxal HCl	0.8 g
Pyridoxamine di-HCl	0.8 g
Riboflavin	0.4 g

Chemicals were dissolved in 140 ml dH₂O and filter sterilised to produce a 1000x solution. This was diluted in dH₂O to make a 1x solution just prior to use in CDM.

2.1.2.3 Solution 3

Adenine Sulphate	0.4 g l ⁻¹
Guanine HCl	0.4 g l ⁻¹

Solution 3 was prepared in 0.1 M HCl.

2.1.2.4 Solution 4

Calcium Chloride Hexahydrate (CaCl ₂ .6H ₂ O)	1 g l ⁻¹
---	---------------------

Ferrous Ammonium Sulphate $((\text{NH}_4)_2\text{Fe}(\text{SO}_4)_2 \cdot \text{H}_2\text{O})$ 0.6 g l⁻¹

Solution 4 was prepared in 0.1 M HCl.

2.1.2.5 Solution 5

Glucose 100 g l⁻¹

Magnesium sulphate Heptahydrate $(\text{MgSO}_4 \cdot 7\text{H}_2\text{O})$ 5 g l⁻¹

2.1.2.6 Preparation of CDM

Solution 1 700 ml

Solution 3 50 ml

Solution 4 10 ml

This mix of solutions was autoclaved under normal conditions. Once cooled to 50°C, 100 ml of Solution 2 at 50°C and 100 ml of solution 5 at 50°C were added to the autoclaved mix.

2.2 Antibiotics

All Antibiotics used are listed in Table 2.1. For antibiotics prepared in dH₂O stock solutions were filter sterilized (0.22µm pore size) and stored at -20°C. When antibiotics were added to agar for plates, agar was cooled to below 50°C prior to addition of the antibiotic.

2.3 Buffers & Solutions

Stock solutions were prepared in dH₂O unless otherwise stated and sterilised by autoclaving whenever required for microbiological work.

2.3.1 Phosphate Buffered Saline

Phosphate Buffered Saline Tablets (Sigma) 5 tablets l⁻¹

2.3.2 Borate Buffer

Boric Acid (H_3BO_3) 0.5M

pH adjusted to 8.7 with NaOH prior to autoclaving

Antibiotic	Stock Concentration (mg ml⁻¹)	Solvent	Working concentration (µg ml⁻¹)
Erythromycin (Ery)	5	100% (v/v) Ethanol	5
Lincomycin (Lin)	25	50% (v/v) Ethanol	25
Spectinomycin (Spec)	50	dH ₂ O	100

Table 2.1 Antibiotics used in this study.

2.3.3 HPLC buffers

All HPLC buffers were made with Milli-Q filtered water and filtered (0.2 µm pore size) prior to use.

2.3.3.1 Buffer A – 10 mM Ammonium Phosphate containing 5 mM sodium azide

Ammonium Phosphate (2.5 M)	4 ml l ⁻¹
Sodium Azide (10% (w/v) stock)	3.27 µl l ⁻¹

Buffer was adjusted to pH 5.6.

2.3.3.2 Buffer B – 10 mM Ammonium Phosphate containing 30% (v/v) Methanol

Ammonium Phosphate (2.5 M)	4 ml l ⁻¹
Methanol	30% (v/v)

Buffer was adjusted to pH 5.6 prior to addition of methanol.

2.3.4 Fixative preparation

2.3.4.1 Preparation of 16% (w/v) paraformaldehyde

100mM sodium phosphate buffer (pH 7.0) was prepared as follows:

Na ₂ HPO ₄ (1M)	57.7 ml
NaH ₂ PO ₄ (1M)	42.3 ml

Final volume was adjusted to 1 l.

For 16% (w/v) paraformaldehyde:

100 mM sodium phosphate buffer (pH 7.0)	50 ml
Paraformaldehyde	8.0 g

The solution was heated to 60°C with stirring for 20mins. Maintaining heat and agitation NaOH (≥ 5M) solution was added drop wise until the solution cleared. The solution was stored at 4°C for up to 3 months.

2.3.4.2 Fixative

16% (w/v) Paraformaldehyde	0.5 ml
PBS	2 ml

2.3.5 Click-iT® reaction buffer mix

All buffer components were made up as per instructions from Molecular Probes.

Click-iT® cell reaction buffer	440 µl
Copper (II) sulphate (100 mM)	10 µl
Click-iT® cell buffer additive	50 µl

2.3.6 STORM imaging buffers

2.3.6.1 50 mM Tris buffer containing 10 mM NaCl (pH 8.0)

Tris base	6.057 g l ⁻¹
NaCl	584.4 mg l ⁻¹

The pH was adjusted to 8.0 prior to autoclaving.

2.3.6.2 MEA

Mercaptoethylamine (MEA)	77.15 g l ⁻¹
--------------------------	-------------------------

MEA was dissolved in 50 mM Tris containing 10 mM NaCl to produce 1M MEA stock. 1 M MEA was diluted 1:10 to 100 mM for normal working concentration in 50 mM Tris containing 10 mM NaCl. Stock was stored for up to 1 month at -20°C, once diluted it was kept for up to 6 hours on ice.

2.3.6.3 GLOX

Glucose oxidase stock	5 mg ml ⁻¹
Catalase stock	4 mg ml ⁻¹

To 100 µg glucose 100 µl glucose oxidase stock (0.5 mg ml⁻¹) and 10 µl catalase stock (40 µg ml⁻¹) were added and the volume made up to 1ml with 50 mM Tris buffer containing 10 mM NaCl (pH 8.0). GLOX buffer lasts for approximately 2 hours before efficiency reduced.

2.3.6.4 GLOX MEA

MEA was added to GLOX (Chapter 2.3.6.3) at either 10 or 100 mM. GLOX MEA buffer lasts for 2 hours before efficiency reduced.

2.3.7 Tris/EDTA/NaCl Buffer (TES)

Tris Base	2.42 g l ⁻¹
EDTA	1.86 g l ⁻¹
NaCl	5.84 g l ⁻¹

The pH was adjusted to 8.0 before autoclaving

2.4 Bacterial strains and growth

Staphylococcus aureus strains used in this study are listed in Table 2.2. Strains were grown on BHI Agar plates, containing antibiotics where necessary to maintain selection markers. For short-term storage strains were stored on agar plates at 4°C and for longer-term storage strains were stored on Microbank Beads at -80°C.

Standard growth in liquid culture was aerobic growth at 37°C. A single colony was used to inoculate 10ml liquid BHI in a sterile 25ml universal tube, and grown overnight at 37°C with shaking at 250 rpm. This was then used to inoculate fresh media in a sterile conical flask at an OD₆₀₀ of ~0.05. Cultures were typically grown to mid-exponential phase (OD₆₀₀ 0.3-0.8) at 37°C, 250 rpm.

2.5 Chemicals & enzymes

All chemicals were of analytical grade and are shown in Table 2.3.

2.6 Centrifugation

A number of different centrifuges were used in the course of this study, their details are shown in Table 2.4.

2.7 Determination of bacterial cell density

2.7.1 Optical density measurements

To determine the bacterial yield of a culture spectrophotometric measurements were taken at 600 nm (OD₆₀₀). Measurements were taken using a Biochrom WPA Biowave DNA spectrophotometer. Whenever necessary a 1:10 dilution was made in sterile culture media.

Strain	Genotype	Source
SH1000	Functional <i>rsbU</i> ⁺ derivative of 8325-4	(Horsburgh et al., 2002)
Sa113 Δ <i>dltA</i>	Sa113 with <i>dltA</i> gene replaced by spectinomycin resistance gene, SpecR	(Peschel et al., 1999)
Sa113 Δ <i>tagO</i>	<i>tagO::Ery</i>	Andreas Peschel
JE2	MRSA - Parental strain of Nebraska Mutant Library. Also known as USA300 JE2	Centre for Staphylococcal Research, University of Nebraska Medical Centre
NE267	Transposon insertion mutant in SAUSA300_1676 (<i>sgtA</i>)	Centre for Staphylococcal Research, University of Nebraska Medical Centre
NE596	Transposon insertion mutant in SAUSA300_1855 (<i>mgt</i>)	Centre for Staphylococcal Research, University of Nebraska Medical Centre
NE1598	Transposon insertion mutant in SAUSA300_2040 (homologous to FtsW, member of FtsW, RodA, SpoVE family - <i>rodA</i>)	Centre for Staphylococcal Research, University of Nebraska Medical Centre
NE420	Transposon insertion mutant in SAUSA300_1512 (<i>pbp3</i>)	Centre for Staphylococcal Research, University of Nebraska Medical Centre
NE679	Transposon insertion mutant in SAUSA300_0629 (<i>pbp4</i>)	Centre for Staphylococcal Research, University of Nebraska Medical Centre
4421 (<i>pbp3</i>)	NE420 transduced into SH1000	Kasia Wacnik
4425 (<i>pbp4</i>)	NE679 transduced into SH1000	Kasia Wacnik
4424 (<i>pbp3pbp4</i>)	SH1000 with both <i>pbp3</i> and <i>pbp4</i> contain transposon insertion	Kasia Wacnik
FtsZ-eYFP	SH1000 P _{Spac} - <i>ftsZ</i> -eYFP	Christa Walther

Table 2.2 *S. aureus* strains used in this study.

Stock Solution	Concentration	Dissolved in	Storage
Lysostaphin	2 mg ml ⁻¹	20mM Sodium acetate (pH 4.6)	-20°C
Mutanolysin (Sigma)	1 mg ml ⁻¹	25mM sodium phosphate containing 0.1mM MgCl ₂ (pH 5.7)	-20°C
Pronase (Sigma)	10 mg ml ⁻¹	TES pH 8.0	-20°C
HADA (Hydroxycoumerin 3-amino-D-alanine)	100 mM	DMSO	-20°C, in dark
NADA (Nitrobenzofurazan 3-amino-D-alanine)	100 mM	DMSO	-20°C, in dark
TADA (Tetramethylrhodamine 3-amino-D-alanine)	100 mM	DMSO	-20°C, in dark
ADA (3-azido-D-alanine) (Iris Biotechnology)	100 mM	DMSO	-20°C
Dipeptide (3-azido-D-alanine-D-alanine)	100 mM	DMSO	-20°C
Alkyl Dyes (Molecular Probes)	0.5 mg ml ⁻¹	DMSO	-20°C, in dark
Vancomycin	100mM	DMSO	-20°C
NHS-647 (Molecular Probes)	4mM	DMSO	-20°C, in dark
NHS-Cy3b (GE Healthcare)	2mM	DMSO	-80°C long term, -20°C short term, in dark
D-serine (Sigma)	2.5M	dH ₂ O	Room temperature
Wheat germ agglutinin, Alexa Fluor® 488 conjugate (Molecular Probes)	1 mg ml ⁻¹	PBS	-20°C in dark
IPTG (Isopropyl-D-1-thiogalactopyranoside)	1 M	dH ₂ O	-20°C

Table 2.3 Chemicals & enzymes used in this study.

Centrifuge	Max Volume	Max Speed
Eppendorf Centrifuge 5424	2 ml	14,680 rpm
Sigma Centrifuge 4K15C	50 ml	5,100 rpm

Table 2.4 Centrifuges used in this study.

Antibiotic	Minimum inhibitory concentration (MIC)
D-Cycloserine	50 $\mu\text{g ml}^{-1}$
Penicillin G	0.5 $\mu\text{g ml}^{-1}$
Moenomycin	0.5 $\mu\text{g ml}^{-1}$
PC190723	1 $\mu\text{g ml}^{-1}$

Table 2.5 Minimum inhibitory concentrations (MICs)

2.8 Antibiotic minimum inhibitory concentration (MIC) determination

S. aureus overnight culture was used to inoculate a series of Universal tubes at an OD₆₀₀ of 0.05. Universals contained 10ml liquid media plus a serial dilution of antibiotic concentration. Tubes were incubated at 37°C with aeration at 250 rpm for 24h. The MIC was determined as the lowest concentration which prevented growth, judged by OD₆₀₀ values, in comparison to an antibiotic-free control tube. Determined MIC for antibiotics used are shown in Table 2.5.

2.9 Growth of *S. aureus* with antibiotic treatment

An overnight culture of *S. aureus* was used to inoculate a conical flask containing sterile BHI liquid media at an OD₆₀₀ of ~ 0.05. This was incubated at 37°C, 250 rpm for 90 min to reach an OD₆₀₀ of ~ 0.3. Antibiotics were then added at required concentration, generally 10 x MIC. Cultures were then continued to be incubated at 37°C, 250 rpm while samples were taken for further analysis.

2.10 Labelling peptidoglycan

2.10.1 Labelling with fluorescent D-amino acids (FDAAs)

Non-commercially available FDAAs were synthesised by members of Dr. Simon Jones' group from the Chemistry Department, University of Sheffield as per the methods described previously (Kuru et al., 2012, 2015).

To label inserted peptidoglycan with FDAAs, *S. aureus* cultures were grown to mid-exponential phase (as described in Chapter 2.4). 1ml aliquots were then added to FDAA at the appropriate concentration (generally 500 µM unless otherwise stated). Samples were incubated at 37°C for the required labelling time. Cells were harvested by centrifugation and the pellet washed once in PBS prior to further use.

2.10.2 Click-iT® reaction

For FDAAs that contain an azide group rather than an intrinsic fluorophore the Click reaction is required to add alkyne containing fluorescent dyes in order to visualise FDAA localisation. The Click reaction was carried out on samples fixed as described below (Chapter 2.12.1). Cells were incubated with 0.5ml Click-iT reaction buffer mix (Chapter 2.3.5) & 5 µg ml⁻¹ alkyne-containing fluorescent dye for 30 mins at room temperature.

2.10.3 Labelling the cell surface with NHS-ester dyes

A 1ml sample of *S. aureus* was centrifuged and the pellet resuspended in 250 μ l PBS containing 1 μ l NHS ester stock. Sample was incubated for 5 mins at room temperature on a rotator for mixing. Labelled cells were then collected by centrifugation and fixed using the method described in Chapter 2.12.1.

2.10.4 Vancomycin labelling

2.10.4.1 Production of fluorescent vancomycin

To produce fluorescent vancomycin a 1:1 mix of 2 mM NHS ester fluorescent dye (e.g. Alexa Fluor dyes) and 2mM vancomycin was created and 5 μ l triethylamine added to 200 μ l of the mix. This was incubated on a rotator at room temperature for 24 h. The resultant mix was left in open air to evaporate any excess trimethylamine before 800 μ l 1M Tris-HCl (pH 7.0) was added to react with any remaining NHS groups within the Alexa Fluor Dye. This method is modified from Daniel and Errington (2003).

2.10.4.2 Labelling peptidoglycan with fluorescent vancomycin

Fluorescent vancomycin was used to label either live or fixed cells, the procedure remained the same. 1 ml culture or cell pellet re-suspended in 1 ml PBS was incubated with 10 μ l fluorescent vancomycin for 30 min at room temperature with mixing. Labelled cells were then collected by centrifugation and fixed if required.

2.11 Labelling Protocols

2.11.1 Labelling 5 minutes peptidoglycan synthesis with FDAAs for diffraction limited microscopy & STORM

An SH1000 overnight culture was used to inoculate 50 ml BHI at OD₆₀₀ of 0.05 and grown at 37°C, 250 rpm for 90 mins to an OD₆₀₀ of ~0.3-0.5. 1 ml aliquots were taken and FDAA added at a concentration of 500 μ M (1 mM for dipeptide). Samples were then incubated at 37°C on a rotary shaker for mixing for 5 minutes. Cells were then pelleted by centrifugation and fixed as per Chapter 2.12.1. For cells labelled with azide containing FDAAs the alkyne fluorophore was added to the FDAA via the Click reaction (Chapter 2.10.2) on fixed cells.

2.11.2 Labelling 5 minutes peptidoglycan synthesis with FDAAs for SIM

An SH1000 overnight culture was used to inoculate 50 ml BHI at OD₆₀₀ of 0.05 and grown at 37°C, 250 rpm for 90 mins to an OD₆₀₀ of ~0.3-0.5. 1 ml aliquots were taken

and FDAA added at a concentration of 5 mM. Samples were then incubated at 37°C on a rotary shaker for mixing for 5 minutes. Cells were then pelleted by centrifugation and fixed as per Chapter 2.12.1

2.11.3 Labelling 2 minutes peptidoglycan synthesis with FDAAs for STORM

An SH1000 overnight culture was used to inoculate 50 ml BHI at OD₆₀₀ of 0.05 and grown at 37°C, 250 rpm for 90 mins to an OD₆₀₀ of ~0.3-0.5. 1 ml aliquots were taken and FDAA added at a concentration of 500 µM. Samples were then incubated at 37°C on a rotary shaker for mixing for 2 minutes. Cells were then pelleted by centrifugation and fixed as per Chapter 2.12.1. For cells labelled with azide containing FDAAs the alkyne fluorophore was added to the FDAA via the Click reaction (Chapter 2.10.2) on fixed cells.

2.11.4 Labelling peptidoglycan synthesis during antibiotic treatment

An SH1000 overnight culture was used to inoculate 50 ml BHI at OD₆₀₀ of 0.05 and grown at 37°C, 250 rpm for 90 mins to an OD₆₀₀ of ~0.3-0.4. A 1ml sample was taken for labelling prior to addition of required antibiotic to the culture. 1 ml samples were taken at 5 minute intervals and FDAA added at a concentration of 500 µM (1 mM for dipeptide). Samples were then incubated at 37°C on a rotary shaker for mixing for 5 minutes. Cells were then pelleted by centrifugation and fixed as per Chapter 2.12.1. For cells labelled with azide containing FDAAs the alkyne fluorophore was added to the FDAA via the Click reaction (Chapter 2.10.2) on fixed cells.

2.11.5 Labelling nascent peptidoglycan synthesis with vancomycin

To label newly inserted peptidoglycan with fluorescent vancomycin a *S. aureus* overnight was created in BHI containing 0.125M D-serine. This was used to inoculate a conical flask containing BHI with 0.125M D-serine at an OD₆₀₀ of ~0.05. This was incubated at 37°C, 250 rpm for 90 min to reach an OD₆₀₀ of ~0.3, samples were centrifuged and re-suspended in BHI lacking excess D-serine. Samples were allowed to grow for the required labelling time before samples were taken and labelled with fluorescent vancomycin as per previous method (Chapter 2.10.4.2).

2.11.6 Labelling whole peptidoglycan with vancomycin

An SH1000 overnight culture was used to inoculate 50 ml BHI at OD₆₀₀ of 0.05 and grown at 37°C, 250 rpm for 90 mins to an OD₆₀₀ of ~0.3-0.5. 1 ml aliquots were

harvested by centrifugation and fixed as per Chapter 2.12.1. The fixed cell pellets were then resuspended in 1ml PBS and labelled with fluorescent vancomycin at 1 mM (Chapter 2.10.4.2).

2.11.7 Dual labelling with dipeptide & vancomycin

An SH1000 overnight culture was used to inoculate 50 ml BHI at OD₆₀₀ of 0.05 and grown at 37°C, 250 rpm for 90 mins to an OD₆₀₀ of ~0.3-0.5. 1 ml aliquots were taken and dipeptide added at a concentration of 1 mM. Samples were then incubated at 37°C on a rotary shaker for mixing for 5 minutes. Cells were then pelleted by centrifugation and fixed as per Chapter 2.12.1. The Click reaction was then carried out to link the alkyne-containing fluorophore (5 µg ml⁻¹). Following completion of the Click reaction cells were pelleted by centrifugation and resuspended in 1 ml PBS and labelled with fluorescent vancomycin at 1 mM (Chapter 2.10.4.2).

2.11.8 Chemical treatment of labelled samples

Cells were labelled with FDAAs for 5 minutes as per Chapter 2.11.1 including the fixation step. Samples were then treated with chemicals to remove portions of the cell wall.

- Non-covalently bound proteins – resuspended in 5 % (w/v) SDS & boiled for 15 minutes. Sample was washed multiple times to remove excess SDS.
- Covalently bound proteins – resuspended in 1 ml 50mM Tris-HCl (pH 7.5) containing 2 mg ml⁻¹ pronase & incubated for 90 mins at 60°C.
- Reducing termini – resuspended in borate buffer (Chapter 2.3.2) and approximately 5 mg ml⁻¹ sodium borohydride was added. Sample incubated for 15 min & the reaction halted by addition of phosphoric acid to reduce the pH.
- Teichoic Acids – resuspended in 250 µl 48% (w/v) Hydrofluoric acid for 48 h at 4°C.

2.11.9 Labelling mutant strains to determine off-septal percentage

Overnight cultures were used to inoculate 50 ml BHI at OD₆₀₀ of 0.05 and grown at 37°C, 250 rpm for 90 mins to an OD₆₀₀ of ~0.3-0.5 for each strain. 1 ml aliquots were taken and FDAA added at a concentration of 500 µM (1 mM for dipeptide). Samples were then incubated at 37°C on a rotary shaker for mixing for 5 minutes. Cells were then pelleted by centrifugation and fixed as per Chapter 2.12.1. For cells labelled with

azide containing FDAAs the alkyne fluorophore was added to the FDAA via the Click reaction (Chapter 2.10.2) on fixed cells.

Samples were then imaged ensuring the same conditions across the strains. To determine % off-septal fluorescence average intensity projections of the stacks were created & portions of the cells highlighted and the CTCFs calculated.

2.11.10 **Using the FtsZ-eYFP strain to determine the effect of PC190723**

2.11.10.1 **Growth of FtsZ-eYFP strain**

The FtsZ-eYFP is under the control of an IPTG inducible promoter. Therefore, within the overnight culture and growth culture IPTG was added at 200 μM .

2.11.10.2 **Treatment of FtsZ-eYFP strain with PC190723**

An SH1000 overnight culture was used to inoculate 50 ml BHI containing 200 μM IPTG at an OD_{600} of 0.05 and grown at 37°C, 250 rpm for 90 mins to an OD_{600} of $\sim 0.3-0.4$. PC190723 was then added to the culture at 10 $\mu\text{g ml}^{-1}$.

2.11.10.3 **Labelling FtsZ-eYFP with FDAAs**

1 ml samples were taken and HADA was added at a concentration of 500 μM . Samples were then incubated at 37°C on a rotary shaker for mixing for 5 minutes. Cells were then pelleted by centrifugation and fixed as per Chapter 2.12.1. Cells were only labelled with HADA as fluorescent proteins are not compatible with the Click reaction as the presence of copper renders them incapable of fluorescence.

2.11.11 **Dual Labelling**

2.11.11.1 **2h followed by 5min with FDAAs**

An SH1000 overnight culture was used to inoculate 50 ml BHI at OD_{600} of 0.05 and grown at 37°C, 250 rpm for 90 mins to an OD_{600} of $\sim 0.3-0.5$. 1 ml aliquots were taken and initial FDAA added at a concentration of 5 mM. Samples were then incubated at 37°C on a rotary shaker for mixing for 2 hours. Cells were then pelleted by centrifugation and resuspended in 1 ml pre-warmed BHI containing the second FDAA at 5 mM and incubated at 37°C on a rotary shaker for mixing for 5 minutes. Cells were then harvested by centrifugation and fixed as per Chapter 2.12.1.

2.11.11.2 Sequential 5 minute labelling

An SH1000 overnight culture was used to inoculate 50 ml BHI at OD₆₀₀ of 0.05 and grown at 37°C, 250 rpm for 90 mins to an OD₆₀₀ of ~0.3-0.5. 1 ml aliquots were taken and FDAA added at a concentration of 5 mM. Samples were then incubated at 37°C on a rotary shaker for mixing for 5 minutes. Cells were then pelleted by centrifugation and resuspended in 1 ml pre-warmed BHI containing the second FDAA at 5 mM and incubated at 37°C on a rotary shaker for mixing for 5 minutes. This was then repeated a third time for labelling with the third FDAA. Cells were then pelleted by centrifugation and fixed as per Chapter 2.12.1.

2.11.11.3 Sequential 30 minute labelling

Prior to this experiment a growth curve of SH1000 growth was determined and the generation time calculated to be 30 minutes under conditions used.

An SH1000 overnight culture was used to inoculate 50 ml BHI at OD₆₀₀ of 0.05 and grown at 37°C, 250 rpm for 90 mins to an OD₆₀₀ of ~0.3-0.5. 1 ml aliquots were taken and FDAA added at a concentration of 500 µM. Samples were then incubated at 37°C on a rotary shaker for mixing for 30 minutes (single generation time). Cells were then pelleted by centrifugation and resuspended in 1 ml pre-warmed BHI containing the second FDAA at 500 µM and incubated at 37°C on a rotary shaker for mixing for 5 minutes. This was then repeated a third time for labelling with the third FDAA. Cells were then pelleted by centrifugation and fixed as per Chapter 2.12.1. For cells labelled with azide containing FDAAs the alkyne fluorophore was added to the FDAA via the Click reaction (Chapter 2.10.2) on fixed cells

2.12 Preparation of samples for fluorescence microscopy

2.12.1 Fixation

Collected cell pellets were re-suspended in 0.5 ml dH₂O and 0.5 ml fixative (Chapter 2.3.4) for 30 min at room temperature on a rotator for mixing. Fixed cells were then washed in dH₂O and the pellet collected by centrifugation.

2.12.2 Sample preparation for diffraction limited microscopy

An approximate sample dilution was made of fixed cells in dH₂O and 5 µl was applied gently to a poly-L-lysine slide (Sigma) and left to air dry. The slide was then washed with dH₂O and dried with Nitrogen. A coverslip was then mounted with 5 µl imaging

buffer and sealed with clear nail polish. Typical imaging buffers used were SlowFade Gold antifade mountant (Molecular Probes) or water (LC-MS CHROMASOLVE®, Fluka).

2.12.3 Sample preparation for STORM

2.12.3.1 Preparation of coverslips

High-precision coverslips (No. 1.5H, 22 x 22mm, 170±5 µm, Marienfeld) were cleaned by sonicating in 1M KOH for 20 min. The KOH was then rinsed off and the coverslips covered by 2 ml poly-L-lysine (0.01% w/v in H₂O, Sigma) and incubated for 30 min at room temperature. Coverslips were then washed and dried with nitrogen before being mounted with a bacterial sample

2.12.3.2 Preparation of sample for BigSTORM

To a prepared coverslip (Chapter 2.12.3.1) 5 µl of a 1:1000 dilution of TetraSpeck™ (0.1 µm, blue/green/orange/dark red, Molecular Probes) were applied and dried with Nitrogen. An appropriate sample dilution was made of fixed cells in HPLC grade water (LC-MS CHROMASOLVE®, Fluka) and this was applied to the coverslip on top of the TetraSpeck™ and dried with nitrogen. The coverslip was then washed with dH₂O and dried with nitrogen. The coverslip was mounted in the centre of a poly-L-lysine slide with 5 µl STORM imaging buffer (Chapter 2.3.6) and sealed with clear nail polish.

2.12.3.3 Preparation of sample for N-STORM

An appropriate sample dilution was made of fixed cells in HPLC grade water (LC-MS CHROMASOLVE®, Fluka) and 5 µl added to a prepared coverslip (Chapter 2.12.3.1). The sample was dried by nitrogen gas, washed in dH₂O and dried once again with nitrogen. Coverslip was mounted on depression slides (76 x 26 x 1.35 mm, 90° ground edges, 1 cavity, 15-18 mm, depth 0.6-0.8 mm, Marienfeld) with approximately 100 µl STORM Imaging Buffer (Chapter 2.3.6) and sealed with clear nail polish just prior to imaging.

2.12.3.4 Preparation of calibration slide for N-STORM

TetraSpeck™ (0.1 µm, blue/green/orange/dark red, Molecular Probes) were diluted 1:1000 in 1 x PBS (1 X PBS pH 7.4, Life Technologies), approximately 100 µl was added to a depression slide (76 x 26 x 1.35 mm, 90° ground edges, 1 cavity, 15-18 mm, depth 0.6-0.8 mm, Marienfeld), covered with High-Precision coverslip (No. 1.5H, 22 x 22mm, 170±5 µm, Marienfeld) and sealed with clear nail polish.

2.12.4 Sample preparation for SIM

An appropriate sample dilution was made of fixed cells in HPLC grade water (LC-MS CHROMASOLVE®, Fluka) and 5 µl added to a High-Precision coverslip prepared as per Chapter 2.12.3.1. The sample was dried by nitrogen gas, washed in dH₂O and dried once again by Nitrogen. The coverslip was mounted in the centre of a poly-L-lysine slide with 5 µl SlowFade® Diamond Antifade Mountant (Molecular Probes) and sealed with clear nail polish.

2.13 Fluorescence microscopy

2.13.1 DeltaVision microscopy

Fluorescence Microscopy was carried out using a DeltaVision deconvolution microscope (Applied Precision) equipped with filters required for imaging of fluorophore used in this study (Table 2.6). Objective used was a UplanSApo 100x oil (NA 1.4) and images were detected using a Photometrics CoolsnapHQ CCD camera. When required images were deconvolved using Softworx and all images were processed using Fiji processing package (v 1.50).

2.13.2 Nikon dual-camera microscopy

Following acquisition of a Nikon dual-cam microscope all standard resolution microscopy was carried out using this microscope. Microscopy was carried out on a Nikon Ti inverted microscope fitted with a Lumencor SpectraX light engine (395 nm, 440 nm, 470 nm, 508 nm, 561 nm, 640 nm) and Emission filters for DAPI, GDP, RFP, Cy5 and Quad(DAPI/GFP/RFP/Cy5). Single emission filters were used whenever possible. Images were using a 100x PlanApo (1.4 NA) oil objective using 1.518 RI oil and detected by an Andor Zyla sCMOS camera. Images were acquired using NIS Elements software including deconvolution where required.

2.13.3 OMX microscopy

Widefield deconvolution and structured illumination microscopy (SIM) was carried out using a GE Healthcare Life Sciences DeltaVision OMX Blaze microscope.

2.13.3.1 Widefield microscopy

For widefield microscopy samples were illuminated using a 6 colour solid state illuminator (LED) with standard filters (Table 2.7). Objective was a 60x 1.42 oil planapochromat lens. Focus was controlled using a UltimateFocus hardware Autofocus

Module. Z-stacks taken using a fast piezo -z-axis system on the nanomotion sample stage. Microscope was controlled and images deconvolved using DeltaVision OMX SoftWoRx 6.1.3.

2.13.3.2 Structured illumination microscopy

SIM samples were illuminated using laser illumination (Table 2.8). Objective and filters were the same as for widefield microscopy. For each z slice, samples were imaged in 5 phase shifts and 3 angles of the illumination pattern, z steps were 0.125 nm.

Images were reconstructed using SoftWoRx version 6.1.3 and optical transfer functions (OTFs) were made according to GE recommendations for image reconstruction.

2.13.4 Image rendering

All diffraction-limited and OMX images were processed and rendered using Fiji, an ImageJ based image processing software. Where 2 or more channels were used each channel was false coloured. When colours overlap usually an intermediate colour is shown, however when this overlap occurs at an area of high intensity or saturation this area was depicted as white. All intensity calculations were carried out using tools within Fiji on z-projections in single channels. Cell size was determined using DIC images and Fiji measurement tool calibrated by image pixel/mm ratio.

2.13.5 Stochastic optical reconstruction microscopy (STORM)

2.13.5.1 BigSTORM

2.13.5.1.1 Hardware setup

Direct STORM localisation microscopy imaging was used (Heilemann et al., 2008). Lasers were focussed onto the back-plane of a 60× 1.4 NA oil immersion objective mounted in an Olympus IX71 inverted optical microscope (Table 2.9). A filter cube containing an appropriate long-pass dichroic filter and band-pass emission filter was inserted. A piezoelectric motor (Physik Instrumente) was used to adjust focus. An image expander comprising a 35 mm and a 100 mm lens was used to project the image onto a Hamamatsu ImagEM camera. A 1 m focal length cylindrical lens was inserted between the image expander lenses to allow for compensation of drift perpendicular to the focal plane (Huang et al., 2008). Focus was maintained by repeatedly localising a fiducial particle and adjusting the objective position using the piezo to maintain a constant ratio of the fitted full-width half maxima (FWHM) in perpendicular directions.

Laser power was adjusted to maximize signal without saturating the charge-coupled device. The camera and piezo were controlled using Labview.

2.13.5.1.2 **Image reconstruction**

Image processing was conducted using localization microscopy methodology as previously described (Huang et al., 2008). Data were processed by fitting Gaussian functions to individual molecule fluorescence using Matlab. Drift in the focal plane was corrected retrospectively by tracking a fiducial particle throughout the acquisition sequence and offsetting localizations against its position.

2.13.5.1.3 **Image rendering**

Images were rendered using ThunderSTORM ImageJ/Fiji plugin (Ovesný et al., 2014). Data points were plotted on a 256 x 256 pixel area histogram with 100 nm z steps from -500 nm to 500 nm. For 2D projections, maximum intensity projections were created. For 3D data, points were false coloured according to their z step prior to creation of a maximum intensity projection.

2.13.5.2 **N-STORM**

N-STORM was carried out using a Nikon Ti-NS N-STORM version 1 with 3D capability. Objective used was a SR Apo TIRF 100x and images detected using EM-CCD (Andor DU-897) camera. Microscope control is via the NIS elements software with the N-STORM module.

2.13.5.2.1 **Calibration**

A sample of fluorescent beads (See Chapter 2.12.3.4) was imaged over an 800 nm shift in z using the 3D calibration tool in the software. The shape of the beads was then used to determine the localisation of fluorescent signal in the z plane.

Filter	Compatible Fluorophores	Excitation	Emission
FITC/YFP	NADA, AlexaFluor488, eYFP	490/20	528/38
DAPI	HADA	360/40	457/50
mRFP	TADA, TMR, Amersham Cy3B	580/20	630/60
Cy5	AlexaFluor647	640/20	685/40

Table 2.6 DeltaVision Filters

Filters	Compatible Fluorophores
436/31	HADA
528/48	NADA
609/37	TADA
638/40	Alexa Flour 647

Table 2.7 OMX Filters

Laser Line	Compatible Fluorophores
445 nm	HADA
488 nm	NADA
568 nm	TADA
642 nm	Alexa Flour 647

Table 2.8 OMX SIM Laser Lines

Laser model & wavelength (nm)	Maximum power (mW)	Filter cube dichroic (nm)	Filter cube emission (nm)	Compatible Fluorophores
OBIS 405	50	NA	NA	NA
Sapphire 514	75	514	542 (27)	YFP
Sapphire 561	75	561	593 (40)	Tetramethyl-rhodamine (TMR)
OBIS 647	120	662	676 (29)	Alexa Flour 647

Table 2.9. Details for Laser lines used in BigSTORM.

2.13.5.2.2 Data acquisition

Data was acquired for ~80,000 frames and focus was kept using the Nikon perfect focussing system. Imaging lasers used were 647 nm for Alexa Fluor 647 at 100% and 568 nm for Amersham Cy3B at ~50%. The 405 nm laser was used for activation and adjusted according to the number of events per frame either manually or using the AutoLP function. The N-STORM filter-cube was used for single colour experiments, collecting light above 675 nm. For dual colour the red/far red cube was used collecting 575-625 nm and above 660 nm and images were taken by consecutive switching between the two channels which is the standard multicolour imaging mode in N-STORM imaging.

2.13.5.2.3 Data processing

Localisation of events was carried out by the N-STORM module of the Nikon NIS elements software version 4.20.02 using default settings for screening minimum and maximum height. Images were rendered using the same system as BigSTORM (Chapter 2.13.5.1.3)

2.14 Purification of cell walls

2.14.1 Extraction of cell walls

An overnight culture was used to inoculate a conical flask containing liquid BHI to an OD₆₀₀ of ~0.05. This was incubated at 37°C, 250 rpm until required OD₆₀₀ was achieved (generally OD₆₀₀ ~ 0.6). Cultures were then boiled for 10 min to kill the cells before being collected by centrifugation. Pellets were re-suspended in 5% (w/v) SDS at 55°C and boiled for 30 min to remove non-covalently bound cell wall components. Cells were collected by centrifugation and re-suspended in 4% (w/v) SDS and boiled for 15 min. Material was then washed six times in dH₂O at 60°C and collected by centrifugation to remove excess SDS. Pellets were re-suspended in 50 mM Tris-HCl (pH 7.5) containing 2 mg ml⁻¹ pronase and incubated at 60°C for 90 min to remove covalently attached proteins. Additional cell wall polymers were removed by incubation in 250 µl 48% (w/v) hydrofluoric acid (HF) at 4°C for 48 h. The purified peptidoglycan was washed at least six times in dH₂O and once in Tris-HCl (pH 7.5) until the pH decreased beyond 5.0. Purified sacculi were stored as pellets at -4°C.

2.14.2 Breaking cells for imaging

When broken cells were required for imaging of sacculi breakage occurred immediately following the first boiling step (Chapter 2.14.1). Cells were broken by FastPrep. Thick suspensions of boiled cells were added to lysing matrix tubes containing 0.1 mm silica spheres (Lysing Matrix B, MP Biomedicals). These samples were mechanically sheared six times at 6.0 m s^{-1} for 30 s using an MP Biomedicals FastPrep 24 Homogeniser at 4°C , ensuring samples did not over heat. Amount of breakage was assessed by microscopy and further mechanical shearing was carried out if required. Cells were recovered by centrifugation for 30 s at 1000 rpm to remove beads from the cell suspension.

2.15 Preparation of cell walls for biochemical analysis

2.15.1 Preparation of fluorescently labelled sacculi

Overnight cultures were used to inoculate conical flasks containing liquid BHI to an OD_{600} of 0.05 and were grown at 37°C , 250 rpm until exponential phase ($\text{OD}_{600} \sim 0.3\text{-}0.4$). HADA was added to cultures at 1mM and cultures were incubated for 30 min at 37°C , 250 rpm. Peptidoglycan was then extracted as described in Chapter 2.14.

2.15.2 Digestion of peptidoglycan to produce soluble muropeptides

Fluorescently labelled & unlabelled peptidoglycan was freeze dried. Peptidoglycan ($\sim 1\text{mg}$) was then re-suspended in 250 μl mutanolysin (1 mg ml^{-1}) made up to 1 ml with 25 mM sodium phosphate buffer containing 0.1 mM MgCl_2 (pH 5.7). This was incubated at 37°C for 18h and was boiled for 5 min to stop the reaction. The soluble peptidoglycan was collected by centrifugation and collection of the supernatant. To this was added 40 μl lysostaphin (2 mg ml^{-1}) and 20 μl 1M Tris HCl (pH 8.3) to adjust pH to 7. This was incubated at 37°C overnight and was boiled for 5 min the stop the reaction.

2.15.3 Sodium borohydride reduction of soluble peptidoglycan material

The resolution of HPLC separation is reduced in the presence of α - and β - anomers of peptidoglycan. Following solubilisation reduction of peptidoglycan with sodium borohydride was carried out. The pH of soluble peptidoglycan was raised by addition of borate buffer (Chapter 2.3.2) and approximately 10 mg ml^{-1} sodium borohydride

was added. The sample was incubated for 15 min at room temperature and the reaction halted by adjusting the pH to pH 4 using phosphoric acid.

2.15.4 HPLC separation of muropeptides

The pH of solubilised peptidoglycan samples was adjusted to pH 5.6 and samples were filtered (0.2 μm , Spartan 13/0.2, GE Healthcare). A Thermo Scientific Hypersil GOLD aQ column (250 x 4.6 mm, 3 μm particle size) was pre-equilibrated with Buffer A (Chapter 2.3.3.1) in a Waters HPLC system. Muropeptides were eluted at a flow rate of 0.5 ml min^{-1} , using a linear gradient 0-100% Buffer B (Chapter 2.3.3.2) containing 30% (v/v) methanol over 140 min. Elution of muropeptides was detected by monitoring absorbance at 202 nm and fluorescence (Excitation 360 nm, Emission 457 nm for HADA). Peaks were collected manually for further analysis.

2.16 Incorporation of ^{14}C -labelled *N*-acetylglucosamine into cell wall peptidoglycan

The rate of peptidoglycan synthesis was determined by measuring incorporation of ^{14}C -GlcNAc (Maki et al., 2001). *S. aureus* was grown overnight in CDM and used to inoculate fresh CDM to an OD_{600} of 0.05 and grown to early exponential phase. At this point 5 μM ^{14}C -GlcNAc (45 $\mu\text{Ci mmol}^{-1}$) was added to cultures as supplied. At 30 min intervals 0.5 ml samples were transferred to a microfuge tube containing 0.5 ml ice-cold 10% (w/v) Trichloroacetic acid (TCA) and incubated at 90°C for 15 mins and placed on ice for 30 min. Samples were then filtered on Glass Microfibre filters followed by 5% (w/v) TCA washing. Filters were then immersed in 10 ml Ultima Gold™ (Perkin Elmer) and radioactivity was counted with a liquid scintillation analyser (Packard Liquid Scintillation Analyzer Model Tri-Carb 31007R) using direct disintegrations per minute (DPM) counts with a count time of 10 min per sample.

Chapter 3

Use of fluorescent D-amino acids to analyse peptidoglycan synthesis in *Staphylococcus aureus*

The work in this chapter was carried out in collaboration with Stéphane Mesnage (biochemical analysis of muropeptides) and Christa Walther & Robert Turner (STORM & SIM microscopy).

3.1 Introduction

3.1.1 Labelling peptidoglycan synthesis

Investigation into the localisation of peptidoglycan synthesis within bacteria has been limited by the availability of labelling tools (Daniel and Errington, 2003). Initial studies into peptidoglycan synthesis used electron microscopy (EM) to localise synthesis within extracted cell walls. This was achieved either by autoradiography of radiolabelled sacculi or uranyl acetate staining of thin sections (Merad et al., 1989; de Pedro et al., 1997). However, these methods are limited since they can be used on sacculi only and topology of insertion can therefore be difficult to assess (Daniel and Errington, 2003).

More recently a method was developed that utilizes the ability of bacteria, such as *E. coli* to incorporate a variety of D-amino acids into the peptide sidechain of peptidoglycan (de Pedro et al., 1997). Media supplemented with D-cysteine allows for the exchange of the terminal D-amino acid via a reaction within the periplasm. The thiols within D-cysteine can be detected using immuno-detection and labels compatible with either fluorescence or electron microscopy. This method is limited to use with sacculi and, at concentrations above 1 mg ml⁻¹, D-cysteine is toxic to bacteria.

To overcome problems from both these methods Daniel and Errington developed a labelling method using a fluorescent derivative of vancomycin (Daniel and Errington, 2003). Vancomycin is a glycopeptide antibiotic that binds tightly to the terminal D-ala-D-ala in the peptidoglycan peptide side chain (Sheldrick et al., 1978). In most cases the terminal D-ala-D-ala in bacteria is protected from binding by rapid processing either

into peptidoglycan crosslinks or hydrolysis, therefore vancomycin is thought to specifically bind to nascent peptidoglycan (Daniel and Errington, 2003). However *S. aureus* has naturally low carboxypeptidase activity, hence in order to use fluorescent vancomycin, *S. aureus* must be incubated in excess D-serine (Scheffers and Pinho, 2005). D-serine is incorporated into the terminal stem peptide position and is not recognised by fluorescent vancomycin. A short pulse of growth with D-ala allows new peptidoglycan synthesised during the pulse to be labelled by vancomycin (Scheffers and Pinho, 2005). While labelling with fluorescent vancomycin has allowed greater insight into localisation of peptidoglycan synthesis, a probe that allowed direct labelling of new peptidoglycan and would be usable in live cells was still necessary.

In 2012 Michael VanNieuwenhze and colleagues developed fluorescent derivatives of D-alanine as labels of nascent peptidoglycan. Small fluorophores were attached to D-alanine to produce fluorescent D-amino acids (FDAAs) which were found to label the peptidoglycan of a variety of bacterial species (Kuru et al., 2012). This labelling was found to require viable cells & the D-enantiomer suggesting active incorporation into the peptidoglycan. Chemical analysis of mucopeptides suggested that incorporation was via periplasmic exchange reactions into position 4 of Gram negative bacteria and position 5 of Gram positive bacteria (Kuru et al., 2012). FDAAs provide a tool for the labelling of peptidoglycan synthesis sites in a wide variety of bacteria that is applicable with any fluorescence detection technique, particularly fluorescence microscopy.

3.1.2 Super resolution microscopy

3.1.2.1 Fluorescence microscopy

Fluorescence is the emission of photons by atoms or molecules following excitation of electrons following absorption of energy, usually in the form of an absorbed photon. When a photon of an appropriate wavelength is absorbed by a fluorescent molecule an electron is excited to a higher energy state and almost immediately falls back to the ground state. In this process the energy is released as a photon, but given some energy will be lost from this system the released photon is generally of a longer wavelength (Murphy and Davidson, 2013). This process can be visualised using a Jablonski diagram (Figure 3.1). In fluorescence microscopy the sample is illuminated by light of a specific

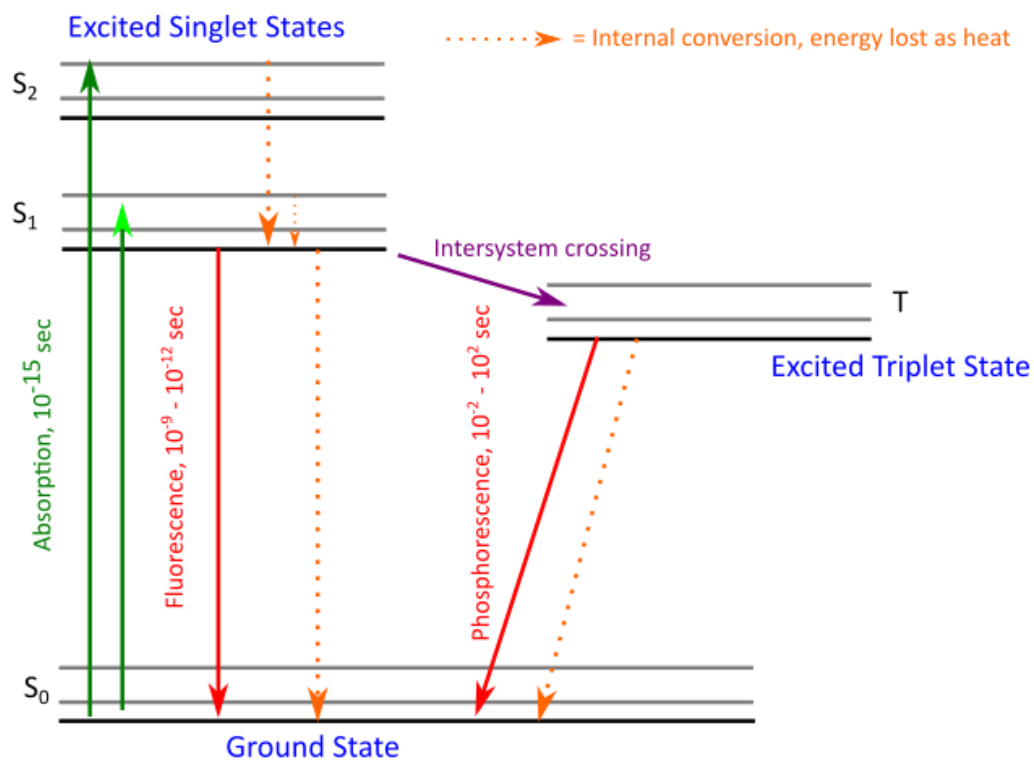


Figure 3.1. Jablonski diagram showing energy levels occupied by an excited electron within a fluorescent molecule. Adapted from (Murphy and Davidson, 2013).

wavelength, that is a wavelength that will be absorbed by the fluorescent molecule used, this is usually selected by an excitation filter that removes all other wavelengths from the excitation light (Figure 3.2). This is then directed through the objective and onto the sample. This is different to light microscopy where the light is transmitted through the sample to the objective. The released fluorescent signal from the sample is then collected by the objective and sent to the camera detector.

3.1.2.2 **The diffraction limit**

When light is focussed it does not converge to an infinitely sharp point rather a blurry focal spot occurs due to diffraction. In a similar fashion a single point emitter, such as a fluorescent molecule, appears as a blurry spot with a finite size (Huang et al., 2010). This defines the point spread function (PSF) of the microscope and if two emitters are localised within a distance of half the point spread function then they will appear as if they were a single object. This resolution limit was recognised by Ernst Abbe and is defined by the wavelength of light used (λ) and the numerical aperture of the objective used (NA) (Rego et al., 2012). This gives a resolution limit of ~ 250 nm in x & y and ~ 550 nm in z given a high NA objective (Huang et al., 2010). Many subcellular functions fall within this size limit and so if these are to be imaged a way to circumvent this limit was required.

3.1.2.3 **Super-resolution microscopy**

A wide range of instruments and methods have been introduced in order to improve the spatial resolution of fluorescence microscopy, these fall mainly into two classes.

1. Patterned illumination to spatially modulate the behaviour of molecules
 2. Single molecule imaging due to stochastic activation of individual molecules
- (Huang et al., 2010).

3.1.2.4 **Patterned illumination**

When a patterned light field is applied to a sample it manipulates the fluorescence emission. Positive patterned illumination occurs when the light field used for imaging is itself patterned while negative patterned illumination uses an additional patterned light field to reduce the population of fluorophores that can emit fluorescence.

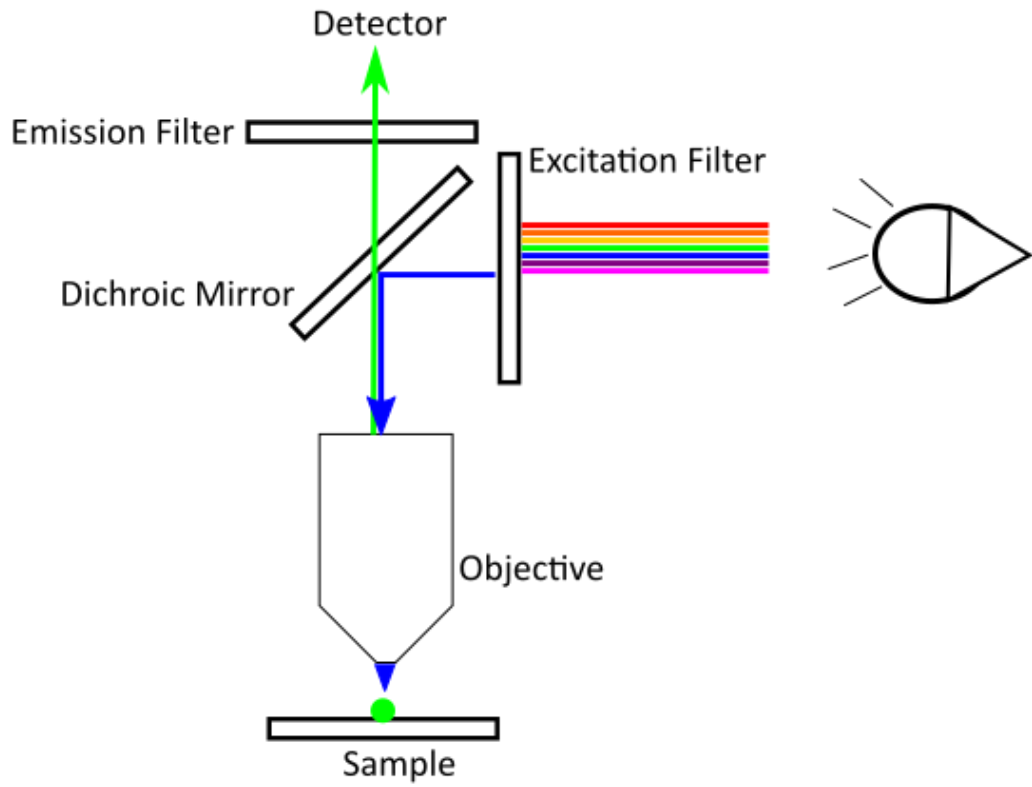


Figure 3.2. Diagram depicting the general features of a fluorescence microscope.

Structured illumination microscopy (SIM) uses a positive pattern of light to illuminate the sample, this is typically a sinusoidal pattern created from the combination of two light beams. Using such a patterned light source means that an image of the sample is taken only of the illuminated subsection of the field and the resultant image is composed of both the sample structure and the patterned light structure (Huang et al., 2010). By taking multiple images using the patterned light by both scanning and rotating the light source additional spatial resolution can be acquired (Chapter 3.2.3.2; Gustafsson, 2000). In practise this means that for each slice in z , images are taken for 5 lateral shifts and 3 angles resulting in 15 images per slice. While in theory any fluorophore is compatible with the system since no special photophysics are required, stable bright fluorophores are advantageous as bleaching during the acquisition process can interfere with the reconstruction algorithm (Huang et al., 2010). SIM is still limited by diffraction therefore only a doubling of resolution is possible, however using the saturated response of fluorophores, it has been possible to achieve resolutions of 50 nm using saturated SIM (SSIM) (Gustafsson, 2005).

In contrast stimulated emission depletion (STED) uses negative patterned illumination (Hell and Wichman, 1994). A secondary light source, the depletion light, brings an excited electron back down to the ground state without the emission of a photon (i.e. fluorescence) (Figure 3.1). The depletion light surrounds the focal spot of the excitation laser reducing the size of illuminated region of molecules. By scanning this sharpened focal spot across the sample and image of greater resolution can be acquired without any post acquisition processing (Huang et al., 2010). The depletion light is created by diffraction limited optics therefore enhancement is in theory limited. However, STED uses the same saturated response of fluorophores as Saturated SIM i.e. the number of fluorophores that are capable of generating fluorescence approaches zero once the depletion laser intensity is above the saturation level (Murphy and Davidson, 2013). When a ring-shaped depletion light above the saturation level is applied to the sample only a very small region of the sample near the centre of the ring can generate a fluorescent signal (Huang et al., 2010).

3.1.2.5 Single-molecule localisation microscopy

Problems arise from the diffraction limit due to overlapping emission from multiple fluorophores such that they cannot be distinguished from one another. By controlling

emission such that only one molecule is emitting at a time it is possible to achieve higher resolution than with standard fluorescence microscopy (Betzig et al., 2006). In 2006, two separate techniques were developed which used this principle to image at higher resolutions; photoactivated localisation microscopy (PALM) was developed using fluorescent proteins (Betzig et al., 2006), while stochastic optical reconstruction microscopy (STORM) was developed for synthetic fluorescent dyes (Rust et al., 2009). However this difference in probes initially used is the only major difference in the two techniques such that they are generally referred to as PALM/STORM microscopy (Murphy and Davidson, 2013). PALM/STORM images are constructed from a series of imaging cycles where in each cycle only a subset of molecules are switched on. This requires the use of lasers of power 50 to 200 milliwatts (mW) to provide sufficient energy to induce single-molecule photoswitching (Murphy and Davidson, 2013).

PALM imaging uses continuous excitation by a laser of wavelength near excitation maximum for the photoactivatable fluorescent protein used. Whenever the proportion of single molecules within the field is reduced a pulse of light from a second laser, often at 405 nm, is capable of activating inactive fluorescent proteins to increase the density of activated fluorescent proteins but still at a resolvable level (Betzig et al., 2006). This cycle is repeated to create thousands of imaging frames.

STORM was first used with a Cy3-Cy5 dye pair. Red laser light produces fluorescent emission from Cy5, forming a stable dark state while green laser light converts Cy5 back to a potential fluorescent state at a higher efficiency in the presence of Cy3 (Rust et al., 2009). Under conditions where single molecule detection can occur this switch can be cycled hundreds of times before permanent photobleaching occurs (Rust et al., 2009). A version of STORM is known as dSTORM (direct STORM) where single fluorescent dyes can be driven into the photoswitchable states with reducing reagents under oxygen depletion (Murphy and Davidson, 2013). In this case single fluorophores can be switched between the states through the use of a single laser. This requires the use of a single fluorescent dye and therefore simplifies the process.

Following acquisition of several thousand images the precise localisation of each of the fluorophores is determined. Each single molecule produces a blurry fluorescent spot. By statistical fitting of an ideal PSF to this spot the centre of the detected emission

light can be determined giving the precise localisation of the molecule (Betzig et al., 2006). Once this has been done for each of the frames the image can be reconstructed through combination of the frames to produce a high resolution plot of fluorophore localisation.

Due to the requirements of STORM, there is a limit to the fluorescent dyes & proteins that are compatible with this technique. Probes require three properties to be a suitable STORM fluorophore. Firstly they must have both a “light” and “dark” state where at a specific range of wavelengths light is only emitted in the light state (Huang et al., 2010). Secondly they must be able to emit a high number of photons before becoming dark in order to achieve high resolution. And finally, a low spontaneous activation is also advantageous, this reduces the likelihood of more than one fluorophore being in the “light” state within a single diffraction limited area (Huang et al., 2010).

Blinking of fluorophores is achieved through the cycling of the fluorophore between a number of different energetic states (Figure 3.1). Stochastic photoswitching is achieved when a fluorophore cycles between photon emission state transitions (i.e. cycling between ground and singlet excited state) and temporary arrest in the triplet state (T) (Henriques et al., 2011). At this point fluorophores are sensitive to permanent photobleaching if exposed to molecular oxygen, therefore oxygen is depleted in imaging samples e.g. by the use of enzyme catalysed oxygen scavenging buffers. Recovery of ionized fluorophore to allow continued photoswitching is often achieved by the addition of millimolar concentrations of reducing agents into the buffer (Henriques et al., 2011).

In order to achieve 3D STORM single molecules must be accurately localised in the axial plane in addition to the lateral plane (Huang et al., 2010). This is achieved through the application of astigmatism, whereby light propagating from different planes has different focal points. A cylindrical lens inserted into the imaging path causes a shape change in the detected light. It is possible to determine the lateral position from the centre of the signal and axial position from the ellipticity of the signal (Huang et al., 2010).

3.1.3 Aims of the chapter

1. To establish fluorescent D-amino acid labelling of peptidoglycan insertion in *S. aureus*.
2. To determine the mechanism of FDAA labelling in *S. aureus*.
3. To establish super-resolution microscopy for the analysis of peptidoglycan synthesis.

3.2 Results

3.2.1 Fluorescent D-amino acid labelling in *S. aureus*

3.2.1.1 Fluorescent D-amino acids

Fluorescent D-amino acids (FDAA) used within this thesis were synthesised by Dr Simon Jones' group (University of Sheffield, Department of Chemistry) when unavailable commercially.

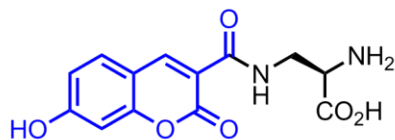
The FDAA's used fall largely into two groups; FDAAs that were intrinsically fluorescent and those that contained azide groups for attachment of fluorophores following insertion into peptidoglycan. All FDAAs used can be seen in Figure 3.3. The FDAAs with intrinsic fluorophores used were HADA, NADA and TADA (Figure 3.3 A-C) which have 7-hydroxycoumarin-3-carboxylic acid (emission 450 nm), 4-chloro-7-nitrobenzofurazan (emission 538 nm) and tetramethylrhodamine (emission maximum 576 nm) fluorophores respectively (Kuru et al., 2012).

The azide containing FDAAs (Figure 3.3 D&E), also known as "clickable" D-amino acids allow the use of fluorophore not compatible with labelling, e.g. due to size/charge to be used as peptidoglycan labels. Alkyne containing fluorophores (Figure 3.3 F & G) can be attached to azido-FDAAs via copper catalysed azide-alkyne cycloaddition (Baskin and Bertozzi, 2007). An azide containing dipeptide FDAA was also utilised (Figure 3.3 E). This is a conjugated azido D-alanine and a second unlabelled D-alanine with the labelled D-alanine in position 1, therefore the fluorophore is proposed to label position 4 within the peptide sidechain.

3.2.1.2 Determining concentration of FDAAs required for *S. aureus* labelling

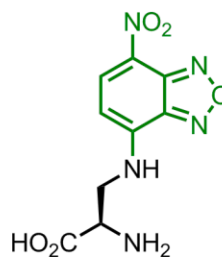
Prior to use of FDAAs for peptidoglycan labelling it was important to determine the optimal labelling conditions. Previous work had shown that labelling in bacteria was

A



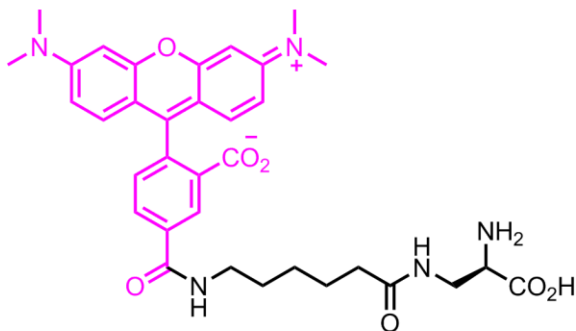
HADA

B



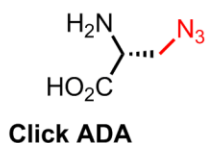
NADA

C



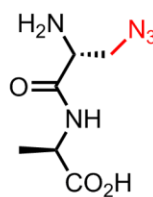
TADA

D



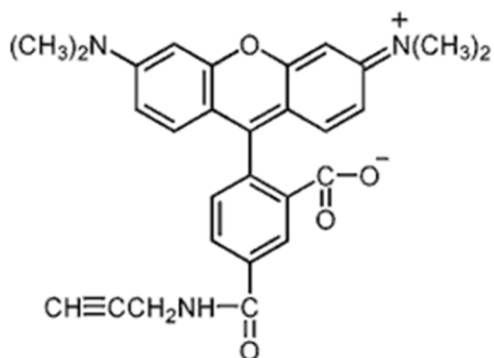
Click ADA

E



Click Dipeptide

F



G

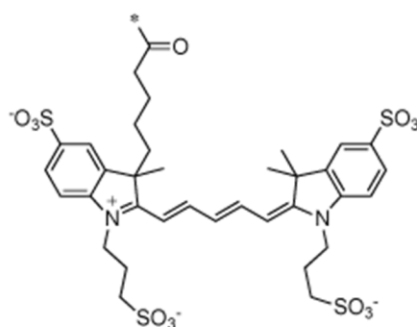


Figure 3.3. Chemical structures of FDAAs & Alkyne Dyes. (A) HADA, (B) NADA, (C) TADA, (D) ADA, (E) dipeptide. Coloured portions represent the fluorophores or reactive groups while black represents the D-amino acid backbone and linker structure. (F) Tetramethylrhodamine alkyne dye structure. (G) Alexa Fluor 647 structure. Exact structure of alkyne derivative not known.

achieved by addition of FDAA's into growth media at a concentration of 0.25-1 mM (Kuru et al., 2012). Concentrations of 100 μ M – 1mM were tested for each of the FDAA's available (Figure 3.4 - Figure 3.9) and it was determined that a concentration of 500 μ M was optimal for each of the FDAAs. This was determined as the lowest concentration of FDAA that gave a good fluorescence signal across the different labels. The concentration of alkyl dye used within the “click” reaction was also examined (Figure 3.8). The Click reaction was carried out following incorporation of the azide containing into the peptidoglycan. A concentration of 5 μ g ml⁻¹ dye was sufficient for azide FDAA labelling within diffraction limited (Figure 3.8) and STORM microscopy (data not shown). The optimal concentration of labelling was also tested for the dipeptide label; this was found to be 1 mM (Figure 3.9).

3.2.1.3 Pattern of FDAA labelling over time

S. aureus was incubated with FDAAs for various times (5 – 30 min) to assess their ability to label synthesis of peptidoglycan (Figure 3.10). At 5 min incubation, clear division septa are labelled by the FDAAs showing septal rings and plates. This pattern continues on increased time incubation however there is also an increase in labelling throughout the cell wall suggesting that material remains labelled and that concentrations used is sufficient for labelling of synthesis over longer periods. This pattern was consistent across all FDAAs used (Appendix I).

3.2.1.4 Mechanism of FDAA labelling in *S. aureus*

3.2.1.4.1 Fluorescent D-amino acids label peptidoglycan

FDAAs have been shown to label peptidoglycan covalently within both *B. subtilis* and *E. coli* through retention of fluorescence in purified sacculi of labelled cells (Kuru et al., 2012). To ensure that this was also the case within *S. aureus*, peptidoglycan was extracted from FDAA labelled cultures and counterstained with Wheat Germ Agglutinin(WGA) Alexa Fluor 488 conjugate, a lectin that binds GlcNAc molecules (Figure 3.11) (Wheeler et al., 2015). A strong fluorescence signal from the FDAA label was present and it was also possible to identify some features of septal labelling such as septal rings. Therefore, FDAAs label the peptidoglycan sacculus of *S. aureus*.

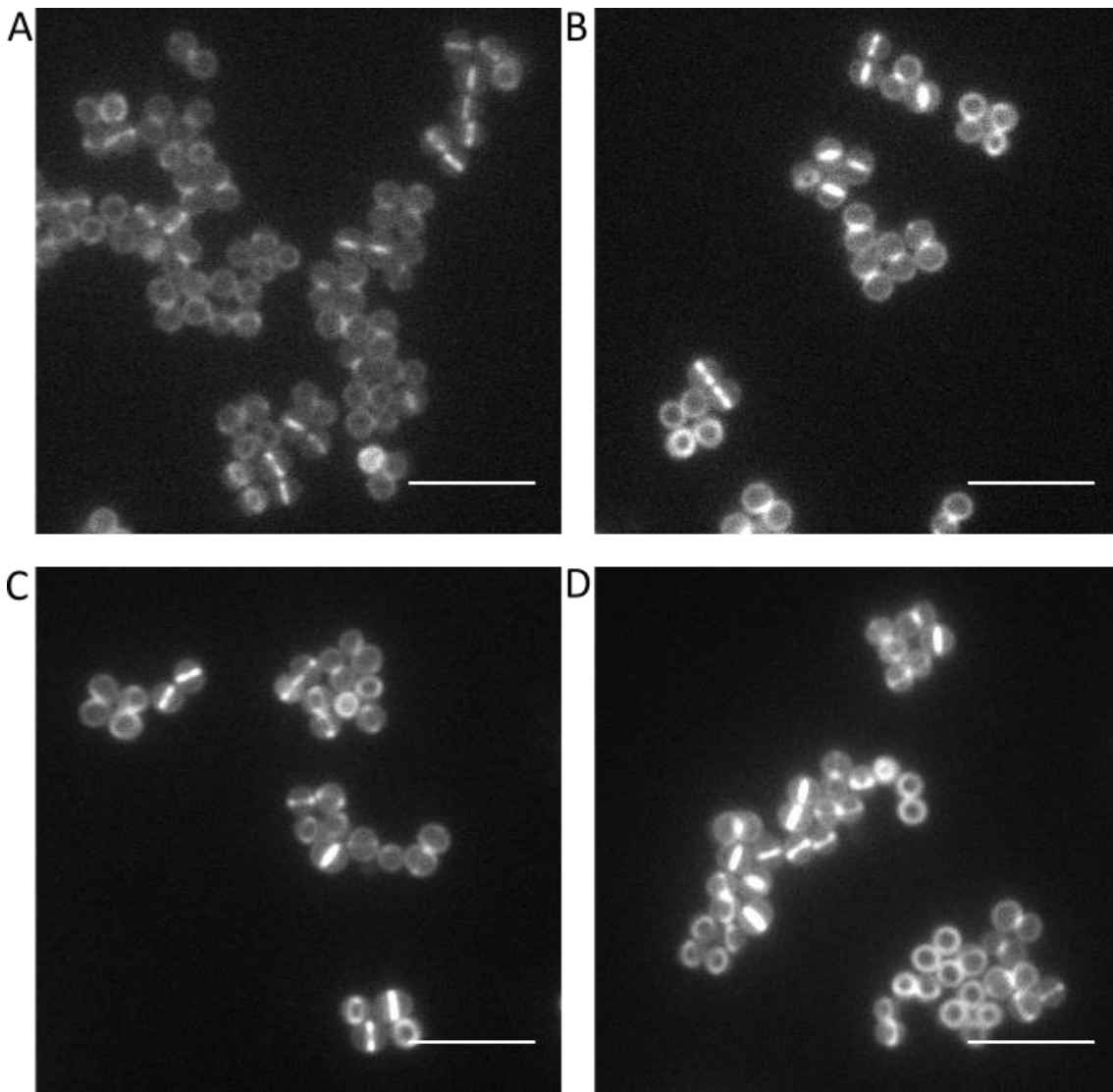


Figure 3.4. Testing increasing concentrations of HADA to determine optimal labelling conditions. All *S. aureus* samples were labelled for 5 minutes and analysed by fluorescence microscopy. (A) 100 μM HADA, (B) 200 μM HADA, (C) 500 μM HADA, (D) 1 mM HADA. (Scale bar 5 μm).

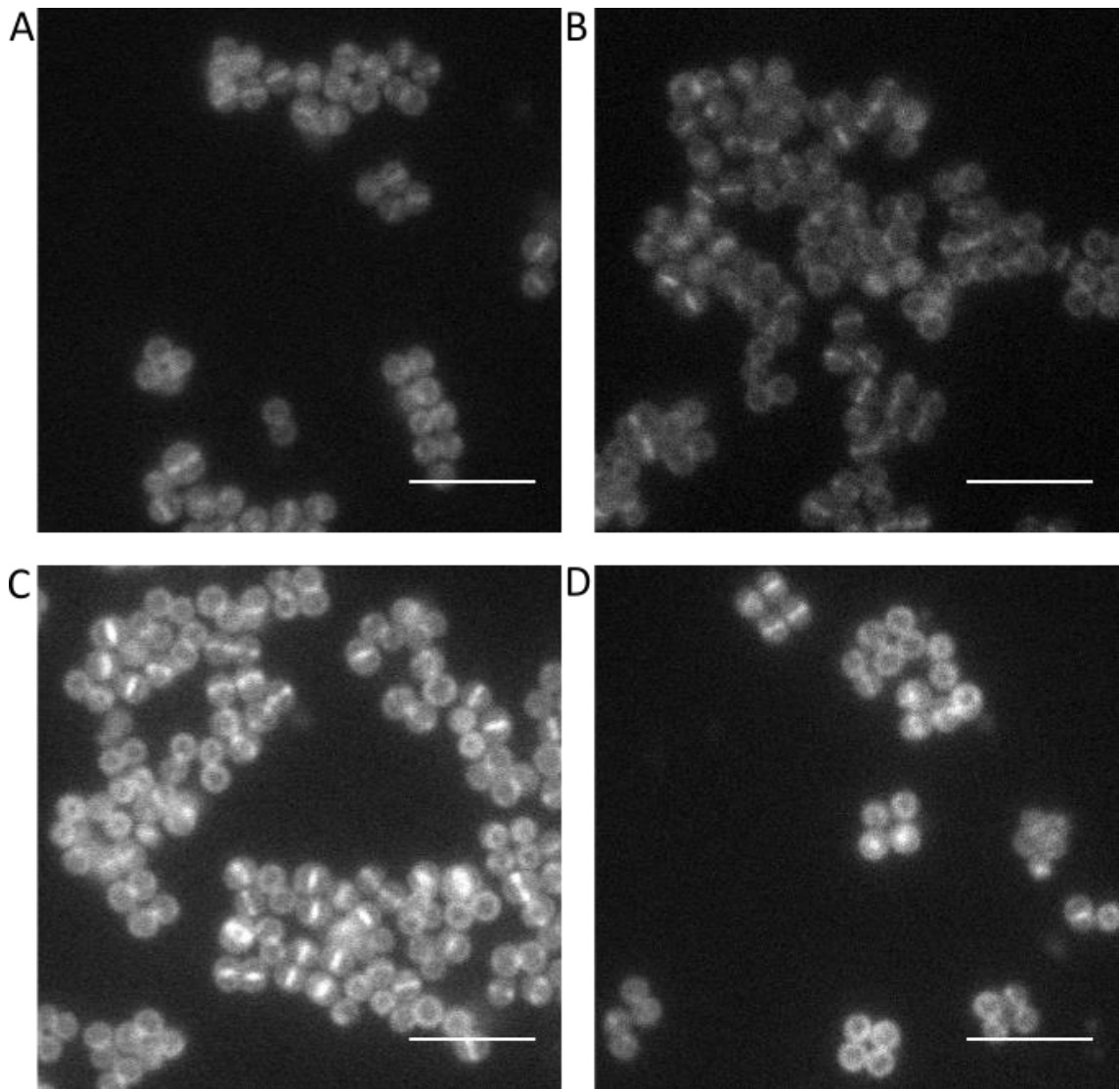


Figure 3.5. Testing increasing concentrations of NADA to determine optimal labelling conditions. All samples were labelled for 5 min. (A) 100 μ M NADA, (B) 200 μ M NADA, (C) 500 μ M NADA, (D) 1 mM NADA. (Scale bar 5 μ m).

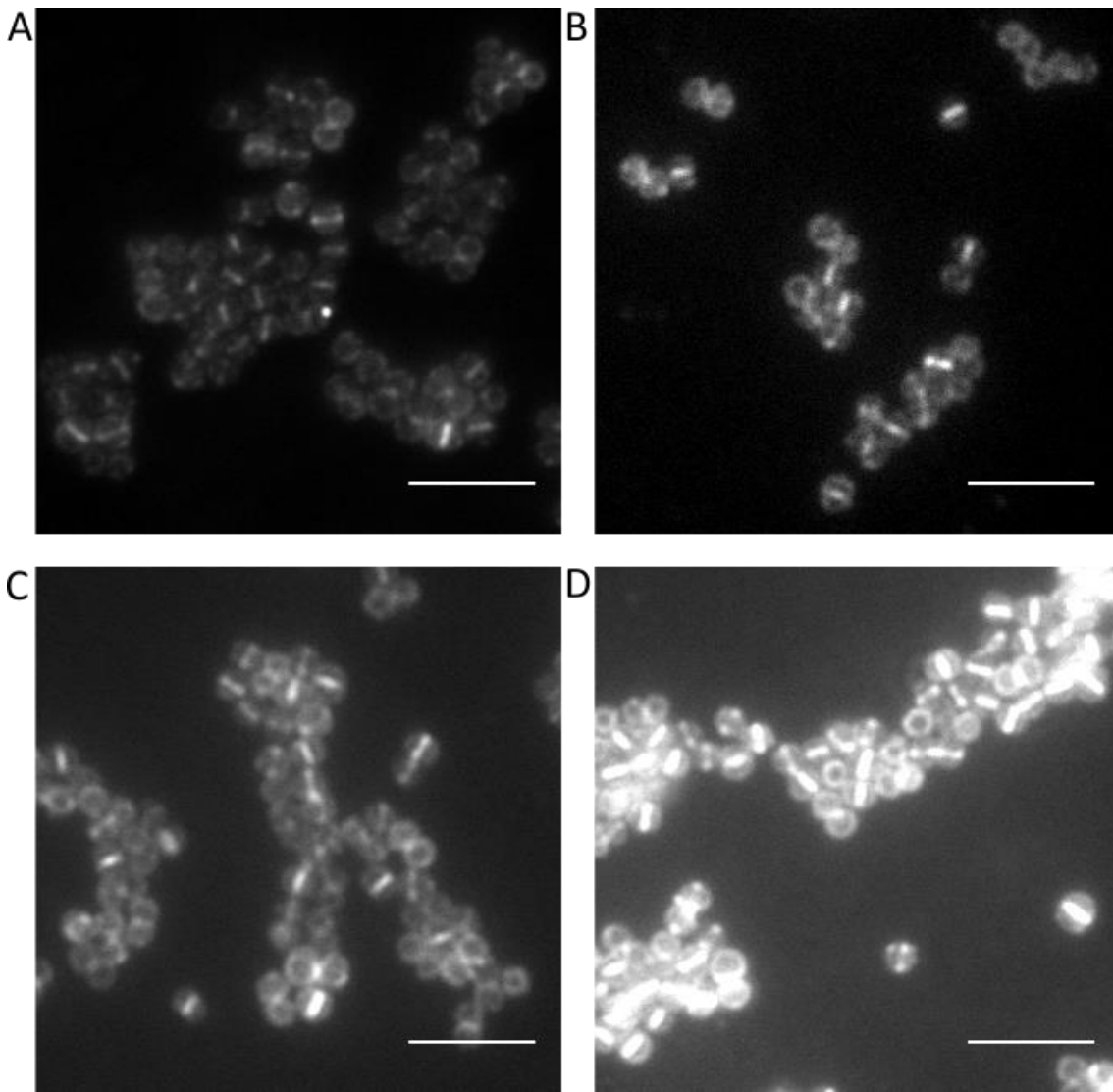


Figure 3.6. Testing increasing concentrations of TADA to determine optimal labelling conditions. All samples were labelled for 5 min. (A) 100 μ M TADA, (B) 200 μ M TADA, (C) 500 μ M TADA, (D) 1 mM TADA. (Scale bar 5 μ m).

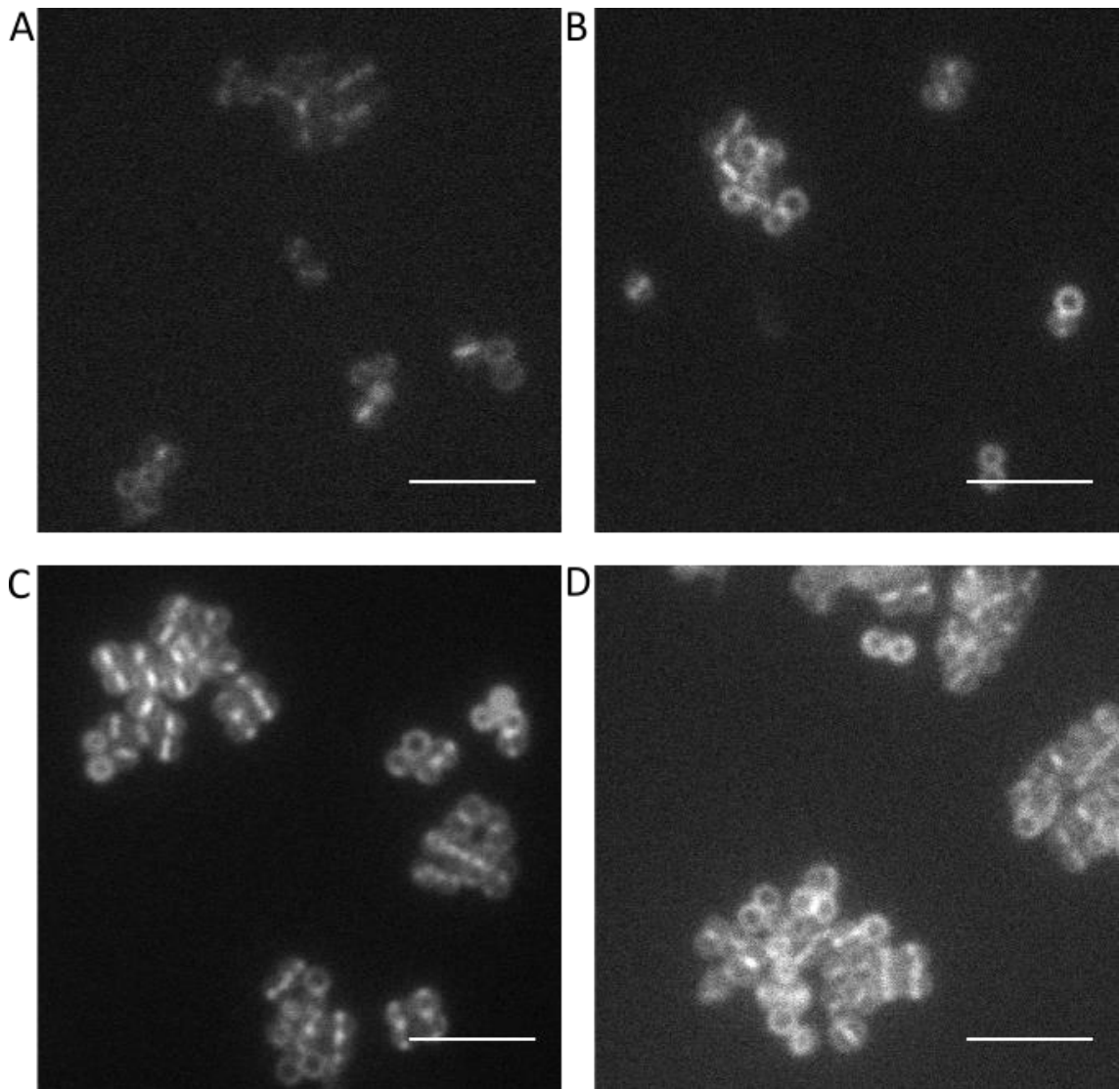


Figure 3.7. Testing increasing concentrations of ADA to determine optimal labelling conditions. All samples were labelled for 5 min and a post-fixation click reaction was carried out with alkyne Alexa Fluor 647 at $5 \mu\text{g ml}^{-1}$. (A) $100 \mu\text{M}$ ADA, (B) $200 \mu\text{M}$ ADA, (C) $500 \mu\text{M}$ ADA, (D) 1 mM ADA. (Scale bar $5 \mu\text{m}$).

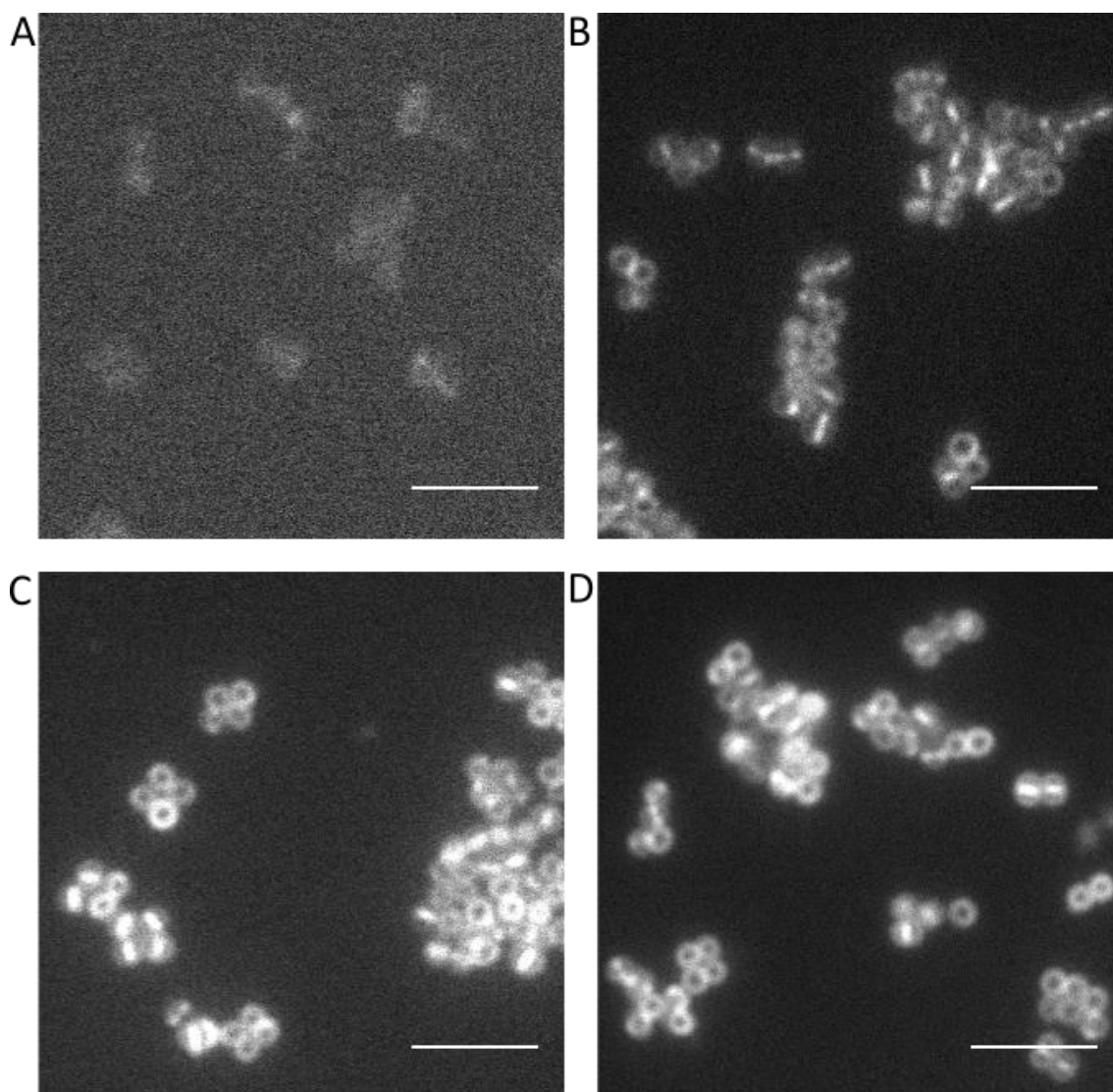


Figure 3.8. Testing increasing concentrations of alkyne Alexa Fluor 647 in the click reaction with ADA at 500 μM to determine optimal conditions for labelling. (A) 0.5 $\mu\text{g ml}^{-1}$, (B) 5 $\mu\text{g ml}^{-1}$, (C) 50 $\mu\text{g ml}^{-1}$, (D) 0.5 mg ml^{-1} . (Scale bar 5 μm).

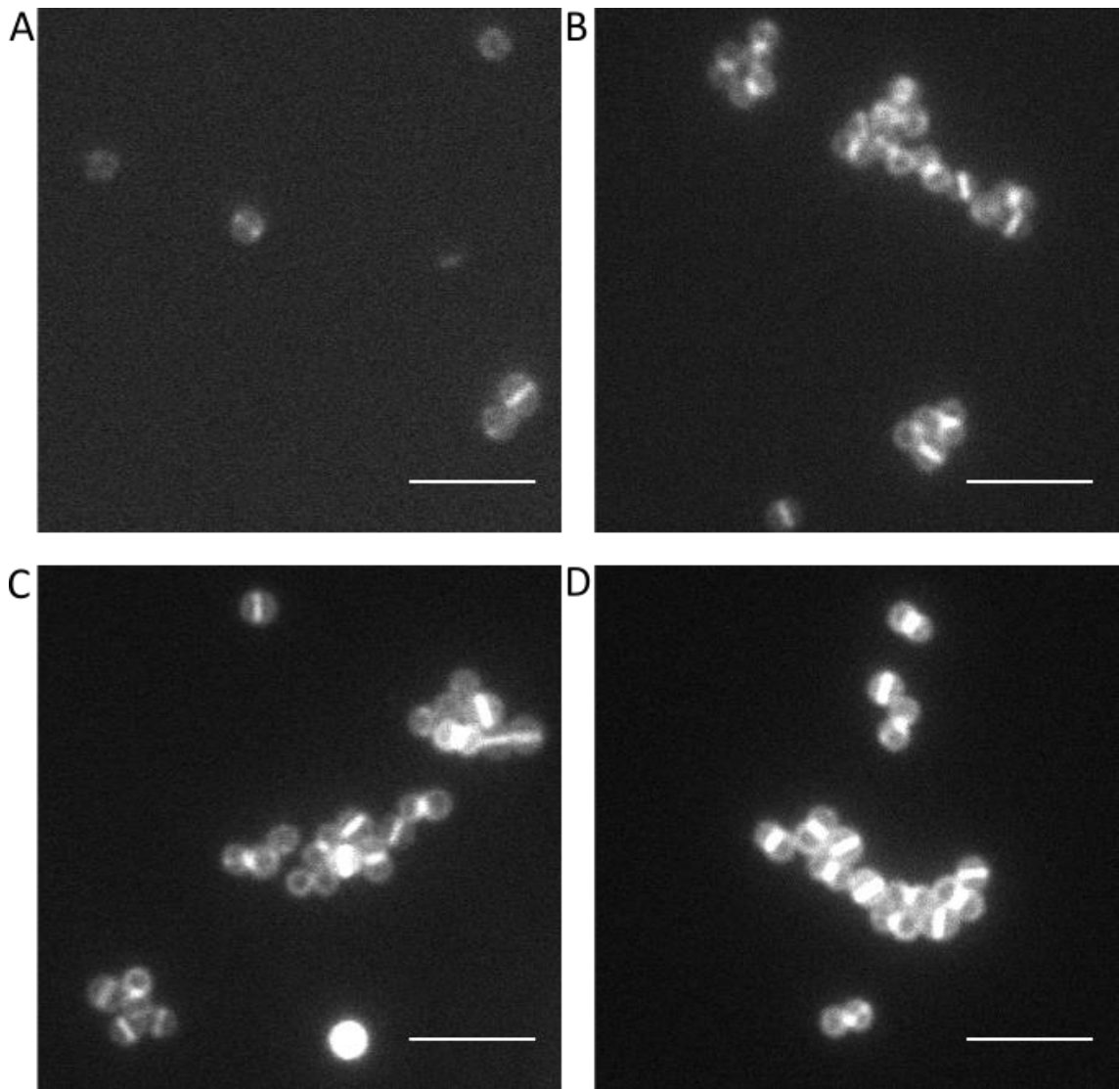


Figure 3.9. Testing increasing concentrations of dipeptide to determine optimal conditions for labelling peptidoglycan insertion. All samples were labelled for 5 minutes and post-fixation click reaction was carried out with alkyne Alexa Fluor 647 at $5 \mu\text{g ml}^{-1}$. (A) $500 \mu\text{M}$ dipeptide, (B) 1 mM dipeptide, (C) 1.5 mM dipeptide, (D) 2 mM dipeptide. (Scale bar $5 \mu\text{m}$).

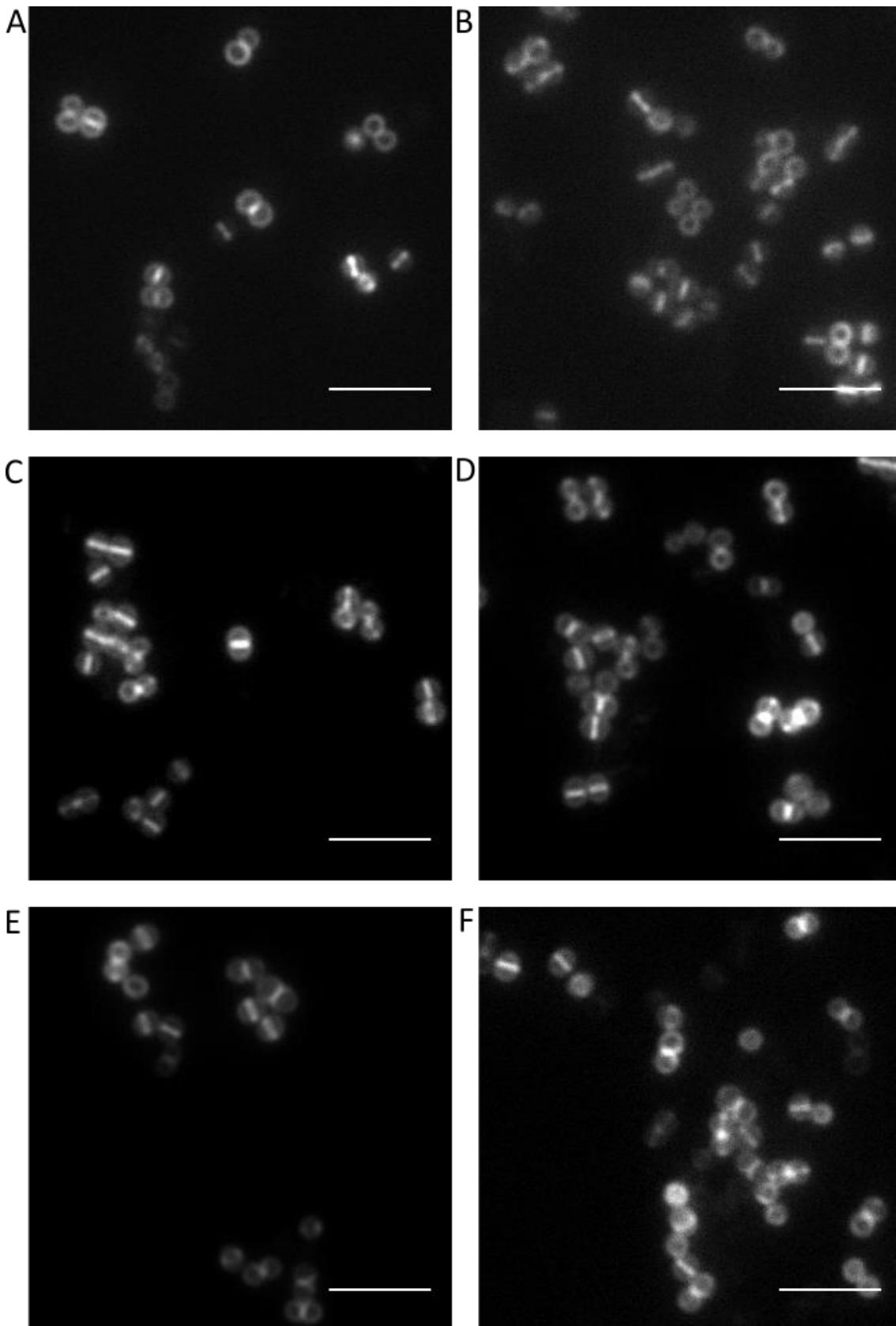
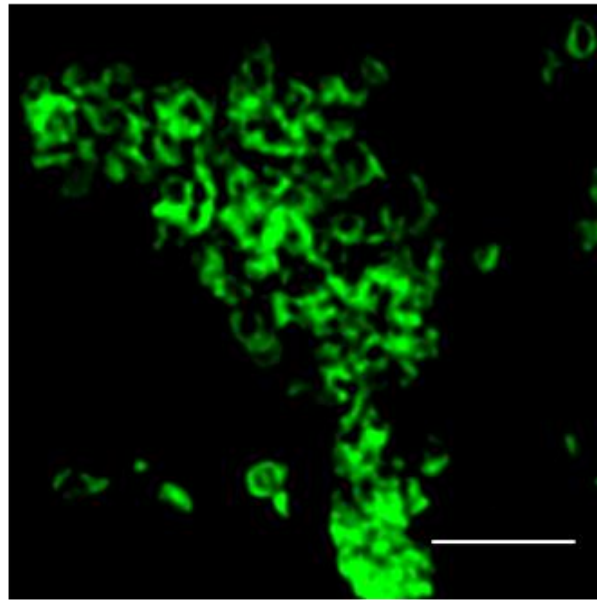
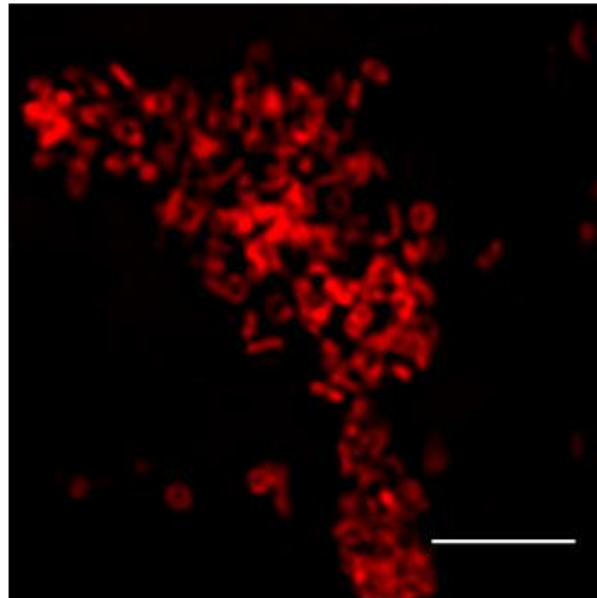


Figure 3.10. Incorporation of ADA over time. (A) 5 min, (B) 10 min, (C) 15 min, (D) 20 min, (E) 25 min, (F) 30 min ADA Labelling. (Scale bar 5 μ m).

WGA



ADA



Merge

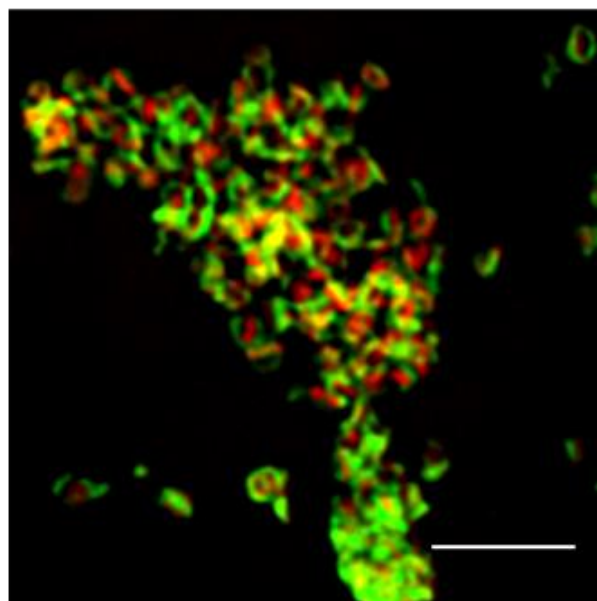


Figure 3.11. Labelling of peptidoglycan sacculi. Peptidoglycan was extracted from ADA labelled *S. aureus* SH1000 (5 minutes labelling at 500 μ M). Following extraction, the click reaction with Alexa Fluor 647 and counter staining with WGA Alexa Fluor 488 carried out. (Scale bar 5 μ m, Images were deconvolved using SoftWoRx).

3.2.1.4.2 Active growth is required for labelling

To determine that FDAAs were actively incorporated during peptidoglycan synthesis rather than labelling through other means, cells in stationary phase were labelled for 5 min with ADA (Figure 3.12). In order to visualise cells samples were counterstained with WGA-488. These cells were seen to have no fluorescence signal from the FDAA, showing that active synthesis of new peptidoglycan is required for FDAA labelling of peptidoglycan within *S. aureus*.

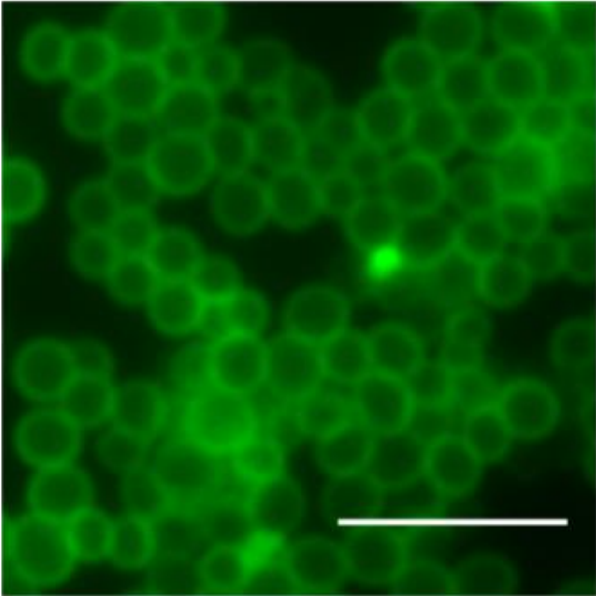
3.2.1.4.3 Effect of peptidoglycan synthesis antibiotics on labelling

Peptidoglycan biosynthesis is an important target for a number of antibiotics such as penicillin (Bugg et al., 2011). Using these antibiotics, it is possible to investigate the incorporation pathway of FDAAs through inhibition of individual steps.

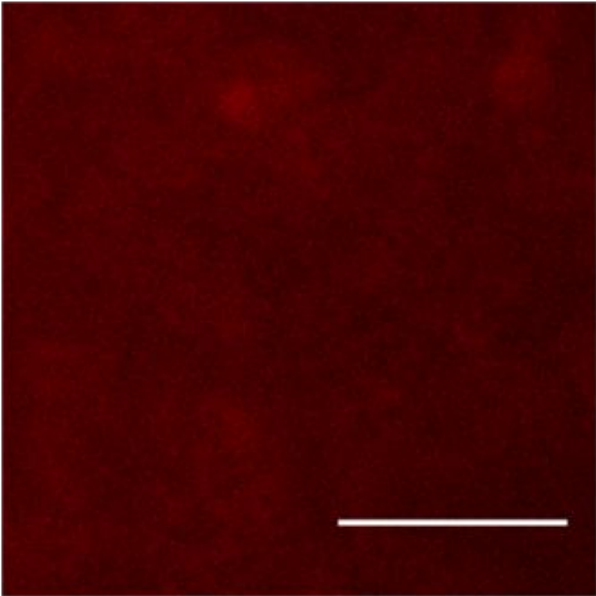
The most common peptidoglycan biosynthesis targeted antibiotics are β -lactam antibiotics. This class of antibiotics covalently bind the serine residues within the transpeptidase active sites of penicillin binding proteins (PBPs), thereby preventing the assembly of the peptidoglycan layer (Jovetic et al., 2010). During treatment of *S. aureus* with 10 x minimum inhibitory concentration (MIC) penicillin G, peptidoglycan synthesis was labelled with HADA (Figure 3.13) and dipeptide (Figure 3.14) for 5 minutes. Even at 30 minutes post treatment incorporation occurs with the same pattern for both HADA and dipeptide however with a decreased level of labelling.

Transglycosylation reactions in the assembly of the peptidoglycan cell wall are inhibited by moenomycin (Braddick et al., 2014). Moenomycin binds the transglycosylase active site of PBPs where the elongating glycan chain would normally bind (Rebets et al., 2013). Treatment of *S. aureus* with 10 x MIC moenomycin, while peptidoglycan insertion was labelled for 5 minute intervals with HADA, showed no change to insertion pattern over 30 minutes suggesting that blocking transglycosylation has no effect on the insertion of FDAAs (Figure 3.15). When labelling peptidoglycan synthesis with the dipeptide label there is a reduction in signal following treatment. However, the pattern of labelling remains consistent (Figure 3.16).

WGA



ADA



Merge

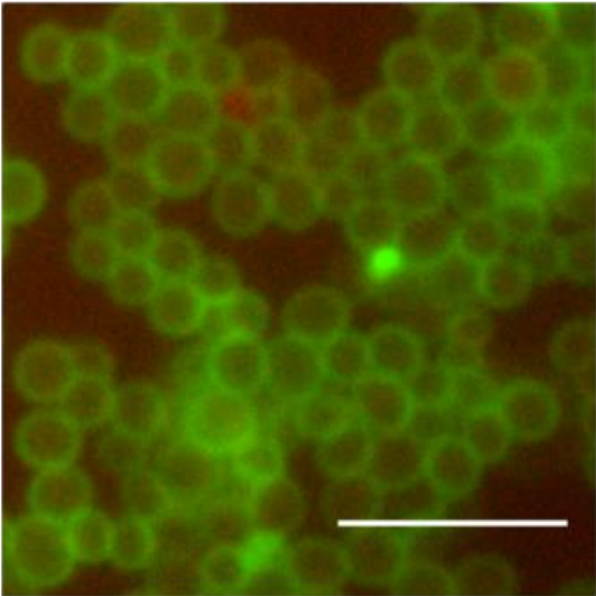


Figure 3.12. FDAA labelling requires active growth. *S. aureus* SH1000 in stationary phase was labelled with ADA for 5 min (500 μ M) and click labelled to Alexa Fluor 647 post fixation. Cells were counter labelled with WGA Alexa Fluor 488. (Scale bar 5 μ m).

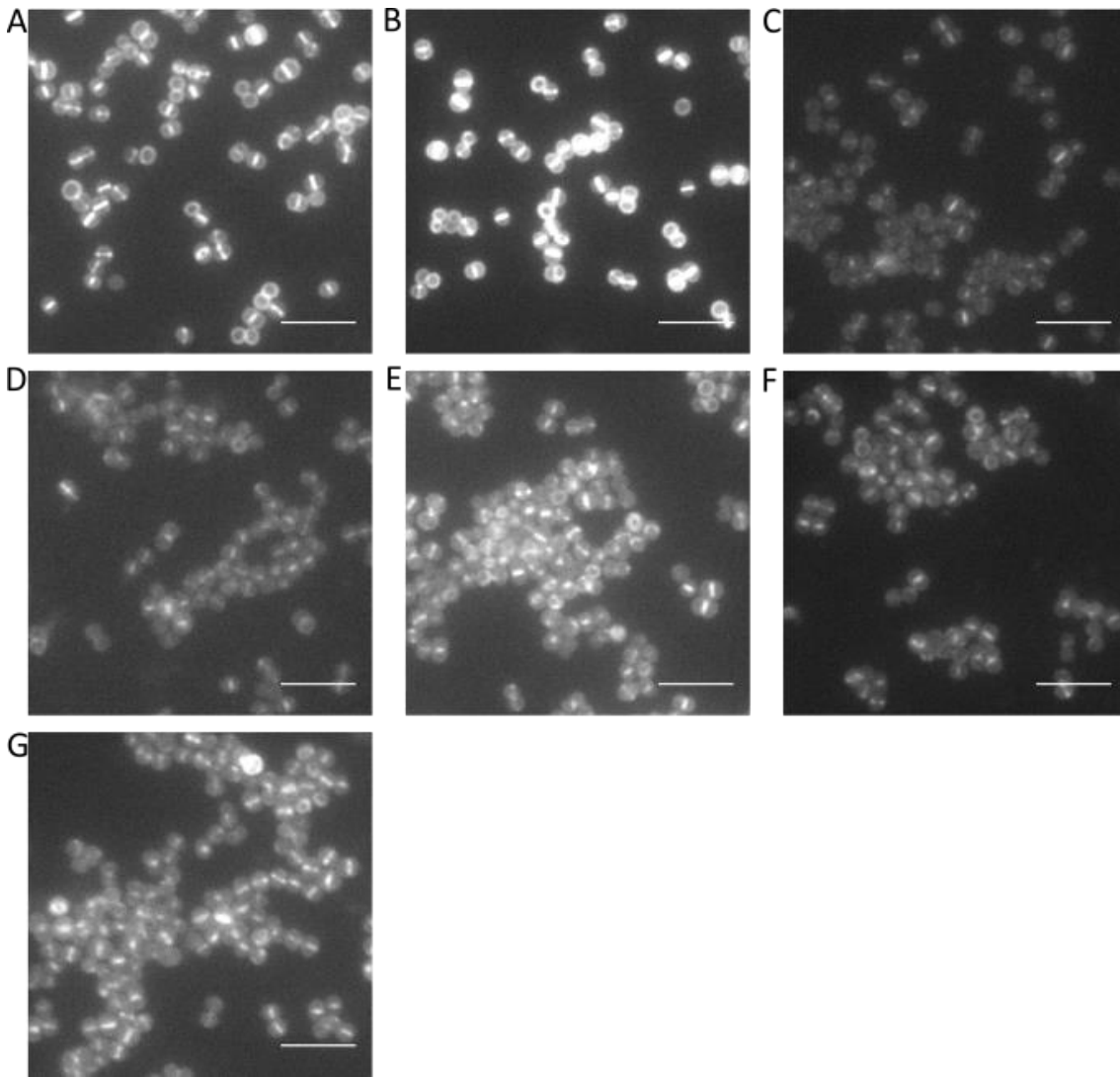


Figure 3.13. Labelling peptidoglycan synthesis in *S. aureus* SH1000 with HADA (500 μM) during treatment with 10 x MIC penicillin G ($5 \mu\text{g ml}^{-1}$). Labelling was carried out for 5 minutes during treatment. (A) No penicillin G, (B) 0-5 min treatment, (C) 5-10 min treatment, (D) 10-15 min treatment, (E) 15-20 treatment, (F) 20-25 min treatment, (G) 25-30 min treatment. (Scale bar 5 μm).

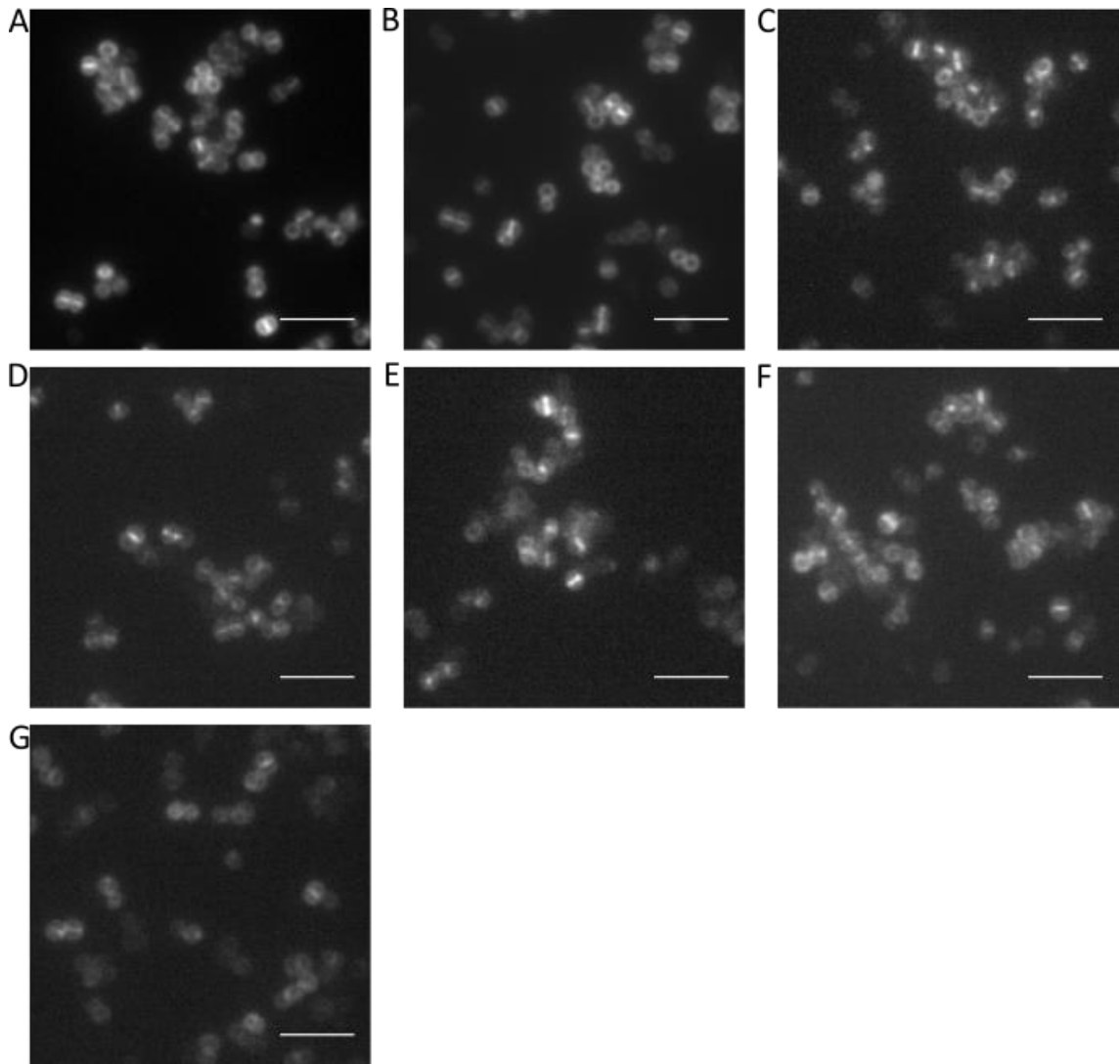


Figure 3.14. Labelling peptidoglycan synthesis in *S. aureus* SH1000 with dipeptide (1 mM) during treatment with 10 x MIC penicillin G ($5 \mu\text{g ml}^{-1}$). Labelling was carried out for 5 minutes during treatment. (A) No penicillin G, (B) 0-5 min treatment, (C) 5-10 min treatment, (D) 10-15 min treatment, (E) 15-20 treatment, (F) 20-25 min treatment, (G) 25-30 min treatment. (Scale bar $5 \mu\text{m}$).

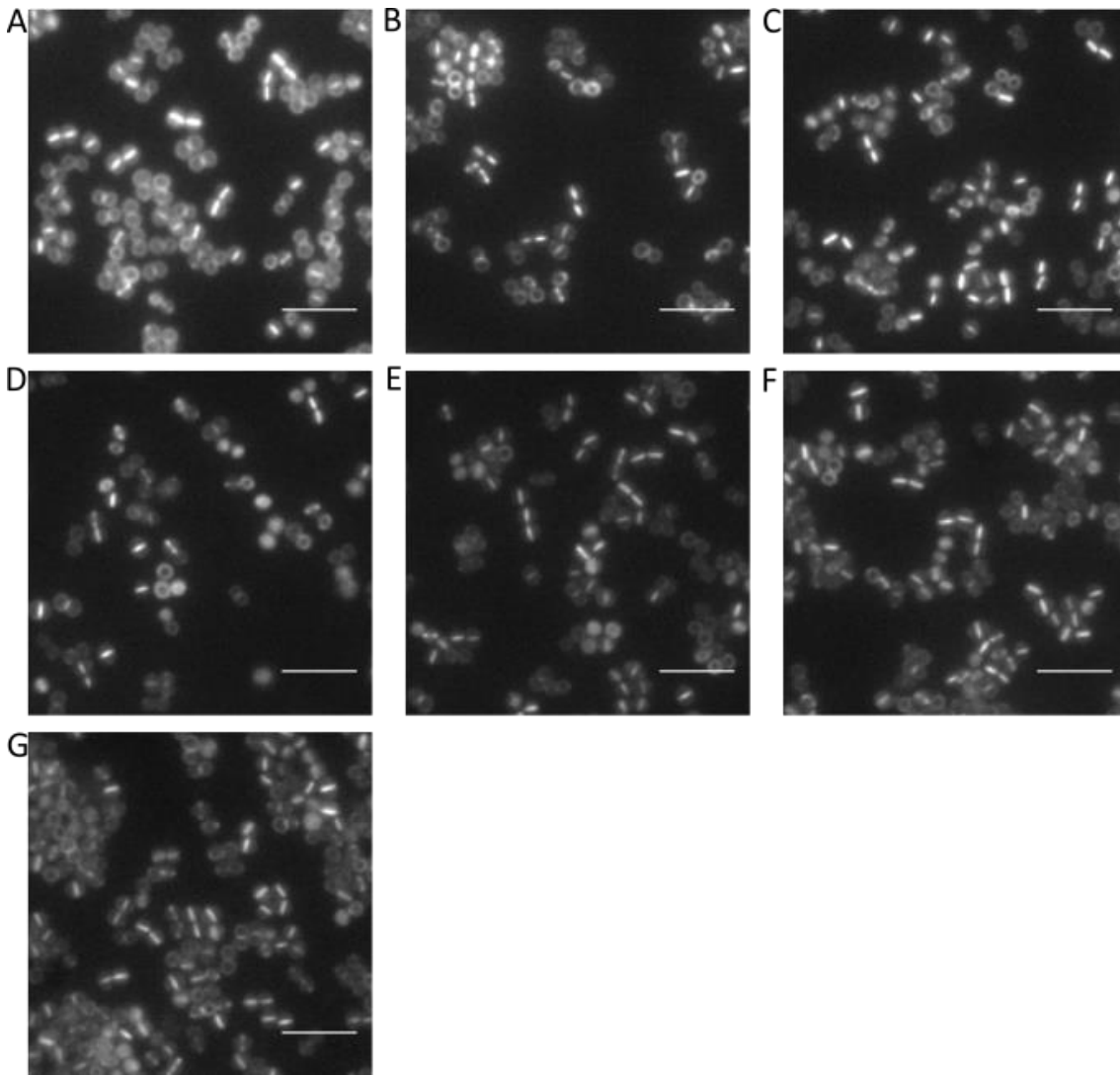


Figure 3.15. Labelling peptidoglycan synthesis in *S. aureus* SH1000 with HADA (500 μM) during treatment with 10 x MIC moenomycin (5 $\mu\text{g ml}^{-1}$). Labelling was carried during treatment. A) No moenomycin, (B) 0-5 min treatment, (C) 5-10 min treatment, (D) 10-15 min treatment, (E) 15-20 treatment, (F) 20-25 min treatment, (G) 25-30 min treatment. (Scale bar 5 μm).

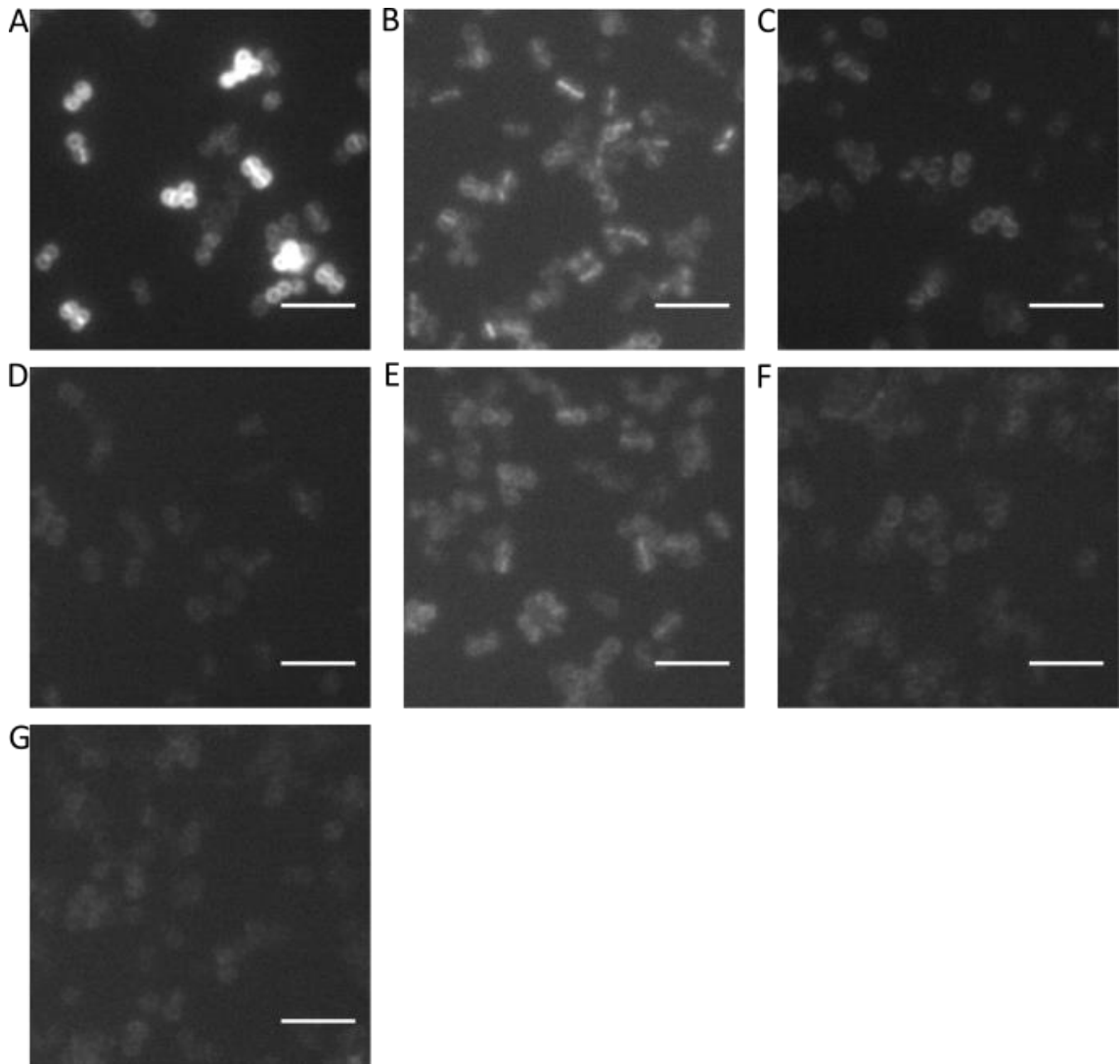


Figure 3.16. Labelling peptidoglycan synthesis in *S. aureus* SH1000 with dipeptide (1 mM) during treatment with 10 x MIC moenomycin ($5 \mu\text{g ml}^{-1}$). Labelling was carried out for 5 minutes during treatment. (A) No moenomycin, (B) 0-5 min treatment, (C) 5-10 min treatment, (D) 10-15 min treatment, (E) 15-20 treatment, (F) 20-25 min treatment, (G) 25-30 min treatment. (Scale bar $5 \mu\text{m}$).

D-cycloserine is an inhibitor of the alanine racemase and D-alanine-D-alanine ligase (Ddl) thus blocking synthesis of the peptidoglycan precursors (Liechti et al., 2013). Treatment of *S. aureus* with 10 x MIC D-cycloserine while concurrently labelling 5 minutes of peptidoglycan synthesis with HADA shows labelling is inhibited at 5 minutes incubation with D-cycloserine (Figure 3.17). Conversely labelling with the dipeptide probe, which should enter the cytoplasmic steps of synthesis after the inhibited processes, continues as normal until 20 minutes incubation (Figure 3.18). At 20 minutes post-treatment the toxic effects of D-cycloserine are apparent. Concentrations of dipeptide used are not sufficient to restore growth, therefore changes in labelling pattern at later stages are likely an effect of the bactericidal drug action as opposed to inhibition of labelling.

3.2.1.4.4 Biochemical analysis of labelled peptidoglycan

Peptidoglycan from *S. aureus* labelled with HADA for 30 min was compared to unlabelled peptidoglycan to further characterise FDAA labelling of peptidoglycan. Prior to analysis via reverse phase C₁₈ HPLC, peptidoglycan was digested with mutanolysin and lysostaphin to produce soluble muropeptides. Muropeptides were separated by HPLC and the elution monitored by absorbance at 202 nm for the presence of muropeptides and fluorescence for the presence of HADA. Comparison of profiles obtained through absorbance monitoring showed no discernible difference between the unlabelled and HADA labelled peptidoglycan (Figure 3.19 A). This is likely due to the small percentage of total peptidoglycan labelled, approximately 0.2-2.8% of total peptidoglycan (Kuru et al., 2012). However, analysis of the fluorescence trace indicated the presence of additional HADA labelled muropeptides within the peptidoglycan, of note a single peak with a fluorescence value of 4×10^5 counts (retention time = 19.7 mins) (Figure 3.19 B). Both the labelled and unlabelled were analysed by Mass Spectrometry (MS) however it was not possible to identify the fluorescently labelled muropeptide and therefore the position of HADA.

3.2.2 Using STORM in *Staphylococcus aureus*

3.2.2.1 Selecting imaging conditions for STORM in *S. aureus*

In order to utilise STORM with *S. aureus* a number of different dyes that have been used previously for STORM were tested within available systems. Initial tests were carried out with tetramethylrhodamine (TMR) which has been used previously in

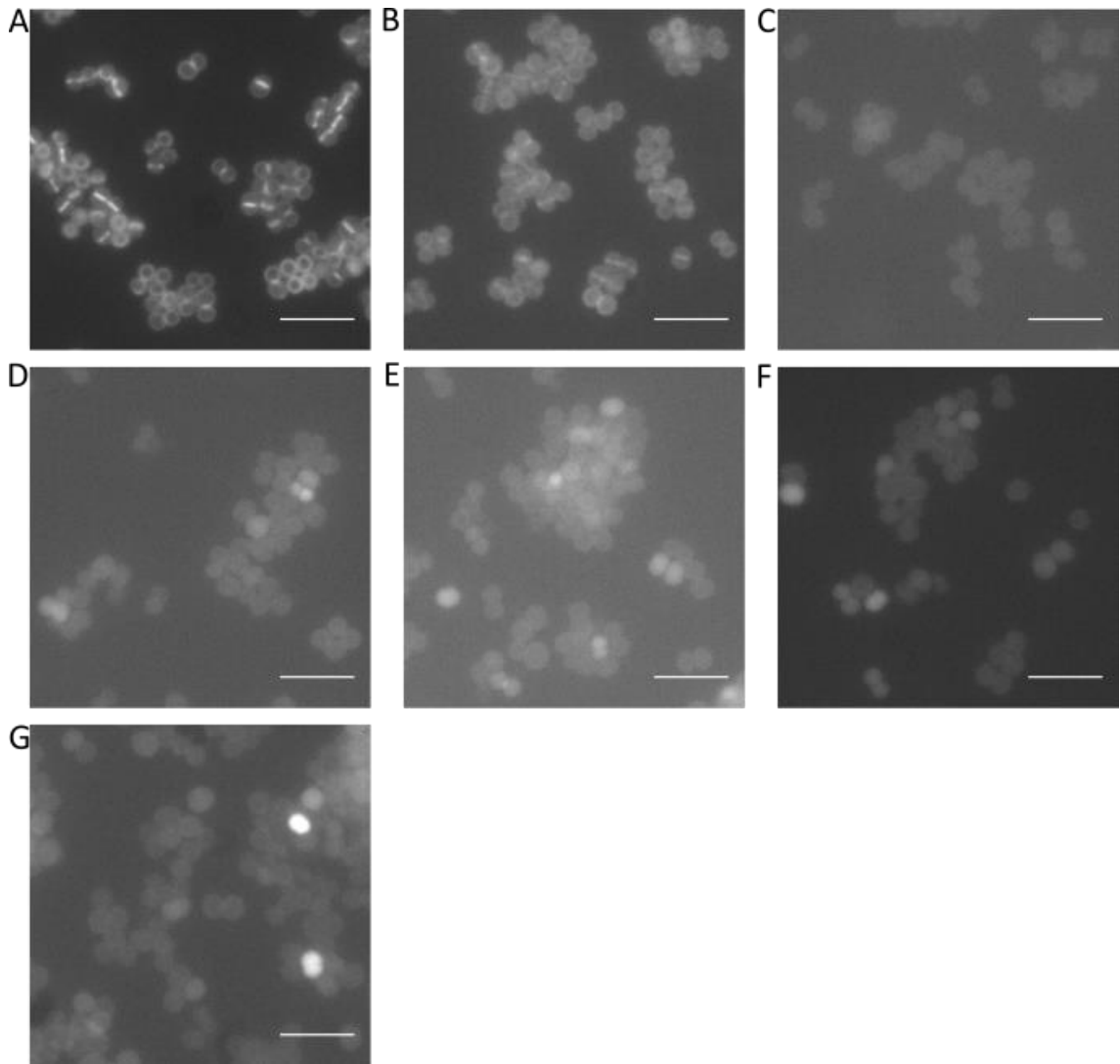


Figure 3.17. Labelling *S. aureus* SH1000 peptidoglycan synthesis with HADA (500 μM) during treatment with D-cycloserine at 10 x MIC (500 $\mu\text{g ml}^{-1}$). Labelling was carried out for 5 minutes during treatment. (A) No D-cycloserine, (B) 0-5 min treatment, (C) 5-10 min treatment, (D) 10-15 min treatment, (E) 15-20 treatment, (F) 20-25 min treatment, (G) 25-30 min treatment. (Scale bar 5 μm).

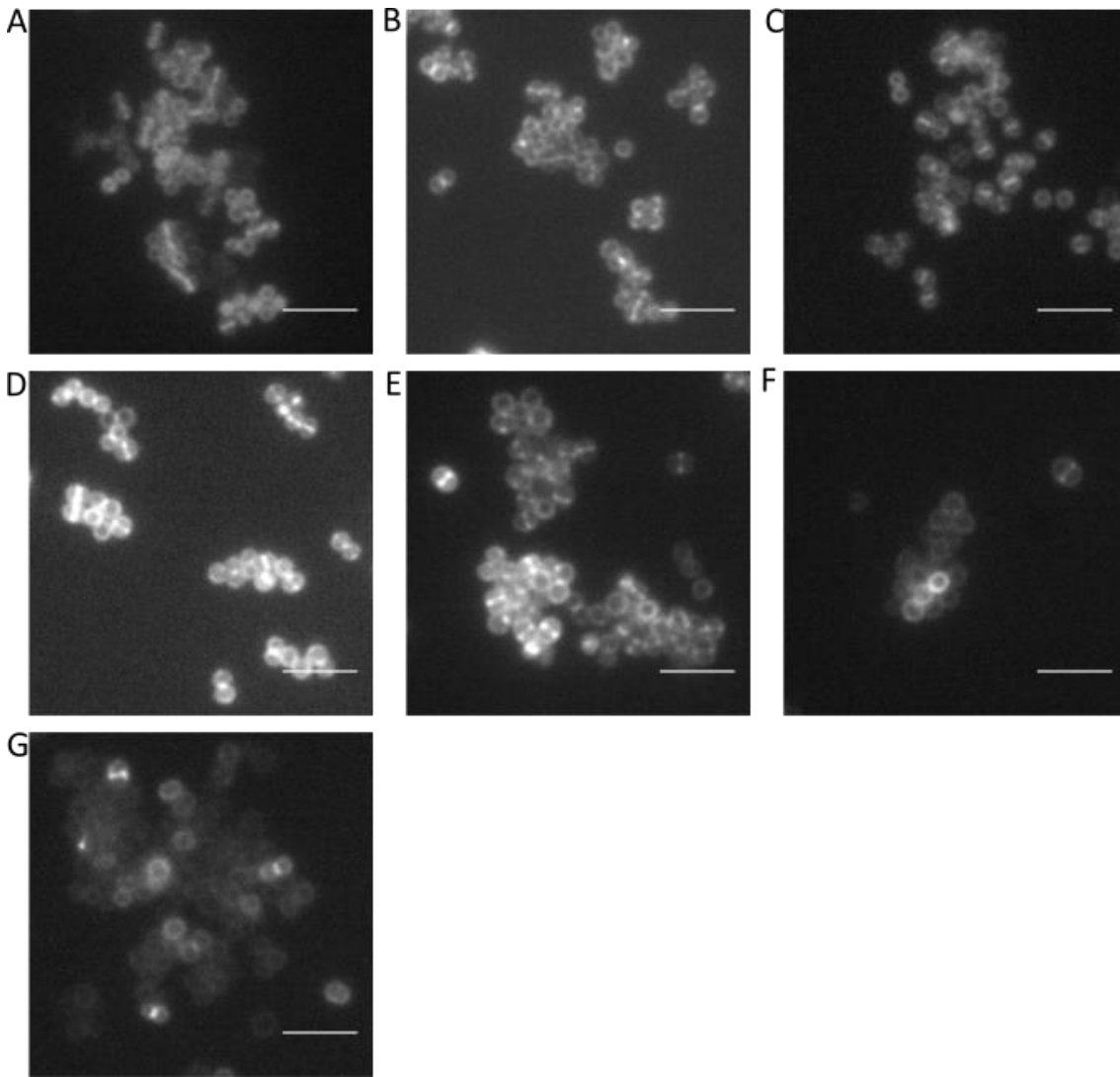


Figure 3.18. Labelling *S. aureus* SH1000 peptidoglycan synthesis with dipeptide (1 mM) during treatment with D-cycloserine at 10 x MIC (500 µg ml⁻¹). Labelling was carried out for 5 minutes during treatment. (A) No D-cycloserine, (B) 0-5 min treatment, (C) 5-10 min treatment, (D) 10-15 min treatment, (E) 15-20 treatment, (F) 20-25 min treatment, (G) 25-30 min treatment. (Scale bar 5 µm).

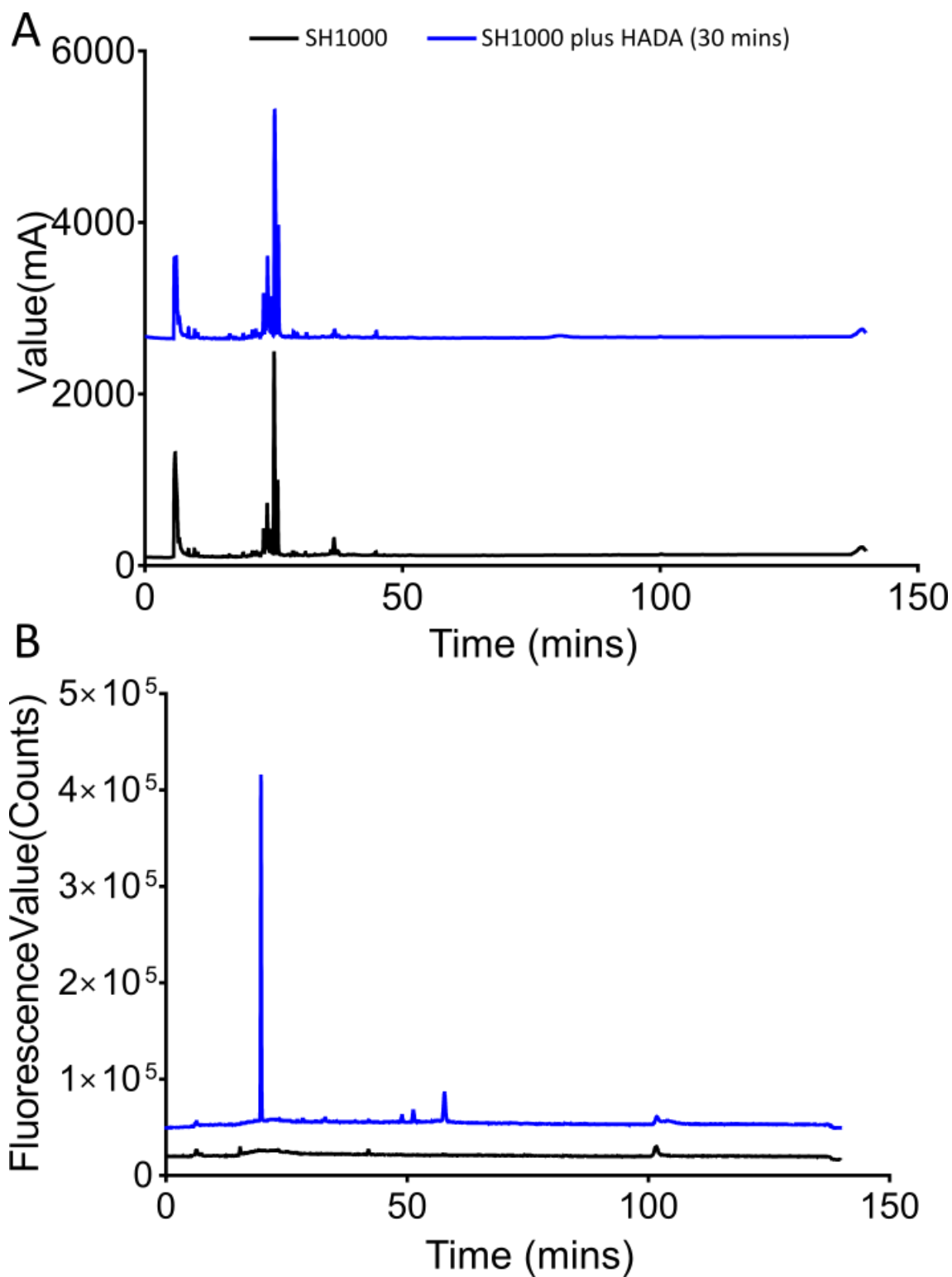
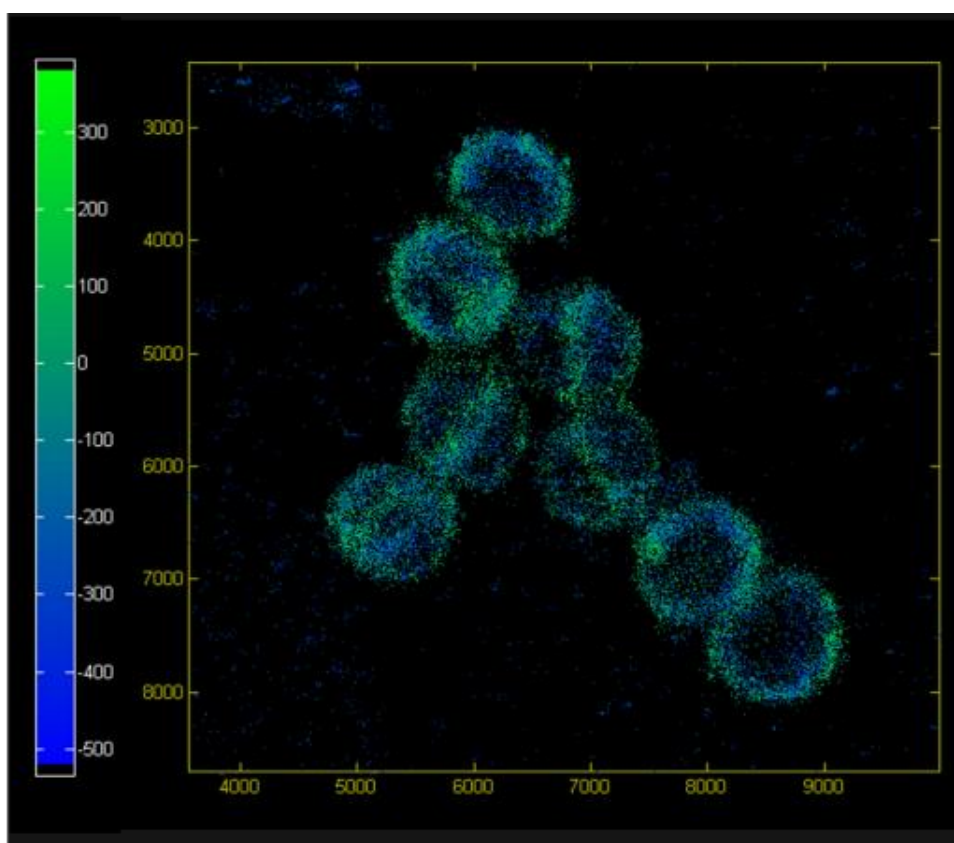
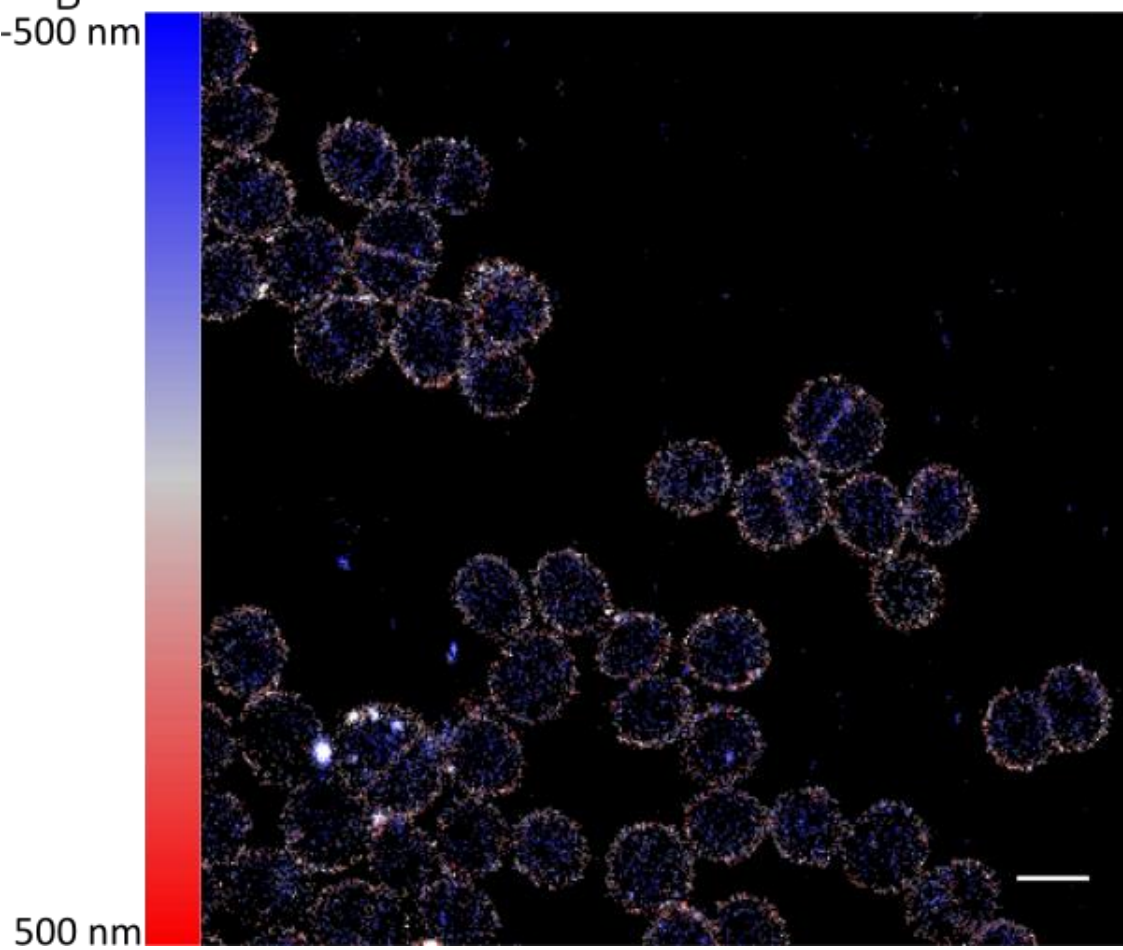


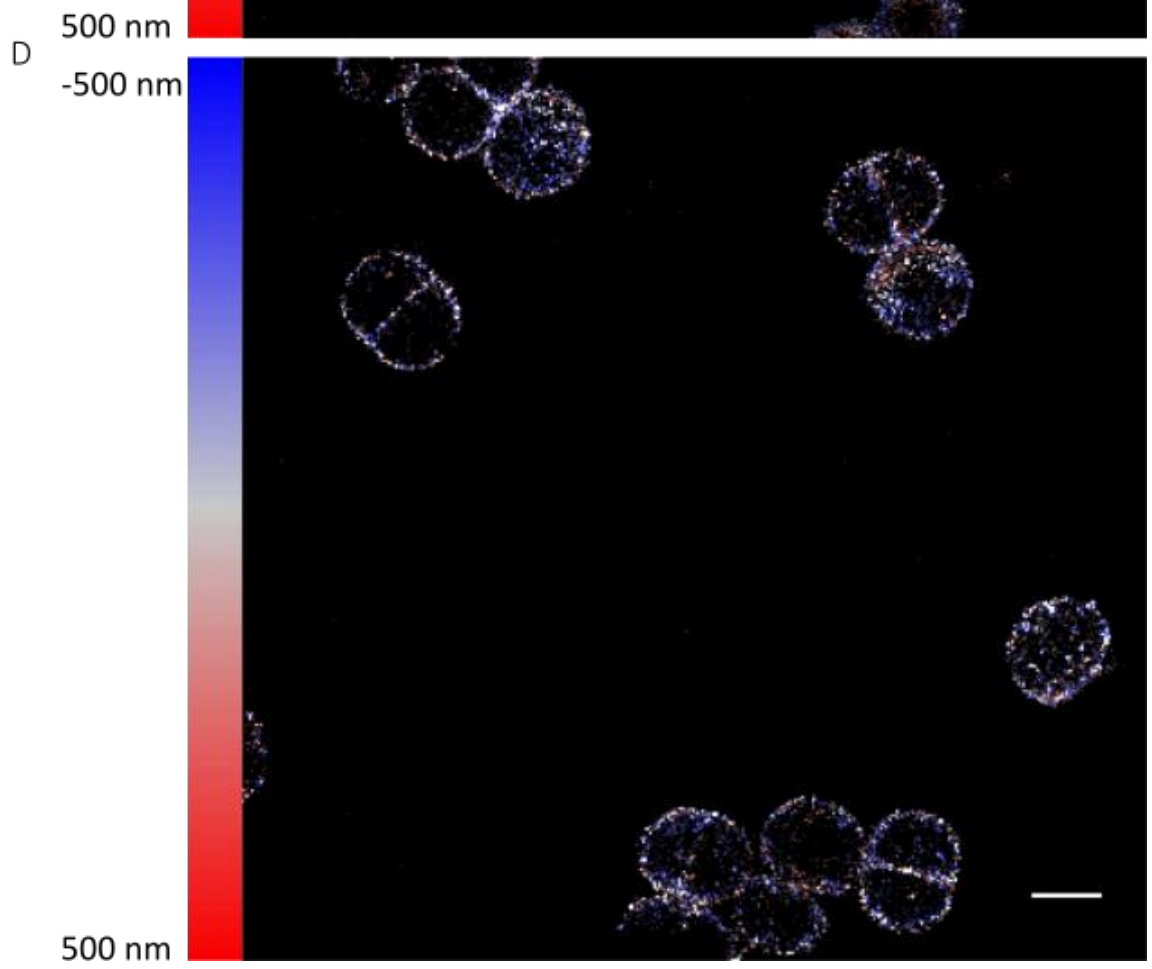
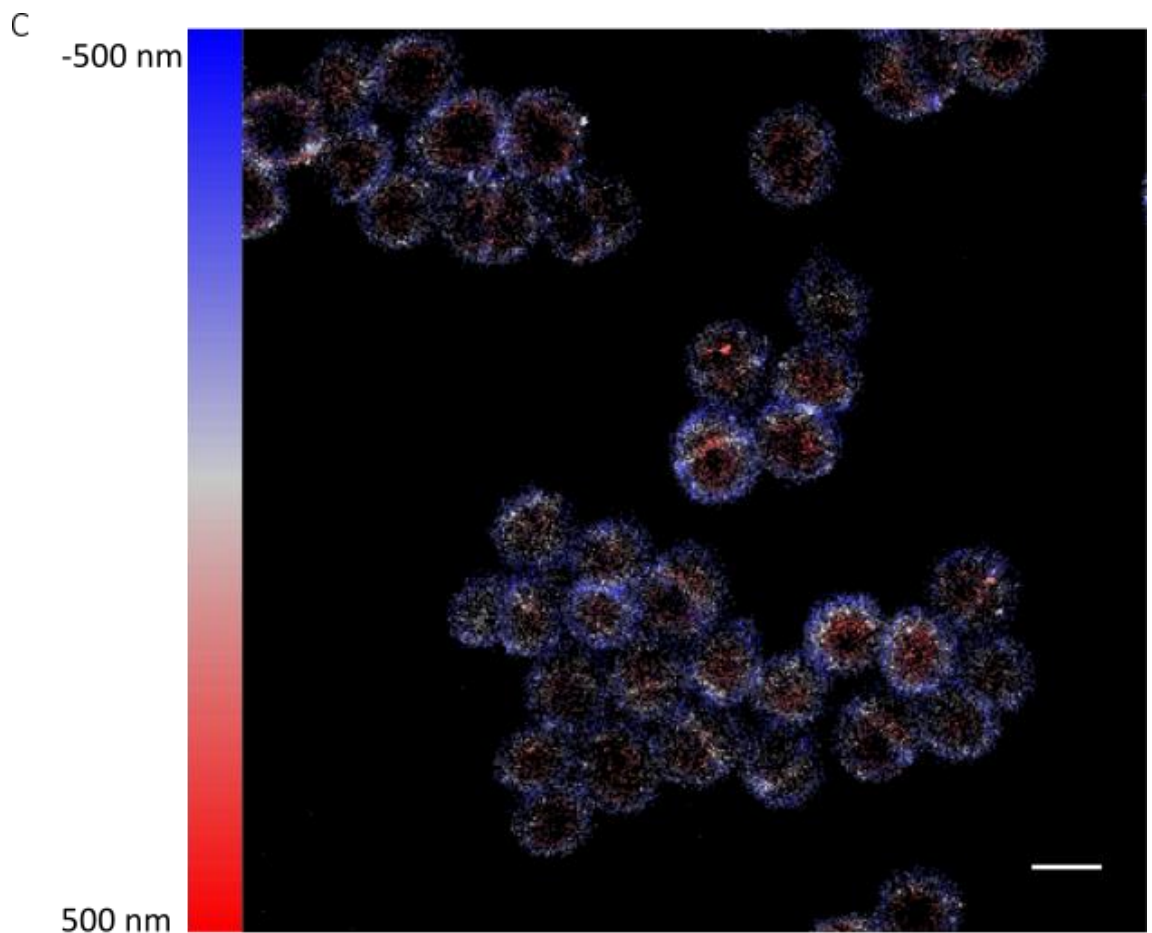
Figure 3.19. Biochemistry of FDAA labelling of *S. aureus* peptidoglycan. Reverse phase C_{18} HPLC Traces of SH1000 peptidoglycan (Black) and 30 min HADA (500 μ M) labelled SH1000 peptidoglycan (Blue) following digestion with mutanolysin and lysostaphin A) UV absorbance at 202 nm, B) fluorescence value (Excitation 360 nm, Emission 457 nm).

A



B
-500 nm





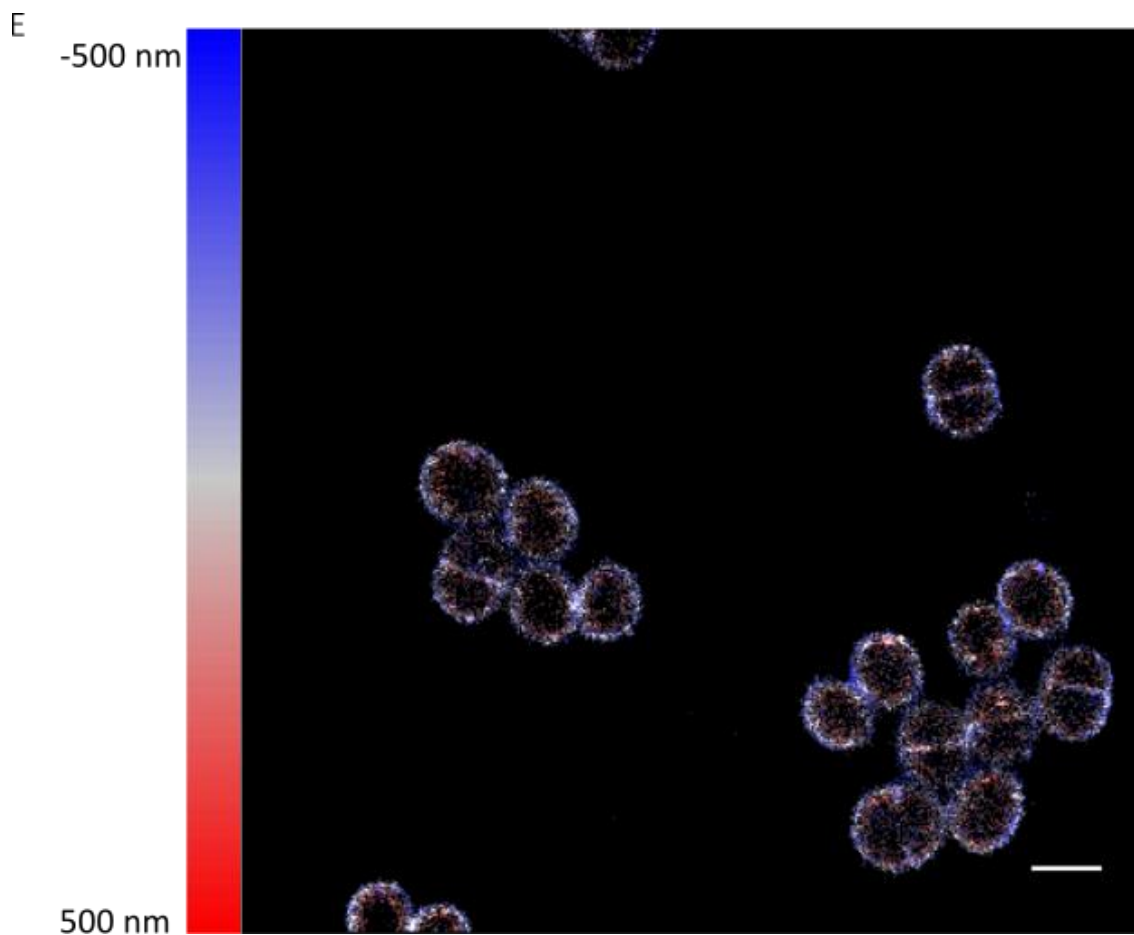


Figure 3.20. Testing fluorescent dyes in STORM. (A) Tetramethylrhodamine (TMR) (Linked to ADA labelled *S. aureus* via Click reaction, 5 minutes labelling with ADA at 500 μM). (B) Alexa Fluor 647 (NHS-ester labelled *S. aureus*, 8 μM). (C) Alexa Fluor 647 vancomycin at 1 mM (GLOX 100 mM MEA). (D) Alexa Fluor 647 vancomycin at 1 mM (GLOX 10 mM MEA) (E) Amersham Cy3B (NHS-ester labelled *S. aureus*, 16 μM). (Scale bar 1 μm).

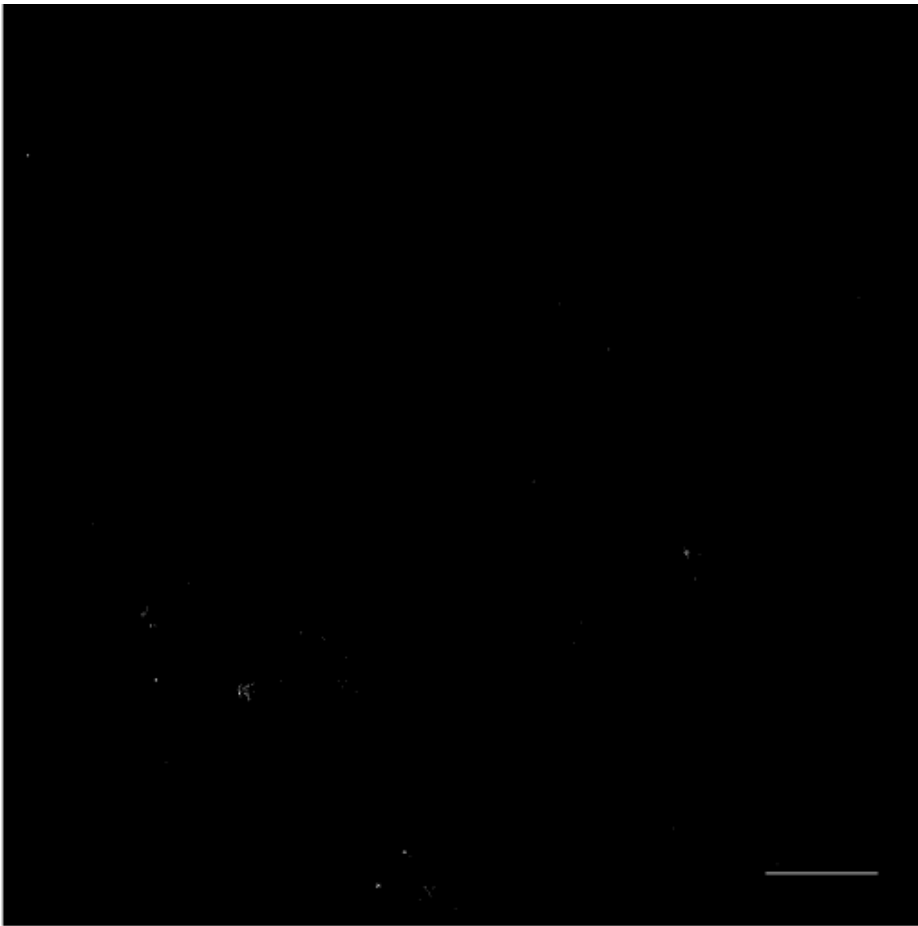
dSTORM (Jones et al., 2011). TMR was attached to the *S. aureus* cell wall via click reaction to ADA and imaged by dSTORM (Figure 3.20 A). Despite investigation with a number of different buffer conditions (50mM Tris containing 10 mM NaCl (pH 8.0), 100 mM MEA, GLOX, GLOX containing 100 mM MEA) imaging with TMR could not be improved from the example shown. Another well studied group of dyes for use in STORM include cyanine based dyes such as Alexa Fluor 647 (Henriques et al., 2011; Jones et al., 2011). Using an Alexa Fluor 647 NHS ester to label the cell surface, *S. aureus* cells were imaged using the NSTORM system (Figure 3.20 B). With this dye it was possible to achieve good resolution in both lateral and axial dimensions. Previous work had shown optimal imaging conditions in GLOX buffer containing 10mM mercaptoethylamine (MEA) (Dempsey et al., 2011). When Alexa Fluor 647 was used within some labelling systems, such as when Click labelled to FDAAs and in use as an NHS ester it was beneficial to increase MEA concentration to 100 mM. Conversely when AlexaFluor 647 was linked to vancomycin image reconstruction was improved with the lower MEA concentration (Figure 3.20 C & D).

In order to explore dual colour STORM it was necessary to have a second STORM compatible dye spectrally compatible with Alexa Fluor 647 and functional in GLOX MEA buffer. One of the possible compatible dyes was Amersham Cy3B. When testing the NHS ester version of this dye to label the bacterial cell surface, it was possible to achieve good resolution and image reconstruction within GLOX 100 mM MEA (Figure 3.20 E). Therefore, in dual colour STORM experiments Amersham Cy3B and Alexa Fluor 647 were used as the two dyes.

3.2.2.2 Controls for STORM

With a sensitive microscopy technique such as STORM it is important to determine the presence and contribution of localisations in the absence of the imaging label so that they may be taken into account when analysing data. To determine the presence of autofluorescence at imaging wavelengths, *S. aureus* that was not labelled with any fluorophores were imaged under the same imaging conditions as in other experiments (Figure 3.21). The number of identified autofluorescence molecules were for Alexa Fluor 647 imaging <500 and for Amersham Cy3B imaging ~3,000. Those within Amersham Cy3B were found to be cell associated. However, this signal was determined not to be at a level at interfere with analysis of labelling pattern.

A



B

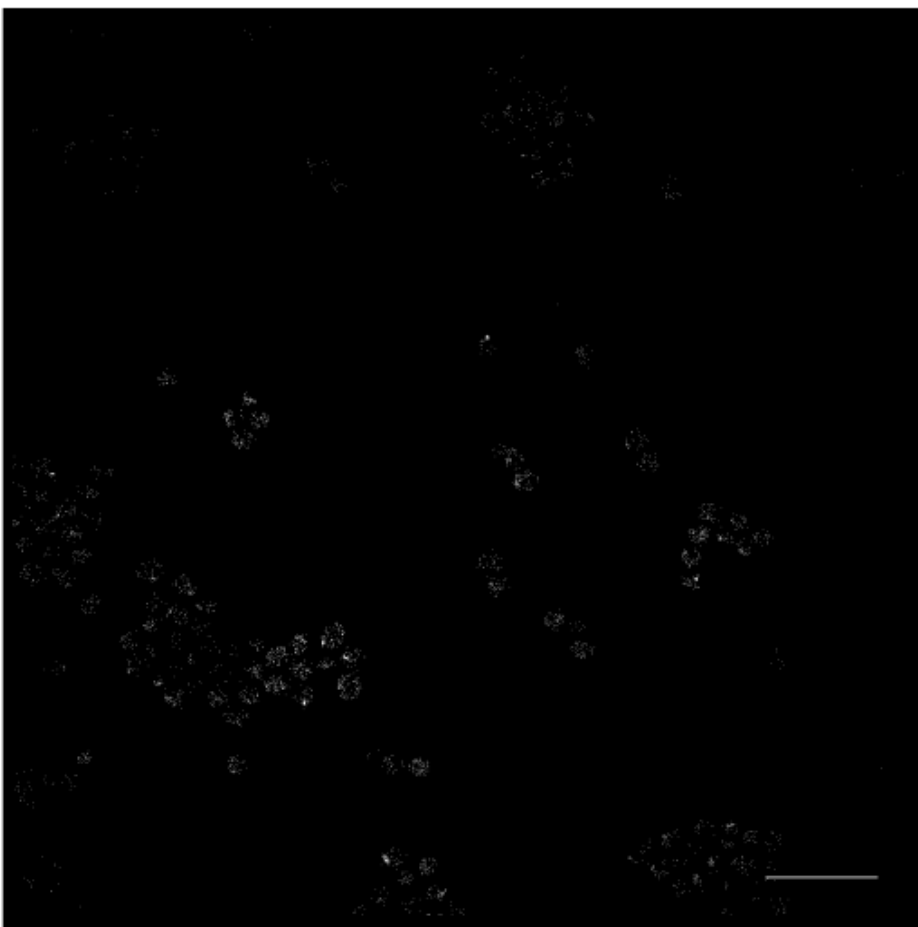


Figure 3.21. Autofluorescence detection in STORM. SH1000 without attached fluorescence were imaged using imaging conditions for both (A) Alexa Flour 647 and (B) Amersham Cy3B. Number of molecules detected were 388 and 3941 respectively. (Scale bar 5 μm).

The amount of cross talk for each of the dyes used was determined by imaging NHS ester-Cy3B or Vancomycin-Alexa Fluor 647 labelled cells under standard imaging conditions for both 538 nm and 647 nm (Figure 3.22). The cross talk seen was cell associated however, was not deemed to be significant enough to cause misinterpretation during dual colour STORM experiments. Another source of non-specific localisations within STORM samples could come from binding of the Alexa Fluor dyes to *S. aureus* during the click reaction used to attach STORM dyes to FDAAs. To determine any background pattern *S. aureus* that was not labelled with any FDAAs was click labelled with Alexa Fluor 647 and STORM imaged using normal imaging conditions. The resultant plot showed that while there is fluorescent signal associated with the cells there is no pattern of labelling (Figure 3.23).

3.2.3 Using SIM in *Staphylococcus aureus*

3.2.3.1 Testing FDAAs in SIM

The synthetic fluorescent dyes attached to FDAAs are promising SIM compatible dyes however when *S. aureus* labelled with FDAAs at normal labelling conditions (from Chapter 3.2.1.2) were imaged using SIM the samples bleached before acquisition of the z-stack was completed. This prevents the processing algorithm from reconstructing images that accurately represent the sample. Since FDAAs are apparently non-toxic to cells labelling was carried out with increased concentrations of FDAAs and imaged using SIM. It was found that labelling for 5 minutes with FDAAs at 10 x normal labelling conditions (i.e. 5 mM) allowed for reconstruction of images within SIM (Figure 3.24). This was true for the three FDAAs with intrinsic fluorophores however was not the case for Alexa Fluor 647 (Figure 3.24 D). It would be possible to use the ADA or dipeptide labels and attach a different fluorophore however since a fourth label was not required this was not pursued further.

3.2.3.2 The problem with SIM

While in theory SIM increases resolution by a factor of 2 and therefore can increase the spatial information we can gain from microscopy images, when interpreting structures close to the resolution limit it is important to be aware of the appearance of artefacts within the image (Georgieva and Nollmann, 2015; Gustafsson, 2005). In particular, the appearance of a residual stripe pattern originating from the illumination grating (Schaefer et al., 2004). One way to determine the presence of an underlying

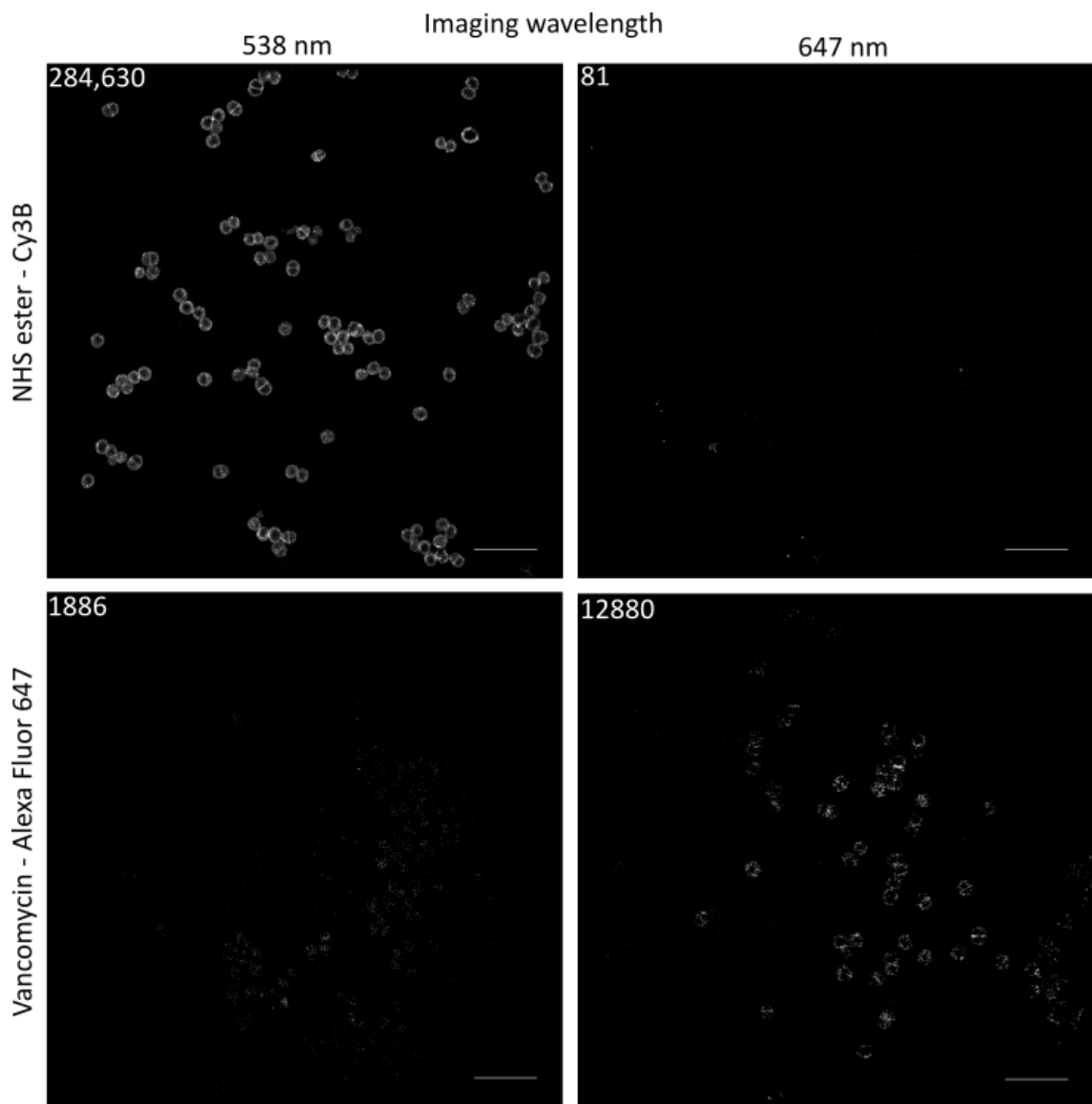


Figure 3.22. Determining crosstalk of Alexa Fluor 647 and Amersham Cy3B. *S. aureus* labelled with either NHS ester-Cy3B (16 μ M, Top Row) or Vancomycin-647 (1 mM, bottom row) were imaged under normal conditions for both 538 nm (left hand column) and 647 nm (right hand column). Numbers in the top left hand side of each image indicates the number of identified molecules. (Scale bar 5 μ m).

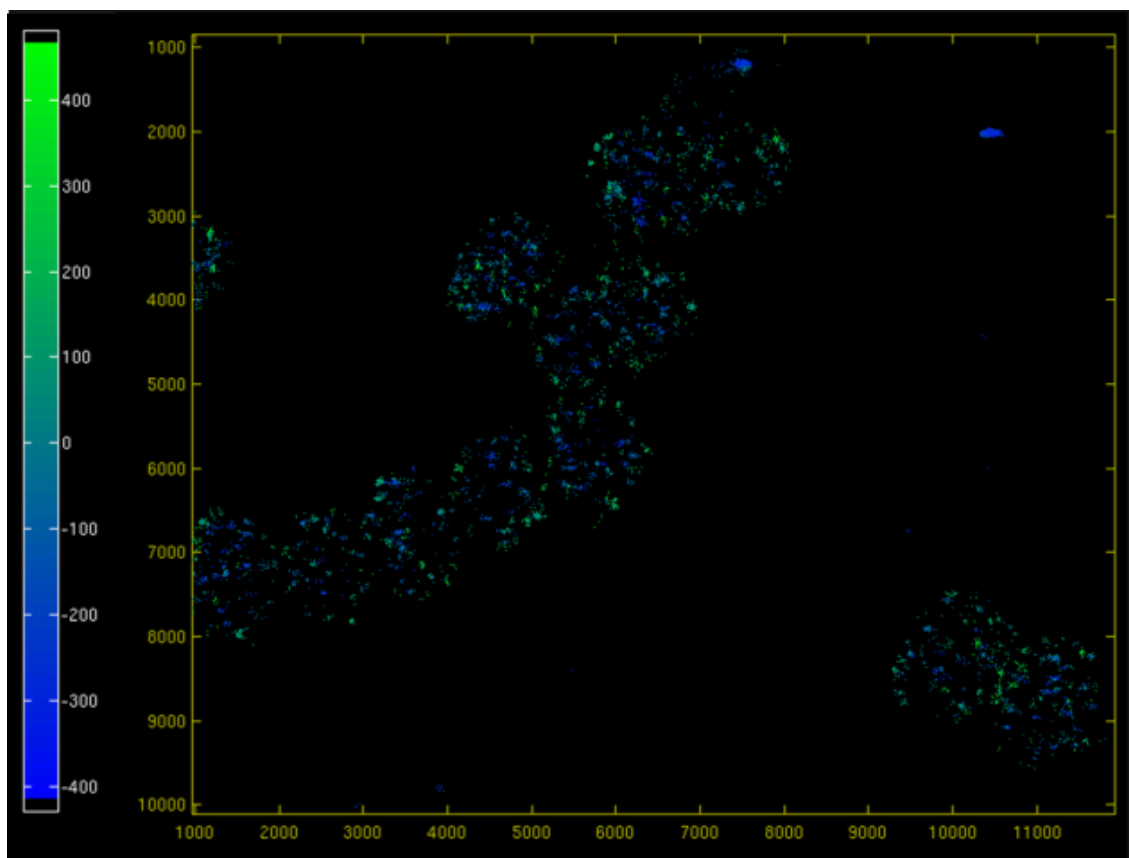


Figure 3.23. STORM of SH1000 labelled by the Click reaction in the absence of Click compatible FDAA. Click reaction containing Alexa Fluor 647 alkyne at $5 \mu\text{g ml}^{-1}$.

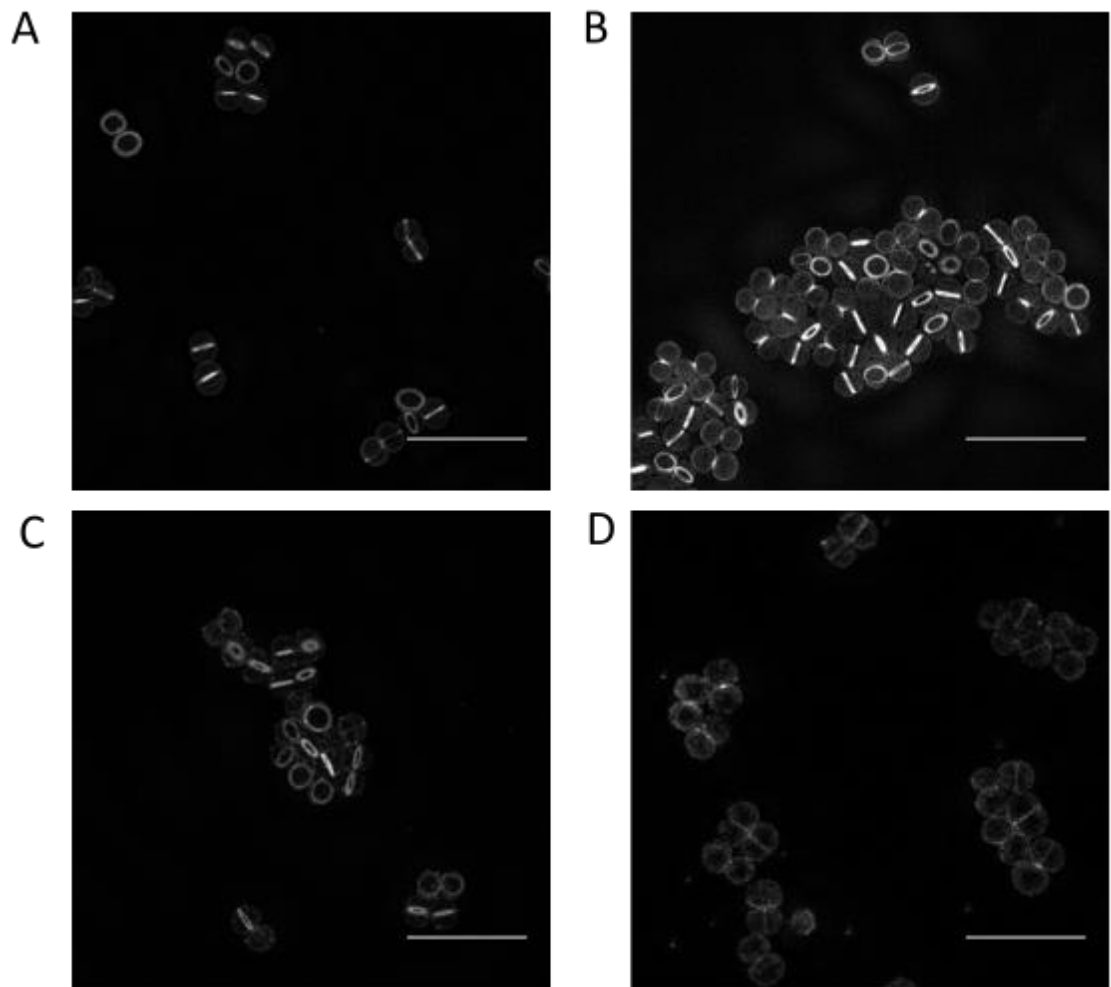


Figure 3.24. Testing peptidoglycan labels in structured illumination microscopy.

Images are shown as maximum intensity projections A) HADA at 5 mM, B) NADA at 5 mM, C) TADA at 5 mM, D) 0.1 μ M vancomycin-647. Scale bar 5 μ m.

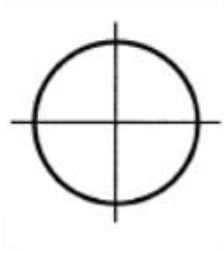
pattern within an image, such as that derived from illumination, is to carry out a Fourier transform of an image. Fourier transforms plot sample structure in reciprocal space. Therefore in resultant Fourier transformed images low resolution information is plotted close to the origin and higher resolution information is plotted further away (Gustafsson, 2000). For example, when a Fourier transform of a diffraction limited image is taken this is plotted as a circle of the observable region in reciprocal space (Figure 3.25 A). However, when structured illumination is used the Fourier transform image has a petal shape for this observable region (Figure 3.25 C). This is because the lateral shifts of the grating result in moiré fringes of the circle from diffraction limited (Figure 3.25 B) and this is repeated for each angle. Therefore, information has been gathered for a region double the size of what can be gathered from a diffraction limited image, hence the increase in resolution. Within these transformed images it is possible to see any underlying structure within the image. For example, the Fourier transform of the HADA labelled sample from Figure 3.24 is shown in Figure 3.25 D-F. While the Fourier transform of the middle of the z-stack (Figure 3.25 D) shows limited structure, Fourier transforms from the bottom (Figure 3.25 E) and Top (Figure 3.25 F) show more distinct patterns such as lines and repeating dots in imaging angles. This suggests an underlying pattern and therefore caution must be used in analysis of this data. For all SIM data found in this thesis corresponding Fourier transforms can be found in Appendix II. In practice therefore SIM can be used to crisp up diffraction limited images however should not be used to determine any new biology, particularly regarding an underlying pattern of fluorescent signal.

3.3 Discussion

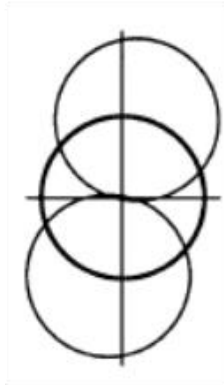
3.3.1 Labelling peptidoglycan synthesis in *S. aureus*

Since the development of FDAAs in 2012 they have been found to be a useful tool in the field of bacterial cell wall research. Compared to previous techniques FDAAs provide a direct and covalent means of labelling peptidoglycan synthesis (Kuru et al., 2012). Unlike D-cysteine or fluorescent antibiotic labelling of peptidoglycan synthesis, FDAAs are compatible with live cell labelling since fixation is not required for imaging. Also of advantage is the application of different coloured FDAAs in virtual time-lapse since the addition of each new probe indicates the location of peptidoglycan synthesis during the labelling period (Kuru et al., 2012). The dynamics of peptidoglycan synthesis

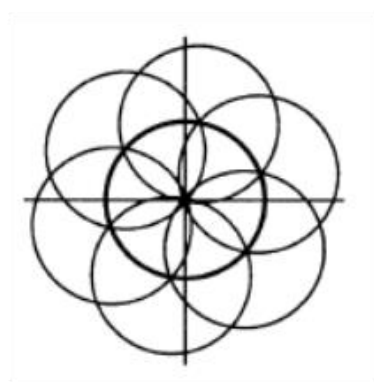
A



B

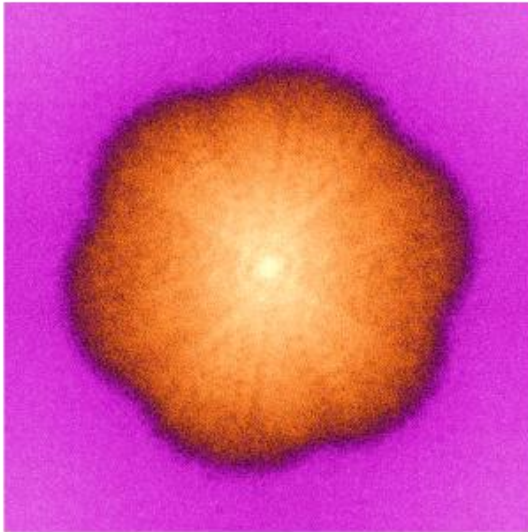


C



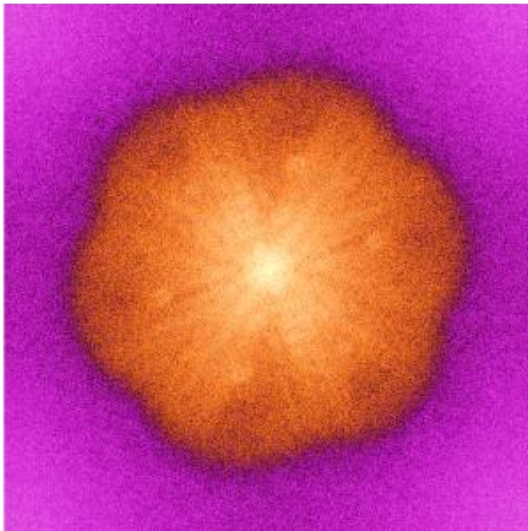
D

Middle of z stack



E

Bottom of z stack



F

Top of z stack

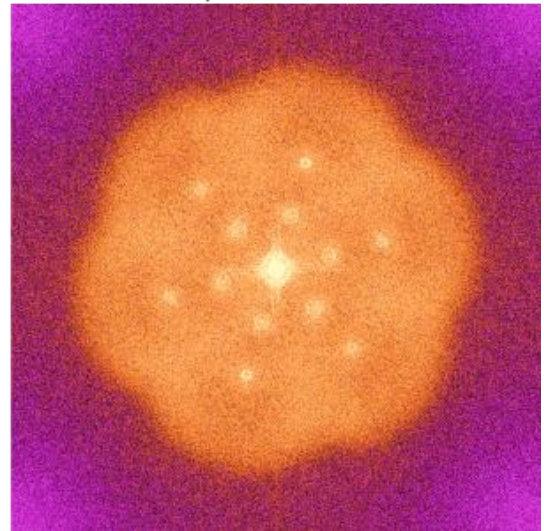


Figure 3.25. Fourier transforms can detect underlying structure in SIM images.

Schematic of Fourier transforms of (A) a diffraction limited image, (B) Moiré fringes due to shifting of the grating pattern and (C) the petal pattern resulting from the use of 3 angles during image acquisition. Adapted from (Gustafsson, 2000). Fourier transform of the z-stack of the HADA labelled sample shown in Figure 3.24 A, from the middle (D), bottom (E) and top (F) of the stack.

can now be assessed over much longer periods of time than previously possible as well as in detail at shorter timescales.

Taxonomically diverse bacteria have been shown to have tolerance for the incorporation of FDAAs, therefore FDAAs have been used across bacterial species to investigate new features of peptidoglycan synthesis. For example, application of FDAAs and 3D SIM in *Streptococcus pneumoniae* discovered a new mode of peptidoglycan synthesis within elongation (Cadby and Lovering, 2014). Peripheral synthesis in *S. pneumoniae* is different from that in rod shaped organisms as it has been shown to occur at the pinched site near the septum. Using FDAAs within *S. pneumoniae* at the mid-to-late stage of cell division peptidoglycan synthesis was located to an outer ring and an inner spot of synthesis with the inner spot associated with PBP2x activity (Tsui et al., 2014).

Another example of FDAAs being used to investigate peptidoglycan within bacterial species has been in the application of FDAAs to the so-called “chlamydial anomaly” (Liechti et al., 2013; Pilhofer et al., 2013). Chlamydial species have been known to contain peptidoglycan synthetic genes within their genomes and are susceptible to cell wall targeting antibiotics (e.g. D-cycloserine and penicillin) however peptidoglycan has not previously been found within *Chlamydia*. Using single amino acids FDAAs it was not possible to detect PG, however the development of a D-alanyl-D-alanine dipeptide probe allowed replicating chlamydiae to be labelled, presumably via incorporation into peptidoglycan (Kuru et al., 2015; Liechti et al., 2013).

However, despite the applications of FDAAs in peptidoglycan synthesis labelling, a consensus is yet to be reached concerning the labelling mechanism. The promiscuity of peptidoglycan metabolic enzymes across bacterial species to the incorporation of both natural and unnatural D-amino acids is well known (Cava et al., 2011; Shieh et al., 2014). Non-canonical D-amino acids (NCDAAAs) are produced by bacteria in stationary phase and their incorporation into peptidoglycan is thought to be important in the control of cell wall metabolism (Lam et al., 2009). Control of peptidoglycan metabolism is proposed to occur via both their incorporation into the peptidoglycan peptide stem and via regulation of peptidoglycan modification enzymes. There are two distinct processes by which NCDAAAs (and therefore FDAAs) may incorporate into

peptidoglycan; either by periplasmic editing of mature peptidoglycan or via incorporation into peptidoglycan subunits in the cytosol (Cava et al., 2011). NCDAAs have been found in both position 4 and 5 in the peptide stem of peptidoglycan via HPLC, the two different positions suggest different incorporation pathways. Formation of NCDAAs in position 4 is dependent upon L,D-transpeptidase reaction in multiple Gram negative species. However NCDAAs were not found in position 4 in Gram positive species tested but instead in position 5 (Cava et al., 2011). For position 5 incorporation within *B. subtilis* the process was determined to be via an extracytoplasmic process catalysed by a D-D-peptidyl transferase. Within the tested Gram negative species formation of NCAAs in position 5 was found to likely occur via peptidoglycan precursors. Since other Gram positive species were not tested it is not possible to determine whether this mechanism is specific to *B. subtilis* or more general, especially since Ddl and MurF are conserved among bacteria suggesting this difference may be attributed to transport mechanisms as opposed to ability of cytoplasmic proteins to incorporate NCDAAs (Cava et al., 2011).

There have been several reported mechanisms for the labelling of peptidoglycan with D-amino acid derivatives. FDAAs were found to incorporate in position 4 in *E. coli* and *Agrobacterium tumefaciens* and in position 5 in *B. subtilis* (Kuru et al., 2012). Comparing this with previous work on NCDAAs it was hypothesized that FDAAs label via extracytoplasmic reactions mediated by L,D-transpeptidases (Ldts) in Gram negatives and PBPs in Gram positives. At the same time as FDAAs were developed, a second group utilised D-amino acids functionalised with azide and alkyl groups to label peptidoglycan *in vivo* (Siegrist et al., 2013). They postulated that these D-amino acids were incorporated via the biosynthetic pathway with the same two possible pathways as hypothesized for NCDAAs. They determined that the pathway used would determine the position that D-amino acid reporters would be located on the peptide sidechain; periplasmic editing of mature peptidoglycan would result in labelling in either the 4th or 5th position while cytosolic incorporation into precursors would result in labelling in position 5 only (Siegrist et al., 2013). Since in many bacteria the 5th position is rapidly processed, the presence of labelled D-amino acids in position 5 is presumed to be labelling of new peptidoglycan irrespective of the labelling

mechanism. However since *S. aureus* has low carboxypeptidase activity the picture is not as clear (Scheffers and Pinho, 2005; Siegrist et al., 2013).

In this thesis I was unable to identify the position of FDAAs within the *S. aureus* peptidoglycan despite identification of a fluorescent peak during HPLC analysis. This is most likely due to the low abundance of material. It is presumed that FDAAs will label only a small proportion of the peptidoglycan, particularly since the presence of such a big additional group is likely to interfere with the processing of peptidoglycan. There are a number of different approaches to take in order to resolve this including increasing the portion of labelled material by incubating *S. aureus* cultures with a saturating concentration of HADA. In addition, this could be done in the presence of a D-alanine racemase inhibitor or a mutant strain however, this may prove toxic to the cells. Other approaches include using different enzymes for peptidoglycan digestion or the use of a radioactive derivative of HADA as detection and quantification of radioactivity is easier than the detection of fluorescence using the analysis systems available. It may also be possible to increase the amount of labelling in a mutant strain that had increased labelling for example an autolysin mutant or strain with decreased crosslinking. However, a strain with increased FDAA labelling has not yet been identified.

The complete blockage of FDAA labelling by antibiotics that inhibit the early stages of peptidoglycan synthesis (D-cycloserine) while treatment with antibiotics that inhibit the extracytoplasmic assembly enzymes (penicillin) allows a mechanism of FDAA labelling in *S. aureus* to be proposed. The majority of peptidoglycan labelling is due to synthesis of precursors, the single FDAA is joined into a dipeptide by the D-alanine-D-alanine ligase (Ddl) and then attached to the precursor via MurF. This MurF step is also the proposed incorporation step of the dipeptide label. However, one cannot rule out the possibility of FDAA labelling occurring via an extracytoplasmic exchange reaction catalysed by the PBPs (Kuru et al., 2012, 2015; Qiao et al., 2014). The dipeptide label has to be incorporated by synthesis, while single FDAAs may be incorporated by both pathways (Liechti et al., 2013). Complete removal of labelling by D-cyloserine suggests that the single FDAA does indeed insert via the cytoplasmic steps, however since D-cyloserine is a substrate analog it is also possible that its presence can inhibit any potential exchange reaction. The decrease in signal from dipeptide labelling during

moenomycin treatment, while fluorescence is maintained with the HADA label suggests that insertion of the dipeptide label requires transglycosylase action whereas HADA incorporation does not. Once moenomycin is added, the transglycosylase reaction will be inhibited and the rest of the synthesis pathway will also stop to prevent build-up of excess lipid II, preventing dipeptide incorporation. However, HADA will be free in the periplasm where it can be incorporated via the exchange reaction. This suggests that even with the inhibition of synthesis the level of labelling is maintained due to an increase in exchange reaction.

There are 4 PBPs in *S. aureus*, with PBP4 being the most plausible candidate for D-amino acid exchange. PBP4 is a low molecular weight PBP, however surprisingly it has transpeptidase activity both *in vitro* and *in vivo* (Qiao et al., 2014). It is a promiscuous enzyme that can interact with both new peptidoglycan and lipid II monomers, suggesting a biological role in incorporating additional crosslinks to increase rigidity, indeed peptidoglycan from a strain lacking PBP4 has reduced crosslinking (Curtis et al., 1980; Qiao et al., 2014). Both *in vivo* and *in vitro* studies show that PBP4 can use both lipid II and peptidoglycan as a substrate for FDAA probes (Qiao et al., 2014). It is possible to suggest that both cytoplasmic incorporation of FDAAs and extracytoplasmic exchange mediated by PBP4 are involved in FDAA peptidoglycan labelling in *S. aureus*. This poses the question, do FDAAs still label peptidoglycan synthesis within *S. aureus*? Since PBP4 was shown to bind and activate nascent peptidoglycan and lipid II it is reasonable to assume that all labelling mediated by PBP4 occurs only at the sites of new peptidoglycan therefore all detected fluorescent signal from FDAA labelling can be attributed to the location of peptidoglycan synthesis (Qiao et al., 2014).

One approach to avoiding any complications from multiple labelling mechanisms is to use a label which solely labels via the cytoplasmic labelling pathway. The D-alanyl-D-alanine dipeptide probe developed by Kuru and colleagues can be used as a synthesis only label (Kuru et al., 2015). The dipeptide probe bypasses the Ddl enzyme and enters the cytoplasmic pathway via MurF (Liechti et al., 2013). By comparing labelling patterns of cells labelled with single FDAAs and with dipeptide it is possible to determine if there are any additional patterns that do not arise from peptidoglycan synthesis during. This is of particular use since currently the dipeptide is only available

with functionalized groups and therefore does not have as widespread an application as the single FDAAs.

A further approach to deciphering labelling mechanisms is to use an *in vitro* analysis to assess the ability of enzymes within the peptidoglycan biosynthesis pathway to use FDAAs as substrates. Thereby it may be possible to determine the ability of PBP4, Ddl and MurF from *S. aureus* to use FDAAs without the complexity of whole cell systems. Looking at the *in vitro* ability of purified systems to incorporate labels into peptidoglycan can unravel mysteries surrounding incorporation pathways as well as informing future development of peptidoglycan labels (Lebar et al., 2014).

Following the success of FDAAs in labelling peptidoglycan synthesis it is wise to question whether there are any other means of labelling peptidoglycan synthesis. Particularly by using a similar approach i.e. fluorescent or functionalised derivatives of components of bacterial muropeptides. Due to the presence of L-amino acids in a large number of structures labelling any L-enantiomers in the peptide sidechain would lead to high background labelling of proteins and other structures. The same is true for labelling of the peptide crossbridge, which in *S. aureus* is attached to the muropeptide before it traverses the membrane by the Fem system (Münch et al., 2012). This leaves the D-glutamic acid in position 2 as a possible site for labelling. However, this amino acid is amidated at the α -carboxyl to produce D-iso-glutamine by the essential GatD/MurT enzyme complex suggesting that labelling at this position may prove lethal (Figueiredo et al., 2012; Münch et al., 2012).

The other structure which can be probed for peptidoglycan synthesis is the sugar backbone. This repeating GlcNAc-MurNAc structure is produced via the same process across bacterial species (Typas et al., 2012) suggesting that sugar labelling would be a universal peptidoglycan synthesis probe. However, during the synthesis of peptidoglycan GlcNAc goes through a number of different reactions limiting the sites at which a functionalised group can be added (Navarre and Schneewind, 1999). Other possibilities include labelling of MurNAc either on the sugar or within the lactyl group, however there is unlikely to be a transport protein that will allow the ingress of these labels into the cytoplasm. In the same manner, feeding cells with labelled lipid II is unlikely to lead to labelled peptidoglycan. Despite the many possible limitations, these

sugar-based probes should not be dismissed out of hand. An azide derivative of GlcNAc (GlcNAz) has been successfully used to label *S. aureus* (Mommel et al., 2013). However, this probe has the ability to label glycoproteins, glycolipids and extracellular polysaccharides in addition to peptidoglycan and the specificity of labelling from this probe has not yet been determined.

3.3.2 Using super-resolution microscopy in *S. aureus*

Due to the small size of bacterial cells, super-resolution techniques have proved particularly powerful. Light microscopy is limited by resolution which restricts localisation within bacterial cells. Electron microscopy has been able to increase resolution due to the subnanometre wavelength of electrons however identification of specific structures (e.g. individual proteins) is not always possible and EM is not compatible with live cells (Coltharp and Xiao, 2012). Recent advances in super-resolution microscopy techniques have achieved resolutions of 10-50 nm while taking advantage of labelling specificity and live cell compatibility that is possible with light based microscopy techniques.

The first developed super-resolution microscopy technique was stimulated-emission-depletion microscopy (STED) (Hell and Wichman, 1994). A depletion pattern surrounds the excitation laser, bringing excited fluorophores to ground state before it can emit fluorescence thereby reducing the area of molecules that can fluoresce (Hell and Wichman, 1994). In theory this system has unlimited resolution however aberrations in optics, scattering from the sample and photostability of fluorophores means that the current maximum achieved resolution is 6 nm. However, this occurred studying fluorescent defects in diamonds, a process with minimal photobleaching. In biological samples the best resolutions achieved are 20 nm with organic dyes and 50-70 nm with fluorescent proteins (Huang et al., 2010). A further advantage of STED is the application with live samples, especially when sample size is small for example imaging bacteria. *S. aureus* labelled with any of the FDAAs would be ideal samples for STED however since complex instrumentation is required it was not possible to test this.

Structured illumination microscopy (SIM) also uses patterned illumination to achieve super-resolution however it uses a positive pattern of illumination (Huang et al., 2010). Patterned light is passed across the sample so that each point on the sample is

illuminated, with multiple images taken per slice. The resultant images are processed via a reconstruction algorithm to produce an image of the sample with greater resolution. The advantage of SIM is that no special photophysics are required for fluorescent probes and similarly to diffraction limited microscopy, it is easily applicable to live cell microscopy (Huang et al., 2010). Despite this it is important to note that most practical applications of SIM suffer from the introduction of artefacts into images (Schaefer et al., 2004). Often these artefacts take the form of residual stripe patterns from the illumination and if not recognised they can influence analysis of images. With SIM it is often not possible to use it to discover new biology however images can make features seen in diffraction limited microscopy clearer.

The third super-resolution technique uses single molecule localisation technology. There are two main types: photoactivation localisation microscopy (PALM) and stochastic optical reconstruction microscopy (STORM). Probes cycle between a dark and light state such that in each frame only a subset of molecules are in a light state, allowing the centre of molecules to be precisely localised and a resolution of ~ 25 nm in the lateral dimension is therefore achievable (Jones et al., 2011). The advantage of such high resolution is that processes can be localised to within molecular resolution, however due to the high number of frames required for this high resolution it is limited in its application with live cells and therefore in the dynamics of structures (Coltharp and Xiao, 2012). Recent developments in reconstruction software and camera sensors allow for high throughput STORM by reducing image acquisition time and increasing fields of view suggest that live cell STORM may be more widely applicable in the future (Almada et al., 2015). Another limitation in the application is the availability of dyes and proteins compatible with STORM/PALM since they must be able to undergo special photophysics in order to be compatible (Henriques et al., 2011). This is particularly problematic within fluorescent proteins. However, there are currently a number of synthetic dyes compatible with STORM that can be used in conjunction with cell wall labelling.

Future development of super-resolution microscopy is currently focussed on the development of correlative light and EM or AFM microscopy, such that the advantages of protein/structure localisation of super-resolution microscopy can be applied to the high-resolution images possible with EM and AFM (Coltharp and Xiao, 2012; Watanabe

et al., 2011). This has already been applied to EM where both STED and PALM microscopy has been correlated with EM within a number of different eukaryotic cell types (Watanabe et al., 2011). The application of correlative microscopy would be particularly advantageous in the investigation into the architecture of bacterial peptidoglycan to link what is known about the synthesis and chemistry of peptidoglycan with the overall cell wall structure seen by EM and AFM (Turner et al., 2014).

Chapter 4

Analysis of the pattern of peptidoglycan synthesis in *Staphylococcus aureus*

The work in this chapter was carried out in collaboration with Christa Walther & Robert Turner (STORM & SIM microscopy).

4.1 Introduction

4.1.1 Cell wall architecture in *S. aureus*

Peptidoglycan architecture is important in maintaining cell morphology and viability (Wheeler et al., 2011). While the biochemical composition of peptidoglycan is well understood, it is only in recent years that the architecture and dynamics of the cell wall have begun to be resolved.

Traditionally peptidoglycan architecture was thought of in terms of glycan strand and peptide side chain orientation. Two opposing models were proposed; the first layered model (and modifications of that model) suggested that glycan strands were arranged parallel to the cytoplasmic membrane (Koch, 1998a; Verwer et al., 1978), whilst the second (scaffold model) suggested glycan strands were arranged perpendicular to the membrane (Dmitriev et al., 2003). While there has been greater support of the layered model neither is perfect and in the light of recent high resolution techniques it is apparent that peptidoglycan architecture is diverse across bacterial species (Turner et al., 2014; Vollmer and Höltje, 2004).

In Gram negative bacteria, particularly *E. coli*, the architecture of peptidoglycan was proposed to comprise of glycan strands parallel to the plasma membrane running circumferentially around the cell in a disorganised hoop-like fashion (Gan et al., 2008). More recently atomic force microscopy (AFM) studies has suggested that glycan strands are parallel to the cell surface but have no general orientation despite large scale circumferential organisation (Turner et al., 2013). This disordered architecture was found to appear in all tested Gram negative species, suggesting a common architecture throughout Gram negatives.

On the other hand Gram positive bacteria have been shown to have a number of different peptidoglycan architectures (Hayhurst et al., 2008; Turner et al., 2010a, 2014; Wheeler et al., 2011). AFM studies of *B. subtilis* peptidoglycan suggests the presence of ~50 nm peptidoglycan cables that run across the short axis of the cell (Hayhurst et al., 2008). Similar studies in ovococci bacteria showed that glycan strands preferentially orientate circumferentially, across the short axis and produce parallel bands of material, thought to be several intertwined glycan strands (Wheeler et al., 2011).

S. aureus has a dynamic peptidoglycan architecture consisting of thick bands, rings and knobbls that change as cells progress through division cycles (Turner et al., 2010a). Thick bands of material, known as piecrusts, encircle intact cells on the inner surface of the peptidoglycan sacculus. These thickenings are formed prior to the centripetal assembly of the septal disk and are proposed to specify the siting of division planes (Turner et al., 2010a). The third architectural feature, knobbls, occur due to remodelling of the septal ring architecture through autolysis during cell spitting and expansion of new hemispheres. *S. aureus* peptidoglycan architecture is produced by the balance of peptidoglycan synthesis and hydrolysis (Turner et al., 2010a; Wheeler et al., 2015).

Synthesis of new cell wall material in *S. aureus* has been shown to occur specifically at the cell division site, i.e. the septum (Pinho and Errington, 2003; Turner et al., 2010a). This synthesis occurs via the production of a ring of material (the piecrust) bisecting the cell, then the completion of the septal disk, associated with an apparent spiral septal architecture. In addition to AFM, transmission EM (TEM) of whole cells and extracted fragments has shown the progression of synthesis at the division septum to follow such a pattern (Matias and Beveridge, 2006, 2007). A thick peptidoglycan bridge is synthesised at the septum site in the mother cell wall, this is thought to correspond to the piecrust feature seen in AFM images (Turner et al., 2010). New peptidoglycan is added to the leading edge of the septum which appears to exist as two separate entities (Matias and Beveridge, 2007). As the septum grows in length it is also thickened by additional peptidoglycan synthesis or remodelling.

Previous work on the synthesis has relied on diffraction-limited microscopy, and as such, any models may miss features of peptidoglycan synthesis. In *E. coli* the

application of stochastic optical reconstruction microscopy (STORM) to determine localisation of peptidoglycan synthesis revealed multiple distinct foci of peptidoglycan insertion spread over the cell cylinder in addition to septal peptidoglycan insertion (Turner et al., 2013). Such application of super-resolution microscopy to *S. aureus* may reveal additional features in peptidoglycan synthesis.

4.1.2 *S. aureus* divisome

S. aureus is closely related to *B. subtilis* however, it has an apparently less complex mechanism of growth, in that it lacks an elongation phase. Therefore, while there will be conservation of the divisome, *S. aureus* is likely to be simpler with less redundancy. Homologs of genes essential in *B. subtilis* are putatively essential in *S. aureus* as well as some non-essential genes (Chaudhuri et al., 2009). This is likely due to the lack of genes with overlapping function in *S. aureus*.

Compared with *B. subtilis* and *E. coli*, *S. aureus* has a minimal biosynthetic machinery, likely due to the apparent single mode of synthesis (Pinho and Errington, 2003). *S. aureus* has only 4 PBPs, of these only 2 have been shown to be essential; PBP1 & PBP2 (Pereira et al., 2007; Pinho et al., 2001; Wada and Watanabe, 1998). PBP2 is a class A HMW PBP, with dual transglycosylase and transpeptidase activity while PBP1 is a transpeptidase only. Some evidence suggests that PBP1 essentiality is due only to the presence of the protein not necessarily its transpeptidase activity, however functional transpeptidation is required for normal growth (Pereira et al., 2009). As well as the PBPs, *S. aureus* encodes 4 other proteins with potential peptidoglycan biosynthetic roles: two monofunctional transglycosylases SgtA & MGT, and two auxiliary proteins FmtA & FmtB. All PBPs have been localised primarily to the septum as well as a number of other division proteins such as FtsZ, EzrA & GpsB (Pinho and Errington, 2003, 2005; Scheffers and Pinho, 2005; Steele et al., 2011). In addition to the 4 native PBPs, MRSA strains contain an additional PBP, PBP2A/MecA (Zapun et al., 2008b). In the presence of β -lactam antibiotics MecA is induced and can act as the only transpeptidase as it has low affinity for the drug present. In this case PBP2 remains essential since the transglycosylase activity is required (Pinho and Errington, 2005). Even with such a simplified set of enzymes required for peptidoglycan synthesis *S. aureus* is capable of growth when only 2 of these are expressed (Reed et al., 2015).

These are the 2 essential PBPs and depletion of either of these in the minimal peptidoglycan synthesis strain (COL MIN) results in arrested growth. COL MIN was shown to grow and produce peptidoglycan as normal although response to changes in environment such as virulence and resistance was reduced (Reed et al., 2015). Additionally, the expression of other peptidoglycan interacting enzymes such as autolysins was modulated. While PBP1 and 2 are the only peptidoglycan biosynthetic enzymes required it is not clear what the minimum system of proteins are required for division to successfully take place.

4.1.3 Aims of the Chapter

1. To determine the pattern of peptidoglycan synthesis in *S. aureus*.
2. To determine the effect of FtsZ inhibition on peptidoglycan synthesis.

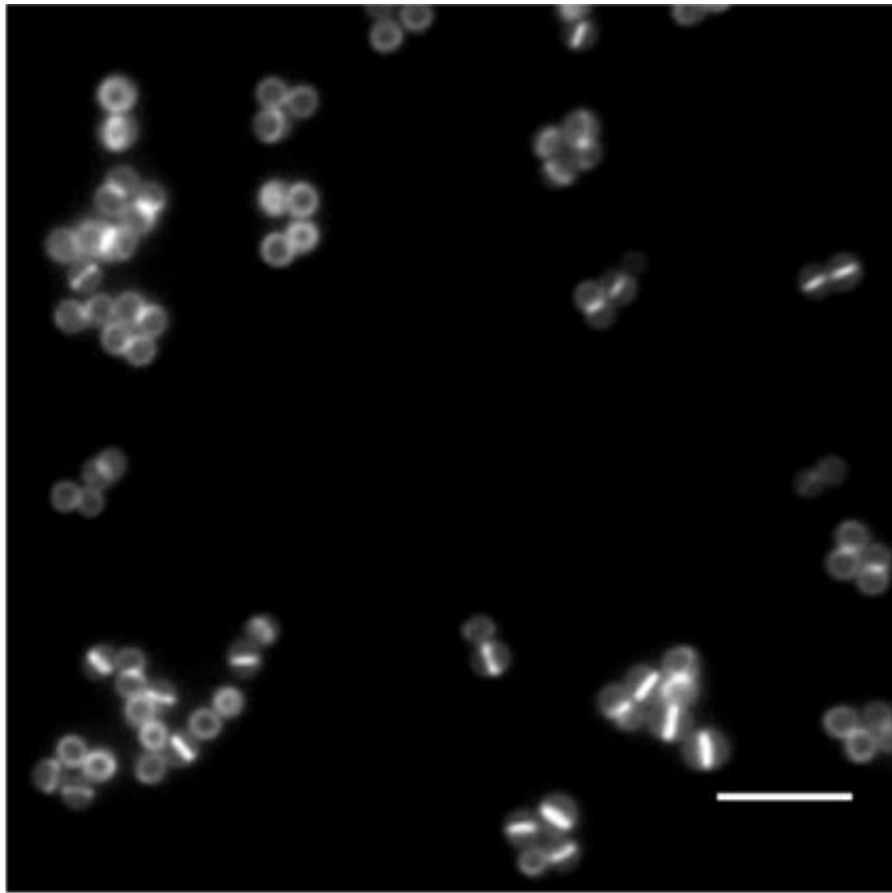
4.2 Results

4.2.1 Localisation of peptidoglycan synthesis in *S. aureus*

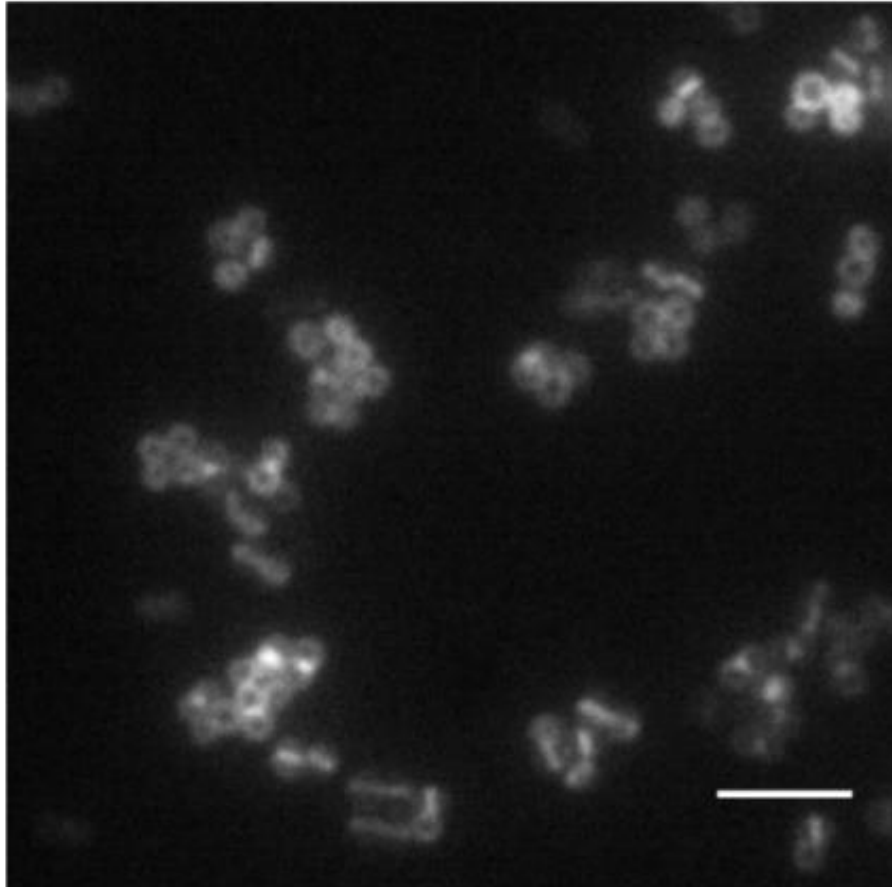
The localisation of peptidoglycan synthesis in *S. aureus* has been presumed to occur primarily, if not exclusively, at the septum (Pinho and Errington, 2003; Turner et al., 2010a). However, this has been based on work using fluorescent vancomycin to label the D-alanine-D-alanine motif, associated with localisation of peptidoglycan synthesis (Daniel and Errington, 2003). *S. aureus* exhibits low carboxypeptidase activity therefore these residues are maintained in the mature peptidoglycan (Scheffers and Pinho, 2005). In order to label newly synthesised peptidoglycan with vancomycin, cultures must be grown in excess D-serine. Therefore, most dipeptide motifs contain D-serine, which is not recognised by vancomycin. Transient incubation in D-serine free media allows nascent peptidoglycan to be labelled by vancomycin (Scheffers and Pinho, 2005). Since the development of FDAAs it has been possible to label synthesis directly (Kuru et al., 2012). Application of this technique in conjunction with super-resolution imaging techniques allows the localisation of peptidoglycan synthesis during division of *S. aureus* at the molecular level.

Localisation of 5 minutes of peptidoglycan synthesis as labelled by both HADA and dipeptide fluorescent labels shows a pattern of peptidoglycan comparable to published data using vancomycin, that is septal synthesis of peptidoglycan (Figure 4.1 A&B)

A



B



C

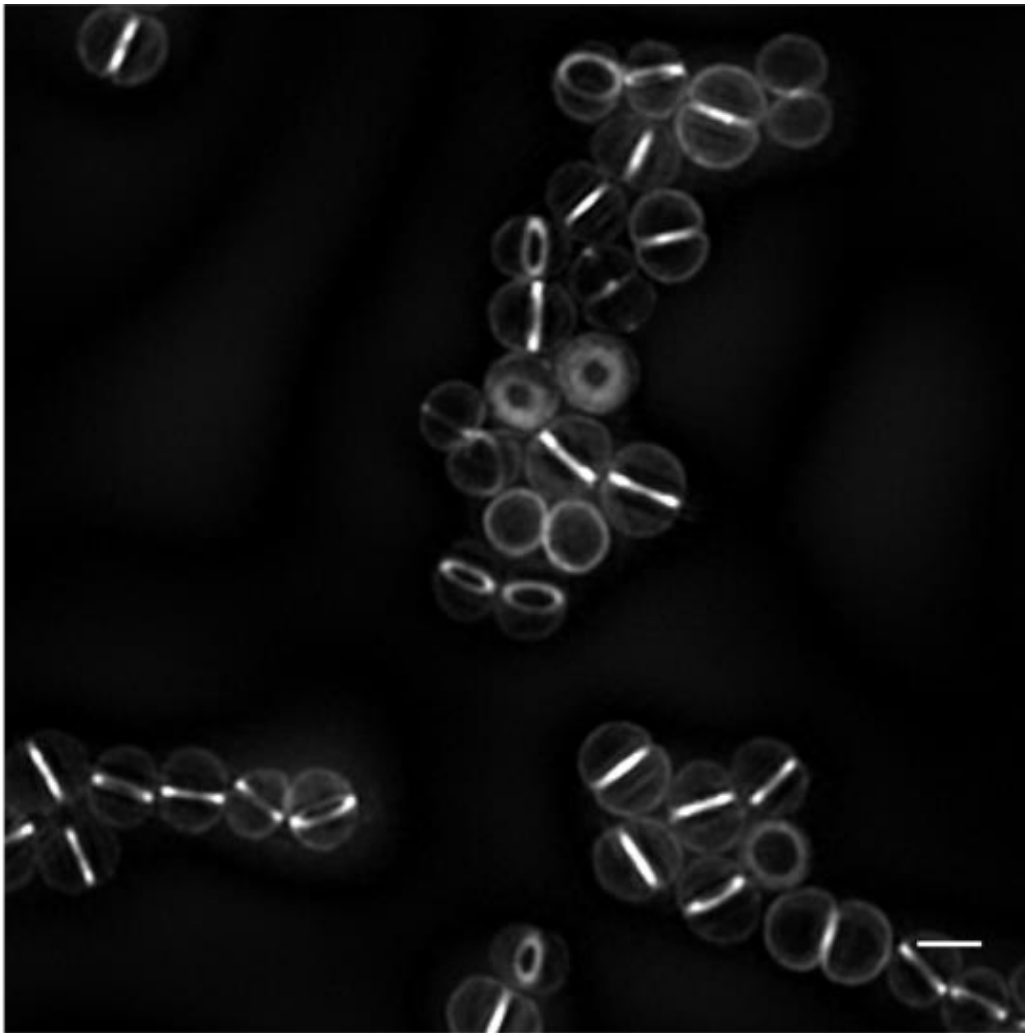


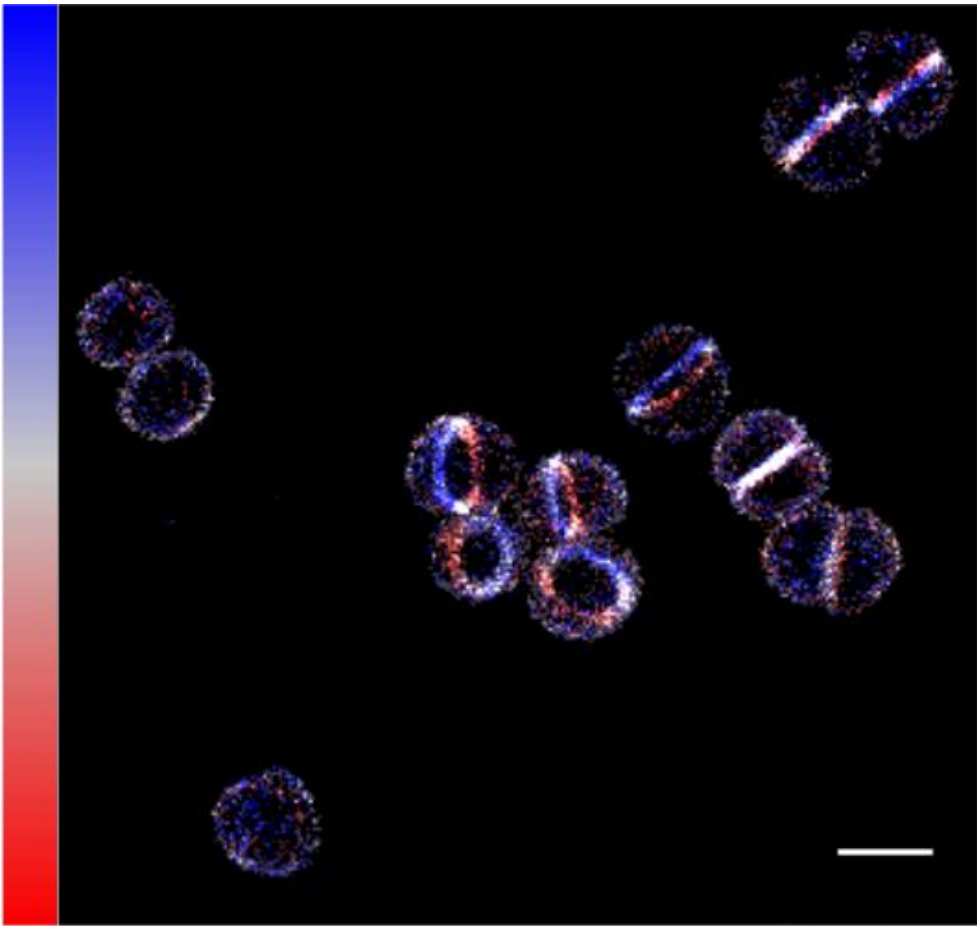
Figure 4.1 Localisation of FDAA Incorporation over 5 minutes. Peptidoglycan synthesis labelled by FDAA incorporation shows a mainly septal localisation when labelled with FDAAs. Images taken using Nikon Dual Cam widefield system (Diffraction limited; A, B) or OMX (structured illumination; C) (A) Synthesis labelled with HADA (500 μM , Scale bar 5 μm , single slice). (B) Synthesis labelled with dipeptide label(1 mM) with Alexa Fluor 647(5 $\mu\text{g ml}^{-1}$) (Scale bar 5 μm , single slice). (C) Structured illumination image of peptidoglycan synthesis labelled with HADA (5 mM, Scale bar 1 μm , average intensity projection).

(Pinho and Errington, 2003; Turner et al., 2014). Diffraction limited microscopy has a resolution of ~250 nm, given that *S. aureus* cells are ~1 µm in diameter it is not possible to learn any further details of peptidoglycan synthesis from previous work, even with the use of FDAA probes (Huang et al., 2010). SIM has increased resolution (to ~125 nm) however in practise this only crisps up diffraction limited images and it is often not possible to glean any new biology from these images (Huang et al., 2010). SIM images of 5 minutes of peptidoglycan synthesis labelled with HADA shows clear septal labelling, however there is also fluorescence outlining the surface of the entire cell (Figure 4.1 C). It is unclear from these images whether this fluorescence surrounding the cell is due to an artefact of SIM microscopy or is due to labelling with FDAAs (Chapter 3.2.3.2 & Appendix Figure 8). For this reason and also for the advantage of the increased resolution available, the pattern of peptidoglycan insertion was then investigated using STORM.

STORM was carried out on mid-exponential phase *S. aureus* labelled for 5 minutes with ADA. Localisation of peptidoglycan synthesis was obtained through 3D imaging using a Nikon N-STORM commercial system and a non-commercial system, resulting in the same localisation patterns (Figure 4.2). There are four features of peptidoglycan synthesis that can be observed and will be discussed in further detail below. These can be identified within fields of cells however, individual cells best representing the features have been enlarged and represented as both 2D images and 3D projections to highlight these features in an easier to interpret form (Figure 4.3). The features are as follows:

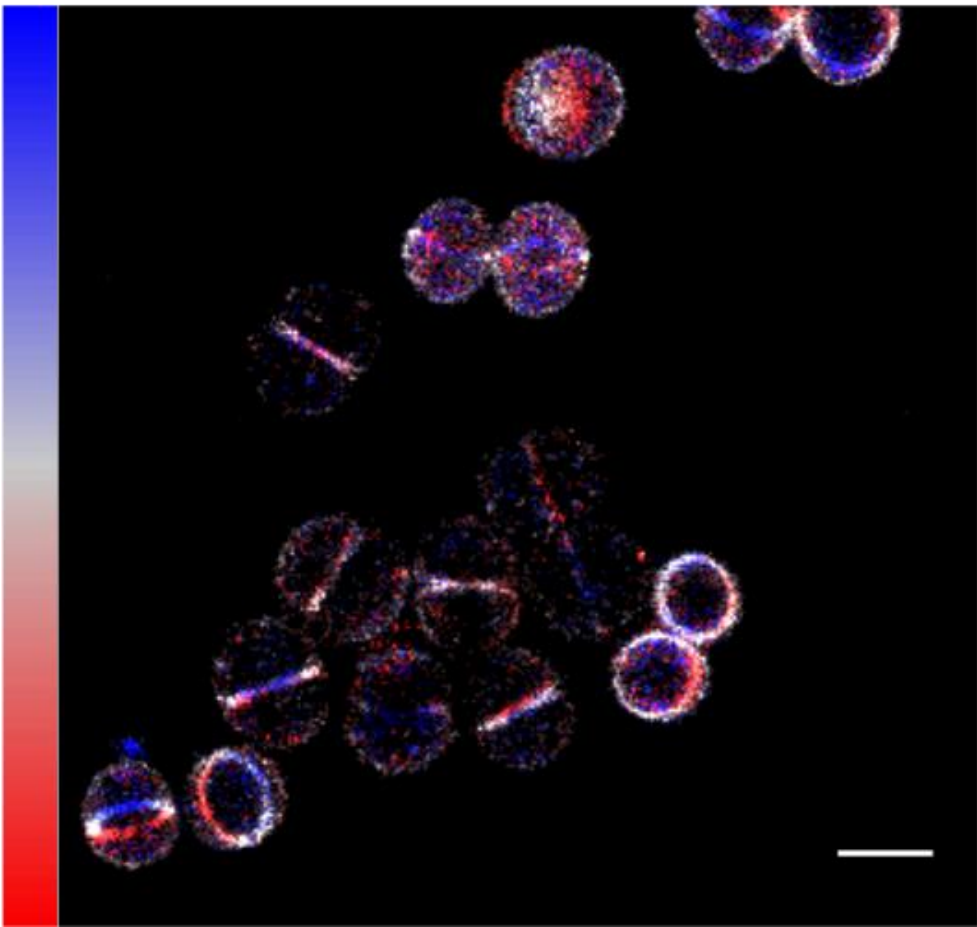
1. Peptidoglycan synthesis at the septum does not occur solely as a focus at the leading edge of the septum.
2. Cells with incomplete septa have an apparent gap in peptidoglycan synthesis at the cross wall junction (Figure 4.3 A).
3. Cells with completed septa prior to cell splitting show 2 separate regions of peptidoglycan synthesis suggesting the presence of two septal plates (Figure 4.3 B).
4. Contrary to previous models peptidoglycan synthesis is not limited to the septum but occurs throughout the cell wall.

-500 nm



500 nm

-500 nm



500 nm

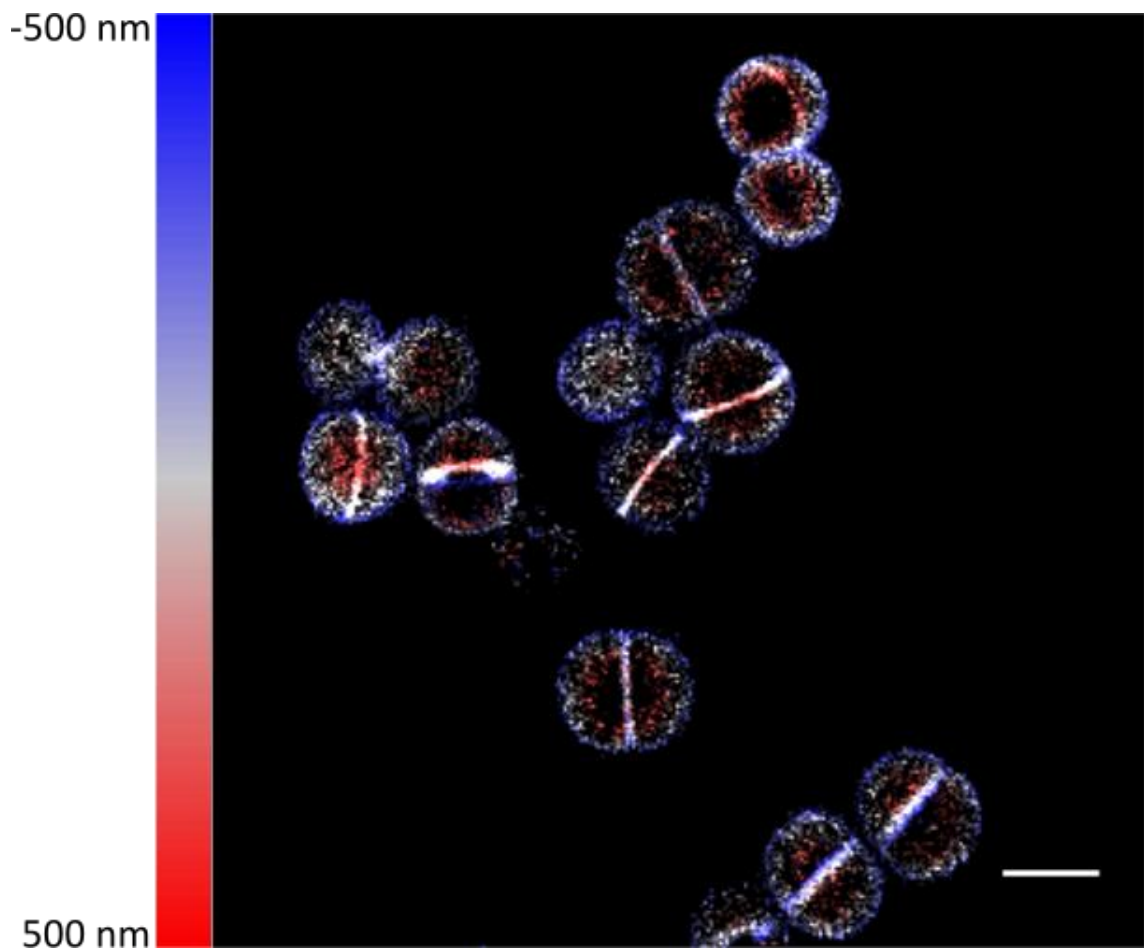
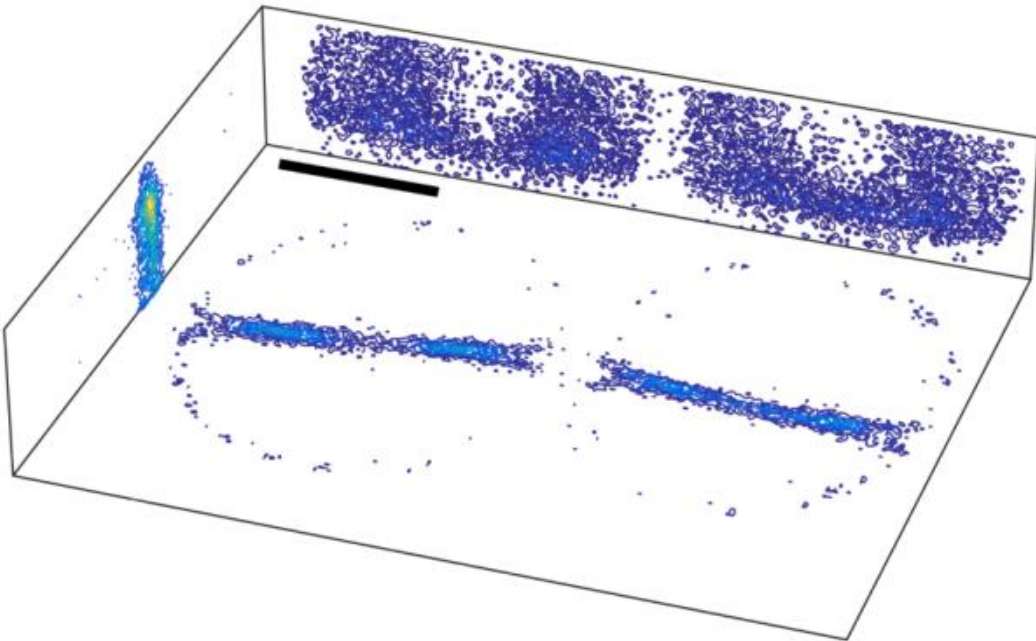
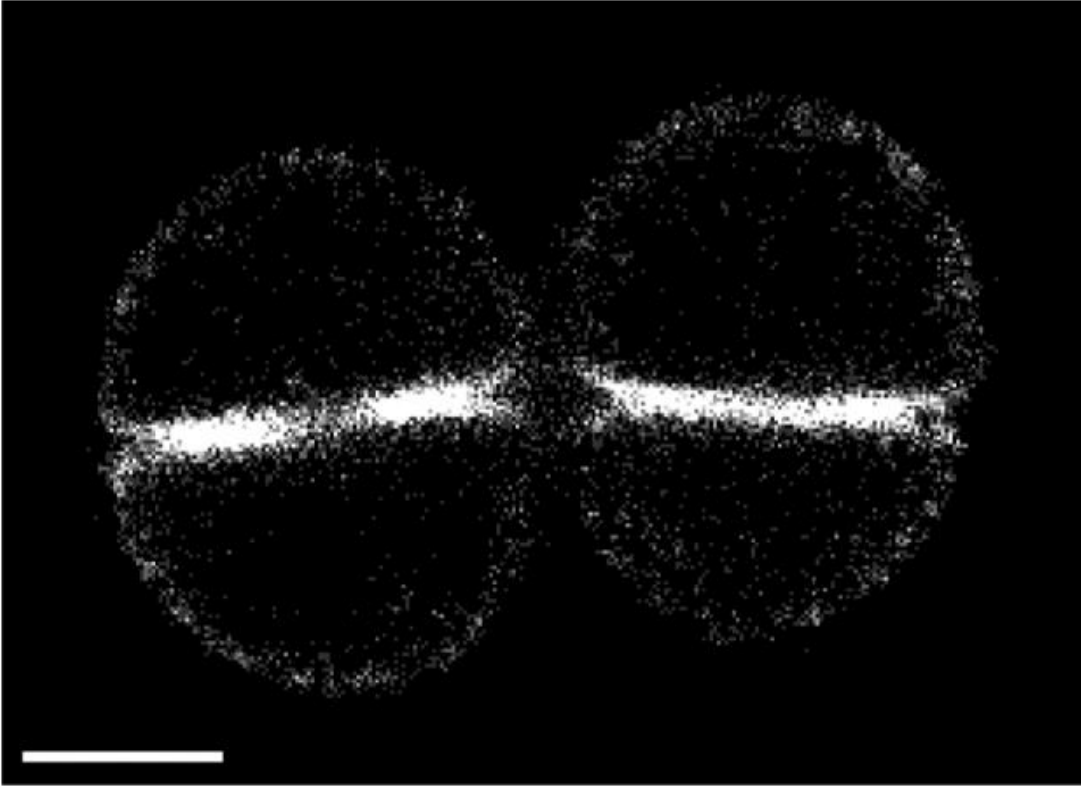


Figure 4.2. Localisation of ADA incorporation over 5 minutes. Labelling shows both a septal and off-septal incorporation pattern. Probe used was ADA Alexa Fluor 647 (ADA at 500 μM , Alexa Fluor 647 at 5 $\mu\text{g ml}^{-1}$ in Click reaction). 3D localisation of synthesis is represented by colour table in 100 nm slices from 500 nm behind the plane of focus (-500 nm, blue) to 500 nm in front of plane of focus (500 nm, red). (Scale bar, 1 μm).

A



B

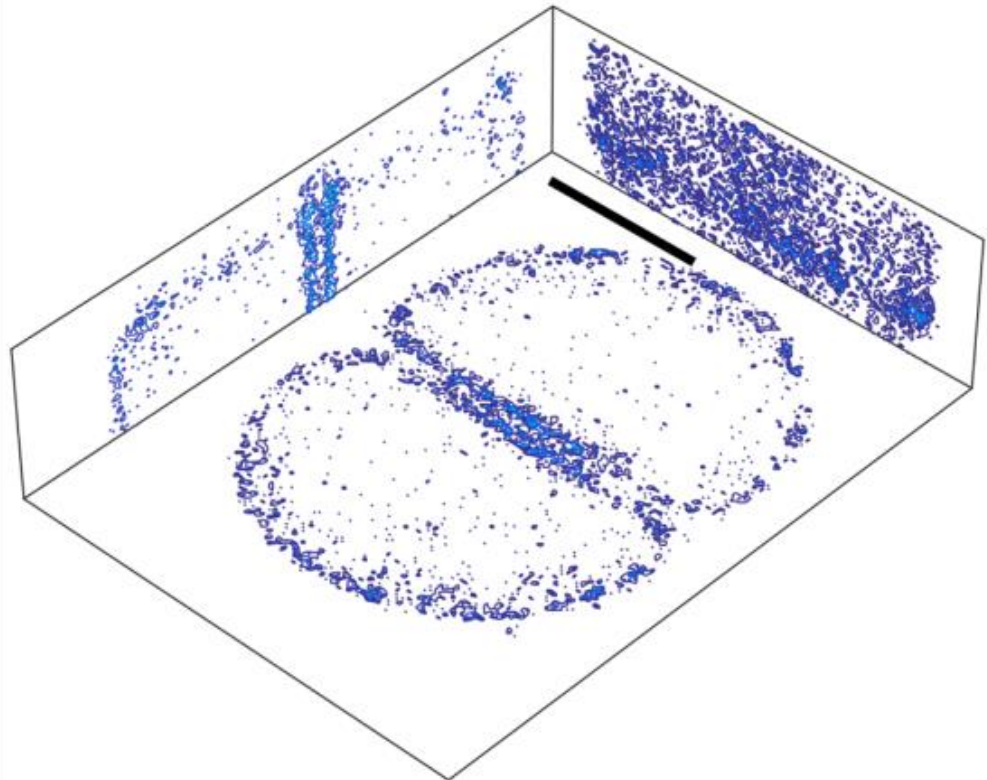
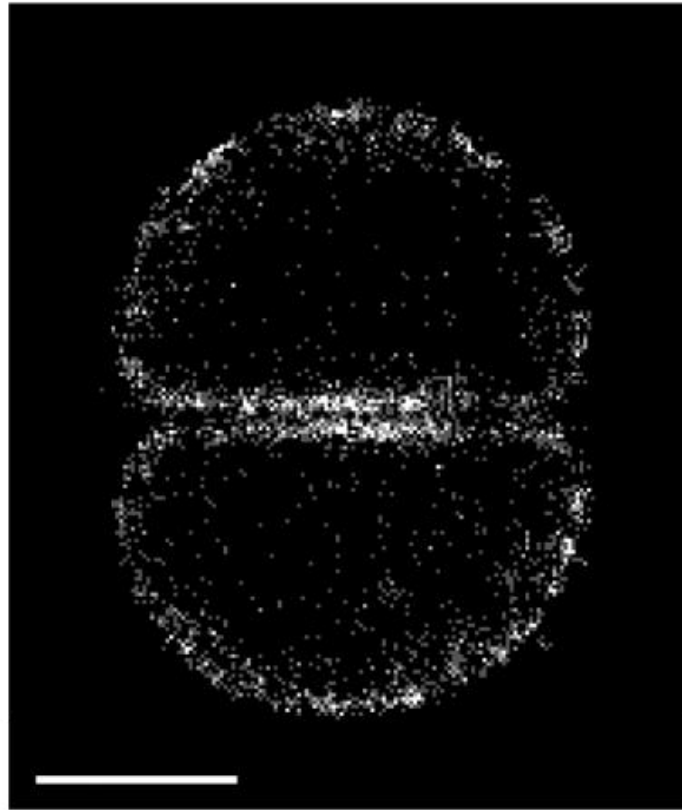


Figure 4.3. 2D images and 3D projections of selected cells to highlight features of peptidoglycan incorporation. Labelling with ADA (500 μM , Alexa Flour 647 at 5 $\mu\text{g ml}^{-1}$

in Click reaction) for 5 minutes. (A) Two cells, both with incomplete septa. (B) Single cell with a completed septum, presumably just prior to cell splitting. In each case a 2D image and 3D contour plot are shown. 2D images are rendered using a 2D histogram with bin dimensions of 10 by 10 nm and number of localisations indicated by grey level. 3D renders are Matlab contour plots with a fixed number of 10 contours per plane. (Scale bar 500 nm).

The same labelling pattern was also seen in cells labelled with the dipeptide FDAA label (Figure 4.4) and with fluorescent vancomycin following incubation with excess D-serine (Figure 4.5). Quality of fluorescent vancomycin labelling is not of the same standard as those labelled with FDAAs however, the labelling pattern shows the same information. This lesser quality is plausibly due to attachment of Alexa Fluor 647 to vancomycin altering the photophysics of the fluorophore thereby reducing the number of localisable events during image acquisition. Identical labelling patterns with 3 different methods of labelling synthesis allows some assurance that observed pattern is due to peptidoglycan synthesis rather than an artefact of the labelling technique.

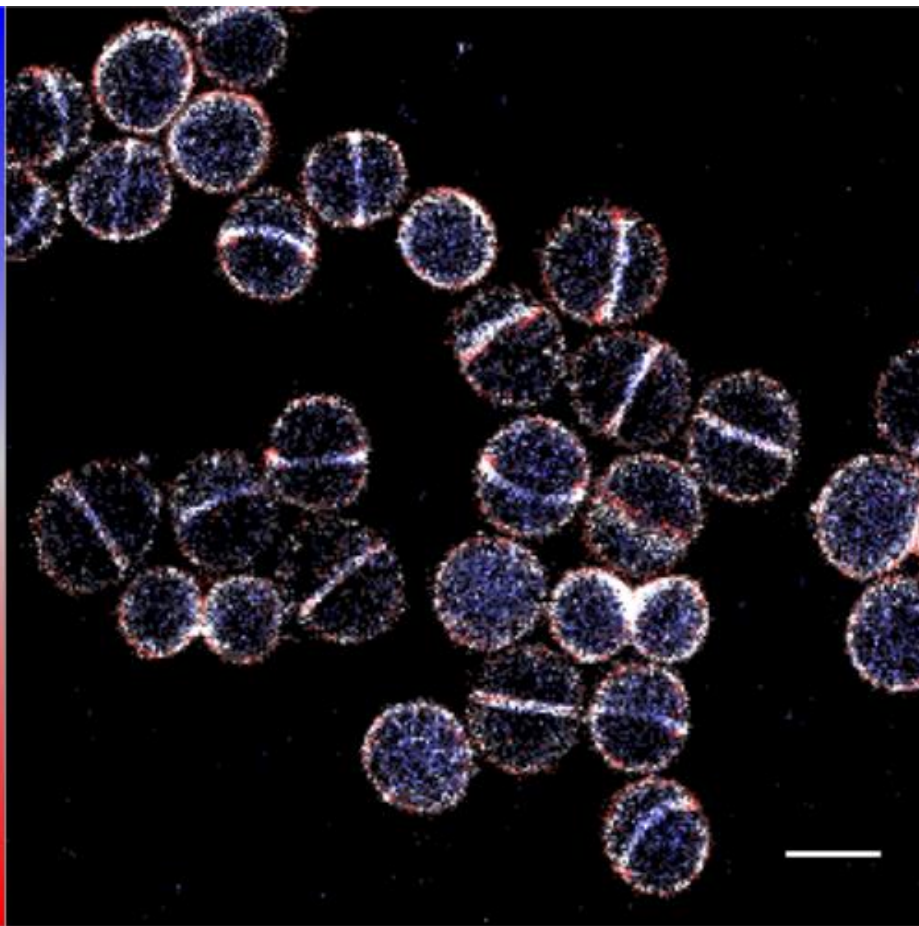
4.2.2 Peptidoglycan synthesis occurs as a zone at the septum

Peptidoglycan synthesis was hypothesised to occur at the leading edge of the septum. However, labelling with ADA has demonstrated that this is not the case since synthesis appears to occur all across the new septum (Figure 4.3 A). Initial suggestions were that labelling 5 minutes of peptidoglycan synthesis was too long to catch insertion just at the leading edge since all peptidoglycan synthesised during the experiment would be labelled. When labelling time is reduced to 2 minutes the amount of labelling throughout the cell was reduced since less new peptidoglycan is synthesised yet the labelling pattern still suggests that peptidoglycan synthesis does not occur only at the leading edge (Figure 4.6). It is therefore postulated that peptidoglycan synthesis occurs as a zone at the septum.

4.2.3 Apparent splitting of septum prior to daughter cell separation

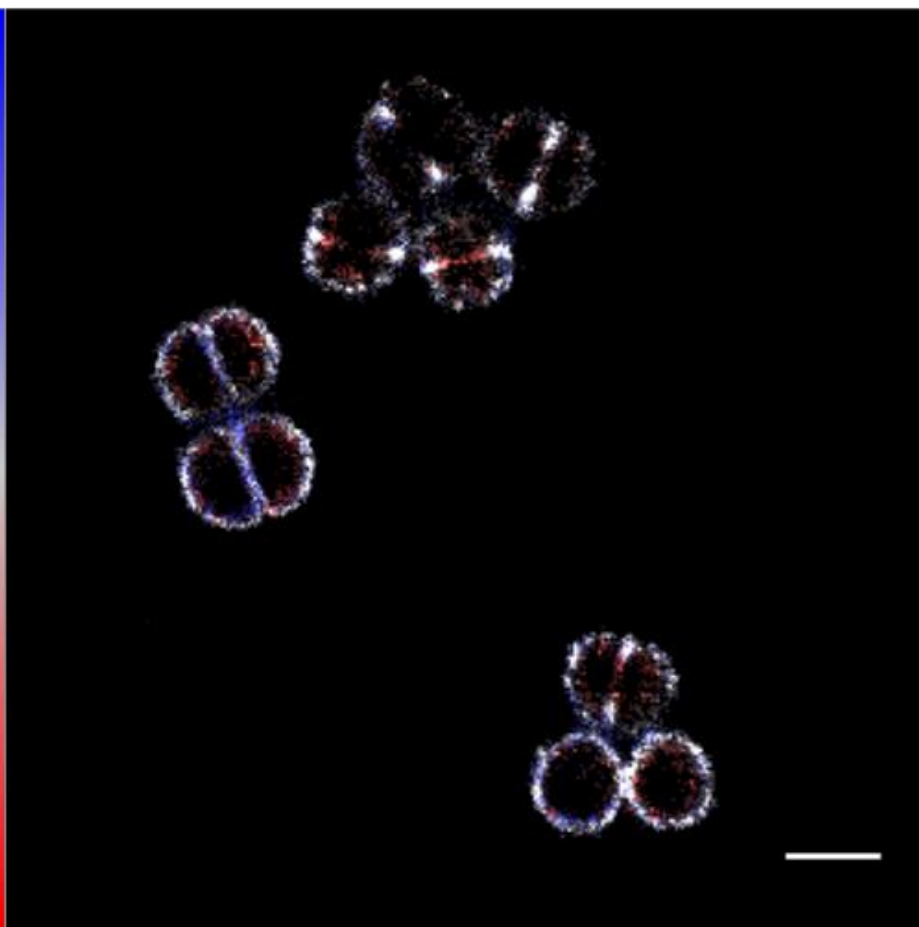
The final stage of *S. aureus* cell division is the splitting into two daughter cells (Zhou et al., 2015). It is at this stage that the septum is split between the daughter cells, the connecting cross wall is broken and the septum expands to form daughter cells of the same shape as the mother cell (Matias and Beveridge, 2007; Wheeler et al., 2015; Zhou et al., 2015). Nascent peptidoglycan labelling reveals a split within the septum towards the mother cell wall edge. In many cases this can be seen to occur prior to completion of septation (Figure 4.3 A & Figure 4.7). It is unlikely that this lack of labelling is due to initiation of the separation process since the incomplete septa would render the cell prone to lysis. Therefore, this apparent gap is likely to be plugged with peptidoglycan and is due to the lack of synthesis of peptidoglycan in this region during

-500 nm



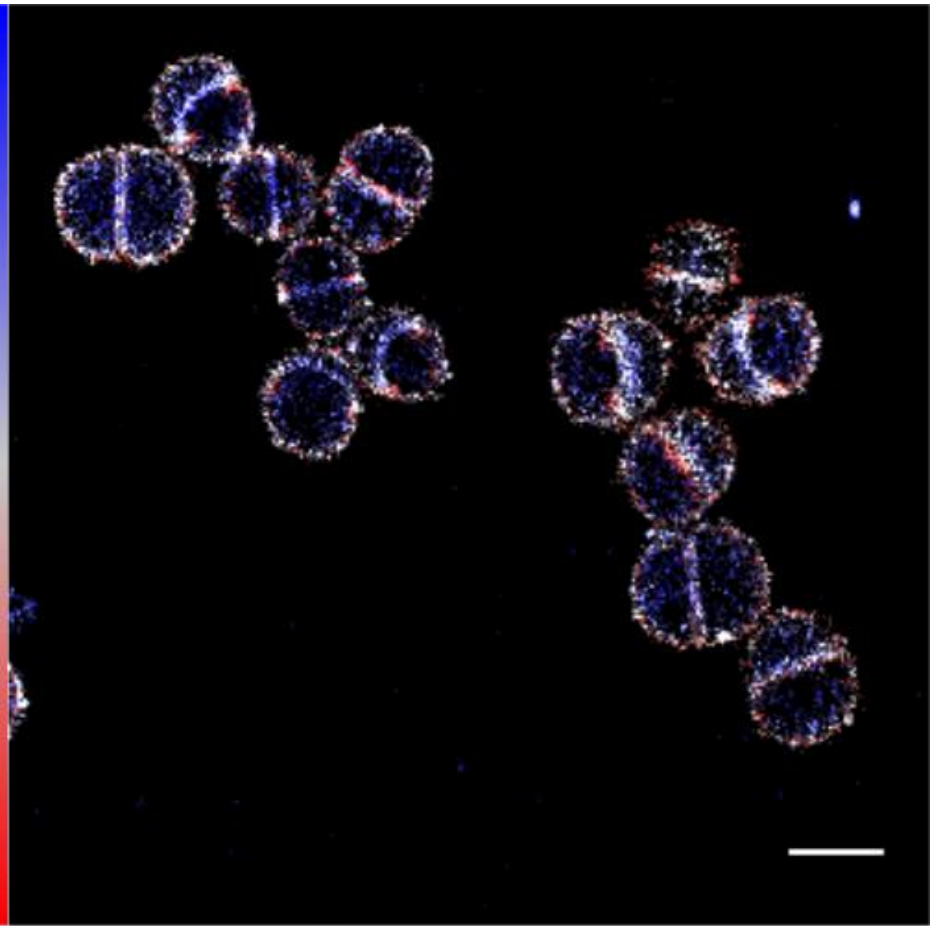
500 nm

-500 nm



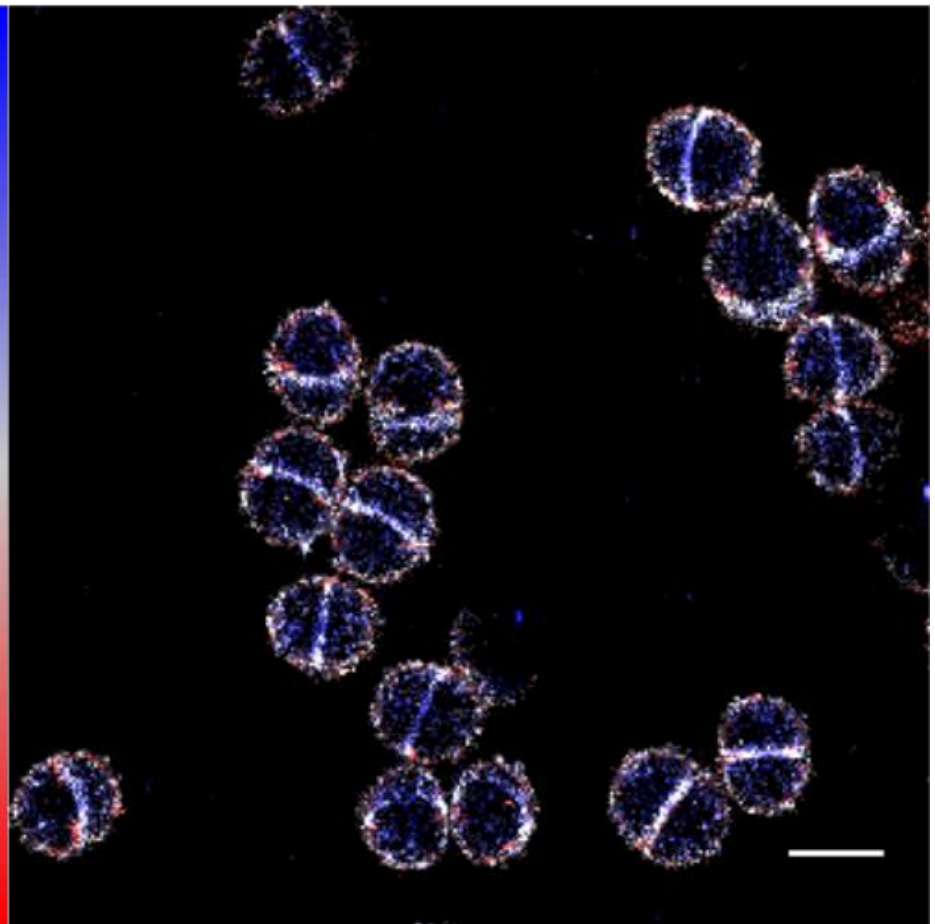
500 nm

-500 nm



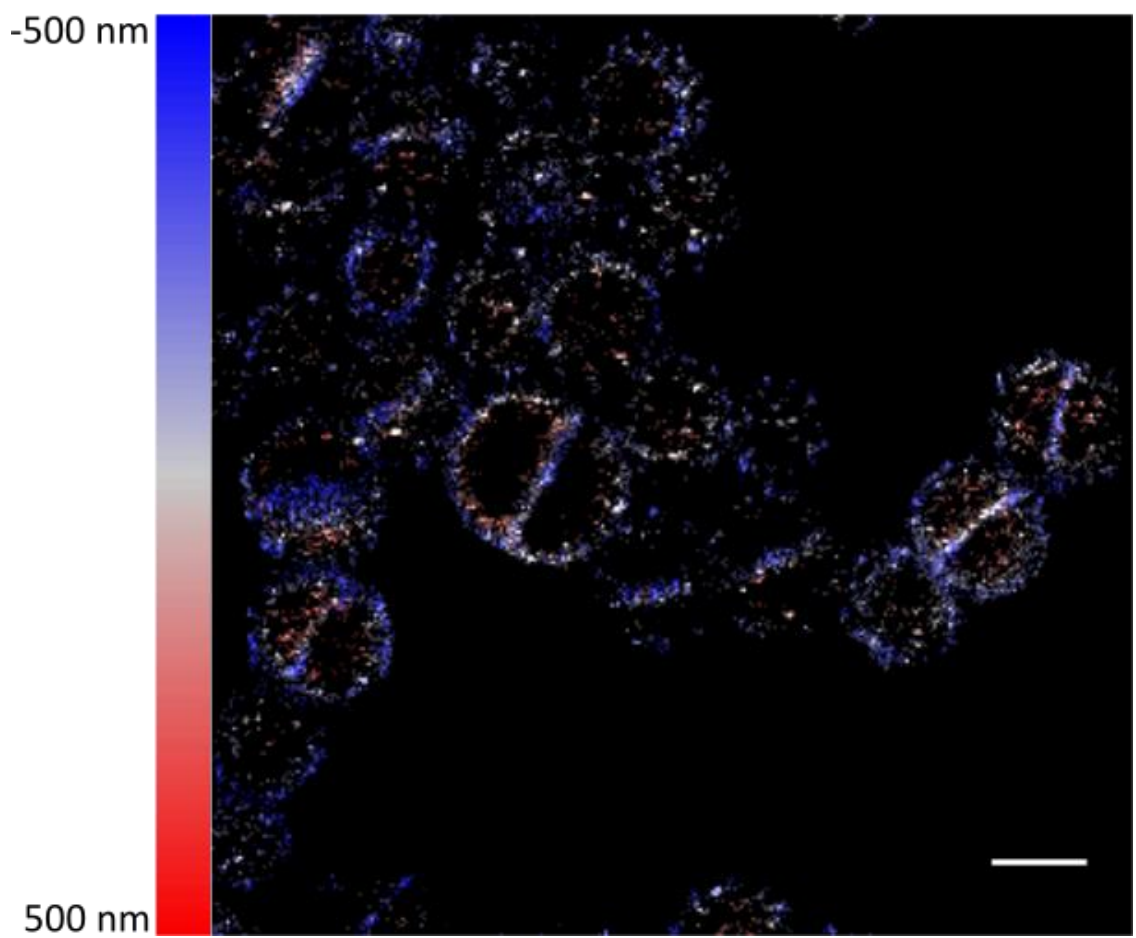
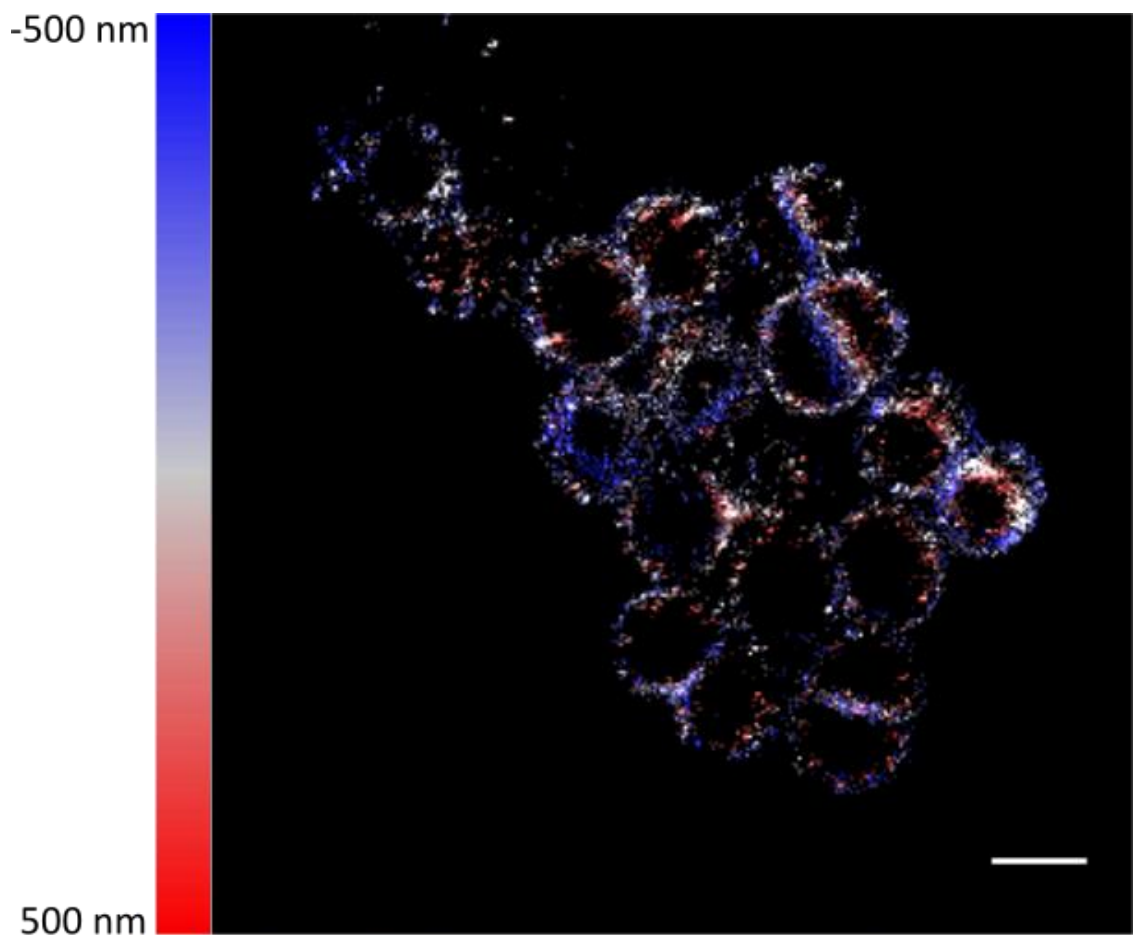
500 nm

-500 nm

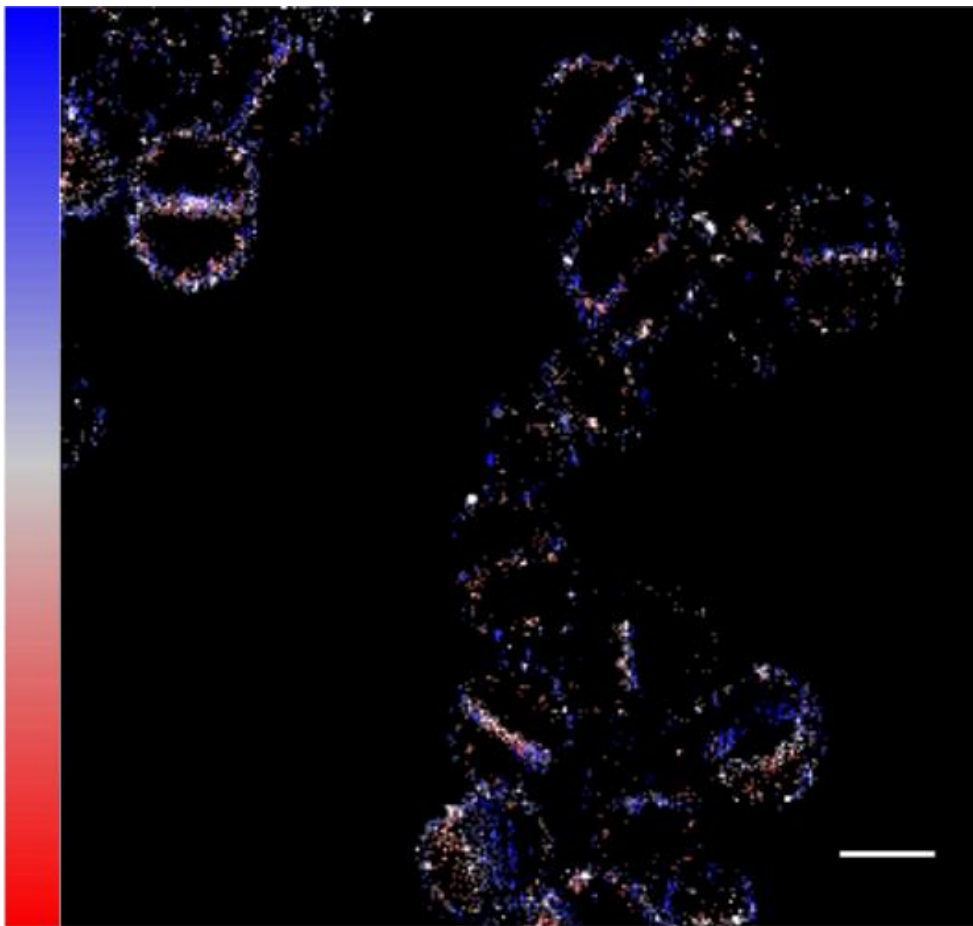


500 nm

Figure 4.4. Localisation of dipeptide incorporation over 5 minutes. Dipeptide labelling shows both a septal and off-septal pattern. Dipeptide at 1 mM, Alexa Flour 647 at 5 $\mu\text{g ml}^{-1}$ in Click reaction. 3D localisation of incorporation is represented by colour table in 100 nm slices from 500 nm behind the plane of focus (-500 nm, blue) to 500 nm in front of plane of focus (500 nm, red). (Scale bar, 1 μm).



-500 nm



500 nm

-500 nm

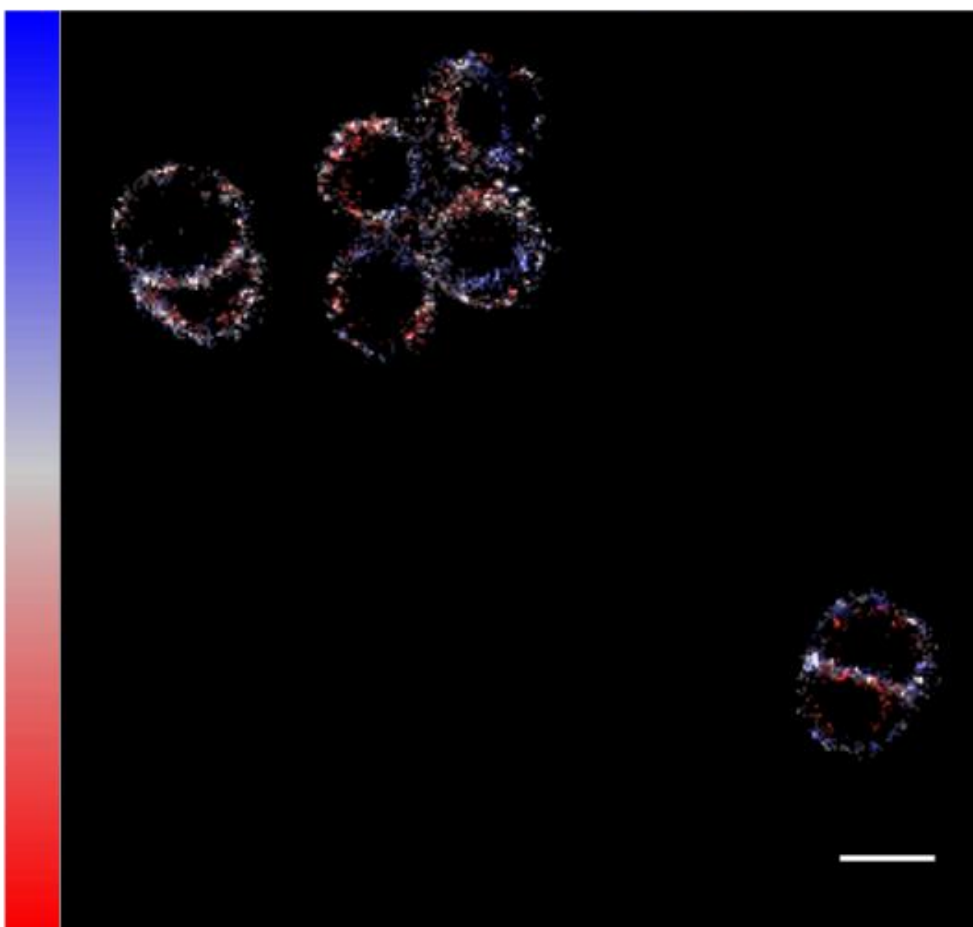
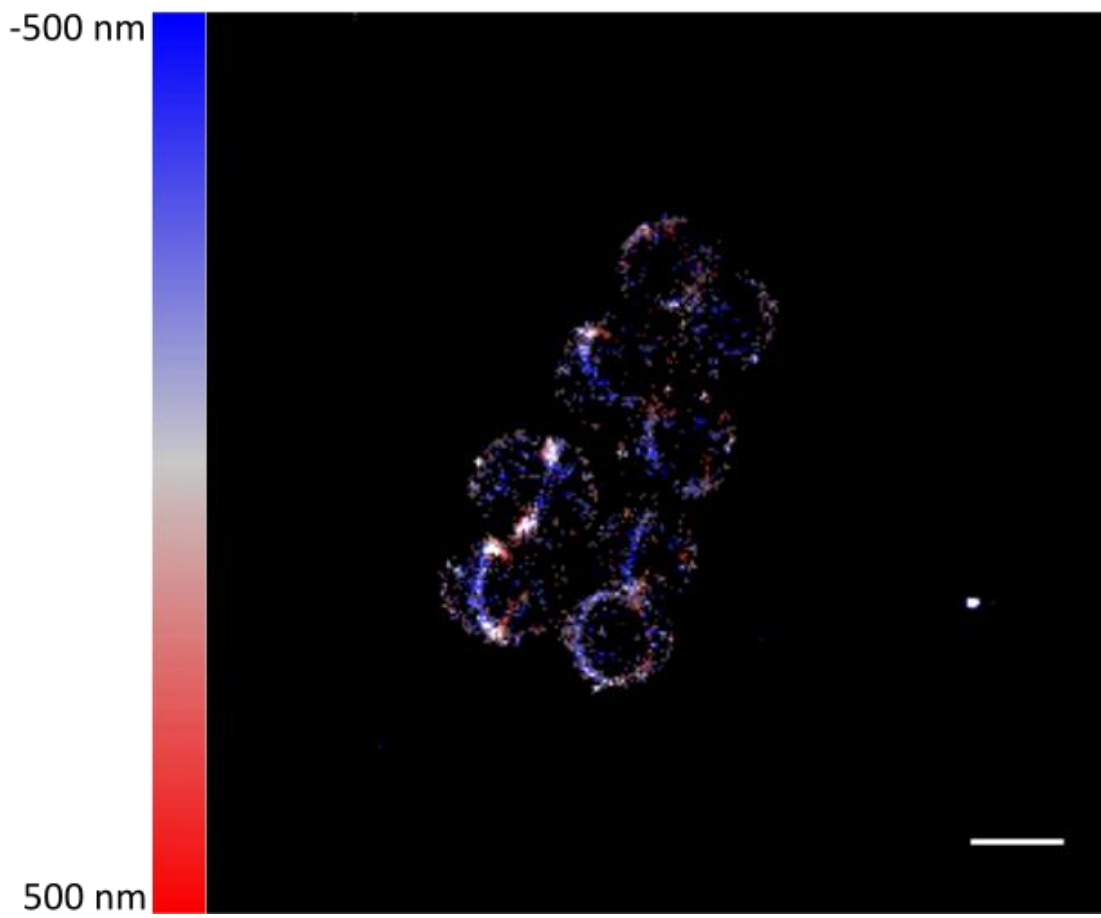
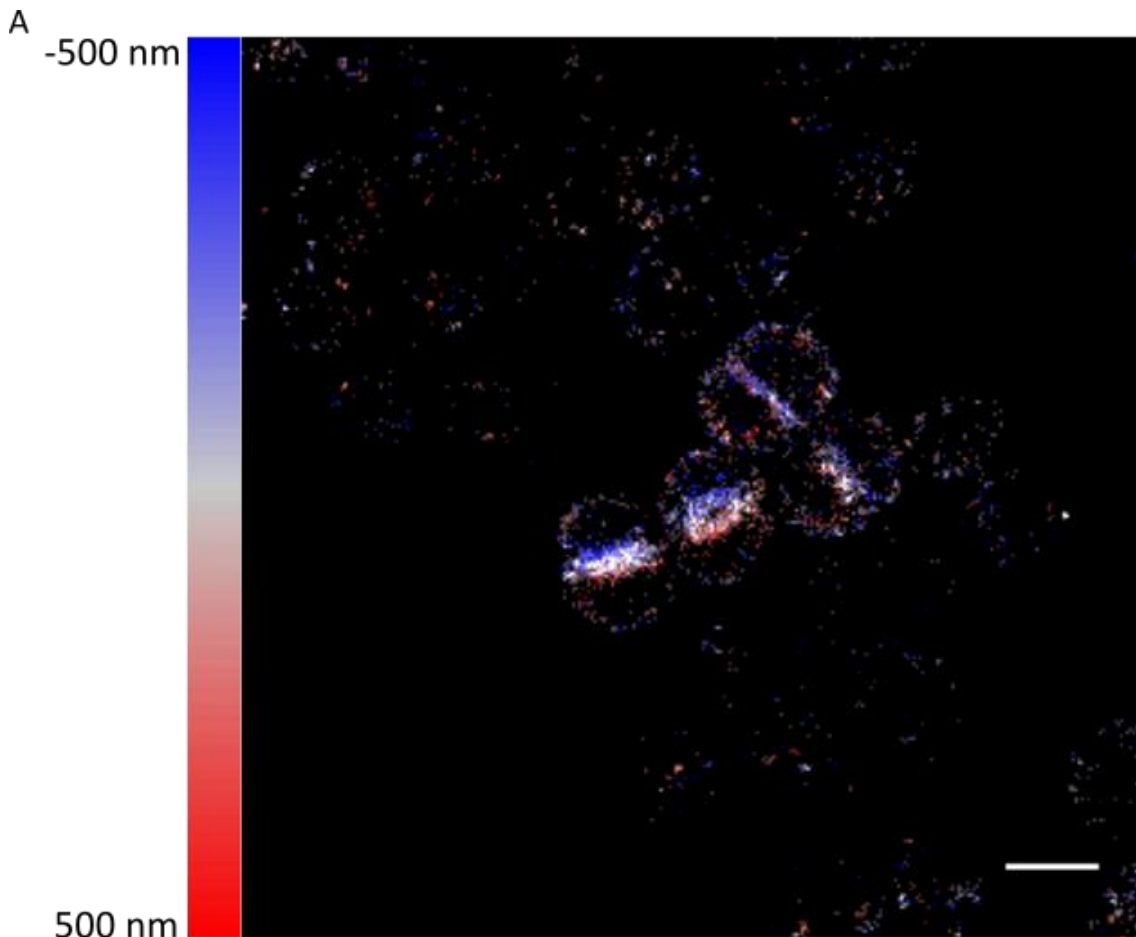


Figure 4.5. Fluorescent vancomycin labelling of nascent peptidoglycan following incubation in excess D-serine demonstrates septal and off-septal labelling. Synthesis is labelled with vancomycin conjugated to Alexa Fluor 647 (1 mM) following 5 minutes incubation in D-serine free media to allow labelling of 5 minutes peptidoglycan synthesis. 3D localisation of synthesis is represented by colour table in 100 nm slices from 500 nm behind the plane of focus (-500 nm, blue) to 500 nm in front of plane of focus (500 nm, red). (Scale bar, 1 μ m).



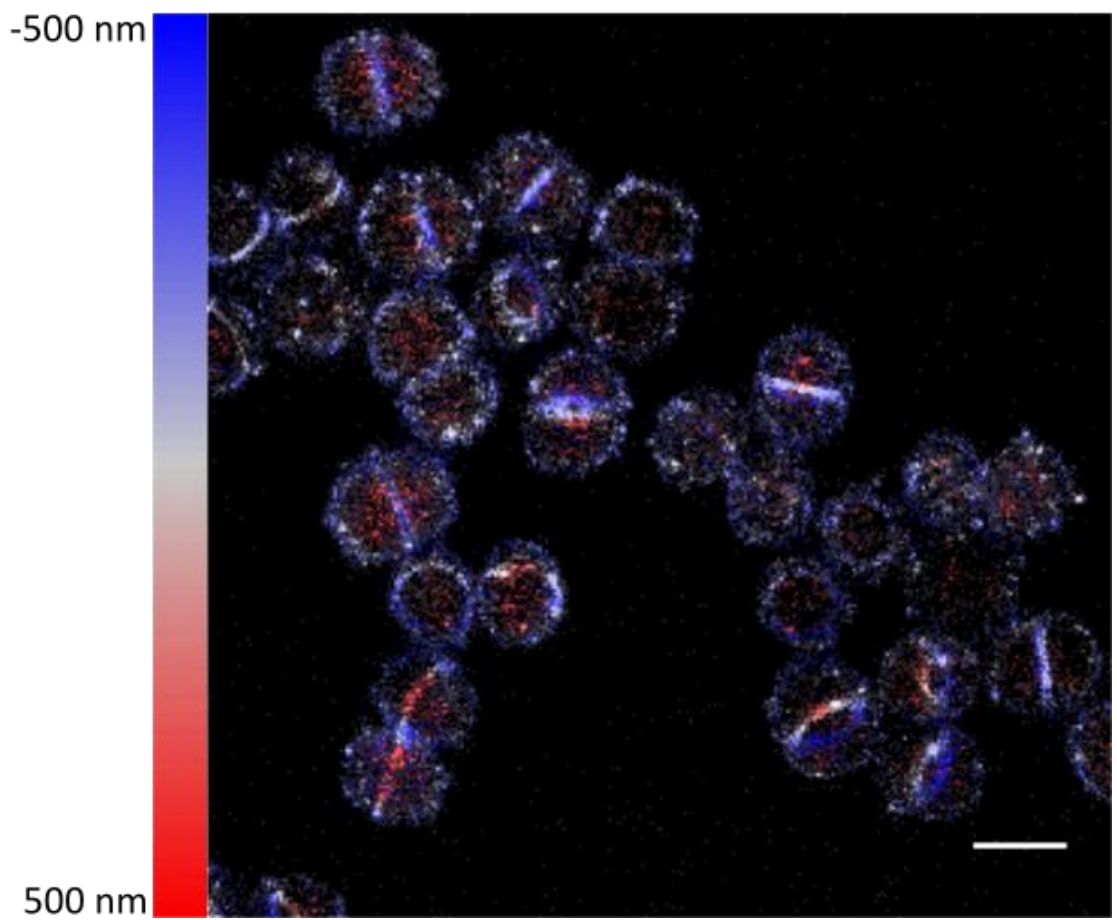
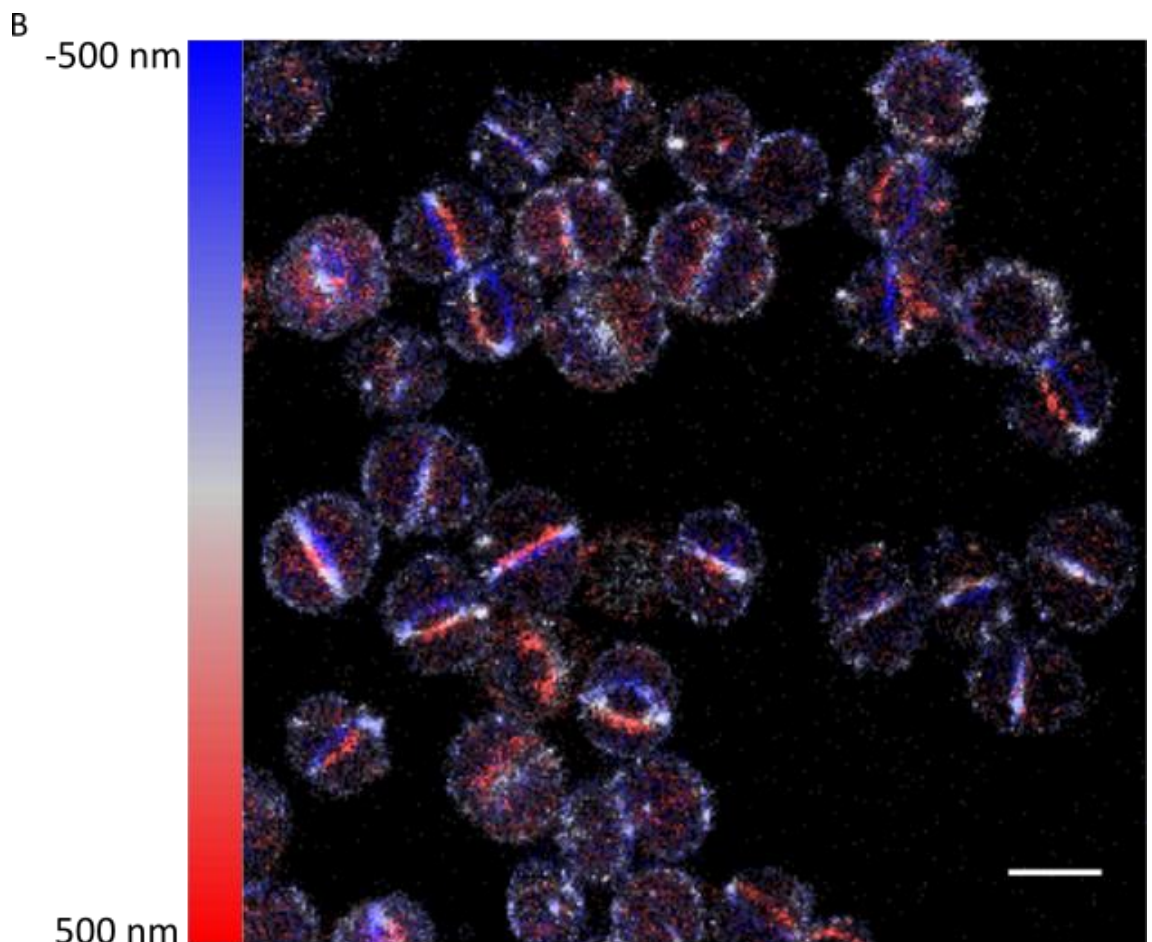
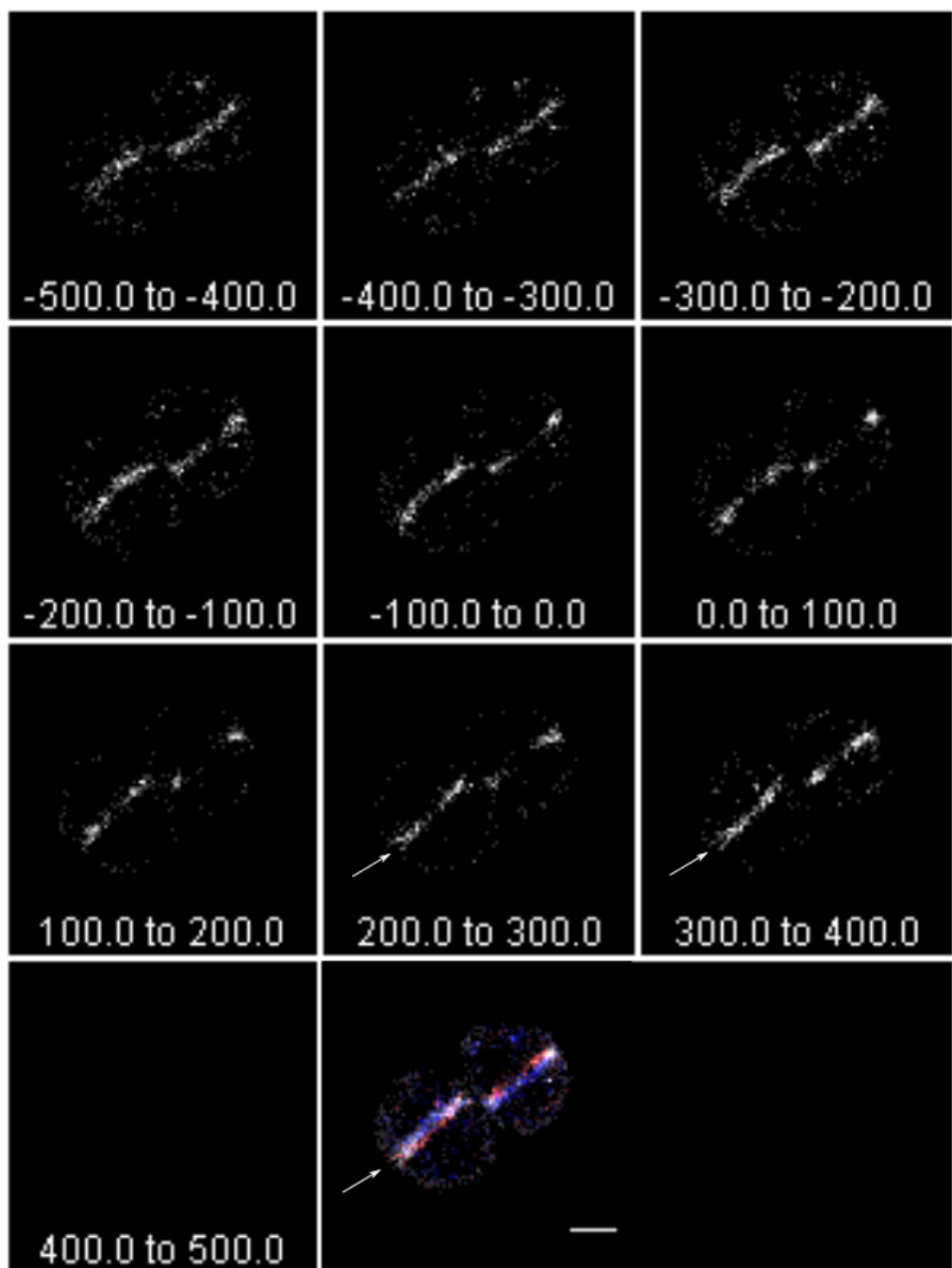


Figure 4.6. Reduced labelling time shows zone of synthesis at septum. Synthesis is labelled with (A) ADA (500 μM) and (B) dipeptide (1 mM) (Alexa Flour 647 at 5 $\mu\text{g ml}^{-1}$ in Click reaction). 3D localisation of synthesis is represented by a colour table in 100 nm slices from 500 nm behind the plane of focus (-500 nm, blue) to 500 nm in front of plane of focus (500 nm, red). (Scale bar, 1 μm).

A



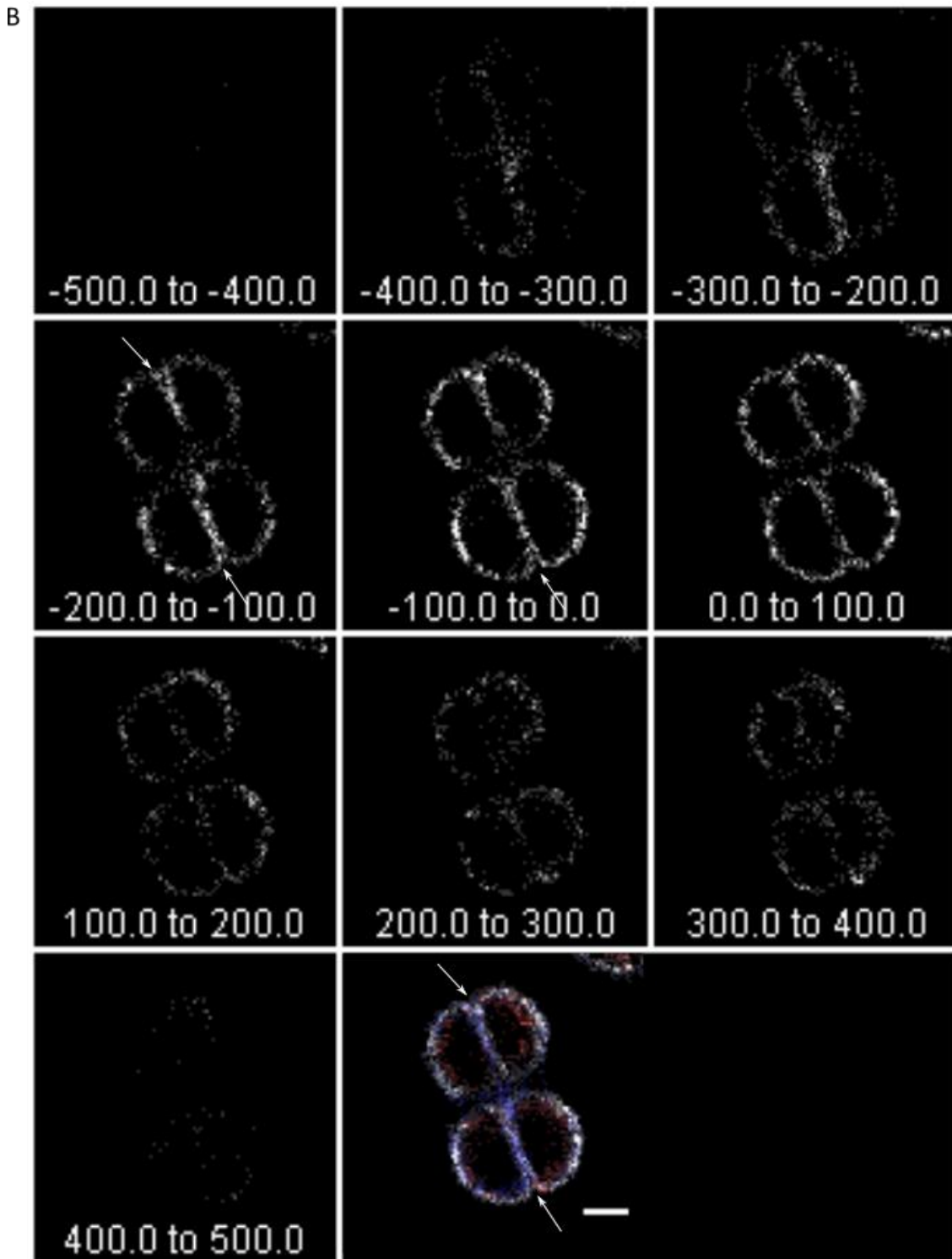


Figure 4.7. Cells show gap in peptidoglycan synthesis labelling at septum & mother cell interface prior to cell splitting. Synthesis of peptidoglycan labelled for 5 minutes with (A) ADA ($500 \mu\text{M}$) and (B) dipeptide (1 mM) (Alexa Flour 647 at $5 \mu\text{g ml}^{-1}$ in Click reaction). Arrows indicate presence of the split at the mother cell edge of the septum. Z slices through the cell is shown in 100 nm segments showing gap at the outside edge

of the septum. Z projection with z indicated by colour table also shown for comparison. (Scale bar 500 nm).

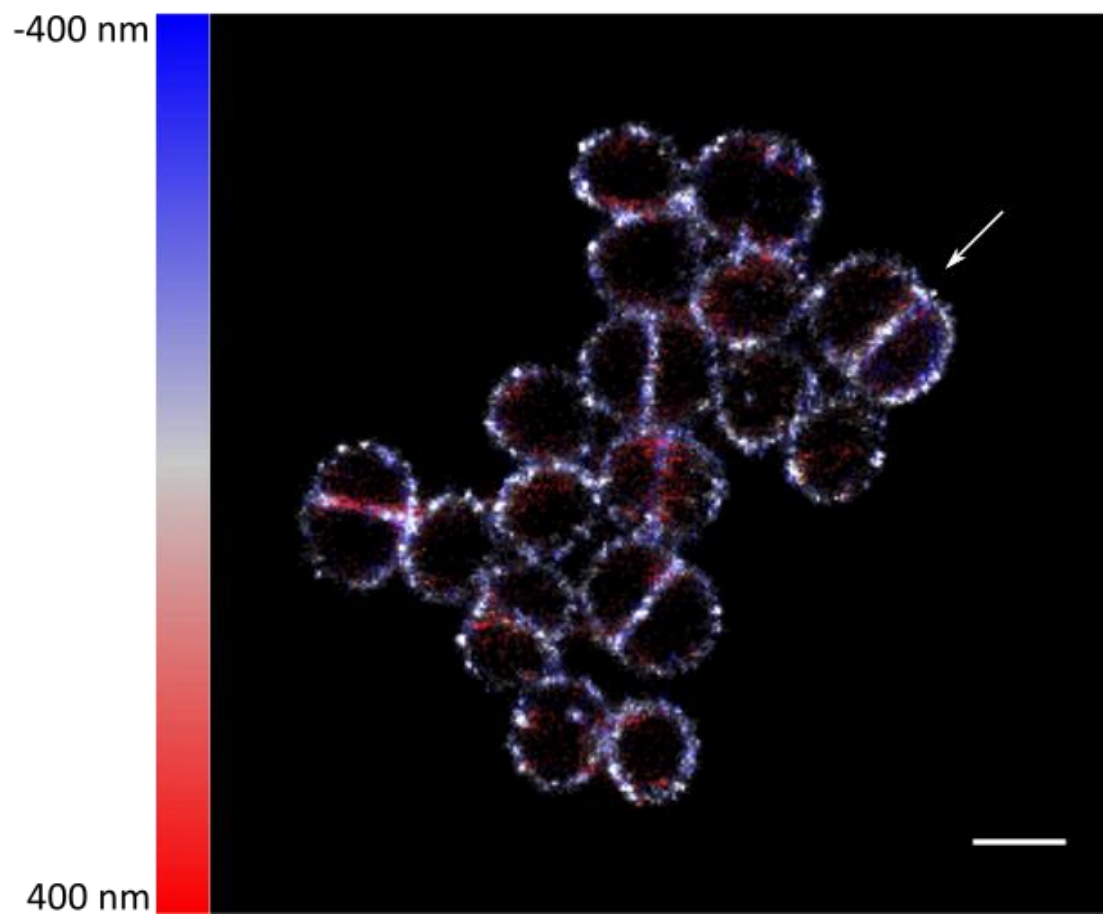
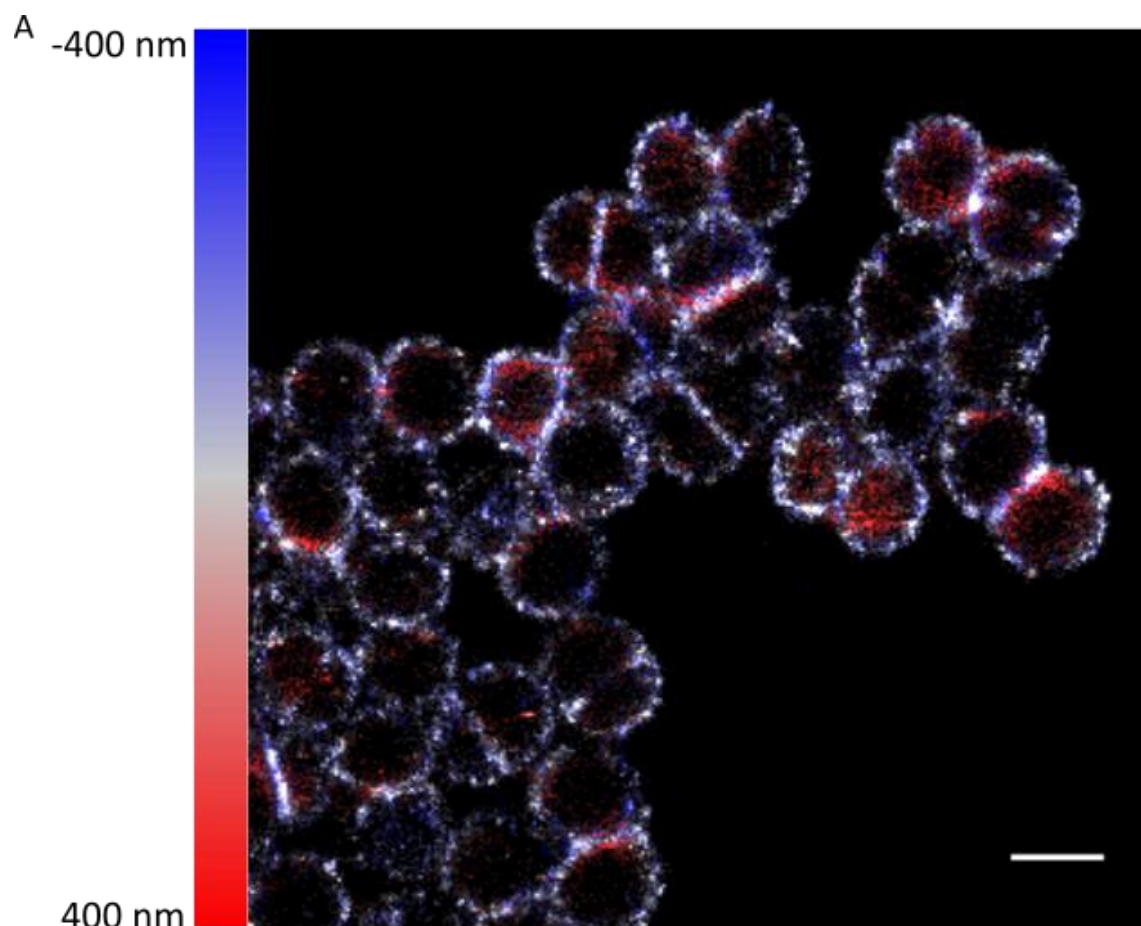
labelling. To determine the presence of peptidoglycan within the apparent gap cells were imaged with vancomycin to stain the cell wall. In the absence of incorporation of excess D-serine vancomycin can be used as a whole cell wall label in *S. aureus*. The split at the outside of the septum is not apparent in vancomycin labelled cells with both incomplete and completed septa suggesting that the split is filled with peptidoglycan (Figure 4.8).

In order to show if the gap in FDAA labelling is in fact filled with peptidoglycan dual-colour STORM was employed with peptidoglycan synthesis labelled with dipeptide and all the cell wall labelled with vancomycin conjugated to the fluorophore Amersham Cy3B. Cells with a gap in labelling with dipeptide have a continuum of peptidoglycan material labelled with vancomycin (Figure 4.9 & Figure 4.10). This shows that the gap is only in peptidoglycan synthesis. Where the septum and mother cell wall join there is a peptidoglycan plug (the piecrust) which remains in place with no further synthesis while the septum is being completed.

In some cells with completed septa the septal plate could be viewed as two separate regions of peptidoglycan synthesis (Figure 4.3). There are a number of different explanations for this;

- The septum is thickened following completion; this occurs only at the two cytoplasmic sides of the peptidoglycan therefore the gap is where the previously synthesised peptidoglycan is situated.
- The septum is synthesized as two separate entities, one for each daughter cell.
- The septum is synthesized as a single entity and then split due to autolytic activity prior to cell separation.

By plotting a grey value profile for a line through the centre of a cell representing this “double septa” phenomenon the gap could be measured as ~ 25 nm (Figure 4.11). This distance is at the limit of resolution achievable by the STORM system. In addition, for the two regions to be visible the cell must be situated such that this gap is more or less parallel to the imaging plane. Therefore, it has not been possible to determine whether this gap is filled with previously synthesised peptidoglycan using dual labelling



B

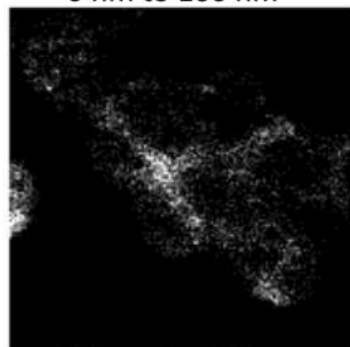
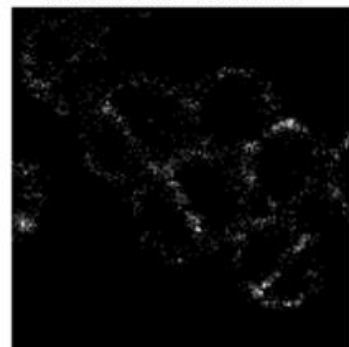
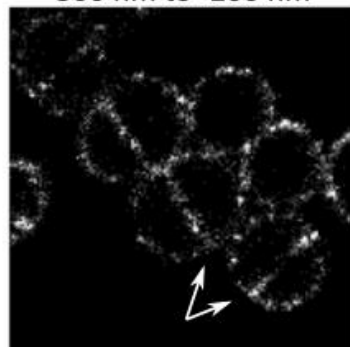
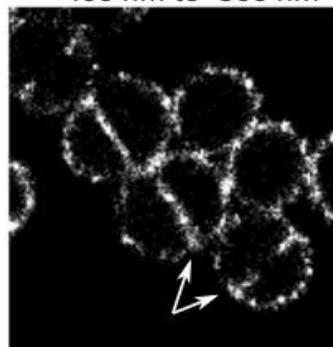
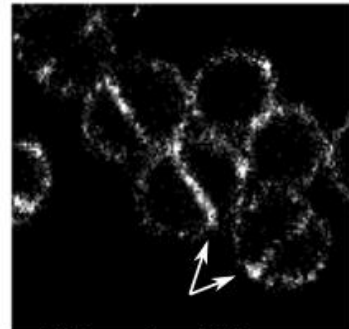
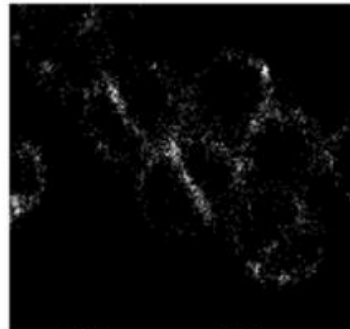
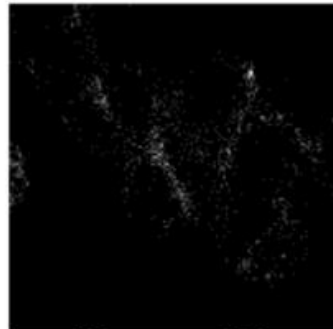
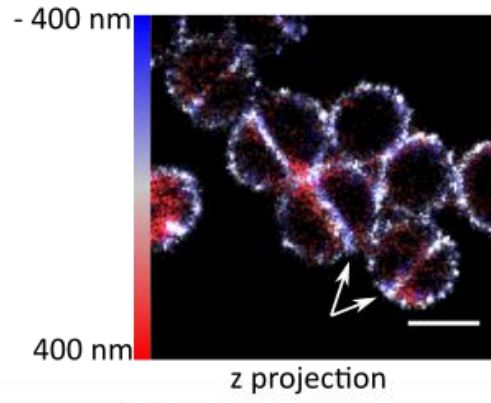
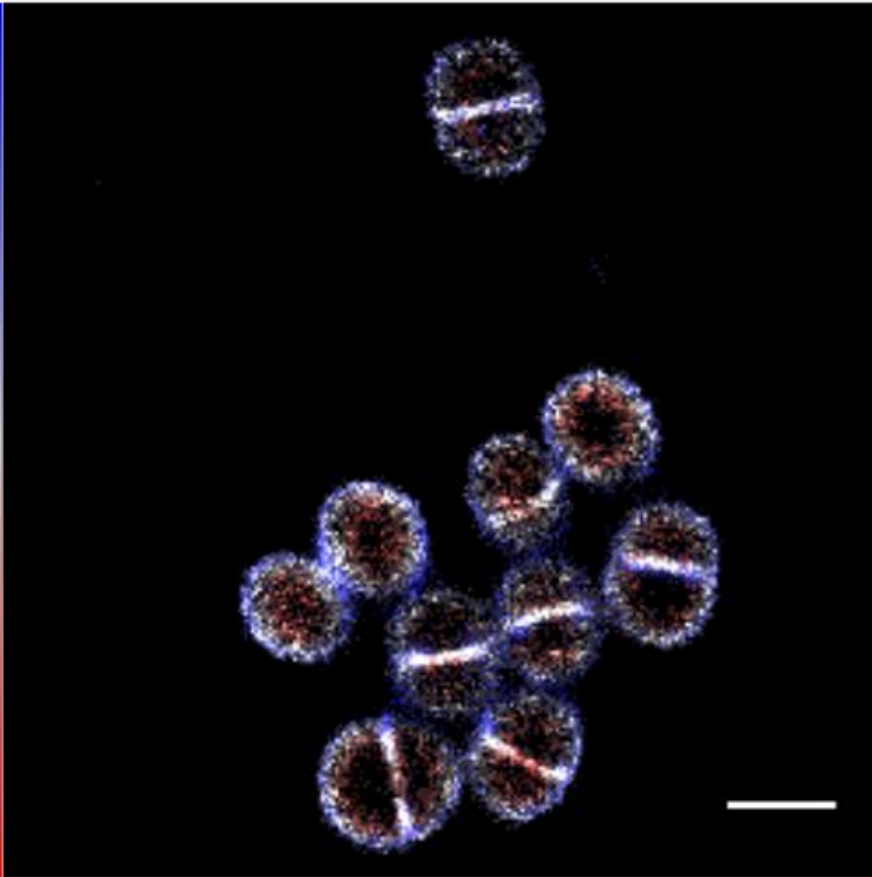


Figure 4.8. The gap in the septum is not apparent in cells when cell wall is labelled with vancomycin. Whole cell wall is labelled by vancomycin (1 mM). (A) Fields of cells labelled with vancomycin. Z- sectioning 800 nm in this example therefore 3D localisation of synthesis is represented by a colour table in 100 nm slices from 400 nm behind the plane of focus (-400 nm, blue) to 400 nm in front of plane of focus (400 nm, red). (Scale bar, 1 μ m). (B) Selection of cells shown to highlight lack of gap in the septum in cells with both completed and incomplete septa prior to cell splitting. Z slices of 100 nm from bottom to top of cells shown along with a Z-projection image for comparison (Scale bar 500 nm).

A

Dipeptide

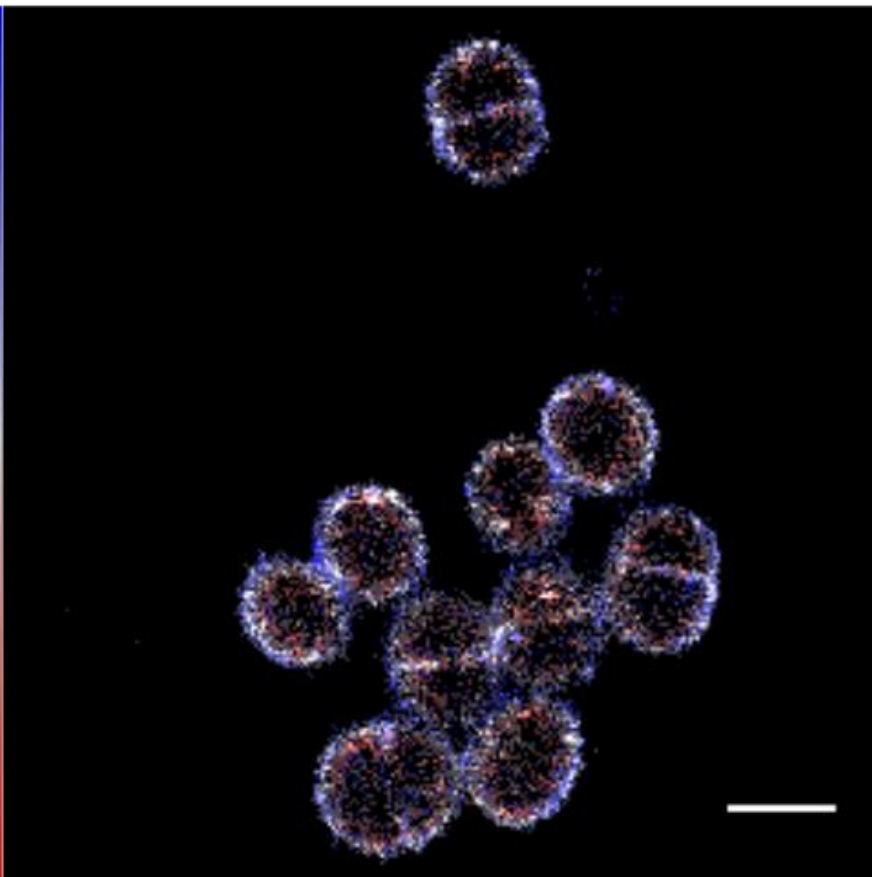
-500 nm



500 nm

Vancomycin

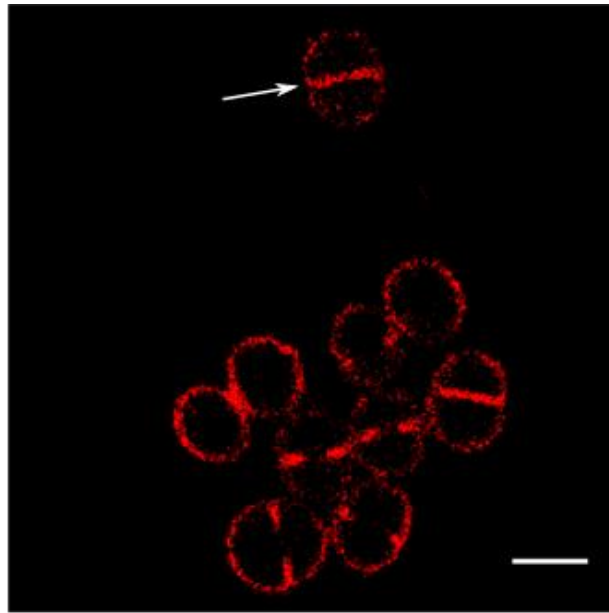
-500 nm



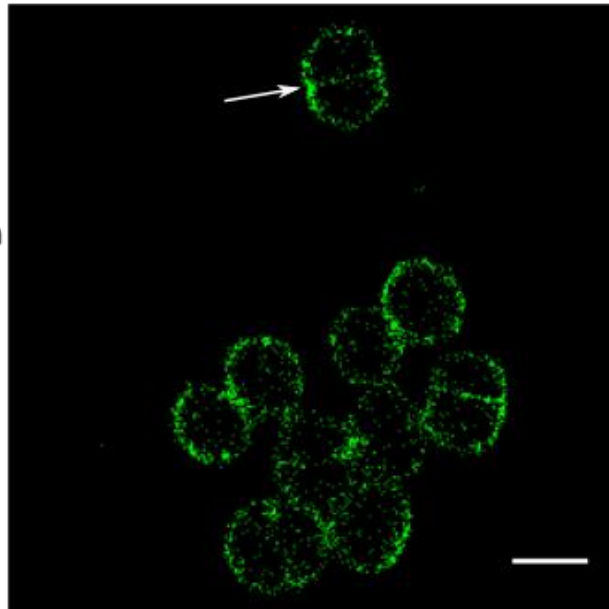
500 nm

B

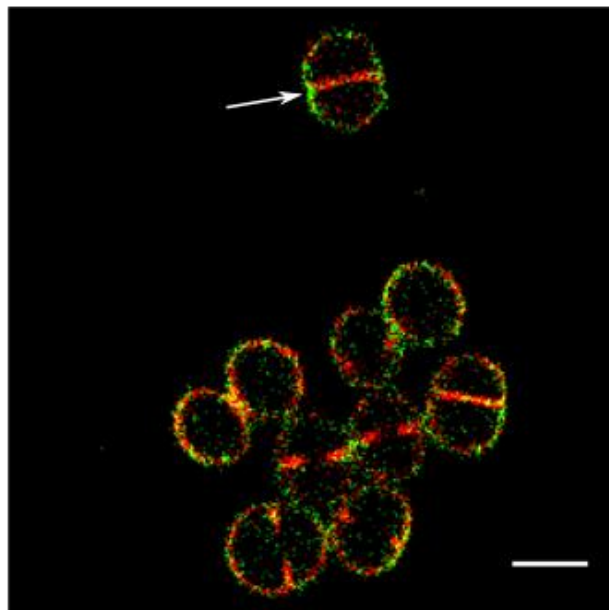
Dipeptide



Vancomycin

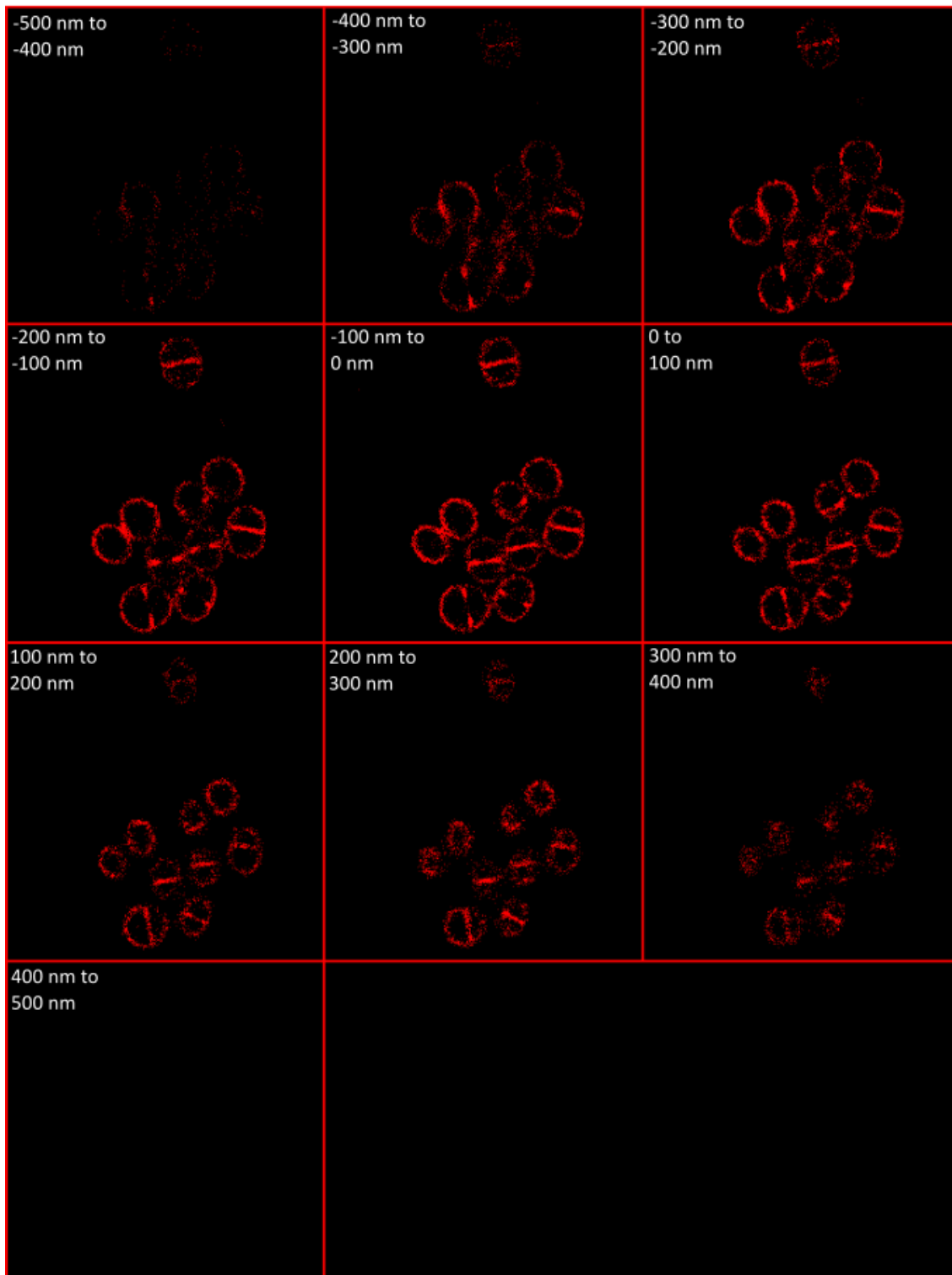


Merge

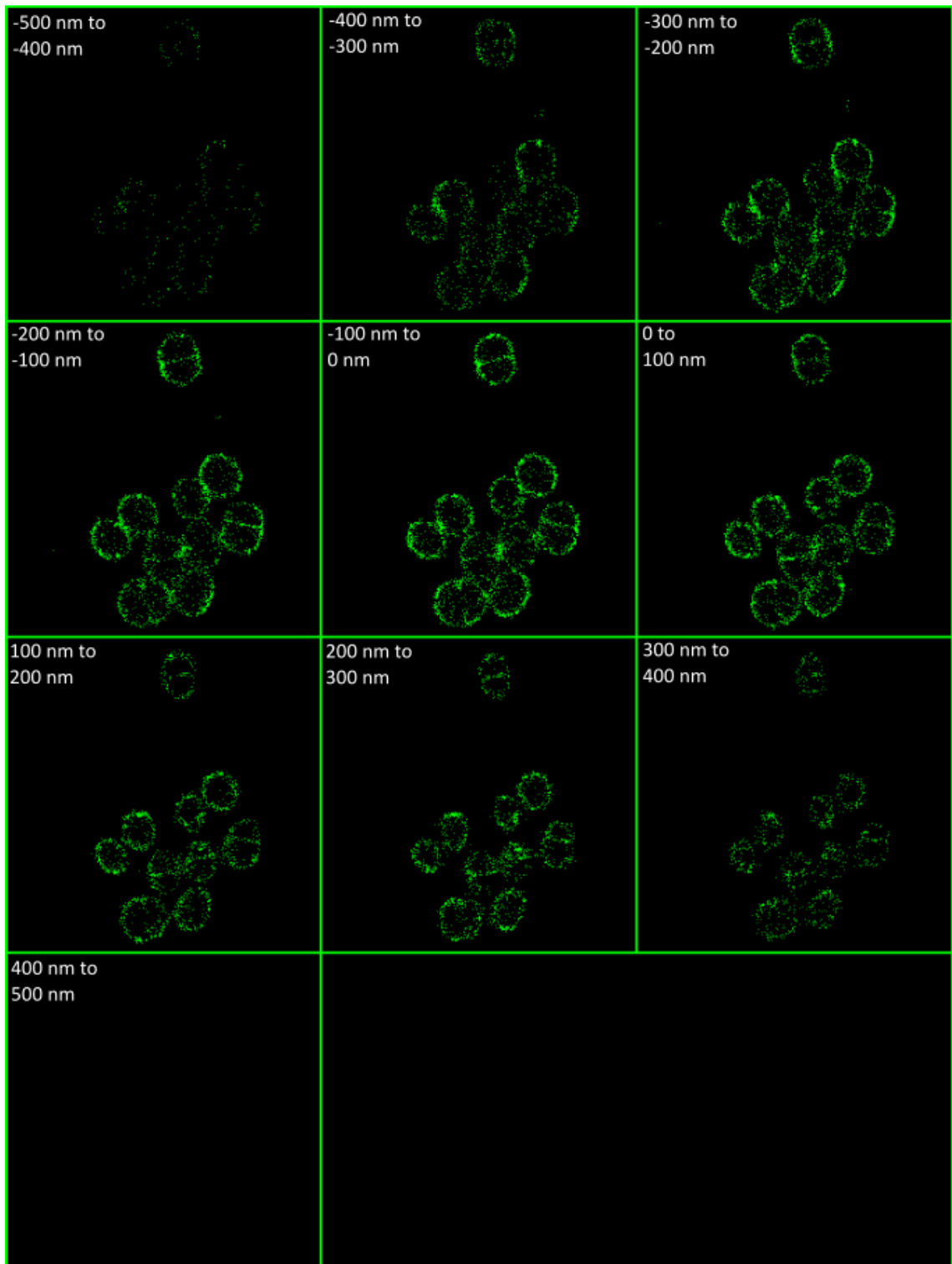


C

Dipeptide



Vancomycin



Merge

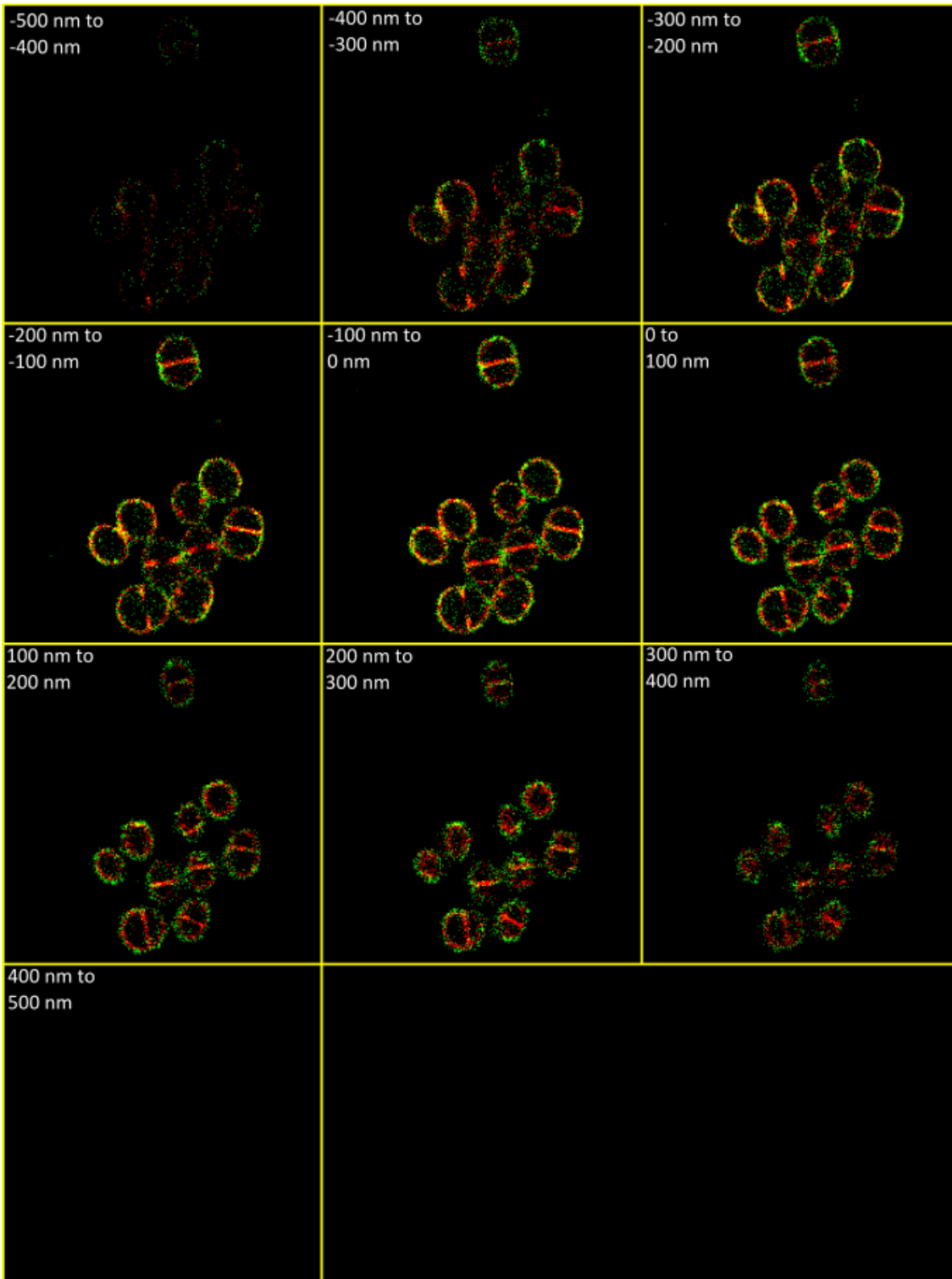
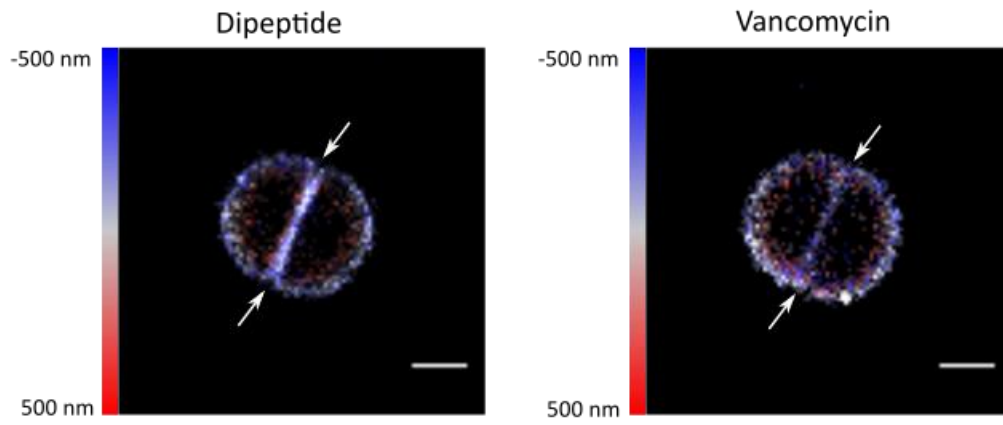


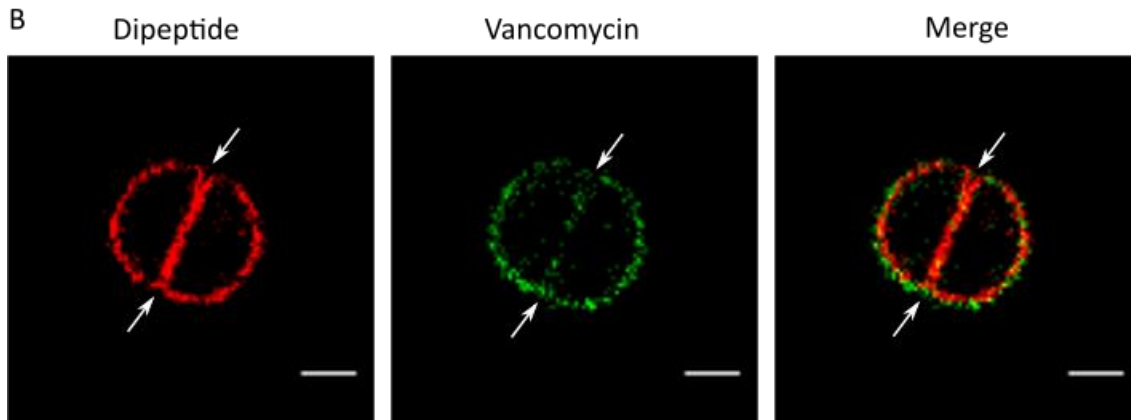
Figure 4.9. STORM of cells dual labelled with dipeptide and vancomycin.

Peptidoglycan synthesis is labelled for 5 minutes with dipeptide (1mM) while the whole cell wall is labelled with vancomycin (1 mM). (A) Dipeptide and vancomycin labels shown separately as z projections with position of molecules in z represented by colour table in 100 nm slices. (B) Single 100 nm slice highlighting presence of peptidoglycan within gaps of peptidoglycan synthesis but not in the peptidoglycan layer (indicated by arrow), dipeptide coloured red & vancomycin coloured green. (C) Z-sectioning of the two labels and the channels merged, split into 100 nm slices. (Scale bar 1 μm).

A

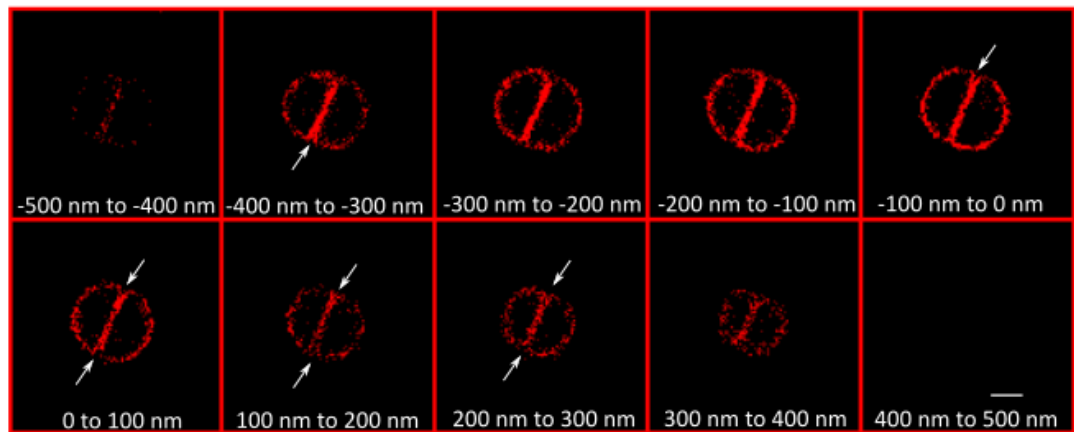


B

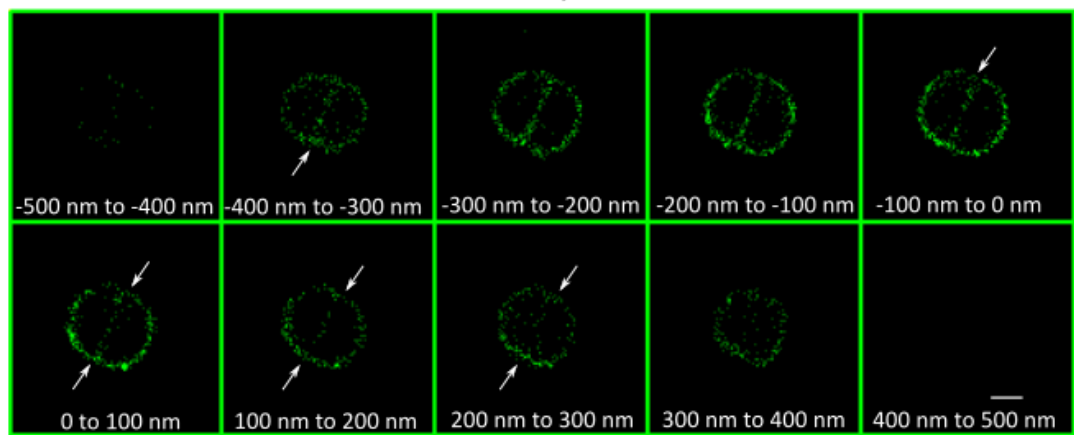


C

Dipeptide



Vancomycin



Merge

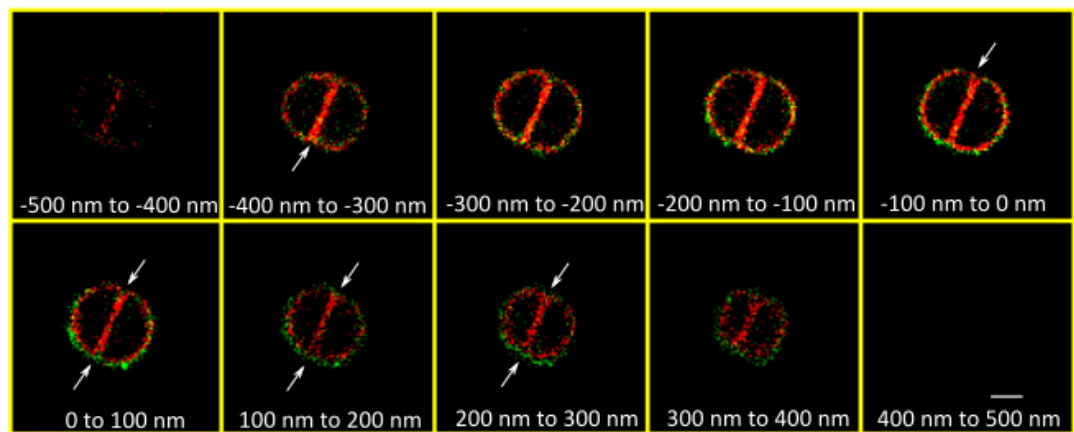


Figure 4.10. STORM of dual dipeptide and vancomycin labelled *S. aureus*.

Peptidoglycan synthesis is labelled for 5 minutes with dipeptide (1 mM) while the whole cell wall is labelled with vancomycin (1 mM). Dipeptide labelling shows a gap at both sides of the septum while vancomycin labelling does not. (A) Dipeptide and vancomycin labels shown separately as z projections with position of molecules in z represented by colour table in 100 nm slices. (B) Single 100 nm slice highlighting presence of peptidoglycan within gaps of peptidoglycan synthesis, dipeptide coloured red & vancomycin coloured green. (C) Z-sectioning of the two labels and the channels merged, split into 100 nm slices. (Scale bar 1 μm).

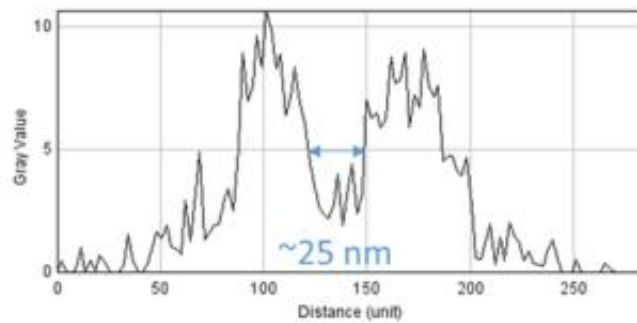
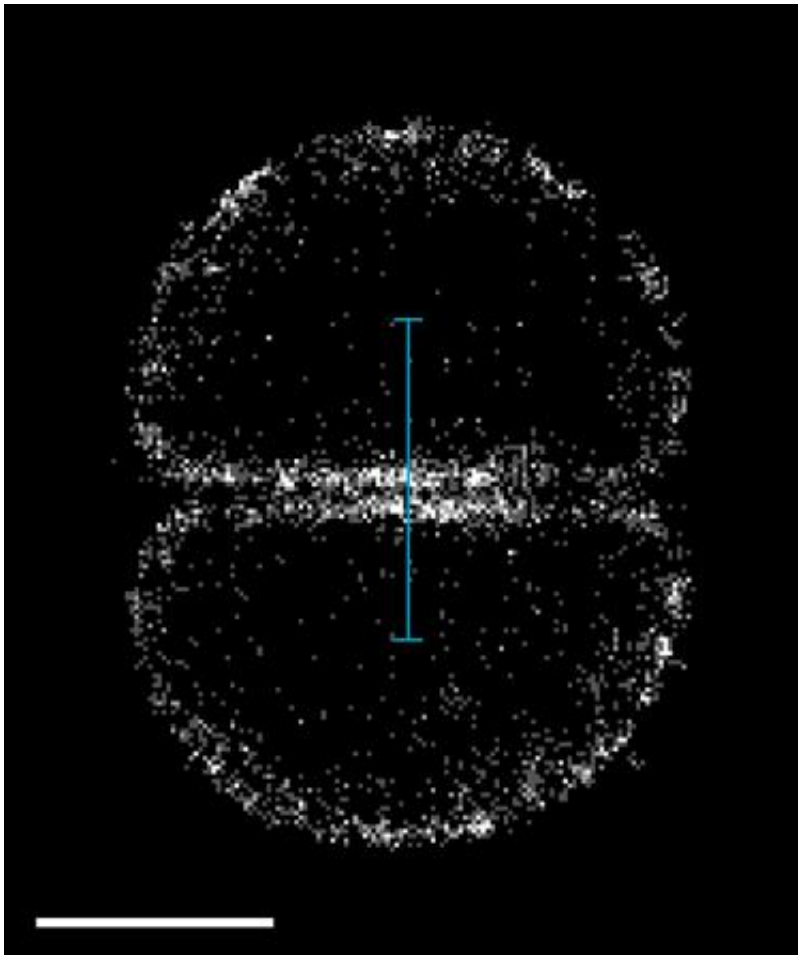


Figure 4.11. Measurement of gap between two areas of peptidoglycan synthesis. A grey value profile was plotted for the line indicated. The gap between the 2 peaks was measured as ~ 25 nm.(Scale bar 500 nm).

with FDAA and vancomycin or whether this phenomenon is present in cells with incomplete septa.

4.2.4 Peptidoglycan insertion is not confined to the septum

Perhaps the most surprising observation was the presence of peptidoglycan synthesis labelling out with the septum as this would suggest that new peptidoglycan synthesis is not limited to septation as previously thought (Pinho and Errington, 2003; Turner et al., 2010a). Further investigation showed that this labelling is present in diffraction limited and SIM images (Figure 4.1). This non-septal peptidoglycan labelling, hereafter referred to as off-septal synthesis or labelling, offers a potential new mode of growth by *S. aureus* and provides further insight into the processes of growth and division in *S. aureus*.

To determine the proportion of fluorescence not associated with septal peptidoglycan synthesis a modified corrected total cell fluorescence (CTCF) protocol was used to calculate the non-septal fluorescence in diffraction limited images (McCloy et al., 2014). Corrected total cell fluorescence is calculated by the following equation:

$$CTCF = \text{Integrated density} - (\text{area of selected cell} \times \text{background mean fluorescence})$$

The CTCF for both the total cell and the septum were calculated and the percentage non-septal fluorescence determined. These calculations were performed on z-projections of diffraction-limited images for ease and because neither SIM nor STORM data should be used for quantitative analysis due to the methods used in image reconstruction.

Calculation for the *S. aureus* wildtype strain, SH1000, estimated non-septal fluorescence at $54 \pm 7\%$. Since there is limited cytosolic labelling with FDAAs this was attributed to off-septal labelling of the cell wall. Before the role of off septal synthesis in the growth of *S. aureus* could be assessed, it was first necessary to determine that the fluorescence signal was due to labelling of peptidoglycan synthesis rather than an artefact of the labelling process.

Chemical treatment of *S. aureus* labelled with ADA-Alexa Fluor 647 to remove different components of the cell wall was carried out in order to determine whether the off-septal incorporation was due to labelling of peptidoglycan or another structure (Figure

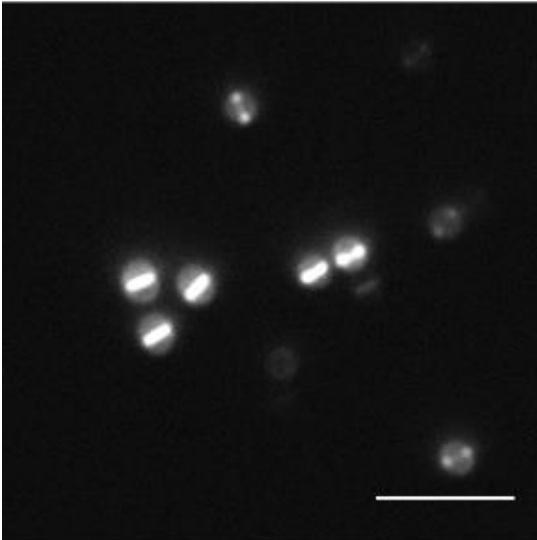
4.12). The treatments used were as follows; SDS to remove any non-covalently bound proteins, pronase to digest any covalently bound proteins, sodium borohydride to reduce the reducing termini of glycan strands and HF to remove teichoic acids. Off-septal labelling remained following these chemical treatments, suggesting that the off-septal labelling occurs in the peptidoglycan (Figure 4.12). In both sodium borohydride and HF treated cells the normal labelling pattern was reduced, in the case of HF treated cells normal labelling was almost completely eliminated. This is most likely due to the harsh effects of chemical treatments on the fluorophore and may be eliminated by carrying out the click reaction following chemical treatment. Another means to determine the presence of off-septal labelling on peptidoglycan is the imaging of purified sacculi (Figure 3.11). However, due to cell breakage during the purification process it is difficult to distinguish between septal and off-septal peptidoglycan.

Teichoic acids are decorated with D-alanine residues and therefore FDAAs may be able to label these structures (Brown et al., 2013). The *dltA* gene of *S. aureus* encodes a D-alanine-D-alanyl carrier protein and the *S. aureus dltA* mutant completely lacks D-alanine in either LTAs or WTAs (Peschel et al., 1999). Labelling the *dltA* mutant with HADA for 5 minutes resulted in similar off-septal labelling as SH1000 (Figure 4.13 A). Deletion of the WTA biosynthetic gene *tarO* produces a strain that is lacking in WTAs (Xia and Peschel, 2008). Once again labelling this mutant for 5 minutes with HADA resulted in no removal or reduction in off-septal labelling (Figure 4.13 A). Calculation of off-septal labelling using the modified CTCF described above determined off-septal labelling to be $57 \pm 7 \%$ and $67 \pm 6 \%$ for the *dltA* and *tarO* mutants respectively. This in fact represents a slight increase in off-septal labelling for these mutants, particularly for the *tarO* mutant (Figure 4.13 B). This increase was coupled with an increase in average CTCF for whole cells and may be due to PBP4 mislocalisation (Figure 4.13 C)(Atilano et al., 2010).

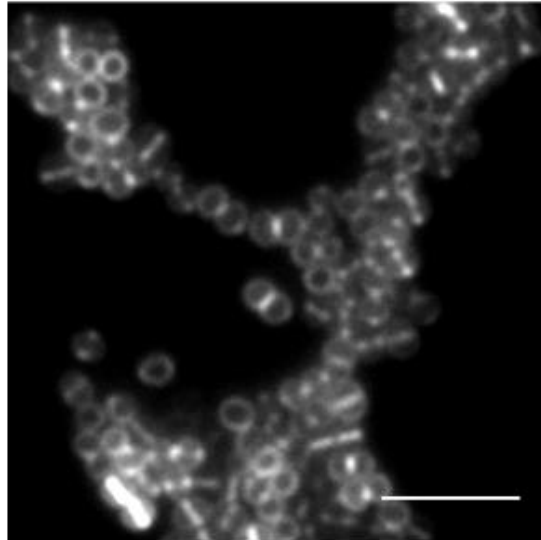
4.2.5 Role of peptidoglycan synthesis enzymes in off-septal labelling of peptidoglycan

Following the demonstration that the off septal labelling is due to peptidoglycan incorporation it was hypothesised that this may be the result of peptidoglycan biosynthetic enzymes. An ordered transposon mutant library exists for *S. aureus*

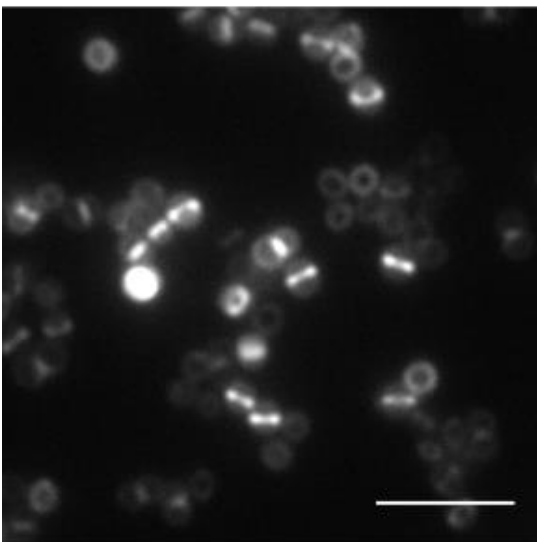
Control



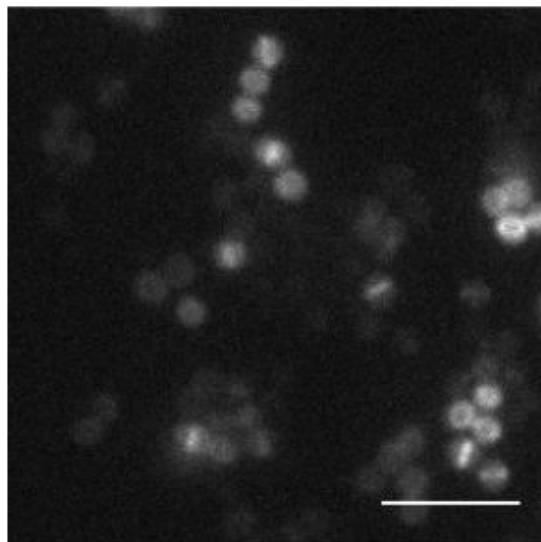
SDS treated



Pronase treated



Sodium borohydride treated



Hydroflouric acid treated

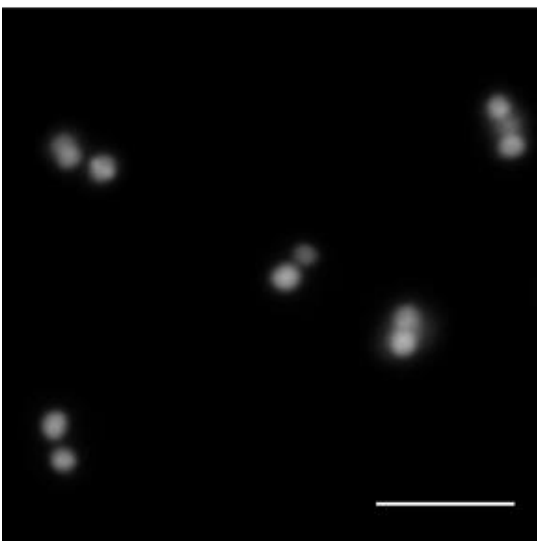
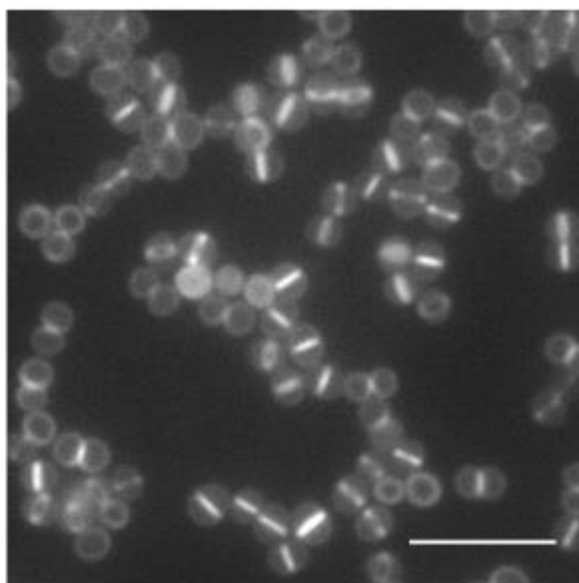


Figure 4.12. Chemical treatment of *S. aureus* to investigate off-septal labelling.

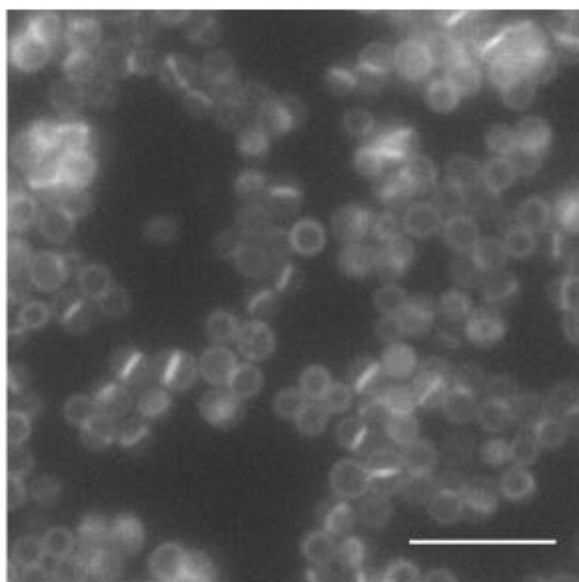
Diffraction limited images of SH1000 labelled with ADA (500 μM)(Alexa Flour 647 at 5 $\mu\text{g ml}^{-1}$ in Click reaction) for 5 minutes then treated with 5% (w/v) SDS for 15 min, 2 mg ml^{-1} pronase for 90 min, 5 mg ml^{-1} sodium borohydride for 15 min or 48% (w/v) hydrofluoric acid for 48 h.

A

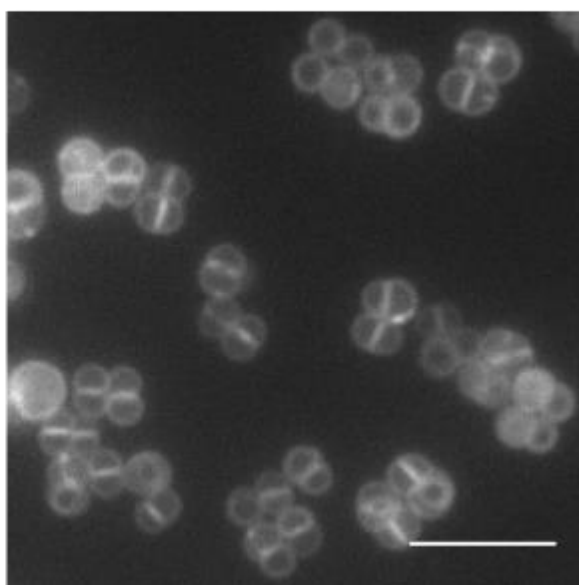
SH1000



ΔdltA



ΔtarO



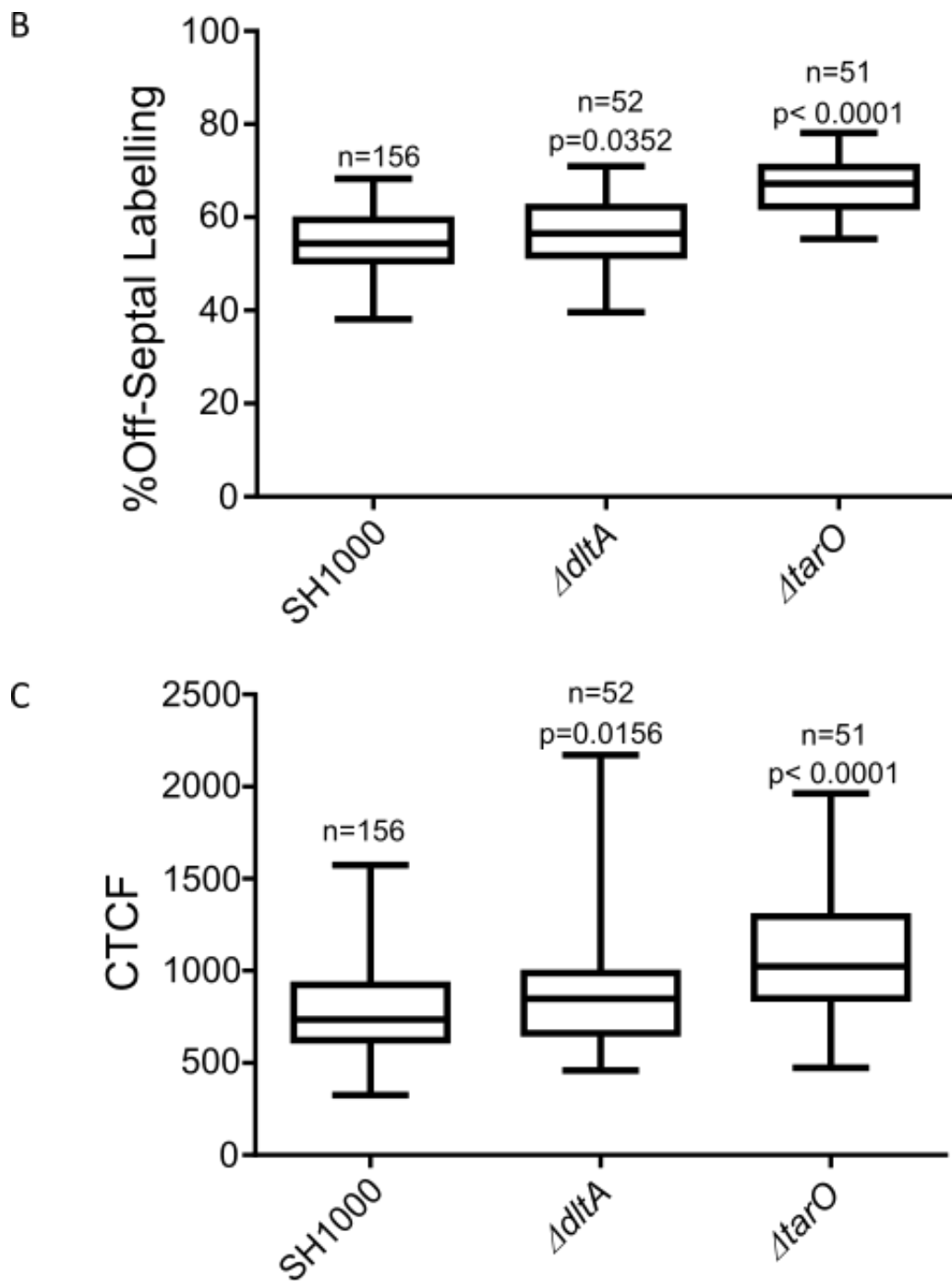


Figure 4.13. Contribution of teichoic acids to off-septal labelling. (A) Diffraction limited images of SH1000, $\Delta dltA$, $\Delta tarO$ labelled for 5 minutes with HADA (500 μ M). (Scale bar 5 μ m). (B) Box plot of % off-septal labelling in SH1000, $\Delta dltA$, $\Delta tarO$. Box extends from 25th to 75th percentiles and midline is plotted at the median. Whiskers are drawn down to the minimum value and up to the maximum value. P values are the result of Mann-Whitney tests comparing mutants with the wildtype (SH1000). (C) Box plot of corrected total cell fluorescence (CTCF). Box and p values same as for off-septal fluorescence.

containing nearly 2,000 strains with non-essential genes disrupted (Fey et al., 2013). Included within this library are mutations in a number of genes coding for cell division and peptidoglycan synthesis components. The five most promising candidates along with the library parental strain, JE2, were labelled for 5 minutes with HADA and the amount of off septal incorporation assessed (Figure 4.14). The five genes chosen for study were the two non-essential PBPs (*pbp3* & *pbp4*), the monofunctional transglycosylases (*sgtA* & *mgt*) and the FtsW homolog (*rodA*). The *rodA* mutant, NE1598, is attributed as a hypothetical protein with the transposon inserted into SAUSA300_2040. This was found to be a homolog of *ftsW*, the lipid II flippase, and has been assigned as *rodA* (http://aureowiki.med.uni-greifswald.de/SAUSA300_2040).

The off-septal labelling of JE2 was found to be 43 ± 6 %, which is lower than that of SH1000. This indicates a degree of variation between the strains. The percentage off-septal labelling for each of the transposon mutants was calculated and compared to JE2 (Figure 4.14 B). The % off-septal labelling for the mutants was not found to be significantly reduced compared to JE2, although there was an increase for the *pbp3*, *sgtA*, *mgt* and *rodA* mutants and a slight decrease for the *pbp4* mutant. This decrease for the *pbp4* mutant may suggest that PBP4 may play some role in the off-septal labelling, however, this small reduction in off-septal labelling is associated with a large reduction in CTCF (Figure 4.14 C). There is also a reduction seen in labelling with the *mgt* mutant. This suggests that both PBP4 and MGT may play a role in the insertion of FDAA labelled precursors into the cell wall rather than a specific role of PBP4 in off-septal synthesis of peptidoglycan.

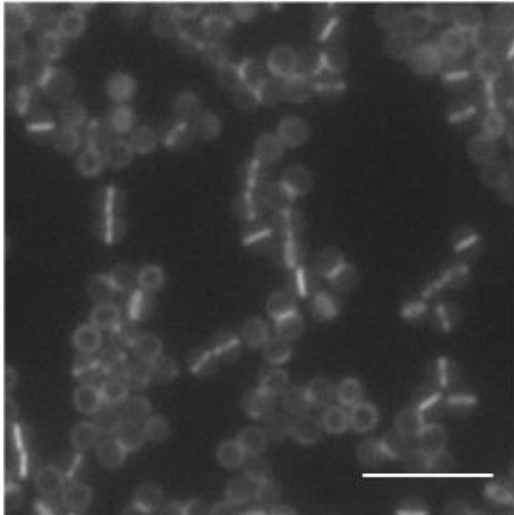
4.2.6 Role of penicillin binding proteins in synthesis of peptidoglycan

The role of the PBPs in peptidoglycan synthesis was further assessed. The *pbp3* and *pbp4* mutants were transduced into the SH1000 background, to give strains 4421 and 4425 respectively, and a *pbp3pbp4* double mutant created (4424). These strains were produced and verified by Kasia Wacnik.

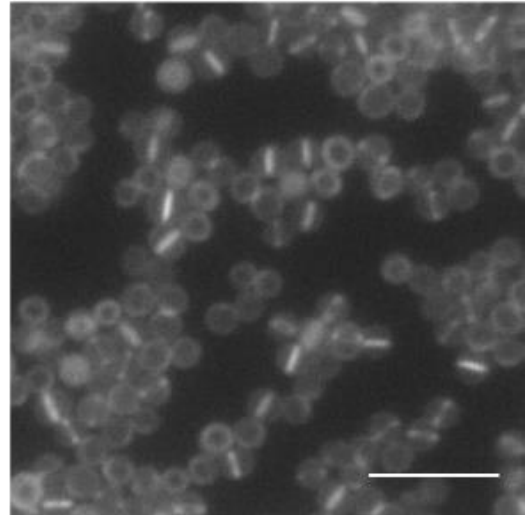
Within the SH1000 background images of both the wildtype and PBP mutant strains have off-septal labelling as in the JE2 background (Figure 4.15). This off-septal labelling

A

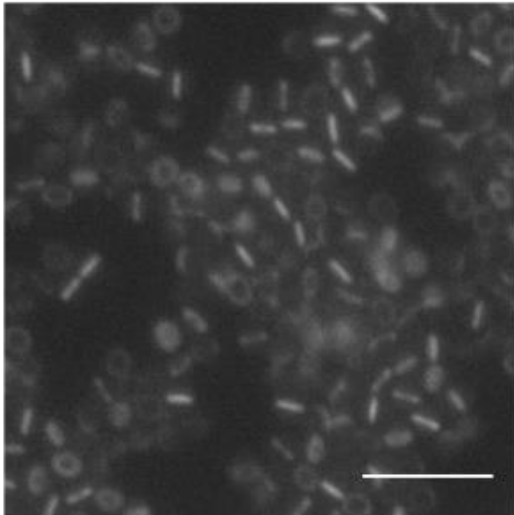
JE2



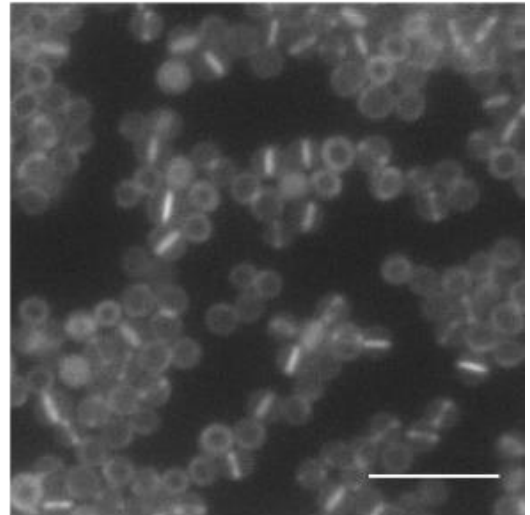
NE420 (*pbp3*)



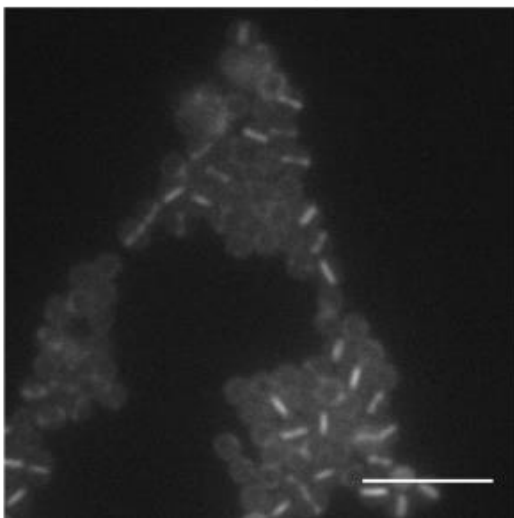
NE679 (*pbp4*)



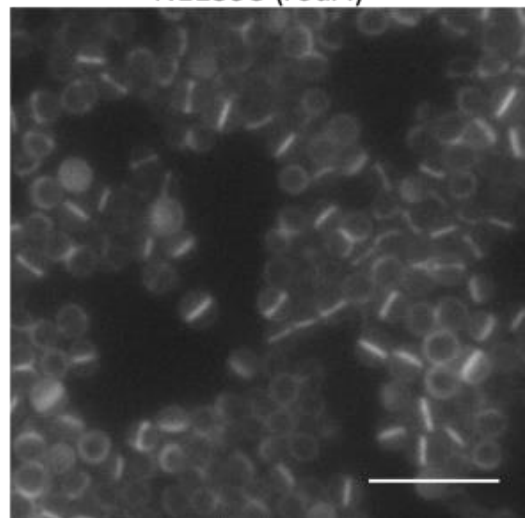
NE267 (*sgtA*)



NE596 (*mgt*)



NE1598 (*rodA*)



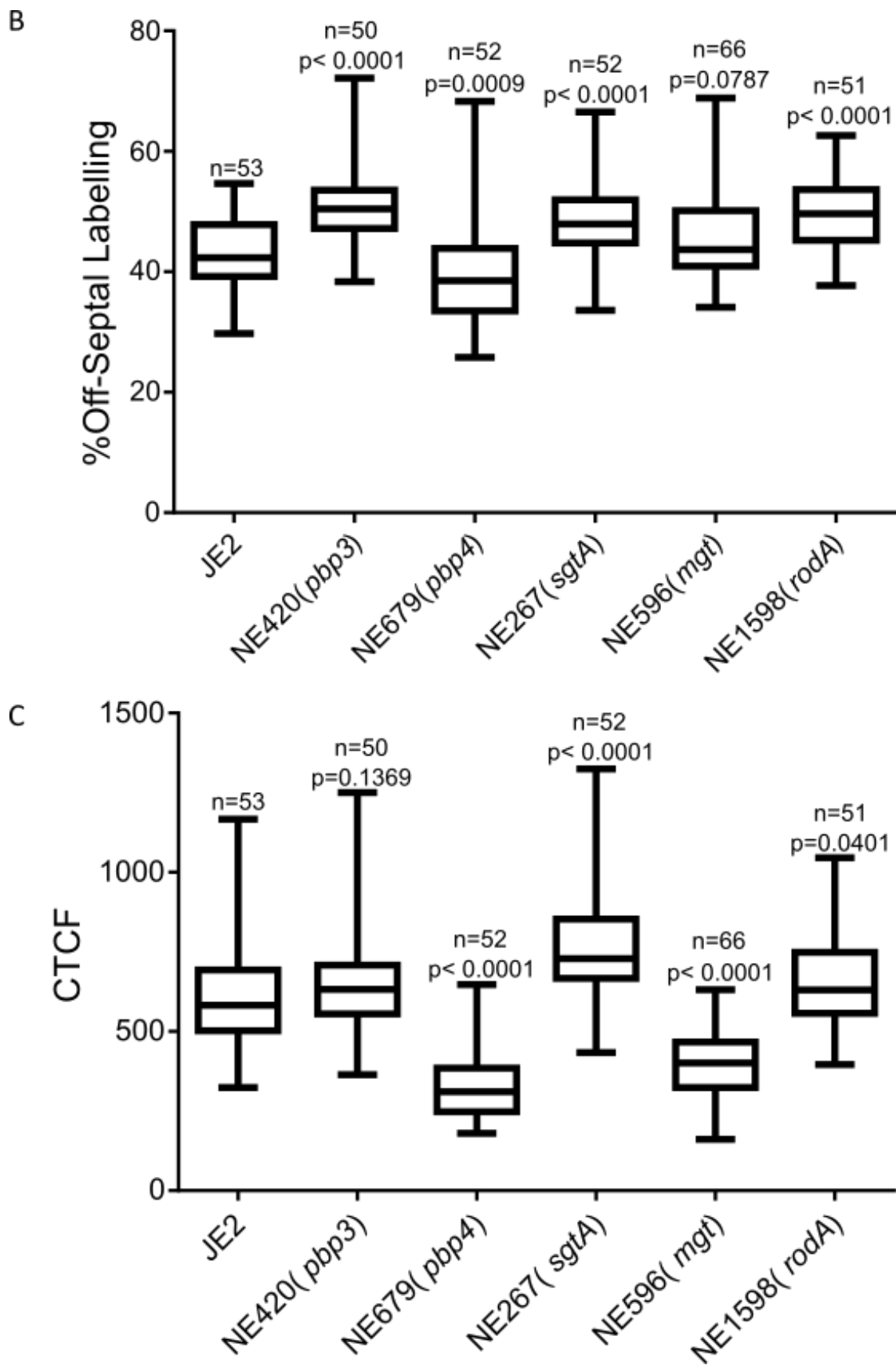


Figure 4.14. Off-septal labelling in Nebraska library mutants. (A) Diffraction limited images of strains labelled for 5 minutes with HADA (500 μ M). (Scale bar 5 μ m). (B) Box

plot of % off-septal labelling for the tested strains. Box extends from 25th to 75th percentiles and midline is plotted at the median. Whiskers are drawn down to the minimum value and up to the maximum value. P values are the result of Mann-Whitney tests comparing mutants with the parental strain (JE2). (C) Box plot of corrected total cell fluorescence (CTCF). Box and p values same as for off-septal fluorescence.

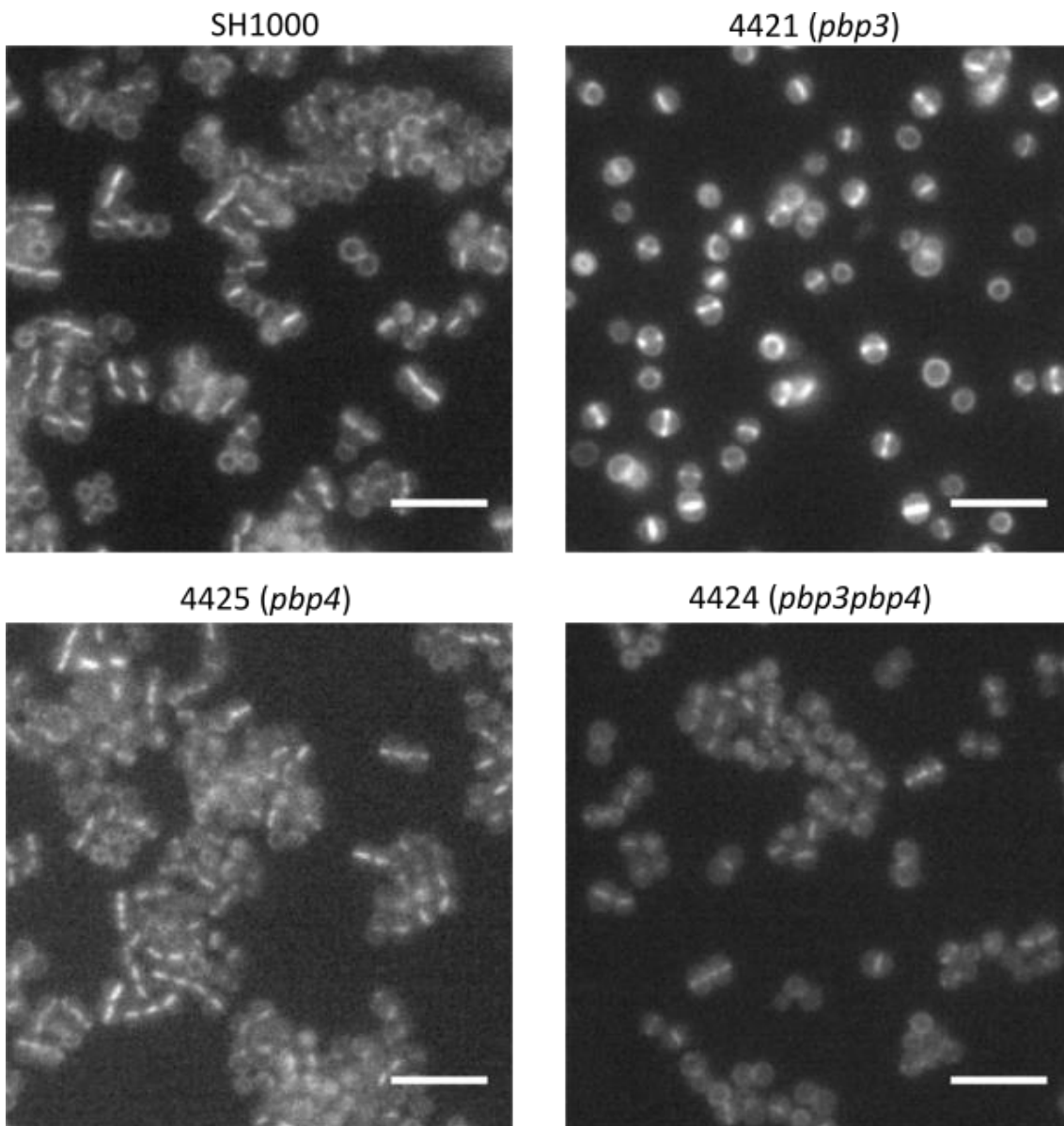
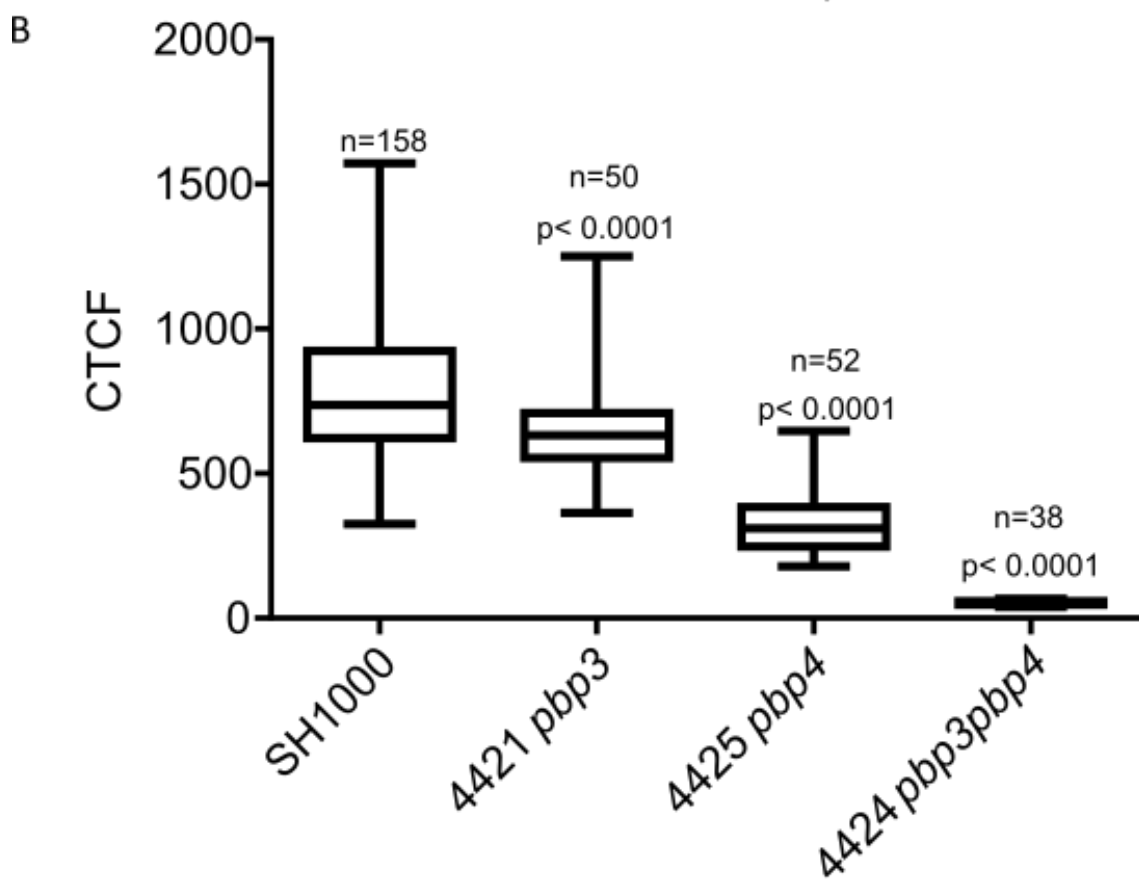
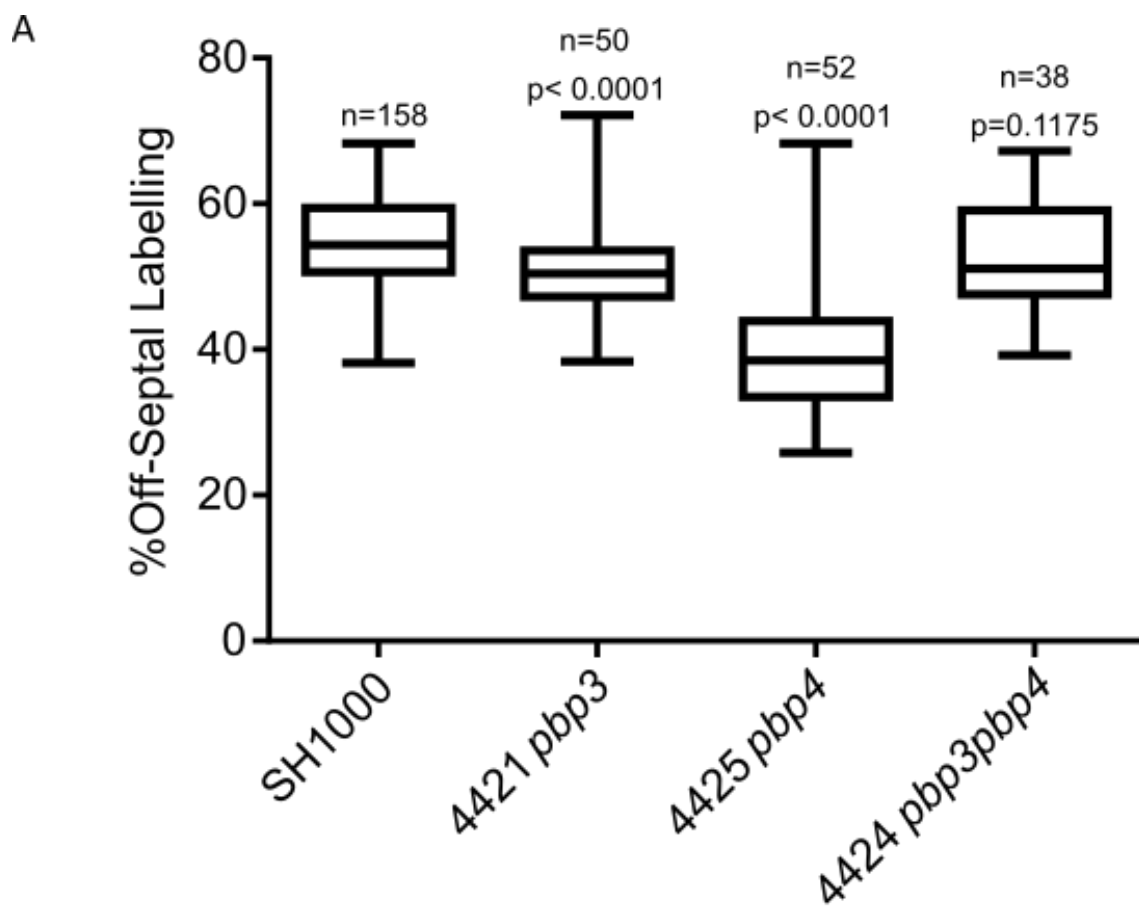


Figure 4.15. Role of PBP3 and PBP4 in off-septal labelling. Diffraction limited images of SH1000, 4421 (*pbp3*), 4425 (*pbp4*) & 4424 (*pbp3pbp4*) labelled with HADA (500 μ M) for 5 minutes. (Scale bar 5 μ m).

is also seen in the double mutant. Quantification of the off-septal labelling gave 55 ± 6 % for SH1000, 51 ± 6 % for 4421 (*pbp3*), 34 ± 7 % for 4425 (*pbp4*) and 53 ± 7 % for 4424 (*pbp3pbp4*) (Figure 4.16 A). The *pbp3* mutant while having a lower mean value shows the same approximate minimum and maximum values for % off-septal labelling suggesting PBP3 does not have a significant role in off-septal labelling. The % off-septal value for 4425 (*pbp4*) is significantly lower than that of SH1000, however the double mutant is not significantly different from SH1000. It is unclear why this may be the case, but may reflect indirect effects of inactivation of both activities. The CTCF of these strains revealed that deletion of the non-essential PBPs results in a reduction in FDAA incorporation into the cell wall (Figure 4.16 B). In the case of the double mutant the CTCF was less than 10% of the SH1000 CTCF. It was hypothesized that this decrease in fluorescence may be due to a reduction in synthesis of peptidoglycan during the labelling period. Comparison of growth rates of SH1000 and the three mutants showed no difference (Figure 4.16 C). Since growth rate is not a factor it may be that the *pbp4* mutant synthesises peptidoglycan at a reduced rate. Peptidoglycan synthesis across the four strains was determined based on the rate of incorporation of ^{14}C GlcNAc over 180 mins. The rate was calculated as DPM per OD unit per minute while cells were growing at exponential phase (Figure 4.16 D). The rate of ^{14}C GlcNAc incorporation whenever *pbp4* was disrupted was not different from that of SH1000 (1634 vs 1727 DPM $\text{OD}_{600}^{-1} \text{min}^{-1}$). The rate for 4421 *pbp3* was higher than that of SH1000 (2124 DPM $\text{OD}_{600}^{-1} \text{min}^{-1}$) however this was not seen in the double mutant (1863 DPM $\text{OD}_{600}^{-1} \text{min}^{-1}$). This shows that the reduction in fluorescence is not due an alteration in peptidoglycan synthesis rather less incorporation of FDAAs when PBP4 is not present. It suggests that the previously mentioned exchange reaction for labelling is mediated by PBP4 (Chapter 3.3.1).

The dipeptide label can only be inserted into peptidoglycan via the synthesis pathway (Liechti et al., 2013). Labelling the PBP mutants with dipeptide therefore would determine if the reduction of CTCF was due to the loss of labelling via the exchange reaction. Both SH1000 and the PBP mutants were labelled for 5 minutes with the dipeptide label and images showed no difference in labelling across the strains (Figure 4.17 A). Quantification of the off-septal labelling showed no reduction in any of the



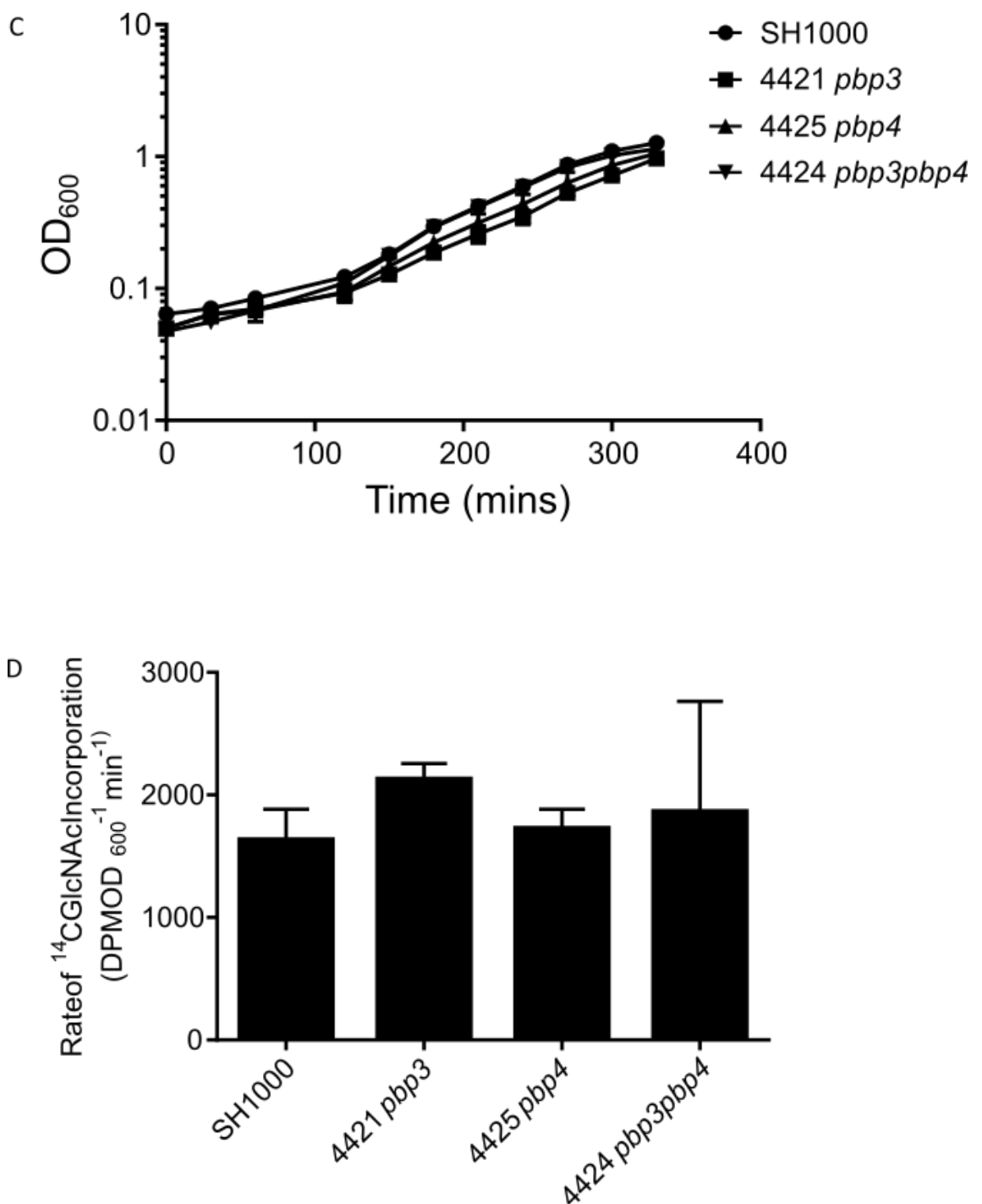
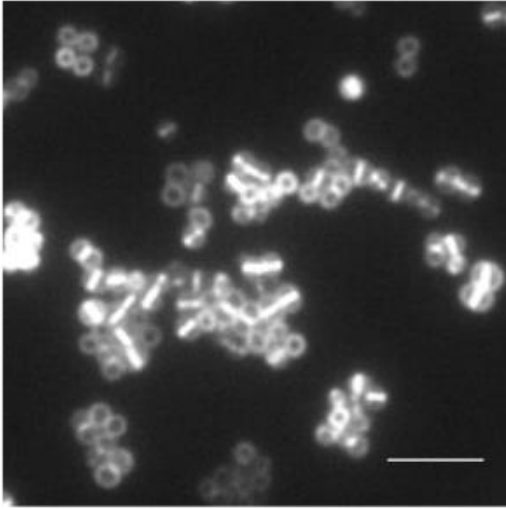


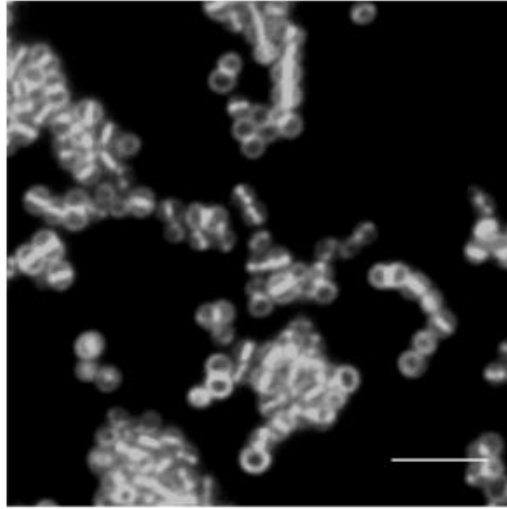
Figure 4.16. Quantification the role of PBP3 and PBP4. (A) Box plot of % off-septal labelling of 5 minutes HADA (500 μ M) incorporation for the PBP mutants. Box extends from 25th to 75th percentiles and midline is plotted at the median. Whiskers are drawn down to the minimum value and up to the maximum value. P values are the result of Mann-Whitney tests comparing mutants with the wildtype. (B) Box plot of corrected total cell fluorescence (CTCF). Box and p values same as for off-septal fluorescence. (C) Growth curve of SH1000 and mutant strains in CDM. (D) Rate of ¹⁴C-GlcNAc Incorporation measured as DPM OD₆₀₀⁻¹ min⁻¹.

A

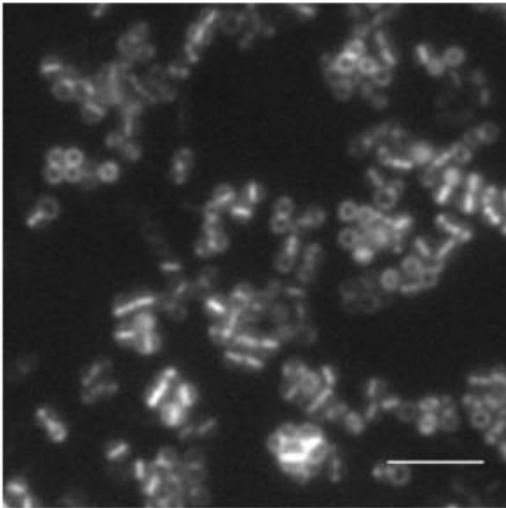
SH1000



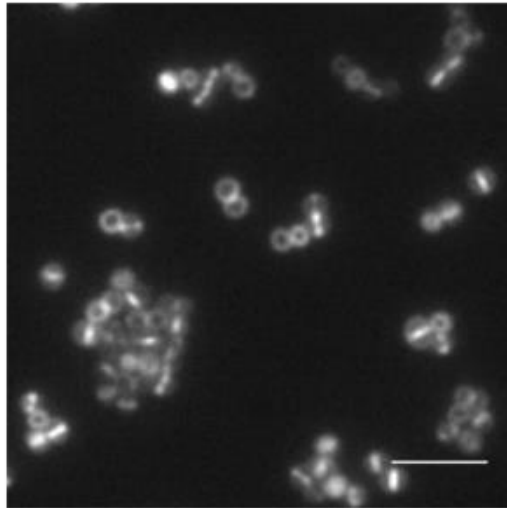
4421 (*pbp3*)



4425 (*pbp4*)



4424 (*pbp3pbp4*)



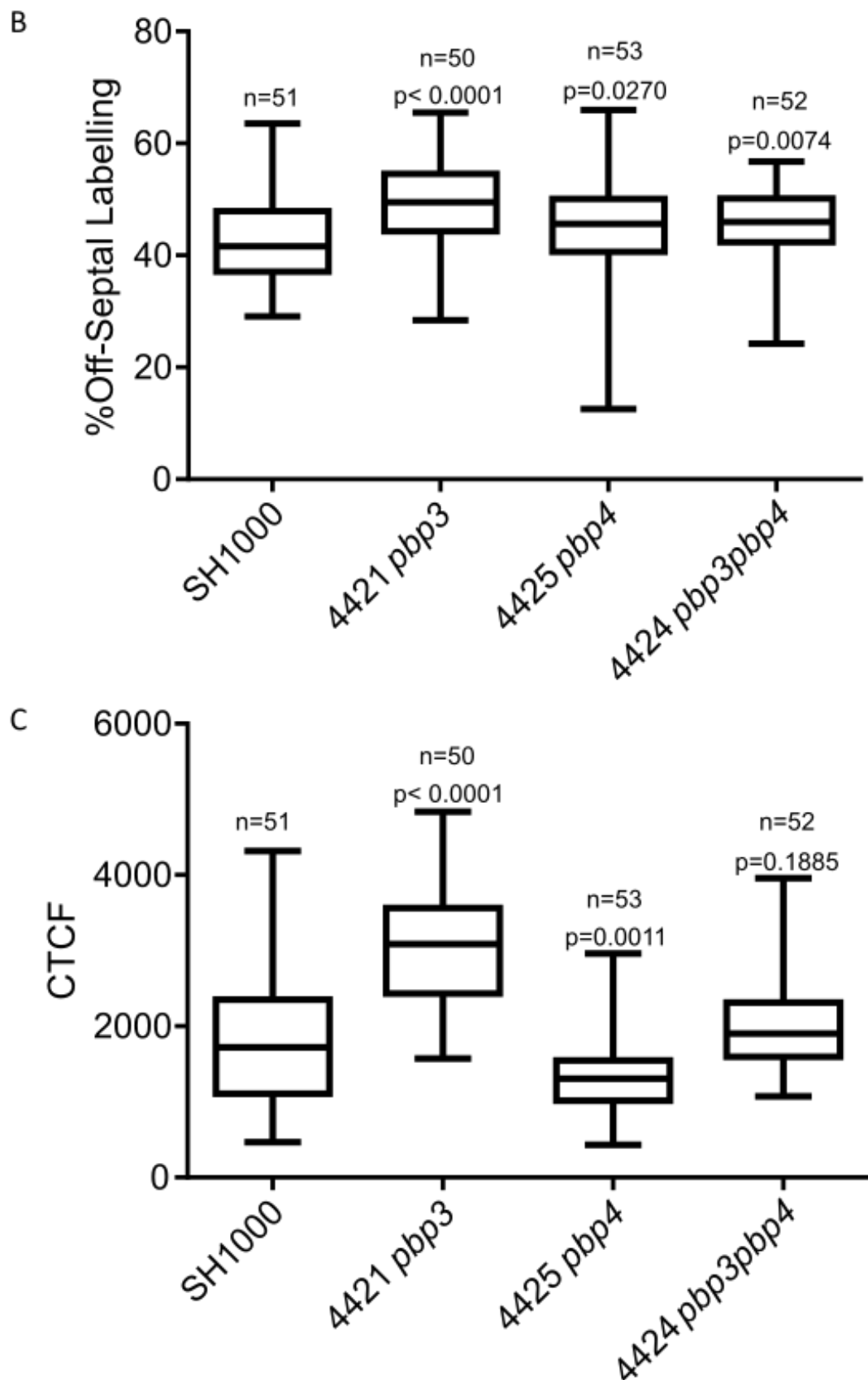


Figure 4.17. Role of PBP3 and PBP4 in off-septal labelling measured via dipeptide incorporation. (A) Diffraction limited images of PBP mutant strains labelled for 5

minutes with dipeptide (1 mM)(Alexa Flour 647 at 5 $\mu\text{g ml}^{-1}$ in Click reaction). (Scale bar 5 μm). (B) Box plot of % off-septal labelling for PBP mutants. Box extends from 25th to 75th percentiles and midline is plotted at the median. Whiskers are drawn down to the minimum value and up to the maximum value. P values are the result of Mann-Whitney tests comparing mutants with the wildtype. (C) Box plot of corrected total cell fluorescence (CTCF). Box and p values as for off septal labelling.

mutant strains, in fact all three were slightly higher than that of SH1000 (Figure 4.17 B). The CTCF for SH1000 and the PBP mutant strains showed a large range of values with 4421 (*pbp3*) showing values significantly higher than SH1000, 4425 (*pbp4*) showing values significantly lower than SH1000 while there was no significant difference in the double mutant 4424 (*pbp3pbp4*) (Figure 4.17 C). This variance is probably due to use of Alexa Fluor 647, an easily bleached fluorophore, within this experimental setup. Contrary to HADA, using dipeptide, PBP4 did not have such a striking role in the level of incorporation.

To determine whether there were any further differences in peptidoglycan synthesis in the PBP mutants the strains were imaged using both SIM and STORM. SIM images of both 4421 (*pbp3*) and 4425 (*pbp4*) showed a similar labelling pattern to SH1000 however the reduction in labelling of these strains made SIM more difficult (Figure 4.18). The reduction in labelling of 4424 (*pbp3pbp4*) meant that reconstruction of images with any cell wall labelling was not possible (Figure 4.18 & Appendix Figure 12). Fourier transforms of SIM image of PBP mutants showed a periodic structure within the images, particularly repetitive dots and stripes in 3 angles, reminiscent of the 3 angles used by the grating during image acquisition (Appendix Figure 9-Appendix Figure 12). To avoid issues with the use of SIM, the PBP mutants were labelled for 5 minutes with ADA and imaged using STORM (Figure 4.19). Within these images the patterns of peptidoglycan synthesis identified previously were present within all strains (Chapter 4.2.1). In particular, the off-septal labelling pattern was seen in all the mutant strains. This result was repeated with 5 minutes labelling of peptidoglycan synthesis with dipeptide (Figure 4.20) thereby showing that these patterns are not due to any exchange reaction mediated by PBP4.

4.2.7 Effect of inhibition of FtsZ by PC190723 on peptidoglycan insertion

4.2.7.1 PC190723

A group of small synthetic antimicrobials have been created with potent bactericidal activity against staphylococcal species and *B. subtilis* however not against other Gram positive and negative bacteria (Haydon et al., 2008). The lead component, PC190723 (

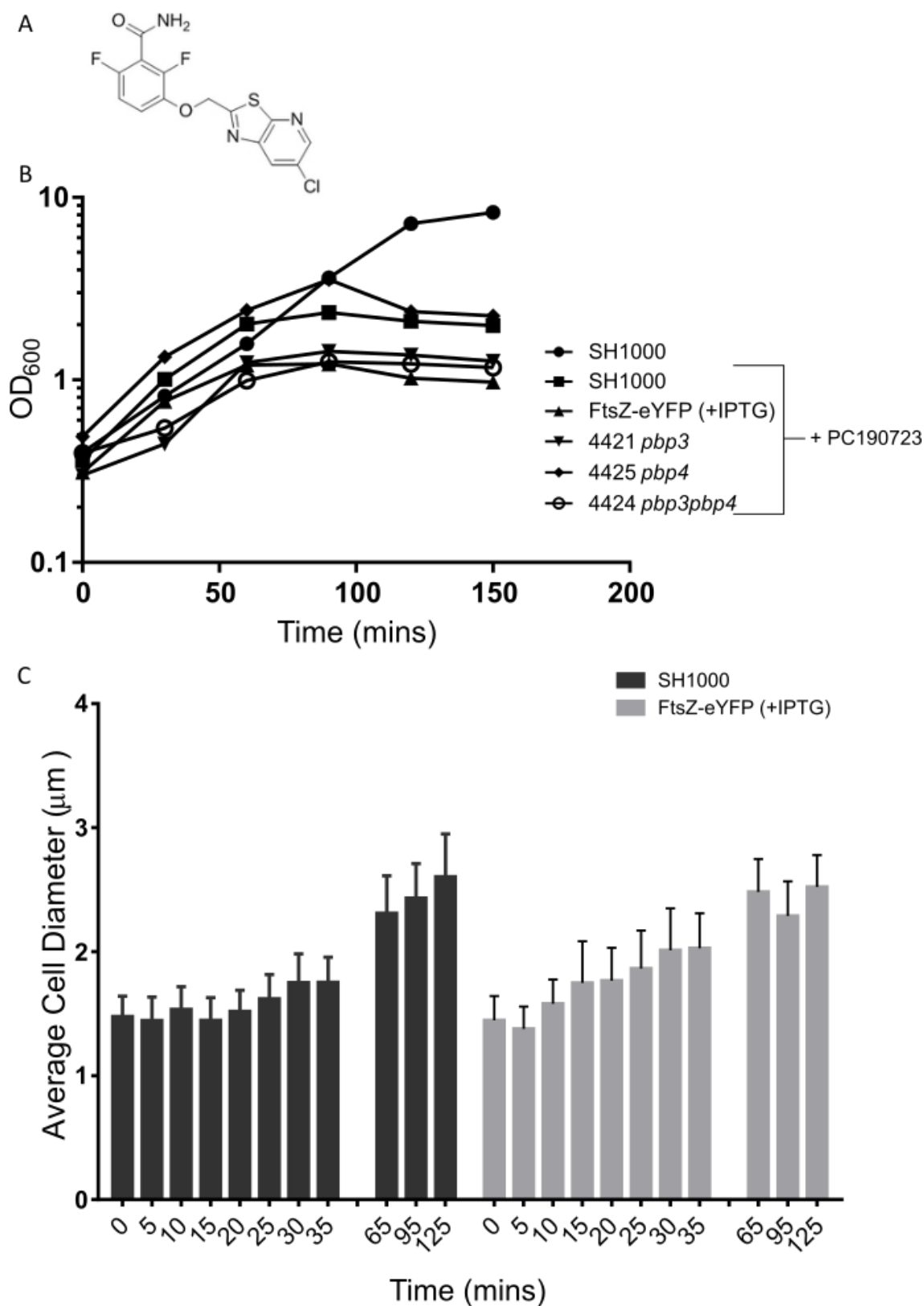


Figure 4.21 A), has been shown to mislocalise FtsZ in *B. subtilis* and *S. aureus* (Haydon et al., 2008; Tan et al., 2012). It has an MIC of 0.5 to 1 $\mu\text{g ml}^{-1}$ against *S. aureus* and an

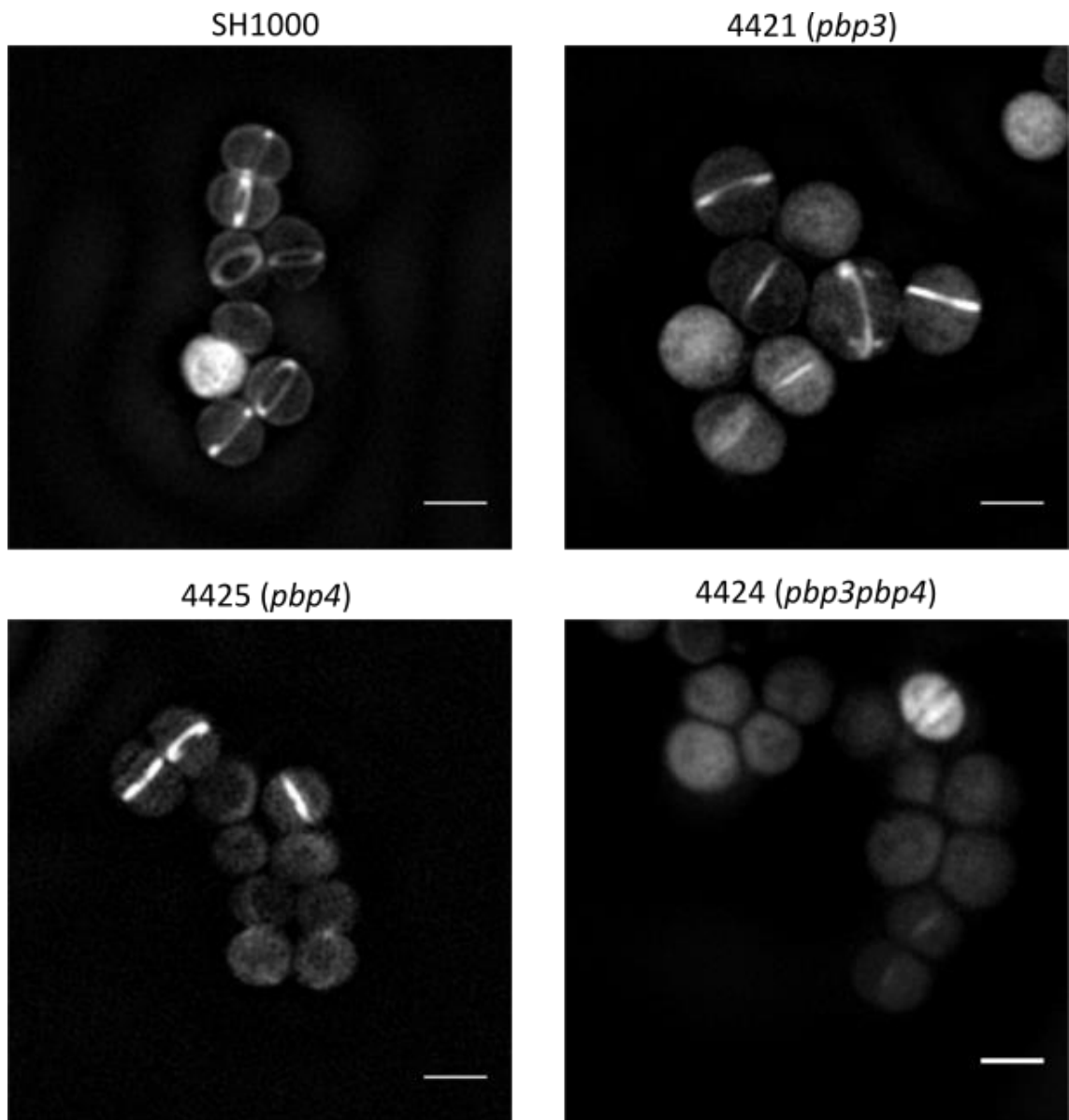
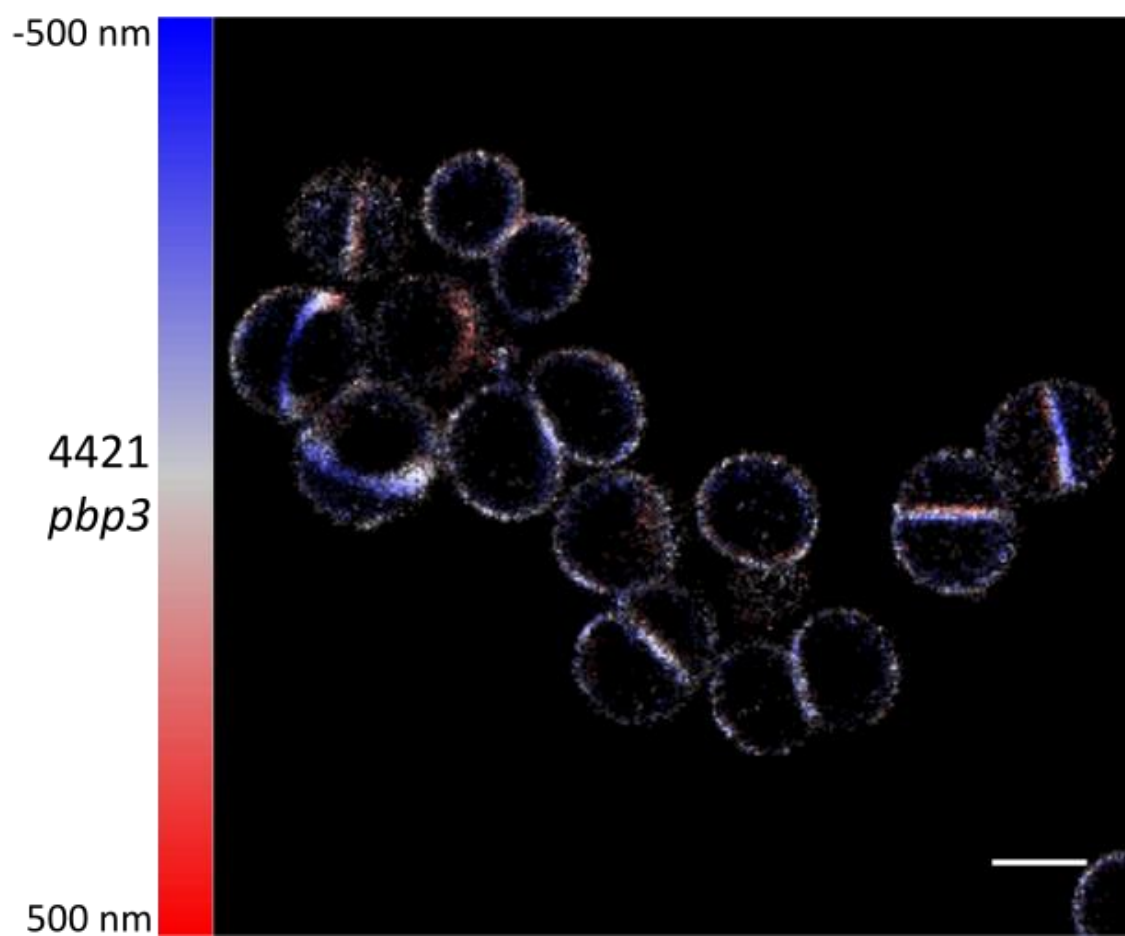
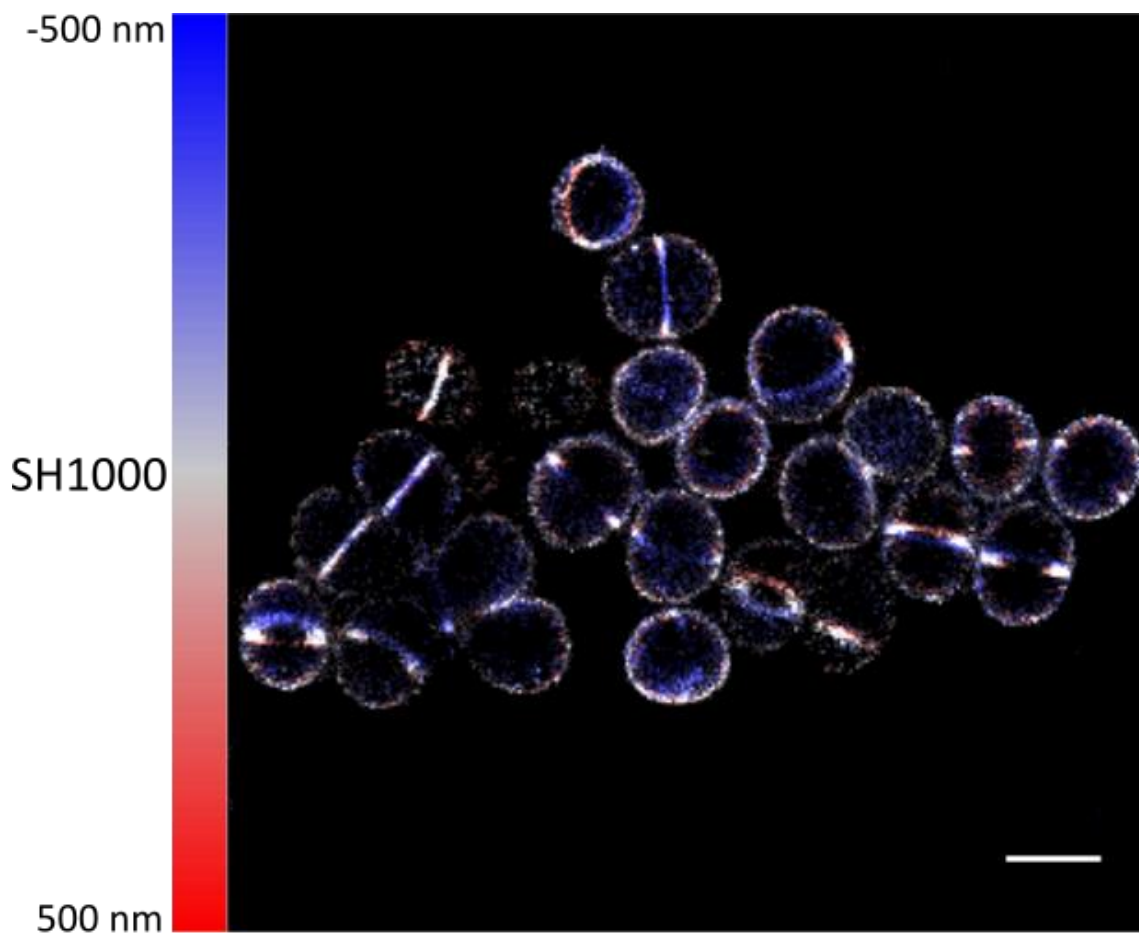


Figure 4.18. SIM of 5 minute HADA labelled PBP mutants. Each strain was labelled for 5 minutes with 5 mM HADA. (Scale bar 1 μ m, average intensity projections).



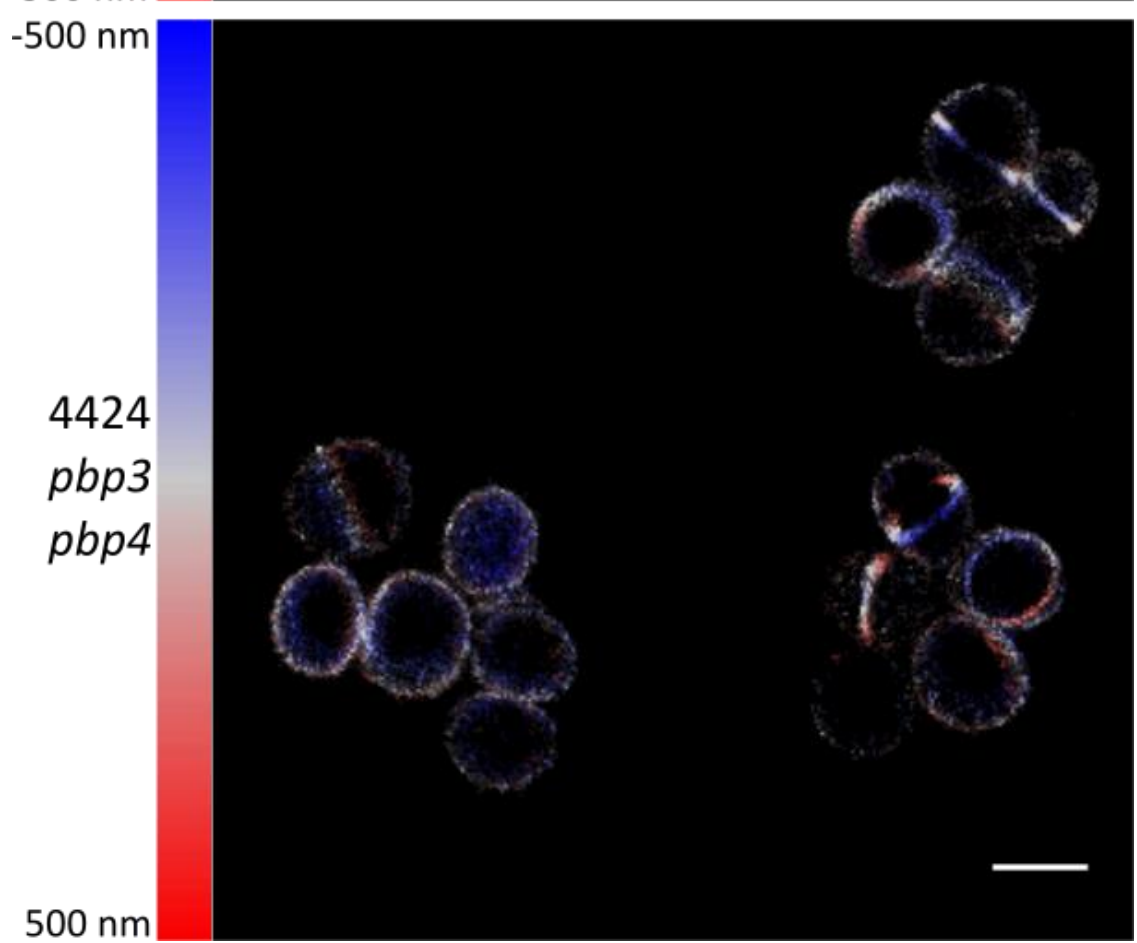
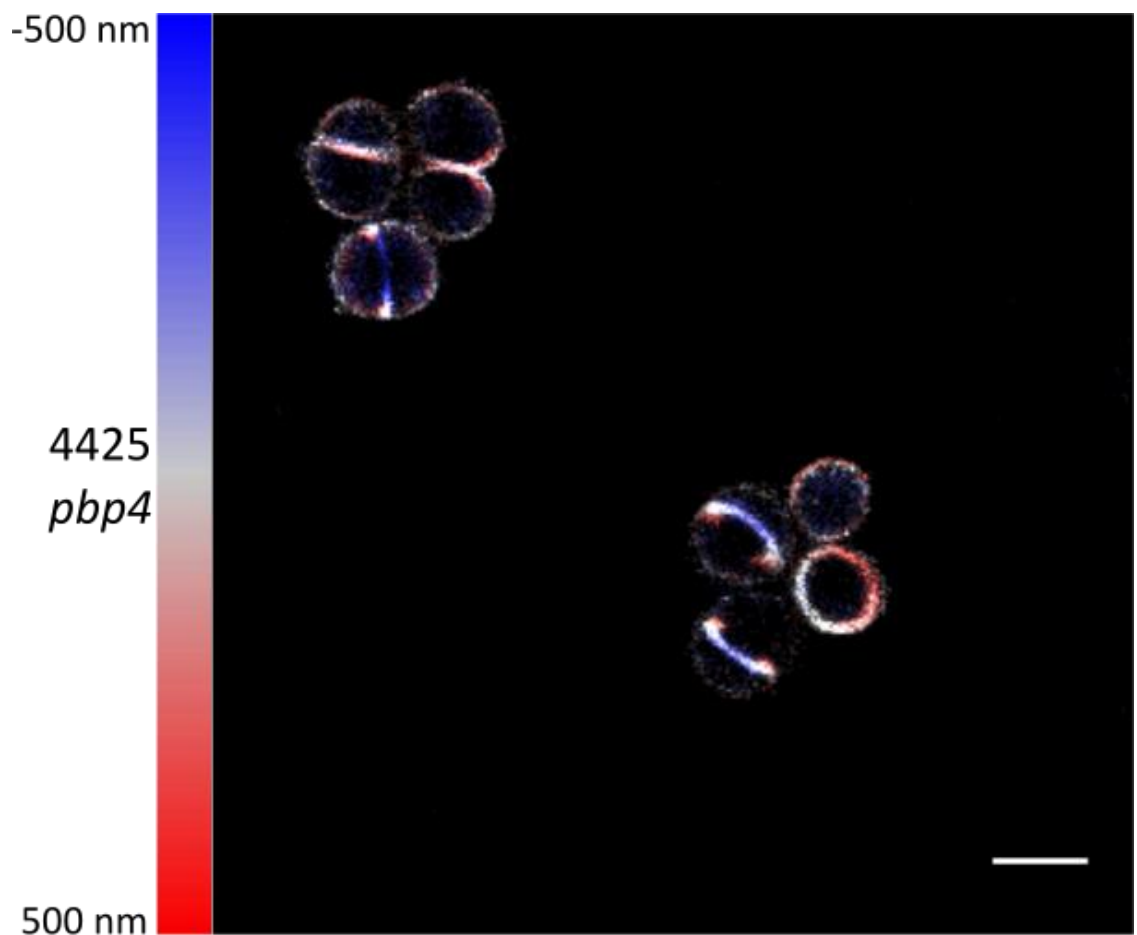
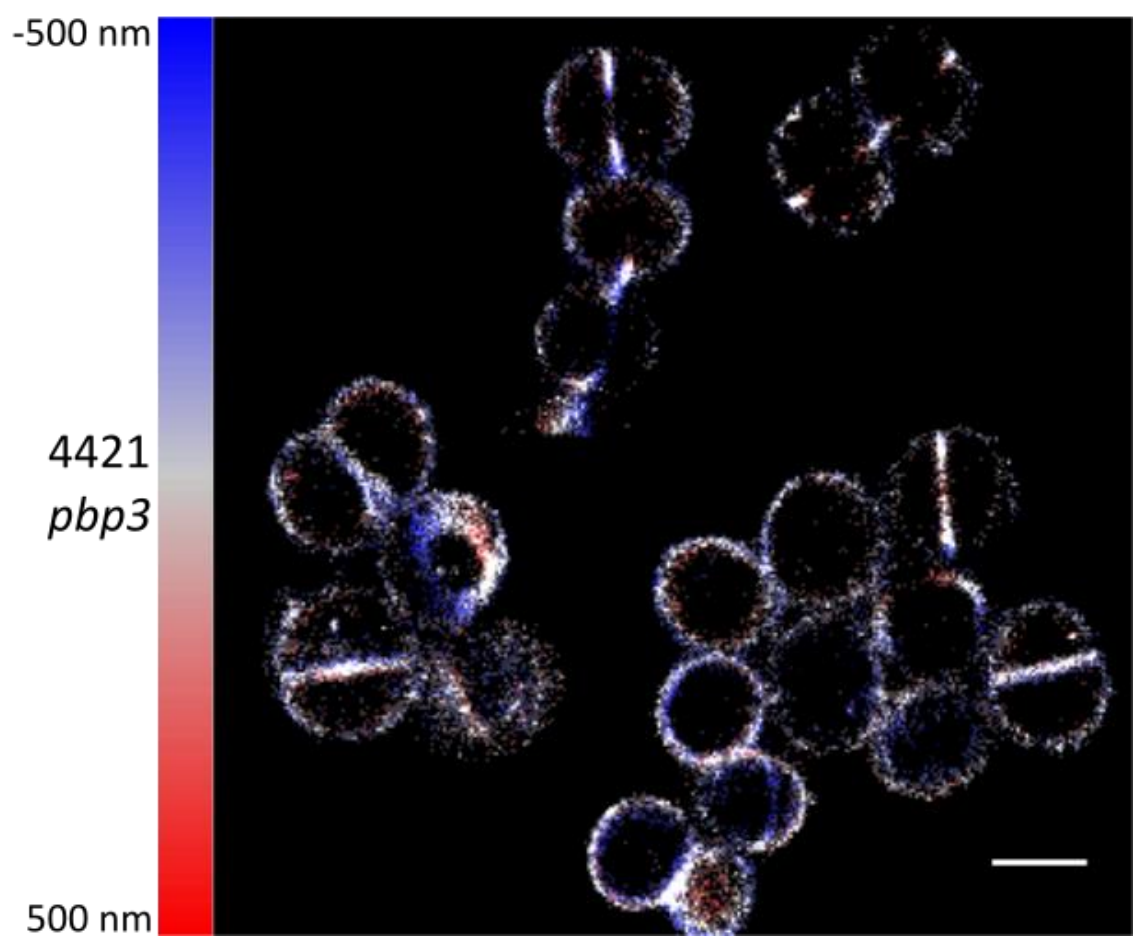
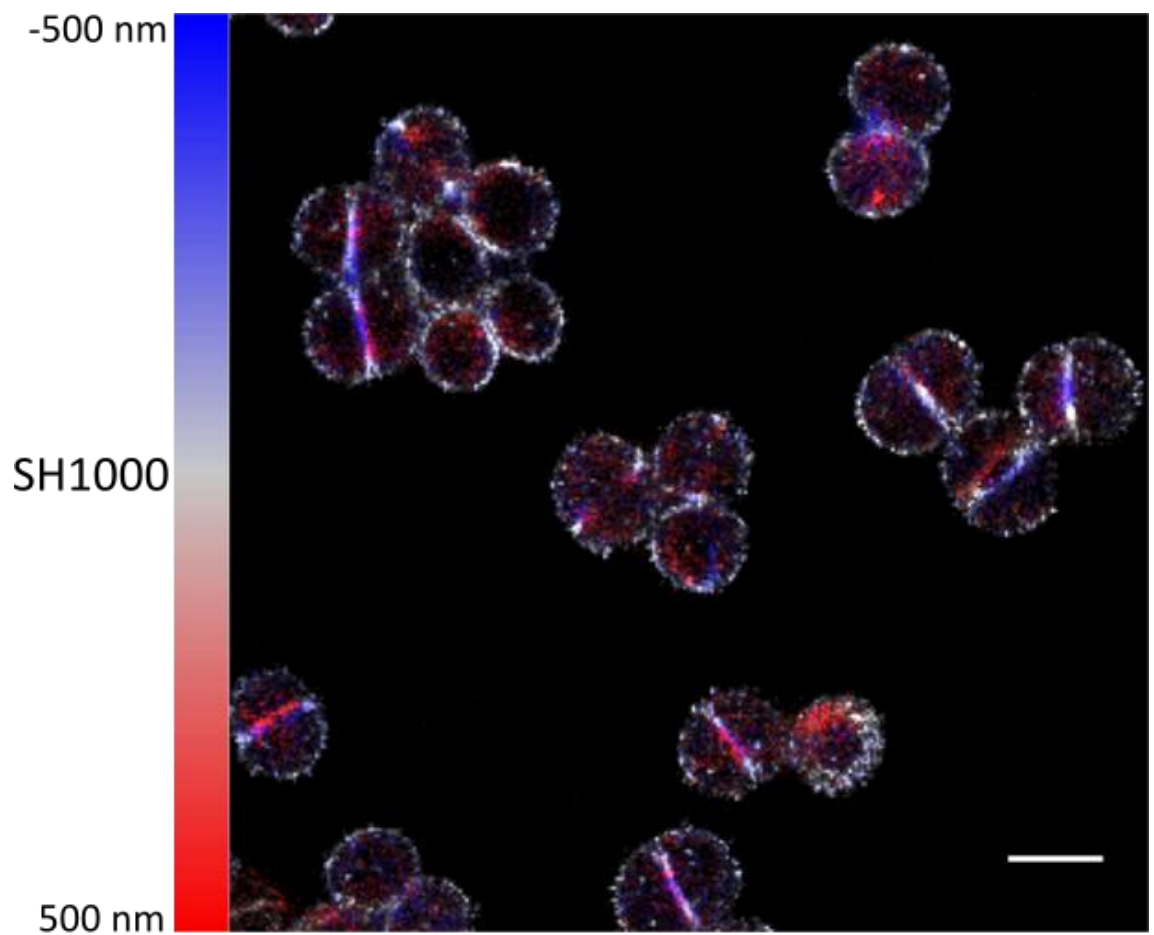


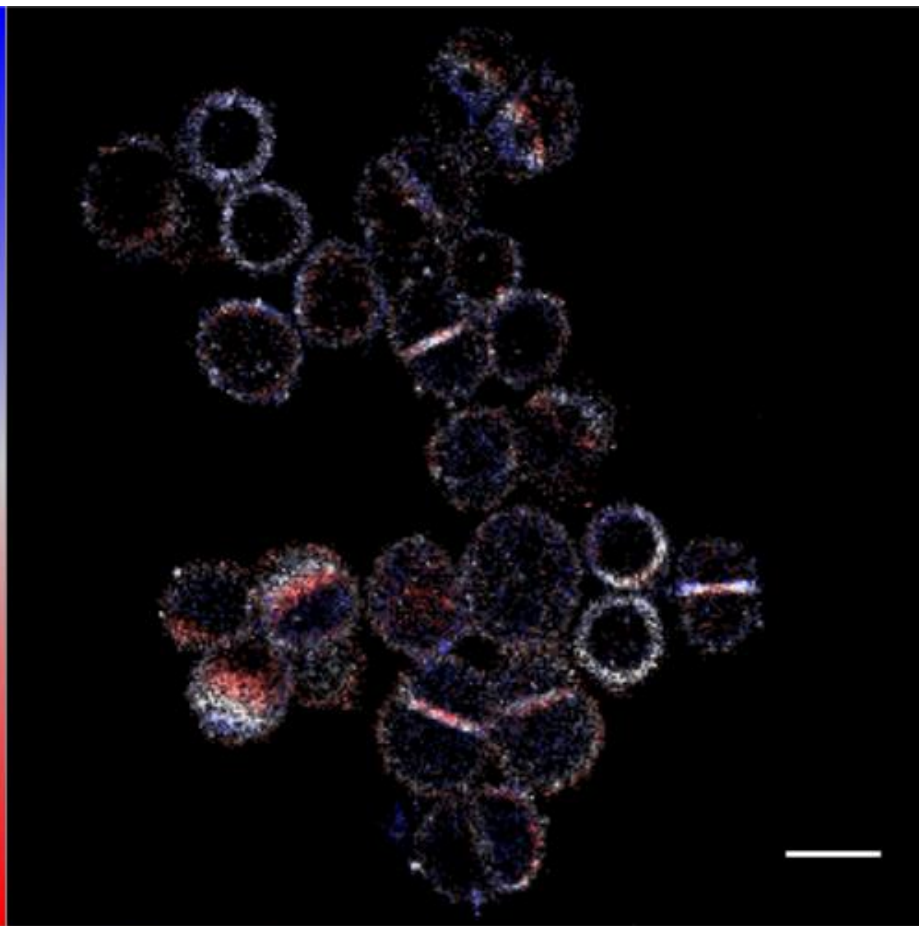
Figure 4.19. STORM of ADA labelled PBP mutants. 5 minutes of peptidoglycan synthesis was labelled with with ADA (500 μM)(Alexa Flour 647 at 5 $\mu\text{g ml}^{-1}$ in Click reaction) in each strain. 3D localisation of synthesis is represented by a colour table in 100 nm slices from 500 nm behind the plane of focus (-500 nm, blue) to 500 nm in front of plane of focus (500 nm, red). (Scale bar, 1 μm).



-500 nm

4425
pbp4

500 nm



-500 nm

4424
pbp3
pbp4

500 nm

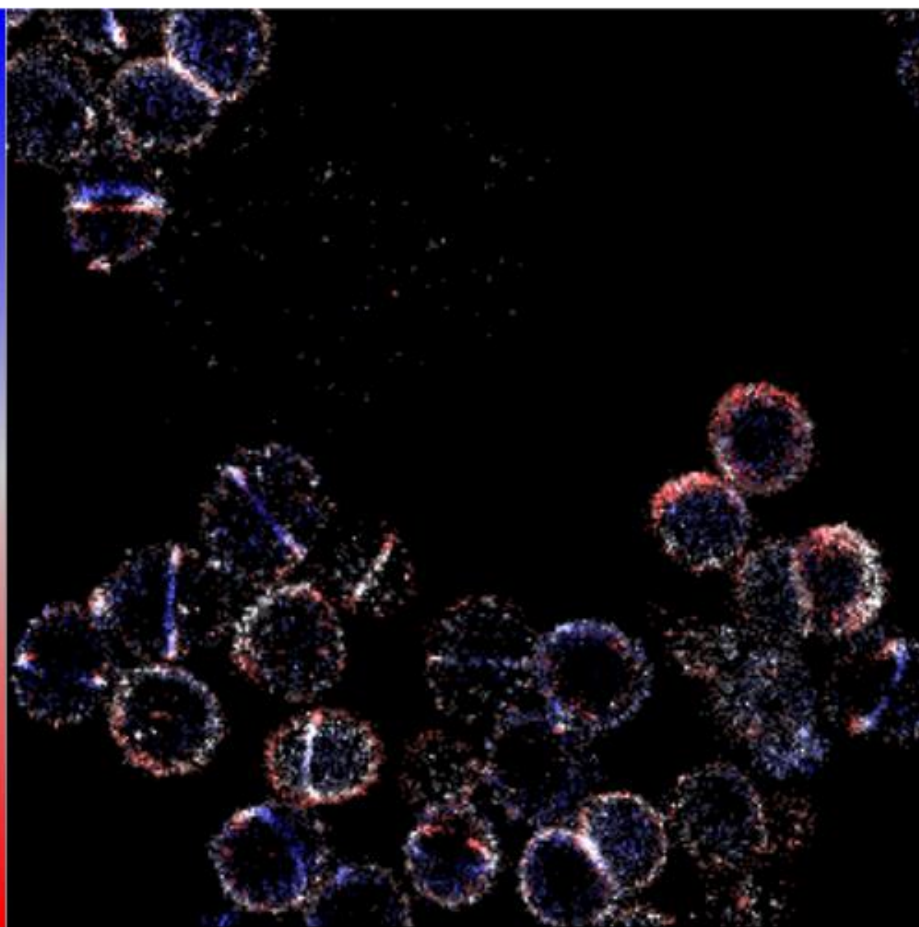


Figure 4.20. STORM of dipeptide labelled PBP mutants. 5 minutes of peptidoglycan synthesis was labelled with dipeptide (1 mM)(Alexa Flour 647 at 5 $\mu\text{g ml}^{-1}$ in Click reaction) in each strain. 3D localisation of synthesis is represented by a colour table in 100 nm slices from 500 nm behind the plane of focus (-500 nm, blue) to 500 nm in front of plane of focus (500 nm, red). (Scale bar, 1 μm).

IC₅₀ of 55ng ml⁻¹.(Haydon et al., 2008) However, the exact mode of action of PC190723 against the FtsZ protein is unclear. It may interact with the GTPase active site preventing GTP hydrolysis or may stabilize FtsZ polymers inducing filament assembly and preventing proper functioning (Andreu et al., 2010; Elsen et al., 2012; Haydon et al., 2008). However, PC190723 has poor drug-like and pharmacokinetic properties so subsequent 1st and 2nd generation pro-drugs have been created with enhanced pharmacokinetics and increased anti-staphylococcal activity *in vivo* (Kaul et al., 2015). Cell division inhibition by PC190723 in *S. aureus* was shown to lead to quick arrest of DNA replication initiation followed by complete arrest of cell growth (Arjes et al., 2014).

In *S. aureus* the drug PC190723 has been shown to cause cell enlargement, typical of FtsZ depletion (Haydon et al., 2008). The localisation of FtsZ has previously been shown to form multiple rings and arcs however the consequent effects on peptidoglycan synthesis have not been studied in *S. aureus* (Tan et al., 2012).

4.2.7.2 Effect of PC190723 on growth & cell size of *S. aureus*

The MIC of PC190723 for SH1000 was determined to be 1 µg ml⁻¹ (Chapter 2.8) therefore all following growth and labelling experiments were carried out at 10 µg ml⁻¹ i.e. 10 x MIC. Following addition of 10 µg ml⁻¹ the growth of *S. aureus* cultures was monitored via OD₆₀₀. PC190723 was shown to cause a growth defect to all strains tested (

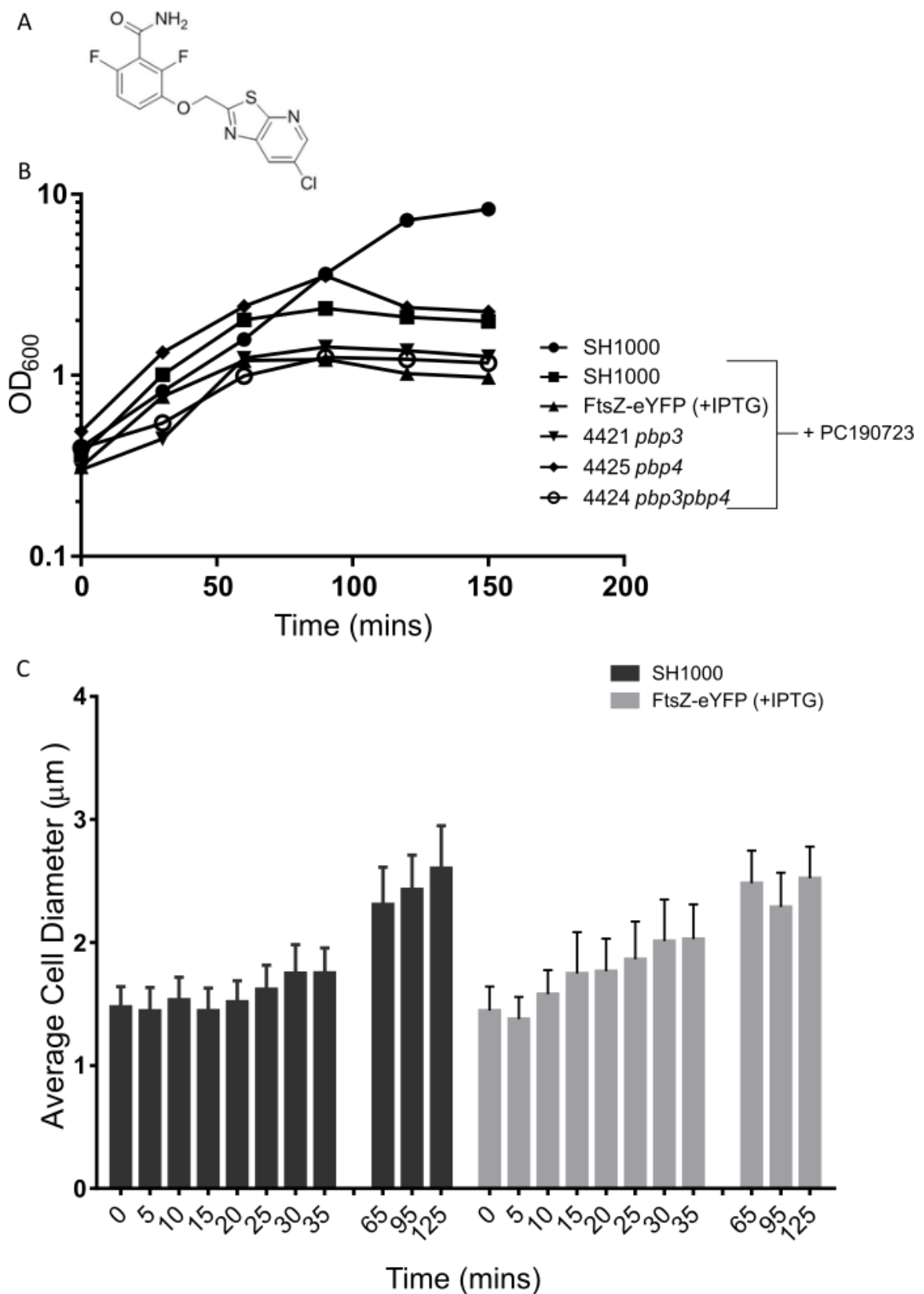


Figure 4.21 B). To determine the localisation of FtsZ, an FtsZ-eYFP fusion was introduced on a plasmid (13ADQETC) with FtsZ-eYFP expression under the control of an inducible promoter (P_{Spac}) (C. Walther, unpublished results). While the MIC of this strain was not tested to determine whether the additional copies of FtsZ had an effect on tolerance to PC190723, addition of $10 \mu\text{g ml}^{-1}$ PC190723 to a growing culture of the

FtsZ-eYFP strain resulted in cessation of growth, as for SH1000 (

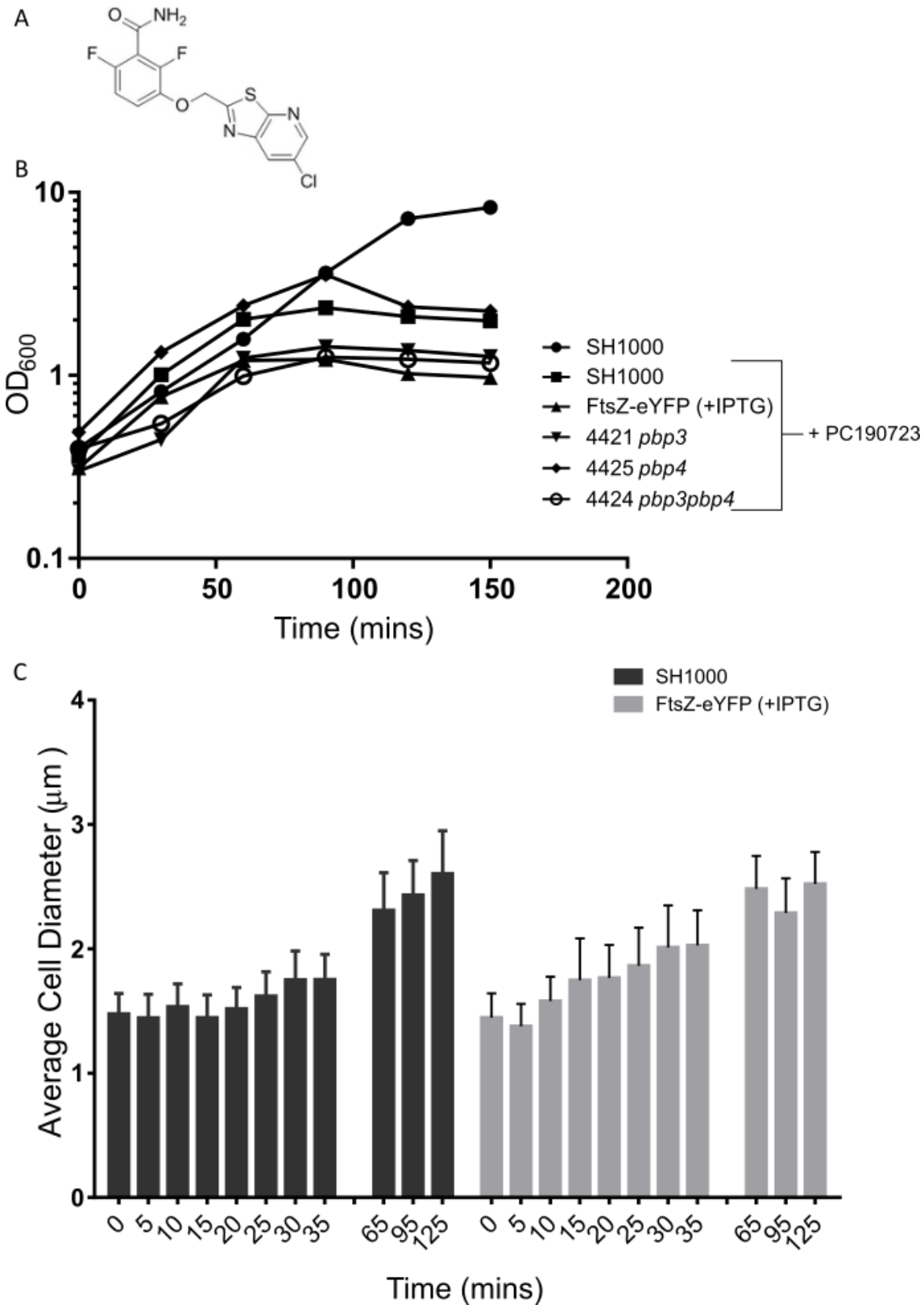


Figure 4.21 B).

The average cell diameters of both SH1000 and the FtsZ-eYFP strain were monitored during treatment with PC190723 (

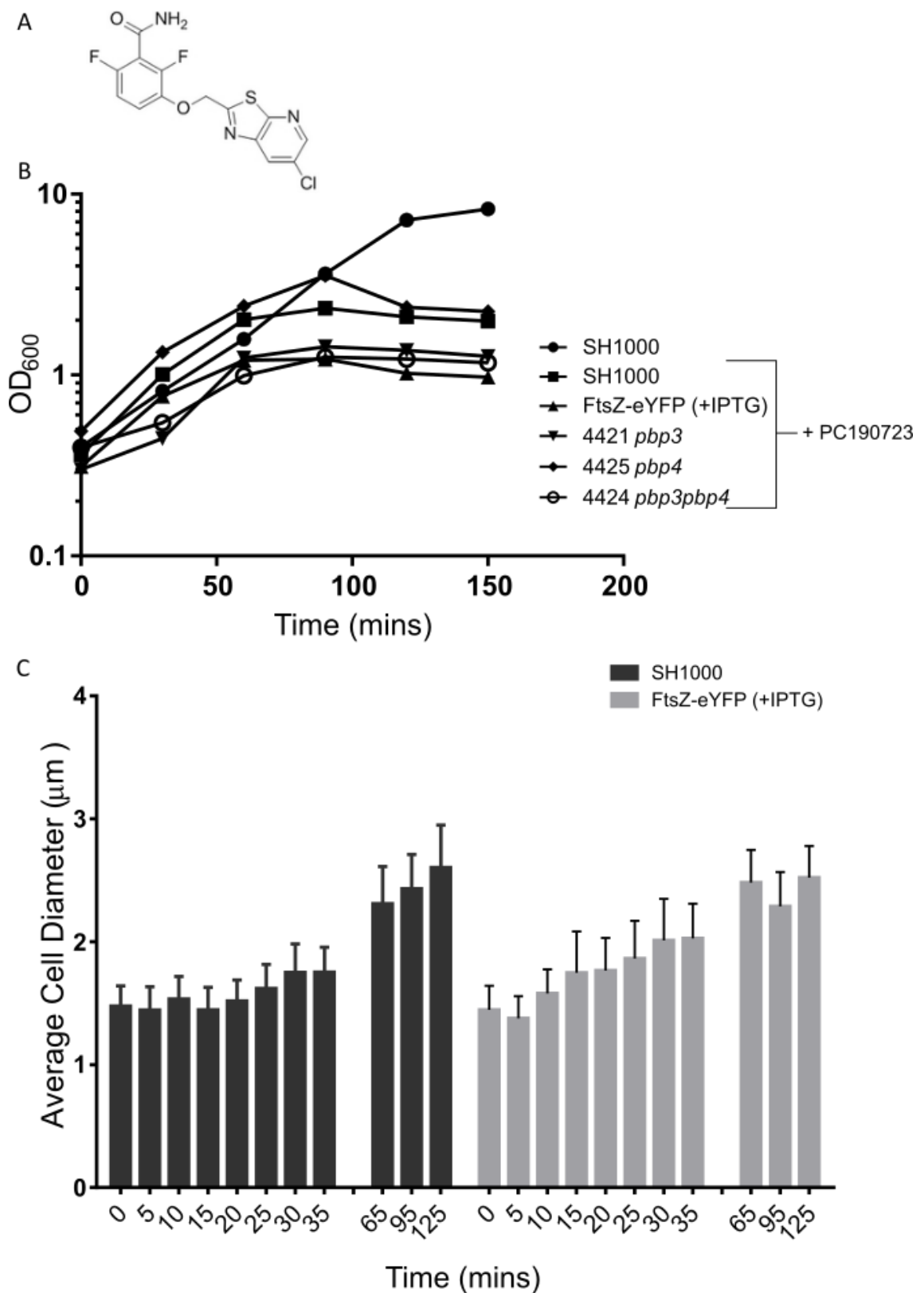


Figure 4.21 C). To achieve this fixed cells were imaged using brightfield and the diameter of cells were measured using Fiji software. Since the diameter of cells will vary throughout the cell cycle at least 150 cells were measured to limit the effects of this variation. Treatment with $10 \mu\text{g ml}^{-1}$ PC190723

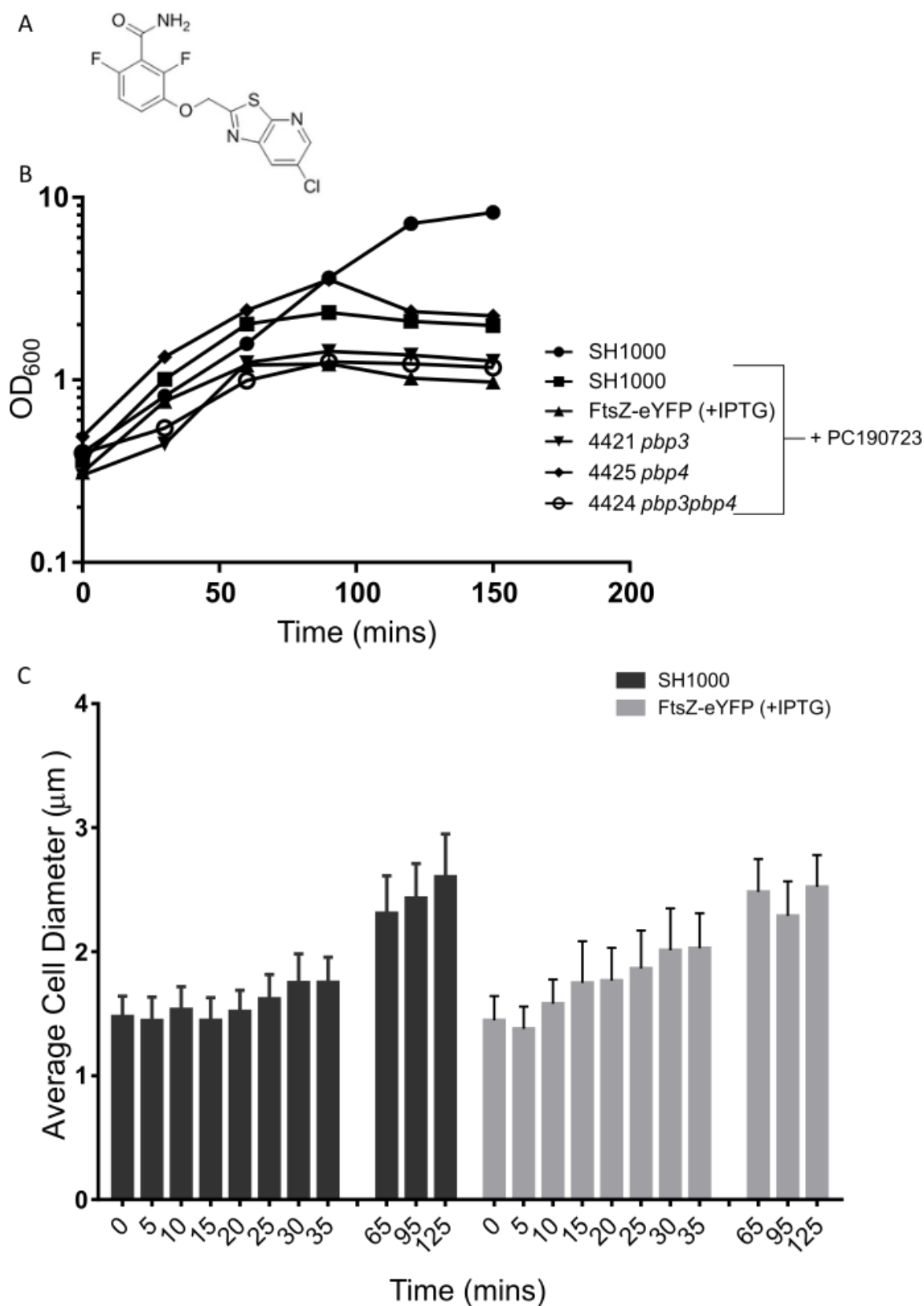


Figure 4.21. Effect of PC190723 on growth and cell diameter. (A) Structure of PC190723. (B) Growth curve in the presence of $10 \mu\text{g ml}^{-1}$ PC190723. (C) Average cell diameter at times shown of SH1000 and FtsZ-eYFP during treatment with $10 \mu\text{g ml}^{-1}$ PC190723.

caused an increase in cell diameter from $1.48 \pm 0.16 \mu\text{m}$ to $2.60 \pm 0.35 \mu\text{m}$ after 125 minutes treatment in SH1000. This pattern was repeated in the FtsZ-eYFP strain in the presence of IPTG with an increase in diameter from $1.45 \pm 0.20 \mu\text{m}$ to $2.52 \pm 0.26 \mu\text{m}$ in the same time period.

4.2.7.3 Effect of PC190723 on FtsZ localisation in *S. aureus*

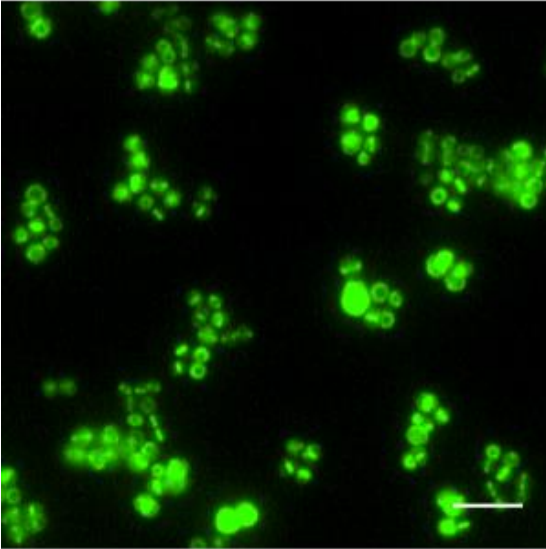
The effect of PC190723 on the FtsZ-eYFP strain was analysed by fluorescence microscopy (Figure 4.22). The localisation patterns of FtsZ were determined and quantified (Figure 4.23). Untreated cells show an FtsZ localisation pattern of rings at the midcell, this ring of different diameters depended on the stage of the cell cycle. After 10 minutes of PC190723 treatment cells began to lose the midcell localisation and FtsZ became localised to discrete foci and arcs, generally at the periphery of the cell. After 10 minutes the midcell localisation and discrete foci/arcs are at approximately 50:50 but by 15 minutes the majority of cells had FtsZ in discrete foci/arcs. This delocalised pattern remained until 95 minutes, over which time cells increase in diameter. At 95 minutes the fluorescent signal from the FtsZ-eYFP strain began to be distributed across the whole cell. The discrete foci of FtsZ is reminiscent of the pattern seen in *B. subtilis* (Haydon et al., 2008).

4.2.7.4 Effect of PC190723 on peptidoglycan synthesis localisation in *S. aureus*

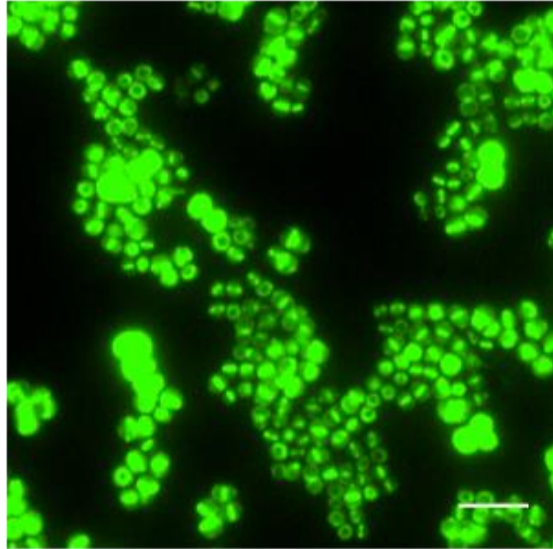
To determine the effect of PC190723 on peptidoglycan synthesis, FtsZ-eYFP was labelled with HADA (Figure 4.24). Quantification of labelling patterns shows that at the interval of 10-15 minutes treatment, insertion of HADA changed from the control synthesis patterns seen previously (e.g septal rings & plates with off septal labelling; Figure 4.1) to exclusive labelling of the peripheral cell wall (Figure 4.25). This change in labelling coincides with the change in FtsZ localisation from septal rings to discrete foci/arcs. At 90-95 minutes and 120-125 minutes HADA labelling in individual cells either remains as peripheral cell wall labelling, labelling is completely removed or the entire cytoplasm is labelled by HADA.

Since the FtsZ-eYFP strain has an increased production of FtsZ, localisation of PG synthesis was also carried out in SH1000 (Figure 4.26). The same change in pattern of peptidoglycan synthesis was observed (Figure 4.24). The control peptidoglycan

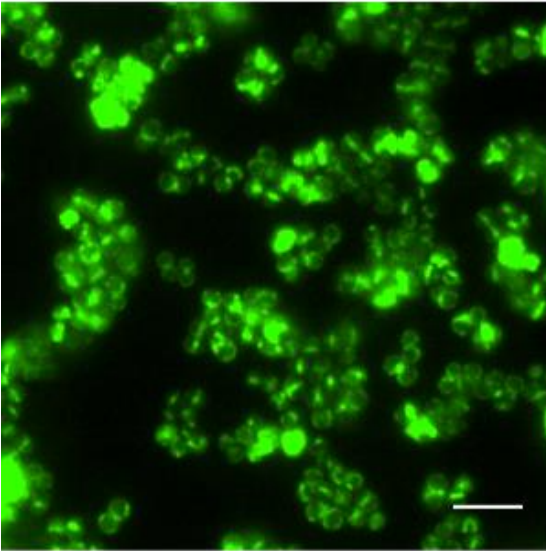
Control



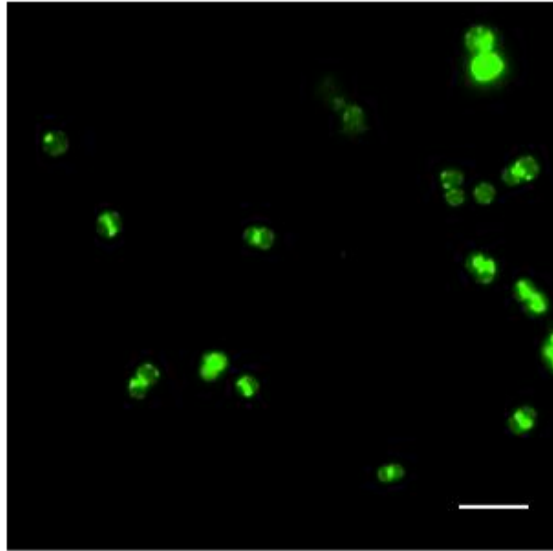
5 minutes



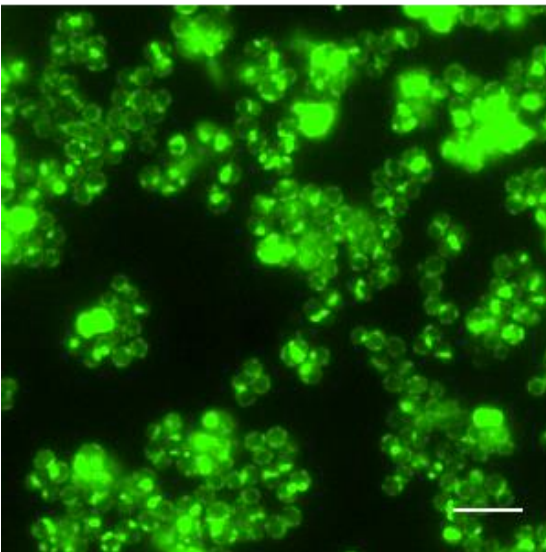
10 minutes



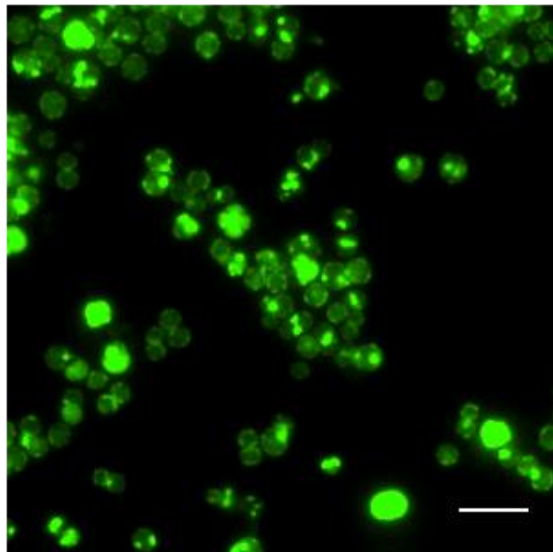
15 minutes



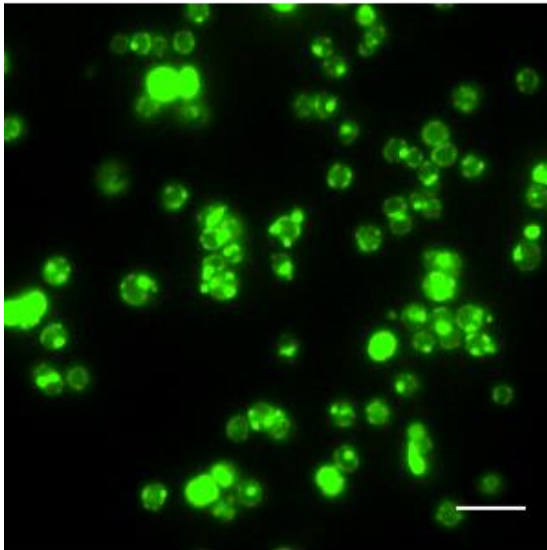
20 minutes



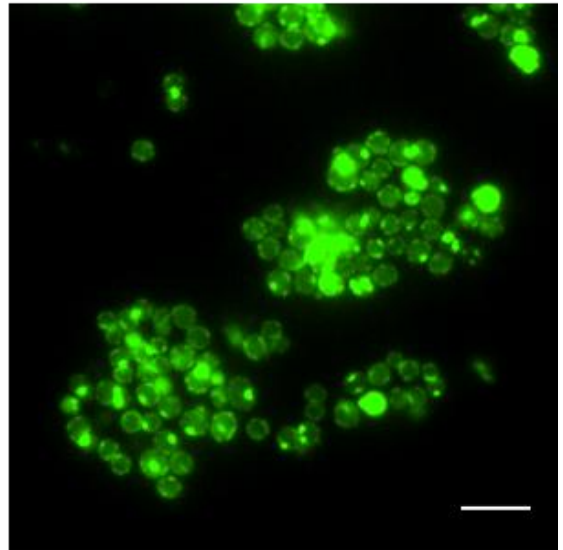
25 minutes



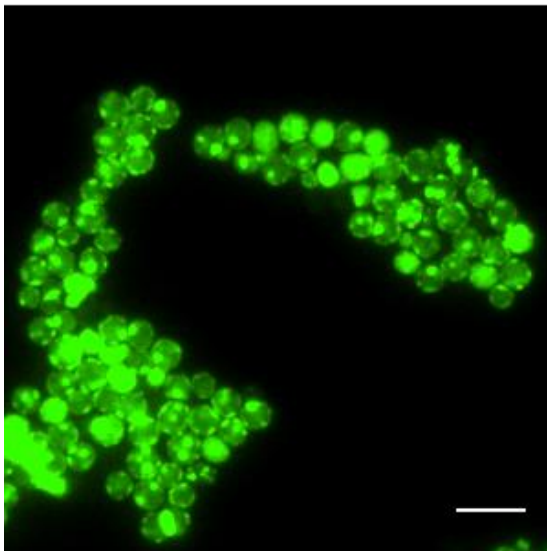
30 minutes



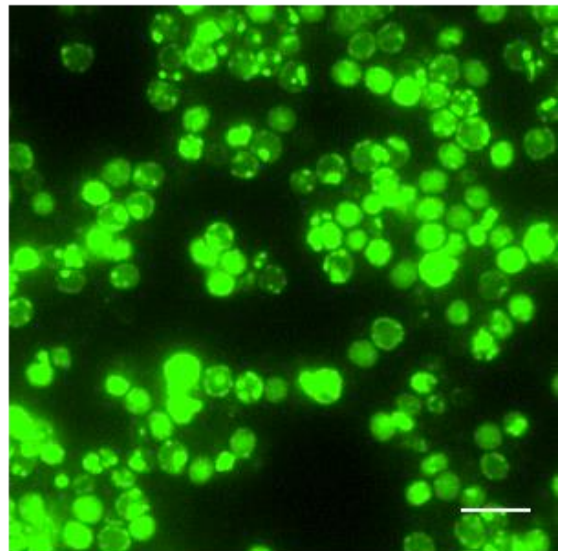
35 minutes



65 minutes



95 minutes



125 minutes

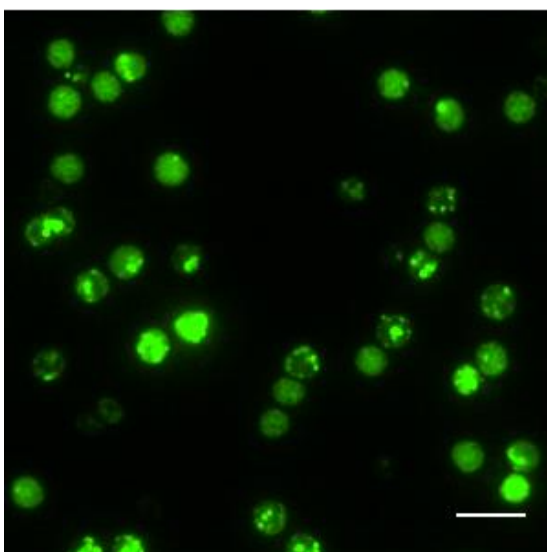


Figure 4.22. Effect of PC190723 on FtsZ localisation in *S. aureus*. FtsZ-eYFP was localised during treatment with $10 \mu\text{g ml}^{-1}$ PC190723. (Scale Bar $5 \mu\text{m}$).

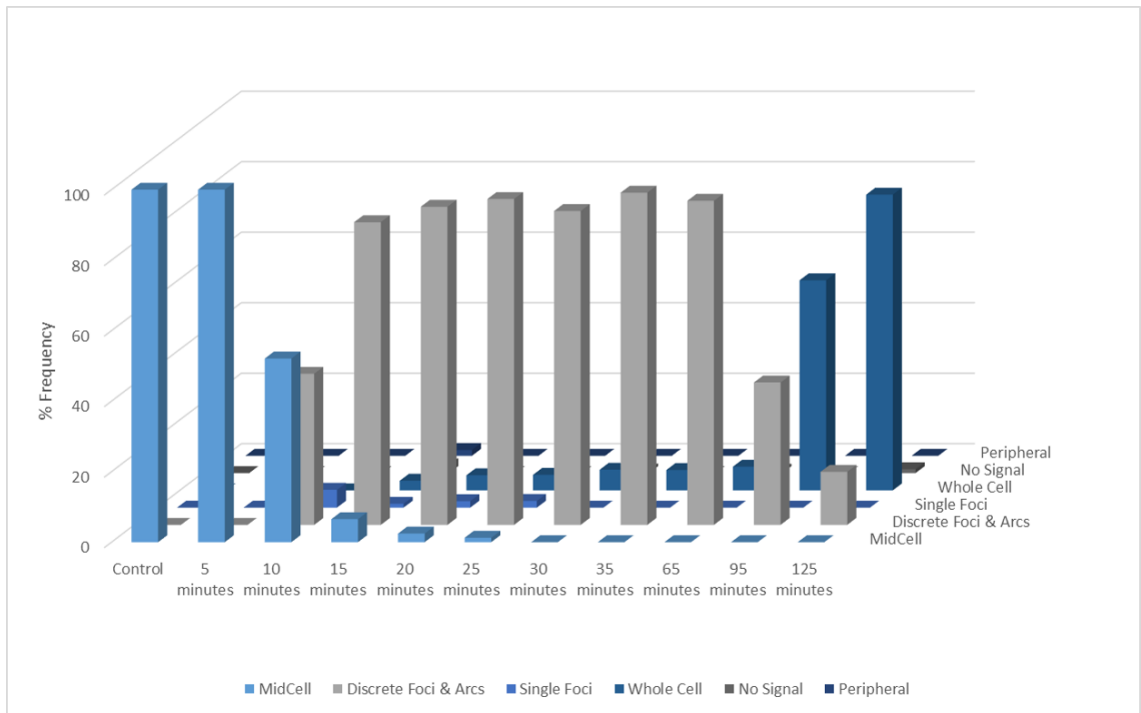
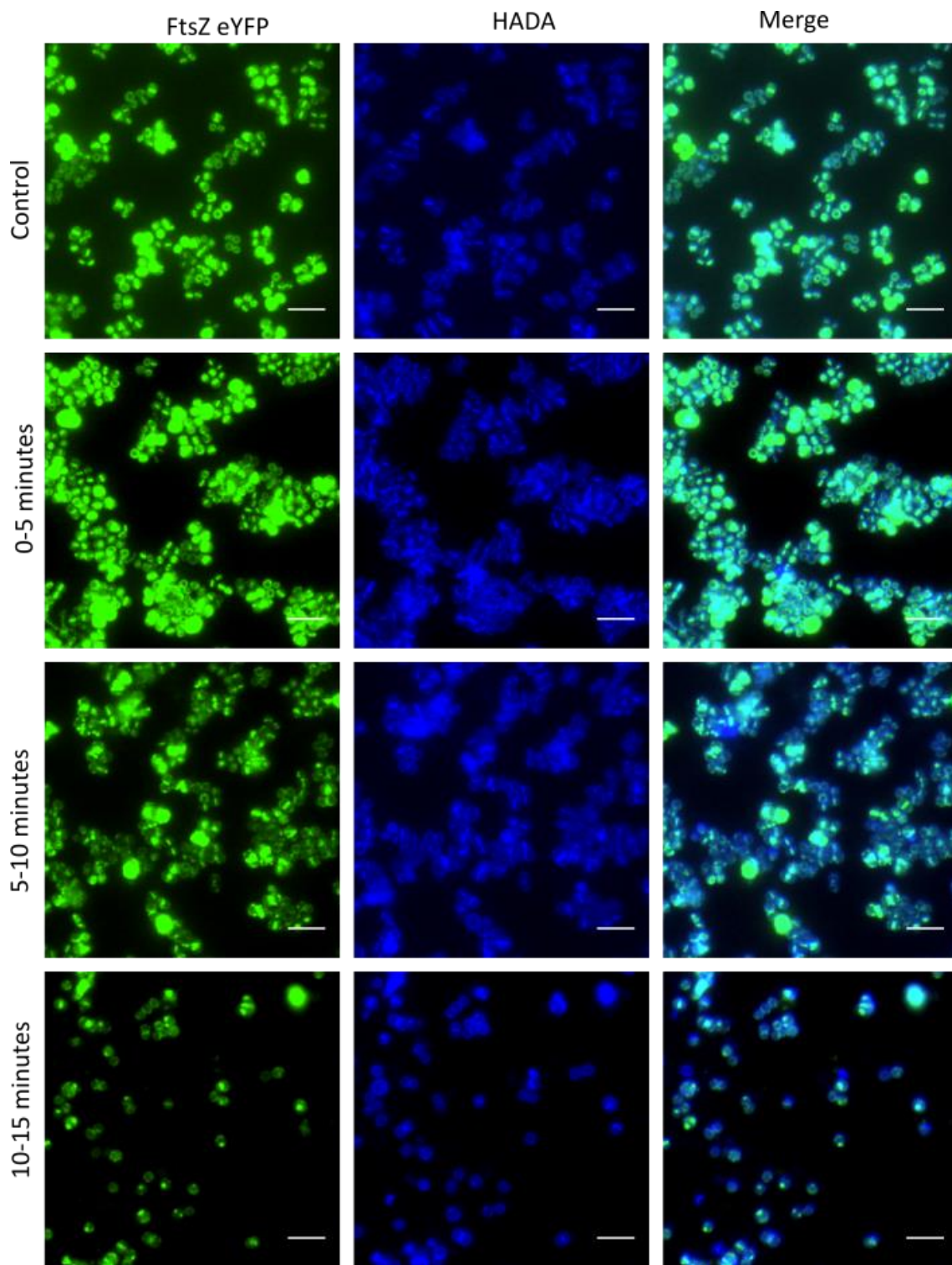
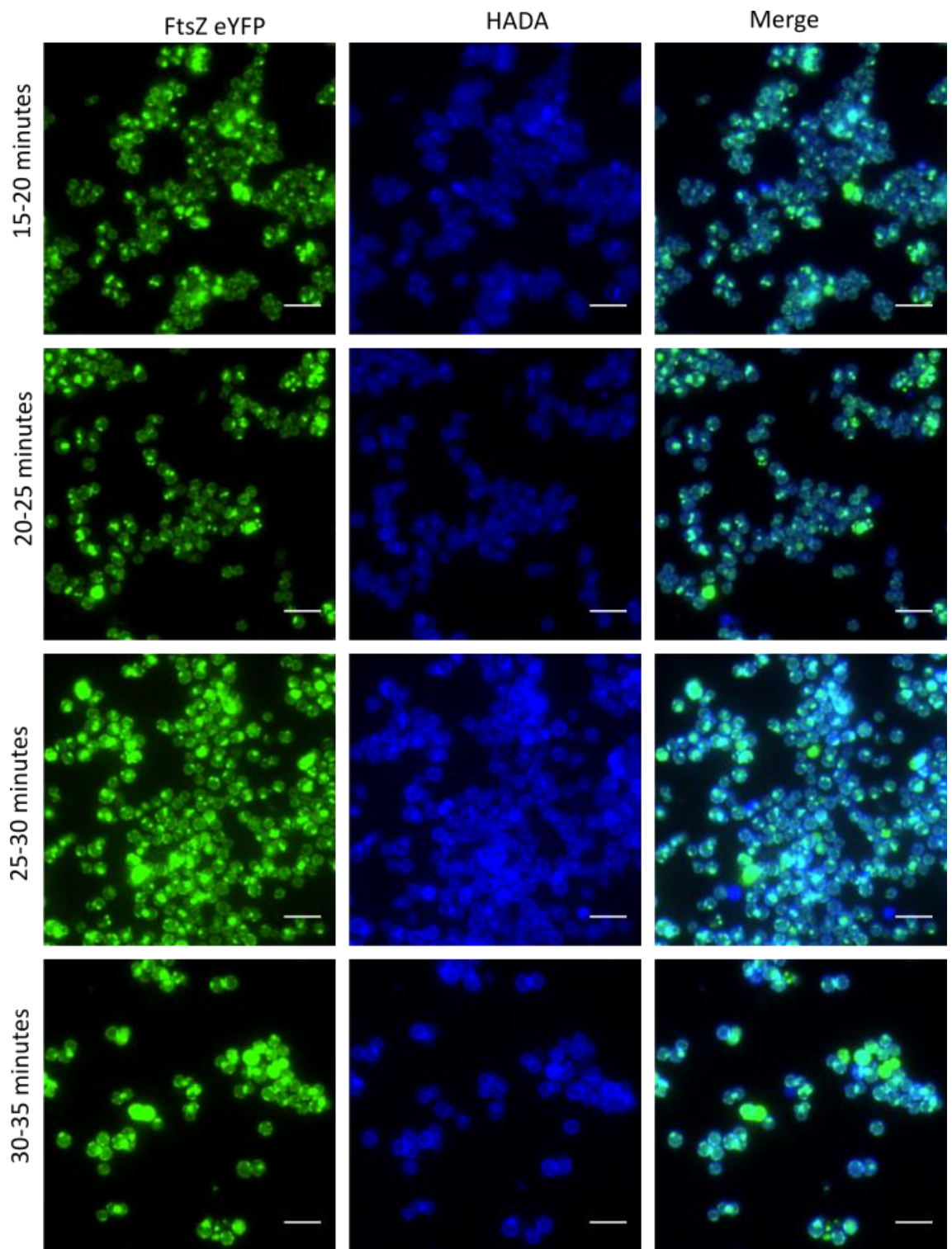


Figure 4.23. Quantification of localisation of FtsZ during PC190723 treatment.

Frequency of FtsZ localisation pattern during treatment with $10 \mu\text{g ml}^{-1}$ PC190723.

Table of frequencies shown in Appendix IV (Appendix Table 1).





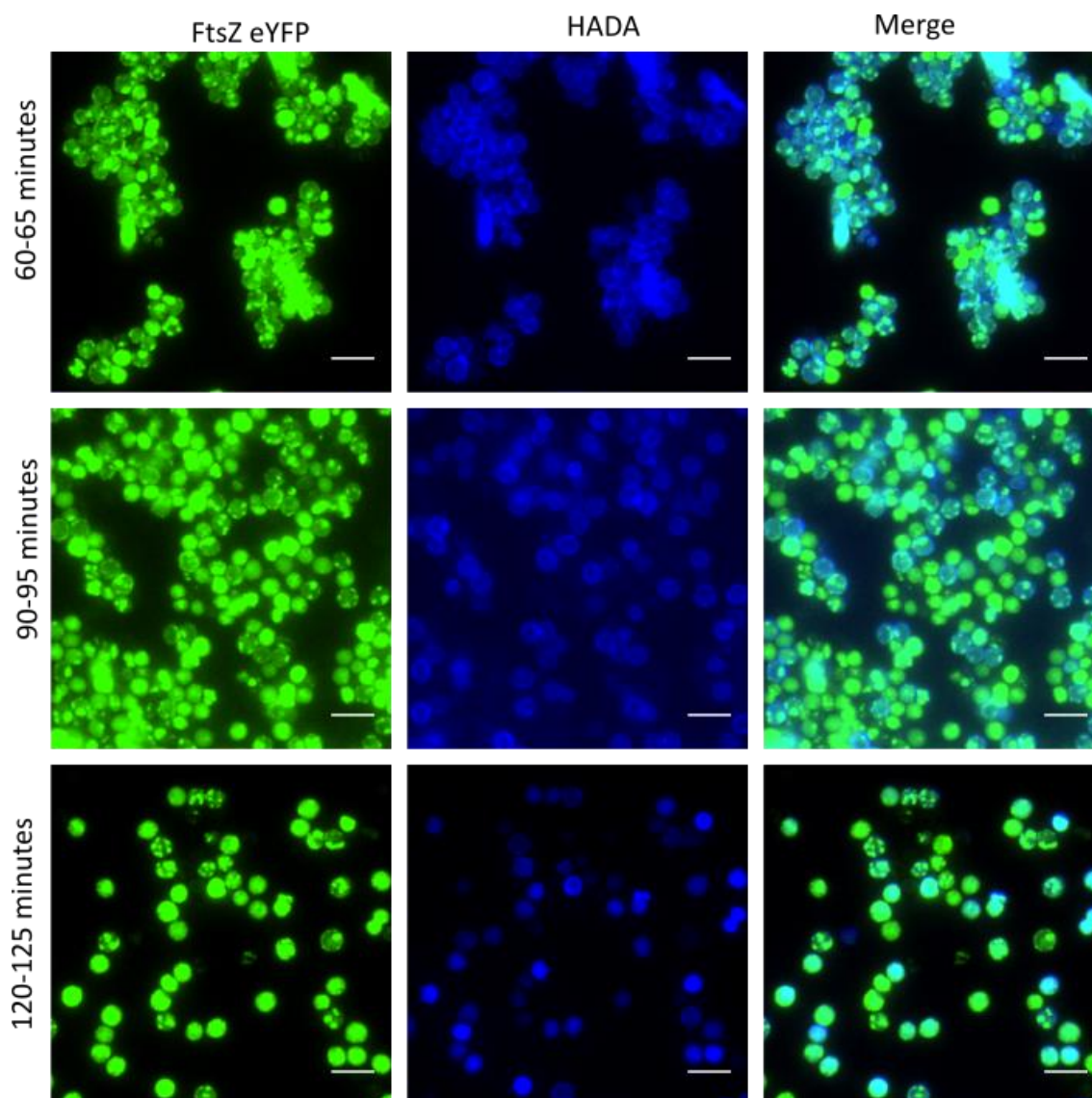


Figure 4.24. Effect of PC190723 on peptidoglycan synthesis in FtsZ-eYFP *S. aureus*.

Peptidoglycan synthesis was labelled over 5 minute windows with HADA (500 μM) and FtsZ-eYFP localised during treatment with 10 $\mu\text{g ml}^{-1}$ PC190723 over 125 minutes. (Scale Bar 5 μm).

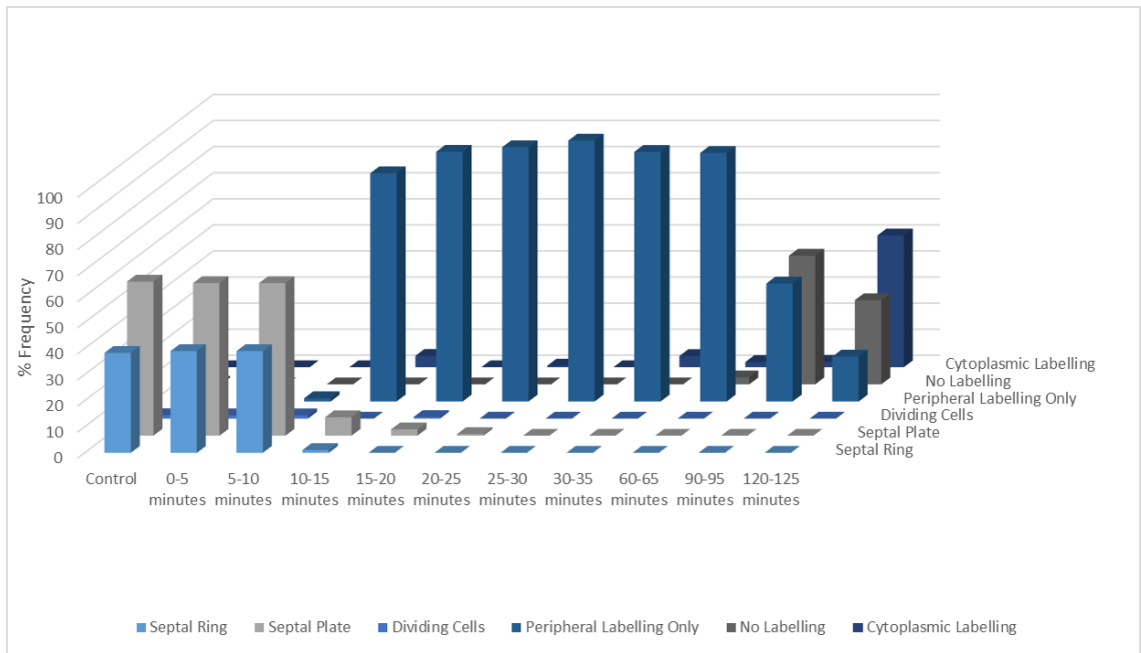
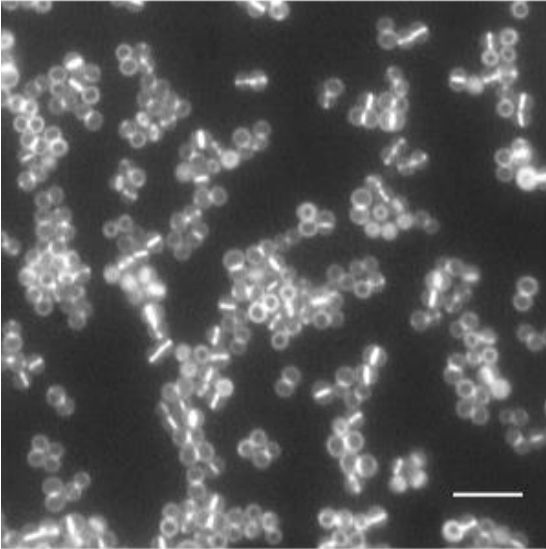
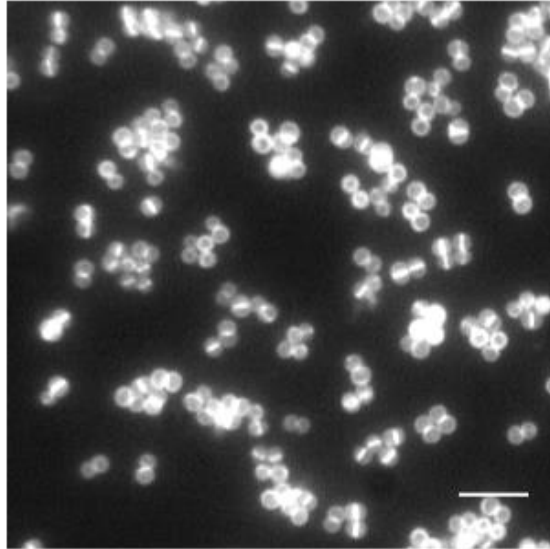


Figure 4.25. Quantification of localisation of peptidoglycan synthesis during inhibition by PC190723 in the FtsZ-eYFP strain. 5 minutes peptidoglycan synthesis was labelled by HADA. The frequency of each HADA localisation pattern during treatment with $10 \mu\text{g ml}^{-1}$ PC190723 was determined. Table of frequencies shown in Appendix IV (Appendix Table 2).

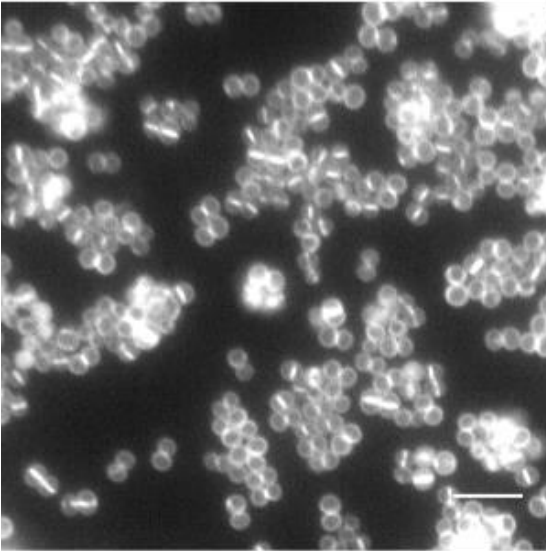
Control



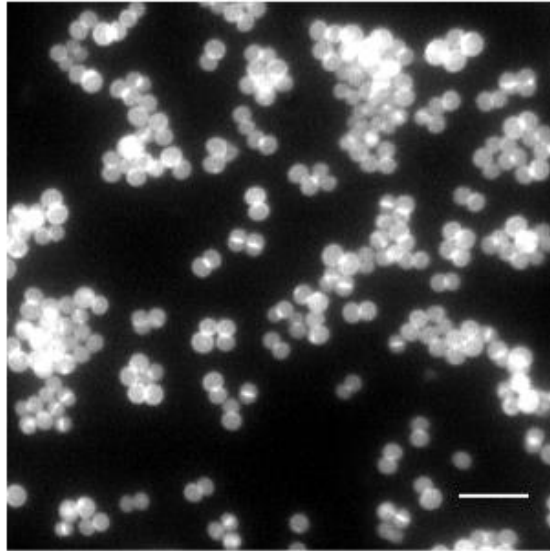
0-5 minutes



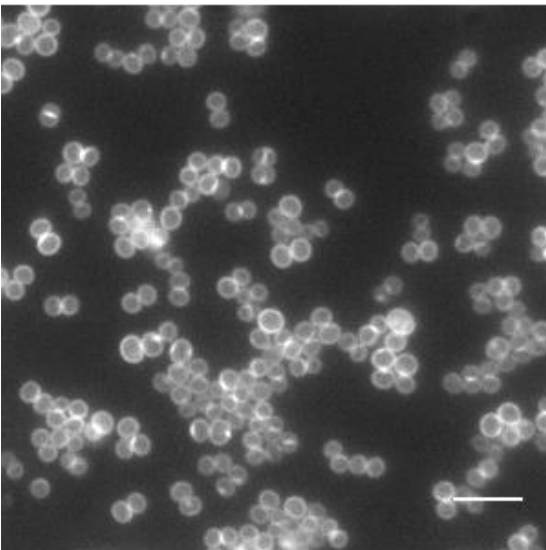
5-10 minutes



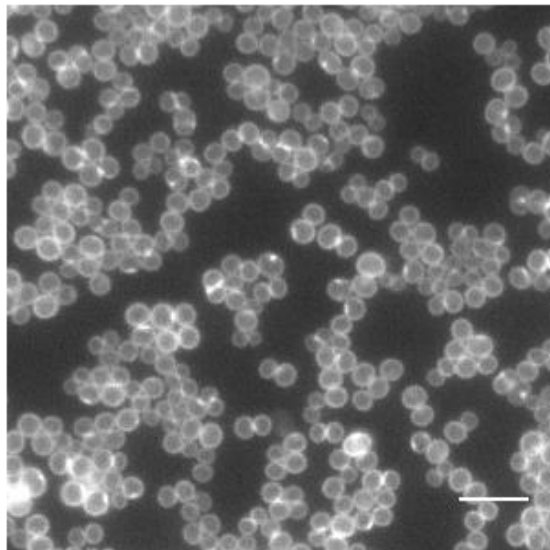
10-15 minutes



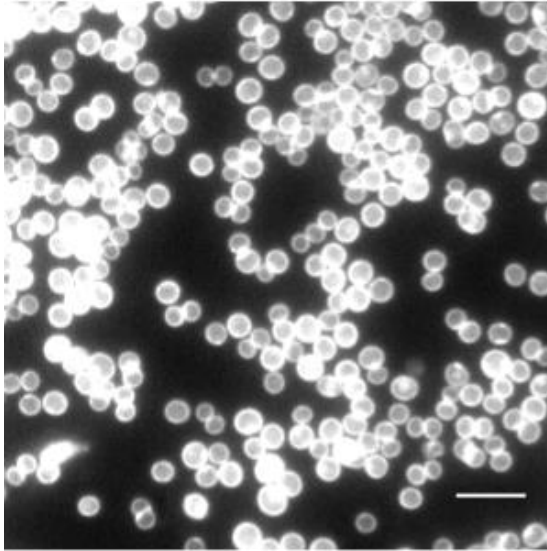
15-20 minutes



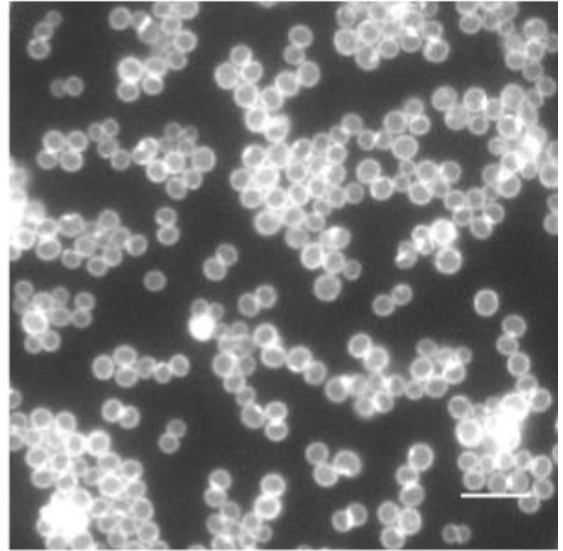
20-25 minutes



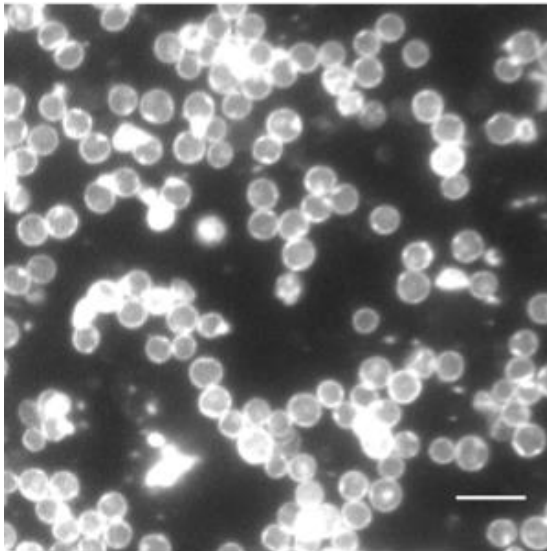
25-30 minutes



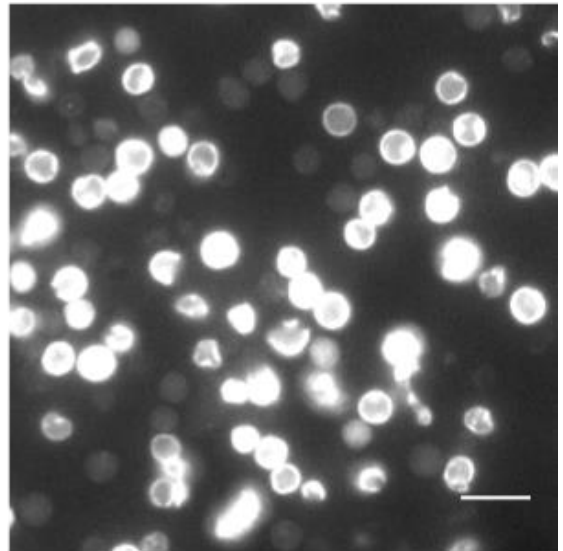
30-35 minutes



60-65 minutes



90-95 minutes



120-125 minutes

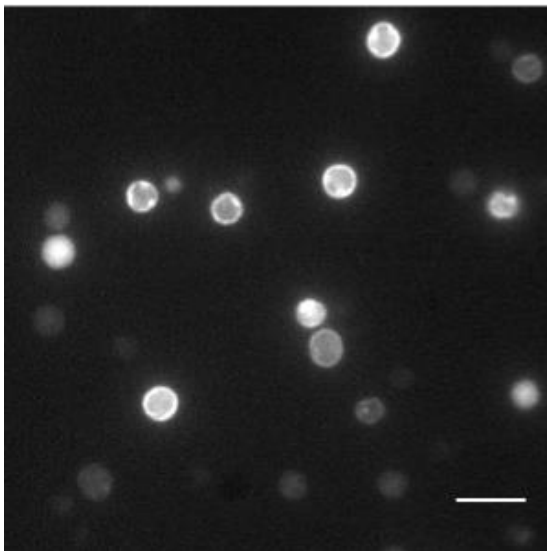


Figure 4.26. Effect of PC190723 on peptidoglycan synthesis in SH1000. 5 minute windows of peptidoglycan synthesis were labelled with HADA (500 μ M) during treatment with 10 μ g ml⁻¹ PC190723. (Scale Bar 5 μ m).

synthesis pattern is lost at approximately 10 minutes after inhibition with PC190723 and peptidoglycan synthesis occurs at the periphery of the cell only until approximately 90 minutes post treatment when cells begin to either entirely lose labelling with HADA or the HADA signal appears throughout the cell (Figure 4.27). To investigate peptidoglycan synthesis during PC190723 treatment in further detail, STORM was used (Figure 4.28). Images show a control phenotype of peptidoglycan synthesis immediately following PC190723 treatment (Figure 4.28 A & B). After 10-15 minutes there is an increase in cells lacking a septum (as expected from the diffraction limited images) and also there are a few enlarged cells with an abnormal phenotype, such as the cell indicated in Figure 4.28 C. After 30 minutes of treatment with PC190723 peptidoglycan synthesis is exclusively at the peripheral cell wall only (Figure 4.28 D & E). Peptidoglycan synthesis appears to occur in a uniform manner suggesting the discrete foci & arcs of FtsZ do not result in a punctate pattern of peptidoglycan synthesis.

The effect of PC190723 on the % off-septal labelling of cells which had initiated septation was measured (Figure 4.29). There was a slight increase in % off-septal labelling (49% to 62%). Therefore, when cells are already septating the addition of PC190723 does not disrupt the pattern of peptidoglycan synthesis.

4.2.7.5 Effect of PBP deletion and PC190723 treatment on peptidoglycan biosynthesis

Deletion of the non-essential PBPs (PBP3 & PBP4) has no effect on either growth or inhibition of growth by PC190723 (Figure 4.16 &

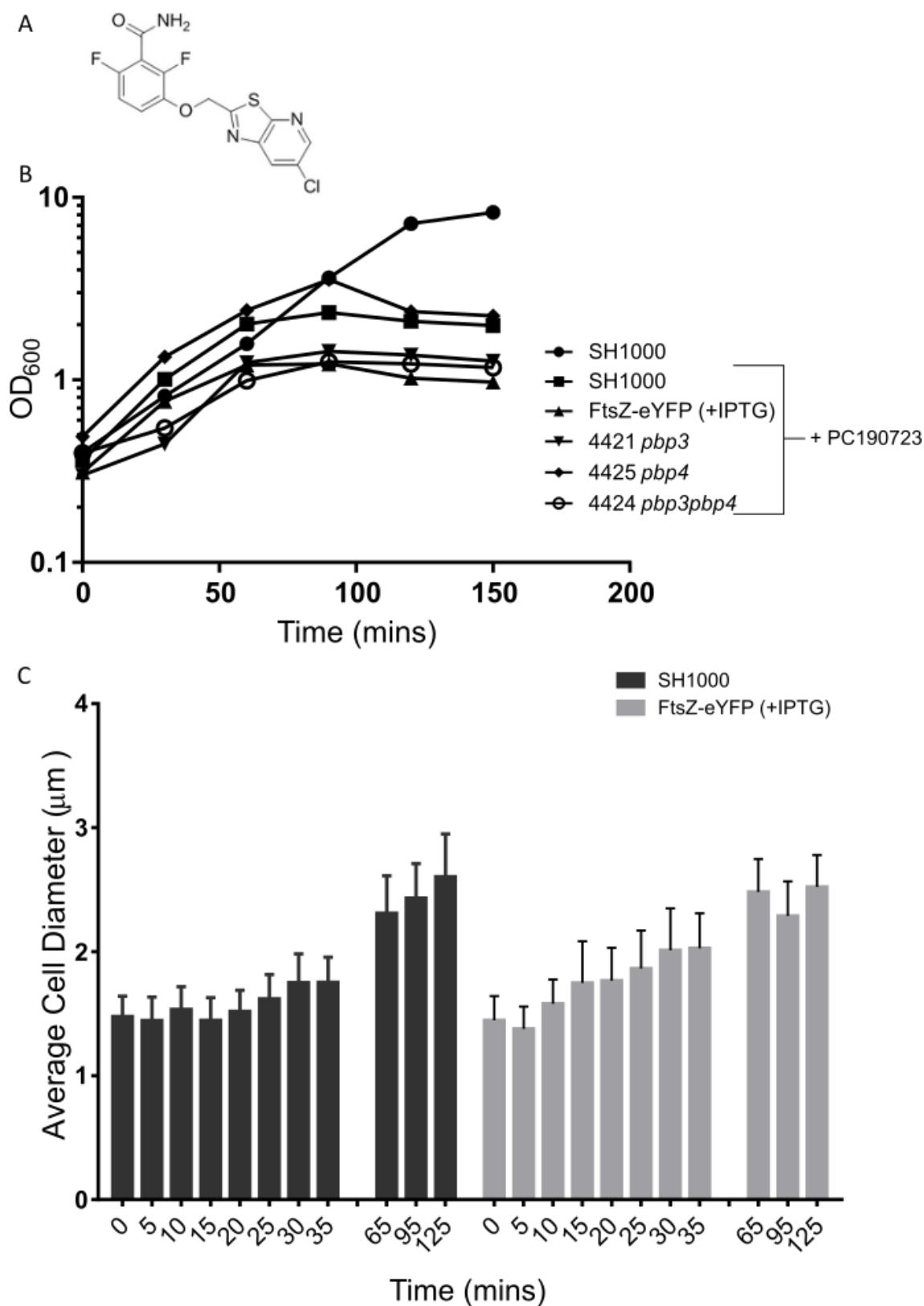


Figure 4.21). The effect of PC190723 on peptidoglycan synthesis in cells missing PBP3 and/or PBP4 was measured. Imaging of peptidoglycan synthesis in 4421 (*pbp3*) (Figure 4.30), 4425 (*pbp4*) (Figure 4.31) or 4424 (*pbp3pbp4*) (Figure 4.32) shows no apparent difference in progression of peptidoglycan synthesis or morphological changes compared to SH1000 (Figure 4.26). Due to the reduction in labelling intensity these

were not able to be followed for the full 125 minutes, especially in the case of 4424 (*pbp3pbp4*).

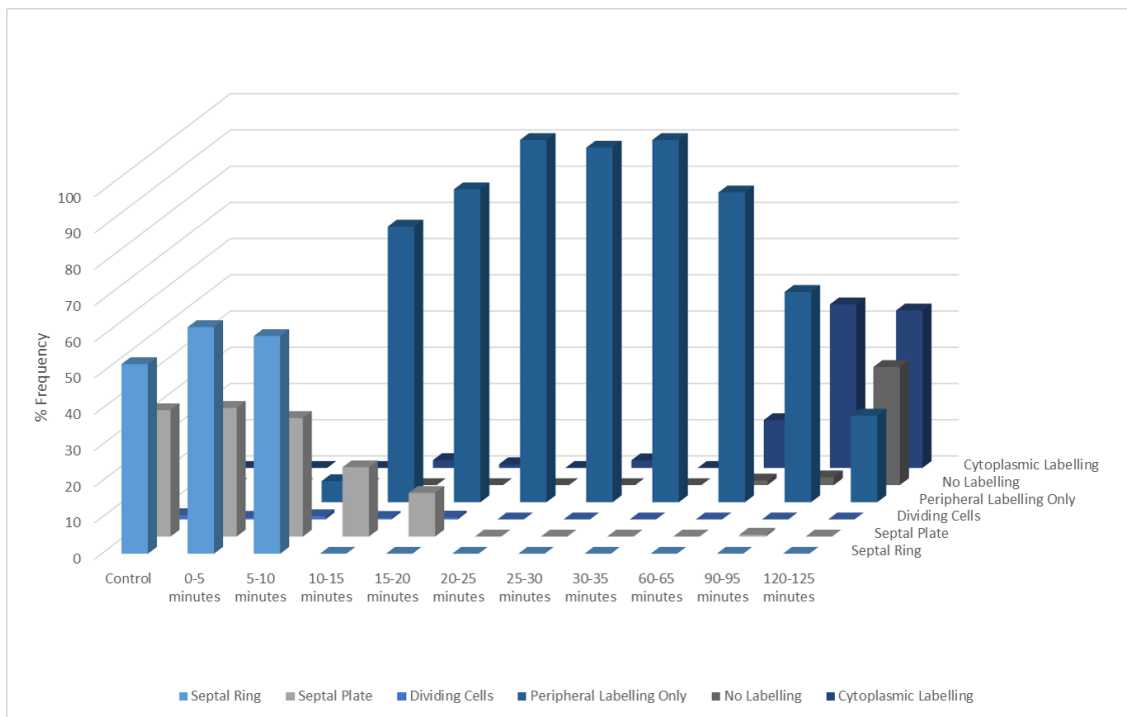
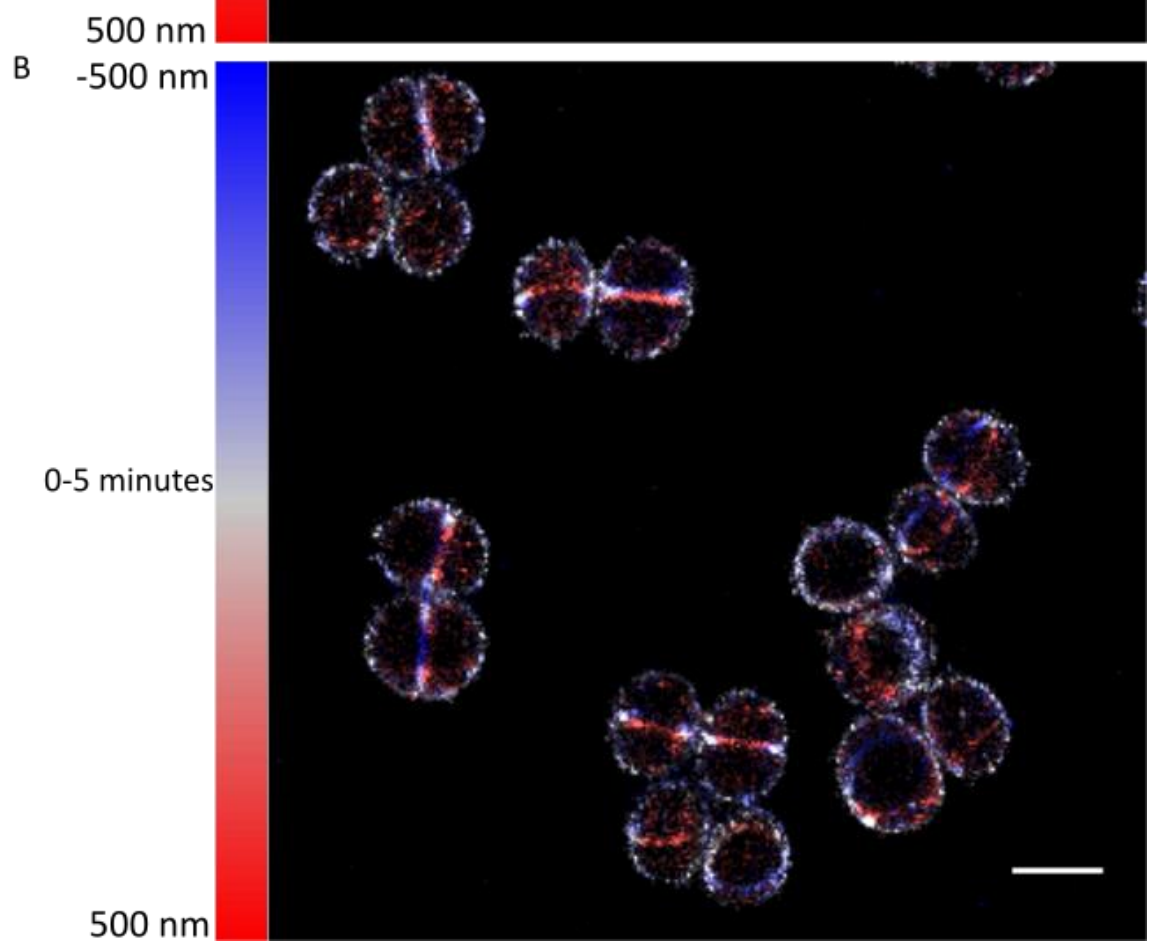
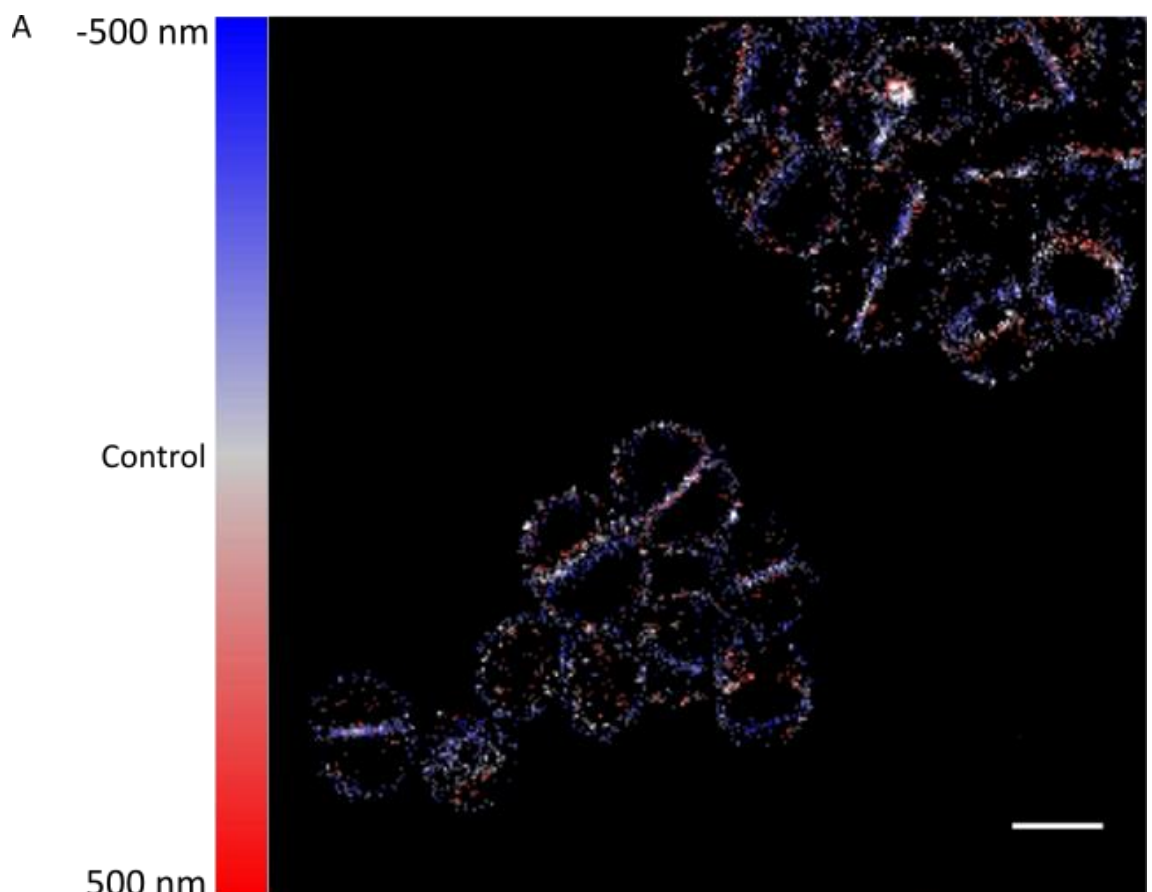
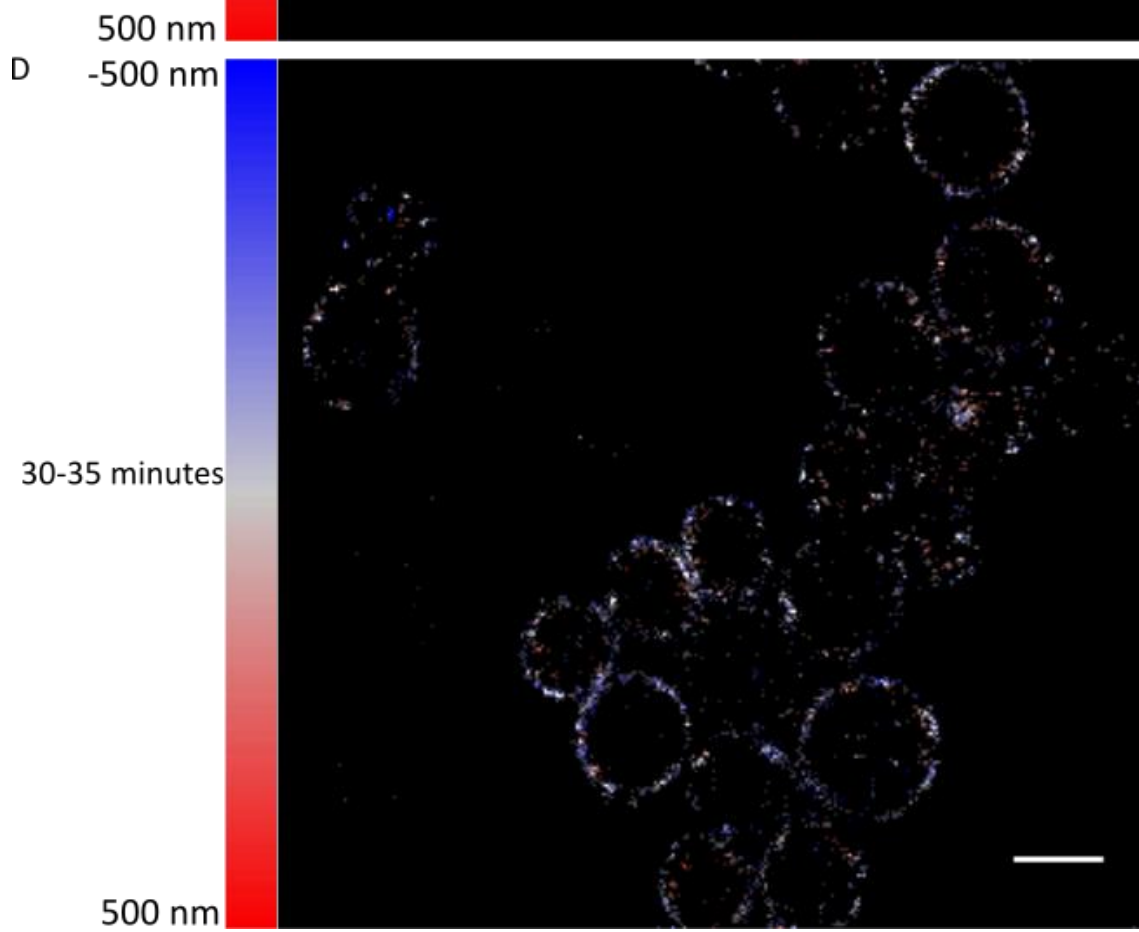
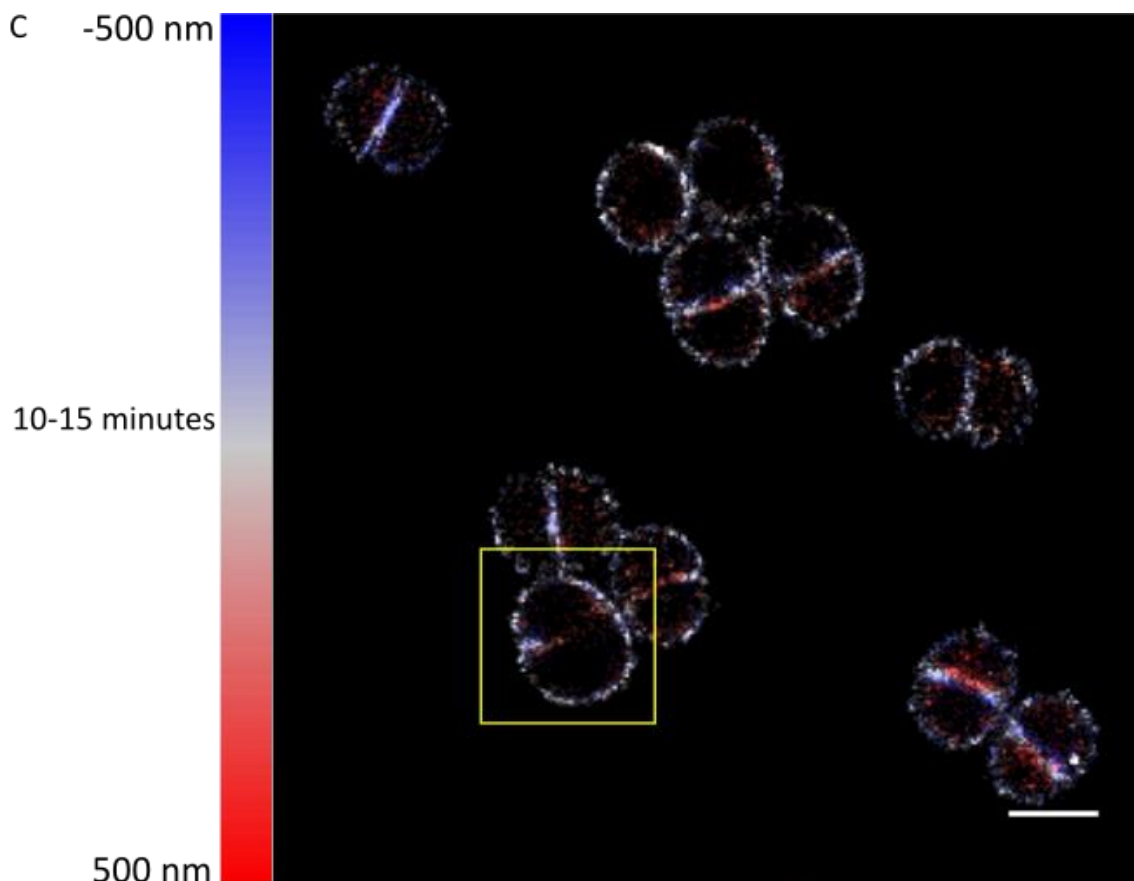


Figure 4.27. Quantification of localisation of PG synthesis during inhibition by PC190723 in SH1000. 5 minute windows of peptidoglycan synthesis labelled by HADA. Frequency of each HADA localisation pattern during treatment with $10 \mu\text{g ml}^{-1}$ PC190723 was determined. Table of frequencies shown in Appendix IV (Appendix Table 3).





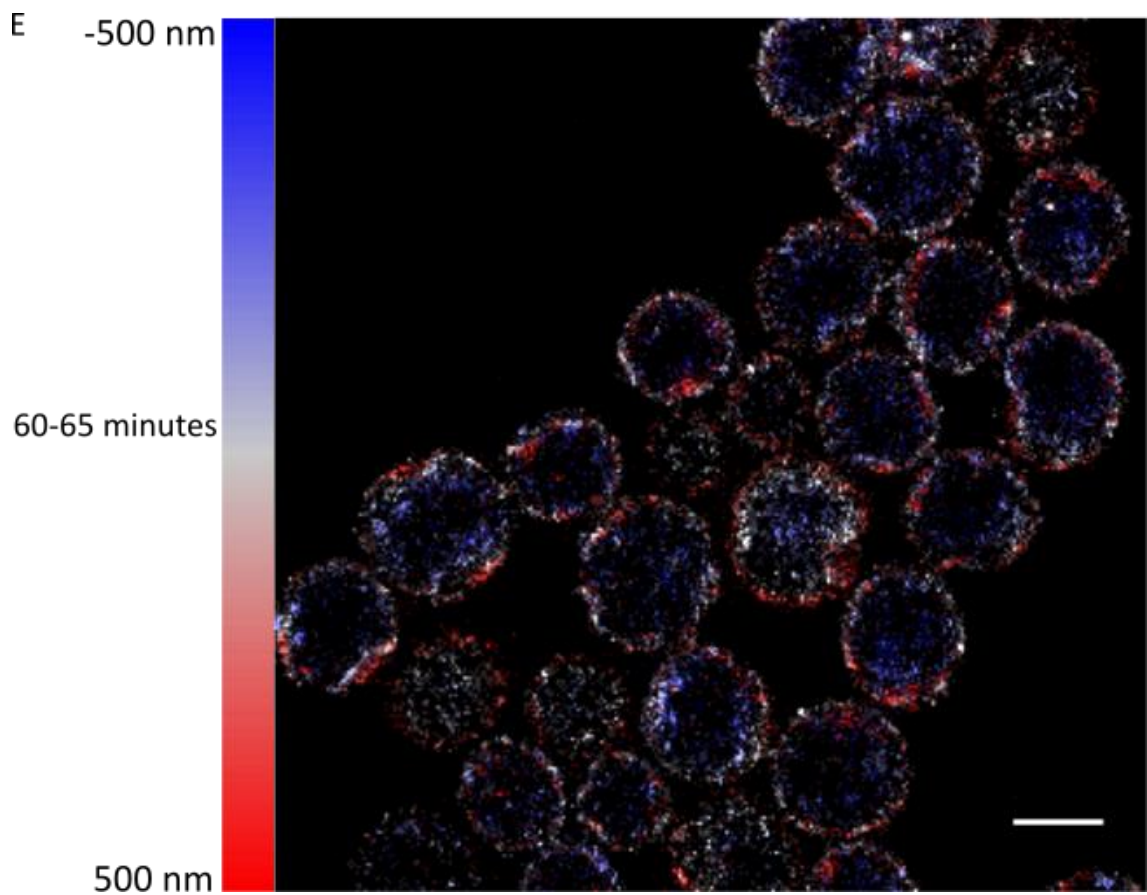


Figure 4.28. Localisation of peptidoglycan synthesis during PC190723 treatment. 5 minutes peptidoglycan synthesis was labelled using ADA (500 μM)(Alexa Flour 647 at 5 $\mu\text{g ml}^{-1}$ in Click reaction) during treatment with 10 $\mu\text{g ml}^{-1}$ PC190723. (A) No PC190723. (B) 0-5 minutes PC190723. (C)10-15 minutes PC190723 with cell of interest highlighted. (D) 30-35 minutes PC190723. (E) 60-65 minutes PC190723. 3D localisation of synthesis is represented by a colour table in 100 nm slices from 500 nm behind the plane of focus (-500 nm, blue) to 500 nm in front of plane of focus (500 nm, red). (Scale bar, 1 μm).

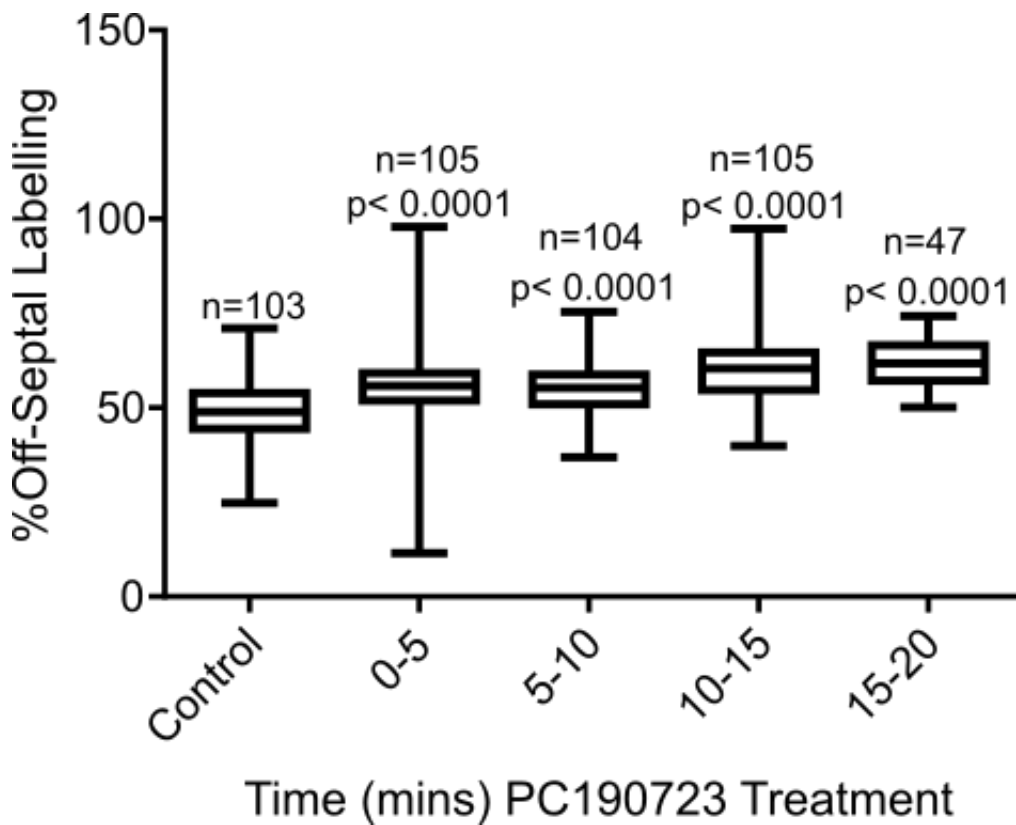
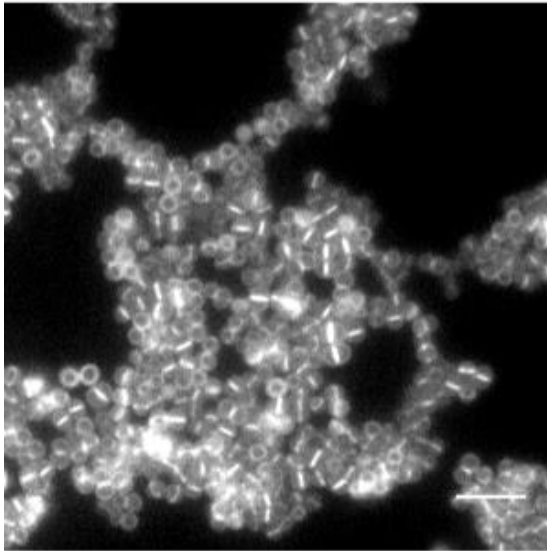
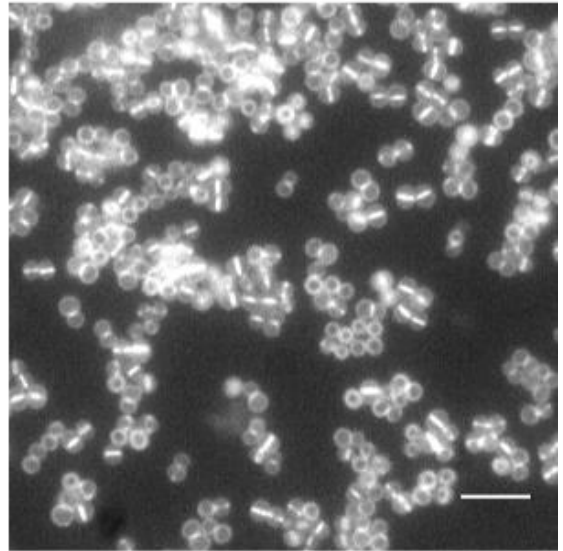


Figure 4.29. Quantification of off-septal labelling during the first 20 minutes of PC190723 treatment. Cells were measured wherever a clear septum was present. Box plot of % off-septal labelling of 5 minutes HADA (500 μ M) incorporation. Box extends from 25th to 75th percentiles and midline is plotted at the median. Whiskers are drawn down to the minimum value and up to the maximum value. P values are the result of Mann-Whitney tests comparing with the control sample. N value for 15-20 minutes was lower due to the smaller portion of cell that were septating following 15 minutes PC190723 treatment.

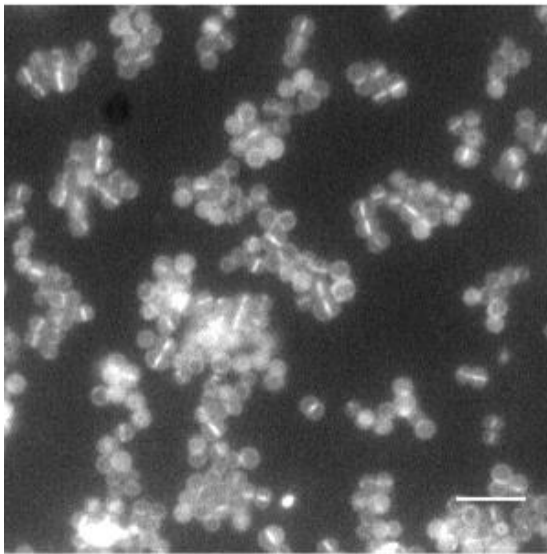
Control



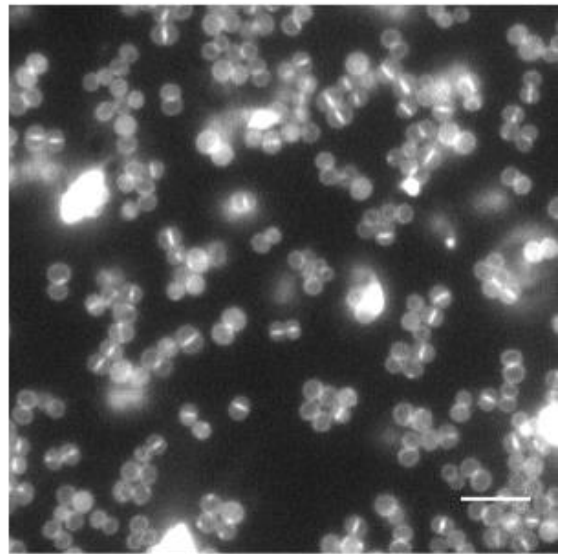
0-5 minutes



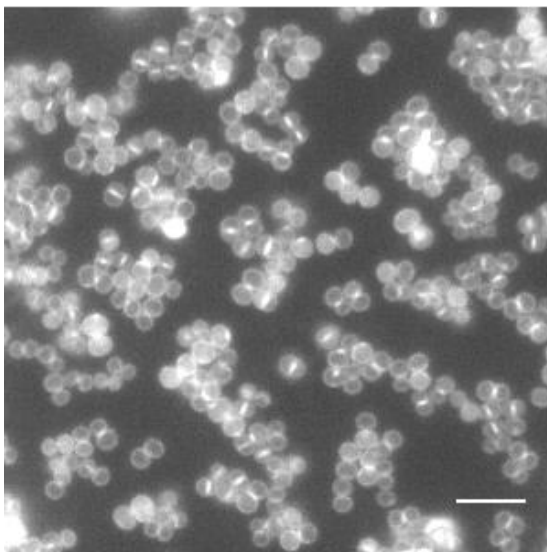
5-10 minutes



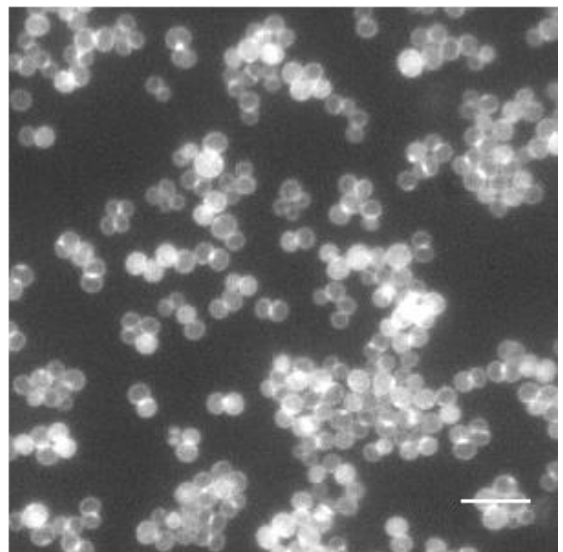
10-15 minutes



15-20 minutes



20-25 minutes



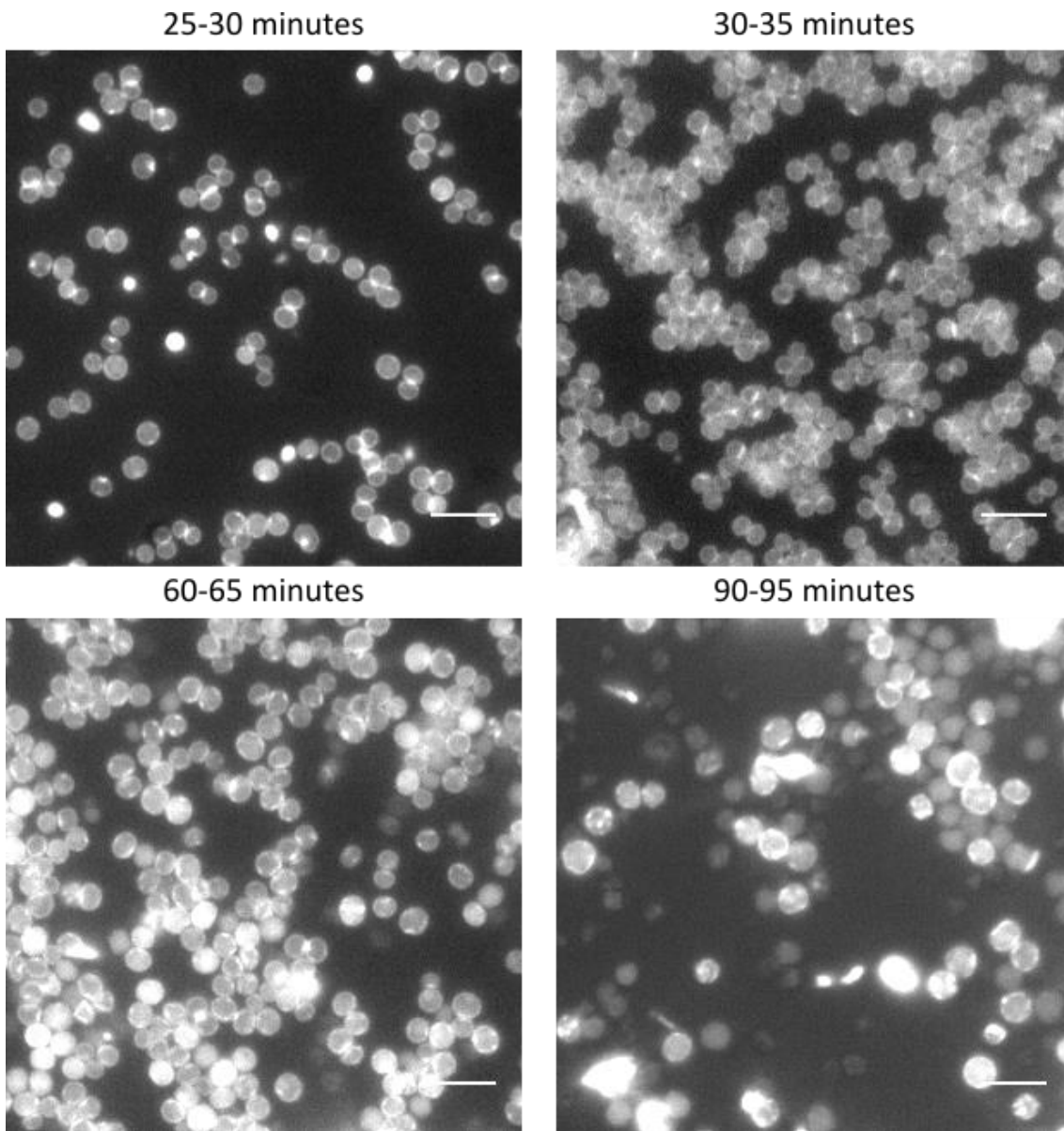
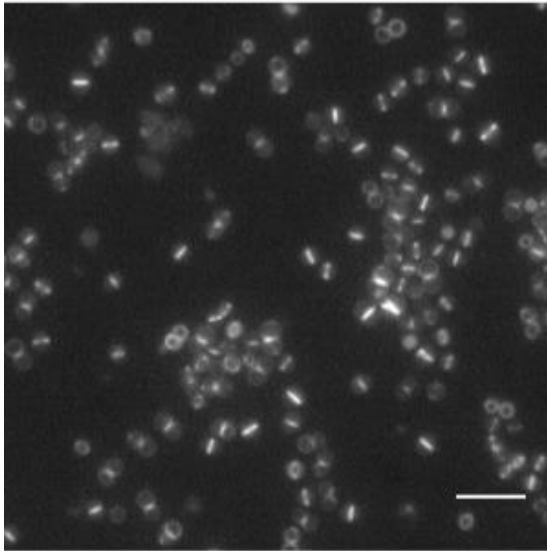
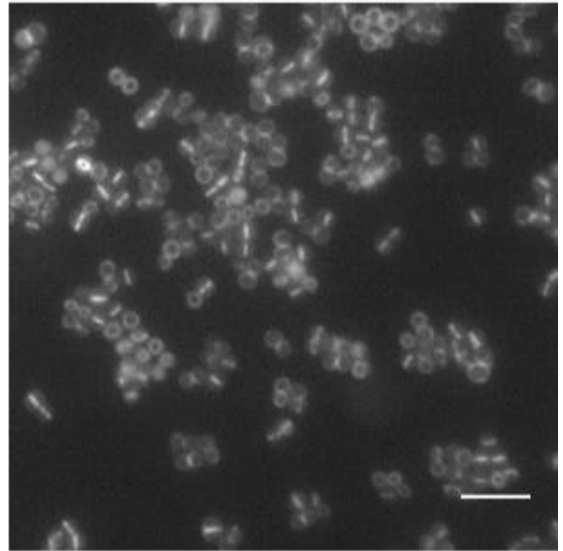


Figure 4.30. Effect of PC190723 on localisation of peptidoglycan synthesis in 4421 (*pbp3*). 5 minute windows of peptidoglycan synthesis were labelled by HADA (500 µM) during treatment with 10 µg ml⁻¹ PC190723. (Scale Bar 5 µm).

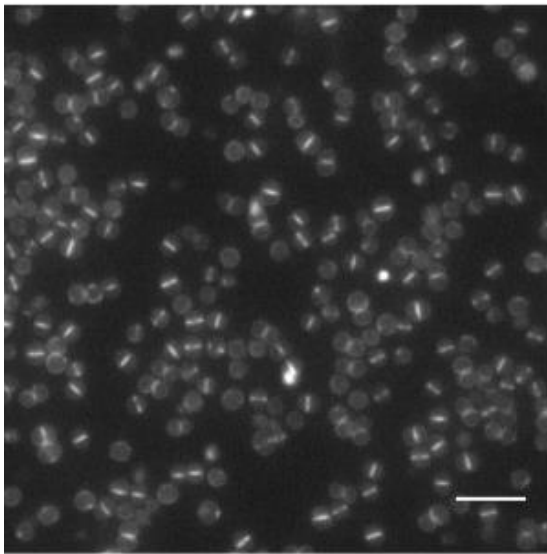
Control



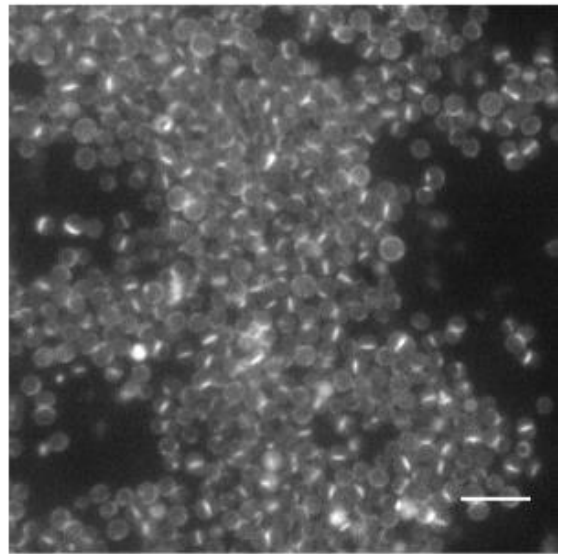
0-5 minutes



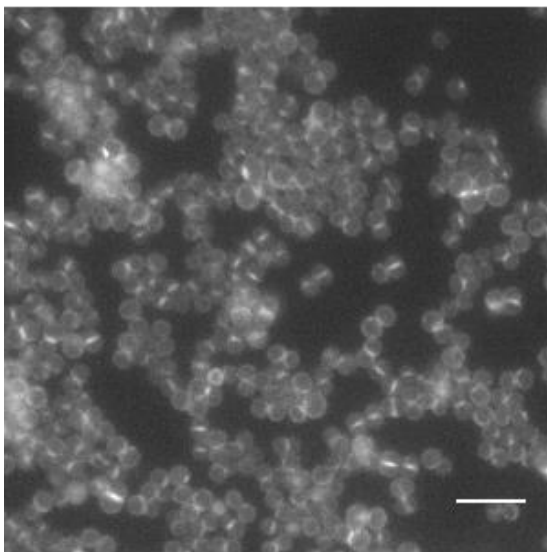
5-10 minutes



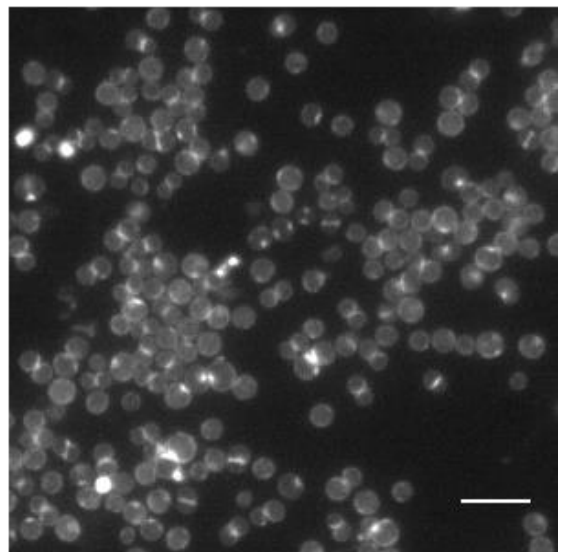
10-15 minutes



15-20 minutes



20-25 minutes



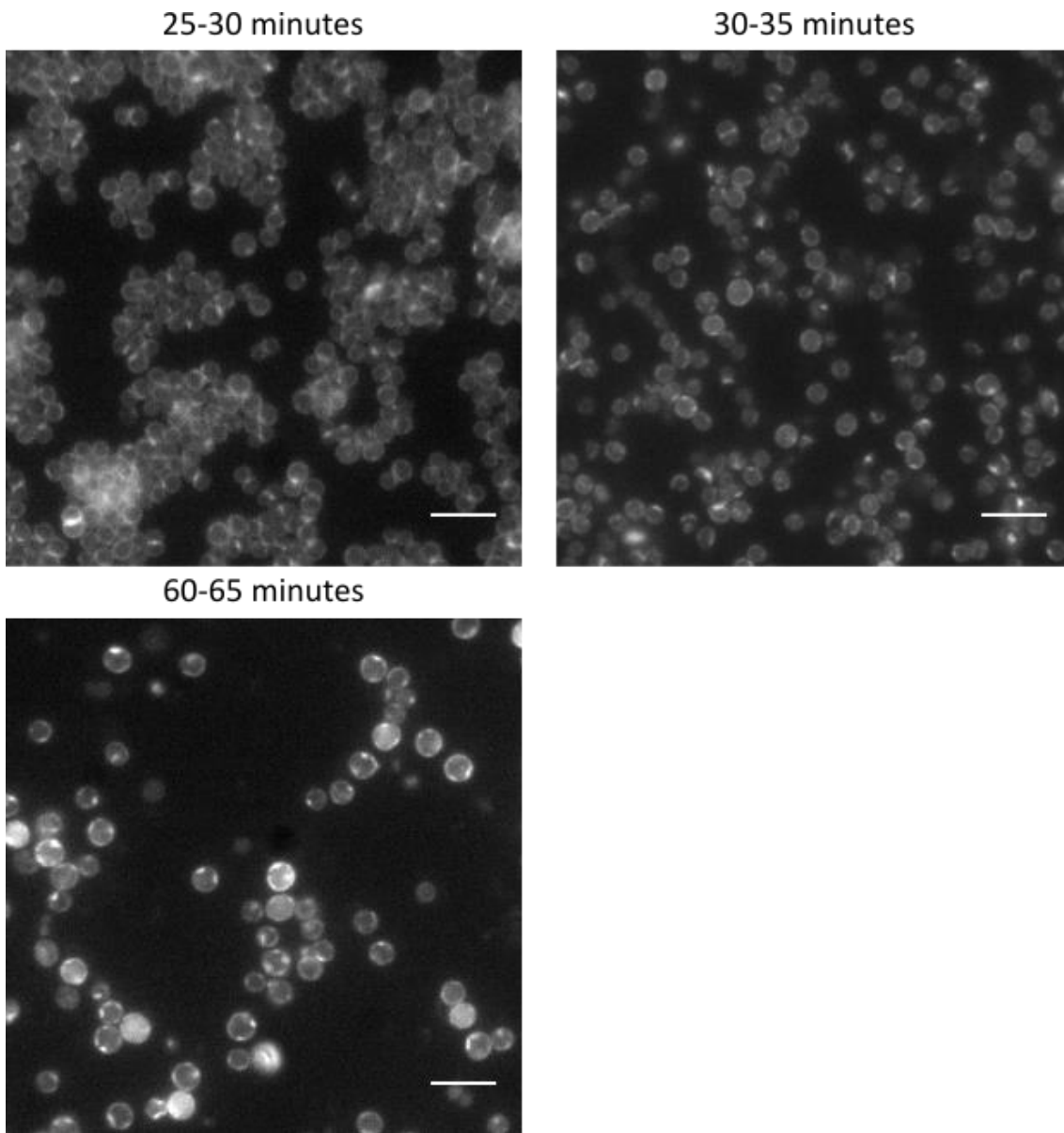
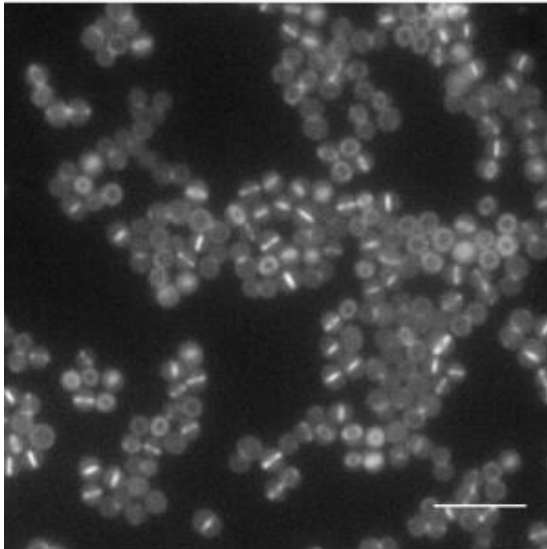
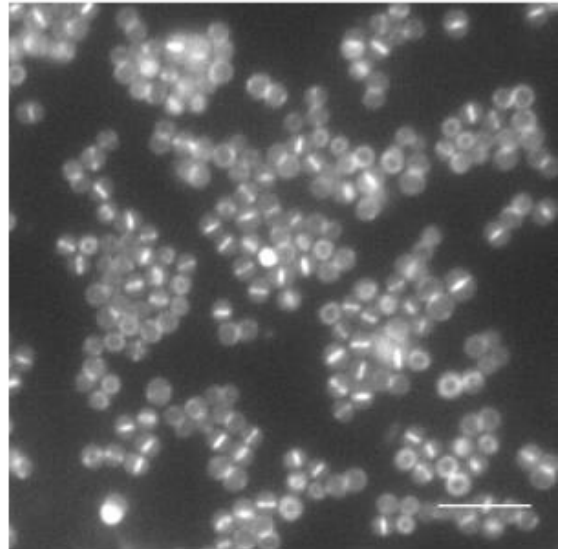


Figure 4.31. Effect of PC190723 on peptidoglycan synthesis in 4425 (*pbp4*). 5 minute windows of peptidoglycan synthesis were labelled by HADA (500 μM) during treatment with 10 $\mu\text{g ml}^{-1}$ PC190723. (Scale Bar 5 μm).

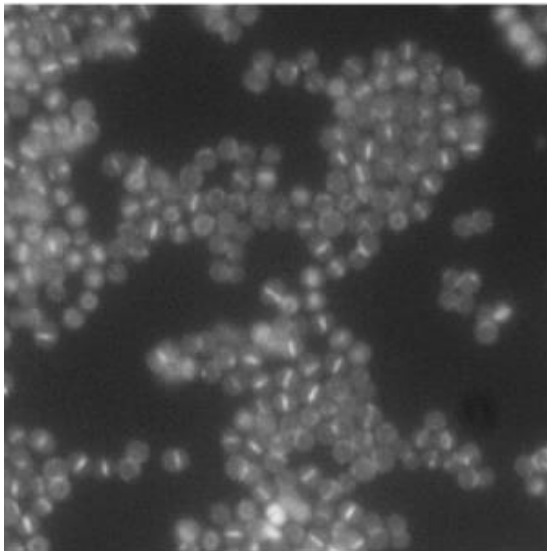
Control



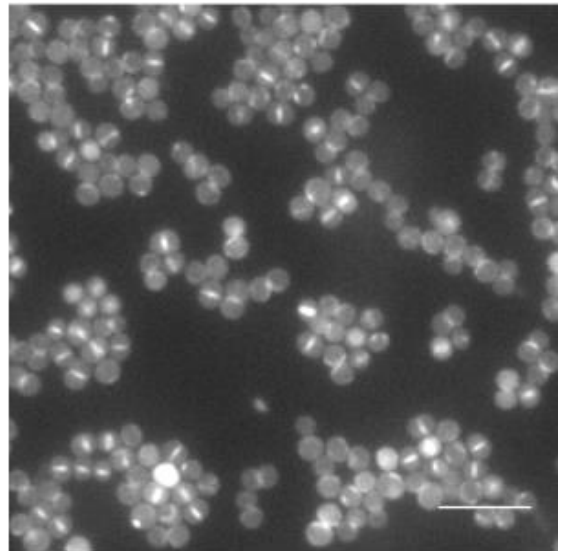
0-5 minutes



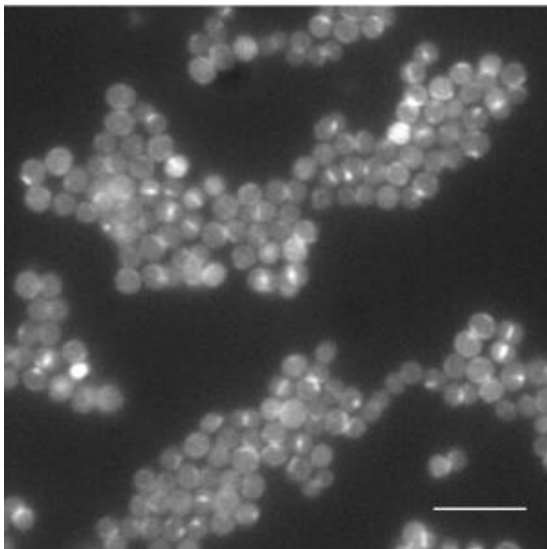
5-10 minutes



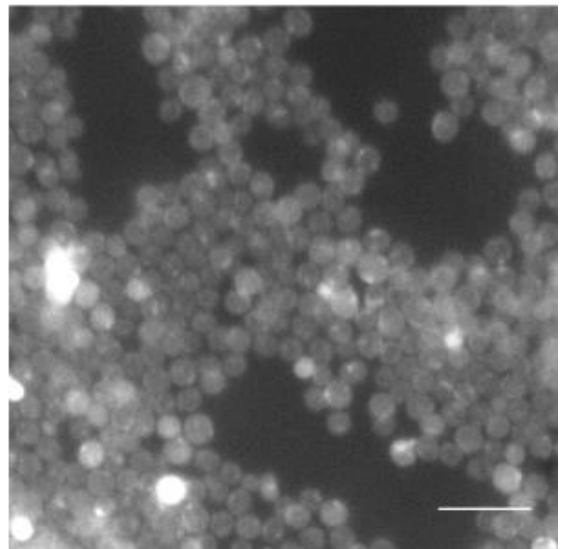
10-15 minutes



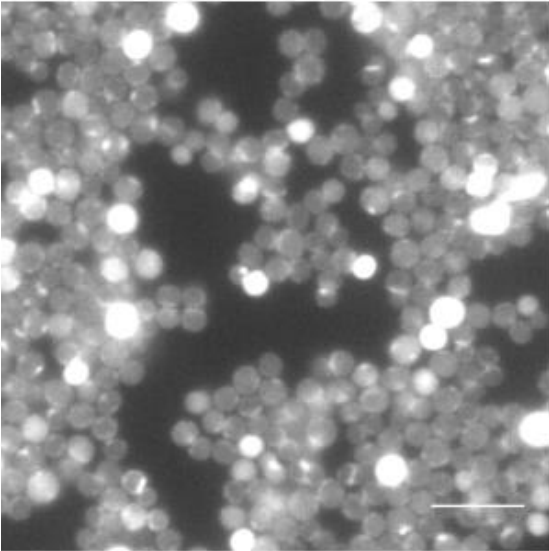
15-20 minutes



20-25 minutes



25-30 minutes



4.3 Figure 4.32. Effect of PC190723 on peptidoglycan synthesis in 4424 (*pbp3pbp4*). 5 minute windows of peptidoglycan synthesis were labelled by HADA (500 μ M) during treatment with 10 μ g ml⁻¹ PC190723. (Scale Bar 5 μ m).

Discussion

4.3.1 Model of septal peptidoglycan synthesis

Features of peptidoglycan synthesis as determined by STORM of FDAA labelled cells allows us to propose a new model of peptidoglycan synthesis within *S. aureus*. Peptidoglycan synthesis was shown to occur as a zone of synthesis toward the leading edge of the septum as opposed to a focus at the leading edge (Chapter 4.2.2). This is in agreement with previous cryo-EM on cell wall fragments that showed the septum flared towards the cross wall (Figure 4.33 A)(Matias and Beveridge, 2007). The septum is synthesised by insertion of new peptidoglycan primarily at the leading edge, however also along the length of the growing septum to produce a complete septum of an appropriate thickness (Figure 4.33 B). The peptidoglycan synthesis enzymes within the divisome are proposed to exist as a gradient around the peptidoglycan synthesis zone denoted by the purple dots within the model (Figure 4.33 B). Indeed, a number of division proteins including FtsZ and EzrA have been shown to have such a localisation (Kasia Wacnik, unpublished results). Eventually the nascent growing septum will reach a cross-section such that its innermost layer can no longer interact with the synthetic machinery. This is also the case at the piecrust where the thick band of peptidoglycan prevents access to the biosynthetic machinery. This does not indicate splitting of the cell prior to completion of the septum as the piecrust at the mother cell wall – septum intersect remains intact. This allows the dividing cell to withstand turgor pressure.

Before or during separation of daughter cells the septum must be split in half such that each daughter cell receives part of the septum as a new hemisphere of cell wall. The intricacies and dynamics of how this happens remains unclear, particularly as this appears to occur at length scales shorter than the resolution of super-resolution microscopy (Zhou et al., 2015). Data from my study shows two separate areas of peptidoglycan synthesis, suggesting 2 separate entities. However, there remains two issues with this model which must be assessed. Firstly, it is possible that the septum exists as a single entity with synthesis occurring at the outer edge of the septal plate thereby leaving a plate of peptidoglycan that is inaccessible to new peptidoglycan synthesis, much like the split that was seen at the cross wall. However, while the split was shown to contain peptidoglycan by the vancomycin labelling experiment it was

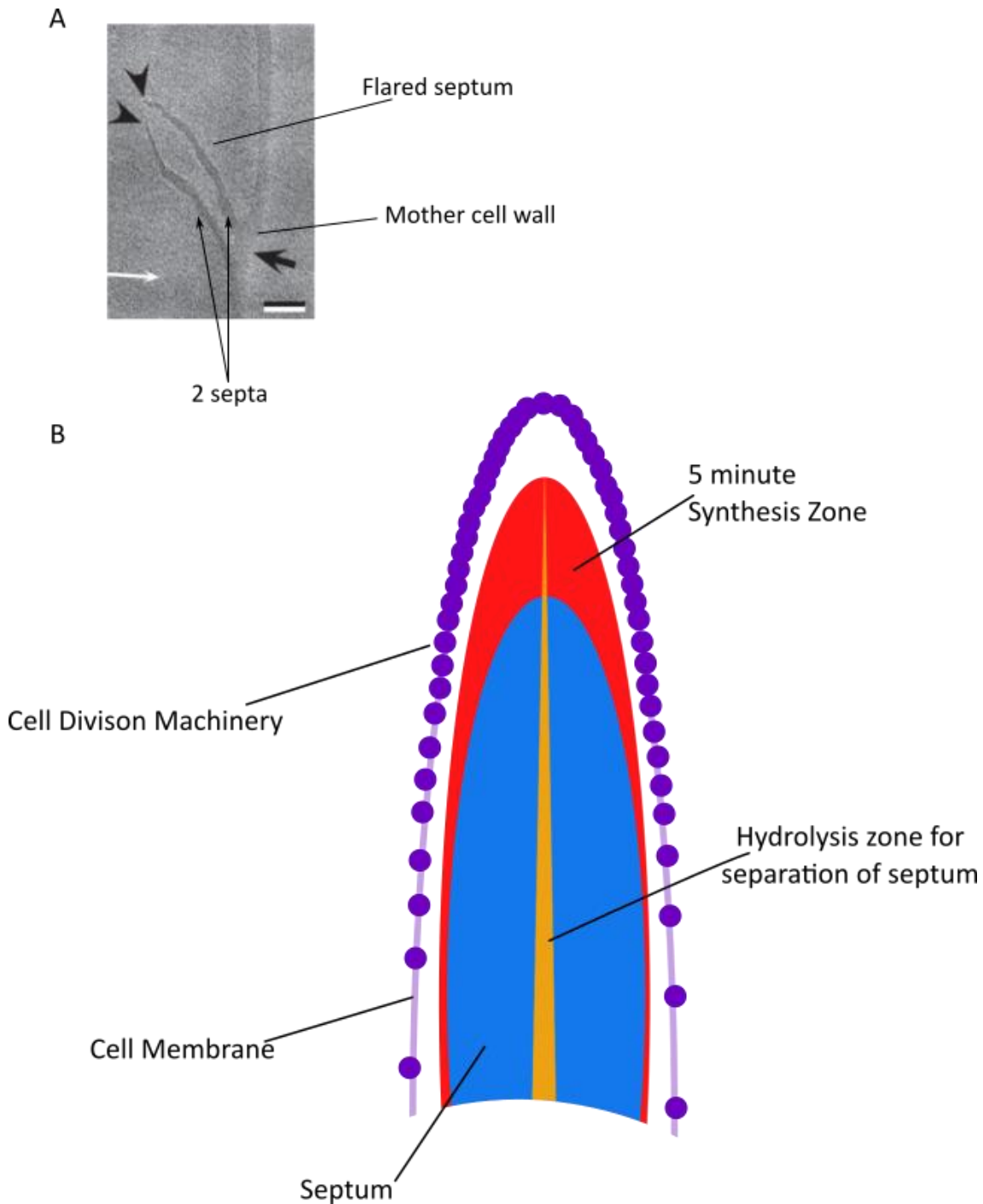


Figure 4.33. Peptidoglycan synthesis occurs as a zone at the septum. (A) TEM of cell wall fragments showing septum flared towards outer cell wall (Matias and Beveridge, 2007). (B) Model of peptidoglycan synthesis at the septum. Red indicates zone of synthesis primarily at the leading edge but also along the length of the growing septum. Cell division machinery (purple dots) also occurs as a gradient.

not possible to resolve the presence or absence of peptidoglycan within the gap between the 2 presumed septal plates. Secondly even if the septum exists as 2 septal plates it is not clear whether the peptidoglycan is synthesized as two separate entities or whether the single septum can be hydrolysed into two, even prior to completion of septal synthesis. Previous work by Matias & Beveridge using cryo-EM showed that the *S. aureus* septum is made of five distinct zones (Matias and Beveridge, 2007). It was suggested that there were two peptidoglycan structures running along the septum with a periplasm-like area between them (Matias and Beveridge, 2007). This provides further evidence that the septum is produced as two entities prior to completion of septation & cell splitting, however it is still not possible to dissect the events that occur at the point of synthesis.

4.3.2 Contribution of off-septal synthesis to growth in *S. aureus*

Unlike rod shaped bacteria *S. aureus* was proposed to only have one mode of growth that is peptidoglycan synthesis during division (Pinho and Errington, 2003). However, labelling peptidoglycan synthesis with FDAAs revealed off-septal labelling which has been attributed to synthesis of peptidoglycan at the peripheral cell wall. Using both chemical and genetic tools it has not been possible to remove or significantly reduce this off-septal labelling as calculated using CTCF values.

The method used for calculation of off-septal labelling results in a wide range of %. This is partially due to difficulties in quantification of subcellular features and variation in the overall labelling between strains. Loss of PBP3, PBP4 and a range of peptidoglycan biosynthetic components did not greatly alter the level of off-septal labelling compared to overall incorporation. This suggests that there is no separate peptidoglycan synthesis machinery responsible for off-septal labelling comparable to the elongasome in rod-shaped organisms. Thus off-septal synthesis is likely carried out by the same machinery as septal synthesis, in particular by PBP2. However, there are a number of additional auxillary proteins involved in peptidoglycan synthesis that could have a role. Of particular interest is FmtA which has been suggested to have weak D-Ala-D-Ala carboxypeptidase activity.

Should off-septal labelling be due to the action of PBP1 and PBP2 there remains a question as to what is the role of this synthesis? Recent work, during the last 12

months, has shown that *S. aureus* is not a true sphere as has been previously suggested but produces an ellipsoidal shape during the cell cycle (Monteiro et al., 2015; Zhou et al., 2015). It is possible that the off-septal synthesis of material may play a role in this shape change. However, it will prove difficult to investigate, as both PBP1 and PBP2 are essential for growth. Conditional lethal expression constructs could allow titration of PBP levels for analysis of their role in off septal labelling.

4.3.3 Response to treatment of *S. aureus* with FtsZ inhibitor PC190723

PC190723 has been shown to stabilize FtsZ polymer formation *in vitro* as well as allowing FtsZ polymers to assemble at lower than normal concentrations (Andreu et al., 2010; Elsen et al., 2012). This prevents the *in vivo* function of FtsZ and thereby poses a means of inhibition of the division process (Andreu et al., 2010). However the mechanism behind cytokinesis inhibition and bactericidal action of PC190723 is not clear (Tan et al., 2012).

Previous work in MRSA has shown PC190723 at 10 x MIC levels to cause an FtsZ-CFP strain to show mislocalisation of FtsZ into multiple rings and arcs (Tan et al., 2012). Within my study a FtsZ-eYFP strain was shown to mislocalise FtsZ into discrete foci and arcs. Strain variation is likely to be the reason for this slightly different pattern. It is unclear why these different strains would produce different localisation patterns. The strains both encode extra copies of fluorescent FtsZ under the control of an inducible promoter. It may be that there is a lower copy number of Ftsz-eYFP than FtsZ-CFP thereby masking multiple rings in addition to the arcs seen. It has proven difficult to substitute the native FtsZ with a fluorescently tagged version.

Imaging of both FtsZ and peptidoglycan synthesis localisation after PC190723 treatment allows its effects to be evaluated. PC190723 promotes FtsZ polymerisation within *S. aureus* cells causing FtsZ to localise to discrete foci & arcs at the periphery of the cell. In turn this causes peptidoglycan synthesis to be recruited to the peripheral cell wall. Insertion of newly synthesised peptidoglycan into the peripheral cell wall without concurrent division causes the characteristic increase in *S. aureus* cell diameter (Pinho and Errington, 2003). This continues until a point at which cells can no longer expand and they die and/or lyse. Without live cell microscopy of cells

undergoing treatment it is unclear whether cells continue expansion until lysis or whether growth will arrest and death eventually occurs via lysis.

The maintenance of control off-septal labelling percentage in cells with a septum suggests that transition to peripheral synthesis is not gradual. In conjunction with the presence of septating cells after the majority of cells altered to a peripheral synthesis pattern suggests that FtsZ mislocalisation by PC190723 only prevents continued cytokinesis before a certain point in the cell cycle. Once cells have passed this point cell division appears to continue however, the next round of division is not possible. This may suggest that FtsZ is only required for the initial stages of cell division and that the process is driven by a separate factor during the later stages, possibly by peptidoglycan synthesis itself. It has been postulated that there is a DivIB checkpoint at the transition between peicrust and septal plate synthesis which may play a role (Bottomley et al., 2014).

It would be interesting to determine the subsequent effect of FtsZ mislocalisation on other proteins within the divisome. For example, EzrA, the negative regulator of FtsZ, was also found to lose its localisation quickly and end up distributed in foci around the cell membrane (K. Wacnik, unpublished results). Another important divisome protein that has been shown to be mislocalised during treatment with PC190723 is PBP2 which localises to broad patches following 30 minutes treatment with PC190723 (Tan et al., 2012). This is particularly important since mislocalisation of PBP2 in MRSA strains can restore sensitivity to β -lactams as the transglycosylase activity of PBP2 is required even in the presence of PBP2A (Pinho and Errington, 2005; Tan et al., 2012). It has been shown that PC190723 can act synergistically with β -lactams therefore PC190723 and other divisome inhibiting compounds may potentiate β -lactam drugs as therapeutics (Tan et al., 2012).

Chapter 5

Dynamics of peptidoglycan insertion in *Staphylococcus aureus*

The work in this chapter was carried out in collaboration with Christa Walther (SIM microscopy).

5.1 Introduction

It has been challenging to determine peptidoglycan dynamics at the subcellular level within bacteria due to the lack of tools to easily visualise peptidoglycan synthesis. However, in recent years the development of FDAA probes has begun to open up this area (Kuru et al., 2012; Siegrist et al., 2013).

Using D-cysteine labelling in conjunction with immunodetection of thiol groups on Gram negative sacculi the dynamics of peptidoglycan insertion was determined (de Pedro et al., 1997). For *E. coli*, the transition of elongation to septation is correlated with a modification of peptidoglycan insertion pattern. Elongation is associated with diffuse and “random” incorporation of precursors over the cylindrical portion of the sacculus (de Pedro et al., 1997). On initiation of septation, insertion changes to localised insertion at the pre-septal area. Additionally, it was determined that following completion of the septa and cell separation the new cell poles (old septa) become metabolically inert suggesting a stable peptidoglycan configuration with neither hydrolysis or synthesis occurring (Vollmer and Bertsche, 2008). In *C. crescentus* the shift from swarmer to stalked phase is coupled with a change to the peptidoglycan insertion pattern. Initial diffuse incorporation of precursors during most of the cell cycle is relocated to the future division site prior to cell constriction, unlike in *E. coli* where constriction is apparent at the shift in incorporation pattern (Aaron et al., 2007; Vollmer and Bertsche, 2008). This pre-septal growth from the midcell contributes to cell elongation prior to cell division.

Rod-shaped organisms, such as *B. subtilis* have two modes of peptidoglycan synthesis, during septation and elongation (Szwedziak and Löwe, 2013). Previous work has concentrated on the dynamics of synthesis proteins as opposed to the dynamics of actual peptidoglycan insertion. Using fluorescent vancomycin, peptidoglycan insertion

in *B. subtilis* was shown to occur in broad bands at division sites as well as on the cylinder of the rod-shape (Daniel and Errington, 2003). The cylinder labelling localisation was reminiscent of the helical pattern previously found for the actin-like proteins MreB and Mbl (Jones et al., 2001). Investigation into the peptidoglycan architecture of both the new septum and wall cylinder suggested a mechanism of insertion of helical cables within the cylinder and in producing the septum as a spiral (Hayhurst et al., 2008). However, both these approaches were limited to static snapshots.

The two modes of peptidoglycan insertion in rod-shaped bacteria are mediated by related but distinct protein complexes; the divisome and elongasome. The divisome is almost universal in bacteria and is responsible for cell division, while the elongasome directs lateral insertion and is a modified version of the divisome, without the FtsZ ring and associated machinery (Szwedziak and Löwe, 2013). The divisome and elongasome are bound to the membrane via actin-like protofilaments FtsA and MreB respectively.

Dynamics of the divisome have often concentrated on the dynamics of FtsZ, a tubulin homolog that organises peptidoglycan synthesis and remodelling at the mid-cell (Szwedziak and Löwe, 2013). FtsZ filaments are also thought to produce the force required for cell constriction during division (Mingorance et al., 2010). The localisation and dynamics of the z-ring was limited by conventional fluorescence microscopy and EM due to the diffraction limit and labelling difficulties (Jennings et al., 2011). Despite this FtsZ has been localised to a band at the mid-cell in a ring-like structure that is dynamic in nature (Romberg and Levin, 2003). More recently the localisation of FtsZ has been determined at higher resolution by super-resolution microscopy techniques (Biteen et al., 2012; Holden et al., 2014; Strauss et al., 2012). Initial studies using 3D SIM showed that the z-ring of *B. subtilis* has a heterogeneous distribution of FtsZ with a possible discontinuous structure due to the presence of “gaps”, areas of the z-ring with little or no visible fluorescence (Strauss et al., 2012). Time-lapse microscopy showed that the distribution and position of FtsZ rapidly changed, however this dynamism was independent of constriction. This was also shown to be the case in *S. aureus*.

Two variations of PALM have been applied to the analysis of FtsZ from *Caulobacter crescentus*, resulting in different models of FtsZ localisation (Biteen et al., 2012; Holden et al., 2014). The first produced images of z-rings that span the cells diameter and were of a thickness to suggest either a compressed helix or similar structure consisting of a high number of FtsZ protofilaments (Biteen et al., 2012). Conversely, Holden et al. found FtsZ to form a patchy ring at the mid-cell (Holden et al., 2014). Using high throughput 3D-PALM and a synchronised population of bacteria, patterns of FtsZ localisation throughout the cell-cycle were determined. Continuous rings were a rare event and although the proportion increased in late-stage division they were never the dominant morphology (Holden et al., 2014). It remains unclear what the shorter timescale dynamics of a patchy z-ring may be. Both a continuous and patchy ring can be modelled to allow FtsZ to produce a force capable of influencing constriction. However, whether force generation is required *in vivo* is still unclear, particularly how it may be linked to peptidoglycan remodelling (Sundararajan et al., 2015). EM tomography of FtsZ indicates a continuous, closed ring formed by overlapping short filaments (Chapter 1.7.1; Szwedziak et al., 2014). It is suggested that the non-continuous rings found by Holden et al. (2014) may be due to the use of tagged proteins since there may be non-functional GTP fusions or that the punctate pattern is an artefact of overexpression (Szwedziak et al., 2014). Additionally, low signal-to-noise may cause overlapping regions of filaments to be over emphasised.

The location and dynamics of the z-ring does not necessarily directly correspond to the synthesis, one way of determining localisation of synthesis is to locate the main peptidoglycan synthesis enzymes, PBPs (Scheffers and Pinho, 2005). Localisation of nearly all the PBPs within *B. subtilis* vegetative cell division and elongation shows there are 3 main patterns (Scheffers and Pinho, 2005; Scheffers et al., 2003);

1. Dispersed localisation at the peripheral cell wall
2. Specific localisation to division septum
3. Localisation to distinct spots at the periphery – sometimes resolved in short arcs.

However, in recent years there has been limited new insights into the localisation and dynamics of PBPs, in particular those which are located to the septum. In addition, it is

not known which PBPs are actively inserting peptidoglycan at any time. This remains a promising avenue of research, one that would be aided by the use of FDAAs to label new peptidoglycan insertion.

The elongasome-linked actin homolog, MreB, is essential for the maintenance of the rod-shape (van Teeffelen et al., 2011). It contains a canonical actin fold and produces protofilaments (Szwedziak and Löwe, 2013). The dynamics of the elongasome have been determined through the analysis of fluorescently tagged MreB (Domínguez-Escobar et al., 2011; Garner et al., 2011; van Teeffelen et al., 2011). Initial studies on MreB suggested localisation in helical filaments that encircled the cytoplasm and were flexible and highly dynamic (Carballido-López, 2006). More recently MreB has been shown to rotate around the long axis in a manner dependent upon peptidoglycan synthesis as opposed to its own polymerization (van Teeffelen et al., 2011). This has been shown in *E. coli* (van Teeffelen et al., 2011) and *B. subtilis* (Domínguez-Escobar et al., 2011; Garner et al., 2011). Within *B. subtilis* MreB filaments exist in shorter fragments or patches that have continuous movement in both directions. The discontinuous nature means that MreB cannot function as a “cell-spanning” structure but may act as a scaffold for peptidoglycan synthesis or to control the mobility of the elongasome (Domínguez-Escobar et al., 2011). Similarly to FtsZ, knowledge of MreB dynamics is only suggestive of where peptidoglycan synthesis is taking place. In order to determine the localisation of peptidoglycan synthesis both at the septum and within the periphery, FDAAs could be used to label peptidoglycan insertion.

Apparently spherical bacteria, such as *S. aureus* lack MreB homologs and have been previously thought to have only one mode of peptidoglycan insertion, septation (Pinho and Errington, 2003; Scheffers and Pinho, 2005). All the major cell division proteins (FtsZ, PBP1, PBP2 & 2A, EzcA) have been localised to the septum during division although evidence of dynamics is limited (Jorge et al., 2011; Pereira et al., 2007; Pinho and Errington, 2003, 2005; Steele et al., 2011). PBP2 was shown to produce a ring at the future division plane and as the septum closes the localisation of PBP2 changes to a disk co-localised with the septum, this remains throughout cell division even as daughter cells begin to separate (Pinho and Errington, 2005). Using 3D-SIM, PBP2 was found to have a similar localisation pattern to FtsZ, namely a heterogeneous bead-like distribution (Strauss et al., 2012).

There exists a model of peptidoglycan dynamics within *S. aureus* informed by architectural features determined by AFM and vancomycin labelling of nascent peptidoglycan. AFM determined the presence of thick bands (“piecrusts”) of material that encircles cells and surrounded any incomplete septa found (Turner et al., 2010a). These piecrusts are thought to be formed before the centripetal assembly of the septal disk occurs. Vancomycin labelling appears to corroborate this since nascent peptidoglycan appears as a ring or disk in the plane of the septum, with brighter fluorescence indicating the piecrust in some cells. Following the synthesis of the septum, pairs of daughter cells were seen to partially separate before synthesis of orthogonal new growth occurred (Figure 5.1). The stage between septum completion and cell splitting is brief (Turner et al., 2010a).

Due to division of *S. aureus* on 3 sequential and orthogonal planes peptidoglycan in the cell wall can be sectorised by age. If it is taken that after each division daughter cells consist of approximately $\frac{1}{2}$ material from the division that has just occurred and $\frac{1}{2}$ from previous generations then the cell wall can be sectorised as follows (Turner et al., 2010a)(Figure 5.2);

1. $\frac{1}{2}$ peptidoglycan from the most recent division
2. $\frac{1}{4}$ from the second most recent division
3. $\frac{1}{8}$ from the third most recent division
4. $\frac{1}{8}$ from a previous division

However, recently it has been suggested that *S. aureus* may not produce 50% new material but instead 33%. Also further remodelling by autolysins etc. does not affect the ratio of 67% old peptidoglycan:33% new peptidoglycan (Monteiro et al., 2015). How these theoretical models of sectoring translate *in vivo* is still uncertain.

5.1.1 Aims of the Chapter

1. To determine the dynamics of peptidoglycan insertion within the septum.
2. To visualise peptidoglycan sectoring.

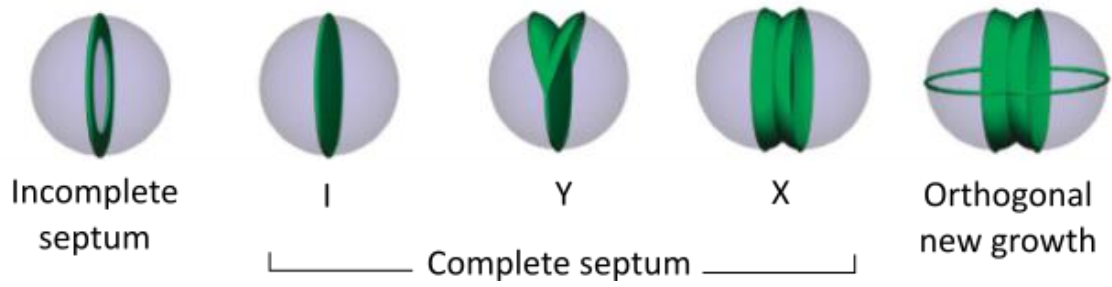


Figure 5.1. Model of dynamics of nascent peptidoglycan insertion. Green indicates localisation of peptidoglycan synthesis. Septum is completed prior to cell splitting and orthogonal new growth. (Taken from Turner et al., 2010).

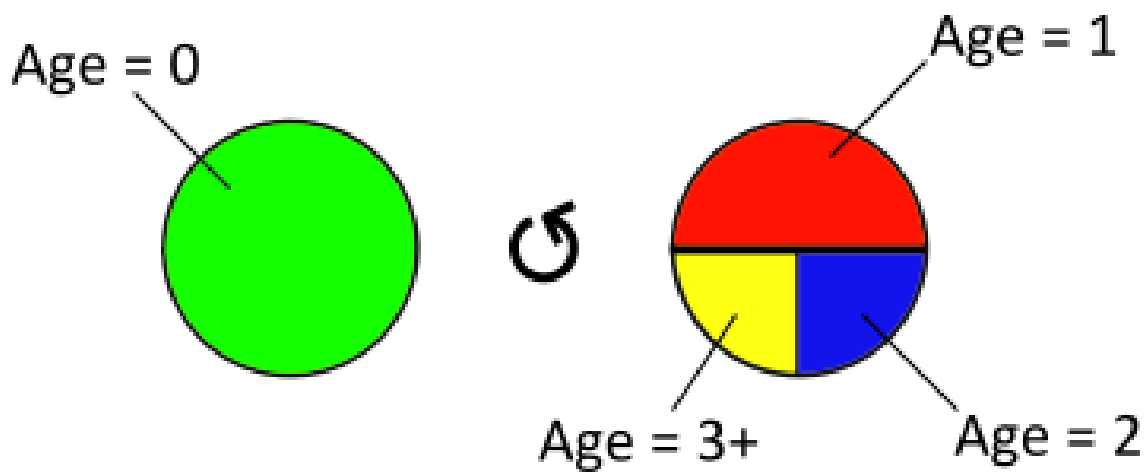


Figure 5.2. Schematic of peptidoglycan age by sectoring of cell-wall during multiple cell division cycles. Two hemispheres of a single cell rotated through 180°. On the left is the recently synthesised hemisphere and the right is the mature hemisphere with age denoted. Age refers to the number of divisions occurred since synthesis.

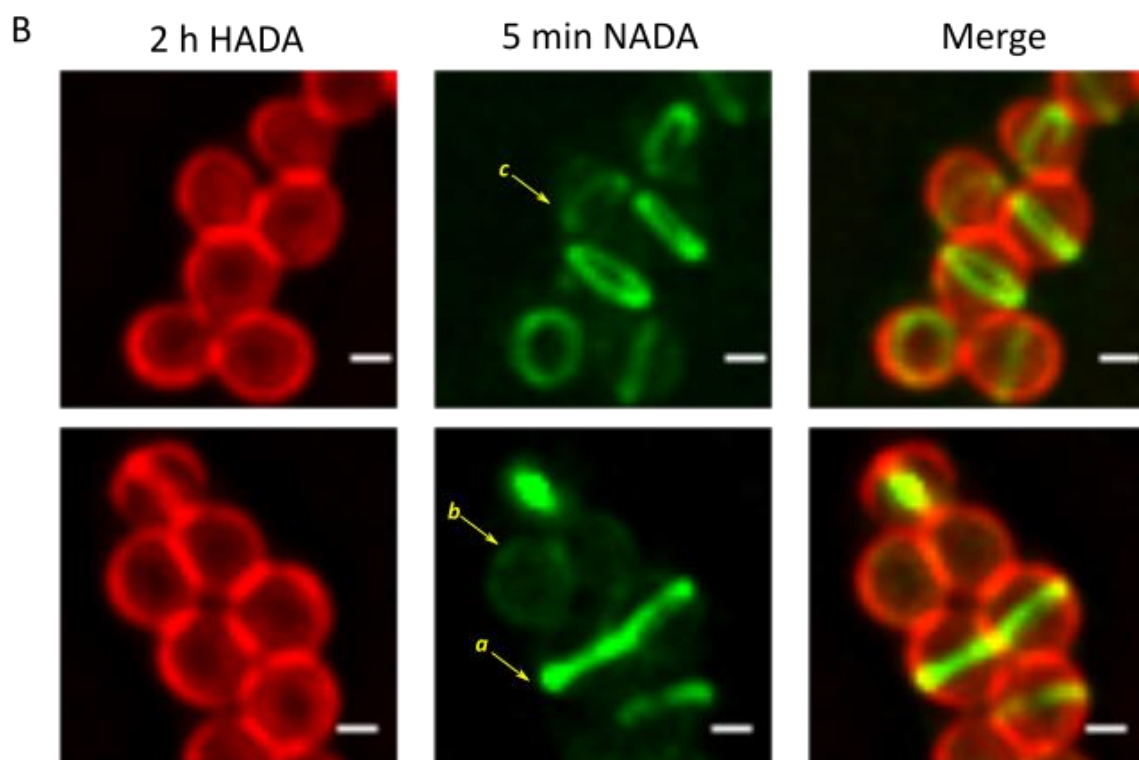
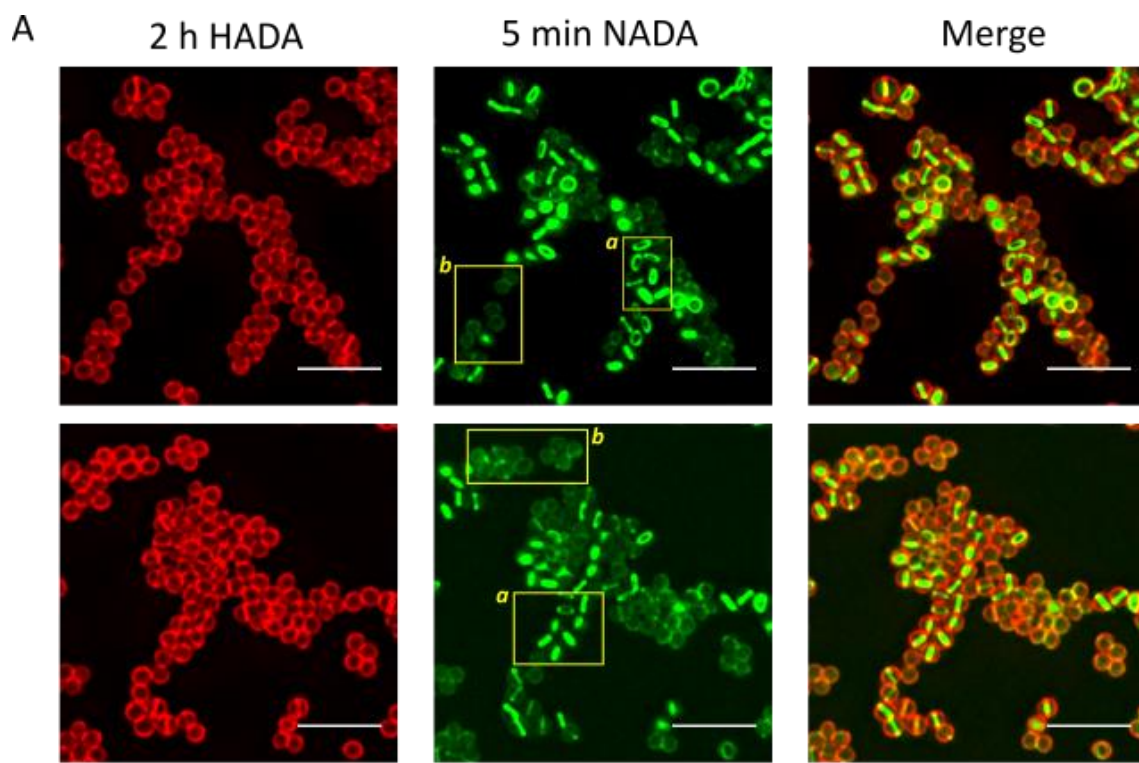
5.2 Results

5.2.1 Dynamics of synthesis by pulse labelling

By labelling peptidoglycan insertion with a long pulse of HADA (2 hours) followed by a short pulse with a second FDAA there are two consequences. Firstly, labelling by the second FDAA should be synthesis only since all available exchange reaction sites should have already exchanged with HADA. Secondly peptidoglycan insertion labelled by the second FDAA can be put into context of the progression of cell division.

Labelling over 5 minutes with NADA following the 2 hour HADA pulse was imaged using widefield deconvolution and structured illumination microscopy (Figure 5.3). NADA labelling has a pattern consistent with previous patterns seen (Figure 4.1; Figure 5.3 A & B), this has two implications; firstly, that 2 hours incubation with HADA has no obvious detrimental effect on cell-division and secondly that previously described incorporation patterns (Chapter 4) are due to peptidoglycan synthesis not the exchange reaction. In addition, off-septal labelling is still present, albeit at a seemingly lower level. This furthers the notion that off-septal labelling is due to synthesis of nascent peptidoglycan at the peripheral cell wall as opposed to an artefact of labelling. During the deconvolution process a portion of the signal is removed from the sample in order to increase signal compared to background, therefore it is not possible to use deconvolved images for quantitative analysis of reduction in off-septal with these images. For quantification to be possible this would need to be repeated using standard widefield microscopy (as used in Chapter 4.2.4).

There also appears to be two populations of cells (Figure 5.3 A, cells marked a & b); one that exhibits a bright ring or plate of fluorescence at the septum (a) and the other with reduced fluorescence (b). The presence of bright rings and plates in septating cells suggests that once a cell is committed to synthesising a septum a large amount of peptidoglycan material is required to be inserted. While many cells that have reduced fluorescence are not in the process of septation, a number have the beginnings of piecrust synthesis labelled with NADA (Figure 5.3 B, cell marked c). This implies that the piecrust may be a temporally consuming stage. The production of the piecrust is thought to be an important stage to be completed prior to the synthesis of the septal plate. Cells lacking in DivIB become stuck at the piecrust stage (Bottomley et al., 2014), suggesting the role of DivIB as a molecular checkpoint for the successful completion of



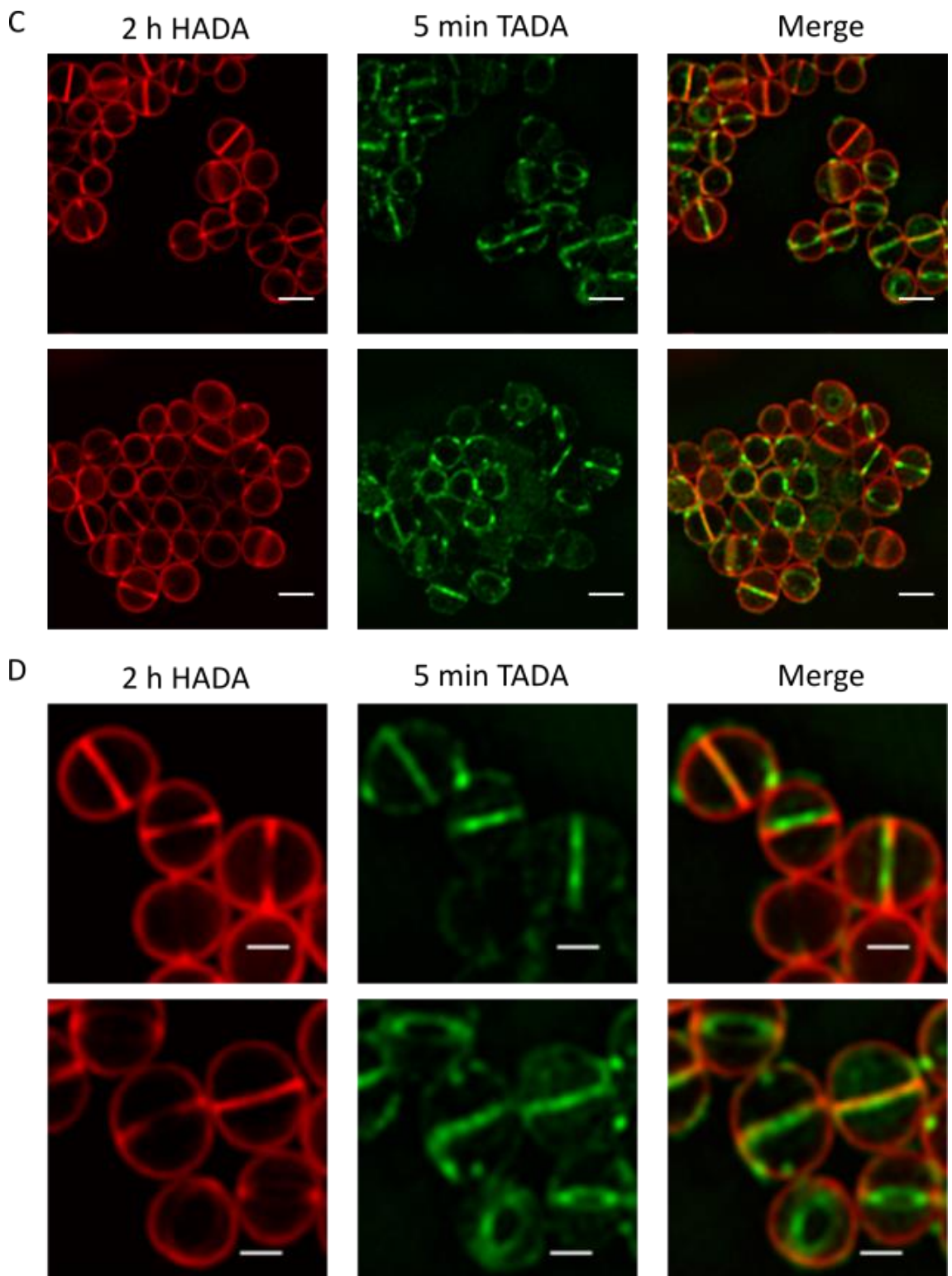


Figure 5.3. Localisation of nascent peptidoglycan synthesis using dual labelling. 5 minutes peptidoglycan synthesis labelled with FDAA following 2 hours labelling with HADA (5 mM). Imaged by OMX widefield microscopy with images deconvolved by Softworx (A&B) or in structured illumination mode (C&D). (A) 2 fields of labelled *S. aureus* cells labelled for 2 hours with TADA (5 mM) and 5 minutes with NADA (5 mM), imaged using OMX widefield. Two patterns of NADA labelling indicated by a & b (Scale bar 5 μm , maximum intensity projection). (B) Selected cells from (A) enlarged to highlight labelling pattern, cells of interest indicated by arrows (Scale bar 0.5 μm , maximum intensity projection). (C) Fields of labelled *S. aureus* labelled for 2 hours with HADA (5 mM) and five minutes with TADA (5 mM) imaged by SIM (Scale bar 1 μm , average intensity projection). (D) Selected cells enlarged to highlight labelling pattern. (Scale bar 0.5 μm , average intensity projection).

the piecrust. Cells throughout the population have a variety of patterns and amounts of peptidoglycan insertion during NADA labelling. This may be due to the different stages of the cell cycle that cells are in during NADA labelling and may suggest a level of heterogeneity in peptidoglycan insertion.

To further investigate the insertion of peptidoglycan samples were imaged using SIM (Figure 5.3 C & D). In this case 2 hour HADA incubation was followed by 5 minute TADA incubation since reconstruction is generally improved with TADA over NADA labelling (Chapter 3.2.3.1). TADA labelled peptidoglycan insertion is found to continue septal synthesis from that incorporated during HADA labelling. This can be seen as the presence of ring and plate structures TADA labelled within initial rings that were HADA labelled. Off-septal labelling is also present in TADA labelled channel, once again indicating that some of the off-septal labelling is due to synthesis. However, it is not possible to infer any pattern in off-septal synthesis due to artefacts arising from the microscopy technique (Chapter 3.2.3.2). These artefacts can be seen from the Fourier transforms in Appendix II (Appendix Figure 13).

The Fourier transforms suggest that both channels include periodic features from the patterned light source. Therefore, the apparent punctate pattern, particularly in the TADA channel is likely an artefact from this rather than a pattern of TADA labelling. In particular, since these puncta are often present where 2 cells meet (e.g Figure 5.3 D, upper panel) where signal density is higher.

To determine short term peptidoglycan synthesis 2 minutes labelling with TADA was used following 2 hours HADA labelling (Figure 5.4). The pattern of incorporation was the same as with 5 minutes labelling. However, the SIM artefact was much more apparent in the images. In addition, the Fourier transform shows significant periodic features (Appendix II, Figure 14). Therefore, any subtle changes in labelling features would be masked.

5.2.2 Septal dynamics by virtual time-lapse

Using previous methods, the dynamics of peptidoglycan synthesis have been difficult to determine. Most of what we know has been inferred from pulse-chase labelling with Vancomycin (Pinho and Errington, 2003; Turner et al., 2010a). FDAAs provide a tool to probe the dynamics of peptidoglycan synthesis by means of virtual time-lapse

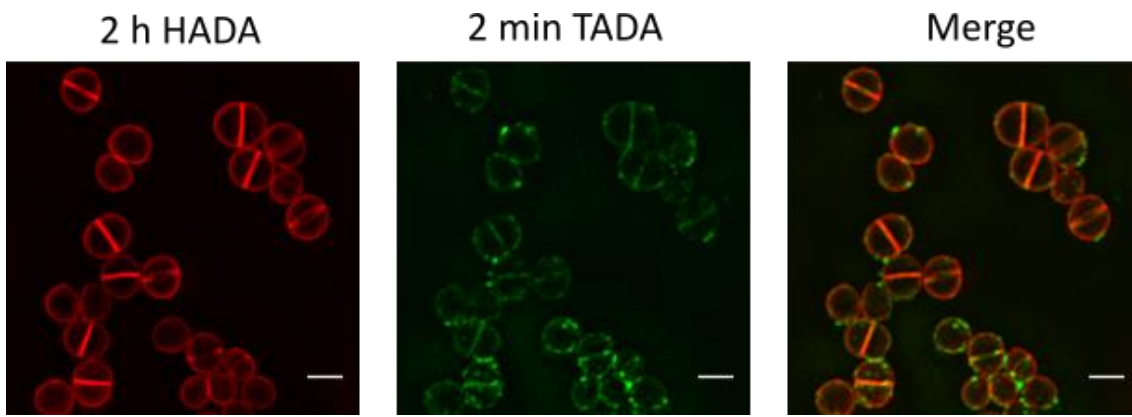


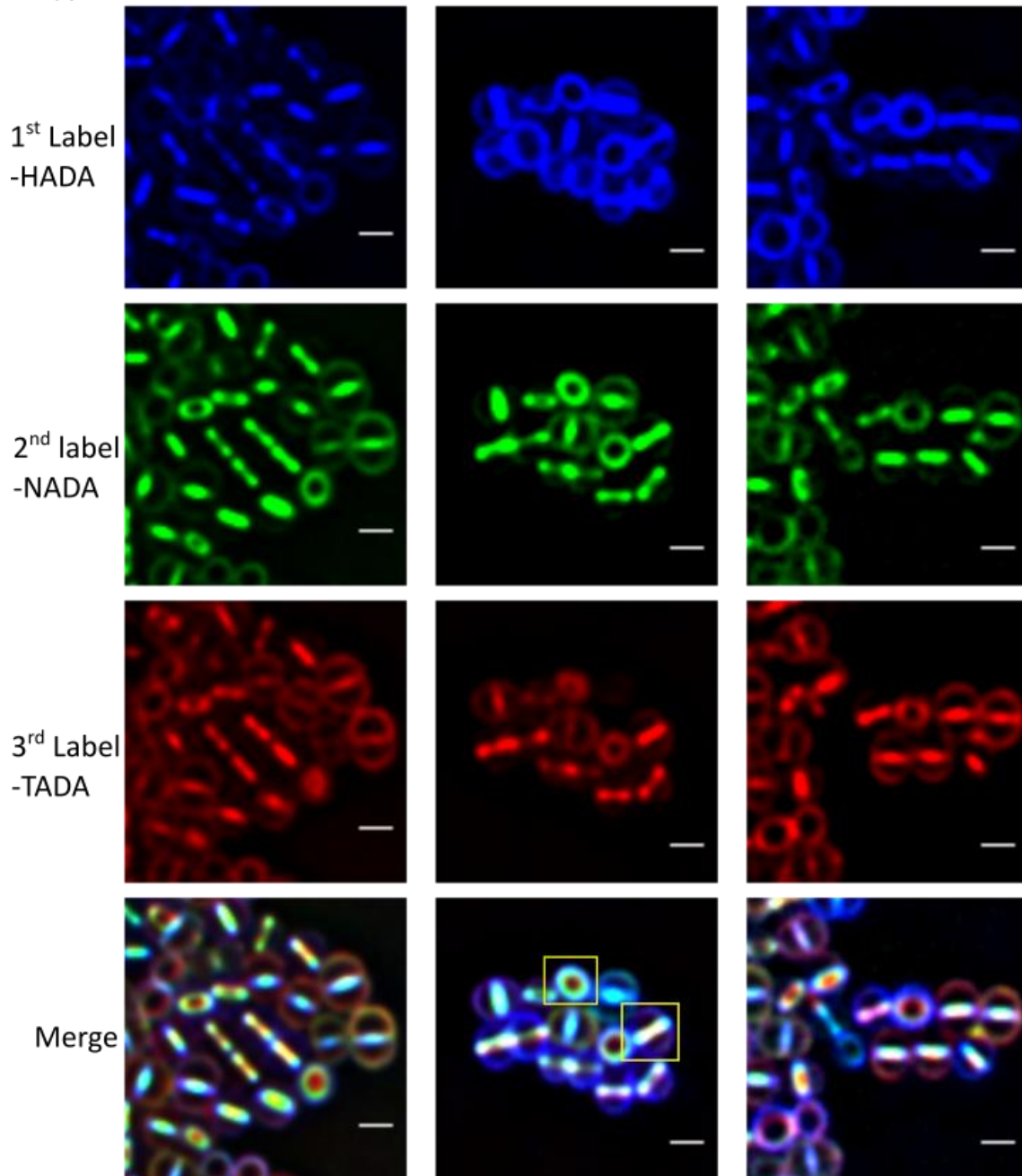
Figure 5.4. Localisation of 2 minutes nascent peptidoglycan synthesis using dual labelling. Following 2 hours labelling of peptidoglycan synthesis with HADA (5 mM) 2 minutes of synthesis was labelled with TADA (5 mM). Resulting cells were imaged using SIM. (Scale bar 1 μm , average intensity projection).

experiments. The location of synthesis during each time period can be marked by the use of spectrally different FDAAs providing a time resolved image of peptidoglycan synthesis (Kuru et al., 2012).

Dynamics of septal peptidoglycan synthesis over 15 minutes were visualised using the virtual time-lapse technique. Mid exponential cultures were consecutively labelled with HADA, NADA and TADA for 5 minutes and imaged using both conventional deconvolution microscopy and SIM (Figure 5.5 & Figure 5.6). To eliminate any probe-mediated effects the experiment was carried out with the FDAAs in different orders, the observed pattern remained consistent. Within cells that were producing a septum during the course of the virtual time-lapse, there appears to be a “rainbow-effect” of FDAA labelling with the first label (coloured blue) on the outer rim of the labelled septum and the final label (coloured red) at the leading edge (Figure 5.5 A). This would seem to suggest overlap of synthesis and a zone of synthesis, consistent with my previous work (Chapter 4.2.2).

Within the population the amount of dye overlap can vary from none to almost complete where it is almost impossible to distinguish differences between the three dyes at available resolutions. Often this occurs since the orientation of cells masks synthesis patterns however, when this is not the case the overlap occurs in an apparent ring, consistent with piecrust synthesis (Figure 5.5 A, highlighted cells). This suggests that individual cells may synthesize the septum at different rates. Within the SIM images, each label appears more distinct than within the deconvolved images yet, areas of overlap are still visible between consecutive labels (Figure 5.5 B, highlighted cells(a)). When images from all three channels are merged it often appears as if each label produces a discrete ring of peptidoglycan synthesis (Figure 5.5 B, highlighted cells (b)), however when individual channels are analysed it is seen that while most labelling occurs at the leading edge to produce the new septum, there is a lesser amount of synthesis labelled within the previously synthesised portion of the septum (Figure 5.6 B, highlighted cell). In all cases the septum is synthesised processively from the outer edge to centre of the septum, suggesting that synthesis occurs as a single process of synthesis and thickening to correct thickness as opposed to an initial synthesis of the septum and subsequent thickening. On the few occasions where a later dye is seen outside of previous events it is almost exclusively in the pattern seen in Figure 5.6 A

A



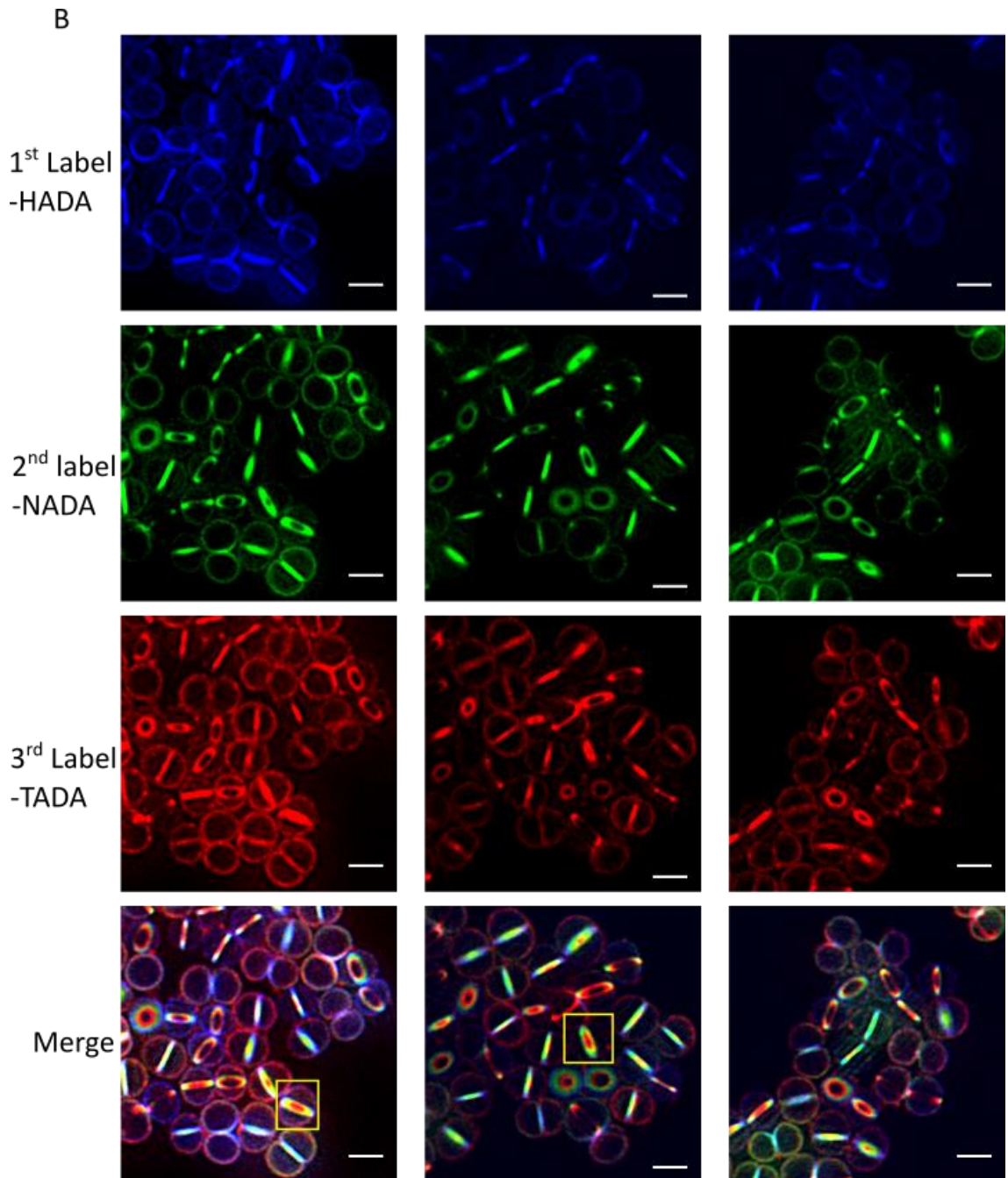
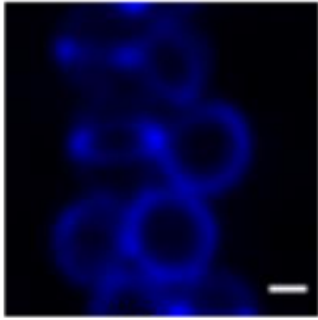


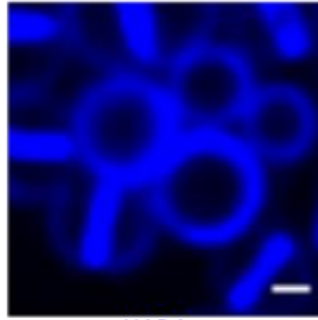
Figure 5.5. Septal dynamics by virtual time-lapse. Dynamics labelled via consecutive incubation with 3 different FDAAs in the following order; HADA, NADA & TADA (all at 5 mM). Samples were imaged by OMX widefield microscopy with images deconvolved by Softworx (A) or in structured illumination mode (B). Septa are produced via sequential peptidoglycan synthesis from the outer edge to the centre & off-septal synthesis continues throughout cell cycle. (Scale bar 1 μ m, average intensity projection).

A

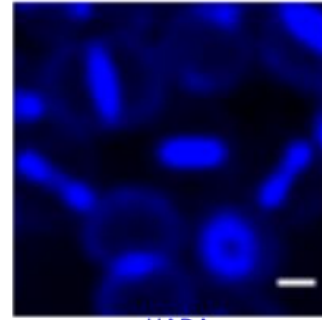
1st Label



HADA

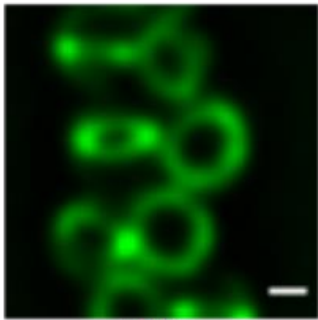


HADA

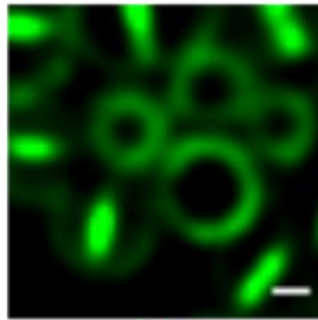


HADA

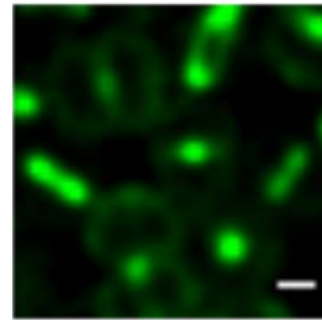
2nd label



TADA

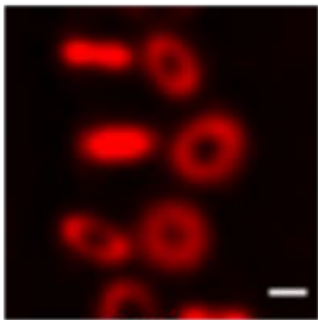


TADA

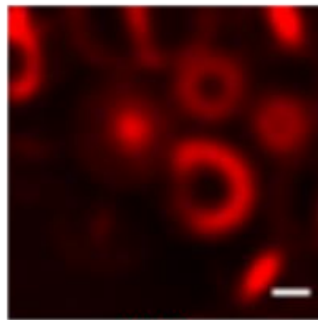


NADA

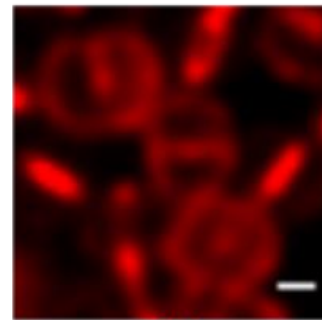
3rd Label



NADA

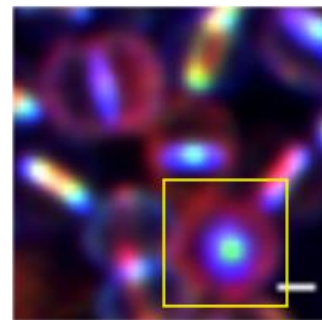
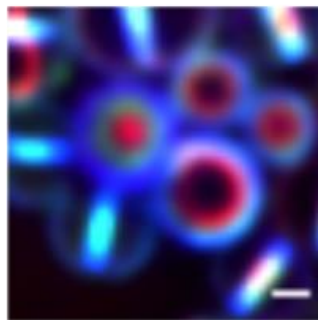
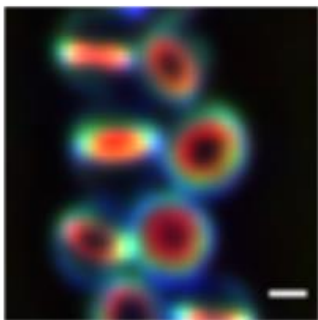


NADA



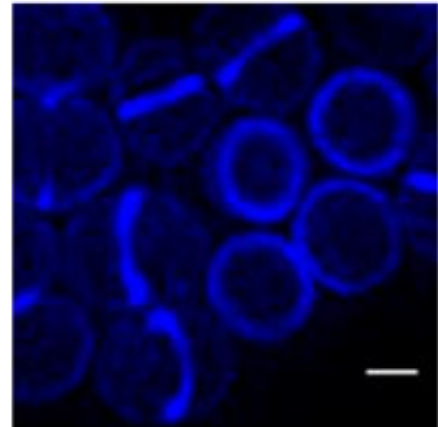
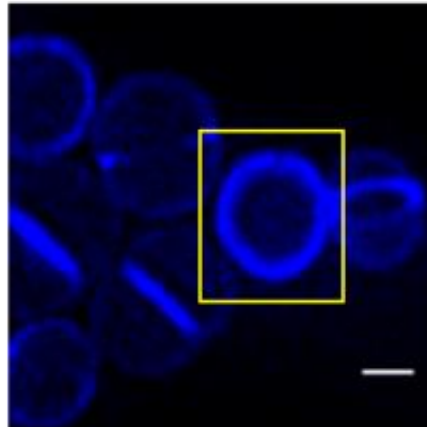
TADA

Merge

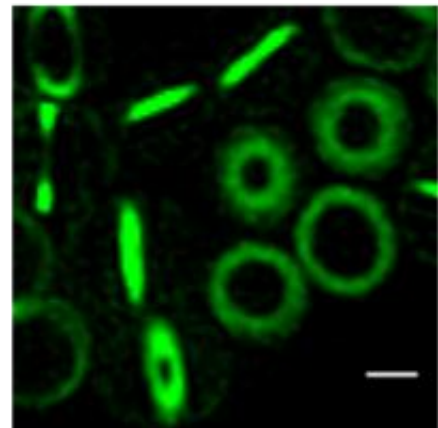
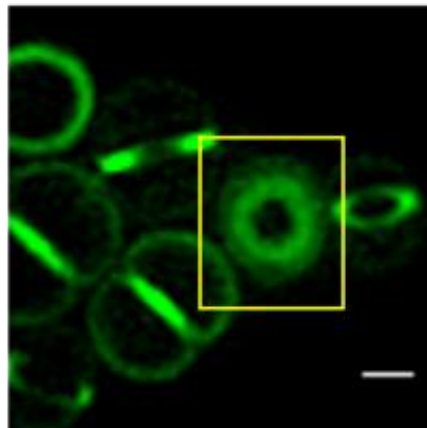


B

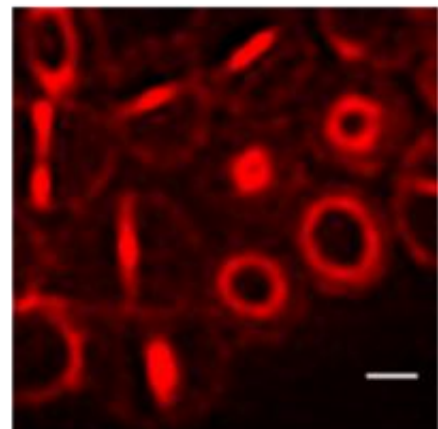
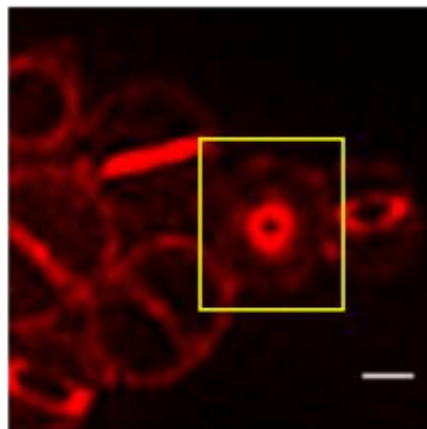
1st Label
-HADA



2nd label
-NADA



3rd Label
-TADA



Merge

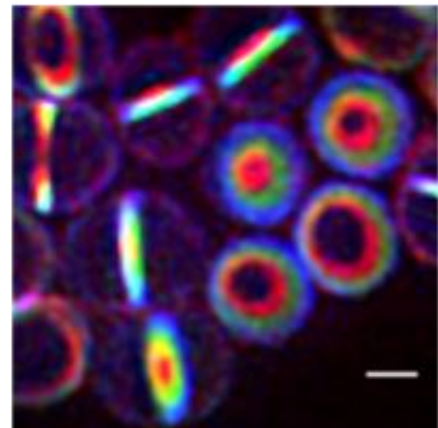
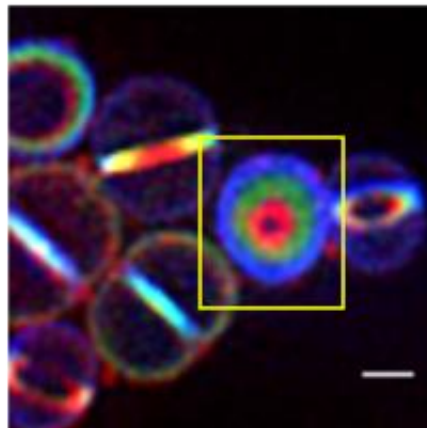


Figure 5.6. Features of dynamics in septal formation. Cells labelled consecutively with three FDAAs in 5 minute periods as in Figure 5.5 enlarged to highlight labelling pattern. (A) OMX widefield images that have been deconvolved using Softworx. Order of FDAAs used indicates below each image, false colour is consistent with order of label rather than label used. (B) SIM images, Samples labelled in order HADA, NADA, TADA. (Scale bar 0.5 μm , average intensity projection).

(highlighted cell). In this case the septum has been completed during labelling with the second FDAA as can be seen by the dot of green labelling of the cell with the septum parallel to the imaging plane. In this case cells are believed to have just split or begun the process of splitting and labelling with the third FDAA due to off-septal synthesis. In a number of cases off-septal synthesis appears to be almost non-existent. However, this could be a limitation of the microscopy technique used for both the deconvolution and SIM cannot adjust for large variations in signal intensity, therefore low intensity light can be lost, such as the signal from off-septal synthesis. Where off-septal labelling is visible, all 3 labels are generally present, regardless of the stage of the cell, suggesting that off-septal synthesis occurs throughout the cell cycle. Due to the limitations of the microscopy techniques used and since the FDAAs are not normalised, quantification of labelling is not possible. However, it is tempting to speculate that the amount of off-septal synthesis is at a consistent level throughout the cell cycle.

5.2.3 Inheritance of peptidoglycan over several generations

Peptidoglycan synthesis at the septum with division in 3 orthogonal planes in *S. aureus* gives a theoretical model of the cell wall of *S. aureus* being sectorised due to age (Turner et al., 2010a). In spite of the presence of synthesis away from the septum the amount of new synthesis at the septum suggests that the cell wall will be sectorised in the manner previously proposed (Figure 5.2). In order to visualise the sectoring cultures were grown in 3 consecutive FDAAs for a generation time, in the case of *S. aureus*, 30 minutes (Figure 5.7). Cells that are dividing can be seen to show a sectoring phenomenon, where the peripheral cell wall is sectorised with the first and second labels, the second showing where the cell has just divided, and the third label marking the septum being synthesised at the point the sample was fixed (Figure 5.8). Since *S. aureus* cannot be made synchronous each cell is in a slightly different phase of the cell cycle when labelling starts, therefore cells with optimal sectoring labelling have been selected to examine the phenomenon (Figure 5.8 B). To highlight peptidoglycan sectoring a pair of sister cell displaying optimal sectoring have had labelling pattern mapped to a schematic of cell division (Figure 5.8 C). A single *S. aureus* cell divided during the first labelling process to produce daughter cells with the new hemisphere labelled. During the second labelling process one of the daughter cells divided again on

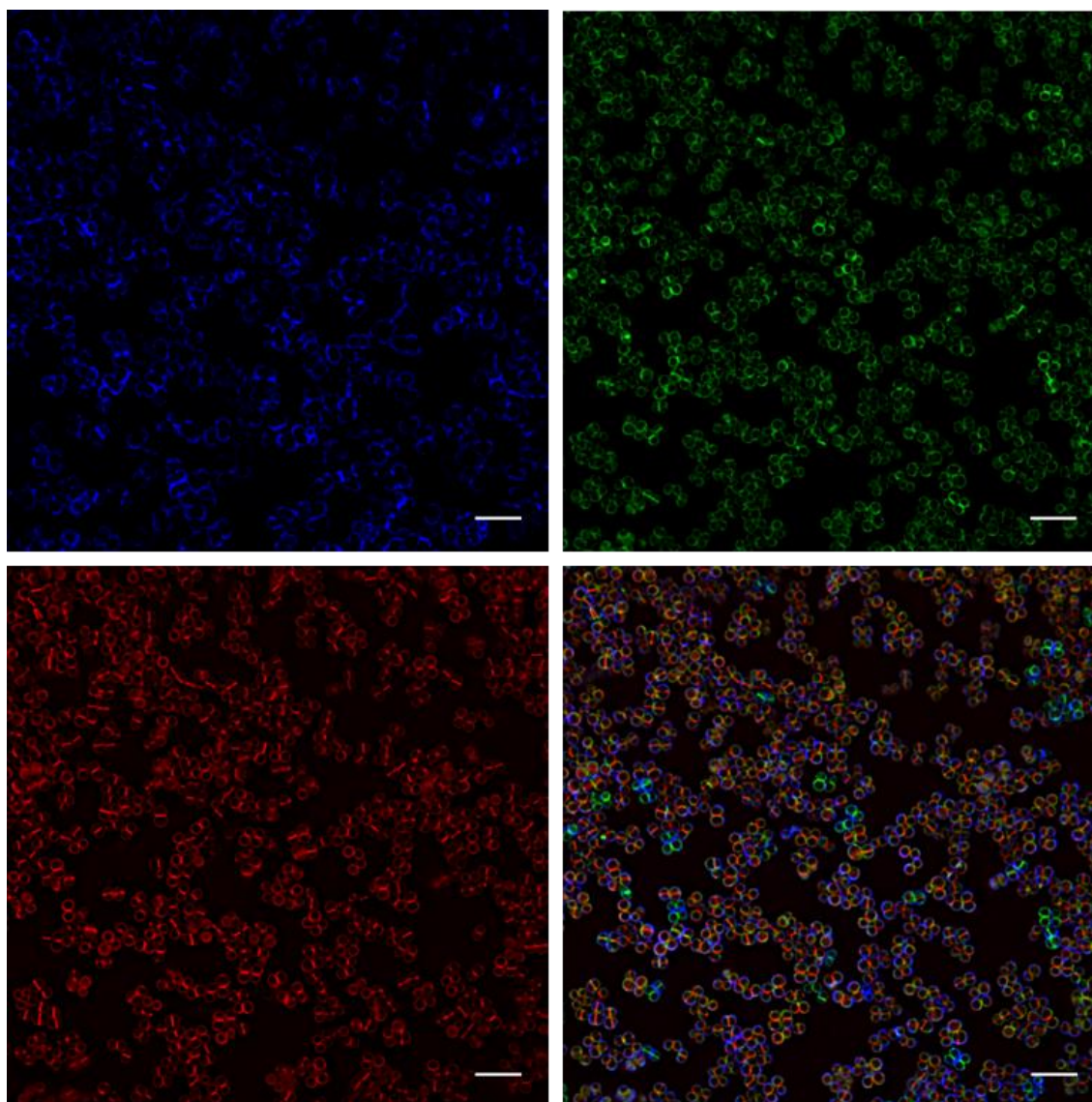
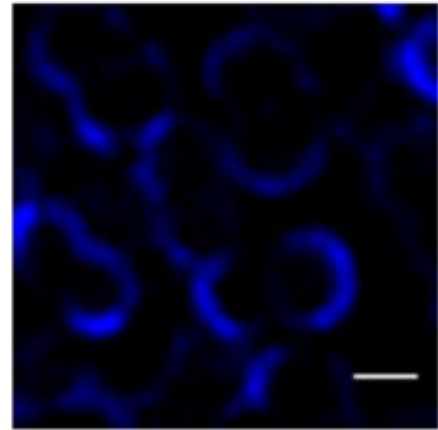
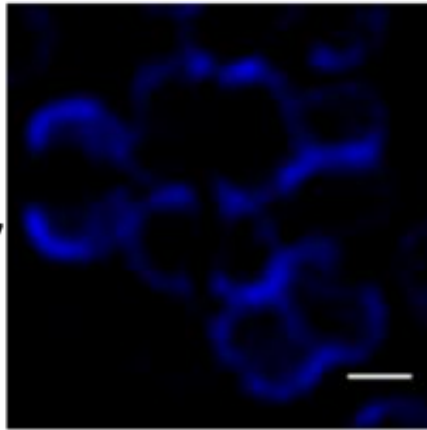


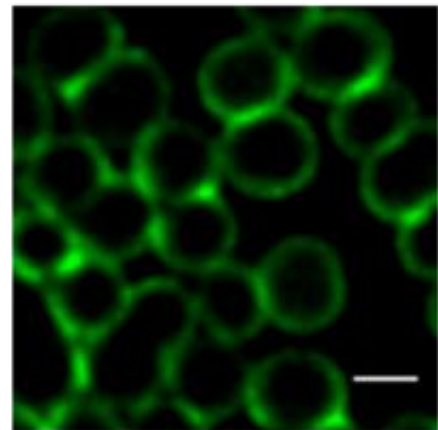
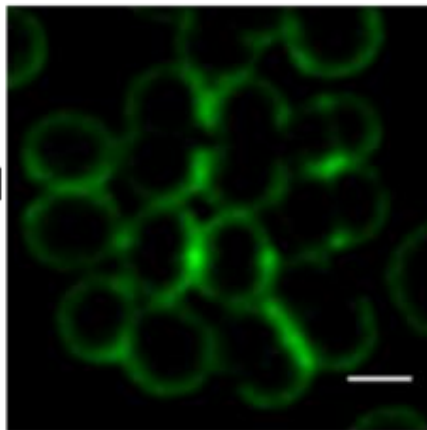
Figure 5.7. Fields of cells labelled consecutively with ADA-647 (blue), NADA (green) and HADA (red) for 30 minutes each (All at 500 μ M).

A

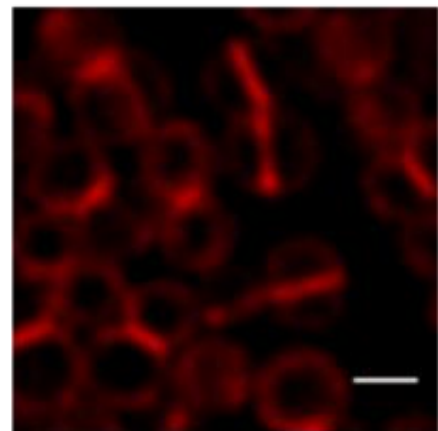
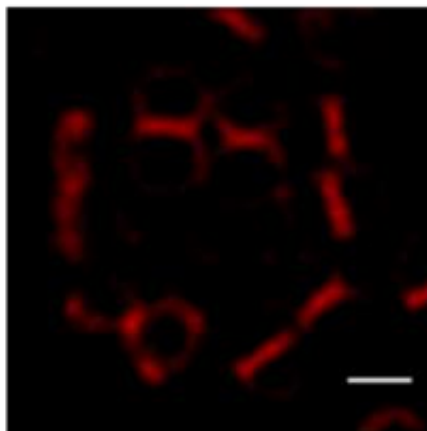
1st Label
- ADA-647



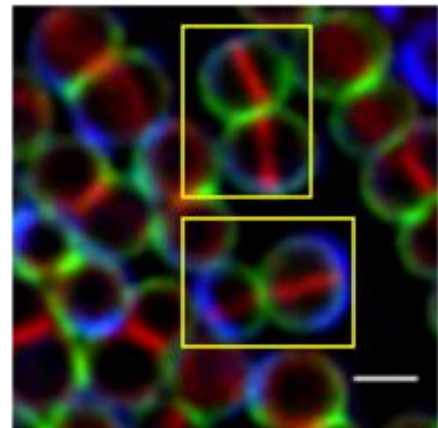
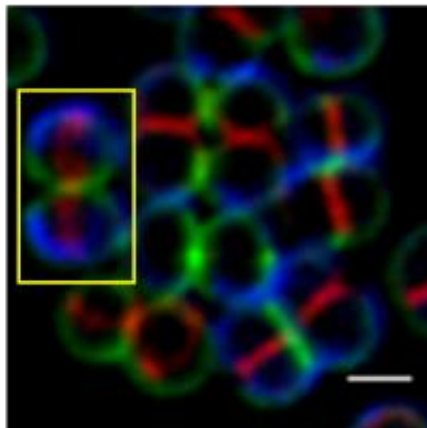
2nd label
-HADA



3rd Label
-NADA

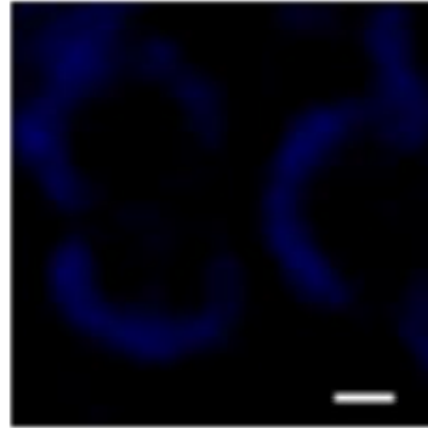
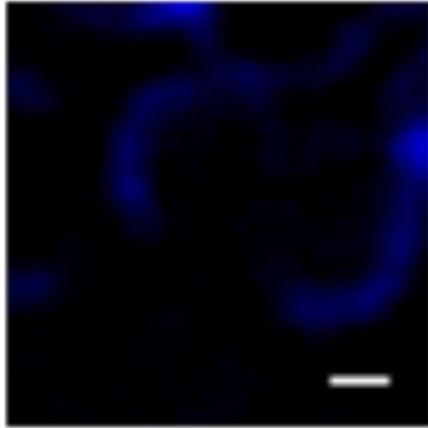


Merge

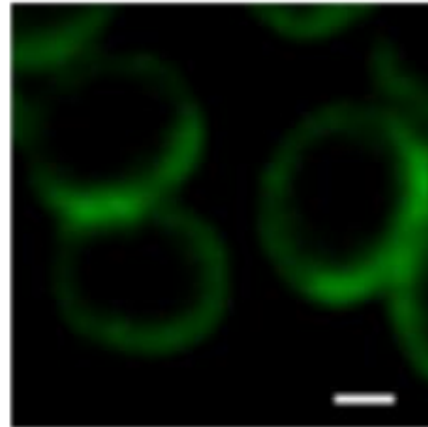
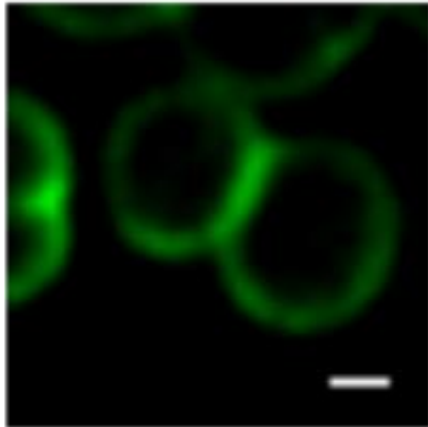


B

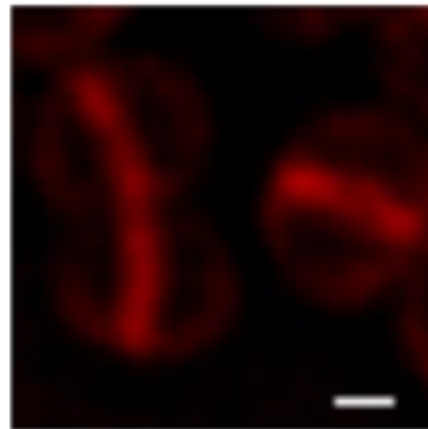
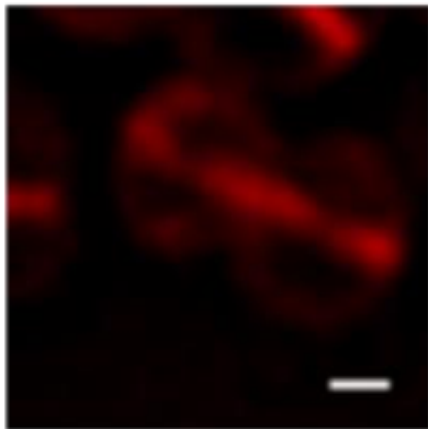
1st Label
- ADA-647



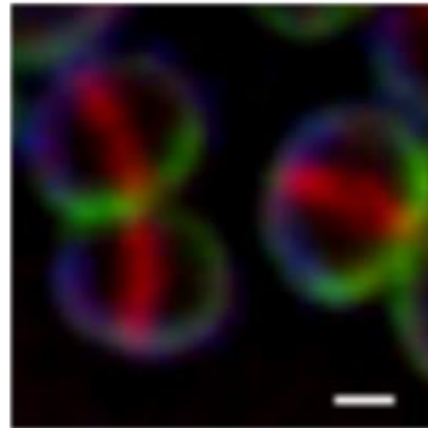
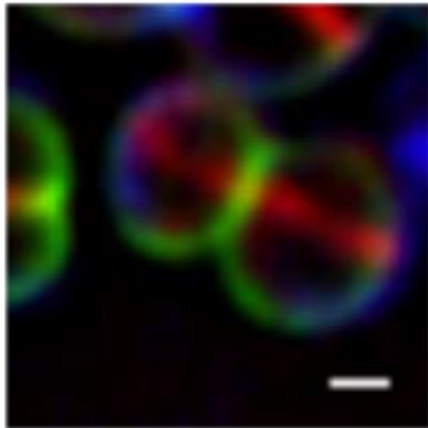
2nd label
- HADA



3rd Label
- NADA



Merge



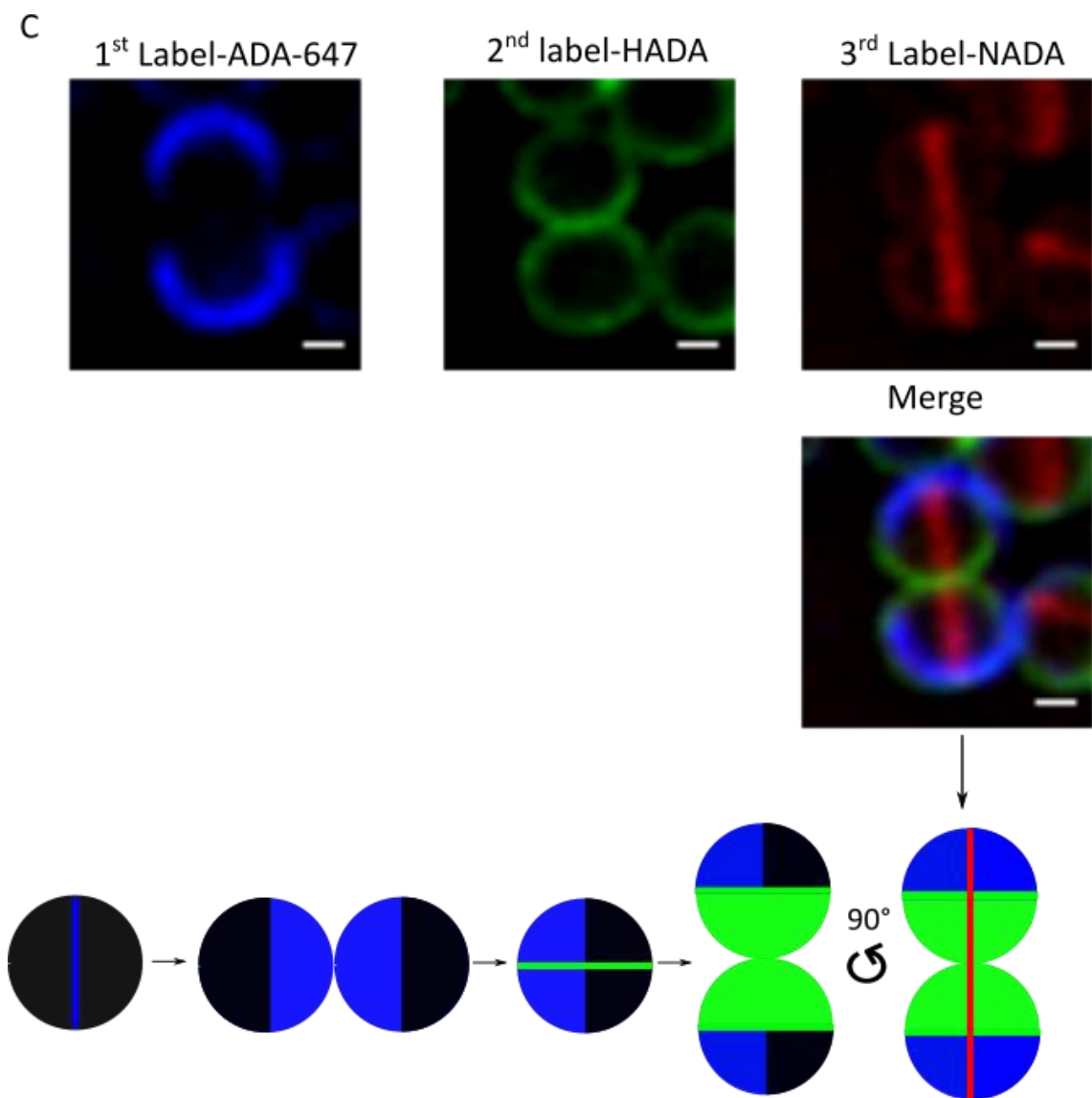


Figure 5.8. Inheritance of peptidoglycan over 3 generations. *S. aureus* cells labelled sequentially by FDAAs for a single generation time each (30 minute) and imaged using DeltaVision deconvolution microscopy and images deconvolved by SoftWoRx. (A) Selections of cells showing characteristic sectoring of peptidoglycan cell wall (Scale bar 1 μm , average intensity projection). (B) Cells enlarged to highlight labelling of sectors (Scale bar 0.5 μm , average intensity projection). (C) Representative cell of optimal peptidoglycan sectoring by age (Scale bar 0.5 μm , average intensity projection) and schematic of events within cell division to produce labelling seen. Schematic represents the external cell wall of *S. aureus* while images are an average projection of slices from around the focal plane. Final schematic is the representative cells rotated 90° to best match the merge image shown.

the orthogonal plane to produce two cells with one hemisphere labelled with the 2nd FDAA and during this process bisecting the old hemisphere such that the sister cells inherited a quarter cell wall labelled with the first FDAA. These sister cells synthesized a new septum on the third orthogonal plane during the third labelling period. However, they did not split prior to the end of the experiment. The final image in the schematic is rotated 90° to best match image and to make visualisation of the final division septum easier. 3D projections of cells that show sectoring (Figure 5.9) indicate the presence of FDAAs on the surface of the cell. The first FDAA used (labelled blue) can be seen to cover approximately one quarter of the total cell wall. This can also be visualised in Movies 1 & 2 (Enclosed CD; Appendix III).

5.2.4 Dynamics reveals heterogeneity in peptidoglycan synthesis

Within a population of *S. aureus* each individual cell is at a slightly different stage of the cell division cycle. 3 labels are used during growth and the incorporation pattern and sectoring can be determined. However, a number of cells within the analysed populations have unexpected labelling suggesting that heterogeneity exists within peptidoglycan synthesis dynamics (Figure 5.10 & Figure 5.11).

FDAA labelling of consecutive 5 minute windows suggests that the rate of peptidoglycan synthesis differs during the cell cycle as specific structures are made; piecrust and septal plate (Figure 5.5 & Figure 5.6). However, there are cells within the population that do not label with an FDAA during a labelling period (Figure 5.10 A). This pause in peptidoglycan synthesis may occur mid septation or just after completion of septation but due to the orientation of cells it is not possible to discern if septation is still in progress. Whilst there may still be some low level peptidoglycan synthesis occurring this is not at a detectable level. Given the proximity of cells with similar phenotypes to each other within an image it may suggest that these cells are related to one another. Therefore, it might be that there is an inherited signal that causes this pause in peptidoglycan synthesis.

Another means by which peptidoglycan synthesis heterogeneity has been identified is by differential labelling patterns in sister cells (Figure 5.10 B). Cells in both panels have completed septation during the first 5 minutes labelling with FDAAs and within sister

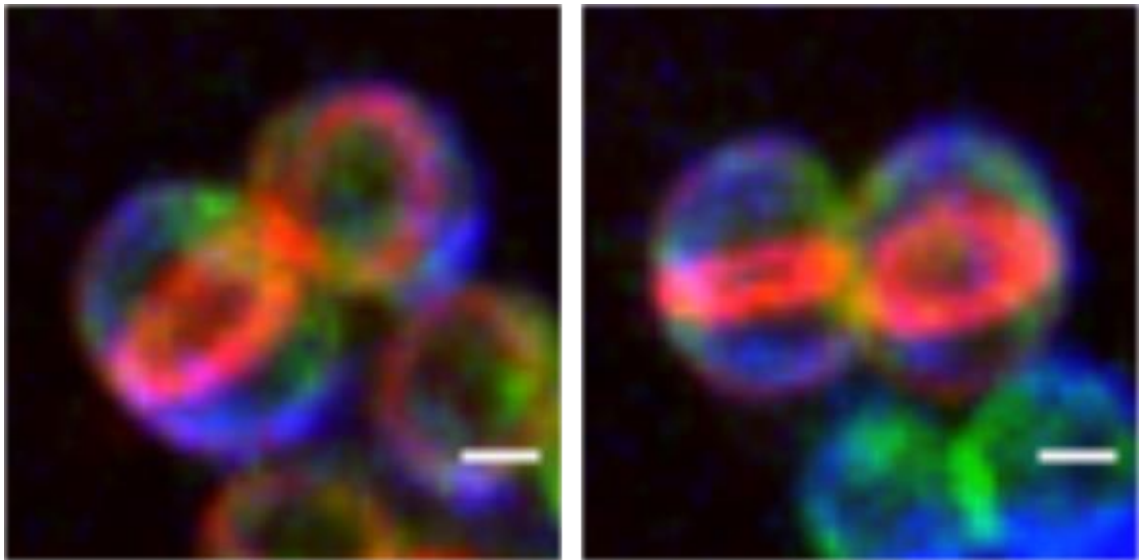
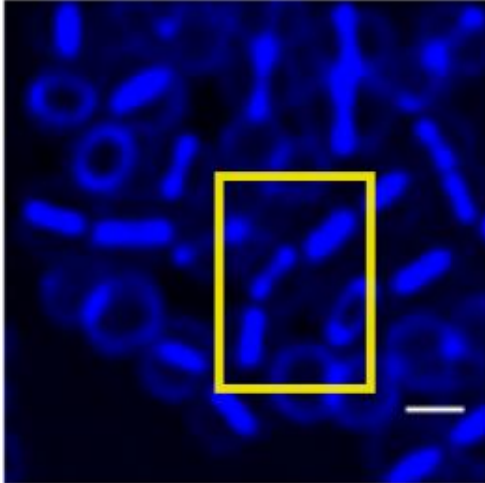


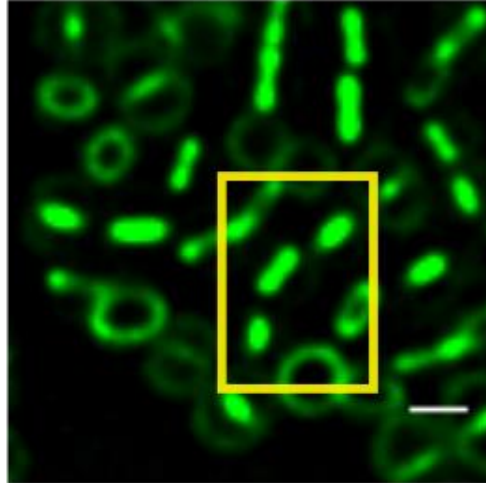
Figure 5.9. 3D Maximum intensity projections of cells labelled for consecutive 30 minute windows with ADA-647 (blue), NADA (green) & HADA (red) (all at 500 μ M).

A

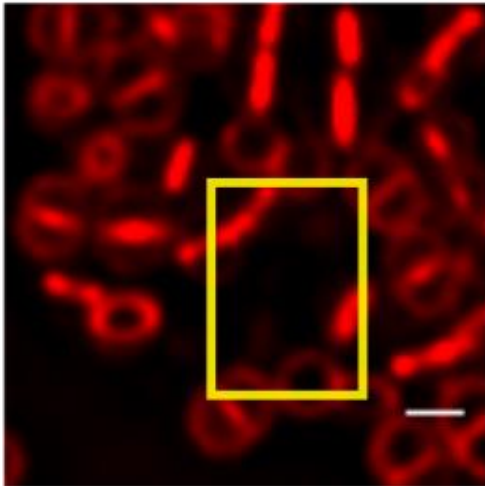
1st Label-HADA



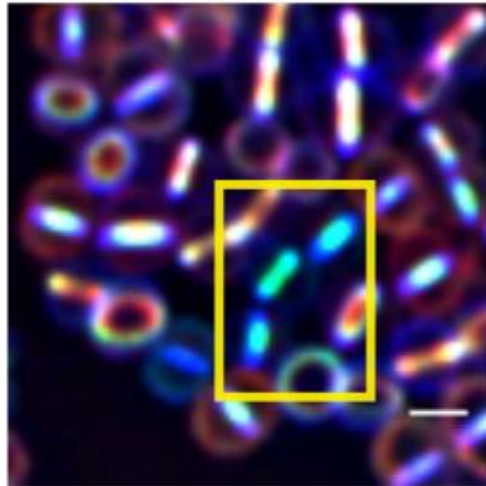
2nd label-NADA



3rd Label-TADA



Merge



B

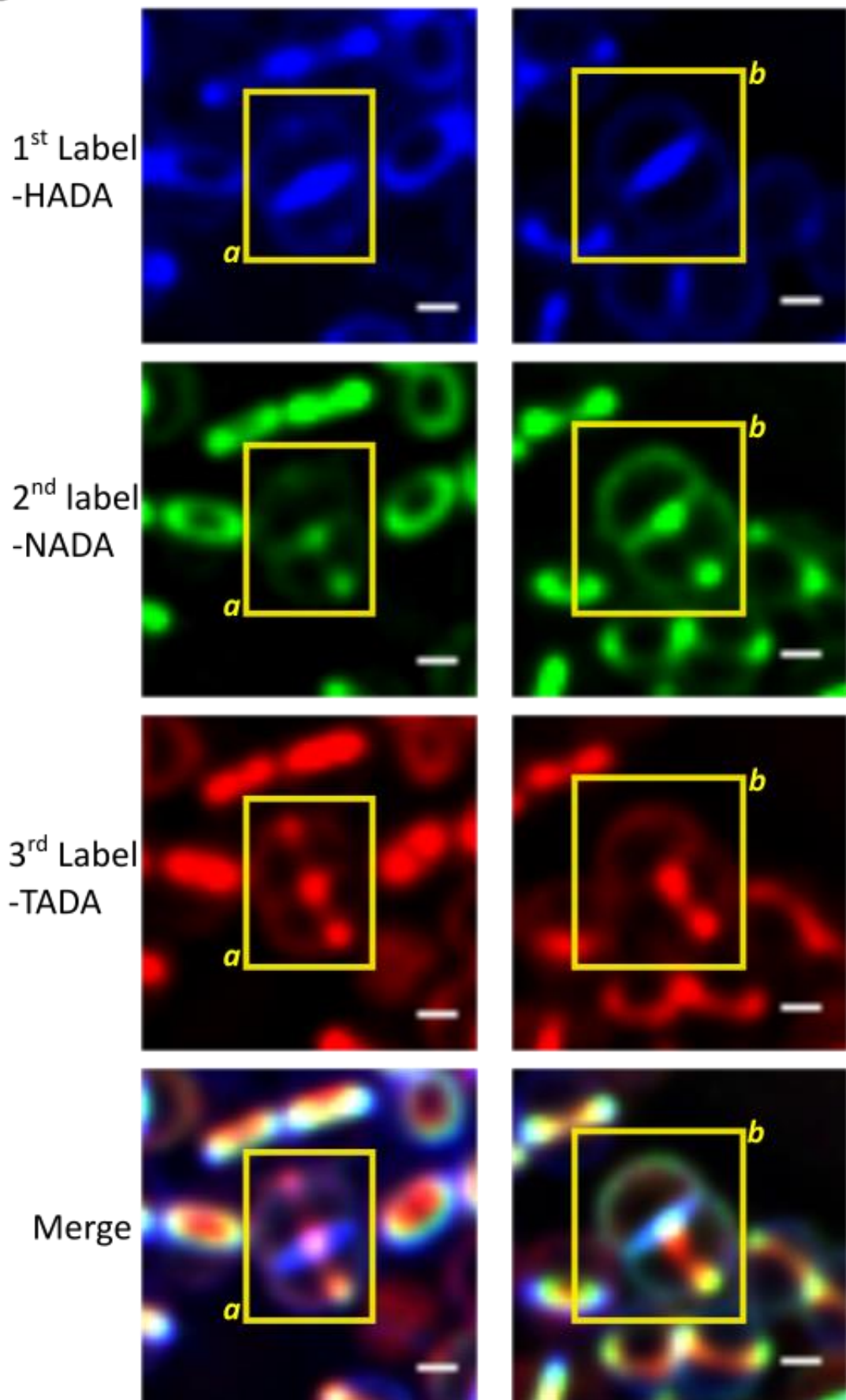
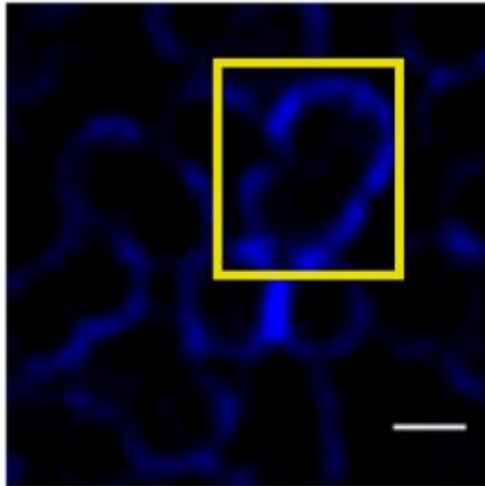


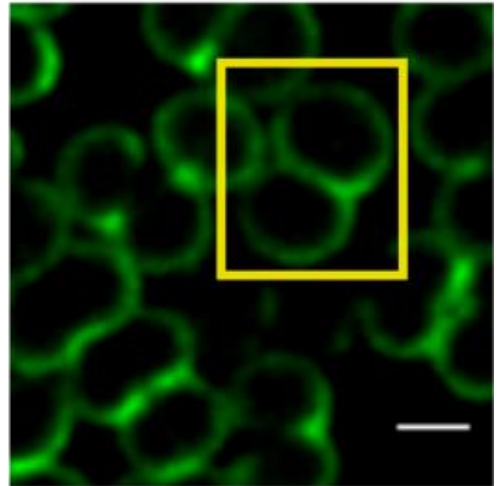
Figure 5.10. Heterogeneity in peptidoglycan synthesis during the cell cycle. Cells labelled sequentially with three FDAAs for 5 minutes each (5 mM). In all cases the first FDAA is coloured blue, second FDAA coloured green and third FDAA labelled red. (A) Cells not labelled with final FDAA, due to a pause in incorporation, suggesting heterogeneity in peptidoglycan synthesis during the cell cycle (Scale bar 1 μm , average intensity projection). (B) Apparent sister cells exhibit different patterns of FDAA incorporation suggesting heterogeneity in synthesis (Scale bar 0.5 μm , average intensity projection).

A

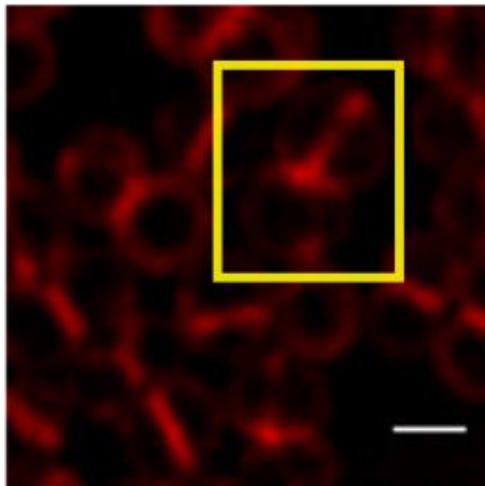
1st Label-ADA-647



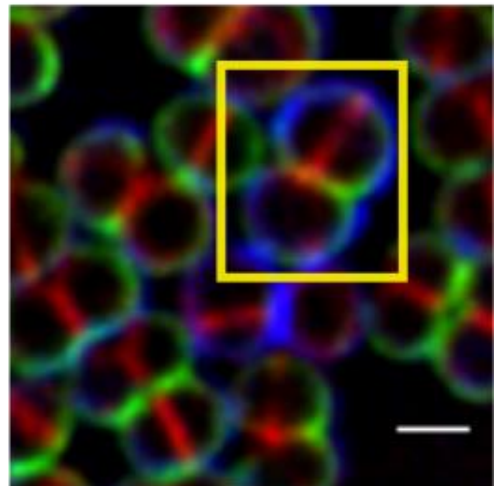
2nd label-HADA



3rd Label-NADA

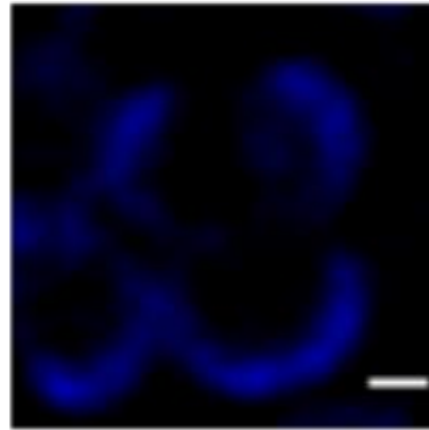
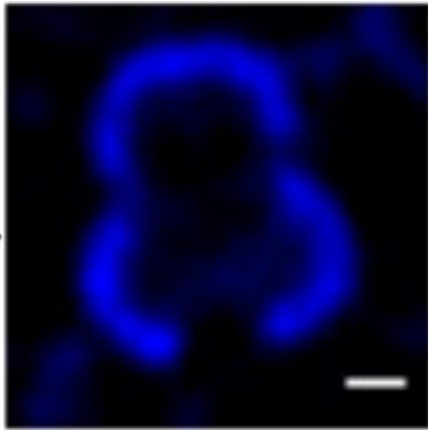


Merge

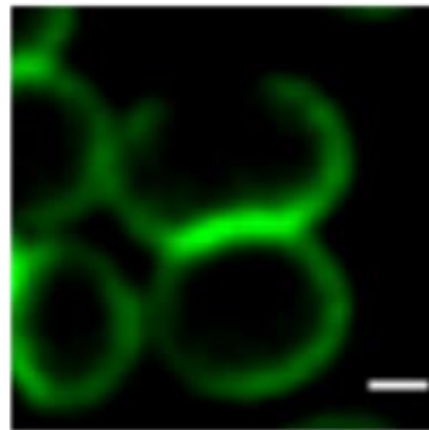
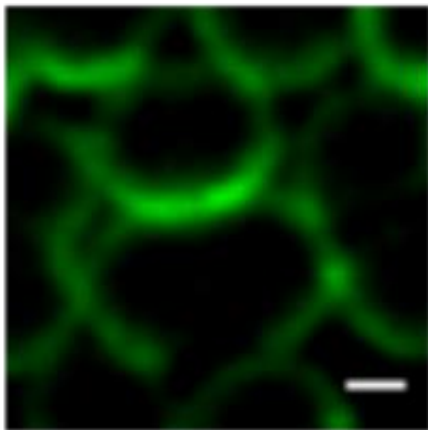


B

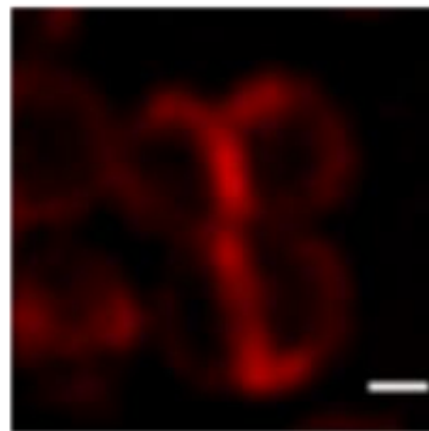
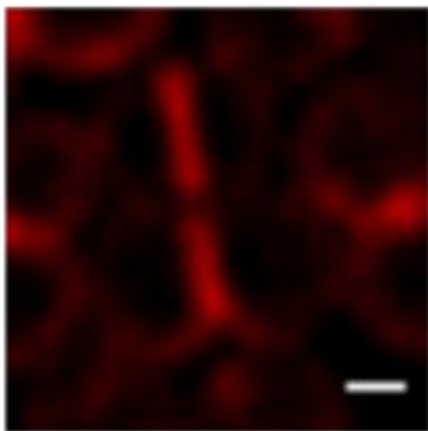
1st Label
-ADA-647



2nd label
-HADA



3rd Label
-NADA



Merge

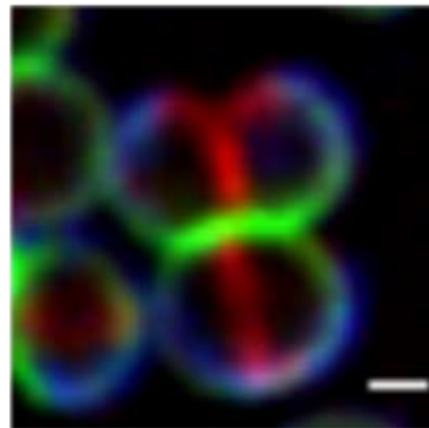
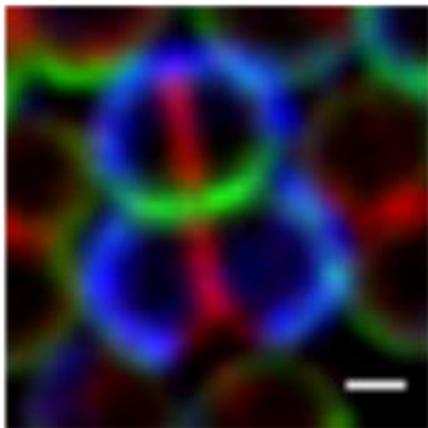


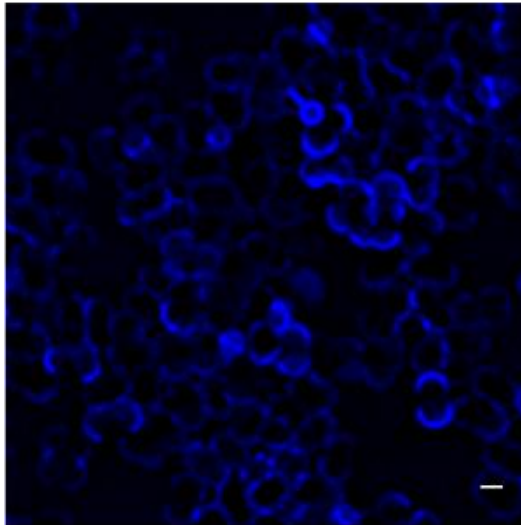
Figure 5.11. Heterogeneous peptidoglycan synthesis within sister cells. Sister cells labelled with 3 FDAA sequentially for 30 minutes exhibit different labelling patterns. In all cases the first FDAA is coloured blue, second FDAA coloured green and third FDAA labelled red (500 μ M). (A) Sister cells indicated by yellow box, one cell has a red septum while the other has not synthesised a septum during generation labelled by the third FDAA (Scale bar 1 μ m, average intensity projections). (B) Sister cells split at different times during labelling experiment. In each pair one sister cell has completed the next synthesis cycle and split while the other sister cell has not (Scale bar 0.5 μ m, average intensity projection).

cells the initiation of peptidoglycan synthesis of the septum in the orthogonal plane occurs at different times. In the cell marked (a) this is a delay of only approximately 5 minutes since initiation of septation in the second daughter cell is labelled by the third FDAA. However, in cell marked (b) septation is not initiated during the course of the experiment. What is important to note is that in both cases the sister cells have off-septal peptidoglycan synthesis throughout the labelling experiment i.e. labelled with all three FDAs. This suggests that there is not global arrest of incorporation but a specific delay in septation in a single daughter cell. Since these cells are in mid-exponential phase with no limitations on growth this delay is likely due to an intrinsic heterogeneity in the cell division progression. This effect is not limited to transient heterogeneity as in cells labelled for a full generation time (30 minutes) with each FDAA also displayed the same effect (Figure 5.11). In this case sister cells were not only identified with delayed septation in a single sister cell (Figure 5.11 A) but also where splitting of cells appears delayed in one sister cell (Figure 5.11 B), either due to a simple delay in separation or due to a delay in completion of the septum. This results in offspring from a single cell becoming asynchronous.

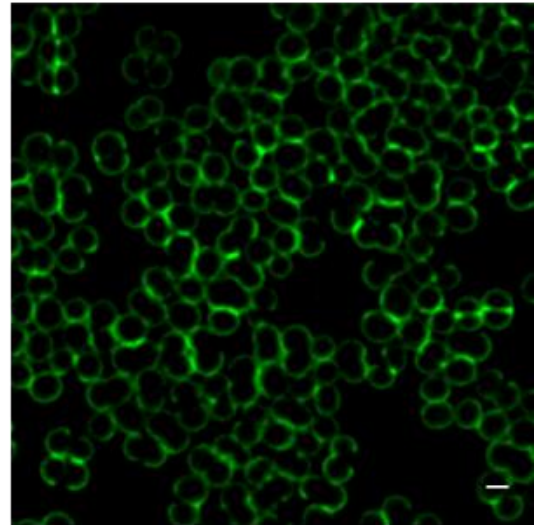
When analysing fields of cells labelled sequentially for 30 minutes with 3 FDAs it is clear that a large number of different labelling patterns are present across the population (Figure 5.12). While many of these patterns are attributable to cells at different stages of cell division at the beginning of the labelling process a subset of cells is seen to completely lack labelling with one or more FDAs. The labelling pattern of cells was analysed and features of peptidoglycan synthesis across a population were revealed (Table 5.1). Of cells analysed 86% were labelled with all 3 FDAs in a pattern compatible with dynamics of peptidoglycan synthesis discussed earlier (Chapter 5.2.3). 0.5 % of counted cells were found to have no labelling whatsoever, these were presumed to be dead, un-lysed cells, a live/dead counterstain would prove this however a reliable one compatible with the FDAs used was not available. A further 13.5% of cells were missing apparent labelling for at least one of the labels used (Figure 5.13 A). In the case when the missing labels were that of the last label, this could be attributed to the death or entrance into a stationary phase state, however within the population some cells were missing either the first or second labels,

A

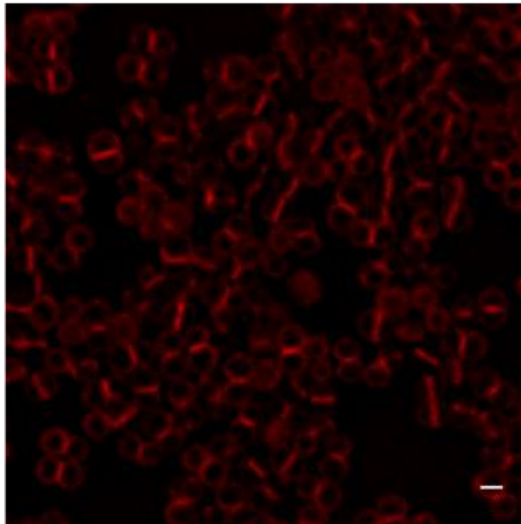
1st Label - ADA-647



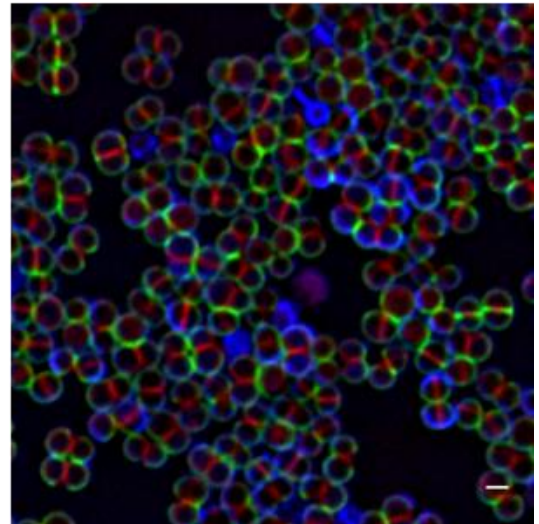
2nd label - HADA



3rd Label - NADA



Merge



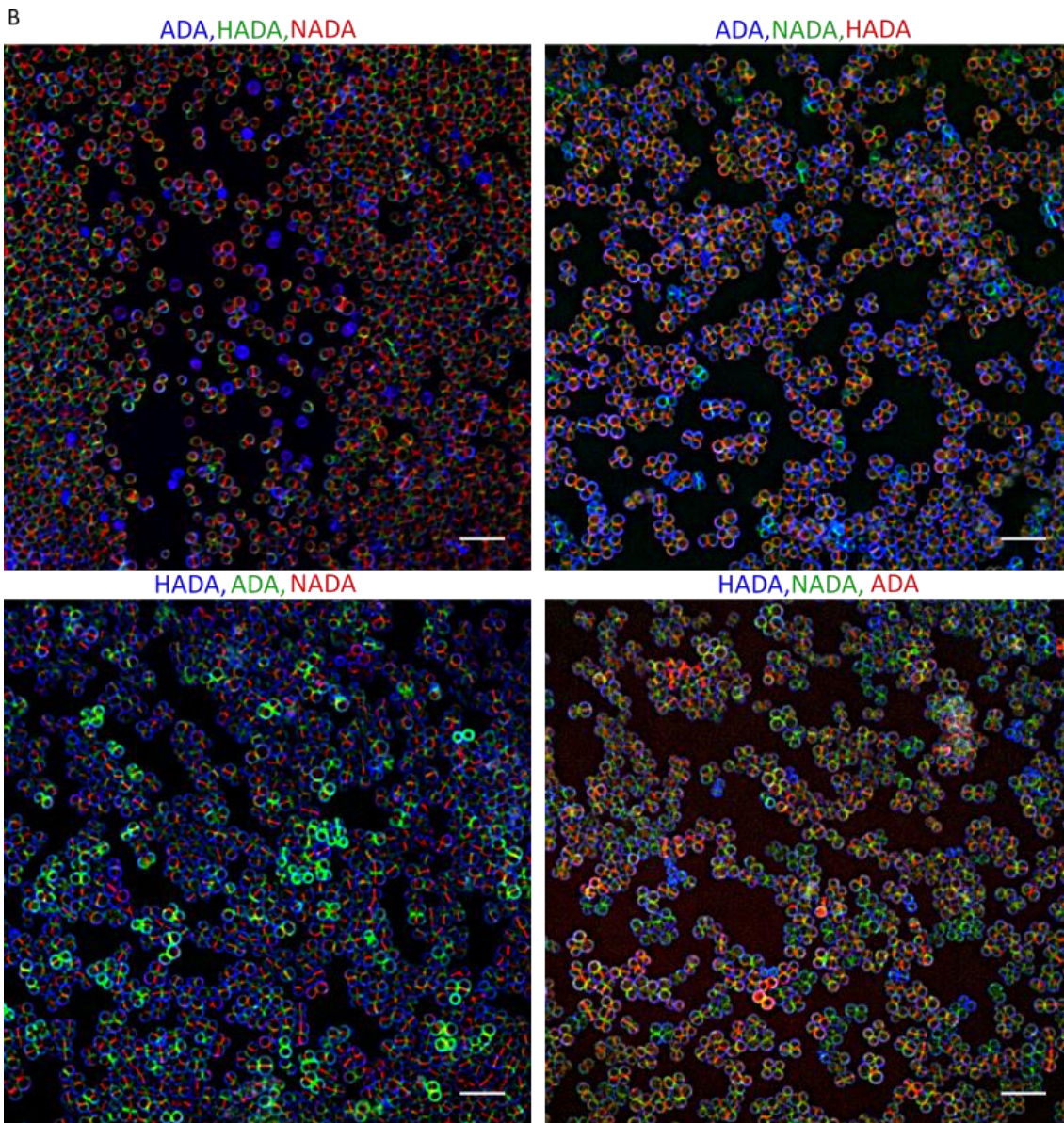
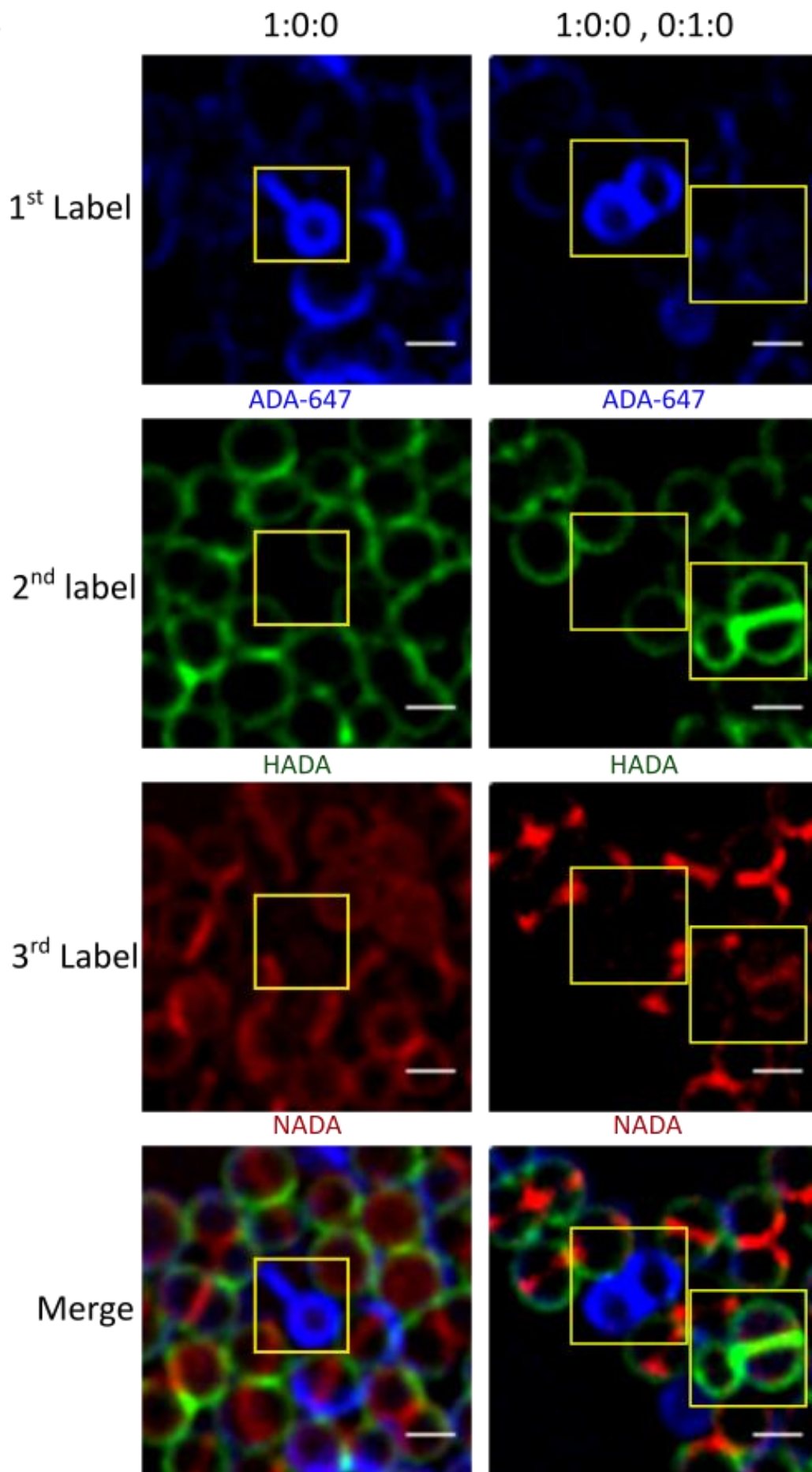


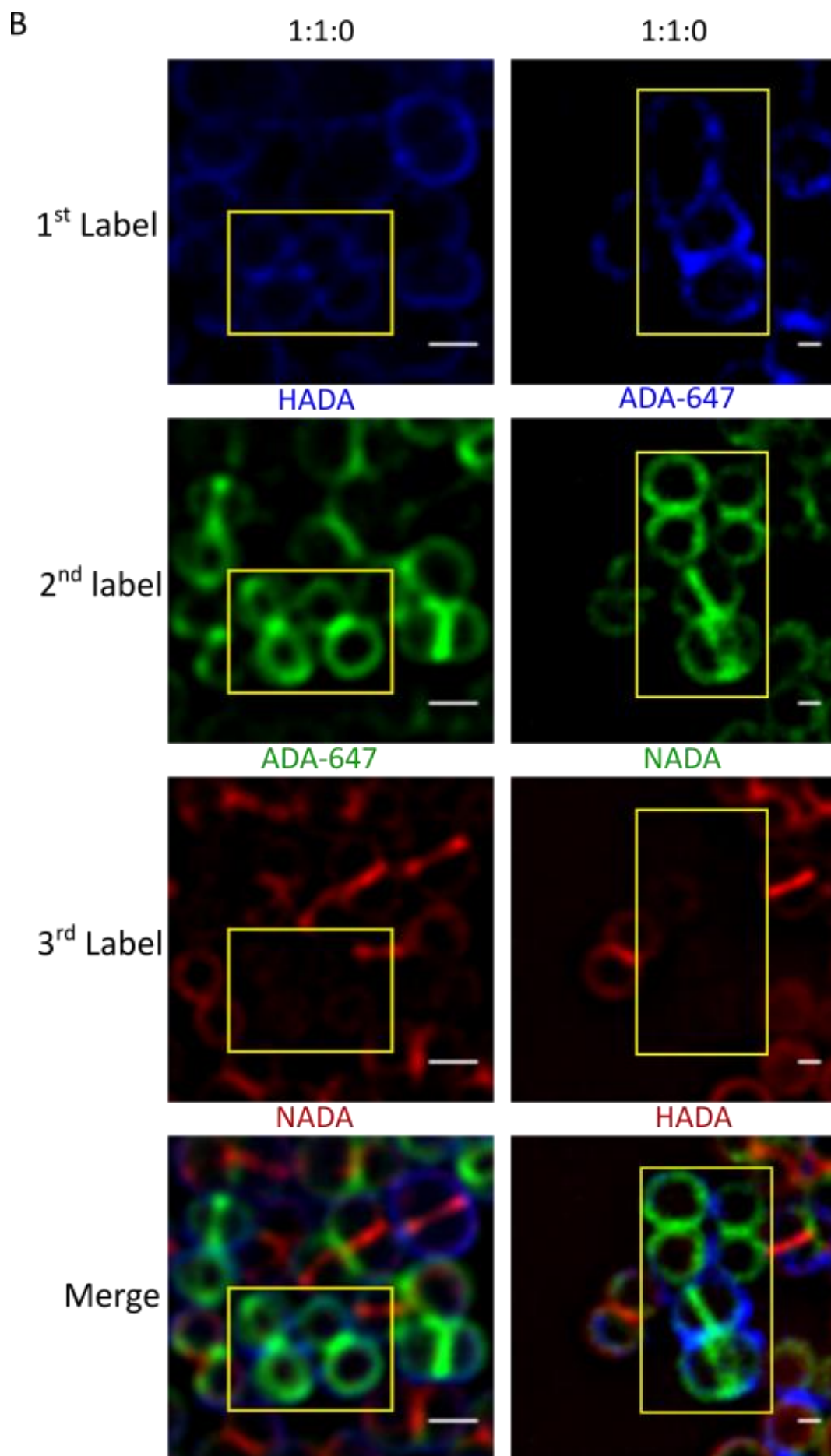
Figure 5.12 Dynamics of peptidoglycan synthesis reveals heterogeneity across a *S. aureus* population. In a population of cells labelled sequentially with 3 FDAA for 30 minutes each a number of different labelling patterns are seen across the population, in particular a subset of cells lacks labelling with one or more FDAA. (A) Field of cells highlighting different labelling patterns across the population. (Scale bar 1 μm). (B) Fields of cells for each of the FDAA labelling orders used, order of FDAA labelling did not affect frequency of labelling patterns. (Scale bar, 5 μm).

Labelling Pattern	Percentage of total cells (n=11,604)
ON → ON→ON	86.0%
OFF→OFF→OFF	0.5%
On (single colour) <ul style="list-style-type: none"> • ON→OFF→OFF • OFF→ON→OFF • OFF→OFF→ON 	1.9% <ul style="list-style-type: none"> • 1.7% • 0.1% • 0.1%
ON (Dual Colour) <ul style="list-style-type: none"> • ON→ON→OFF • OFF→ON→ON • ON→OFF→ON (oscillators) 	11.6% <ul style="list-style-type: none"> • 6.9% • 2.9% • 1.7%

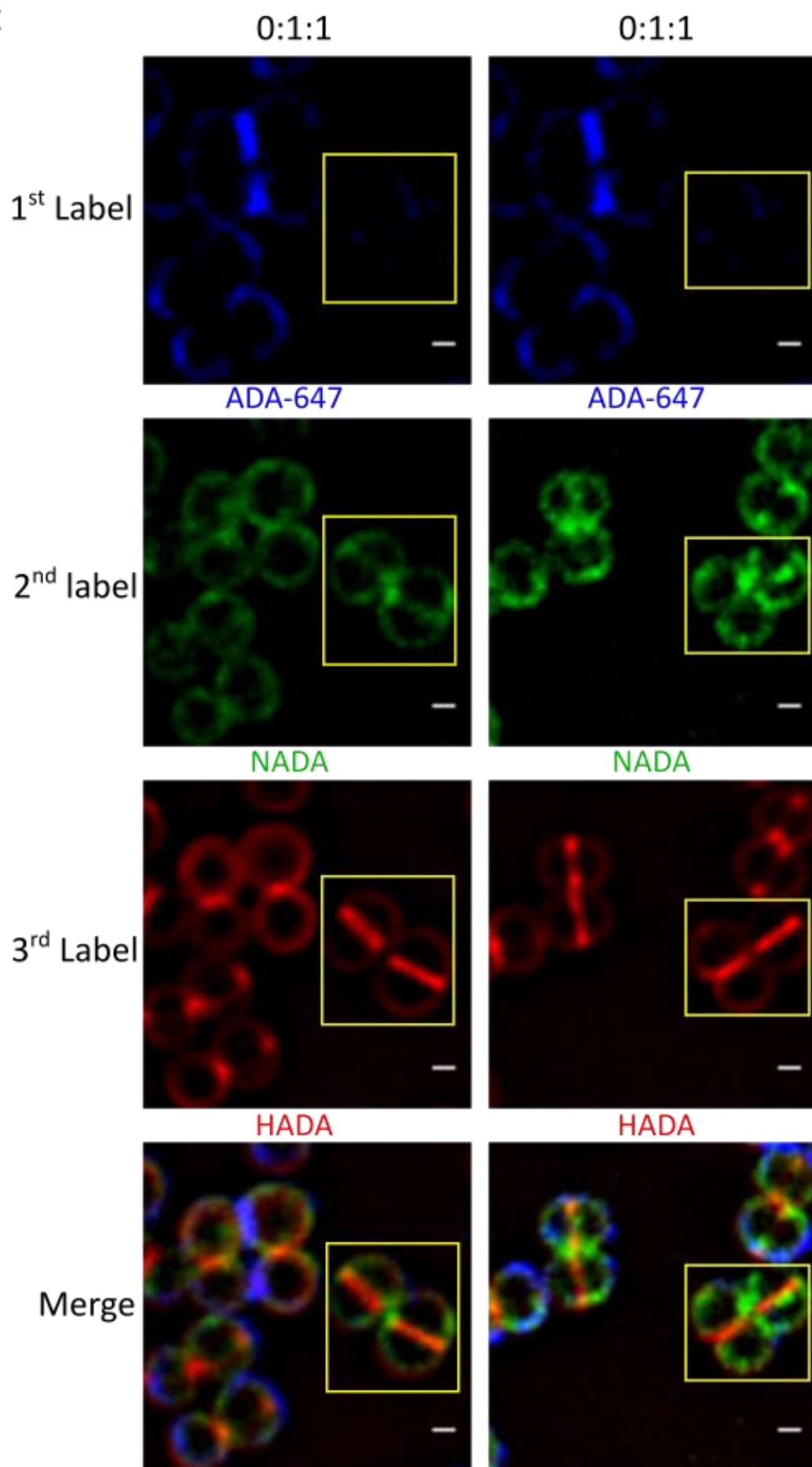
Table 5.1. Distribution of FDAA incorporation over 3 generations in *Staphylococcus aureus*.

A





C



D

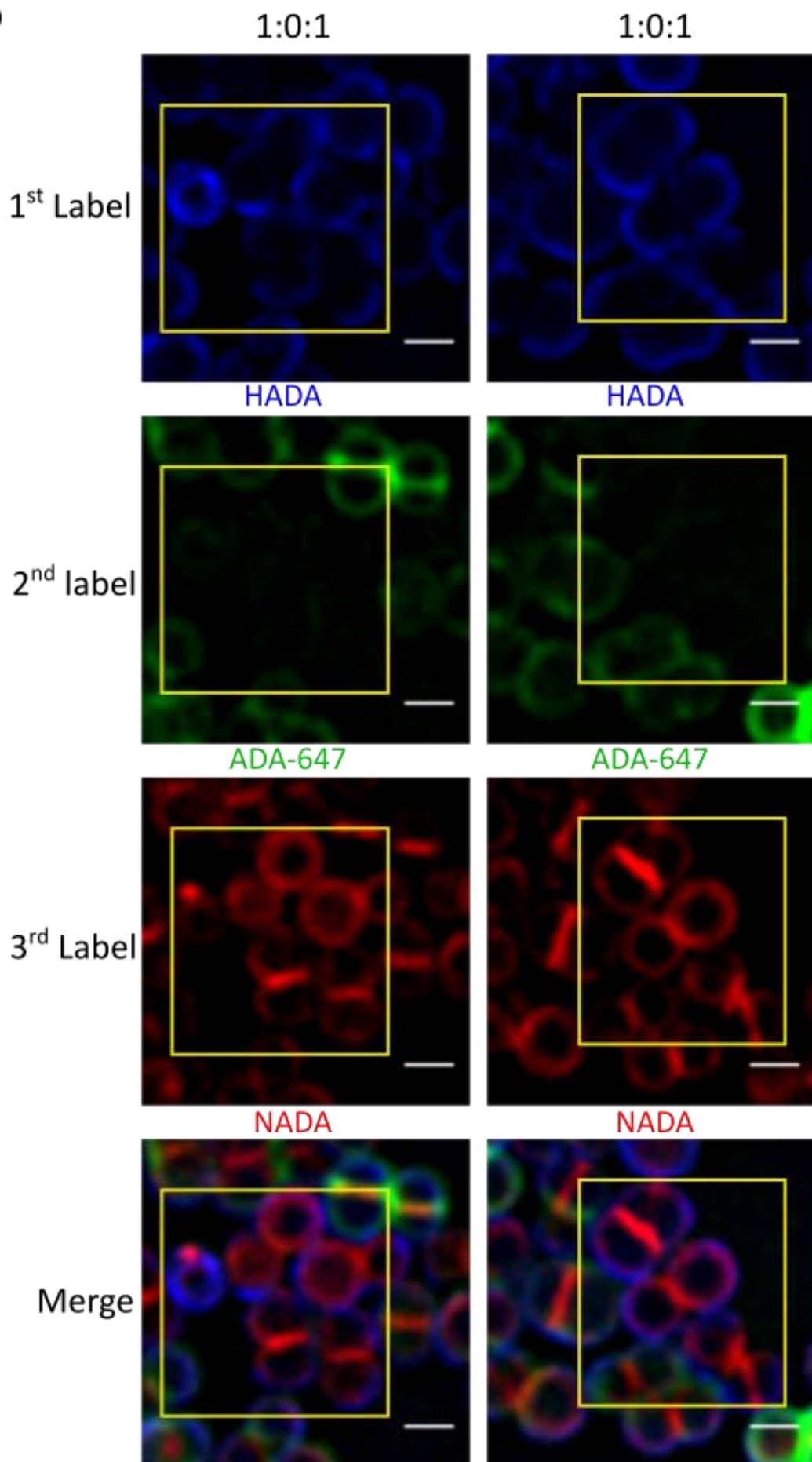


Figure 5.13 Population heterogeneity in peptidoglycan incorporation. Cells labelled sequentially with 3 FDAAs for a generation time each display population heterogeneity. (A) Cells labelled by a single FDAAs (Scale bar 1 μm). (B) & (C) Cells labelled with 2 consecutive FDAAs but not the third (Scale bar 500 nm). (D) Cells labelled with the 1st and 3rd FDAAs but not the 2nd (Scale bar 1 μm).

suggesting that growth (& therefore synthesis of peptidoglycan) restarted from a temporary state of arrest. A feature of this missing labelling is that it isn't only septal labelling that is missing but also off-septal labelling, suggesting a global arrest of peptidoglycan synthesis. Of particular interest are the 1.7% of counted cells which during the course of the experiment were actively incorporating for the first and third labels but not during the 30 minutes of growth with the second label (Table 5.1, final row). These are particularly useful as the pattern of peptidoglycan synthesis before and after pause in synthesis can be visualised (Figure 5.13 D). Peptidoglycan synthesis within these so-called "oscillators" shows no apparent gap in the labelling process despite a lack of labelling with the second FDAA. This suggests that growth is arrested within these individual cells as opposed to the phenomenon being due to the FDAAs or microscopy technique. The experiment was carried out with all permutations of FDAA labelling (Figure 5.12 B; Appendix V), further suggesting that this is not due to the labelling technique but a characteristic of *S. aureus* growth. Thus with an apparently exponentially growing population there are cells that have stopped growing but with the potential to restart.

5.3 Discussion

5.3.1 Septation dynamics

In *S. aureus* septation progression has been followed by transmission electron microscopy (TEM) and atomic force microscopy (AFM) (Matias and Beveridge, 2007; Touhami et al., 2004). Onset of septation occurs when visible growth of wall material was seen protruding into the cytoplasm at the mid-cell by TEM (Touhami et al., 2004). The septum then continues inward growth until it meets in the middle. The movement of the septation process has been described like the closing of a camera aperture (Touhami et al., 2004). Sequential labelling experiments carried out within this chapter have revealed that this is indeed the case with later peptidoglycan synthesis occurring within the ring of older synthesised peptidoglycan. Following completion of the septa, and splitting of cells, daughter cells remain mostly joined with surface features of cell splitting apparent (Touhami et al., 2004).

Previous single colour STORM imaging of the septation process suggested that synthesis does not occur solely at the leading edge of the septum but as a zone across the septum (Chapter 4). SIM images of consecutive 5 minutes labelling with FDAAs show clear concentric rings of FDAA incorporation. While the majority of incorporation occurs at the leading edge forming these concentric rings there is also insertion of peptidoglycan into the existing septal material. In SIM images there appears to be greater contrast between the leading edge and the existing septum incorporation. However, this may be influenced by artefacts from SIM. The consistency between labelling experiments and imaging techniques suggests that the previously described model of a zone of synthesis is compatible with the dynamics of septal formation.

5.3.2 Inheritance of peptidoglycan in sectors

S. aureus is an approximately “spherical” organism that divides on three orthogonal planes (Tzagoloff and Novick, 1977). This influenced the production of models of the bacterial cell wall in sectors for both glycan strand orientation and peptidoglycan age (Dmitriev et al., 2004; Turner et al., 2010a). The sectoring hypothesis was tested using sequential labelling with three FDAAs and was shown to occur in the majority of cells within a population. The sectoring model is therefore maintained despite publications released during the later stages of this project that suggest *S. aureus* is ellipsoid during the division cycle (Monteiro et al., 2015; Zhou et al., 2015). This new observation also affects the percentage of total cell surface area in each sector not the sectoring phenomenon itself, as new peptidoglycan has been shown to account for less than half of the total cell surface following division. In order to further quantify the peptidoglycan sectors super-resolution images of sectorised cells rendered in 3D are required. This would require further 3D SIM images of sector labelled *S. aureus* cells, however care must be taken on the influence of the artefact associated with SIM on these quantifications.

There are a number questions to answer when it comes to the inheritance of cell wall. What percentage of the cell wall of a newly split cell comes from septal peptidoglycan and does this change as the cell cycle continues? This has recently been determined to be less than 50% and is maintained until the next division cycle begins (Monteiro et al., 2015; Zhou et al., 2015). However, the dynamics of this over multiple division cycles was not followed, it remains possible that expansion of the new septum may continue

for multiple generations. Another question to answer is whether the proportions of each cell wall sector need to be recalculated? This question has added complication due to the presence of off-septal synthesis which may or may not contribute to overall cell growth (Chapter 4; Monteiro et al., 2015). However, to assess this question it would first be important to repeat sequential 30 minute labelling with FDAAs with SIM.

5.3.3 Heterogeneity in peptidoglycan synthesis

Peptidoglycan synthesis heterogeneity appears to occur at a number of different levels within *S. aureus*; heterogeneity in progression of synthesis, heterogeneity between individual cells to produce an asynchronous clonal population and population heterogeneity. During the progression of the cell division cycle peptidoglycan synthesis heterogeneity seems to occur in two ways. Firstly, individual cells take different lengths of time to pass various morphological checkpoints within the cell division process. For example, DivIB acts as a molecular checkpoint to ensure synthesis of the ring/band of peptidoglycan is completed prior to completion of the septum (Bottomley et al., 2014). It is required for the synthesis of the septal plate after piecrust formation. Secondly, the actual speed of peptidoglycan synthesis at the different stages of the division cycle and between individual cells does not appear consistent. Individual cells therefore progress through the division process at different rates, most likely dictated by a number of different factors, presumably including availability of peptidoglycan precursors.

The rate of cell division does not appear to be determined by an inherited factor, due to the different progression of cell division observed in sister cells. This produces asynchrony within a clonal population. The presence of cells at different stages in the cell cycle allows continuous expansion of the population and may have advantages in speed of reaction of the population to fluctuations in the environment. It is unclear what may cause heterogeneous sister cells. Stochastic gene expression and partitioning of molecules at division may provide an explanation but are unlikely to be the full story (Elowitz et al., 2002; Huh and Paulsson, 2011). However, while in some cases apparent sister cells had a different incorporation pattern, in other cases cells in close proximity to one another showed the same FDAa incorporation. Cells that are in close proximity may be related to one another. This may suggest that inheritance may

play a role in FDAA incorporation patterns, in particular when cells undergo growth arrest.

Population heterogeneity gives phenotypic diversity in the absence of any apparent genetic or environmental variation (Ackermann, 2015). Even when differences (genetic/environmental) are minimised single cells are still seen to differ from one another e.g. in gene expression and phenotypic traits. The reason for this is that many cellular processes are based on a small number of molecules against a noisy background such that fluctuations within individual cells are inevitable (McAdams and Arkin, 1999). These fluctuations are tolerated since careful control comes at a high energetic cost and the ability of a subset of cells to survive a sudden change in environmental conditions is a selective advantage (Balaban et al., 2013). There are two means by which population heterogeneity generally occurs within bacteria; bet-hedging and division of labour (Ackermann et al., 2008; Philippi and Seger, 1989).

Division of labour occurs when two (or more) phenotypes are encoded by the same genotype & each phenotype relies on the other for some benefit (Ackermann et al., 2008). There are several examples of this within bacteria that occur in both the ability to utilise nutrients and in pathogenesis. For example, *B. subtilis* produces the enzyme subtilisin E to digest extracellular proteins during nutrient deprivation. Only a subset of cells produce subtilisin E, presumably at high energetic cost, while all cells within the population benefit from the additional nutrients (Veening et al., 2008).

Other examples of heterogeneity do not rely on interaction between individual cells to commit to different phenotypes but occur seemingly randomly across a population and therefore allow populations to benefit in fluctuating environments (Ackermann, 2015). There are multiple examples of bet-hedging heterogeneity in bacteria. These include competence in *B. subtilis* and host evasion in *Salmonella typhimurium*. Non-expression of flagellin in *Salmonella* allows evasion of the host immune system however prevents ability of *Salmonella* to migrate to areas of higher nutrients (Stewart et al., 2011). The mechanism controlling the two states of flagellin expression (on or off) impacts on the ability of an individual to cause infection.

Perhaps the best known example of population heterogeneity lies in persistence, the ability of a subset of genetically identical cells to survive extended exposure to

antibiotics without the acquisition of resistance genes. Here, those cells in the *S. aureus* population that cease peptidoglycan synthesis might be persister cells, as they are not growing (See Chapter 5.3.4).

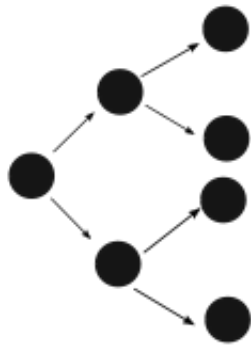
The presence of heterogeneity at multiple levels within a bacterial population emphasises the need for single-cell microbiology techniques. Many current analyses on bacteria rely on techniques based on averages e.g. optical density. In this case both a pause in cell division and individual cell death is masked (Figure 5.14).

5.3.4 Bacterial persistence

When antibiotics are used against a bacterial infection the majority of the population are killed. However, a small proportion (between 0.001-0.1%) survive by entering a “persister-state” (Van den Bergh et al., 2016; Verstraeten et al., 2016). Persisters are phenotypic variants of a genetically clonal population that have entered a dormant state (Levin-Reisman and Balaban, 2016). The dormant state is characterised by decrease in important cellular processes such as DNA replication, protein synthesis and cell wall synthesis, processes that are also important targets for antibiotics (Balaban et al., 2013). Persister cells are thought to be the major cause of recurrence in chronic bacterial infections (Verstraeten et al., 2016). Unlike the production of resistant mutants, cells that are regrown from persistent bacteria remain sensitive to antibiotics (Balaban et al., 2004). The growth state (slow-growth vs. non-growth) and mechanisms behind production of persisters remain largely unknown (Helaine et al., 2014).

There are two types of bacterial persistence. Type I results from stress signals and can be eliminated by keeping cells in exponential phase while Type II occurs when cells stochastically enter a non-growing state presumably in the absence of an external signal (Levin-Reisman and Balaban, 2016). Type II persisters are continuously generated within populations (Balaban et al., 2004). Persistence has been linked to pre-existing heterogeneity in bacterial populations where phenotypic switching produces cells within a population which are “normal” or exhibit reduced growth rates (Balaban et al., 2004). This reduced growth rate was seen to occur prior to the addition

Whole population level



Single cell level

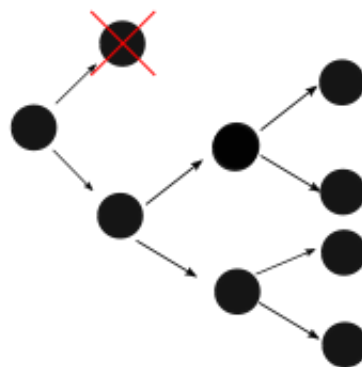
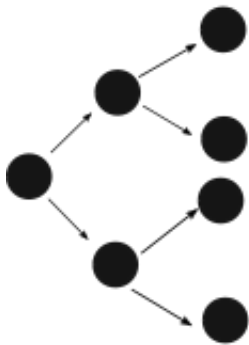
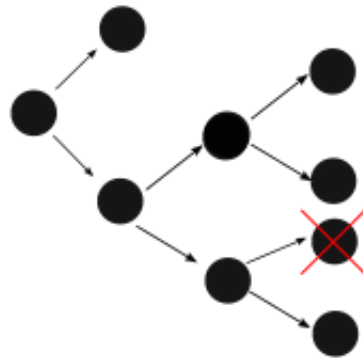


Figure 5.14 Whole population versus single cell analysis. Using average based detection techniques, heterogeneity within a bacterial population is missed. This schematic highlights the different conclusions of the proliferation of 2 cells to form a population of 8 cells measured by whole population and single cell analysis. Whole population analysis misses cell death and dormancy. Adapted from (Helaine and Holden, 2013).

of antibiotics and this heterogeneity is thought to be important in adaptation of a bacterial population to fluctuating environments, such as those encountered during infection (Balaban et al., 2004). Oscillator cells found in my study show that the switch between arrested growth & fast growth also occurs within a *S. aureus* population. This phenomenon allows an increased chance of survival in a rapidly changing environments. The signals that cause a single cell to enter the “persister-state” are still largely unknown, possible candidates include fluctuations in levels of a small number of proteins (possibly due to unequal partitioning of proteins on cell division), differential exposure to nutrient deprivation and bacterial signalling (Helaine and Holden, 2013; Lewis, 2010).

Signals that may trigger cells to enter the persister state can broadly be split into cell-intrinsic and cell-extrinsic signals (Balaban et al., 2013). Cell intrinsic signals may be due to noisy gene expression, an example of this is the involvement of a toxin-antitoxin module in persistence (Verstraeten et al., 2016). In *E. coli* a mutagenesis screen using ethyl methanesulphonate (EMS) led to the discovery of mutations within the *hipA* gene that caused high levels of persistence (Verstraeten et al., 2016). The *hipBA* locus encodes a toxin-antitoxin (TA) module. TA modules encode a fragile antitoxin that controls the activity of a stable toxin, usually targeted to an essential cellular process (Verstraeten et al., 2016). The levels of both the toxin HipA and antitoxin HipB during normal cell growth are in balance such that the toxin is unable to cause an effect, however under stress HipB is degraded by the Lon protease such that HipA is free to act within the cell (Rowe et al., 2016). Current understanding is that the balance between HipA and HipB is perturbed in a subset of cells allowing the toxin level to increase above a threshold causing transient growth arrest as the toxin exerts its effect until HipB levels increase (Balaban et al., 2013). This effect may be due to leaky gene expression of the *hipAB* locus or may be due to a more global mechanism of persister formation based on guanosine tetraphosphate (ppGpp) concentrations. Slow-growing cells often have high concentrations of the bacterial signalling molecule ppGpp, a signal involved in environmental stress response. High p(p)Gpp can activate TA loci through a regulatory cascade (Balaban et al., 2013; Verstraeten et al., 2016). However, since the high ppGpp levels have only been detected once persister cells have been

isolated, it is unclear whether ppGpp has a role in formation or maintenance of the persister state once an environmental stress has occurred.

Many extrinsic signals, particularly environmental stresses, induce the formation of persisters, these include nutrient stresses e.g. starvation and carbon source transition, host signals as well as the presence of antibiotics (Helaine and Kugelberg, 2014). There exists multiple mechanisms of persister formation that may interact with one another (Lewis, 2010). This poses difficulty in the eradication of persisters during infection.

Persisters within infection pose a particular threat not only due to the possibility of recurrence but also since persisters have a high propensity to develop resistance, especially since stressed bacterial cells have a higher than normal mutation rate (Balaban et al., 2013). Recurrence of chronic infection is proposed to be due to a combination of biofilm formation and persister cells. Biofilms are aggregated bacteria within an extracellular matrix that often stick to both biological and non-biological surfaces (Periasamy et al., 2012). In general biofilms are not thought to be less permeable to antibiotics however, they pose a barrier to immune cells (Lewis, 2010). A model of relapsing infection is as follows; The immune system clears both regular and persister cells from the bloodstream while antibiotics kill the majority of other bacterial cells within the host (e.g. in biofilms). Any persister cells located within the biofilm are not cleared. Once antibiotic levels drop these remaining persisters repopulate the biofilm and infection relapses (Lewis, 2010). Within the clinical setting an important question is whether remaining cells are due to ineffectiveness of antibiotics to kill persister cells or whether antibiotics are unable to reach certain cells within the infection (Conlon et al., 2013). Eradication of persisters therefore must rely on the development of drugs that target all cells within a population regardless of growth state or a molecule that can be used in conjunction with standard antibiotics to eliminate persisters through perturbation of the persister state. Since the mechanisms of persister formation are varied possible targets will likely be involved in persister maintenance (Lewis, 2010). Such targets may include processes such as lipid bilayer maintenance which must be continued for a cell to remain viable, indeed reduction in PlsB function, a protein involved in the synthesis of phospholipids, leads to reduction in persister formation (Lewis, 2010). Recent work from the Lewis group discovered a compound that can be used to clear persisters within infections (Conlon et al., 2013).

An acyldepsipeptide (ADEP4) activates the ClpP protease resulting in death of cells. The ClpP protein is involved in the degradation of misfolded protein however the ADEP4-ClpP complex has an open catalytic chamber allowing non-specific degradation in a non ATP-dependent manner of multiple proteins forcing cell death (Conlon et al., 2013). ClpP null mutants were shown to arise however co-treatment with Rifampicin resulted in complete eradication of *S. aureus* even from biofilms (Conlon et al., 2013). A further outcome of this is the observation that persisters are not invulnerable suggesting that recurrent infections are due to pathogen tolerance of antibiotics as opposed to inability of antibiotics to reach all pathogens within an infection (Conlon et al., 2013).

Within my work *S. aureus* were seen to enter into a transient dormant state where no cell wall synthesis occurred. It could be said that these cells are entering a persistent state. Since the experiment was carried out in the complete absence of antibiotics and with cells at mid-exponential phase the oscillator cells are examples of *S. aureus* stochastically entering a persistent state, from which they can return to an active growing state with no apparent ill-effects. However, there remains a number of questions to ask about these cells. Labelling with FDAAs only indicates the state of the cell wall synthesis process, it is unclear whether cells that are in a “dormant-state” also have reduced other cellular processes or whether cell wall synthesis is the only process involved. These two options would suggest two entirely different explanations for the occurrence of oscillators. If this process was only due to peptidoglycan synthesis it would most likely be due to a checkpoint in cell division, where peptidoglycan synthesis is paused until cell division is able to proceed. However, this seems unlikely for two reasons. Firstly, oscillators are seen to pause at entirely different stages in cell division, if this was due to a cell division checkpoint there should be finite points within the cell cycle that cell division is paused. Secondly, it stands to reason that pausing the cell cycle would only result in the pause of septal peptidoglycan synthesis, such as is the case in the production of heterogeneous population mentioned previously (Chapter 5.2.4). Since oscillators completely pause peptidoglycan synthesis for both septal and off-septal synthesis it suggests that lack of synthesis is due to entrance of individual cells into a dormant state comparable with that of persisters.

Another possibility for cells that lack labelling is incomplete transition from stationary to exponential phase in individual cells. Overnight cultures of cells used for inocula within these experiments are in a starvation state therefore there will be a high proportion of persister cells. Increasing single-cell lag time distribution is a mechanism bacterial populations undergo in order to acquire tolerance to antibiotics without the need for acquisition of resistance (Fridman et al., 2014). While this may explain those cells that either lack labelling or are missing the early labels, once a cell has committed to entering exponential phase pauses are likely to be due to transition to persister state due to mechanisms associated with that transition rather than a reversion to stationary phase. Additionally, cultures were grown for 90 minutes in fresh media prior to initiation of labelling. Existing in a dormant state comes at a cost of time available to proliferate. Therefore in conditions with a lack of environmental stress remaining in a dormant state reduces the number of potential offspring for no apparent advantage (Fridman et al., 2014).

Determination of the presence of pre-existing persisters, or “pre-sisters”, within a mid-exponential phase culture of *S. aureus*, which should not be under any environmental stress, opens up a new area of investigation. What causes *S. aureus* to enter into a transient dormant state with no environmental stress? Are oscillators actually persisters? Despite the original observation of persistence occurring within *Staphylococci* there remains very little within the literature surrounding persistence in *S. aureus* (Verstraeten et al., 2016). First would be to confirm the presence of persisters in exponential phase culture by another means, for example using the fluorescence dilution method as described by Helaine (Helaine et al., 2010). This involves the expression of a plasmid with two fluorescent proteins, one under a constitutive promoter and one under an inducible promoter. Following removal of the inducer from culture each division dilutes the intensity of the fluorophore under the inducible promoter, thereby persisters can be identified by retention of this fluorophore (Helaine et al., 2014). Where this method has its advantages over the use of FDAAs is in the ability to combine with live-cell microscopy. Should the presence of persisters be confirmed it would then be possible to begin to assess their contribution to the bacterial population, particularly in survival during antibiotic treatment, as well as investigation into the mechanisms behind persister formation.

Chapter 6

General Discussion

6.1 Growth & division in *S. aureus*

The cell cycle of *S. aureus* has the following overall features. First the division plane is selected and synthesis of the septum is initiated. Next the septum is completed creating two daughter cells still joined together within the mother cell wall. Then the daughter cells split apart before the next round of division takes place at an orthogonal plane (Figure 6.1). This is however a generalised view of the process and there are many questions and models concerning how this process is carried out at the molecular level:

- How are the division planes selected?
- What is the mechanism of peptidoglycan synthesis?
- How is the septum divided between the daughter cells?
- What causes daughter cell separation?
- Are these processes interlinked?
- How does the cell grow in between septation events?

6.1.1 Selection of division plane

Since *S. aureus* divides on 3 orthogonal planes it is not thought that the spatial information driving this can be encoded within the DNA therefore there must be some other epigenetic feature that drives the selection of division plane (Turner et al., 2010a). This is because the factor that specifies division plane must be carried over multiple division cycles before their effect is required, yet change on every division. In rod shaped organisms localisation of the z-ring and therefore the division septum is modified by the Min system which prevents erroneous production of z-rings at cell poles (Wu and Errington, 2011). In addition nucleoid occlusion prevents the formation of the z-ring prior to chromosome segregation (Wu and Errington, 2011). However, apparently spherical bacteria such as *S. aureus* lack the Min system, therefore, the nucleoid occlusion system has been thought to play a role in z-ring placement in

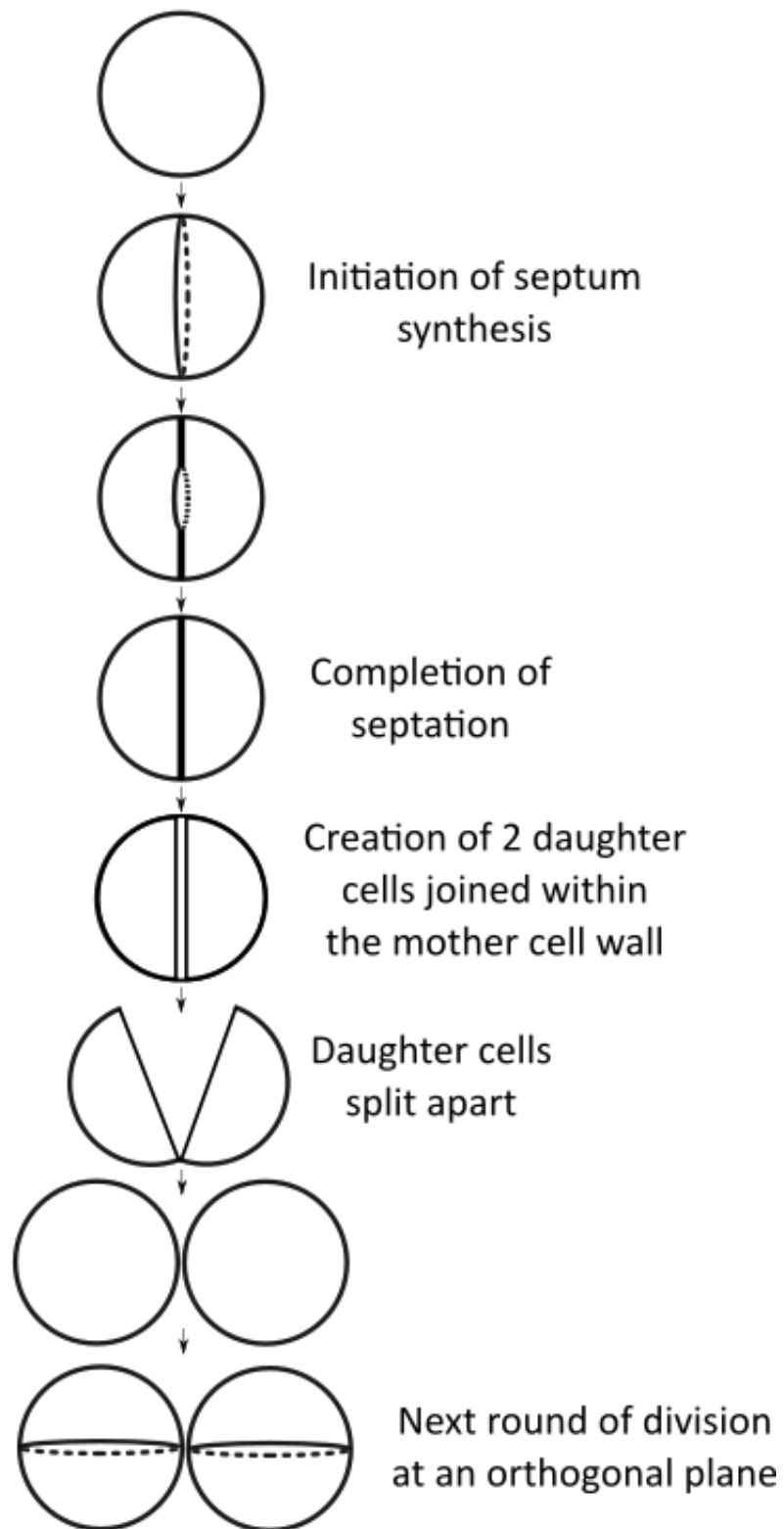


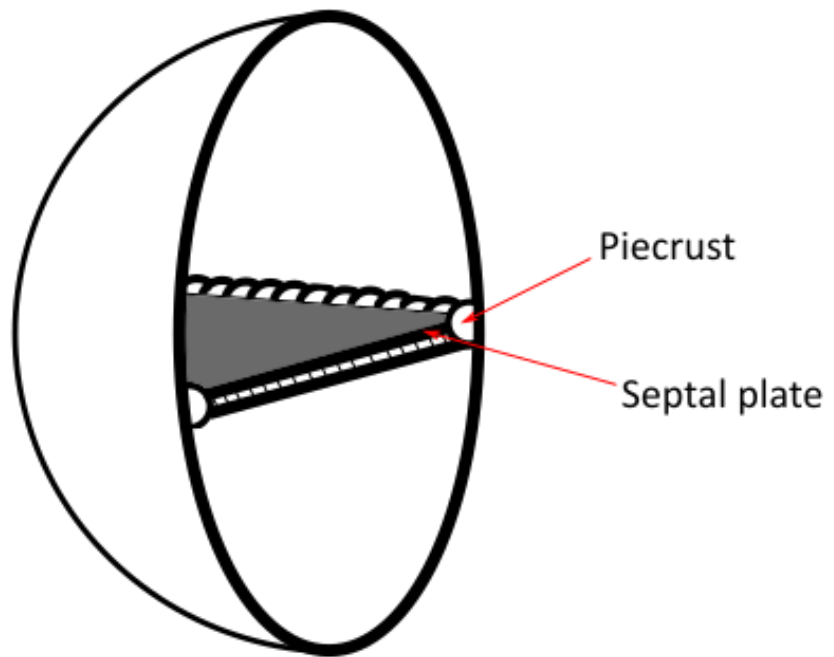
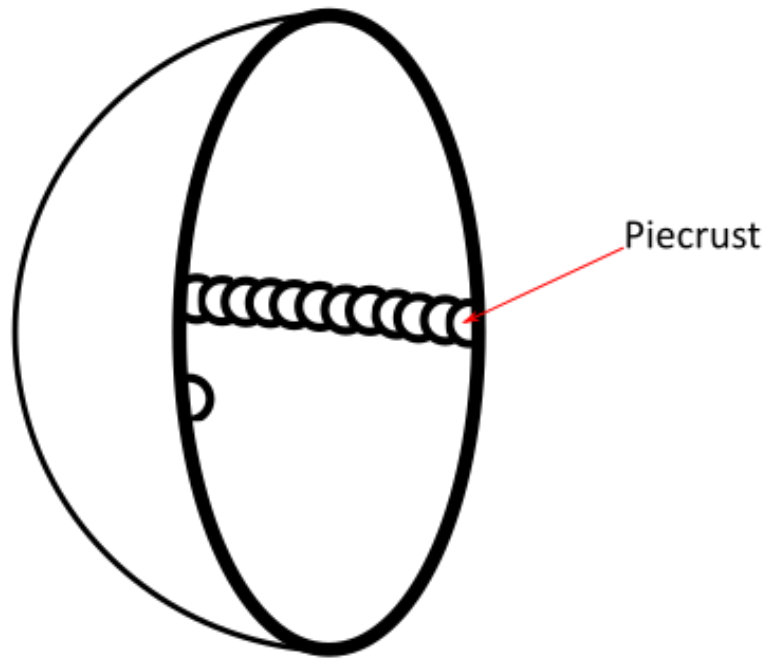
Figure 6.1. General Schematic of cell division in *S. aureus*

spherical organisms (Wu and Errington, 2011). In *S. aureus* the Noc protein co-localises with the nucleoid and prevents bisection of the chromosome during cell division (Veiga et al., 2011). Following chromosome segregation, a space at the *S. aureus* midcell exists where Noc is absent thereby releasing inhibition of z-ring formation.

Additionally, in *S. aureus* Noc deletion results in the formation of multiple rings and arcs of FtsZ, therefore it was suggested that nucleoid occlusion may coordinate localisation of the division plane (Veiga et al., 2011). However, this is not sufficient to allow *S. aureus* to divide on 3 orthogonal planes as a further signal is required either to direct the axis of chromosome segregation or define the division plane (Veiga et al., 2011; Wheeler, 2012). It has been suggested that inherited architectural features of peptidoglycan may play a role in this process (Turner et al., 2010a).

AFM analysis of purified sacculi demonstrated a thick band of peptidoglycan material, the “piecrust”, that encircled the septum and was presumably synthesised as the first step in septum formation (Figure 6.2 A). On division this structure is divided between the 2 daughter cells such that each has a full “rib” of material denoting the division plane that has just been used (Figure 6.2 B). Following the second round of division this rib is divided in half such that each daughter cell inherits a semicircle rib surrounding the old portion of the cell. At the same time daughter cells inherit a second piecrust derived full rib. In the third division the semicircle, or half rib, is divided in half to produce a quarter rib, the full rib is divided in half to produce a half rib and a new full rib is inherited from piecrust material. At the next division (the 4th division) *S. aureus* will divide on the same plane as the first division. This is the plane in which the quarter rib material is present. Therefore, it is possible that there is recognition of the quarter rib (or rejection of the half and full ribs) to determine the plane of division. There are a number of different models for the recognition of the ribs, such that division plane can be specified, these include induced membrane curvature which can be recognised by a protein recruiter, proximity of peptidoglycan to the membrane thereby being favoured by the divisome, recognition of distinct chemistry that may exist within the rib or the pre-existing localisation of proteins or protein anchors to the ribs that may recruit the divisome to the correct plane (Wheeler, 2012).

A



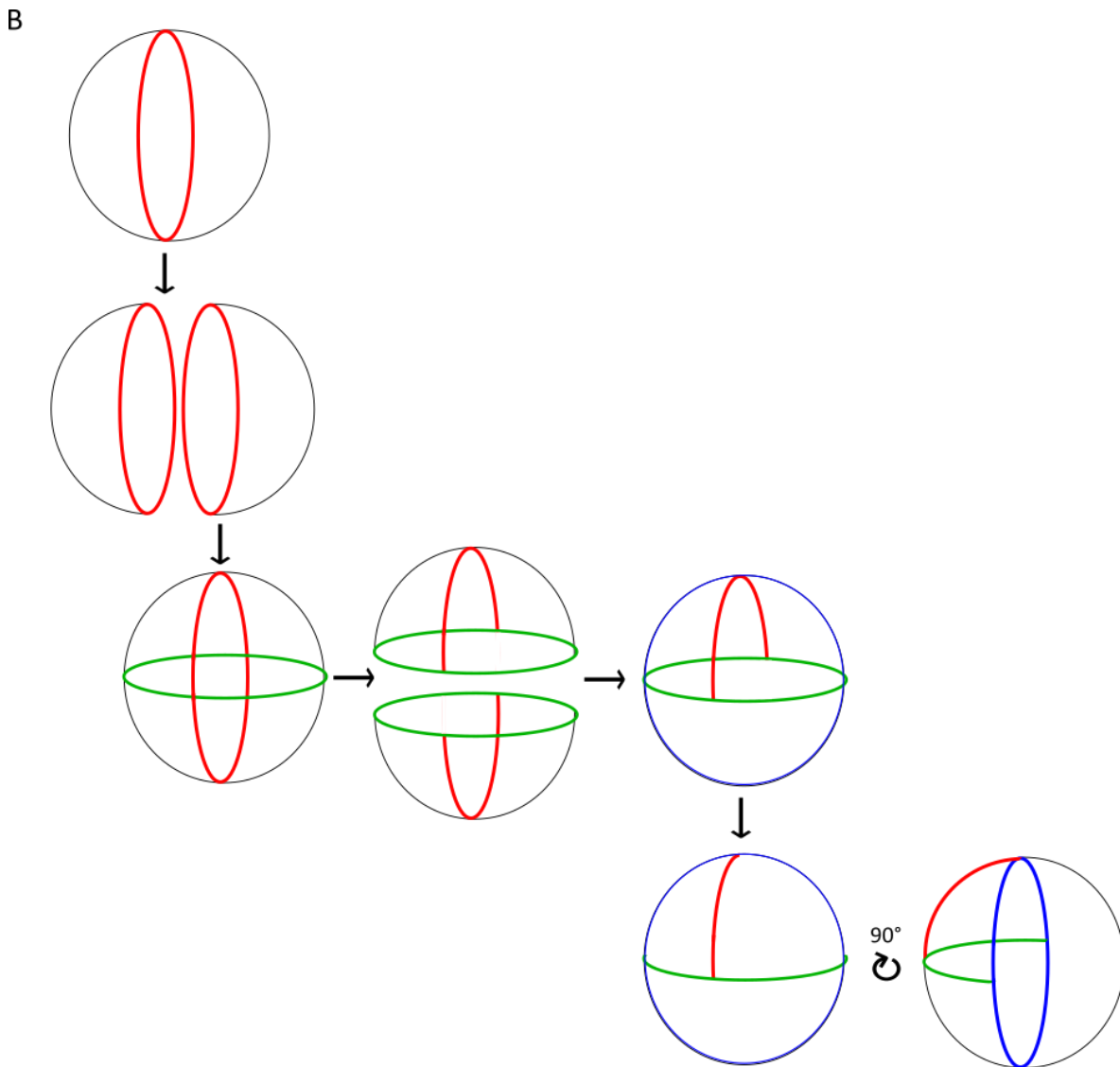


Figure 6.2. Schematic of the piecrust and its subsequent inheritance. (A)

Representative diagram of placement of piecrust. Diagram of a dividing cell cut in half perpendicular to previous division. Following division of the septal plate each daughter will inherit a proportion of the piecrust. (B) Schematic of inheritance of piecrust for 3 divisions. Red indicates the piecrust from the first division, Green indicates piecrust from the second division and blue indicates piecrust from the third division. This shows how piecrust can be inherited such that each offspring inherits a quarter rib from the first division, a half rib from the second division and a full rib from the last division with high fidelity.

6.1.2 Peptidoglycan synthesis

Peptidoglycan synthesis has been thought to occur at the leading edge of the septum (Amako and Umeda, 1984; Touhami et al., 2004), however, super-resolution imaging of FDAA labelled *S. aureus* has indicated that synthesis occurs in a zone across the surface of the septum (Chapter 4). This is corroborated by EM data (Matias and Beveridge, 2007), which showed that incomplete septa were flared in thickness towards the mother cell wall. Once septation has been initiated the piecrust is synthesised, this thick cell wall structure is a time consuming stage (Chapter 5). Following this the septum is synthesised in concentric zones of synthesis, where the majority of synthesis appears to occur at the leading edge however there is still significant synthesis across the rest of septum. Presumably thickening the cell wall such that it is of the correct width at cell splitting to withstand the turgor pressure of the cytoplasm (Matias and Beveridge, 2007). Only once this has occurred will cell splitting take place, however, the mechanisms that may dictate this control are unknown although several models have been proposed

Previous models of *S. aureus* growth have relied upon the presumption that the majority of effective peptidoglycan synthesis in *S. aureus* occurs at the septum and following cell splitting changes in cell shape and volume are due to remodelling of septal peptidoglycan. However two recent observations are in opposition to this model; Firstly cell volume has been shown to continually increase over several generations (Zhou et al., 2015) and secondly the observation of off-septal synthesis during FDAA labelling experiments (Chapter 4.2.4)(Monteiro et al., 2015). Concurrently with these observations it was also revealed by two separate groups that *S. aureus* has an “elongation phase”, that is *S. aureus* does not remain as a sphere throughout the cell cycle (Monteiro et al., 2015; Zhou et al., 2015). Cells start the cell cycle in a spherical shape and become slightly elongated perpendicular to the division plane before initiation of septum formation, during septal synthesis cells do not significantly elongate however following completion of septal synthesis and prior to cell splitting further elongation perpendicular to the division plane occurs (Monteiro et al., 2015).

It is possible to speculate that elongation could be mediated by off-septal peptidoglycan synthesis. Off-septal synthesis could be associated with repair of the mature cell wall or may be productive synthesis in terms of allowing cell volume

expansion. Using the FtsZ inhibitor PC190723 I have shown that off-septal synthesis can lead to productive growth i.e. peripheral synthesis in PC190723 treated cells leads to increased cell diameter. However, whether off-septal synthesis does in fact contribute to growth during normal division process is not straight forward. Additionally, the presence of productive off-septal synthesis must fit with current architectural data. It was suggested that part of the non-essential peptidoglycan biosynthetic machinery may produce the off-septal labelling, in particular PBP4 has been implicated (Gautam et al., 2015). Using *pbp4* mutants I was unable to determine a significant reduction in off-septal labelling using either the single amino acid FDAA or dipeptide probes. This is contrary to evidence from Monteiro et al. (2015) who showed an almost complete loss of peripheral labelling in a $COL\Delta pbpD$ strain which lacks PBP4. My results show that strains lacking PBP4 have a marked reduction in total labelling with single amino acid probes such as NADA used within the published study. Therefore, it is possible that the reduced signal gave the appearance of removal of off-septal labelling. This is particularly relevant for SIM imaging since it generally requires a high signal:noise ratio compared with diffraction limited microscopy. Whether or not a *pbp4* mutant strain lacks off-septal labelling, it has been shown to maintain elongation suggesting that at least PBP4 is not solely responsible for this process. Off-septal peptidoglycan synthesis may involve several redundant biosynthetic components, combining the mutations in both the monofunctional transglycosylase encoding genes and the non-essential PBPs may have an influence on the off-septal synthesis and elongation of *S. aureus*.

6.1.3 Splitting of daughter cells

Separation of daughter cells has long been seen as a “popping” event with very fast intermediate stages (Tzagoloff and Novick, 1977), more recently this process has been shown to occur on a millisecond timescale (Zhou et al., 2015). This speed suggests that separation of the daughter cells cannot rely entirely on enzymatic action but also on mechanical splitting (Zhou et al., 2015). It has been suggested that splitting occurs by mechanical crack propagation from a random point of cell wall failure resulting in the split daughter cells but with a remaining connection or hinge point opposite the initial point of failure (Zhou et al., 2015). Previous models have suggested that cell volume doubles at the point of cell splitting (Seligman and Pincus, 1987), however this seems

unlikely with a millisecond timescale popping event, and indeed volume increase has been shown to increase throughout the cell cycle (Zhou et al., 2015). Immediately following splitting the aspect ratio of cells has been shown to decrease as the cells round up before it once again increases as cells elongate through the next division cycle (Zhou et al., 2015). Neither the role of peptidoglycan synthesis or hydrolysis has yet been determined in the shape change of *S. aureus*.

6.1.4 Requirement of peptidoglycan hydrolysis in cell growth

Growth of the peptidoglycan sacculus cannot be thought of in terms of synthesis alone. Bacteria are known to produce a number of peptidoglycan hydrolases with redundant functions (Heidrich et al., 2001; Smith et al., 2000). Most bacteria have multiple peptidoglycan hydrolases capable of cleaving most bonds within peptidoglycan (Vollmer et al., 2008b). Due to this multiplicity of peptidoglycan hydrolases there is the potential for a degree of redundancy within the hydrolysis system, suggesting an essential role of peptidoglycan hydrolysis in growth of bacteria may involve several enzymes (Heidrich et al., 2002).

During the *S. aureus* cell cycle the newly synthesised septum was found to be stiffer than the surrounding cell wall (Bailey et al., 2014). This implied enzymatic remodelling of the septum is responsible for shape change rather than solely expansion through stretching of the material. This is because a mechanical expansion only process would require the new septum to be soft and stiffen on expansion via stretching (Bailey et al., 2014). It was found that the major enzymes responsible for this remodelling and therefore septum expansion were the peptidoglycan glucosaminidases of which there are 4 known in *S. aureus* (Wheeler et al., 2015). Glucosaminidase activity is required for processing glycans into the characteristic short chains with a concomitant reduction in cell surface stiffness (Wheeler et al., 2015). Deletion & depletion of glucosaminidase activity in *S. aureus* led to the increase in prevalence of hemispherical cells, that is cells that have not been able to remodel the septum (Wheeler et al., 2015). However peptidoglycan synthesis & selection of division plane can still continue. This led to a model where dense, stiff regions of peptidoglycan are formed within the septum and as this is hydrolysed it becomes less dense with reduced stiffness allowing the expansion of the new septum (Wheeler et al., 2015). In another study similar hemispherical cells were seen on the deletion of single peptidoglycan hydrolase Sle1 or

LytM (Monteiro et al., 2015). Sle1 is a N-acetylmuramyl-L-alanine amidase while LytM has glycyglycine endopeptidase activity (Kajimura et al., 2005; Ramadurai et al., 1999). This may suggest that these enzymatic activities are also required for expansion of the septum. It is therefore possible that a combination of different hydrolase activities is required. However whilst glucosaminidase activity is essential for growth both *sle1* and *lytM* mutants are viable and the majority of the cell population exhibit a wildtype morphology (Monteiro et al., 2015). This raises the question as to how these single mutations only dramatically effect a small proportion of the cell population.

6.1.5 Inheritance of cell wall material

Since the determination of an elongation phase and the continual increase in cell volume throughout the cell cycle the previous suggestion that following division the cell wall consists of 50% old and 50% new peptidoglycan was brought into question (Figure 6.3 A) (Seligman and Pincus, 1987; Turner et al., 2010a). In their recent publications both Zhou et al. and Monteiro et al. measured the proportion of old vs. new peptidoglycan in recently split *S. aureus* cells and found new cell wall area to comprise of 25 – 33% of the total cell wall and that this percentage persists throughout the cell cycle (Monteiro et al., 2015; Zhou et al., 2015). However, this would position the scars of cell division (ribs) not at the mid cell but off-centre (Figure 6.3 B). Over the generations, if division occurs on orthogonal planes, this would result in the cell wall being scarred with multiple ribs. This is not seen in AFM images (Turner et al., 2010a). If the septal material remains as less than 50% addition of new material is required or else cells would reduce in size on each division, a process incompatible with life (Zhou et al., 2015). It has been suggested that this growth occurs from synthesis and/or hydrolysis throughout the entire cell wall therefore maintaining the ~33% septal peptidoglycan and ~67% old cell wall. This would also propose off-septal synthesis as productive synthesis required for the increase in cell size.

There is another possibility for cell growth such that the newly synthesised septum may initially form only ~33% of the daughter cell wall however during the next cell cycle this may increase to 50% presumably through hydrolase activity with or without off-septal synthesis (Wheeler et al., 2015). This increase could in theory take longer to reach the full 50% than the division cycle following immediately after. Ribs would

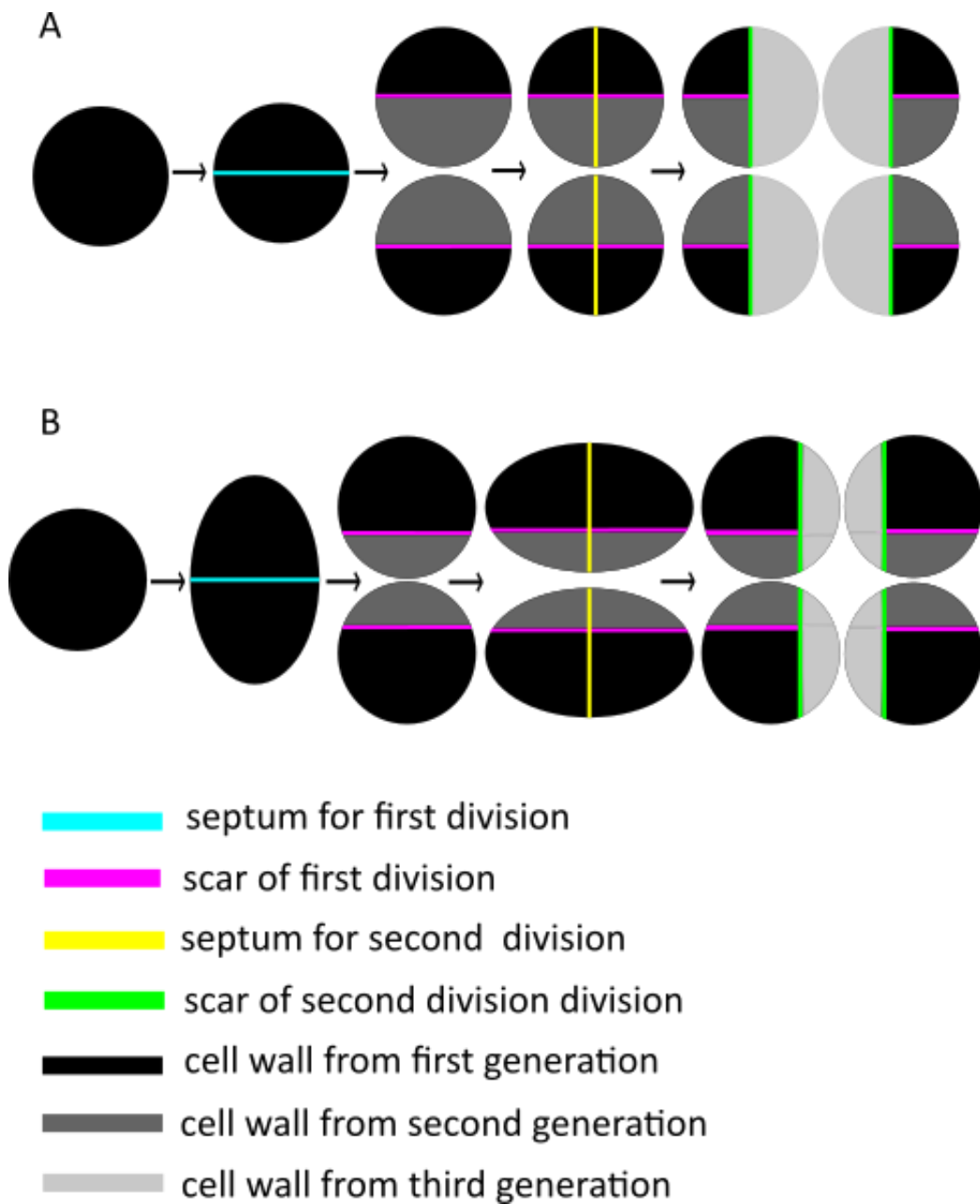


Figure 6.3 Models of cell wall inheritance. (A) 50% new cell wall considering a spherical shape throughout cell division. This results in sectoring of peptidoglycan into $1/2$, $1/4$, $1/8$ etc and place scars & ribs. at the midcell (Turner et al., 2010a). (B) 25% new cell wall with elongation perpendicular to division septum resulting in sectors that do not place scars & ribs at the midcell (Monteiro et al., 2015).

therefore end up at the midcell as has been seen in AFM and are still a viable mechanism for specification of division plane.

6.1.6 Model of septum formation in *S. aureus*

How *S. aureus* produces the septum remains an unanswered question. Although it can now be proposed that the septum is produced by a gradient of synthesis it still remains unclear whether the septum is produced as one or two entities. This may not be resolved until we can utilise higher resolution imaging, possibly with the addition of live-cell application of such a technology, since many of the subtleties of septum formation is thought to occur at length scales below what can currently be resolved. While dynamics of peptidoglycan synthesis has been achieved using virtual time-lapse labelling (Chapter 5) the use of live cell imaging would allow the dynamics of even shorter time periods to be determined and remove any potential labelling artefact from the repeated exchange of growth media to permit multi coloured labelling.

There also remains questions about the cause and control of daughter cell separation in the light of the mechanical crack propagation evidence. If we are to believe that cell splitting is solely due to a stress fault within the peripheral cell wall at the septum site, what is to stop this occurring prior to the completion of septation when the daughter cells are in a state where they can withstand turgor pressure. However, control of autolysin activity, thought to be linked to cell splitting (such as that of Atl) has to occur at locations distant from the finishing septum.

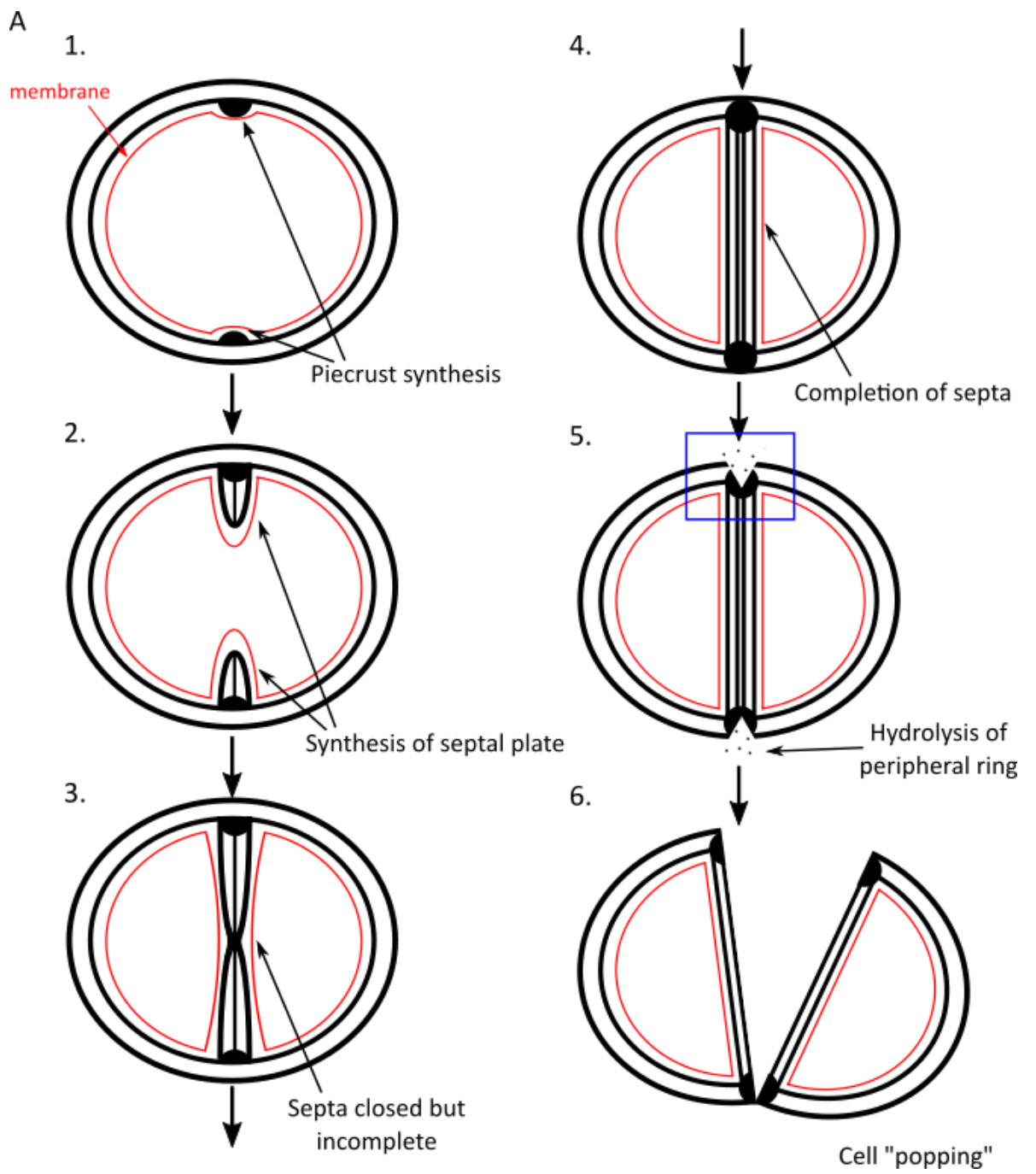
Models of septum formation and subsequent cell splitting are possible for both 1 and 2 septal plates. Firstly, the septum can be thought to be synthesised as one and then hydrolysed into two halves once complete. This is likely not the case since EM has shown incomplete septa consisting of 2 septal plates (Matias and Beveridge, 2007). A modification of this is the model proposed by Matias & Beveridge suggesting septa is synthesised as one then almost immediately hydrolysed into 2. This would require the interaction of hydrolases with the synthesis machinery and tight control such that the septum is divided in half so that each daughter cell receives sufficient material and also to prevent thinning of the septa through hydrolase activity. Subsequent splitting of daughter cells can then occur with control by any of the possible mechanisms suggested below. If the septum is produced as 2 separate entities they can exist either

with nothing between them or associated by a specific feature, this specific feature could act as a checkpoint to prevent initiation of splitting prior to the completion of the septation process.

Splitting of the daughter cells occurs on a millisecond timescale however it must be controlled. Therefore, splitting is probably mediated by both mechanical stress and hydrolase activity. The initial stage of cell division is the production of the piecrust material, following completion of septation this thick band must be split to allow separation of the daughter cells, such that each daughter cell receives a rib of piecrust material. Due to the localisation of hydrolases such as Atl at the division septum, and specifically binding to the piecrust, this splitting is likely due to hydrolase activity (Kent, 2013). Hydrolase activity may result in the thinning of the peripheral ring (piecrust) in a controlled manner to the point where this ring cannot withstand the mechanical force causing daughter cell separation (Zhou et al., 2015). At this point the septal plates will separate. To ensure this occurs at the appropriate time either hydrolases involved in the process are localised to the peripheral ring at the required time or, such as in the case of Atl, activated following completion of the septum via an unknown signalling pathway.

I propose a model whereby completion of the septum results in an increase in mechanical stress altering the 3D conformation of the hydrolase substrate allowing for the digestion of the peripheral ring of peptidoglycan (Figure 6.4). The piecrust is synthesised at the division plane and the septal plate is then synthesised. Within this model the septum can be synthesised as either one or two but exists as 2 separate entities soon after synthesis whether through synthesis or hydrolysis. These septa presumably have no structure between them. On completion of the septa the 2 daughter cells now exert a force upon one another, this mechanical stress can travel up the gap between the septa and result in a change to the orientation or stress upon the piecrust material where hydrolases are localised (Kent, 2013; Yamada et al., 1996). These hydrolases can then be activated by the stressed state of the peptidoglycan, a mechanism that has previously been postulated for autolysin activation (Foster and Johnstone, 1987; Koch, 1985). At some point the peripheral ring fails at a specific point resulting in the “popping” or separation of the daughter cells as described by Zhou et

al. (2015). It is unclear whether this occurs at a random point in the peripheral ring or whether the chemistry of the ring influences the split. For example, where the quarter



B

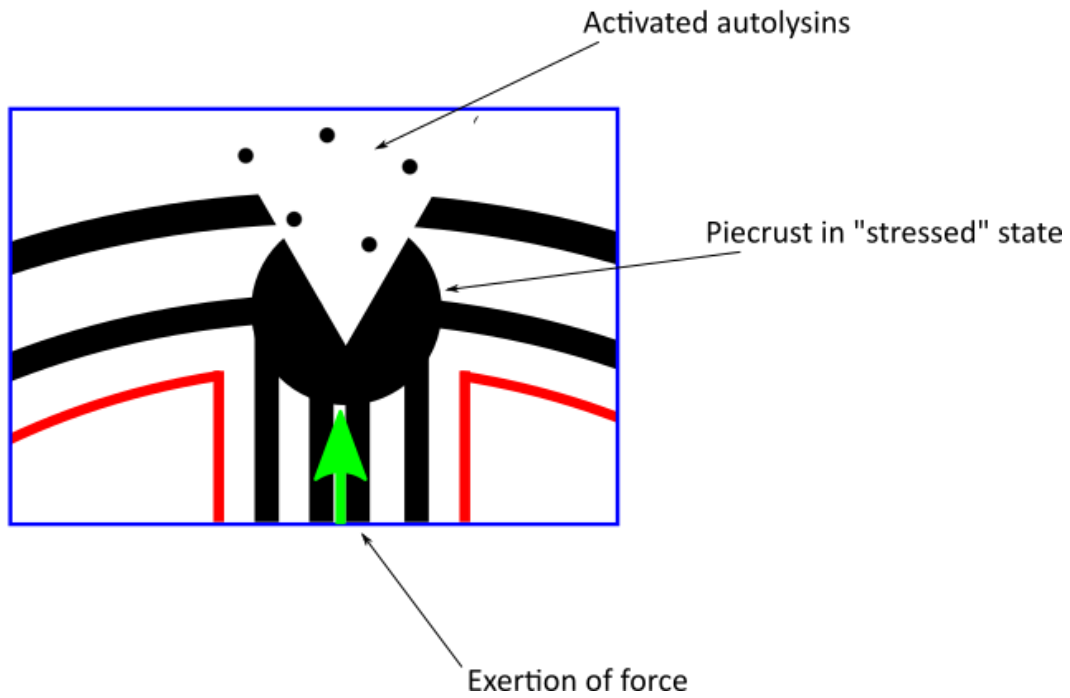


Figure 6.4 Model of *S. aureus* cell division. Division begins by synthesis of the piecrust then subsequent synthesis of the septal plate. This is presumed to occur as 2 plates but may equally be synthesised as one and hydrolysed into two immediately. Following completion of septum, the daughter cells can exert force on each other. This stress is transmitted to the piecrust peptidoglycan (green arrow, B) activating hydrolysis of this material. Hydrolysis of the piecrust and mechanical force between the daughter cells eventually leads to cell splitting. (A) Model of division. (B) Magnified view of area within the blue box to highlight details of model.

rib from a previous division occurs may be stronger or weaker. This may be due to different chemistry i.e. the peptidoglycan is devoid of teichoic acids (Kent, 2013) therefore, the rib section of the outer cell wall on the division plane will lack teichoic acids while the rest of outer cell wall in that plane will contain teichoic acids.

6.2 Heterogeneity of *S. aureus* populations

The discovery of heterogeneous synthesis of the cell wall within a *S. aureus* population has important ramifications for growth and division. Each cell, whilst carrying out the same overall cell cycle acts as an individual with potentially a different growth rate from its siblings. Also cells have the potential to pause the cell cycle presumably occurring due to some signal within an individual cell. This means that analysis of the growth cycle requires the use of single cell biology in addition to culture wide observations. The signals and checkpoints that control cell cycle progression need to be evaluated as such insights into *S. aureus* growth could be relevant in a clinical setting. This is particularly the case for cells that temporarily ceased growth as these have the hallmarks of Type II persisters, that is cells that stochastically enter a transient stationary phase (Levin-Reisman and Balaban, 2016). However, it still remains to be determined whether such cells do indeed persist in an antibiotic environment. If this is the case, then my labelling system provides a mechanism to identify potential persisters before addition of the antibiotic stress.

6.3 Future Directions

6.3.1 Shape change in *S. aureus*

The first important question to answer will be the influence of shape changes during the cell cycle. This will involve thorough investigation of the published models along with existing data including whole cell AFM of cell growth and both scanning and transmission EM. Additionally, it is important to determine whether there are any differences in the models of growth dependent upon whether cell wall or membrane shape is followed. The role of peptidoglycan synthesis and hydrolysis in this shape change must then be determined. Peptidoglycan is either hydrolysed until it reaches a maximally hydrolysed state and becomes permanently inert to maintain cell wall integrity or the alternative is that hydrolysis of all cell wall material happens all the time. This latter hypothesis would not only suggest that the septum may be expanding while it is still being synthesised but would also suggest that synthesis of new material

in old sectors is required to allow the concomitant hydrolysis while maintaining cell wall integrity. It may be possible to determine the role of this hydrolysis by determining cell growth and shape change due to the arrest of all synthesis e.g. through D-cycloserine treatment. Following determination of the features and mechanisms of shape change throughout the cell cycle it will then be possible to investigate the roles of individual division proteins in this process.

6.3.2 Future insights into peptidoglycan using microscopy

Previous studies of the localisation of peptidoglycan synthesis in bacteria have been limited by the microscopy resolution available. FDAAs and super-resolution microscopy techniques, particularly STORM, allows us to begin to dissect the division process at the molecular level. At present this gives us close to the maximum resolution achievable with biological samples and fluorescence microscopy. To further determine the mechanism, it would be useful to be able to combine molecular approaches with live cell imaging, however the tools with which to carry this out are not currently available. Recent work by Stefan Hell & colleagues have developed fluorescent probes that have enabled 1 and 2 colour STED images of 40-60 nm resolution. Live cell imaging of the division process may allow the dynamics of peptidoglycan synthesis to be resolved on time scales not possible with the methods used in my work.

Another important aspect is to begin to link peptidoglycan chemistry with architecture, for example do certain architectural features, such as the piecrust differ in chemical make up? This may begin to be possible with a dual STORM and AFM approach (Chacko et al., 2013). However, this technique is still being developed. Additionally, a range of probes would need to be developed to label not only the D-amino acid side chain at the 4th or 5th position, but also to label glycan strands, crossbridges and other features such as modifications etc.

6.3.3 Role of *S. aureus* division proteins

Growth and division of bacteria involves much more than just the insertion of peptidoglycan into the sacculus. A large number of components are required both directly in the mechanism and in its regulation. How these proteins interact, are controlled, localise within bacteria and effect bacterial growth remains an important but unanswered question. While a number of these interactions have already been

determined in *S. aureus* (Figure 6.5) we do not have a complete picture and also do not understand what the interactions mean in the context of the whole cell. It is not currently understood how hydrolases may interact within the divisome machinery although such interactions seem likely. It has recently been suggested that SagB, the important glucosaminidase, does not interact with PBP2, MGT or SgtA in *S. aureus* (Chan et al., 2016). However, such interactions may be indirect or may occur with other hydrolases. Also hydrolysis of peptidoglycan does not need to occur concomitantly with synthesis to permit growth. All 2-hybrid results need to be verified independently using a system such as FRET (García-Lara et al., 2015) or immunoprecipitation. In addition, these interactions can be further analysed biochemically for example through crystal structures. Along with the determination of interactions it will be important to elucidate the localisation of these interactions within the bacterial cell as well as their outcome e.g. protein activation or repression. It is important to note that interactions do not give information as to the stoichiometry or dynamics of the proteins.

To permit determination of the organisation of proteins within the cell it is possible to utilise the super-resolution techniques used within my work in conjunction with fluorescently tagged proteins. This has been achieved for division proteins using both SIM (Monteiro et al., 2015; Strauss et al., 2012) and PALM/STORM (Fu et al., 2010; Holden et al., 2014). However, there are a number of obstacles to overcome in order to routinely use such techniques. Primarily obstacles have been in finding suitable fluorescent proteins that not only express in *S. aureus* but that work within the PALM/STORM system. In addition to the use of fluorescent proteins, SNAP & CLIP tags can be used to label proteins with synthetic dyes (Gautier et al., 2008; Keppler et al., 2003). Synthetic probes have had more success in super-resolution microscopy however, are often not cell permeable and cannot access cytoplasmic proteins or domains. Due to the increase in resolution gained from super-resolution techniques it is also ideal to create single-copy fluorescent fusions. Since many of the proteins of interest are essential this has proven challenging.

How protein interactions and localisations work at a cellular level is also important. By analysing the effect of deletion or depletion of proteins within the divisome on both cellular morphology, division process and peptidoglycan biochemistry we can begin to

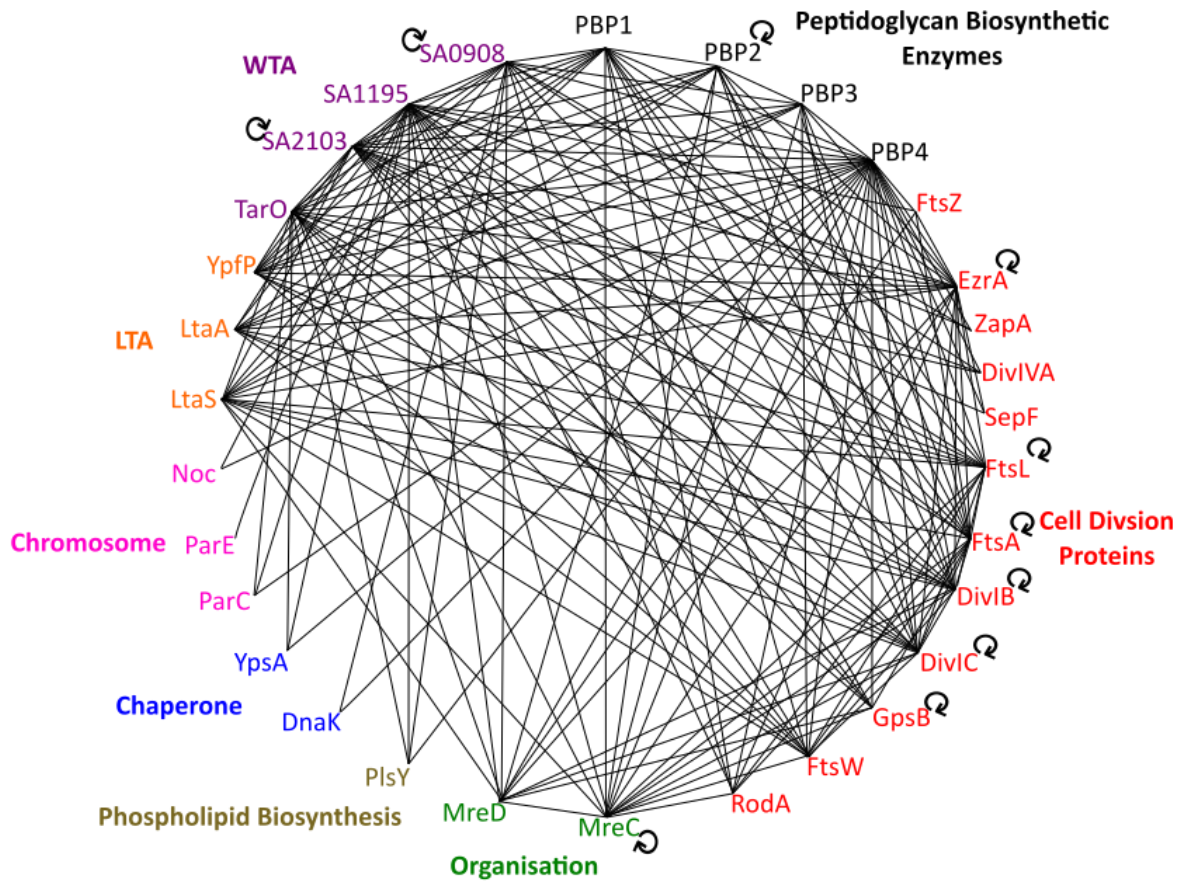


Figure 6.5 Interaction map of proteins involved in the division process. (Bottomley, 2011; Fairclough, 2009; Kent, 2013; Reichmann et al., 2014; X. Ma, personal communication).

dissect the molecular interplay. For example, the role of SagB in both cell wall stiffness and glycan chain length was determined using such a regime (Wheeler et al., 2015). In particular, the role of the peptidoglycan biosynthetic enzymes and their requirement for cell growth will be important. Additionally, the localisation and dynamics of division proteins both in relation to one another and to the cell wall dynamics at the molecular level is crucial.

Using an *in vitro* system it will be possible to determine the roles of the peptidoglycan biosynthetic enzymes in isolation from other cell processes. This will allow the role of individual constituent parts in the building up of the peptidoglycan sacculus to be identified. Recombinant proteins can be reconstituted into liposomes and fed substrates. Resulting peptidoglycan material may be investigated both biochemically and architecturally. This can reveal the actual substrates for each protein. For example, is PBP4 capable of crosslinking lipid II molecules or does it only act on glycan chains of a certain length? Information can also be gathered on the molecular interplay and control of the process at the molecular level including the stoichiometry of the divisome.

6.3.4 Effect of antibiotic treatment and resistance

Finally, *S. aureus* is a clinically important bacteria and therefore determination of how the growth & division system is altered by antibiotics and how resistance mechanisms may affect the growth cycle is of interest. How does treatment with different cell wall-targeting antibiotics effect the peptidoglycan biochemistry including glycan chain length and crosslinking? The same questions can also be asked of the effect of resistance mechanisms both in the presence and absence of the antibiotic. For example, MRSA strains have MecA but both PBP1 & PBP2 are required for high level resistance. The effect of MecA on peptidoglycan synthesis from a biochemical, architectural and localisation standpoint will determine how it is able to render *S. aureus* so resistant to clinically important antibiotics. It is by an increased understanding of peptidoglycan metabolism that new approaches for control of such a formidable pathogen will be determined.

References

- Aaron, M., Charbon, G., Lam, H., Schwarz, H., Vollmer, W., and Jacobs-Wagner, C. (2007). The tubulin homologue FtsZ contributes to cell elongation by guiding cell wall precursor synthesis in *Caulobacter crescentus*. *Mol. Microbiol.* *64*, 938–952.
- Ackermann, M. (2015). A functional perspective on phenotypic heterogeneity in microorganisms. *Nat. Rev. Microbiol.* *13*, 497–508.
- Ackermann, M., Stecher, B., Freed, N.E., Songhet, P., Hardt, W.-D., and Doebeli, M. (2008). Self-destructive cooperation mediated by phenotypic noise. *Nature* *454*, 987–990.
- Almada, P., Culley, S., and Henriques, R. (2015). PALM and STORM: Into large fields and high-throughput microscopy with sCMOS detectors. *Methods* *88*, 109–121.
- Amako, K., and Umeda, A. (1984). Cross Wall Synthesis and the Arrangement of the Wall Polymers in the Cell Wall of *Staphylococcus* spp. *Microbiol. Immunol.* *28*, 1293–1301.
- Amako, K., Umeda, A., and Murata, K. (1982). Arrangement of peptidoglycan in the cell wall of *Staphylococcus* spp. *J. Bacteriol.* *150*, 844–850.
- Andre, G., Kulakauskas, S., Chapot-Chartier, M.-P., Navet, B., Deghorain, M., Bernard, E., Hols, P., and Dufrêne, Y.F. (2010). Imaging the nanoscale organization of peptidoglycan in living *Lactococcus lactis* cells. *Nat. Commun.* *1*, 27.
- Andreu, J.M., Schaffner-Barbero, C., Huecas, S., Alonso, D., Lopez-Rodriguez, M.L., Ruiz-Avila, L.B., Núñez-Ramírez, R., Llorca, O., and Martín-Galiano, A.J. (2010). The antibacterial cell division inhibitor PC190723 is an FtsZ polymer-stabilizing agent that induces filament assembly and condensation. *J. Biol. Chem.* *285*, 14239–14246.
- Angert, E.R. (2005). Alternatives to binary fission in bacteria. *Nat. Rev. Microbiol.* *3*, 214–224.
- Arjes, H.A., Kriel, A., Sorto, N.A., Shaw, J.T., Wang, J.D., and Levin, P.A. (2014). Failsafe Mechanisms Couple Division and DNA Replication in Bacteria. *Curr. Biol.* *24*, 2149–2155.
- Atilano, M.L., Pereira, P.M., Yates, J., Reed, P., Veiga, H., Pinho, M.G., and Filipe, S.R. (2010). Teichoic acids are temporal and spatial regulators of peptidoglycan cross-linking in *Staphylococcus aureus*. *Proc. Natl. Acad. Sci. U. S. A.* *107*, 18991–18996.
- Atrih, A., Zollner, P., Allmaier, G., and Foster, S.J. (1996). Structural analysis of *Bacillus subtilis* 168 endospore peptidoglycan and its role during differentiation. *J. Bacteriol.* *178*, 6173–6183.
- Atrih, A., Bacher, G., Allmaier, G., Williamson, M.P., and Foster, S.J. (1999). Analysis of peptidoglycan structure from vegetative cells of *Bacillus subtilis* 168 and role of PBP 5 in peptidoglycan maturation. *J. Bacteriol.* *181*, 3956–3966.

- Bailey, R.G., Turner, R.D., Mullin, N., Clarke, N., Foster, S.J., and Hobbs, J.K. (2014). The Interplay between Cell Wall Mechanical Properties and the Cell Cycle in *Staphylococcus aureus*. *Biophys. J.* *107*, 2538–2545.
- Balaban, N.Q., Merrin, J., Chait, R., Kowalik, L., and Leibler, S. (2004). Bacterial persistence as a phenotypic switch. *Science* (80-). *305*, 1622–1625.
- Balaban, N.Q., Gerdes, K., Lewis, K., and McKinney, J.D. (2013). A problem of persistence: still more questions than answers? *Nat. Rev. Microbiol.* *11*, 587–591.
- Baskin, J.M., and Bertozzi, C.R. (2007). Bioorthogonal Click Chemistry: Covalent Labeling in Living Systems. *QSAR Comb. Sci.* *26*, 1211–1219.
- Beeby, M., Gumbart, J.C., Roux, B., and Jensen, G.J. (2013). Architecture and assembly of the Gram-positive cell wall. *Mol. Microbiol.* *88*, 664–672.
- Van den Bergh, B., Michiels, J.E., and Michiels, J. (2016). Experimental Evolution of *Escherichia coli* Persister Levels Using Cyclic Antibiotic Treatments. In *Bacterial Persistence: Methods and Protocols*, J. Michiels, and M. Fauvart, eds. pp. 131–143.
- Bernhardt, T.G., and De Boer, P.A.J. (2003). The *Escherichia coli* amidase AmiC is a periplasmic septal ring component exported via the twin-arginine transport pathway. *Mol. Microbiol.* *48*, 1171–1182.
- Bernhardt, T.G., and De Boer, P.A.J. (2005). SlmA, a nucleoid-associated, FtsZ binding protein required for blocking septal ring assembly over chromosomes in *E. coli*. *Mol. Cell* *18*, 555–564.
- Betzig, E., Patterson, G.H., Sougrat, R., Lindwasser, O.W., Olenych, S., Bonifacino, J.S., Davidson, M.W., Lippincott-Schwartz, J., and Hess, H.F. (2006). Imaging intracellular fluorescent proteins at nanometer resolution. *Science* (80-). *313*, 1642–1645.
- Bisicchia, P., Noone, D., Lioliou, E., Howell, A., Quigley, S., Jensen, T., Jarmer, H., and Devine, K.M. (2007). The essential YycFG two-component system controls cell wall metabolism in *Bacillus subtilis*. *Mol. Microbiol.* *65*, 180–200.
- Biswas, R., Voggu, L., Simon, U.K., Hentschel, P., Thumm, G., and Götz, F. (2006). Activity of the major staphylococcal autolysin Atl. *FEMS Microbiol. Lett.* *259*, 260–268.
- Biteen, J.S., Goley, E.D., Shapiro, L., and Moerner, W.E. (2012). Three-Dimensional Super-Resolution Imaging of the Midplane Protein FtsZ in Live *Caulobacter crescentus* Cells Using Astigmatism. *ChemPhysChem* *13*, 1007–1012.
- de Boer, P.A.J., Crossley, R.E., and Rothfield, L.I. (1989). A division inhibitor and a topological specificity factor coded for by the minicell locus determine proper placement of the division septum in *E. coli*. *Cell* *56*, 641–649.
- Boneca, I.G., Huang, Z.-H., Gage, D.A., and Tomasz, A. (2000). Characterization of *Staphylococcus aureus* cell wall glycan strands, evidence for a new beta-N-acetylglucosaminidase activity. *J. Biol. Chem.* *275*, 9910–9918.
- Bottomley, A.L. (2011). Identification and characterisation of the cell division machinery in *Staphylococcus aureus*. University of Sheffield.

Bottomley, A.L., Kabli, A.F., Hurd, A.F., Turner, R.D., García-Lara, J., and Foster, S.J. (2014). Staphylococcus aureus DivIB is a peptidoglycan-binding protein that is required for a morphological checkpoint in cell division. *Mol. Microbiol.* *94*, 1041–1064.

Bouhss, A., Crouvoisier, M., Blanot, D., and Mengin-Lecreulx, D. (2004). Purification and characterization of the bacterial MraY translocase catalyzing the first membrane step of peptidoglycan biosynthesis. *J. Biol. Chem.* *279*, 29974–29980.

Bouhss, A., Trunkfield, A.E., Bugg, T.D.H., and Mengin-Lecreulx, D. (2008). The biosynthesis of peptidoglycan lipid-linked intermediates. *FEMS Microbiol. Rev.* *32*, 208–233.

Braddick, D., Sandhu, S., Roper, D.I., Chappell, M.J., and Bugg, T.D.H. (2014). Observation of the time-course for peptidoglycan lipid intermediate II polymerization by *Staphylococcus aureus* monofunctional transglycosylase. *Microbiology* *160*, 1628–1636.

Bramkamp, M., Emmins, R., Weston, L., Donovan, C., Daniel, R.A., and Errington, J. (2008). A novel component of the division-site selection system of *Bacillus subtilis* and a new mode of action for the division inhibitor MinCD. *Mol. Microbiol.* *70*, 1556–1569.

Brennan, P.J., and Nikaido, H. (1995). The envelope of mycobacteria. *Annu. Rev. Biochem.* *64*, 29–63.

Brown, S., Santa Maria, J.P., and Walker, S. (2013). Wall teichoic acids of gram-positive bacteria. *Annu. Rev. Microbiol.* *67*, 313–336.

Bugg, T.D.H., Braddick, D., Dowson, C.G., and Roper, D.I. (2011). Bacterial cell wall assembly: still an attractive antibacterial target. *Trends Biotechnol.* *29*, 167–173.

Buss, J., Coltharp, C., Huang, T., Pohlmeier, C., Wang, S.C., Hatem, C., and Xiao, J. (2013). *In vivo* organization of the FtsZ-ring by ZapA and ZapB revealed by quantitative super-resolution microscopy. *Mol. Microbiol.* *89*, 1099–1120.

Cadby, I.T., and Lovering, A.L. (2014). Molecular surveillance of the subtle septum: discovering a new mode of peptidoglycan synthesis in streptococci. *Mol. Microbiol.* *94*, 1–4.

Canepari, P., Varaldo, P.E., Fontana, R., and Satta, G. (1985). Different staphylococcal species contain various numbers of penicillin-binding proteins ranging from four (*Staphylococcus aureus*) to only one (*Staphylococcus hyicus*). *J. Bacteriol.* *163*, 796–798.

Carballido-López, R. (2006). The Bacterial Actin-Like Cytoskeleton. *Microbiol. Mol. Biol. Rev.* *70*, 888–909.

Cava, F., de Pedro, M.A., Lam, H., Davis, B.M., and Waldor, M.K. (2011). Distinct pathways for modification of the bacterial cell wall by non-canonical D-amino acids. *EMBO J.* *30*, 3442–3453.

Chacko, J.V., Zanicchi, F.C., and Diaspro, A. (2013). Probing cytoskeletal structures by coupling optical superresolution and AFM techniques for a correlative approach. *Cytoskeleton* *70*, 729–740.

- Chan, Y.G.Y., Frankel, M.B., Missiakas, D.M., and Schneewind, O. (2016). SagB glucosaminidase is a determinant of *Staphylococcus aureus* glycan chain length, antibiotic susceptibility and protein secretion. *J. Bacteriol.* **188**, 00983–15.
- Chastanet, A., and Carballido-López, R. (2012). The actin-like MreB proteins in *Bacillus subtilis*: a new turn. *Front. Biosci.* **17**, 1582.
- Chaudhuri, R.R., Allen, A.G., Owen, P.J., Shalom, G., Stone, K., Harrison, M., Burgis, T.A., Lockyer, M., García-Lara, J., Foster, S.J., et al. (2009). Comprehensive identification of essential *Staphylococcus aureus* genes using Transposon-Mediated Differential Hybridisation (TMDH). *BMC Genomics* **10**, 291.
- Cheng, K.J., and Costerton, J.W. (1977). Ultrastructure of *Butyrivibrio fibrisolvens*: a gram-positive bacterium. *J. Bacteriol.* **129**, 1506–1512.
- Clarke, A.J., and Dupont, C. (1992). O-acetylated peptidoglycan: its occurrence, pathological significance, and biosynthesis. *Can. J. Microbiol.* **38**, 85–91.
- Cleverley, R.M., Barrett, J.R., Baslé, A., Bui, N.K., Hewitt, L., Solovyova, A., Xu, Z.-Q., Daniel, R.A., Dixon, N.E., Harry, E.J., et al. (2014). Structure and function of a spectrin-like regulator of bacterial cytokinesis. *Nat. Commun.* **5**, 5421.
- Collins, L.V., Kristian, S.A., Weidenmaier, C., Faigle, M., Van Kessel, K.P.M., Van Strijp, J.A.G., Götz, F., Neumeister, B., and Peschel, A. (2002). *Staphylococcus aureus* strains lacking D-alanine modifications of teichoic acids are highly susceptible to human neutrophil killing and are virulence attenuated in mice. *J. Infect. Dis.* **186**, 214–219.
- Coltharp, C., and Xiao, J. (2012). Superresolution microscopy for microbiology. *Cell. Microbiol.* **14**, 1808–1818.
- Conlon, B.P., Nakayasu, E.S., Fleck, L.E., LaFleur, M.D., Isabella, V.M., Coleman, K., Leonard, S.N., Smith, R.D., Adkins, J.N., and Lewis, K. (2013). Activated ClpP kills persisters and eradicates a chronic biofilm infection. *Nature* **503**, 365–370.
- Corrigan, R.M., Abbott, J.C., Burhenne, H., Kaefer, V., and Gründling, A. (2011). c-di-AMP is a new second messenger in *Staphylococcus aureus* with a role in controlling cell size and envelope stress. *PLoS Pathog.* **7**, e1002217.
- Courvalin, P. (2006). Vancomycin resistance in gram-positive cocci. *Clin. Infect. Dis.* **42**, S25–S34.
- Coyette, J., and van der Ende, A. (2008). Peptidoglycan: the bacterial Achilles heel. *FEMS Microbiol. Rev.* **32**, 147–148.
- Curtis, N.A.C., Hayes, M. V, Wyke, A.W., and Ward, J.B. (1980). A mutant of *Staphylococcus aureus* H lacking penicillin-binding protein 4 and transpeptidase activity in vitro. *FEMS Microbiol. Lett.* **9**, 263–266.
- van Dam, V., Orlachs, N., and Breukink, E. (2009). Specific labeling of peptidoglycan precursors as a tool for bacterial cell wall studies. *ChemBioChem* **10**, 617–624.
- Daniel, R.A., and Errington, J. (2000). Intrinsic instability of the essential cell division protein FtsL of *Bacillus subtilis* and a role for DivIB protein in FtsL turnover. *Mol.*

Microbiol. 36, 278–289.

Daniel, R.A., and Errington, J. (2003). Control of Cell Morphogenesis in Bacteria: Two Distinct Ways to Make a Rod-Shaped Cell. *Cell* 113, 767–776.

Dempsey, G.T., Vaughan, J.C., Chen, K.H., Bates, M., and Zhuang, X. (2011). Evaluation of fluorophores for optimal performance in localization-based super-resolution imaging. *Nat. Methods* 8, 1027–1036.

Derouaux, A., Wolf, B., Fraipont, C., Breukink, E., Nguyen-Distèche, M., and Terrak, M. (2008). The monofunctional glycosyltransferase of *Escherichia coli* localizes to the cell division site and interacts with penicillin-binding protein 3, FtsW, and FtsN. *J. Bacteriol.* 190, 1831–1834.

Desmarais, S.M., De Pedro, M.A., Cava, F., and Huang, K.C. (2013). Peptidoglycan at its peaks: how chromatographic analyses can reveal bacterial cell wall structure and assembly. *Mol. Microbiol.* 89, 1–13.

Divakaruni, A. V, Baida, C., White, C.L., and Gober, J.W. (2007). The cell shape proteins MreB and MreC control cell morphogenesis by positioning cell wall synthetic complexes. *Mol. Microbiol.* 66, 174–188.

Dmitriev, B.A., Toukach, F. V, Schaper, K., Holst, O., Rietschel, E.T., and Ehlers, S. (2003). Tertiary Structure of Bacterial Murein : the Scaffold Model. *J. Bacteriol.* 185, 3458–3468.

Dmitriev, B.A., Toukach, F. V, Holst, O., Rietschel, E.T., and Ehlers, S. (2004). Tertiary Structure of *Staphylococcus aureus* Cell Wall Murein. *J. Bacteriol.* 186, 7141–7148.

Domínguez-Escobar, J., Chastanet, A., Crevenna, A.H., Fromion, V., Wedlich-Soldner, R., and Carballido-López, R. (2011). Processive Movement of MreB-Associated Cell Wall Biosynthetic Complexes in Bacteria. *Science* (80-.). 333, 225–228.

Donachie, W.D., and Begg, K.J. (1989). Cell length, nucleoid separation, and cell division of rod-shaped and spherical cells of *Escherichia coli*. *J. Bacteriol.* 171, 4633–4639.

Durand-Heredia, J.M., Yu, H.H., De Carlo, S., Lesser, C.F., and Janakiraman, A. (2011). Identification and characterization of ZapC, a stabilizer of the FtsZ ring in *Escherichia coli*. *J. Bacteriol.* 193, 1405–1413.

Elowitz, M.B., Siggia, E.D., Levine, A.J., and Swain, P.S. (2002). Stochastic Gene Expression in a Single Cell. *Sci. Reports* 297, 1183–1187.

Elsen, N.L., Lu, J., Parthasarathy, G., Reid, J.C., Sharma, S., Soisson, S.M., and Lumb, K.J. (2012). Mechanism of action of the cell-division inhibitor PC190723: Modulation of FtsZ assembly cooperativity. *J. Am. Chem. Soc.* 134, 12342–12345.

Errington, J., Daniel, R.A., and Scheffers, D.-J. (2003). Cytokinesis in bacteria. *Microbiol. Mol. Biol. Rev.* 67, 52–65, table of contents.

Fairclough, V.R. (2009). Functional Analysis of Novel Genes of *Staphylococcus aureus*. University of Sheffield.

- Feucht, A., Lucet, I., Yudkin, M.D., and Errington, J. (2001). Cytological and biochemical characterization of the FtsA cell division protein of *Bacillus subtilis*. *Mol. Microbiol.* **40**, 115–125.
- Fey, P.D., Endres, J.L., Yajjala, V.K., Widhelm, T.J., Boissy, R.J., Bose, J.L., and Bayles, K.W. (2013). A genetic resource for rapid and comprehensive phenotype screening of nonessential *Staphylococcus aureus* genes. *MBio* **4**, 1–8.
- Figueiredo, T.A., Sobral, R.G., Ludovice, A.M., de Almeida, J.M.F., Bui, N.K., Vollmer, W., de Lencastre, H., and Tomasz, A. (2012). Identification of genetic determinants and enzymes involved with the amidation of glutamic acid residues in the peptidoglycan of *Staphylococcus aureus*. *PLoS Pathog.* **8**.
- Firtel, M., Henderson, G., and Sokolov, I. (2004). Nanosurgery: Observation of peptidoglycan strands in *Lactobacillus helveticus* cell walls. *Ultramicroscopy* **101**, 105–109.
- Foster, S.J., and Johnstone, K. (1987). Purification and properties of a germination-specific cortex-lytic enzyme from spores of *Bacillus megaterium* KM. *Biochem. J.* **242**, 573–579.
- Foster, T.J., and Hook, M. (1998). Surface protein adhesins of *Staphylococcus aureus*. *Trends Microbiol.* **6**, 484–488.
- Frankel, M.B., and Schneewind, O. (2012). Determinants of murein hydrolase targeting to cross-wall of *Staphylococcus aureus* peptidoglycan. *J. Biol. Chem.* **287**, 10460–10471.
- Fridman, O., Goldberg, A., Ronin, I., Shores, N., and Balaban, N.Q. (2014). Optimization of lag time underlies antibiotic tolerance in evolved bacterial populations. *Nature* **513**, 418–421.
- Fu, G., Huang, T., Buss, J., Coltharp, C., Hensel, Z., and Xiao, J. (2010). In Vivo structure of the *E. coli* FtsZ-ring revealed by photoactivated localization microscopy (PALM). *PLoS One* **5**, 1–16.
- Fuchs-Cleveland, E., and Gilvarg, C. (1976). Oligomeric intermediate in peptidoglycan biosynthesis in *Bacillus megaterium*. *Proc. Natl. Acad. Sci. U. S. A.* **73**, 4200–4204.
- Galli, E., and Gerdes, K. (2010). Spatial resolution of two bacterial cell division proteins: ZapA recruits ZapB to the inner face of the Z-ring. *Mol. Microbiol.* **76**, 1514–1526.
- Gan, L., and Jensen, G.J. (2012). Electron tomography of cells. *Quarterly Rev. Biophys.* **45**, 27–56.
- Gan, L., Chen, S., and Jensen, G.J. (2008). Molecular organization of Gram-negative peptidoglycan. *105*, 18953–18957.
- García-Lara, J., Weihs, F., Ma, X., Walker, L., Chaudhuri, R.R., Kasturiarachchi, J., Crossley, H., Golestanian, R., and Foster, S.J. (2015). Supramolecular structure in the membrane of *Staphylococcus aureus*. *Proc. Natl. Acad. Sci.* 201509557.
- Garner, E.C., Bernard, R., Wang, W., Zhuang, X., Rudner, D.Z., and Mitchison, T. (2011).

- Coupled, Circumferential Motions of the Cell Wall Synthesis Machinery and MreB Filaments in *B. subtilis*. *Science* (80-). 333, 222–225.
- Gautam, S., Kim, T., and Spiegel, D.A. (2015). Chemical Probes Reveal an Extraseptal Mode of Cross-Linking in *Staphylococcus aureus*. *J. Am. Chem. Soc.* 150602131608004.
- Gautier, A., Juillerat, A., Heinis, C., Correa, I.R., Kindermann, M., Beaufils, F., and Johnsson, K. (2008). An Engineered Protein Tag for Multiprotein Labeling in Living Cells. *Chem. Biol.* 15, 128–136.
- Georgieva, M., and Nollmann, M. (2015). Superresolution microscopy for bioimaging at the nanoscale: from concepts to applications in the nucleus. *Res. Rep. Biol. Volume 6*, 157.
- Ghuysen, J. (1968). Use of Bacteriolytic Enzymes in Determination of Wall Structure and Their Role in Cell Metabolism. *Bacteriol. Rev.* 32, 425–464.
- Giesbrecht, P., Kersten, T., Maidhof, H., and Wecke, J. (1997). Two alternative mechanisms of cell separation in staphylococci: one lytic and one mechanical. *Arch. Microbiol.* 167, 239–250.
- Giesbrecht, P., Kersten, T., Maidhof, H., and Wecke, J. (1998). Staphylococcal cell wall: morphogenesis and fatal variations in the presence of penicillin. *Microbiol. Mol. Biol. Rev.* 62, 1371–1414.
- Glauner, B., Höltje, J.V., and Schwarz, U. (1988). The composition of the murein of *Escherichia coli*. *J. Biol. Chem.* 263, 10088–10095.
- Goley, E.D., Comolli, L.R., Fero, K.E., Downing, K.H., and Shapiro, L. (2010). DipM links peptidoglycan remodelling to outer membrane organization in *Caulobacter*. *Mol. Microbiol.* 77, 56–73.
- Le Gouëllec, A., Roux, L., Fadda, D., Massidda, O., Vernet, T., and Zapun, A. (2008). Roles of pneumococcal DivIB in cell division. *J. Bacteriol.* 190, 4501–4511.
- Gründling, A., and Schneewind, O. (2007). Synthesis of glycerol phosphate lipoteichoic acid in *Staphylococcus aureus*. *Proc. Natl. Acad. Sci. U. S. A.* 104, 8478–8483.
- Gustafsson, M.G.L. (2000). Surpassing the lateral resolution limit by a factor of two using structured illumination microscopy. *198*, 82–87.
- Gustafsson, M.G.L. (2005). Nonlinear structured-illumination microscopy: wide-field fluorescence imaging with theoretically unlimited resolution. *Proc. Natl. Acad. Sci. U. S. A.* 102, 13081–13086.
- Hamoen, L.W., Meile, J.C., De Jong, W., Noirot, P., and Errington, J. (2006). SepF, a novel FtsZ-interacting protein required for a late step in cell division. *Mol. Microbiol.* 59, 989–999.
- Hanaki, H., Kuwahara-Arai, K., Boyle-Vavra, S., Daum, R.S., Labischinski, H., and Hiramatsu, K. (1998). Activated cell-wall synthesis is associated with vancomycin resistance in methicillin-resistant *Staphylococcus aureus* clinical strains Mu3 and Mu50. *J. Antimicrob. Chemother.* 42, 199–209.

- Harz, H., Burgdorf, K., and Höltje, J.V. (1990). Isolation and separation of the glycan strands from murein of *Escherichia coli* by reversed-phase high-performance liquid chromatography. *Anal. Biochem.* *190*, 120–128.
- Hashimoto, M., Ooiwa, S., and Sekiguchi, J. (2012). Synthetic lethality of the *lytE* *cwlo* genotype in *Bacillus subtilis* is caused by lack of D, L-endopeptidase activity at the lateral cell wall. *J. Bacteriol.* *194*, 796–803.
- Haydon, D.J., Stokes, N.R., Ure, R., Galbraith, G., Bennett, J.M., Brown, D.R., Baker, P.J., Barynin, V. V., Rice, D.W., Sedelnikova, S.E., et al. (2008). An inhibitor of FtsZ with potent and selective anti-staphylococcal activity. *Science* (80-). *321*, 1673–1675.
- Hayhurst, E.J., Kailas, L., Hobbs, J.K., and Foster, S.J. (2008). Cell wall peptidoglycan architecture in *Bacillus subtilis*. *Proc. Natl. Acad. Sci. U. S. A.* *105*, 14603–14608.
- Heidrich, C., Templin, M.F., Ursinus, A., Merdanovic, M., Schwarz, H., de Pedro, M.A., and Höltje, J.V. (2001). Involvement of N -acetylmuramyl- L -alanine amidases in cell separation and antibiotic-induced autolysis of *Escherichia coli*. *Mol. Microbiol.* *41*, 167–178.
- Heidrich, C., Ursinus, A., Berger, J., Schwarz, H., and Höltje, J.V. (2002). Effects of multiple deletions of murein hydrolases on viability, septum cleavage, and sensitivity to large toxic molecules in *Escherichia coli*. *J. Bacteriol.* *184*, 6093–6099.
- van Heijenoort, J. (2007). Lipid intermediates in the biosynthesis of bacterial peptidoglycan. *Microbiol. Mol. Biol. Rev.* *71*, 620–635.
- Heilemann, M., Van De Linde, S., Schüttpelz, M., Kasper, R., Seefeldt, B., Mukherjee, A., Tinnefeld, P., and Sauer, M. (2008). Subdiffraction-resolution fluorescence imaging with conventional fluorescent probes. *Angew. Chemie - Int. Ed.* *47*, 6172–6176.
- Helaine, S., and Holden, D.W. (2013). Heterogeneity of intracellular replication of bacterial pathogens. *Curr. Opin. Microbiol.* *16*, 184–191.
- Helaine, S., and Kugelberg, E. (2014). Bacterial persisters: Formation, eradication, and experimental systems. *Trends Microbiol.* *22*, 417–424.
- Helaine, S., Thompson, J.A., Watson, K.G., Liu, M., Boyle, C., and Holden, D.W. (2010). Dynamics of intracellular bacterial replication at the single cell level. *Proc. Natl. Acad. Sci. U. S. A.* *107*, 3746–3751.
- Helaine, S., Cheverton, A.M., Watson, K.G., Faure, L.M., Matthews, S.A., and Holden, D.W. (2014). Internalization of *Salmonella* by Macrophages Induces Formation of Nonreplicating Persisters. *Science* (80-). *343*, 204–208.
- Hell, S.W., and Wichman, J. (1994). Breaking the diffraction resolution limit by stimulated emission: stimulated-emission-depletion fluorescence microscopy. *Opt. Lett.* *19*, 780–782.
- Henriques, R., Griffiths, C., Hesper Rego, E., and Mhlanga, M.M. (2011). PALM and STORM: Unlocking live-cell super-resolution. *Biopolymers* *95*, 322–331.
- Holden, S.J., Pengo, T., Meibom, K.L., Fernandez Fernandez, C., Collier, J., and Manley,

- S. (2014). High throughput 3D super-resolution microscopy reveals *Caulobacter crescentus* in vivo Z-ring organization. *Proc. Natl. Acad. Sci. U. S. A.* *111*, 4566–4571.
- Holmes, N.E., Johnson, P.D.R., and Howden, B.P. (2012). Relationship between vancomycin-resistant *Staphylococcus aureus*, vancomycin-intermediate *S. aureus*, high vancomycin MIC, and outcome in serious *S. aureus* infections. *J. Clin. Microbiol.* *50*, 2548–2552.
- Höltje, J.V. (1998). Growth of the stress-bearing and shape-maintaining murein sacculus of *Escherichia coli*. *Microbiol. Mol. Biol. Rev.* *62*, 181–203.
- Höltje, J.V., and Heidrich, C. (2001). Enzymology of elongation and constriction of the murein sacculus of *Escherichia coli*. *Biochimie* *83*, 103–108.
- Höltje, J.V., Mirelman, D., Sharon, N., and Schwarz, U. (1975). Novel type of murein transglycosylase in *Escherichia coli*. *J. Bacteriol.* *124*, 1067–1076.
- Hoppert, M., and Mayer, F. (1999). Principles of macromolecular organization and cell function in bacteria and archaea. *Cell Biochem. Biophys.* *31*, 247–284.
- Horsburgh, M.J., Aish, J.L., White, I.J., Shaw, L., Lithgow, J.K., and Foster, S.J. (2002). σ^B Modulates Virulence Determinant Expression and Stress Resistance: Characterization of a Functional rsbU Strain Derived from *Staphylococcus aureus* 8325-4. *J. Bacteriol.* *184*, 5457–5467.
- Howden, B.P., Davies, J.K., Johnson, P.D.R., Steinar, T.P., and Grayson, M.L. (2010). Reduced vancomycin susceptibility in *Staphylococcus aureus*, including vancomycin-intermediate and heterogeneous vancomycin-intermediate strains: Resistance mechanisms, laboratory detection, and clinical implications. *Clin. Microbiol. Rev.* *23*, 99–139.
- Hu, Z., and Lutkenhaus, J. (1999). Topological regulation of cell division in *Escherichia coli* involves rapid pole to pole oscillation of the division inhibitor MinC under the control of MinD and MinE. *Mol. Microbiol.* *34*, 82–90.
- Huang, B., Wang, W., Bates, M., and Zhuang, X. (2008). Three-Dimensional Super-Resolution Reconstruction Microscopy. *Science* (80-.). *319*, 810–813.
- Huang, B., Babcock, H., and Zhuang, X. (2010). Breaking the diffraction barrier: super-resolution imaging of cells. *Cell* *143*, 1047–1058.
- Huh, D., and Paulsson, J. (2011). Non-genetic heterogeneity from stochastic partitioning at cell division. *Nat. Genet.* *43*, 95–100.
- Jennings, P.C., Cox, G.C., Monahan, L.G., and Harry, E.J. (2011). Super-resolution imaging of the bacterial cytokinetic protein FtsZ. *Micron* *42*, 336–341.
- Jones, L.J.F., Carballido-López, R., and Errington, J. (2001). Control of cell shape in bacteria: Helical, actin-like filaments in *Bacillus subtilis*. *Cell* *104*, 913–922.
- Jones, S.A., Shim, S.-H., He, J., and Zhuang, X. (2011). Fast, three-dimensional super-resolution imaging of live cells. *8*, 499–505.

- Jorge, A.M., Hoiczky, E., Gomes, J.P., and Pinho, M.G. (2011). EzrA contributes to the regulation of cell size in *Staphylococcus aureus*. *PLoS One* *6*, e27542.
- Jovetic, S., Zhu, Y., Marcone, G.L., Marinelli, F., and Tramper, J. (2010). β -Lactam and glycopeptide antibiotics: first and last line of defense? *Trends Biotechnol.* *28*, 596–604.
- Kajimura, J., Fujiwara, T., Yamada, S., Suzawa, Y., Nishida, T., Oyamada, Y., Hayashi, I., Yamagishi, J., Komatsuzawa, H., and Sugai, M. (2005). Identification and molecular characterization of an N-acetylmuramyl-L-alanine amidase Sle1 involved in cell separation of *Staphylococcus aureus*. *Mol. Microbiol.* *58*, 1087–1101.
- Kamio, Y., and Nikaido, H. (1976). Outer membrane of *Salmonella typhimurium*: accessibility of phospholipid head groups to phospholipase c and cyanogen bromide activated dextran in the external medium. *Biochemistry* *15*, 2561–2570.
- Kaul, M., Mark, L., Zhang, Y., Parhi, A.K., Lyu, Y.L., Pawlak, J., Saravolatz, S., Saravolatz, L.D., Weinstein, M.P., LaVoie, E.J., et al. (2015). TXA709: A FtsZ-Targeting Benzamide Prodrug with Improved Pharmacokinetics and Enhanced In Vivo Efficacy against Methicillin-Resistant *Staphylococcus aureus*. *Antimicrob. Agents Chemother.* AAC.00708–00715.
- Kent, V. (2013). Cell wall architecture and the role of wall teichoic acids in *Staphylococcus aureus*. University of Sheffield.
- Keppler, A., Gendreizig, S., Gronemeyer, T., Pick, H., Vogel, H., and Johnsson, K. (2003). A general method for the covalent labeling of fusion proteins with small molecules *in vivo*. *Nat. Biotechnol.* *21*, 86–89.
- Kim, S.J., Singh, M., Preobrazhenskaya, M., and Schaefer, J. (2013). *Staphylococcus aureus* Peptidoglycan Stem Packing by Rotational-Echo Double Resonance NMR Spectroscopy. *Biochemistry*.
- Kim, S.J., Chang, J., and Singh, M. (2014). Peptidoglycan architecture of Gram-positive bacteria by solid-state NMR. *Biochim. Biophys. Acta* 1–13.
- Koch, A.L. (1985). Bacterial wall growth and division or life without actin. *Trends Biochem. Sci.* *10*, 11–14.
- Koch, A.L. (1998a). Orientation of the peptidoglycan chains in the sacculus of *Escherichia coli*. *Res. Microbiol.* *149*, 689–701.
- Koch, A.L. (1998b). The three-for-one model for Gram-negative wall growth: A problem and a possible solution. *FEMS Microbiol. Lett.* *162*, 127–134.
- Kraft, A.R., Prabhu, J., Ursinus, A., and Höltje, J.V. (1999). Interference with murein turn over has no effect on growth but reduces β -lactamase induction in *Escherichia coli*. *J. Bacteriol.* *181*, 7192–7198.
- Kuroda, M., Ohta, T., Uchiyama, I., Baba, T., Yuzawa, H., Kobayashi, I., Cui, L., Oguchi, A., Aoki, K., Nagai, Y., et al. (2001). Whole genome sequencing of methicillin-resistant *Staphylococcus aureus*. *Lancet Infect. Dis.* *357*, 1225–1240.
- Kuru, E., Hughes, H.V., Brown, P.J., Hall, E., Tekkam, S., Cava, F., de Pedro, M.A., Brun,

- Y. V, and VanNieuwenhze, M.S. (2012). In Situ probing of newly synthesized peptidoglycan in live bacteria with fluorescent D-amino acids. *Angew. Chemie Int. Ed.* *51*, 12519–12523.
- Kuru, E., Tekkam, S., Hall, E., Brun, Y. V, and VanNieuwenhze, M.S. (2015). Synthesis of fluorescent D-amino acids and their use for probing peptidoglycan synthesis and bacterial growth in situ. *Nat. Protoc.* *10*, 33–52.
- Lam, H., Oh, D.-C., Cava, F., Takacs, C.N., Clardy, J., de Pedro, M.A., and Waldor, M.K. (2009). D-Amino Acids Govern Stationary Phase. *Science* (80-.). *325*, 1552–1555.
- Leaver, M., and Errington, J. (2005). Roles for MreC and MreD proteins in helical growth of the cylindrical cell wall in *Bacillus subtilis*. *Mol. Microbiol.* *57*, 1196–1209.
- Lebar, M.D., May, J.M., Meeske, A.J., Leiman, S.A., Lupoli, T.J., Tsukamoto, H., Losick, R., Rudner, D.Z., Walker, S., and Kahne, D. (2014). Reconstitution of peptidoglycan cross-linking leads to improved fluorescent probes of cell wall synthesis. *J. Am. Chem. Soc.*
- Lee, T.K., and Huang, K.C. (2013). The role of hydrolases in bacterial cell-wall growth. *Curr. Opin. Microbiol.* *16*, 760–766.
- Lenarcic, R., Halbedel, S., Visser, L., Shaw, M., Wu, L.J., Errington, J., Marenduzzo, D., and Hamoen, L.W. (2009). Localisation of DivIVA by targeting to negatively curved membranes. *EMBO J.* *28*, 2272–2282.
- Levin, P.A., Kurtser, I.G., and Grossman, A.D. (1999). Identification and characterization of a negative regulator of FtsZ ring formation in *Bacillus subtilis*. *Proc. Natl. Acad. Sci. U. S. A.* *96*, 9642–9647.
- Levin-Reisman, I., and Balaban, N.Q. (2016). Quantitative Measurements of Type I and Type II Persisters Using ScanLag. In *Bacterial Persistence: Methods and Protocols*, J. Michiels, and M. Fauvart, eds. pp. 75–81.
- Lewis, K. (2010). Persister cells. *Annu. Rev. Microbiol.* *64*, 357–372.
- Li, Z., Trimble, M.J., Brun, Y. V, and Jensen, G.J. (2007). The structure of FtsZ filaments in vivo suggests a force-generating role in cell division. *EMBO J.* *26*, 4694–4708.
- Liechti, G.W., Kuru, E., Hall, E., Kalinda, A., Brun, Y. V, VanNieuwenhze, M.S., and Maurelli, A.T. (2013). A new metabolic cell-wall labelling method reveals peptidoglycan in *Chlamydia trachomatis*. *Nature*.
- Llewelyn, M., and Cohen, J. (2002). Superantigens: Microbial agents that corrupt immunity. *Lancet Infect. Dis.* *2*, 156–162.
- Loose, M., and Mitchison, T.J. (2014). The bacterial cell division proteins FtsA and FtsZ self-organize into dynamic cytoskeletal patterns. *Nat. Cell Biol.* *16*, 38–46.
- Lovering, A.L., de Casro, L.H., Lim, D., and Strynadka, N.C.J. (2007). Structural Insight into the Transglycosylation Step of Bacterial Cell-Wall Biosynthesis. *Science* (80-.). *1402315*, 1402–1405.

- Lovering, A.L., Safadi, S.S., and Strynadka, N.C.J. (2012). Structural perspective of peptidoglycan biosynthesis and assembly. *Annu. Rev. Biochem.* *81*, 451–478.
- Löwe, J., and Amos, L.A. (1998). Crystal structure of the bacterial cell-division protein FtsZ. *Nature* *391*, 203–206.
- Maki, H., Miura, K., and Yamano, Y. (2001). Katanosin B and plusbacin A(3), inhibitors of peptidoglycan synthesis in methicillin-resistant *Staphylococcus aureus*. *Antimicrob. Agents Chemother.* *45*, 1823–1827.
- Margolin, W. (2000). Themes and variations in prokaryotic cell division. *FEMS Microbiol. Rev.* *24*, 531–548.
- Marshall, J.H., and Wilmoth, G.J. (1981). Pigments of *Staphylococcus aureus*, a series of triterpenoid carotenoids. *J. Bacteriol.* *147*, 900–913.
- Matias, V.R.F., and Beveridge, T.J. (2006). Native cell wall organization shown by cryo-electron microscopy confirms the existence of a periplasmic space in *Staphylococcus aureus*. *J. Bacteriol.* *188*, 1011–1021.
- Matias, V.R.F., and Beveridge, T.J. (2007). Cryo-electron microscopy of cell division in *Staphylococcus aureus* reveals a mid-zone between nascent cross walls. *Mol. Microbiol.* *64*, 195–206.
- McAdams, H., and Arkin, A. (1999). It's a noisy business: Genetic regulation at the nanomolecular scale. *Trends Genet.* *15*, 65–69.
- McCloy, R.A., Rogers, S., Caldon, C.E., Lorca, T., Castro, A., and Burgess, A. (2014). Partial inhibition of Cdk1 in G₂ phase overrides the SAC and decouples mitotic events. *Cell Cycle* *13*, 1400–1412.
- McDonough, M.A., Anderson, J.W., Silvaggi, N.R., Pratt, R.F., Knox, J.R., and Kelly, J.A. (2002). Structures of two kinetic intermediates reveal species specificity of penicillin-binding proteins. *J. Mol. Biol.* *322*, 111–122.
- Memmel, E., Homann, A., Oelschlaeger, T.A., and Seibel, J. (2013). Metabolic glycoengineering of *Staphylococcus aureus* reduces its adherence to human T24 bladder carcinoma cells. *Chem. Commun.* *49*, 7301–7303.
- Merad, T., Archibald, A.R., Hancock, I.C., Harwood, C.R., and Hobot, J.A. (1989). Cell wall assembly in *Bacillus subtilis*: visualization of old and new wall material by electron microscopic examination of samples stained selectively for teichoic acid and teichuronic acid. *J. Gen. Microbiol.* *135*, 645–655.
- Mercer, K.L.N., and Weiss, D.S. (2002). The *Escherichia coli* cell division protein FtsW is required to recruit its cognate transpeptidase, FtsI (PBP3), to the division site. *J. Bacteriol.* *184*, 904–912.
- Migocki, M.D., Freeman, M.K., Wake, R.G., and Harry, E.J. (2002). The Min system is not required for precise placement of the midcell Z ring in *Bacillus subtilis*. *EMBO Rep.* *3*, 1163–1167.
- Mingorance, J., Rivas, G., Vélez, M., Gómez-Puertas, P., and Vicente, M. (2010). Strong

FtsZ is with the force: mechanisms to constrict bacteria. *Trends Microbiol.* **18**, 348–356.

Mohammadi, T., van Dam, V., Sijbrandi, R., Vernet, T., Zapun, A., Bouhss, A., Diepeveen-de Bruin, M., Nguyen-Distèche, M., de Kruijff, B., and Breukink, E. (2011). Identification of FtsW as a transporter of lipid-linked cell wall precursors across the membrane. *EMBO J.* **30**, 1425–1432.

Moll, A., Schlimpert, S., Briegel, A., Jensen, G.J., and Thanbichler, M. (2010). DipM, a new factor required for peptidoglycan remodelling during cell division in *Caulobacter crescentus*. *Mol. Microbiol.* **77**, 90–107.

Monteiro, J.M., Fernandes, P.B., Vaz, F., Pereira, A.R., Tavares, A.C., Ferreira, M.T., Pereira, P.M., Veiga, H., Kuru, E., VanNieuwenhze, M.S., et al. (2015). Cell shape dynamics during the staphylococcal cell cycle. *Nat. Commun.* **6**, 8055.

Morath, S. (2001). Structure-Function Relationship of Cytokine Induction by Lipoteichoic Acid from *Staphylococcus aureus*. *J. Exp. Med.* **193**, 393–398.

Moynihán, P.J., and Clarke, A.J. (2011). O-Acetylated peptidoglycan: Controlling the activity of bacterial autolysins and lytic enzymes of innate immune systems. *Int. J. Biochem. Cell Biol.* **43**, 1655–1659.

Moynihán, P.J., and Clarke, A.J. (2013). Assay for peptidoglycan O-acetyltransferase: A potential new antibacterial target. *Anal. Biochem.* **439**, 73–79.

Münch, D., Roemer, T., Lee, S.H., Engeser, M., Sahl, H.G., and Schneider, T. (2012). Identification and in vitro analysis of the GatD/MurT enzyme-complex catalyzing lipid II amidation in *Staphylococcus aureus*. *PLoS Pathog.* **8**, 1–11.

Murphy, D.B., and Davidson, M.W. (2013). *Fundamentals of Light Microscopy and Electronic Imaging* (Wiley-Blackwell).

Navarre, W.W., and Schneewind, O. (1999). Surface proteins of gram-positive bacteria and mechanisms of their targeting to the cell wall envelope. *Microbiol. Mol. Biol. Rev.* **63**, 174–229.

Nelson, D.E., and Young, K.D. (2001). Contributions of PBP 5 and dd-Carboxypeptidase Penicillin Binding Proteins to Maintenance of Cell Shape in *Escherichia coli*
Contributions of PBP 5 and DD -Carboxypeptidase Penicillin Binding Proteins to Maintenance of Cell Shape in *Escherichia coli*. *J. Bacteriol.* **183**, 3055–3064.

Neu, H.C. (1992). The crisis in antibiotic resistance. *Science* (80-.). **257**, 1064–1073.

Neuhaus, F.C., and Baddiley, J. (2003). A continuum of anionic charge: structures and functions of D-alanyl-teichoic acids in gram-positive bacteria. *Microbiol. Mol. Biol. Rev.* **67**, 686–723.

Ohnishi, R., Ishikawa, S., and Sekiguchi, J. (1999). Peptidoglycan hydrolase LytF plays a role in cell separation with Cw1F during vegetative growth of *Bacillus subtilis*. *J. Bacteriol.* **181**, 3178–3184.

Osawa, M., Anderson, D.E., and Erickson, H.P. (2008). Reconstitution of contractile FtsZ

rings in liposomes. *Science* (80-). *320*, 792–794.

Ovesný, M., Křížek, P., Borkovec, J., Svindrych, Z., and Hagen, G.M. (2014). ThunderSTORM: a comprehensive ImageJ plug-in for PALM and STORM data analysis and super-resolution imaging. *Bioinformatics* *30*, 2389–2390.

Paradis-Bleau, C., Markovski, M., Uehara, T., Lupoli, T.J., Walker, S., Kahne, D., and Bernhardt, T.G. (2010). Lipoprotein cofactors located in the outer membrane activate bacterial cell wall polymerases. *Cell* *143*, 1110–1120.

de Pedro, M.A., Quintela, J.C., Höltje, J.V., and Schwarz, H. (1997). Murein segregation in *Escherichia coli*. *J. Bacteriol.* *179*, 2823–2834.

Pereira, S.F.F., Henriques, A.O., Pinho, M.G., de Lencastre, H., and Tomasz, A. (2007). Role of PBP1 in cell division of *Staphylococcus aureus*. *J. Bacteriol.* *189*, 3525–3531.

Pereira, S.F.F., Henriques, A.O., Pinho, M.G., de Lencastre, H., and Tomasz, A. (2009). Evidence for a dual role of PBP1 in the cell division and cell separation of *Staphylococcus aureus*. *Mol. Microbiol.* *72*, 895–904.

Periasamy, S., Joo, H.-S., Duong, A.C., Bach, T.-H.L., Tan, V.Y., Chatterjee, S.S., Cheung, G.Y.C., and Otto, M. (2012). How *Staphylococcus aureus* biofilms develop their characteristic structure. *Proc. Natl. Acad. Sci. U. S. A.* *109*, 1281–1286.

Peschel, A., Otto, M., Jack, R.W., Kalbacher, H., Jung, G., and Gotz, F. (1999). Inactivation of the *dlt* Operon in *Staphylococcus aureus* Confers Sensitivity to Defensins, Protegrins, and Other Antimicrobial Peptides. *J. Biol. Chem.* *274*, 8405–8410.

Philippi, T., and Seger, J. (1989). Hedging one's evolutionary bets, revisited. *Trends Ecol. Evol.* *4*, 41–44.

Pichoff, S., and Lutkenhaus, J. (2002). Unique and overlapping roles for ZipA and FtsA in septal ring assembly in *Escherichia coli*. *EMBO J.* *21*, 685–693.

Pilhofer, M., Aistleitner, K., Biboy, J., Gray, J., Kuru, E., Hall, E., Brun, Y. V., VanNieuwenhze, M.S., Vollmer, W., Horn, M., et al. (2013). Discovery of chlamydial peptidoglycan reveals bacteria with murein sacculi but without FtsZ. *Nat. Commun.* *4*, 2856.

Pinho, M.G., and Errington, J. (2003). Dispersed mode of *Staphylococcus aureus* cell wall synthesis in the absence of the division machinery. *Mol. Microbiol.* *50*, 871–881.

Pinho, M.G., and Errington, J. (2005). Recruitment of penicillin-binding protein PBP2 to the division site of *Staphylococcus aureus* is dependent on its transpeptidation substrates. *Mol. Microbiol.* *55*, 799–807.

Pinho, M.G., Filipe, S.R., de Lencastre, H., and Tomasz, A. (2001). Complementation of the essential peptidoglycan transpeptidase function of penicillin-binding protein 2 (PBP2) by the drug resistance protein PBP2A in *Staphylococcus aureus*. *J. Bacteriol.* *183*, 6525–6531.

Plomp, M., Leighton, T.J., Wheeler, K.E., Hill, H.D., and Malkin, A.J. (2007). In vitro high-

resolution structural dynamics of single germinating bacterial spores. *Proc. Natl. Acad. Sci. U. S. A.* *104*, 9644–9649.

Poggio, S., Takacs, C.N., Vollmer, W., and Jacobs-Wagner, C. (2010). A protein critical for cell constriction in the Gram-negative bacterium *Caulobacter crescentus* localizes at the division site through its peptidoglycan-binding LysM domains. *Mol. Microbiol.* *77*, 74–89.

Popham, D.L. (2013). Visualizing the production and arrangement of peptidoglycan in Gram-positive cells. *Mol. Microbiol.* *88*, 645–649.

Potluri, L.-P., de Pedro, M.A., and Young, K.D. (2012). *E. coli* low molecular weight penicillin binding proteins help orient septal FtsZ, and their absence leads to asymmetric cell division and branching. *Mol. Cell* *44*, 501–526.

Public Health England (2015). Bacteraemia; Voluntary surveillance of *Staphylococcus aureus* bacteraemia in England, Wales and Northern Ireland : 2007-2014.

Qiao, Y., Lebar, M.D., Schirner, K., Schaefer, K., Tsukamoto, H., Kahne, D., and Walker, S. (2014). Detection of Lipid-Linked Peptidoglycan Precursors by Exploiting an Unexpected Transpeptidase Reaction. *J. Am. Chem. Soc.* 8–11.

Ramadurai, L., Lockwood, K.J., Nadakavukaren, M.J., and Jayaswal, R.K. (1999). Characterization of a chromosomally encoded glycyglycine endopeptidase of *Staphylococcus aureus*. *Microbiology* *145*, 801–808.

Raskin, D.M., and de Boer, P. a (1997). The MinE ring: an FtsZ-independent cell structure required for selection of the correct division site in *E. coli*. *Cell* *91*, 685–694.

Rebets, Y., Lupoli, T.J., Qiao, Y., Schirner, K., Villet, R., Hooper, D., Kahne, D., and Walker, S. (2013). Moenomycin Resistance Mutations in *Staphylococcus aureus* Reduce Peptidoglycan Chain Length and Cause Aberrant Cell Division. *ACS Chem. Biol.*

Reed, P., Veiga, H., Jorge, A.M., Terrak, M., and Pinho, M.G. (2011). Monofunctional transglycosylases are not essential for *Staphylococcus aureus* cell wall synthesis. *J. Bacteriol.* *193*, 2549–2556.

Reed, P., Atilano, M.L., Alves, R., Hoiczky, E., Sher, X., Reichmann, N.T., Pereira, P.M., Roemer, T., Filipe, S.R., Pereira-Leal, J.B., et al. (2015). *Staphylococcus aureus* Survives with a Minimal Peptidoglycan Synthesis Machine but Sacrifices Virulence and Antibiotic Resistance. *PLOS Pathog.* *11*, e1004891.

Rego, E.H., Shao, L., Macklin, J.J., Winoto, L., Johansson, G.A., Kamps-Hughes, N., Davidson, M.W., and Gustafsson, M.G.L. (2012). Nonlinear structured-illumination microscopy with a photoswitchable protein reveals cellular structures at 50-nm resolution. *Proc. Natl. Acad. Sci.* *109*, E135–E143.

Reichmann, N.T., Piçarra Cassona, C., Monteiro, J.M., Bottomley, A.L., Corrigan, R.M., Foster, S.J., Pinho, M.G., and Gründling, A. (2014). Differential localization of LTA synthesis proteins and their interaction with the cell division machinery in *Staphylococcus aureus*. *Mol. Microbiol.* *92*, 273–286.

Reynolds, P.E. (1989). Structure, biochemistry and mechanism of action of

- glycopeptide antibiotics. *Eur. J. Clin. Microbiol. Infect. Dis.* **8**, 943–950.
- Romaniuk, J.A.H., and Cegelski, L. (2015). Bacterial cell wall composition and the influence of antibiotics by cell-wall and whole-cell NMR. *Philos. Trans. R. Soc. B Biol. Sci.* **370**, 20150024.
- Romberg, L., and Levin, P.A. (2003). Assembly dynamics of the bacterial cell division protein FtsZ: poised at the edge of stability. *Annu. Rev. Microbiol.* **57**, 125–154.
- Rowe, S.E., Conlon, B.P., Keren, I., and Lewis, K. (2016). Persisters: Methods for Isolation and Identifying Contributing Factors—A Review. In *Bacterial Persistence: Methods and Protocols*, J. Michiels, and M. Fauvart, eds. pp. 17–28.
- Rueff, A.S., Chastanet, A., Domínguez-Escobar, J., Yao, Z., Yates, J., Prejean, M.V., Delumeau, O., Noirot, P., Wedlich-Söldner, R., Filipe, S.R., et al. (2014). An early cytoplasmic step of peptidoglycan synthesis is associated to MreB in *Bacillus subtilis*. *Mol. Microbiol.* **91**, 348–362.
- Ruiz, N. (2015). Lipid Flippases for Bacterial Peptidoglycan Biosynthesis. *Lipid Insights* **8**, 21–31.
- Rust, M.J., Bates, M., and Zhuang, X. (2009). Stochastic optical reconstruction microscopy (STORM) provides sub-diffraction-limit image resolution. *3*, 793–795.
- Sauvage, E., Kerff, F., Terrak, M., Ayala, J.A., and Charlier, P. (2008). The penicillin-binding proteins: structure and role in peptidoglycan biosynthesis. *FEMS Microbiol. Rev.* **32**, 234–258.
- Schaefer, L.H., Schuster, D., and Schaffer, J. (2004). Structured illumination microscopy: artifact analysis and reduction utilizing a parameter optimization approach. *J. Microsc.* **216**, 165–174.
- Scheffers, D.-J., and Driessen, A.J.M. (2010). The Polymerization Mechanism of the Bacterial Cell Division Protein FtsZ. *FEBS Lett.* **506**, 6–10.
- Scheffers, D.-J., and Pinho, M.G. (2005). Bacterial cell wall synthesis: new insights from localization studies. *Microbiol. Mol. Biol. Rev.* **69**, 585–607.
- Scheffers, D.-J., and Tol, M.B. (2015). LipidII: Just Another Brick in the Wall? *PLOS Pathog.* **11**, e1005213.
- Scheffers, D.-J., Jones, L.J.F., and Errington, J. (2003). Several distinct localization patterns for penicillin-binding proteins in *Bacillus subtilis*. *Mol. Microbiol.* **51**, 749–764.
- Schleifer, K.H., and Kandler, O. (1972). Peptidoglycan types of bacterial cell walls and their taxonomic implications. *Bacteriol. Rev.* **36**, 407–477.
- Seligman, S.J., and Pincus, M.R. (1987). A Model for the Three-dimensional Structure of Peptidoglycan in Staphylococci. *J. Theor. Biol.* **124**, 275–292.
- Sham, L.-T., Butler, E.K., Lebar, M.D., Kahne, D., Bernhardt, T.G., and Ruiz, N. (2014). MurJ is the flippase of lipid-linked precursors for peptidoglycan biogenesis. *Science* (80-). **345**, 220–222.

- Sharpe, M.E., Hauser, P.M., Sharpe, R.G., and Errington, J. (1998). Evidence for Active Nucleoid Partitioning Length at Initiation of DNA Replication and Fluorescence Microscopy: Constancy of Cell. *J. Bacteriol.* *180*, 547–555.
- Sheldrick, G.M., Jones, P.G., Kennard, O., Williams, D.H., and Smith, G.A. (1978). Structure of vancomycin and its complex with acetyl-D-alanyl-D-alanine. *Nature* *271*, 223–225.
- Shieh, P., Siegrist, M.S., Cullen, A.J., and Bertozzi, C.R. (2014). Imaging bacterial peptidoglycan with near-infrared fluorogenic azide probes. *Proc. Natl. Acad. Sci. U. S. A.* *111*, 5456–5461.
- Shockman, G.D., and Barrett, J.F. (1983). Structure, Function, and Assembly of Cell Walls of Gram-Positive Bacteria. *Annu. Rev. Microbiol.* *37*, 501–527.
- Siegrist, M.S., Whiteside, S., Jewett, J.C., Aditham, A., Cava, F., and Bertozzi, C.R. (2013). D-amino acid chemical reporters reveal peptidoglycan dynamics of an intracellular pathogen. *ACS Chem. Biol.* *8*, 500–505.
- Silhavy, T.J., Kahne, D., and Walker, S. (2010). The bacterial cell envelope. *Cold Spring Harb. Perspect. Biol.* *2*, a000414.
- Singh, J.K., Makde, R.D., Kumar, V., and Panda, D. (2007). A membrane protein, EzrA, regulates assembly dynamics of FtsZ by interacting with the C-terminal tail of FtsZ. *Biochemistry* *46*, 11013–11022.
- Singh, S.K., Saisree, L., Amrutha, R.N., and Reddy, M. (2012). Three redundant murein endopeptidases catalyse an essential cleavage step in peptidoglycan synthesis of *Escherichia coli* K12. *Mol. Microbiol.* *86*, 1036–1051.
- Singh, S.K., Parveen, S., SaiSree, L., and Reddy, M. (2015). Regulated proteolysis of a cross-link-specific peptidoglycan hydrolase contributes to bacterial morphogenesis. *Proc. Natl. Acad. Sci. U. S. A.* *112*, 10956–10961.
- Smith, T.J., Blackman, S.A., and Foster, S.J. (2000). Autolysins of *Bacillus subtilis*: Multiple enzymes with multiple functions. *Microbiology* *146*, 249–262.
- Snowden, M.A., and Perkins, H.R. (1990). Peptidoglycan cross-linking in *Staphylococcus aureus*. An apparent random polymerisation process. *Eur. J. Biochem.* *191*, 373–377.
- Spratt, B.G., Zhou, J., Taylor, M., and Merrick, M.J. (1996). Monofunctional biosynthetic peptidoglycan transglycosylases. *Mol. Microbiol.* *19*, 639–647.
- Stapleton, M.R., Horsburgh, M.J., Hayhurst, E.J., Wright, L., Jonsson, I.-M., Tarkowski, A., Kokai-Kun, J.F., Mond, J.J., and Foster, S.J. (2007). Characterization of IsaA and SceD, two putative lytic transglycosylases of *Staphylococcus aureus*. *J. Bacteriol.* *189*, 7316–7325.
- Steele, V.R., Bottomley, A.L., García-Lara, J., Kasturiarachchi, J., and Foster, S.J. (2011). Multiple essential roles for EzrA in cell division of *Staphylococcus aureus*. *Mol. Microbiol.* *80*, 542–555.
- Stewart, M.K., Cummings, L.A., Johnson, M.L., Berezow, A.B., and Cookson, B.T. (2011).

- Regulation of phenotypic heterogeneity permits *Salmonella* evasion of the host caspase-1 inflammatory response. *Proc. Natl. Acad. Sci. U. S. A.* *108*, 20742–20747.
- Strauss, M.P., Liew, A.T.F., Turnbull, L., Whitchurch, C.B., Monahan, L.G., and Harry, E.J. (2012). 3D-SIM Super Resolution Microscopy Reveals a Bead-Like Arrangement for FtsZ and the Division Machinery: Implications for Triggering Cytokinesis. *PLoS Biol.* *10*, e1001389.
- Sundararajan, K., Miguel, A., Desmarais, S.M., Meier, E.L., Casey Huang, K., and Goley, E.D. (2015). The bacterial tubulin FtsZ requires its intrinsically disordered linker to direct robust cell wall construction. *Nat. Commun.* *6*, 7281.
- Swoboda, J.G., Campbell, J., Meredith, T.C., and Walker, S. (2010). Wall Teichoic Acid Function, Biosynthesis, and Inhibition. *ChemBioChem* *11*, 35–45.
- Szwedziak, P., and Löwe, J. (2013). Do the divisome and elongasome share a common evolutionary past? *Curr. Opin. Microbiol.* *16*, 745–751.
- Szwedziak, P., Wang, Q., Bharat, T.A.M., Tsim, M., and Löwe, J. (2014). Architecture of the ring formed by the tubulin homologue FtsZ in bacterial cell division. *Elife* *3*, e04601.
- Takahashi, J., Komatsuzawa, H., Yamada, S., Nishida, T., Labischinski, H., Fujiwara, T., Ohara, M., Yamagishi, J., and Sugai, M. (2002). Molecular characterization of an *atl* null mutant of *Staphylococcus aureus*. *Microbiol. Immunol.* *46*, 601–612.
- Tan, C.M., Therien, A.G., Lu, J., Lee, S.H., Caron, A., Gill, C.J., Lebeau-Jacob, C., Benton-Perdomo, L., Monteiro, J.M., Pereira, P.M., et al. (2012). Restoring methicillin-resistant *Staphylococcus aureus* susceptibility to β -lactam antibiotics. *Sci. Transl. Med.* *4*, 126ra35.
- van Teeffelen, S., Wang, S., Furchtgott, L., Huang, K.C., Wingreen, N.S., Shaevitz, J.W., and Gitai, Z. (2011). The bacterial actin MreB rotates, and rotation depends on cell-wall assembly. *Proc. Natl. Acad. Sci.* *108*, 15822–15827.
- Tiyanont, K., Doan, T., Lazarus, M.B., Fang, X., Rudner, D.Z., and Walker, S. (2006). Imaging peptidoglycan biosynthesis in *Bacillus subtilis* with fluorescent antibiotics. *Proc. Natl. Acad. Sci. U. S. A.* *103*, 11033–11038.
- Tocheva, E.I., López-Garrido, J., Hughes, H.V., Fredlund, J., Kuru, E., Vannieuwenhze, M.S., Brun, Y. V, Pogliano, K., and Jensen, G.J. (2013). Peptidoglycan transformations during *Bacillus subtilis* sporulation. *Mol. Microbiol.* *88*, 673–686.
- Todd, J.A., Roberts, A.N., Johnstone, K., Piggot, P.J., Winter, G., and Ellar, D.J. (1986). Reduced heat resistance of mutant spores after cloning and mutagenesis of the *Bacillus subtilis* gene encoding penicillin-binding protein 5. *J. Bacteriol.* *167*, 257–264.
- Touhami, A., Jericho, M.H., and Beveridge, T.J. (2004). Atomic Force Microscopy of Cell Growth and Division in *Staphylococcus aureus*. *J. Bacteriol.* *186*, 3286–3295.
- Tsui, H.-C.T., Boersma, M.J., Vella, S.A., Kocaoglu, O., Kuru, E., Peceny, J.K., Carlson, E.E., VanNieuwenhze, M.S., Brun, Y. V, Shaw, S.L., et al. (2014). PBP2x localises separately from PBP2B and other peptidoglycan synthesis proteins during later stages

of cell division of *Streptococcus pneumoniae* D39. *Mol. Microbiol.* *94*, 21–40.

Turner, R.D., Ratcliffe, E.C., Wheeler, R., Golestanian, R., Hobbs, J.K., and Foster, S.J. (2010a). Peptidoglycan architecture can specify division planes in *Staphylococcus aureus*. *Nat. Commun.* *1*, 26.

Turner, R.D., Thomson, N.H., Kirkham, J., and Devine, D. (2010b). Improvement of the pore trapping method to immobilize vital coccoid bacteria for high-resolution AFM: a study of *Staphylococcus aureus*. *J. Microsc.* *238*, 102–110.

Turner, R.D., Hurd, A.F., Cadby, A., Hobbs, J.K., and Foster, S.J. (2013). Cell wall elongation mode in Gram-negative bacteria is determined by peptidoglycan architecture. *Nat. Commun.* *4*, 1496.

Turner, R.D., Vollmer, W., and Foster, S.J. (2014). Different walls for rods and balls: The diversity of peptidoglycan. *Mol. Microbiol.* *91*, 862–874.

Typas, A., Banzhaf, M., Van Den Berg Van Saparoea, B., Verheul, J., Biboy, J., Nichols, R.J., Zietek, M., Beilharz, K., Kannenberg, K., Von Rechenberg, M., et al. (2010). Regulation of peptidoglycan synthesis by outer-membrane proteins. *Cell* *143*, 1097–1109.

Typas, A., Banzhaf, M., Gross, C.A., and Vollmer, W. (2012). From the regulation of peptidoglycan synthesis to bacterial growth and morphology. *Nat. Rev. Microbiol.* *10*, 123–136.

Tzagoloff, H., and Novick, R.P. (1977). Geometry of cell division in *Staphylococcus aureus*. *J. Bacteriol.* *129*, 343–350.

Uehara, T., and Park, J.T. (2007). An anhydro-*N*-acetylmuramyl-L-alanine amidase with broad specificity tethered to the outer membrane of *Escherichia coli*. *J. Bacteriol.* *189*, 5634–5641.

Varma, A., De Pedro, M.A., and Young, K.D. (2007). FtsZ directs a second mode of peptidoglycan synthesis in *Escherichia coli*. *J. Bacteriol.* *189*, 5692–5704.

Veening, J.-W., Igoshin, O.A., Eijlander, R.T., Nijland, R., Hamoen, L.W., and Kuipers, O.P. (2008). Transient heterogeneity in extracellular protease production by *Bacillus subtilis*. *Mol. Syst. Biol.* *4*, 184.

Veiga, H., Jorge, A.M., and Pinho, M.G. (2011). Absence of nucleoid occlusion effector Noc impairs formation of orthogonal FtsZ rings during *Staphylococcus aureus* cell division. *Mol. Microbiol.* *80*, 1366–1380.

Verstraeten, N., Knapen, W., Fauvart, M., and Michiels, J. (2016). A Historical Perspective on Bacterial Persistence. In *Bacterial Persistence: Methods and Protocols*, J. Michiels, and M. Fauvart, eds. pp. 3–13.

Verwer, R.W.H., and Nanninga, N. (1976). Electron Microscopy of isolated cell walls of *Bacillus subtilis* var. *niger*. *Arch. Microbiol.* *109*, 195–197.

Verwer, R.W.H., Nanninga, N., Keck, W., and Schwarz, U. (1978). Arrangement of glycan chains in the sacculus of *Escherichia coli*. *J. Bacteriol.* *136*, 723–729.

- Vollmer, W. (2006). The prokaryotic cytoskeleton: a putative target for inhibitors and antibiotics? *Appl. Microbiol. Biotechnol.* *73*, 37–47.
- Vollmer, W. (2008). Structural variation in the glycan strands of bacterial peptidoglycan. *FEMS Microbiol. Rev.* *32*, 287–306.
- Vollmer, W., and Bertsche, U. (2008). Murein (peptidoglycan) structure, architecture and biosynthesis in *Escherichia coli*. *Biochim. Biophys. Acta* *1778*, 1714–1734.
- Vollmer, W., and Höltje, J.V. (2004). The Architecture of the Murein (Peptidoglycan) in Gram-Negative Bacteria: Vertical Scaffold or Horizontal Layer(s)? *J. Bacteriol.* *186*, 5978–5987.
- Vollmer, W., and Seligman, S.J. (2010). Architecture of peptidoglycan: more data and more models. *Trends Microbiol.* *18*, 59–66.
- Vollmer, W., Blanot, D., and de Pedro, M.A. (2008a). Peptidoglycan structure and architecture. *FEMS Microbiol. Rev.* *32*, 149–167.
- Vollmer, W., Joris, B., Charlier, P., and Foster, S.J. (2008b). Bacterial peptidoglycan (murein) hydrolases. *FEMS Microbiol. Rev.* *32*, 259–286.
- Wada, A., and Watanabe, H. (1998). Penicillin-binding protein 1 of *Staphylococcus aureus* is essential for growth. *J. Bacteriol.* *180*, 2759–2765.
- Wang, J., Liu, Y., Wan, D., Fang, X., Li, T., Guo, Y., Chang, D., Su, L., Wang, Y., Zhao, J., et al. (2012a). Whole-Genome sequence of *Staphylococcus aureus* strain LCT-SA112. *J. Bacteriol.* *194*, 4124.
- Wang, S., Furchtgott, L., Huang, K.C., and Shaevitz, J.W. (2012b). Helical insertion of peptidoglycan produces chiral ordering of the bacterial cell wall. *Proc. Natl. Acad. Sci. U. S. A.* *109*, E595–E604.
- Wang, X., Huang, J., Mukherjee, A., Cao, C., and Lutkenhaus, J. (1997). Analysis of the interaction of FtsZ with itself, GTP, and FtsA. *J. Bacteriol.* *179*, 5551–5559.
- Ward, J.B., and Perkins, H.R. (1973). The direction of glycan synthesis in a bacterial peptidoglycan. *Biochem. J.* *135*, 721–728.
- Watanabe, S., Punge, A., Hollopeter, G., Willig, K.I., Hobson, R.J., Davis, M.W., Hell, S.W., and Jorgensen, E.M. (2011). Protein localization in electron micrographs using fluorescence nanoscopy. *Nat. Methods* *8*, 80–84.
- Waxman, D.J., and Strominger, J.L. (1983). Penicillin-binding proteins and the mechanism of action of beta-lactam antibiotics. *Annu. Rev. Biochem.* *52*, 825–869.
- Weart, R.B., Lee, A.H., Chien, A.-C., Haeusser, D.P., Hill, N.S., and Levin, P.A. (2007). A metabolic sensor governing cell size in bacteria. *Cell* *130*, 335–347.
- Wertheim, H.F., Melles, D.C., Vos, M.C., van Leeuwen, W., van Belkum, A., Verbrugh, H. a, and Nouwen, J.L. (2005). The role of nasal carriage in *Staphylococcus aureus* infections. *Lancet Infect. Dis.* *5*, 751–762.
- Wheeler, R. (2012). Peptidoglycan Architecture and Dynamics of Gram-Positive

Bacteria. University of Sheffield.

Wheeler, R., Mesnage, S., Boneca, I.G., Hobbs, J.K., and Foster, S.J. (2011). Super-resolution microscopy reveals cell wall dynamics and peptidoglycan architecture in ovococcal bacteria. *Mol. Microbiol.* *82*, 1096–1109.

Wheeler, R., Turner, R.D., Bailey, R.G., Salamaga, B., Mesnage, S., Mohamad, S.A.S., Hayhurst, E.J., Horsburgh, M.J., Hobbs, J.K., and Foster, S.J. (2015). Bacterial Cell Enlargement Requires Control of Cell Wall Stiffness Mediated by Peptidoglycan Hydrolases. *MBio* *6*, 1–10.

Wu, L.J., and Errington, J. (2011). Nucleoid occlusion and bacterial cell division. *Nat. Rev. Microbiol.* *10*, 8–12.

Wyke, A.W., Ward, J.B., Hayes, M. V, and Curtis, N.A.C. (1981). A role in vivo for penicillin-binding protein-4 of *Staphylococcus aureus*. *Eur. J. Biochem.* *119*, 389–393.

Xia, G., and Peschel, A. (2008). Toward the pathway of *S. aureus* WTA biosynthesis. *Chem. Biol.* *15*, 95–96.

Xia, G., Kohler, T., and Peschel, A. (2010). The wall teichoic acid and lipoteichoic acid polymers of *Staphylococcus aureus*. *Int. J. Med. Microbiol.* *300*, 148–154.

Yamada, S., Sugai, M., Komatsuzawa, H., Nakashima, S., Oshida, T., Matsumoto, A., and Suginaka, H. (1996). An Autolysin Ring Associated with Cell Separation of *Staphylococcus aureus*. *J. Bacteriol.* *178*, 1565–1571.

Yao, X., Jericho, M., Pink, D., and Beveridge, T.J. (1999). Thickness and elasticity of gram-negative murein sacculi measured by atomic force microscopy. *J. Bacteriol.* *181*, 6865–6875.

Young, K.D. (2014). A flipping cell wall ferry. *Science* (80-.). *345*, 139–140.

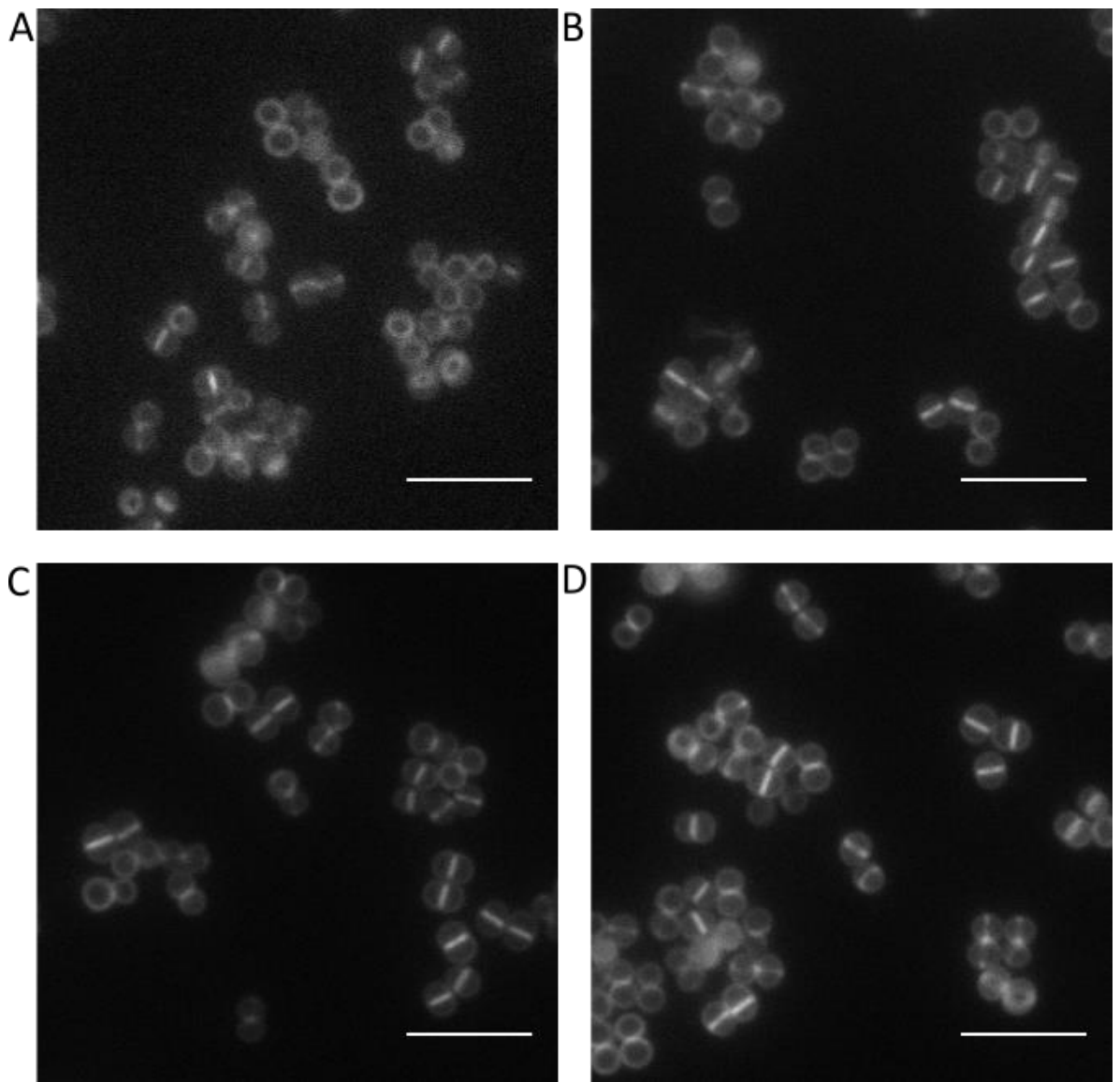
Yunck, R., Cho, H., and Bernhardt, T.G. (2015). Identification of MltG as a potential terminase for peptidoglycan polymerization in bacteria. *Mol. Microbiol.*

Zapun, A., Vernet, T., and Pinho, M.G. (2008a). The different shapes of cocci. *FEMS Microbiol. Rev.* *32*, 345–360.

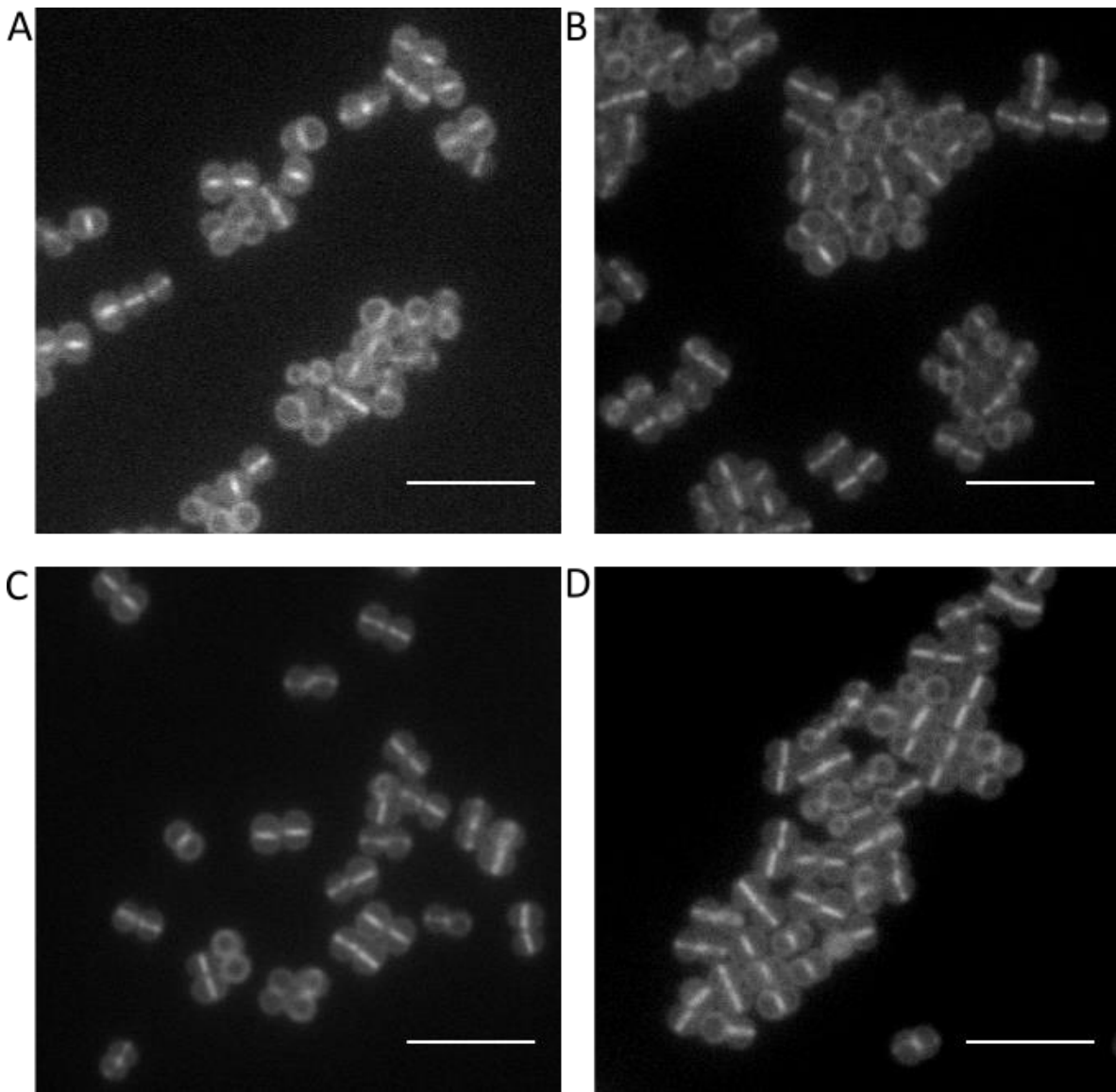
Zapun, A., Contreras-Martel, C., and Vernet, T. (2008b). Penicillin-binding proteins and beta-lactam resistance. *FEMS Microbiol. Rev.* *32*, 361–385.

Zhou, X., Halladin, D.K., Rojas, E.R., Koslover, E.F., Lee, T.K., Huang, K.C., and Theriot, J.A. (2015). Mechanical crack propagation drives millisecond daughter cell separation in *Staphylococcus aureus*. *Science* (80-.). *348*, 574–578.

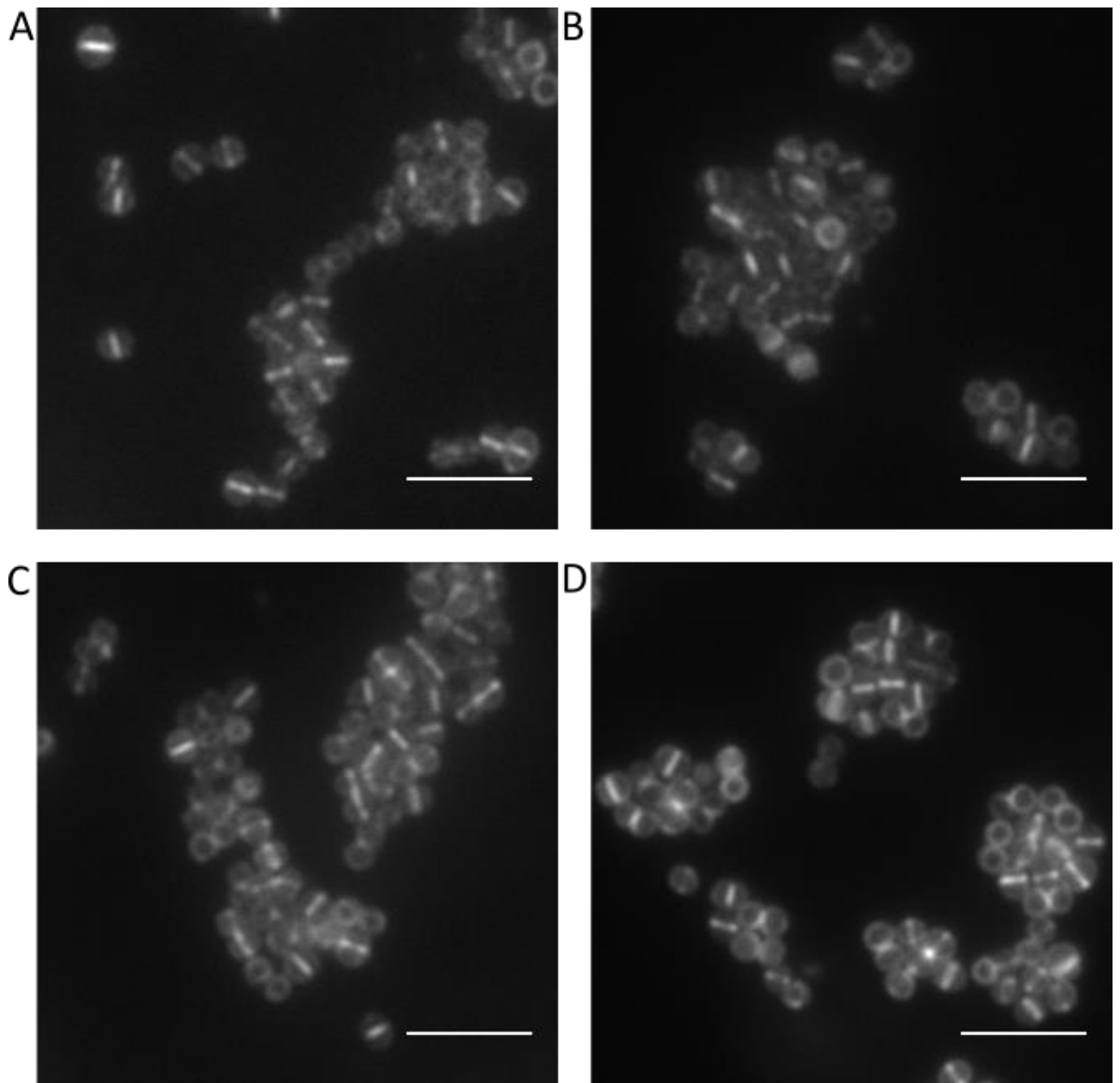
Appendix I - Pattern of FDAA labelling over time



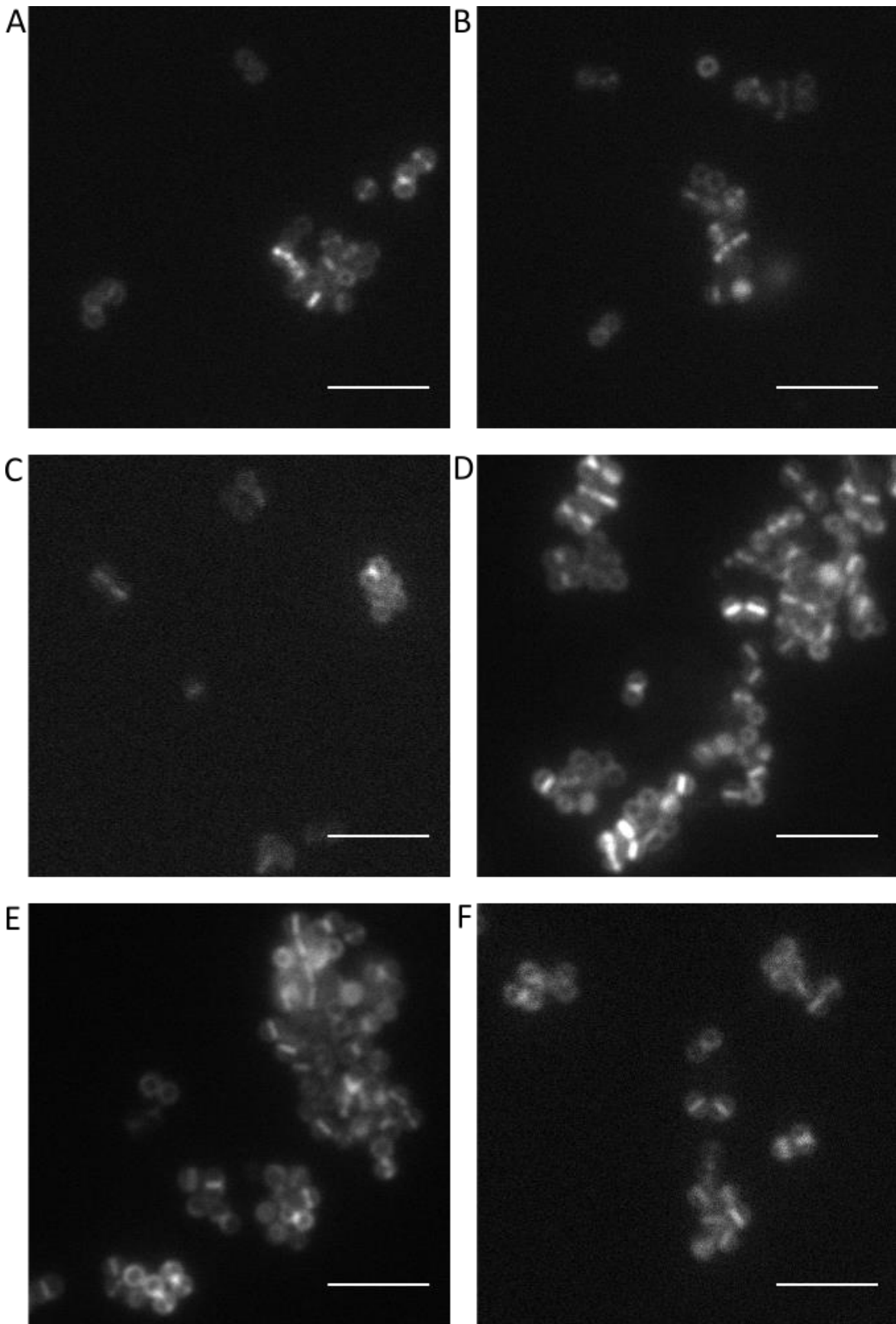
Appendix Figure 1. Incorporation of HADA over time. (A) 5 min. (B) 10 min, (C) 15 min, (D) 20 min HADA labelling. (Scale bar 5 μ m).



Appendix Figure 2. Incorporation of NADA over time. (A) 5min, (B) 10 min, (C) 15 min, (D) 20 min NADA labelling. (Scale bar 5 μ m).

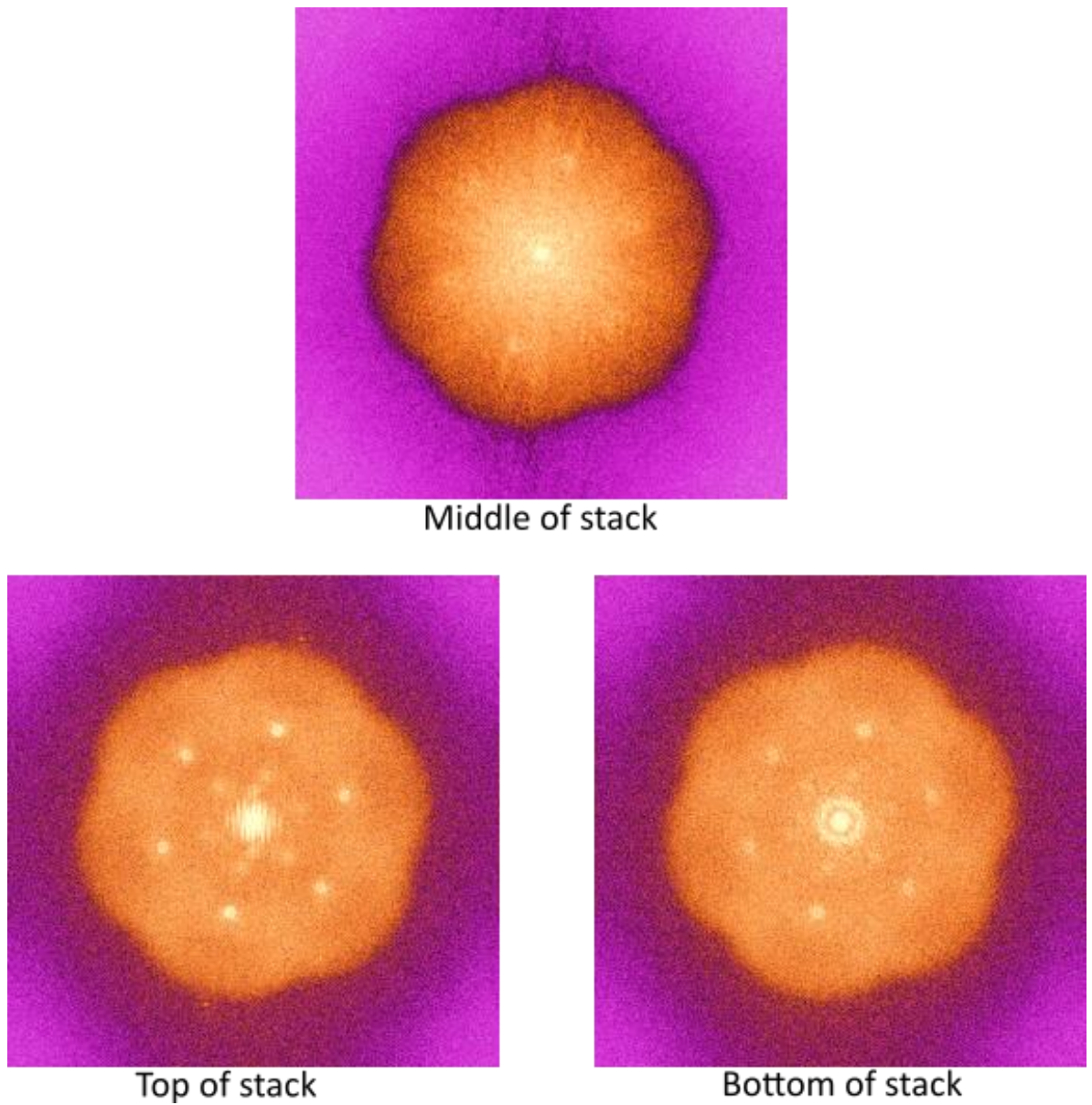


Appendix Figure 3. Incorporation of TADA over time. (A) 5min, (B) 10 min, (C) 15 min, (D) 20 min TADA labelling. (Scale bar 5 μ m).

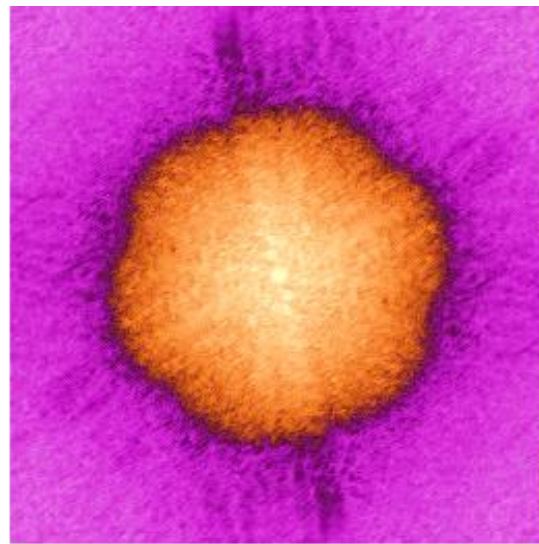


Appendix Figure 4. Incorporation of dipeptide over time. (A) 5min, (B) 10 min, (C) 15 min, (D) 20 min, (E) 25 min, (F) 30 min dipeptide labelling. (Scale bar 5 μ m).

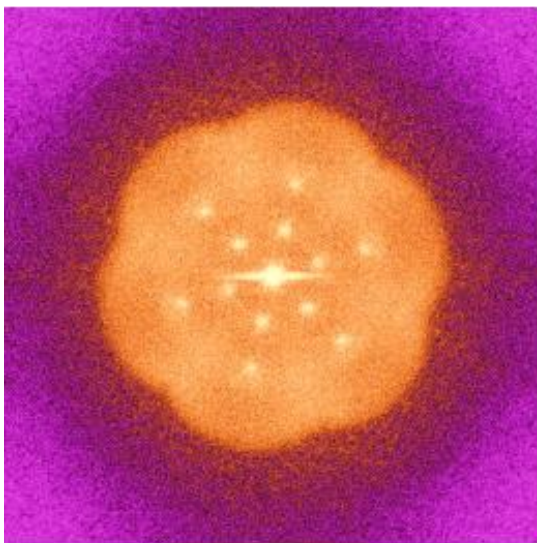
Appendix II - Fourier transform of SIM images



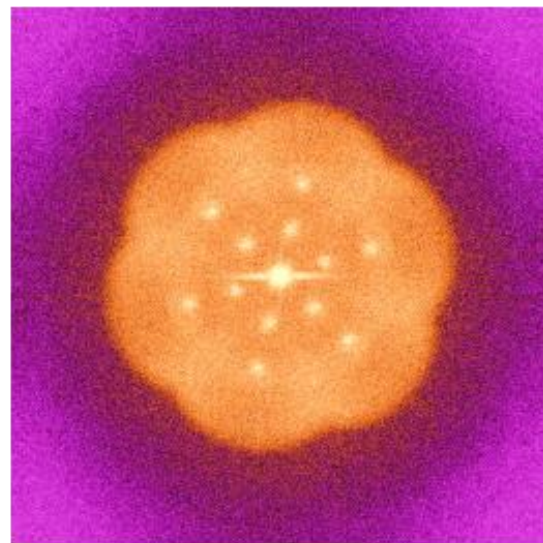
Appendix Figure 5. Fourier Transform of SH1000 labelled with NADA from Figure 3.24
B. Fourier transforms of slices from the top, middle and bottom of the z stack showing periodic structures. Far extents of z-stack were removed from projection within the figure.



Middle of stack

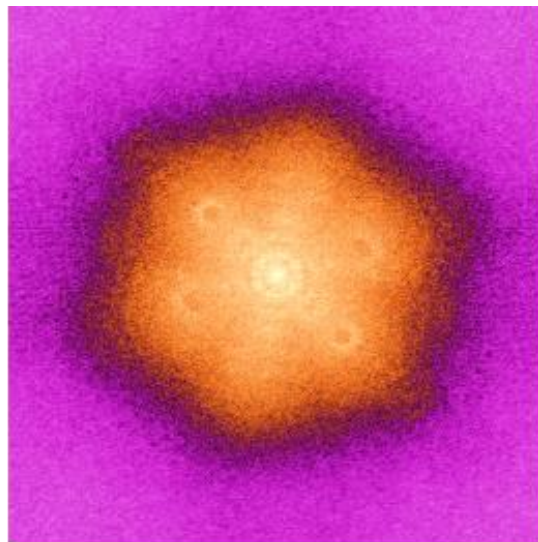


Top of stack

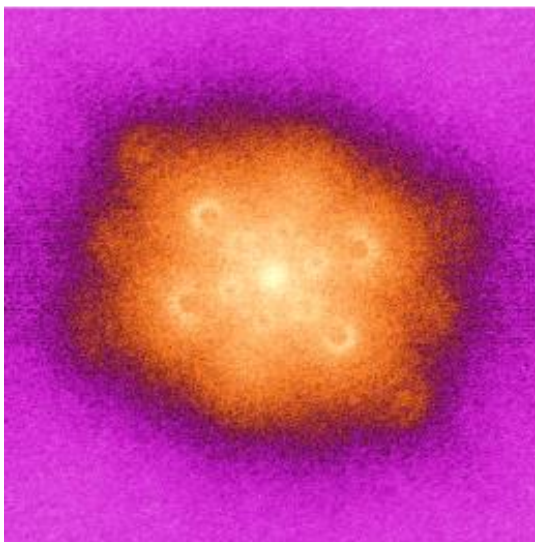


Bottom of stack

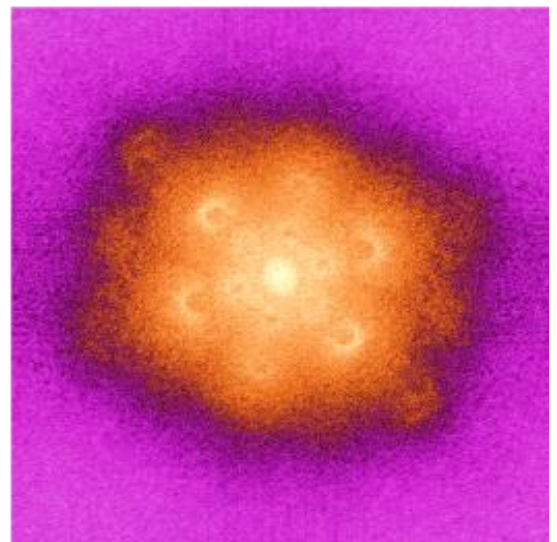
Appendix Figure 6. Fourier Transform of SH1000 labelled with TADA from Figure 3.24
C. Fourier transforms of slices from the top, middle and bottom of the z stack showing periodic structures.



Middle of stack

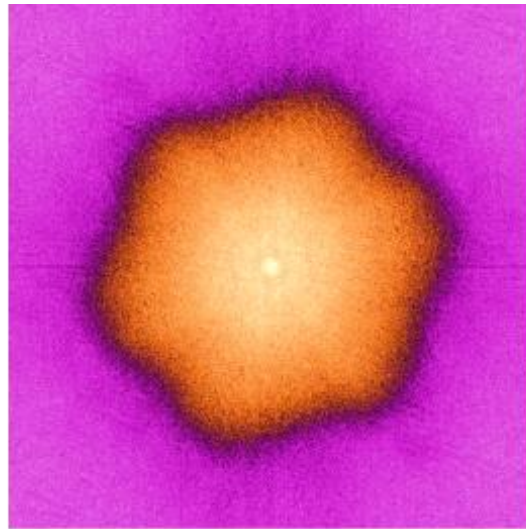


Top of stack

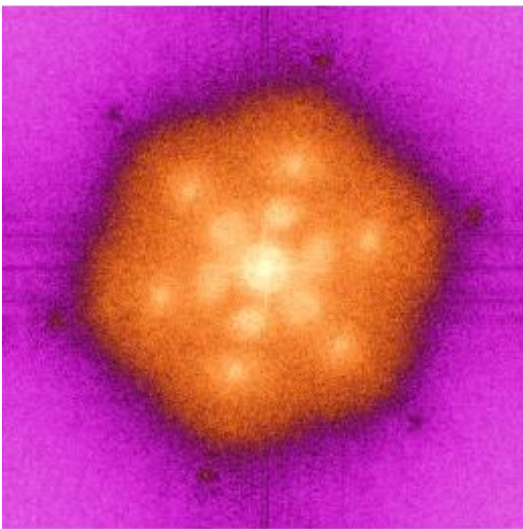


Bottom of stack

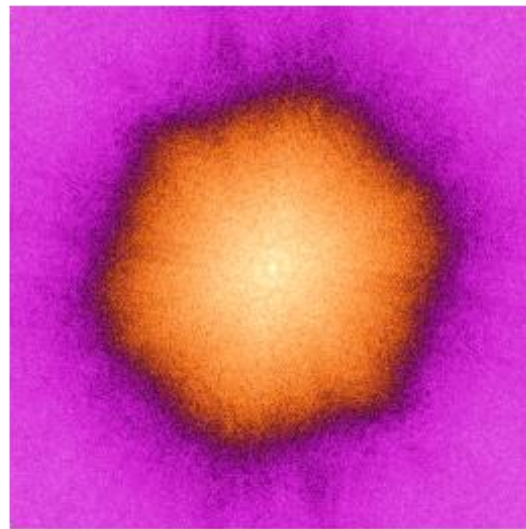
Appendix Figure 7. Fourier Transform of SH1000 labelled with Alexa Fluor 647 from Figure 3.24 D. Fourier transforms of slices from the top, middle and bottom of the z stack showing not only periodic features but also lacking in the petal shape suggesting missing spatial information from images, probably due to the bleaching of Alexa Fluor 647.



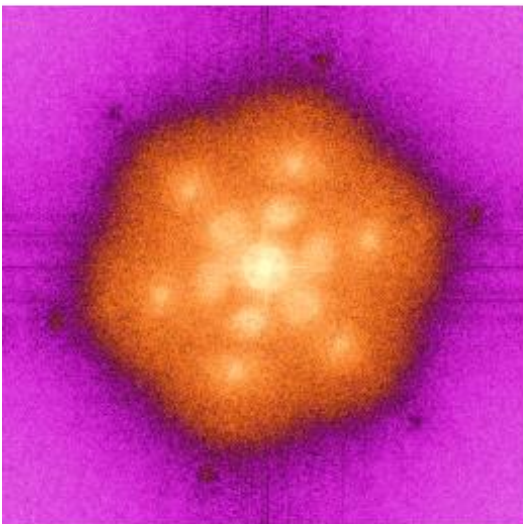
Middle of stack



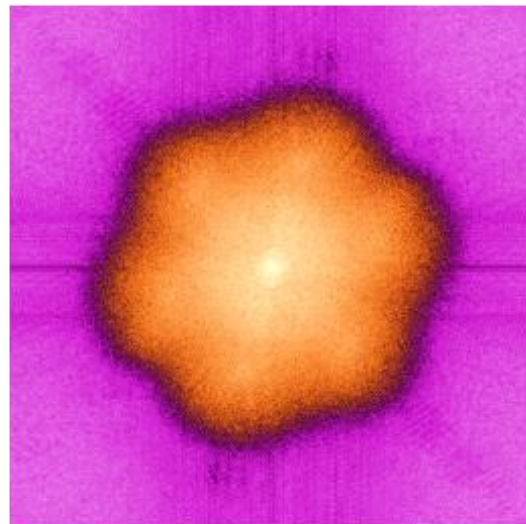
Top of full stack



Top of stack used



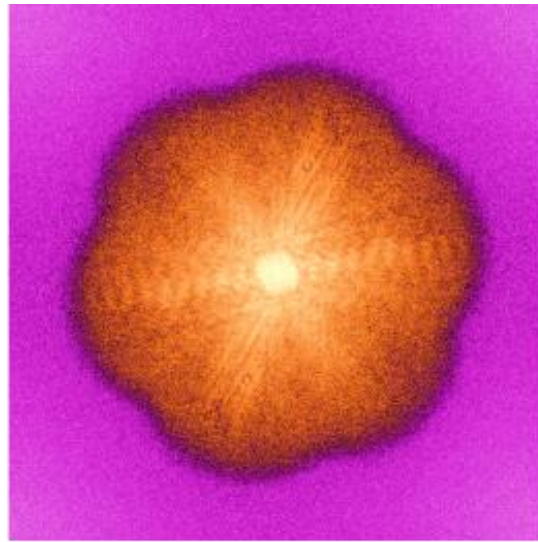
Bottom of full stack



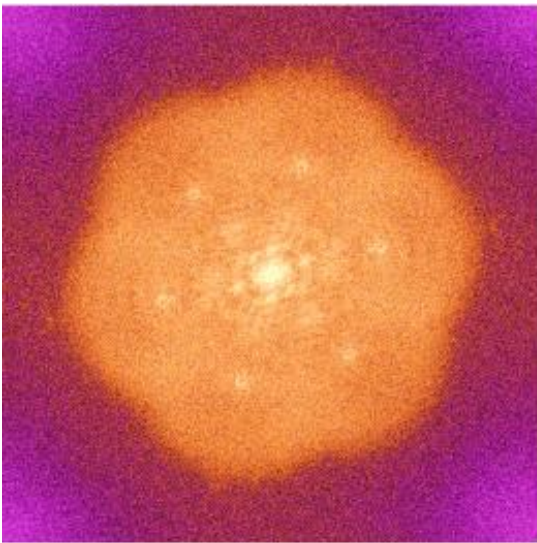
Bottom of stack used

Appendix Figure 8. Fourier Transform of SH1000 from Figure 4.1. Fourier transforms of slices from the top, middle and bottom of the z stack showing periodic structures.

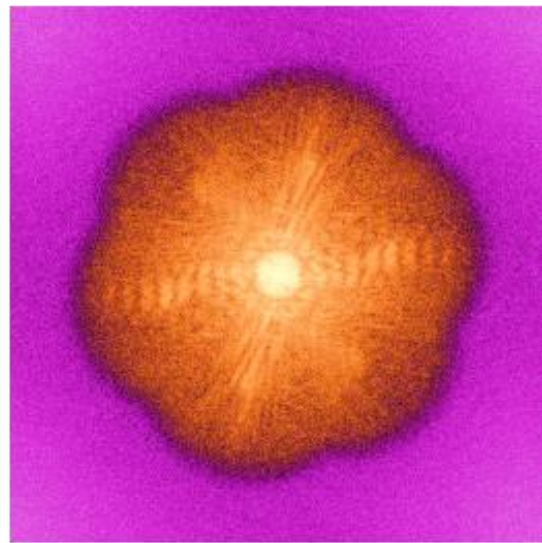
Due to extent of structures in the top and bottom of the full stack a reduced stack was used which minimises the appearance of periodic structures within the Fourier transform.



Middle of stack

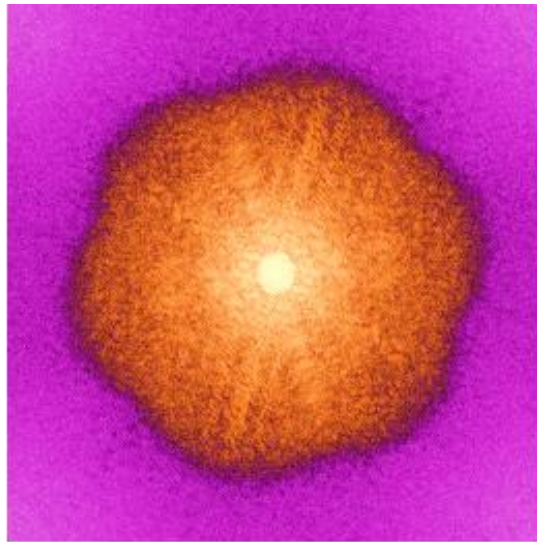


Top of stack

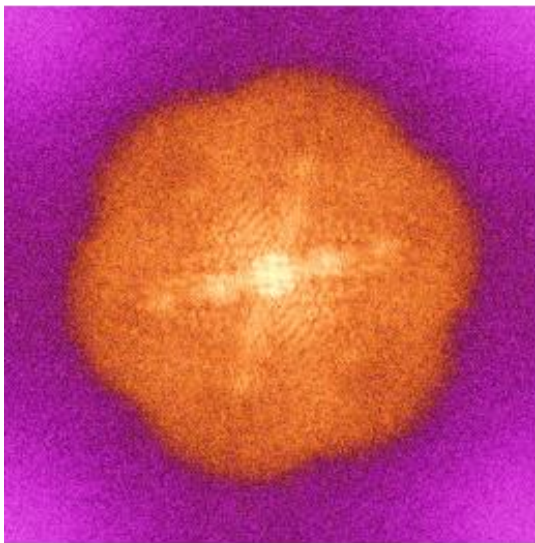


Bottom of stack

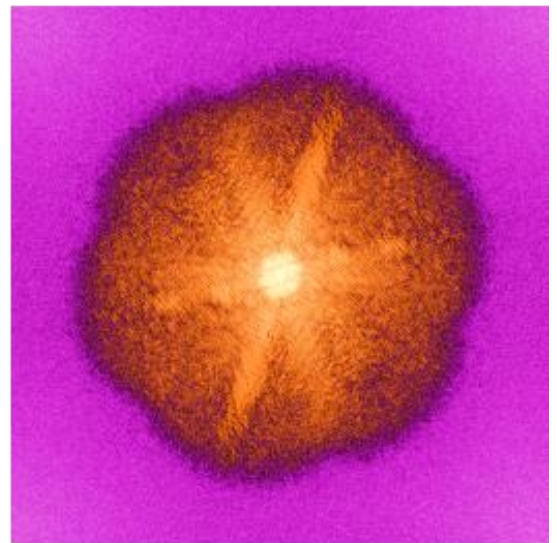
Appendix Figure 9. Fourier Transform of SH1000 from Figure 4.18. Fourier transforms of slices from the top, middle and bottom of the z stack showing periodic structures.



Middle of stack

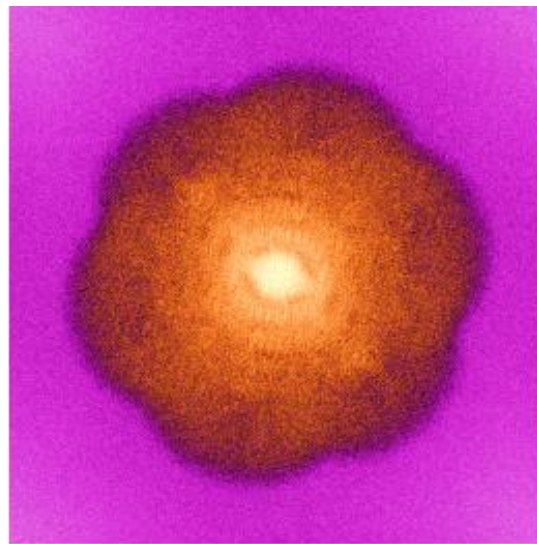


Top of stack

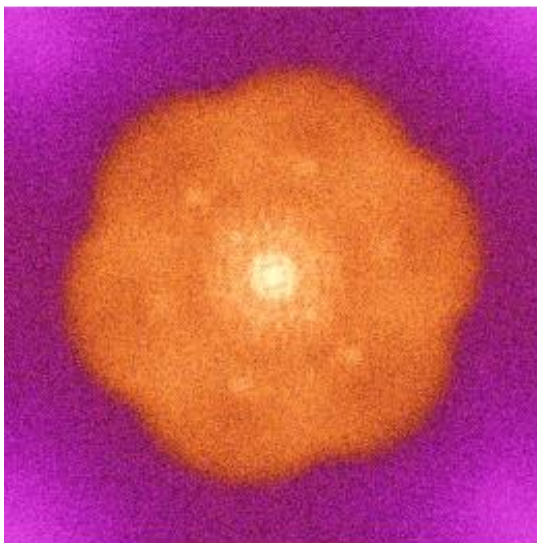


Bottom of stack

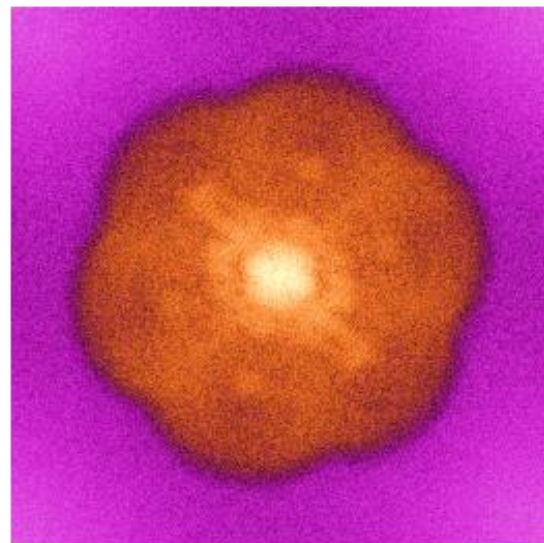
Appendix Figure 10. Fourier Transform of 4421 (*pbp3*) from Figure 4.18. Fourier transforms of slices from the top, middle and bottom of the z stack showing periodic structures.



Middle of stack

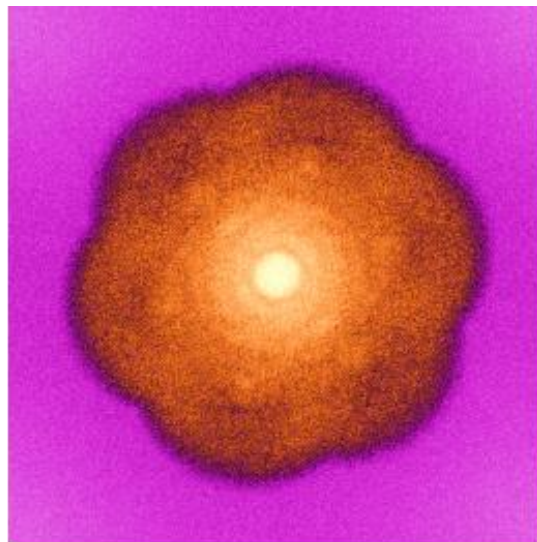


Top of stack

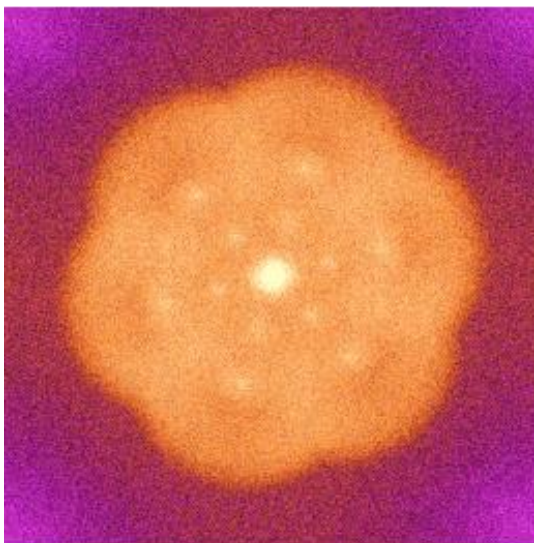


Bottom of stack

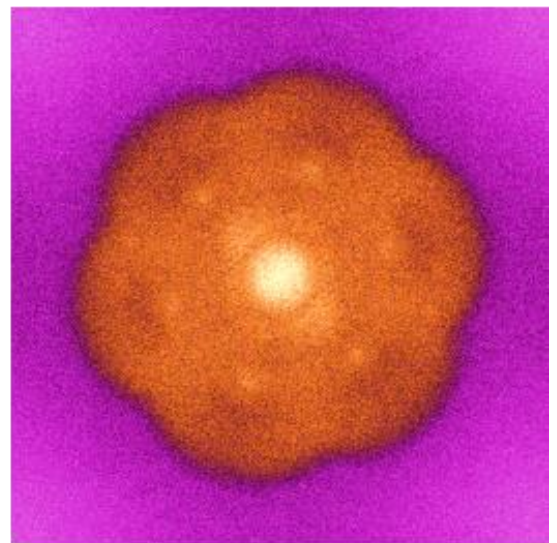
Appendix Figure 11. Fourier Transform of 4425 (*pbp4*) from Figure 4.18. Fourier transforms of slices from the top, middle and bottom of the z stack showing periodic structures.



Middle of stack



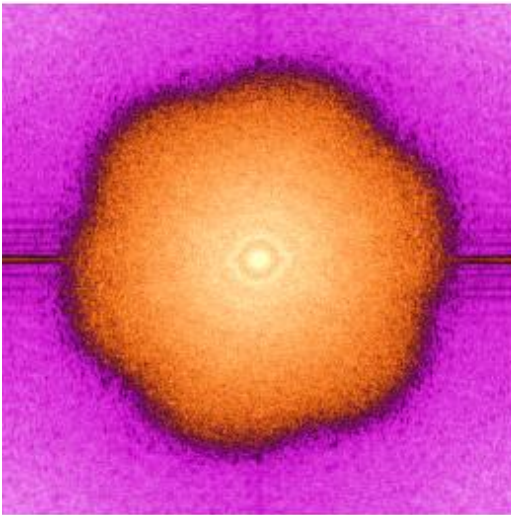
Top of stack



Bottom of stack

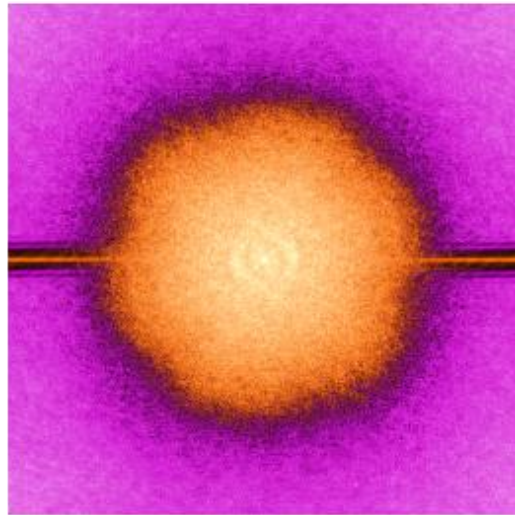
Appendix Figure 12. Fourier Transform of 4424 (*pbp3pbp4*) from Figure 4.18. Fourier transforms of slices from the top, middle and bottom of the z stack showing periodic structures.

HADA

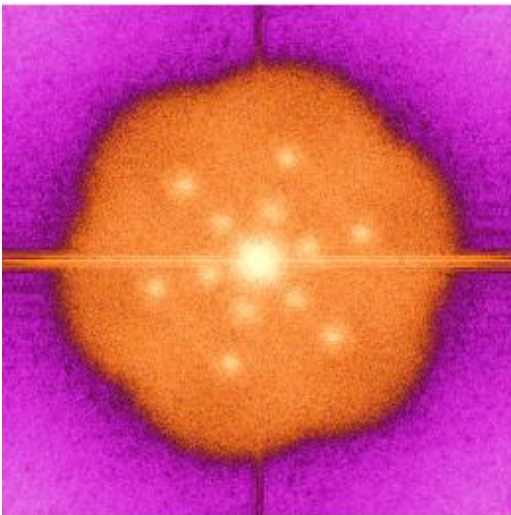


Middle of stack

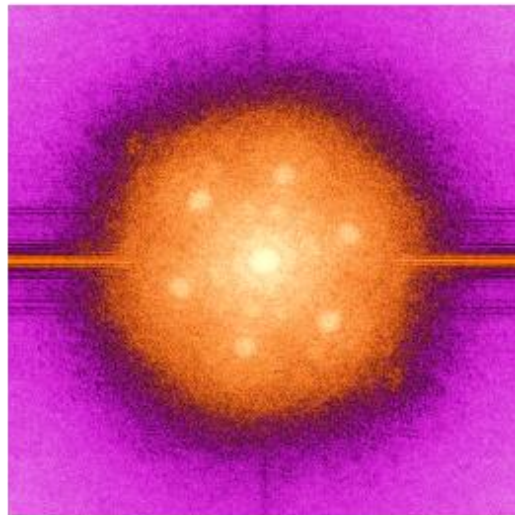
TADA



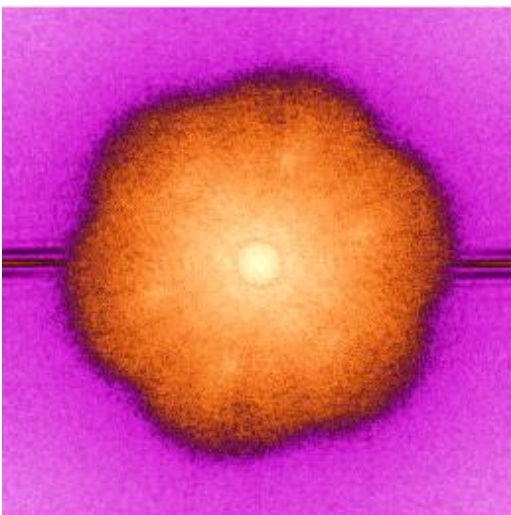
Middle of stack



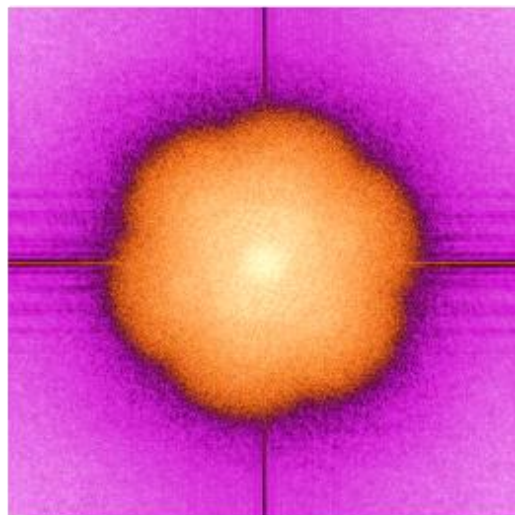
Top of stack



Top of stack



Bottom of stack

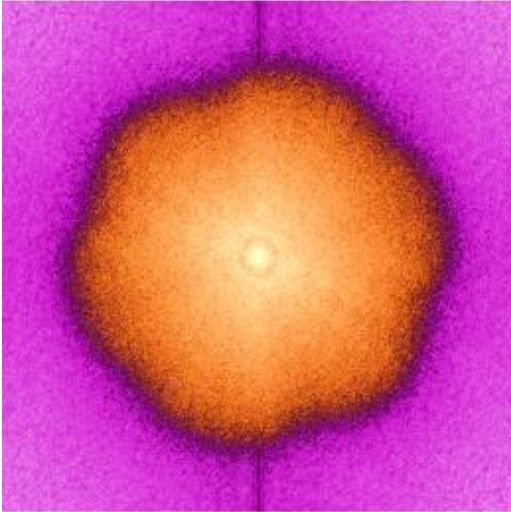


Bottom of stack

Appendix Figure 13. Fourier Transform of dual labelled *S. aureus*. Labelling for 2 hours with HADA and 5 minutes with TADA. Example Fourier transform for a field

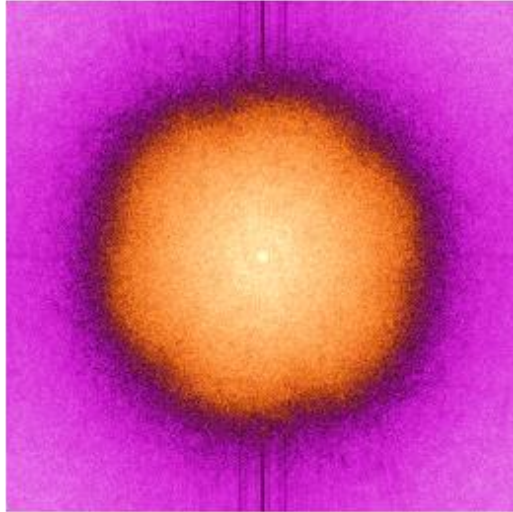
shown in **Figure 5.3**. Fourier transforms of slices from the top, middle and bottom of the z stack showing periodic structures.

HADA

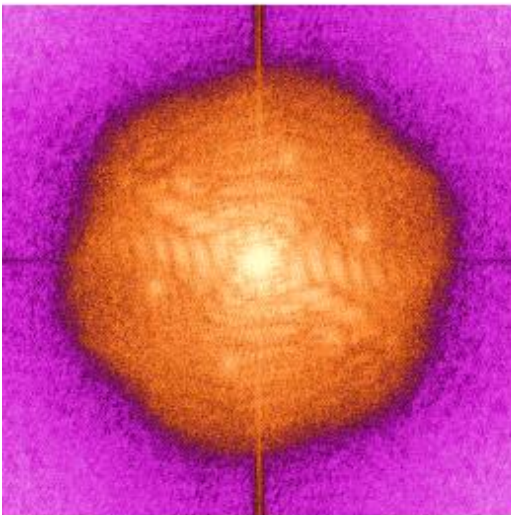


Middle of stack

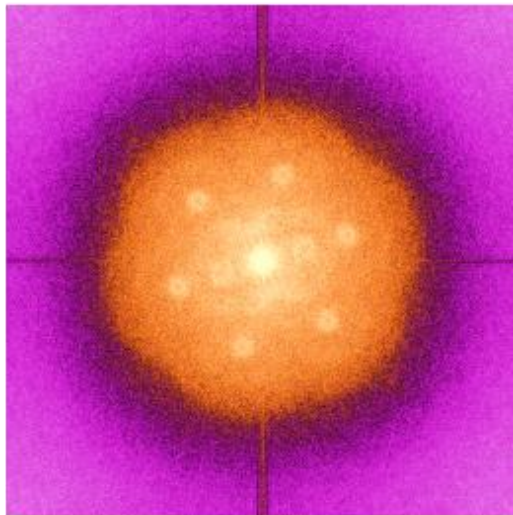
TADA



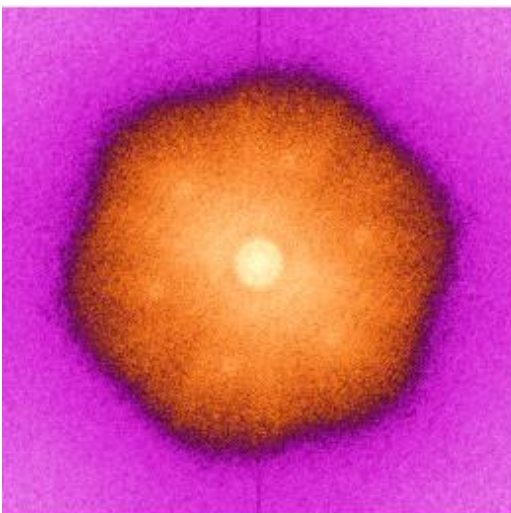
Middle of stack



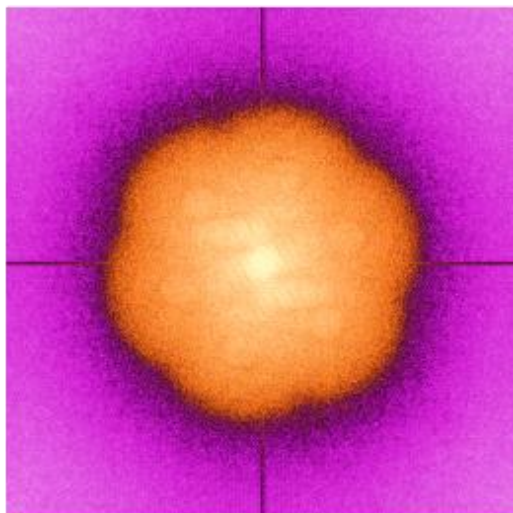
Top of stack



Top of stack



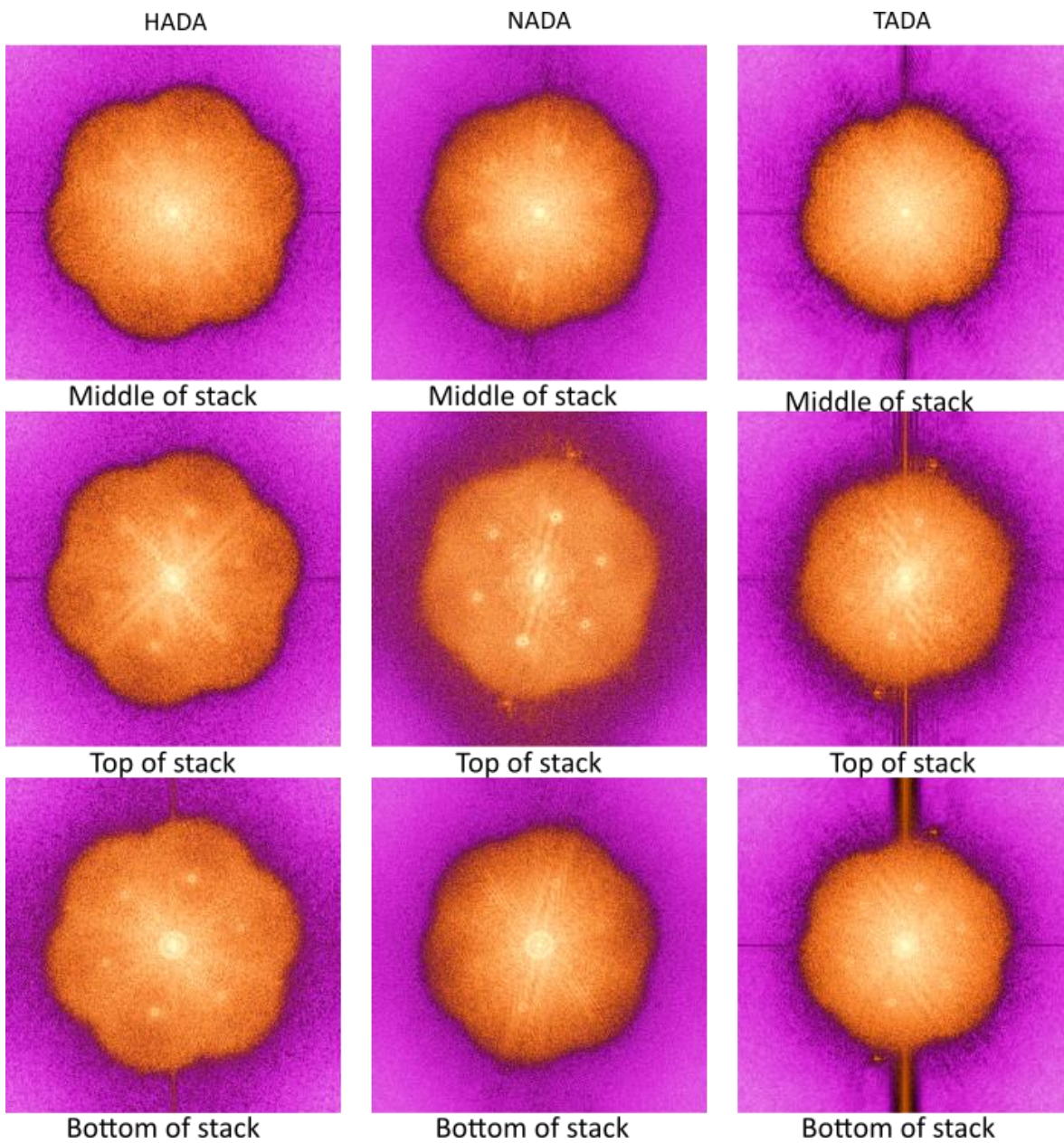
Bottom of stack



Bottom of stack

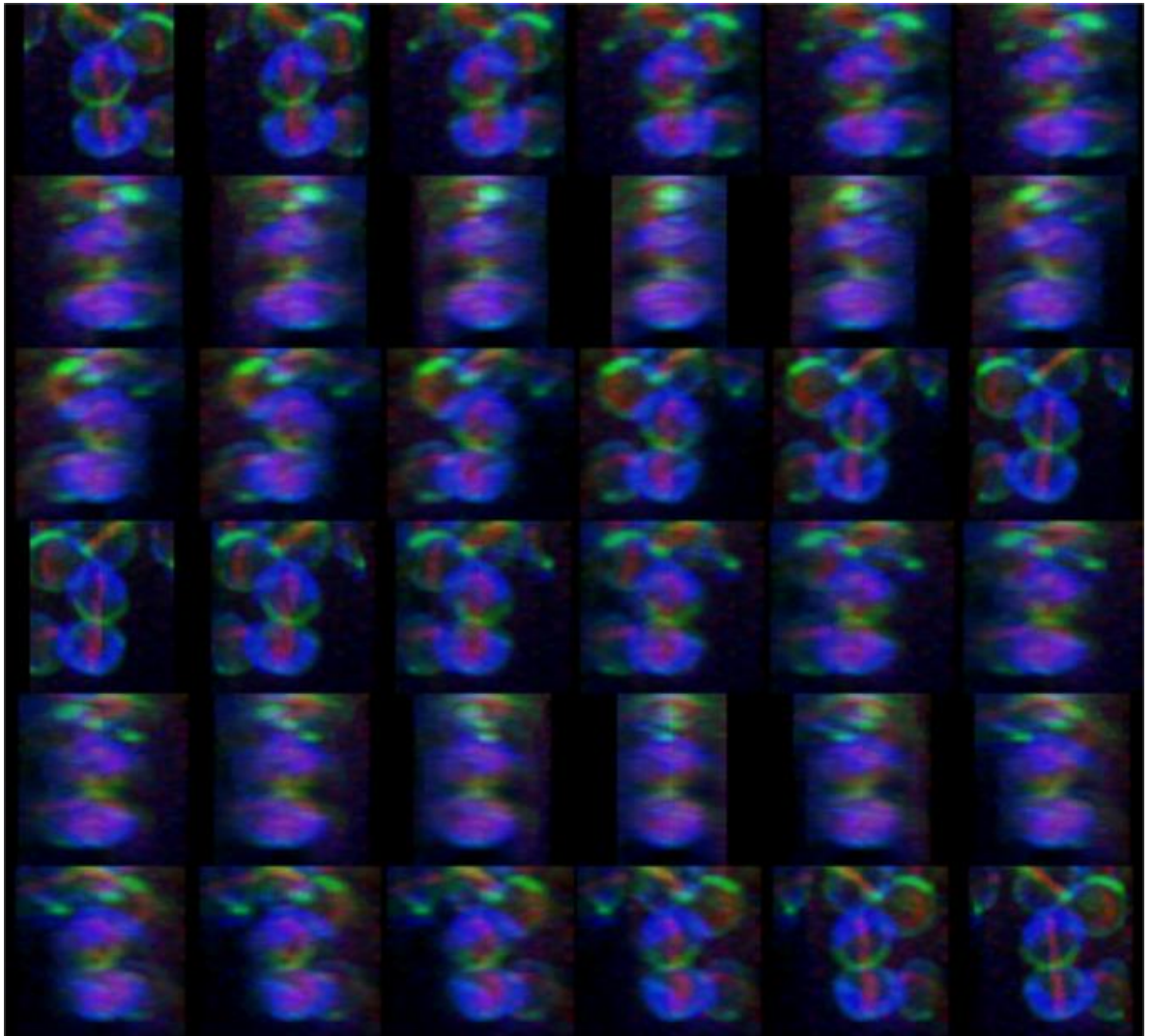
Appendix Figure 14. Fourier Transform of dual labelled *S. aureus* from Figure 5.4.

Labelling for 2 hours with HADA and 2 minutes with TADA. Fourier transforms of slices from the top, middle and bottom of the z stack showing periodic structures.

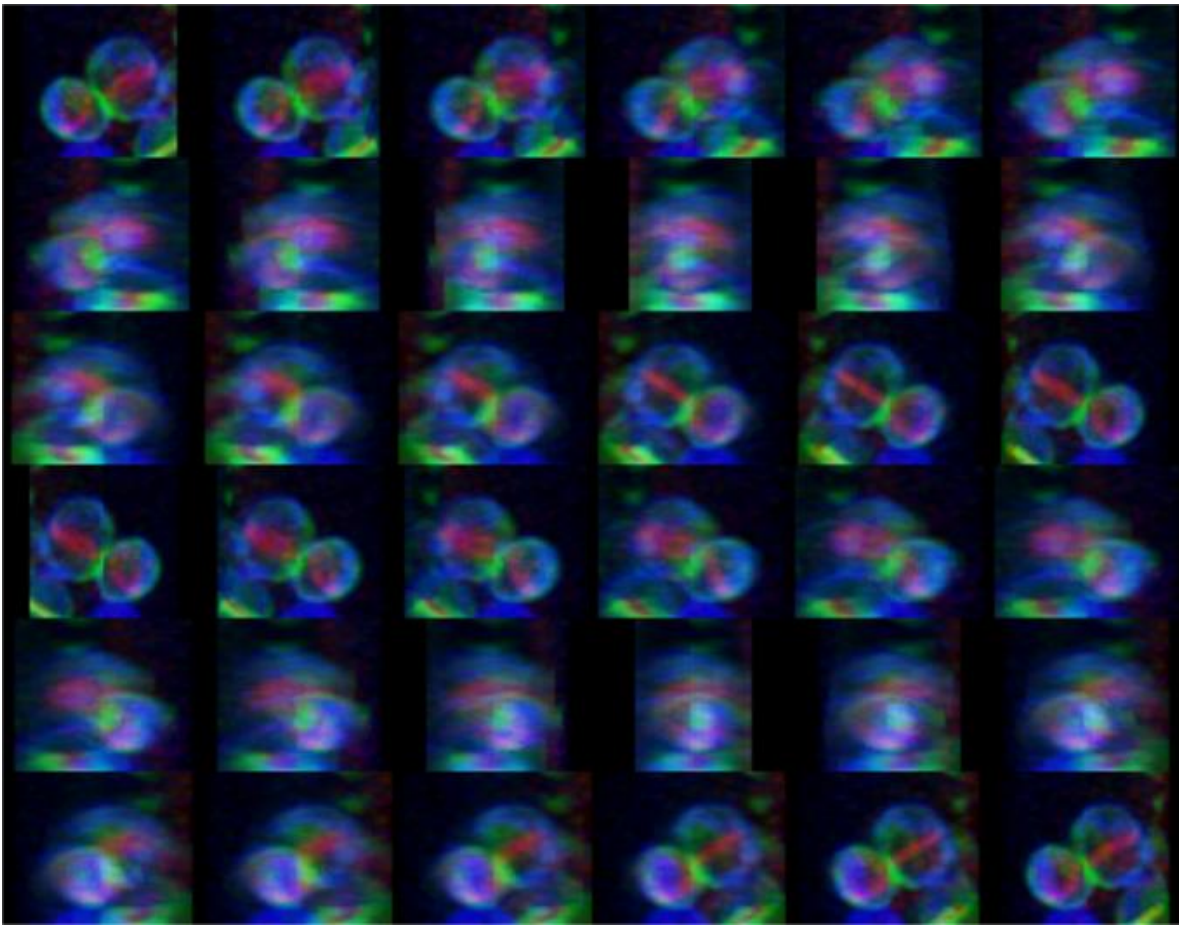


Appendix Figure 15. Fourier transform of triple labelled *S. aureus*. Cells labelled consecutively with HADA, NADA & TADA for 5 minutes. Fourier transforms of slices from the top, middle and bottom of the z stack showing periodic structures. Fourier transforms shown are representative of images used in Figure 5.5 & Figure 5.6.

Appendix III - Stills from movies 1 & 2



Appendix Figure 16. Stills of each frame of Movie 1.



Appendix Figure 17. Stills of each frame of Movie 2.

Appendix IV - Frequency tables for FtsZ & HADA localisations

Time	MidCell	Discrete Foci & Arcs	Single Foci	Whole Cell	No Signal	Peripheral
No PC190723	100	0	0	0	0	0
5 minutes PC190723	100	0	0	0	0	0
10 minutes PC190723	52.1008403	42.85714286	5.042016807	0	0	0
15 minutes PC190723	6.52173913	85.86956522	1.086956522	2.717391304	2.173913043	1.630434783
20 minutes PC190723	2.43902439	90.24390244	1.829268293	4.268292683	0	0
25 minutes PC190723	1.25786164	92.45283019	1.886792453	4.402515723	0	0
30 minutes PC190723	0	89.05109489	0	5.839416058	0.729927007	0
35 minutes PC190723	0	94.24460432	0	5.755395683	0	0
65 minutes PC190723	0	91.94630872	0	6.711409396	0.67114094	0
95 minutes PC190723	0	40.4109589	0	59.5890411	0	0
125 minutes PC190723	0	15.05376344	0	83.87096774	1.075268817	0

Appendix Table 1. Frequencies of FtsZ localisation during PC190723 treatment.

Time	Septal Ring	Septal Plate	Dividing Cells	Peripheral Labelling Only	No Labelling	Cytoplasmic Labelling
No PC190723	38.3116883	59.09090909	1.298701299	0.649350649	0.649350649	0
0-5 minutes PC190723	38.9937107	58.49056604	1.257861635	1.257861635	0	0
5-10 minutes PC190723	38.9937107	58.49056604	1.257861635	1.257861635	0	0
10-15 minutes PC190723	1.08695652	7.065217391	0	87.5	0	4.347826087
15-20 minutes PC190723	0	2.43902439	0.609756098	95.73170732	0	0
20-25 minutes PC190723	0	0.628930818	0	97.48427673	0	0.628930818
25-30 minutes PC190723	0	0	0	100	0	0
30-35 minutes PC190723	0	0	0	95.68345324	0	4.316546763
60-65 minutes PC190723	0	0	0	95.30201342	2.684563758	2.013422819
90-95 minutes PC190723	0	0	0	45.20547945	49.31506849	2.054794521
120-125 minutes PC190723	0	0	0	17.20430108	32.25806452	50.53763441

Appendix Table 2. Frequencies of HADA localisation (peptidoglycan synthesis) for FtsZ-eYFP strains during PC190723 treatment.

Time	Septal Ring	Septal Plate	Dividing Cells	Peripheral Labelling Only	No Labelling	Cytoplasmic Labelling
No PC190723	52.3255814	34.88372093	1.162790698	0	0	0
0-5 minutes PC190723	62.5528367	35.51401869	0.46728972	0	0	0
5-10 minutes PC190723	60.0896861	32.73542601	0.896860987	5.829596413	0	0
10-15 minutes PC190723	0	19.13043478	0.434782609	76.08695652	0	2.173913043
15-20 minutes PC190723	0	12.04188482	0.523560209	86.38743455	0	1.047120419
20-25 minutes PC190723	0	0	0	100	0	0
25-30 minutes PC190723	0	0	0	97.88359788	0	2.116402116
30-35 minutes PC190723	0	0	0	100	0	0
60-65 minutes PC190723	0	0	0	85.53459119	1.257861635	13.20754717
90-95 minutes PC190723	0	0.537634409	0	58.06451613	2.150537634	45.16129032
120-125 minutes PC190723	0	0	0	23.91304348	32.60869565	43.47826087

Appendix Table 3. Frequencies of HADA localisation (peptidoglycan synthesis) for SH1000 during PC190723 treatment.

Appendix V - Quantification of population heterogeneity

Label Pattern	Repeat 1 % of cells (n=689)	Repeat 2 % of cells (n=1159)	Repeat 3 % of cells (n= 1581)	% of Total Cells (n=3429)	Mean % across 3 biological repeats	St dev
No Label	0	0.09	0.38	0.20	0.16	0.20
1 st Label only	0	0.17	0.25	0.17	0.14	0.13
2 nd Label only	0	0	0	0	0	0
3 rd Label only	0	0	0.32	0.15	0.11	0.18
1 st & 2 nd Labels	22.06	8.46	8.10	11.02	12.87	7.96
1 st & 3 rd Labels	0	0.09	0.89	0.44	0.33	0.49
2 nd & 3 rd Labels	0.72	0.17	0.06	0.23	0.32	0.35
All 3 Labels	77.21	91.03	90.01	87.78	84.42	7.70

Appendix Table 4. Quantification of 30 minute HADA, NADA, ADA labelled cells

Label Pattern	Repeat 1 % of cells (n=751)	Repeat 2 % of cells (n=671)	Repeat 3 % of cells (n=1141)	% of Total Cells (n=2736)	Mean % across 3 biological repeats	St dev
No Label	0	0.15	0.46	0.26	0.20	0.23
1 st Label only	1.07	0.45	1.37	1.06	0.96	0.47
2 nd Label only	0	0	0.08	0.04	0.03	0.05
3 rd Label only	0.40	0	0	0.11	0.13	0.23
1 st & 2 nd Labels	4.26	2.83	7.53	5.48	4.87	2.41
1 st & 3 rd Labels	2.40	3.28	3.27	3.03	2.98	0.51
2 nd & 3 rd Labels	0	0.30	0.46	0.29	0.25	0.23
All 3 Labels	91.88	92.99	86.83	89.73	90.57	3.28

Appendix Table 5. Quantification of 30 minute HADA, ADA, NADA labelled cells.

Label Pattern	Repeat 1 % of cells (n=602)	Repeat 2 % of cells (n=775)	Repeat 3 % of cells (n=1038)	% of Total Cells (n=2415)	Mean % across 3 biological repeats	St dev
No Label	0.17	0	0.96	0.46	0.38	0.51
1 st Label only	6.48	3.87	8.38	4.46	6.24	2.26
2 nd Label only	0	0	0	0	0	0
3 rd Label only	0	0	0	0	0	0
1 st & 2 nd Labels	0	0.26	0.19	0.17	0.15	0.13
1 st & 3 rd Labels	8.47	2.84	0.87	3.40	4.06	3.94
2 nd & 3 rd Labels	18.60	2.06	2.12	6.21	7.59	9.53
All 3 Labels	66.28	90.97	87.48	83.31	81.58	13.36

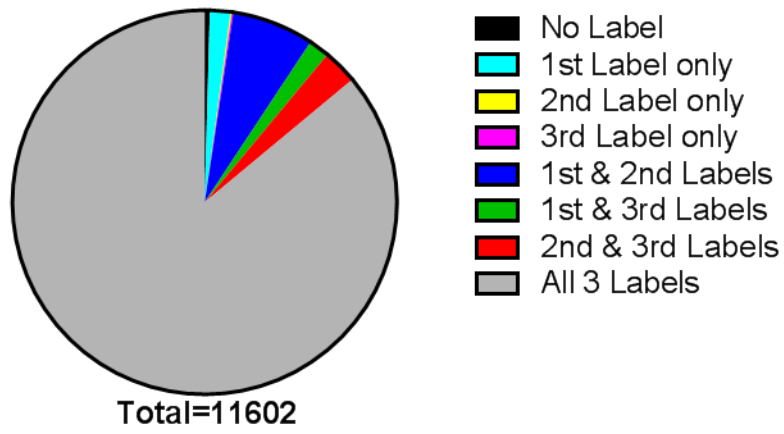
Appendix Table 6. Quantification of 30 minute ADA, HADA, NADA labelled cells.

Label Pattern	Repeat 1 % of cells (n=1066)	Repeat 2 % of cells (n= 487)	Repeat 3 % of cells (n=1421)	% of Total Cells (n=2974)	Mean % across 3 biological repeats	St dev
No Label	0	0	1.76	0.84	0.59	1.02
1 st Label only	0.19	0	0.56	0.34	0.25	0.28
2 nd Label only	0.56	0.62	0.21	0.40	0.46	0.22
3 rd Label only	0	0	0.42	0.20	0.14	0.24
1 st & 2 nd Labels	13.41	7.60	2.81	7.40	7.94	5.31
1 st & 3 rd Labels	0.09	0	1.41	0.71	0.5	0.79
2 nd & 3 rd Labels	9.76	9.45	1.69	5.58	6.97	4.57
All 3 Labels	75.98	82.34	91.14	84.26	83.15	7.61

Appendix Table 7. Quantification of 30 minute ADA, NADA, HADA labelled cells.

Label Pattern	HADA_ NADA_ ADA (n=3429)	HADA_ ADA_ NADA (n=2736)	ADA_ HADA_ NADA (n=2415)	ADA_ NADA_ HADA (n=2974)	% of Total Cells (n=11602)	Mean % across all Labelling Orders	St dev
No Label	0.20	0.26	0.46	0.84	0.43	0.44	0.29
1 st Label only	0.17	1.06	4.46	0.34	1.73	1.51	2.01
2 nd Label only	0	0.04	0	0.40	0.11	0.11	0.19
3 rd Label only	0.15	0.11	0	0.20	0.12	0.12	0.09
1 st & 2 nd Labels	11.02	5.48	0.17	7.40	6.90	6.02	4.52
1 st & 3 rd Labels	0.44	3.03	3.40	0.71	1.73	1.90	1.54
2 nd & 3 rd Labels	0.23	0.29	6.21	5.58	2.93	3.08	3.26
All 3 Labels	87.78	89.73	83.31	84.26	86.04	86.27	3.00

Appendix Table 8. Overall quantification of 30 minute triple labelled cells.



Appendix Figure 18. Pie chart of combined quantification of triple labelled cells.